A biomimetic approach to *in vitro* dentinogenesis inspired by the mechanobiology of dental pulp

Laura Lee Elsie Whitehouse

Submitted in accordance with the requirements for the degree of Doctor of Philosophy

The University of Leeds

School of Dentistry

November 2023

INTELLECTUAL PROPERTY AND PUBLICATION STATEMENTS

The candidate confirms that the work submitted is her own, except where work which has formed part of jointly authored publications has been included. The contribution of the candidate and the other authors to this work has been explicitly indicated below. The candidate confirms that appropriate credit has been given within the thesis where reference has been made to the work of others.

This work makes reference to a publication published during the PhD period. The details of this publication are below:

Whitehouse, L. L. E., Thomson, N. H., Do, T., & Feichtinger, G. A. (2021, July 1). BIOACTIVE MOLECULES FOR REGENERATIVE PULP CAPPING. *European Cells and Materials*. AO Research Institute Davos. https://doi.org/10.22203/eCM.v042a26

This work was authored and devised by the candidate. The other authors provided input on structure, content and format as well as reviewing the manuscript. This work is referenced in Chapter 1, INTRODUCTION AND BACKGROUND.

ACKNOWLEDGEMENTS

No man (or woman) is an island, and although this work is my own, it would not have been possible without the help, support and input of many people.

Firstly, I need to thank my funders: The Pathological Society of Great Britain and Ireland, The Royal college of Surgeons (England) and The British Society of Oral and Maxillofacial Pathology for their research funding. The research costs of this PhD were gathered in a piecemeal fashion from these bodies and without their generosity and understanding with regards to altering deadlines in the light of the COVID-19 pandemic, this work would not have been possible. Small research grants such as the ones I was awarded are vital for early career researchers and I hope more funding becomes available in the future to support early-career academics, particularly in basic science as this is where every innovation begins. I also need to thank the University of Leeds for my Leeds Doctoral Scholarship, and the School of Dentistry for putting me forwards for this award; without this I would not have been able to afford the time away from my clinical work to complete this PhD.

Secondly, I would like to thank my supervisors, mentors and examiners. My supervisors Thuy and Jing have offered unwavering optimism and great technical support with complex laboratory procedures and statistics respectively. Neil has always provided a level-headed approach and quick replies to my numerous lengthy emails, and he has always had time to support me with the many grant applications, thesis revisions and issues that have arisen during the PhD journey. I have been entirely dependent on their support and guidance throughout this process, and I cannot thank them enough. They have remained patient, understanding and empathetic throughout the last four years and I have valued their wisdom, experience and expertise in trying times. When I doubted myself, they never once questioned whether I would complete this work. My mentor, Nick West (University of Leeds), has given me sound guidance throughout the PhD and I'm grateful for the advice he has provided. I also need to thank my examiners for taking time from their busy schedules to read my thesis and examine my work.

Thirdly, I need to thank my fellow PhD students, post-doctoral researchers, and laboratory staff in Oral Biology, Pathology and Physics. Particular recognition must go to Michael Brooks for his help with the scanning electron microscopy, Sarah Myers for her help with the tissue bank and cell culture and Emma Black for her support with tissue culture.

Fourthly, I have to thank my family and friends. I am incredibly blessed to have such wonderful people in my life. My parents and brother always offer me unwavering support even when they do not understand what I'm doing. They have made me the 'determined little bugger' that I am and I will never be able to repay their love, kindness and support.

Niall, my husband, best friend and side-kick for life, puts up with far more than he should have to. Over the past four years, he has supported us financially, been the primary carer for our daughter, and made

countless cups of tea and coffee. I would be lost without you. You are my anchor in every stormy sea and my home, wherever we end up.

Finally, I must end with an apology to my amazing, beautiful, smart, funny, mischievous, joy-filled daughter Kitty. I should have been there more for you over the first two years of your life. And for this, I am sorry. I will never regain the time together we have lost through working long days, short maternity leave and hours working from home, but I will try to be the best parent I can be going forwards. It is tough balancing being a parent and working, but you make everyday special and magical.

ABSTRACT

Dental caries is a global burden. When a tooth is badly damaged by caries, reparative dentine may be produced, sealing the pulp from harmful external stimuli. Reparative dentine is produced following odontoblast death, where a new generation of odontoblast-like cells are created following the migration and differentiation of dental pulp stem cells. Although we have some awareness of the mechanisms behind this, we do not fully understand the physical and biological changes that may be occurring in the pulp to influence reparative dentine production.

This project has explored, for the first time, the elastic modulus of the dental pulp of carious and sound teeth at the nano and micro level and found it to have a clear non-monotonic gradient behaviour, with the core having a statistically lower elastic modulus than the coronal and apical areas. Statistical differences between carious and sound teeth were also identified close to the dentine-pulp junction. To link the mechanical changes identified in the pulp to the underlying biology, RNA next generation sequencing and histomorphometric analysis of pulpal collagen bundles was completed. For RNA sequencing, more genes were upregulated in carious teeth than sound, with genes pertaining to neural functioning, signalling and inflammation being the most commonly differentially expressed genes. The histomorphometric analysis identified a reduction in the width and volume of collagen fibres towards the centre of the pulp. More fibres generally in sound teeth than carious were also identified, correlating to the elastic modulus findings.

Agarose hydrogel scaffolds with a range of elastic moduli were created, guided by the dental pulp outcomes. These scaffolds were used to successfully produce hard tissue *in-vitro* and facilitate differentiation of dental pulp stem cells. Agarose has not been used before to facilitate odontogenic differentiation. This work can be taken forwards for therapeutic applications such as dental pulp capping.

CONTENTS

Lists of Tables and Illustrative Material

Tables

Figures

1. INTRODUCTION AND BACKGROUND

4. CHARACTERISATION AND CORRELATION OF THE ELASTIC MODULUS OF THE DENTAL PULP, THE PULP TRANSCRIPTOME AND COLLAGEN BUNDLES IN SOUND AND CARIOUS TEETH

Equations

4. ATOMIC FORCE MICROSCOPY, RNA SEQUENCING AND HISTOMORPHOMETRIC CONFOCAL MICROSCOPY OF THE PULP IN CARIOUS AND SOUND TEETH

Abbreviations

A	Adenine
AB	Alamar Blue
AFM	Atomic Force Microscopy
AKT	v-Akt Murine Thymoma Viral Oncogene
ALP	Alkaline Phosphatase
AM	Acetomethoxy
BMP2	Bone Morphogenetic Protein 2
BMP4	Bone Morphogenetic Protein 4
BMP7	Bone Morphogenetic Protein 7
BSA	Bovine serum albumin
BrdU	Bromodeoxyuridine
BSE	Back Scatter
BSP	Bone sialoprotein
C	Cytosine
cDNA	Complementary DNA
CP	Crossing Point
cPCR	Comparative PCR
DAB	3,3'-diaminobenzidine
DAPI	4′,6-diamidino-2-phenylindole
DFPC	Dental follicle progenitor cells
DMEM	Dulbecco's Modified Eagle Medium
DMP1	Dentin matrix acidic phosphoprotein
DMSO	Dimethyl sulfoxide
DNA	Deoxyribonucleic acid
DPC	Dentino-pulp complex
DPSC	Dental Pulp Stem Cells
DPX	Dibutylphthalate Polystyrene Xylene
DSPP	Dentine sialophosphoprotein
ECM	Extra cellular matrix
EDS	Energy Dispersive X-ray Spectrometry
EDTA	Ethylenediaminetetraacetic acid
EGF	Epidermal growth factor
EH	Ethidium homodimer I
FBS	Fetal bovine serum

FGF2	Fibroblast growth factor 2
FP	Floor of pulp
FVM	Force volume map
G	Guanine
GCSF	Granulocyte-colony stimulating factor
H	Hydrogen
H3342	Hoechst 3342
HEPES	4--1-piperazineethanesulfonic acid
HLA	Human leukocyte antigen
HPLL	High molecular weight poly-l-lysine
IDPSC	Immature dental pulp stem cells
IF	Immunofluorescence
IGF-1	Insulin-like growth factor 1
IHC	Immunohistochemistry
InvOLS	Inverse Optical Lever Sensitivity
IQR	Inter-quartile range
JNK	Jun amino-terminal kinases
LDH	Lactate dehydrogenase
LIPUS	Low intensity pulsed ultrasound
LPDL	Low molecular weight poly-d-lysine
LPLL	Low molecular weight poly-l-lysine
MA	Mean average
MAPK	Mitogen-activated protein kinase
MP	Mid pulp
MRN	Median ratio normalization
mRNA	Messenger RNA
MTA	Mineral Trioxide Aggregate
mTOR	Mammalian target of rapamycin
Na	Sodium
NF-κB	Nuclear factor kappa light chain enhancer of activated B cells
NGS	Next generation sequencing
padj	Adjusted p-value
PBS	Phosphate buffered saline
PBST	Phosphate buffered saline with 0.1% Tween 20
PC	Principal component

PCA	Pulp Capping Agent
PCR	Polymerase chain reaction
PDL	Poly-d-lysine
PDLSC	Periodontal ligament stem cells
PGA	Polyglycolic acid
PI3K	Phosphoinositide 3-kinase
PLA	Polylactic acid
PLGA	Poly(lactic-co-glycolic) acid
PLL	Poly-l-lysine
qPCR	Quantitative PCR
RIN	RNA integrity number
RLE	Relative log expression
RNA	Ribonucleic acid
RNAseq	RNA sequencing
ROS	Reactive oxygen species
rRNA	Ribosomal RNA
RT-PCR	Reverse transcription PCR
SCAP	Stem cells from apical papilla
SCF	Stem cell factor
scRNA-seq	Single cell RNA sequencing
SD	Standard deviation
SE	Standard error
SEM	Scanning electron microscopy
SHED	Stem cells from exfoliated deciduous teeth
SIBLING	Small integrin-binding ligand N-linked glycoprotein
T	Thymine
TGF-β1	Transforming growth factor beta 1
TMM	Trimmed Mean of M-values
UV	Ultra-violet
VEGF	Vascular endothelial growth factor
Wnt	Wingless and Int-1
α-MEM	α-Modified Eagle Medium

1. INTRODUCTION AND BACKGROUND

1.1 DENTINE AND DENTAL CARIES

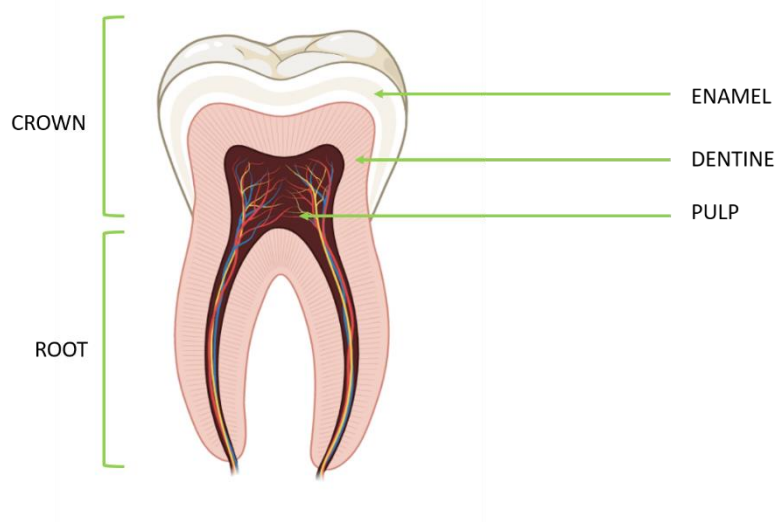

Figure 1.1 1: Basic structure of a molar tooth, demonstrating the hard enamel and dentine and soft inner pulp. Created with BioRender.com.

Caries (dental decay) is the most prevalent non-communicable human disease. The Global Burden of Disease Study estimated that 3.58 billion people worldwide have untreated caries (1). Caries is linked to low quality of life (2) and depression (3). In 2015, the global direct cost of caries (e.g. cost of dental treatment due to decay) was estimated at being $356.80 billion, with indirect costs (e.g. absence from work) estimated at $187.61 billion (4), highlighting the significant impact caries has at a global level. If left untreated, caries will eventually cause the tooth to become non-vital. A non-vital tooth can lead to further dental pathologies such as acute/chronic periapical periodontitis, periapical granuloma, radicular cyst, acute/chronic apical abscess, and life-threatening Ludwig's angina.

The crowns of teeth comprise enamel, dentine and pulpal tissue (Figure 1.1 1). Enamel is the strongest substance the body can produce and is acellular (and therefore incapable of cellular repair). Enamel has a complex, prismatic, lattice-like structure, and is up to 98% inorganic content by weight, with hydroxyapatite ($Ca_{10}(PO_4)_6(OH)_2$) making up ~92% of the mineral content (5).

Below the enamel layer is dentine. Dentine is softer than enamel, with a higher organic content (approximately 20%), predominantly made up of collagen Type I (90% of the organic content), with the remaining organic content being made up of non-collagenous proteins (for example; dentine phosphoproteins) and lipids (6). Dentine is a living structure, and the inorganic content is relatively similar to bone, being predominantly hydroxyapatite, and calcium and phosphate salts (6).

Odontoblasts ('dentine producing cells') are responsible for the production of the organic content of dentine (predominantly type I collagen), and its subsequent mineralisation both during tooth

development and after eruption (7). During primary dentinogenesis (initial dentine production during which teeth are formed), odontoblasts firstly produce fibronectin, and collagen type III, which calcifies as the odontoblast matures. Once the odontoblast is mature, it begins depositing collagen type I which acts as the framework for dentine prior to mineralisation (6).

Mineralisation of dentine occurs when the secreted organic matrix is typically 20-30µm thick (7). Odontoblasts have a long cytoplasmic extension that resides within fine tubules that run throughout the dentine, from the enamel-dentine junction to the pulp. The cytoplasmic projection gradually extends as dentine is produced and the odontoblast cell body is pushed towards the centre of the tooth by the deposited dentine behind it. Cytoskeleton filaments, such as microtubules and intermediate filaments are the main components of the cytoplasmic projection (7). After primary dentinogenesis, the odontoblast's nucleus and remainder of the cytoplasm resides at the periphery of the pulp, adjacent to a layer of predentine (the organic, dentine matrix deposited prior to mineralisation, composed of collagens, proteoglycans and glycoproteins) (Figure 1.1 2) (7). Histologically, odontoblasts have a polarised morphology, with secretion of predentine happening at the end opposite to the nucleus (7,8). Although dentine is similar in its molecular make-up to bone, odontoblasts are different to osteoblasts (bone-producing cells), because they deposit dentine in a unilateral progressive manner and thus do not get fully encased by the mineral they produce (as occurs with Volkmann's canals and Haversian canals in bone). This means that, unlike bone, no physiological remodelling or repair can occur in dentine that has already been produced (8).

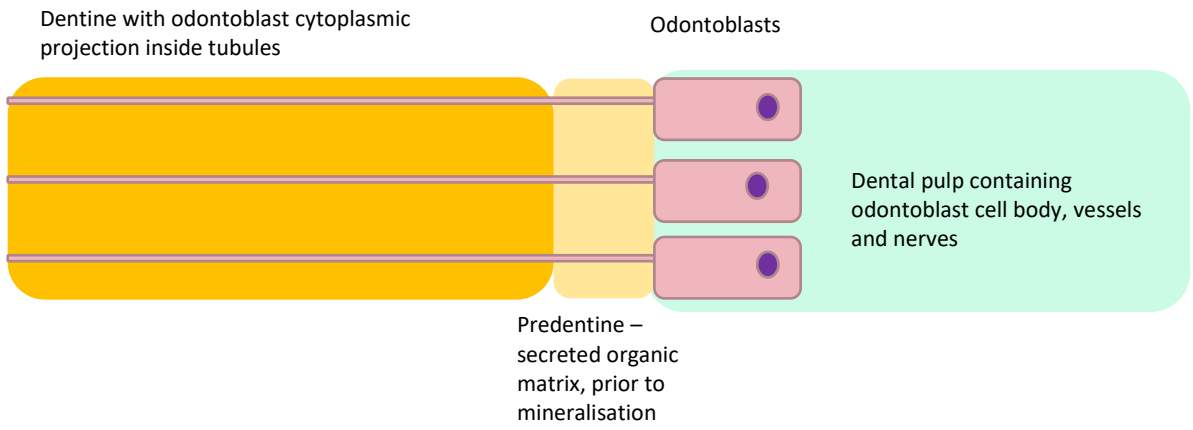

Figure 1.1 2: Schematic diagram of the dentine-pulp complex

The dental pulp contains the vessels and nerves that maintain the vitality of the tooth, in addition to the odontoblast cell body. The pulp is a soft structure made up of loose connective tissue (75% water, 25% organic matrix)(6). The main protein found in the pulp is collagen type I, followed by collagen type III (6). In addition to collagens, numerous other proteins are present, such as; decorin, biglycan, and fibronectin, to name but a few. These proteoglycans and glycoproteins, coupled with collagen, can influence cell migration, proliferation, adhesion, differentiation, and function by acting on the cells

present within the dental pulp (6). The complex framework of collagens and their association with resident proteoglycans and glycoproteins stabilises the structure of the pulp, giving it unique "gel-like properties" (6).

The most common cell type in the dental pulp is the fibroblast, however the pulp is also home to stem cells (termed 'Dental Pulp Stem Cells' (DPSCs), first isolated by Gronthos *et al*.(9)), and leukocytes (white blood cells). In health, leukocytes are less than 1% of the total cell population of the pulp, with granulocytes and neutrophils being the main subtype, followed by T lymphocytes, monocytes, dendritic cells, natural killer cells and B lymphocytes (8). Although leukocytes are integral to the immune response of the pulp to caries and trauma, odontoblasts act as the first line of defence against caries by providing an barrier function due to the tight junctions between the odontoblasts and through the production of antibacterial products (for example, cationic host defense peptides – released following binding of bacterial products with toll-like receptors on the odontoblast) (8) . (8)

The pulp has historically been separated into histologically distinct zones. Beneath the odontoblast layer is a 'cell-free zone', largely consisting of vascular and neuronal complexes (for example, the plexus of Raschkow, which is a dense neuronal complex, with projections into the dentinal tubules, running alongside odontoblastic processes; it is presumed there is cross-talk between the two structures (6,8)). This is followed by a 'cell-rich zone' which again is rich in vessels, but also contains pulpal fibroblasts and some DPSCs. The final zone is the 'central core', this again contains fibroblasts, DPSCs and vessels (6). The pulpal vascular and neuronal networks enter the pulp via apical foramina at the end of the roots and arise from the adjacent alveolar bone of the mandible and maxilla (6,8).

As alluded to above, dentine and pulp are inextricably linked (termed together 'dentino-pulp-complex' (DPC)). They share embryological origin (as they are both derived from the cranial neural crest (8)) and both release factors acting on the other (10). DPC maintains the tooth's vitality and is the only part of the tooth with *in-vivo* regenerative potential and is being increasingly studied as a potential for biological scaffold production (11–15), as the reparative process of one cannot be considered without the other.

In health, odontoblasts are largely inactive after primary dentinogenesis and tooth formation. Over time and as the individual ages, they lay down a low volume of dentine termed 'secondary dentine'; this is very slow (up to 10 times slower than primary dentinogenesis, at 0.4µm per day)(6). Over time, this leads to the pulp chamber becoming smaller as an individual ages. However, following mild injury to the pulp (for example due to caries or less likely, trauma), odontoblasts do play a role in wound healing in the form of tertiary dentinogenesis (specifically reactionary dentine), whereby the odontoblasts lay down dentine more quickly to seal the vital pulp from the insult. Should the injury be great enough to kill the odontoblasts, a new generation of 'odontoblast-like' cells will migrate to the site of injury and begin laying down dentine, resulting in a tertiary dentine bridge (reparative dentine). These

'odontoblast-like' cells are widely thought to arise from resident DPSCs and this is largely due to the knowledge that DPSCs are capable of differentiating into odontoblast-like cells *in vitro* and the presence of cells resembling odontoblastic morphology adjacent to tertiary dentine in healthy teeth used for pulp capping studies (16) , though some controversy exists as to whether this hard tissue is actually produced by fibroblasts (8,16). The belief that reparative dentine is produced by fibroblasts has some backing in the scientific community for numerous reasons such as: 1) Mesenchyme-derived tissues often display histological increases in collagen production from fibroblasts, which leads to dystrophic calcifications (e.g. dental pulp stones), 2) The lack of a tubular architecture characteristic of dentine in reparative dentine, 3) The odontoblast-like cells found adjacent to tertiary dentine in teeth exposed to caries often have a flattened morphology, not in-keeping with the traditional columnar appearance of an odontoblast (16). A less popular theory is that the odontoblast-like cells derive from daughter cells, the production of the last mitoses of odontoblasts during tooth development, theoretically located in the cell-rich zone of the pulp (7).

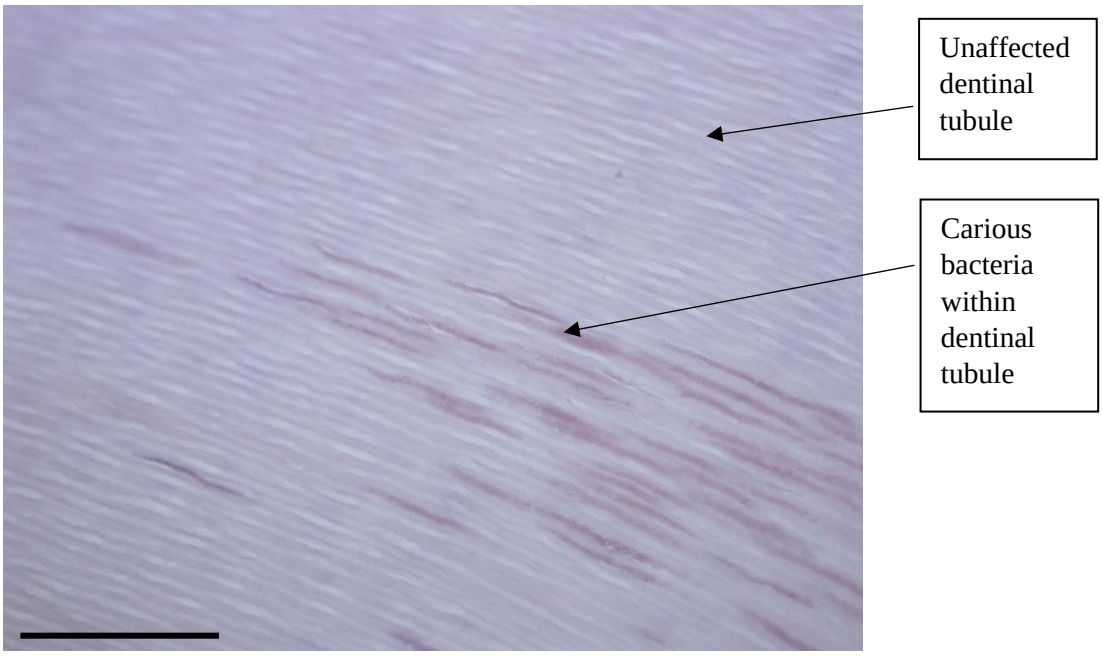

Figure 1.1 3: Histological image of carious ingress into dentine tubules. Haematoxylin and eosin stain (H and E), scale bar = 20µm

Caries is a broad term given to describe dental decay. Caries is understood to be the result of a long-standing interaction between acid-producing micro-organisms and fermentable carbohydrates, though the exact oral microenvironment and host differences are believed to influence progression (17). Dental biofilms are complex networks composed of extracellular polymers (mainly polysaccharides) and polymicrobial communities. No one organism is understood to be responsible for caries, with species of *Streptococcus*, *Lactobacillus*, *Actinomyces*, *Scardovia* and *Bifidobacterium* all implicated in either acid-production or addition to the biofilm polysaccharides (17). See Figure 1.1 3 for a histological image of carious bacteria invading dentine tubules.

Caries develops through complex biological interactions between acidogenic bacteria, fermentable carbohydrates and a suitable tooth surface(18). Bacteria reside on the tooth surface within a biofilm, and whilst biofilms develop in all humans, they only become cariogenic following the consumption of fermentable carbohydrates (19). Biofilms are a community of bacteria enmeshed within a polysaccharide matrix, composed of numerous different bacterial species that synthesise extra-cellular polymeric substances (including glycoproteins, proteins and glycolipids) that aid in protection of the bacterial population, influence their bacteria-to-bacteria interactions and adhesion to both the tooth surface and each other (19). Within the oral cavity, a biofilm develops following adhesion of the carious bacteria to the pellicle (a thin layer of salivary proteins on a surface) (19). The bacteria metabolise fermentable carbohydrates to produce extracellular polysaccharides, which increase adhesion and protect the developing bacterial colony (19). The biofilm typically has low oxygen levels available for metabolism, so anaerobic glycolysis is frequently used, leading to adenosine triphosphate production (necessary for bacterial growth and metabolism) and lactic acid as a by-product(19). Lactic acid causes demineralisation of the tooth surface, resulting in tooth structure damage(19). As caries advances through the enamel, dentine and pulp, the biofilm adapts to the increasingly anaerobic environment, with a higher bacterial diversity observed (20).

Dentinogenesis by odontoblasts in response to caries (reactionary dentinogenesis) is complex and multifactorial, being affected by numerous molecular events and pathways, collated and discussed in a comprehensive review by da Rosa *et al.* (21). Briefly, seven key pathways are involved in secretion of dentine by odontoblasts; 1) p38 MAPK Pathway, 2) TGFβ-Smad Pathway, 3) PI3K/AKT/mTOR Pathway, 4) Wnt/β-catenin Pathway, 5) NF-κB Pathway 6) MAPK/ERK Pathway, 7) JNK Pathway (21).

Reactionary dentinogenesis may display distinct patterns, such as sclerotic reactionary dentine (where the tubules are progressively occluded due to deposition of minerals (22)) and circumpulpal reactionary dentine (new dentine deposited adjacent to the pulp (23)), depending on the degree of odontoblast injury. Reactionary dentinogenesis is widely believed to be upregulated by release of bioactive molecules that have been sequestered in dentine during primary dentinogenesis and released during dentine matrix breakdown caused by caries or trauma, and these have been shown to have a dose-dependent response on the volume of dentine produced (7,24,25).

Assuming reparative dentinogenesis occurs as a result of DPSC migration and differentiation into odontoblast-like cells, this process would include complex cytological steps, such as DPSC recruitment, cytological differentiation and upregulation of secretion (10). Understandably, this process will be slower than reactionary dentinogenesis. The interplay between regeneration and inflammation is a delicate balance in the carious pulp. Some inflammation is deemed necessary to instigate the reparative process, though too much inflammation tips the balance away from regeneration resulting in eventual

pulpal necrosis. In carious pulp exposures, bacterial irritation and the host inflammatory responses of the pulp usually adversely affect reparative dentinogenesis, compromising pulp vitality and opportunities for DPC repair and regeneration (7,8,10). Reparative dentinogenesis is significantly driven by the release of bioactive molecules (including growth factors, cytokines and other matrix molecules) sequestered within dentine during primary dentinogenesis and released following dentine damage. The exact pathways utilised in reparative dentinogenesis are still being discovered, but to date are believed to include Wnt/β Catenin (26), Notch (27), p38 MAPK(28) and NFκB (down-regulated) (26). Intervention is typically needed to remove bacterial irritation and improve the regenerative process to increase reparative dentine deposition and seal the dental pulp (i.e. caries removal and restoration placement).

Reparative dentine, in contrast to primary and secondary dentine has an irregular, amorphous structure, often lacking regular tubular architecture. See Figure 1.1 4 which demonstrates the difference between normal dentine and reparative dentine.

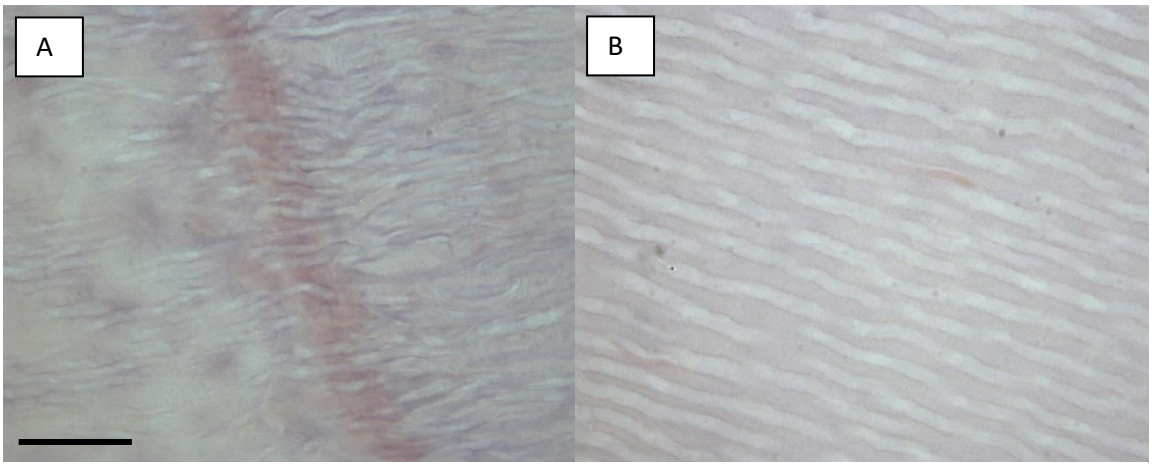

Figure 1.1 4: Comparison of histological features of reparative dentine (A) demonstrating irregular, stunted, dentinal tubules and normal dentine (B) with regular, evenly spaced, parallel dentinal tubules. H and E stain. Scale bar = 10µm

It is generally believed that sub-infection levels of bacteria may enhance the infiltration and function of neutrophils and macrophages, promoting healing, however on-going infection will compromise the inherent protecting inflammation of the pulp and impair healing (29). Progression of caries can result in varying cellular responses within the pulp and as such different patterns of dentine formation, which in turn signals towards different bacterial biofilm growth conditions within each carious lesion (29).

For DPSCs (or indeed, fibroblasts) to migrate to the area of pulp injury, modification of the local pulpal extracellular matrix occurs, with deposition of collagen type III and fibronectin (7). The immune response to dental caries will also cause degradation of extracellular matrix locally, making cellular migration easier (although also causing damage to host cells in the vicinity (8)). Various bioactive

molecules sequestered in dentine that may be released have a chemotactic ability to recruit DPSCs to the site of injury (for example, TGF-β1and FGF2 (30)). Once at the site of injury, the cells adhere to adjacent dentine and begin deposition of collagens type I and type III and fibronectin (7). The dentine that is produced often contains trapped cells, is atubular, contains high levels of bone-associated proteins, and is less mineralised than primary and secondary dentine; in this way, reparative dentine closely resembles bone and is sometimes termed 'osteodentine'(7). This layer of mineralised tissue is adhesive to further migrating cells, and once the remaining pulp is sealed from the carious irritation, odontoblast-like cells differentiate (7). These odontoblast-like cells lay down orthodentine, which is molecularly similar to osteodentine, but has more tubules than osteodentine (though these tubules may be less in number and have a more irregular arrangement than primary and secondary dentine) (7). The process of osteodentine production and orthodentine production may be simultaneous and it is often difficult to differentiate between the types of dentine produced (7). It is currently unclear whether the different morphology of reparative dentine (when compared to primary or secondary dentine) is due to the hasty and less tightly regulated deposition of dentine, or due to the cell type producing it (i.e. not an odontoblast, but an odontoblast-like cell or fibroblast) (8).

DPSCs are believed to reside in a series of niches within the pulp. Numerous studies have looked at classifying DPSCs, and currently it is believed that there are several different subpopulations of DPSCs within the dental pulp, with different populations possibly localising in specific niches and having differing levels of pluripotency, and potentially behaving differently in response to carious stimuli (31). It is generally thought that there are likely three main areas that DPSCs reside – perivascular and perineural niches, the sub-odontoblast cell rich area and the central pulp. The population at the sub-odontoblast layer is thought to be home to daughter cells from the final mitosis of odontoblasts during tooth development (7,31).

Mesenchymal stem cells are generally defined by their ability to produce different types of tissue - osteogenic differentiation, adipogenic differentiation and chondrogenic differentiation in addition to displaying set surface antigens (32) .

DPSCs are just one type of dental stem cell used for regenerative research. Other sources include; SHED (stem cells from exfoliated deciduous teeth) , PDLSC (periodontal ligament stem cells), SCAP (stem cells from apical papilla), IDPSC (immature DPSCs) and DFPC (dental follicle progenitor cells) (33). They each have different expression profiles and have been used for various types of regenerative medicine research (both within the oral and maxillofacial region and more generally) and are covered in several comprehensive reviews (33–35).

DPSCs are frequently used as a mesenchymal stem cell population for *in vitro* tissue regeneration, likely due to the ease of which they can be isolated. Gronthos *et al*(9) were the first to isolate and characterise the stem cells in the dental pulp, and since then studies have set to determine whether the state of the

tooth (36,37), the age of the patient (38) and cell isolation method (39) have any bearing on the stem cells harvested in terms of their antigenic expression and differentiation potentials. DPSCs have also been compared to mesenchymal stem cells from other sources, such as adipose-derived and bone marrow- derived and DPSCs have been shown to have enhanced mineralisation capabilities compared to these other cell types (40,41).

Minimal work has been completed with regards to locating the stem cell niches within the pulp. As earlier mentioned, it is generally believed that they are located in perivascular niches; Téclès *et al.*, and Løvschall *et al.* (42,43) have done vital work in this area. The niches are difficult to locate histologically and immunohistochemically due to the paucity of stem cells in the pulp, the variable antigenic markers expressed by the heterogenous stem cell population and the lack of stem cell specific markers (44).

It has been suggested as far back as the 1980s that the microenvironment of the dental pulp may be integral to the differentiation of DPSCs into odontoblast-like cells during dentine bridge formation (45). More recently, DPSCs have been found to be mechanosensitive cells, and this has been explored in a comprehensive review by Marrelli *et al*. (26). Mechanosensing by cells involves the cell recognising and responding to an external stimulus. This response is typically seen in DPSCs as proliferation or differentiation, and frequently involves the MAPK pathway (26). Odontogenic differentiation of DPSCs has been shown to be sensitive to external mechanical forces such as dynamic hydrostatic pressure (46), cyclical tensile strain (47), cyclical uniaxial compressive stress (48), mechanical compression (49) and substrate stiffness (12). In terms of *in-vivo* applications of these methodologies for DPSC differentiation to odontoblasts, most have limited potential as they would be difficult to instigate chair-side. However, the use of varying substrate stiffness could have potential in the differentiation of DPSCs to instigate reparative dentine deposition in the carious or traumatically exposed pulp.

1.2 PULP CAPPING

Following caries removal, a dental restoration needs to be placed to restore functionality to the tooth. An ideal dental restoration replaces lost tooth tissue and is as close as possible in functional and aesthetic properties to the natural material (namely, dentine and enamel) (50), however many dental materials fail to hit this brief. Dental restorative materials are termed ‘direct’ or ‘indirect’ determined by whether a material is applied chair side or needs to be custom-created in laboratory respectively. Dental filling materials, such as amalgam, glass ionomer and composite are examples of direct restoration materials. Crowns, onlays and inlays are examples of indirect restorative materials.

When a pulp is exposed through iatrogenic means, caries or trauma, the clinician has a choice of whether to attempt to save the pulp (via a direct pulp cap, partial pulpotomy or complete pulpotomy), or not (leading to a root canal treatment (endodontics) or an extraction). Only pulps perceived to have reversible pulpitis are considered suitable for pulp caps and pulpotomies. Irreversible pulpitis requires the tooth to be extracted or to undergo endodontic treatment (see Table 1.2 1).

Other than the status of the pulp, factors that effect this decision may include; the amount of tooth tissue remaining, the oral health of the patient, the general health of the patient, the age of the patient, patient preference, cost/remuneration, the remaining dentition of the patient and access to health services. Root canal treatment and the restoration of an endodontically treated tooth (which typically requires a laboratory made crown or onlay) are costly and result in considerable tooth tissue destruction. Taking into account failure rates, pulp capping has been found to be a more cost-effective long-term choice than root canal treatment in a German healthcare setting (51).

Pulpitis	Signs, symptoms and treatment
Reversible	Pain is on application of stimulus, pulp testing is positive, pain is brief and mild-moderate intensity. Treated by removal of causative issue (for example; caries, fracture) and restoration of tooth. If left untreated, the pulpitis becomes irreversible.
Irreversible	Pain is spontaneous and on application of stimulus, pulp testing is positive (though may have a delayed response), pain is long in duration (lasting beyond removal of stimulus) and moderate-severe intensity. Treated by extraction or root canal treatment. The tooth will eventually become non-vital, potentially leading to apical periodontitis, periapical granuloma, apical abscess or radicular cyst.

Table 1.2 1 : Comparison of reversible and irreversible pulpitis. N.B: Reversible and irreversible pulpitis are part of a spectrum, and the signs and symptoms may overlap as reversible pulpitis progresses and becomes irreversible.

To speed up the process of a tertiary dentine bridge formation in a pulpotomy or pulp cap, a dental pulp capping agent (PCA) is usually placed in the cavity. PCAs may be placed as a ‘direct’ or ‘indirect’ pulp cap, depending upon whether the PCA is placed in direct contact with the pulp, or a small slither of dentine is left between the PCA and the pulp. In an indirect pulp cap scenario, the PCA leeches via the dentinal tubules into the pulp to encourage tertiary dentinogenesis. Direct and indirect pulp caps are only suitable for vital teeth, with or without symptoms of reversible pulpitis (Table 1.2 1). Non-vital teeth, or teeth with irreversible pulpitis are not suitable for pulp capping and in these instances root canal treatment or extraction is indicated.

There has been a recent call for reclassification of pulpitis with defined treatments based upon the symptoms of the patient (52). Under this newer classification, a partial or full pulpotomy is recommended in any tooth with uncontrolled bleeding, with a PCA placed on the remaining pulpal tissue. This method is advised to remove any infected and heavily inflamed dental pulp to facilitate better healing (52).

There are many direct PCAs available commercially, however there is a significant lack of long-term cohort studies and randomised control trials to determine the 'best' PCA (53,54). Different follow-up times, selection criteria, differing populations and commercially funded studies with conflicts of interest all add to the difficulties in comparing studies to determine the success rates of PCAs. Furthermore, clinical studies often do not reflect 'normal' practice with stringent exclusion and inclusion criteria (such as the tooth being free of caries and cracks and young healthy patients); clinical studies also often use split mouth designs on teenagers having sound premolars extracted for orthodontic reasons (54), which further limits the ability of clinicians to determine PCAs with the best outcomes.

Direct pulp caps and pulpotomies can be lengthy and technical to perform successfully and correctly. When a pulp is exposed, the tooth needs to be isolated (ideally with a rubber dam), any bleeding halted, the area disinfected with sodium hypochlorite (including the removal of any further caries), any heavily inflamed or infected pulpal tissue removed (for a pulpotomy, however for a pulp cap this is left in situ), the PCA prepared/mixed, placed and allowed to set (if setting is required), and the cavity restored with either a temporary or permanent restoration (52). If a temporary restoration is placed, it is typical for a permanent restoration to be placed at a later date when any symptoms of pulpitis have resolved and a dentine bridge formed over the pulp, however delays in placing a permanent restoration can lead to fewer successful outcomes. Besides the PCA used, numerous other factors influence the success rates of a pulp cap, such as; bacterial microleakage from the restoration (55), operative debris from the cavity preparation (55), uncontrolled haemorrhage (55), the experience of the operator (56), the position of cavity (interdental or occlusal) (56), the length of time to permanent restoration (57), the type of lavage/haemostasis used (58) and the type of exposure (carious/mechanical/trauma) (56).

A pulp cap is deemed successful if at 75-90 days a dentine bridge has formed and the tooth remains vital (59), though typically a dentine bridge forms sooner than this (around 30 days (60)). Clinically, the presence of a dentine bridge may be assessed radiologically or by direct visualisation. Although it is accepted that the true 'gold standard' for pulpal assessment is histological examination, this can only be achieved through extracting the tooth (54,61), so is infrequently performed in studies. As many clinical trials fail to include histology, this further compounds the issues surrounding which is the best PCA (54), as the true status of the pulp and the dentine bridge is not assessed. No PCAs currently available are perfect as they "fail to satisfy clinical requirements" (62) and, considering the prevalence of caries, it is imperative that cost-effective materials with high success rates, desirable clinical outcomes and suitable handling qualities are available for clinical use.

There are many PCAs available commercially, with $Ca(OH)_2$, Mineral Trioxide Aggregate (MTA) and calcium silicate based cements (e.g. Biodentine™ and Theracal™) being the most commonly used in practice. Other less commonly used PCAs include; zinc oxide eugenol, corticosteroids and antibiotics,

polycarboxylate cement, bonding agents, calcium phosphate and glass ionomers/resin modified glass ionomers (63).

From a Brazilian study, $Ca(OH)_2$ is the preferred material of choice for most general dental practitioners in a community setting, but MTA is preferred by dentists working in academic settings. They also found that dentists who had qualified more recently preferred MTA, whereas those who had qualified some time ago preferred $Ca(OH)_2$ (64). There may also be a cost factor in this decision, as MTA is considerably more costly than $Ca(OH)_2$ (54).

Recent systematic reviews have attempted to determine the 'best' PCA available, and focus on comparing $Ca(OH)_2$ and MTA (65,66), with MTA coming out as the better material in terms of successful clinical outcomes. When calcium silicate cements (specifically Biodentine™) are also compared to $Ca(OH)_2$ and MTA, no significant difference is found between MTA and calcium silicate cements, but both MTA and Biodentine™ outperform $Ca(OH)_2$ (67).

1.2.1 CALCIUM HYDROXIDE

Of the most commonly used PCAs, $Ca(OH)_2$ has been used for the longest period of time (having been first explored in the 1920s) and for many years has been considered the 'gold standard' for a direct pulp cap (54,63). $Ca(OH)_2$ is often considered as a bench-mark to compare newer PCAs against – *in-vivo* and *in-vitro*. Due to its long-term commercial availability, $Ca(OH)_2$ has a wealth of evidence in the literature discussing its pros, cons and efficacy. It has a high pH (approximately 12.5–12.8) (68) and traditionally, $Ca(OH)_2$ pastes have additives to allow for radiopacity, and a vehicle to allow for improved handing capabilities (68). $Ca(OH)_2$ typically comes as a base paste and a catalyst paste, mixed together chair-side and applied directly to the pulpal exposure. The high alkalinity of $Ca(OH)_2$ eliminates micro-organisms, providing a favourable environment for dentinogenesis. The exact mode of action for dentinogenesis in a $Ca(OH)_2$ pulp capped tooth remains contentious, with some people believing the irritation, inflammation and necrosis in the pulp caused by the $Ca(OH)_2$ initiates dentinogenesis via an unknown pathway, and others suggesting that it is due to $Ca(OH)_2$ facilitating release of bioactive molecules sequestered in dentine (54,69), or potentially a combination of the two.

Calcium hydroxide is easy to handle, apply and sets quickly. However, it is also highly soluble, has low compressive strength and provides a poor seal to the pulp (52).

Success rates of pulp caps with $Ca(OH)_2$ vary from 21% to 81% (1-13 years, with times varying study to study (52)), though as previously mentioned, there is a paucity of high quality studies in the literature, making it difficult to determine an accurate figure for general practice use.

1.2.2 CALCIUM SILICATE CEMENTS

1.2.2.1 MTA

MTA is newer to the commercial market than $Ca(OH)_2$, though has been used since the 1990s (70), and is thought to have better success rates than $Ca(OH)_2$ according to several systematic reviews (65–67). However, not all systematic reviews found MTA to be definitively better, with Schwendicke *et al*., concluding that "no firm evidence was reached to strongly support any recommendations" with regards to changing current $Ca(OH)_2$ usage to MTA, citing issues with study design (such as all sound teeth), lack of histological data and a paucity of long term studies (greater than 2 years follow up) as significant issues in comparing the two PCAs (61).

MTA is hydrophilic and requires moisture to set (70). MTA is typically supplied as a powder to be mixed with water, sometimes pre-measured or in easy to mix capsules. The powder is usually a mixture of calcium oxide in the form of tricalcium silicate, dicalcium silicate and tricalcium aluminate, with bismuth oxide (added for radiopacity) (54). When water is added, a colloidal gel, composed of calcium oxide crystals, is formed and $Ca(OH)_2$ is released (70–72). The release of $Ca(OH)_2$ imparts much of MTA's known antimicrobial activity and possibly some of its regenerative qualities (70,73).

Although MTA is considered to have better clinical outcomes than $Ca(OH)_2$, there are some drawbacks to this material, such as long setting times (typically several hours), difficult handling characteristics, tooth discolouration, high cost and pulpal obliteration with dentine (63,70,73–75). The release of $Ca(OH)_2$ by MTA, which is highly alkaline, is also cytotoxic to pulpal cells (71,72). "Blow out" which is the propensity for a cement to breakdown when in contact with body fluids is a further disadvantage to MTA (76) . Mechanically, the compressive and flexural strength of MTA is also less than that of dentine (77).

MTA has undergone various iterations since first introduced to curtail some of the undesirable qualities (such as discolouration and long setting times). Fourth generation versions of MTA are currently on the market, with improved setting times (through the addition of calcium sulphate or sodium hypochlorite, the reduction in particle size, or addition of substances to allow for light curing) and reduced tooth discolouration (70), though long-term studies are needed to confirm these changes are effective over prolonged periods and no reduction of efficacy is seen.

As MTA is considered to generally have better clinical success rates, it has been shown to be more cost-effective (despite its initial high purchase costs) than $Ca(OH)_2$ in a German healthcare setting (78).

When comparing MTA and $Ca(OH)_2$, MTA is believed to produce a more impervious dentine barrier, with fewer tunnel defects, which may be the reason behind more successful clinical outcomes for MTA (74,76).

It has been demonstrated that MTA liberates bioactive molecules from dentine, such as VEGF, IGF-I, EGF and SCF to name but a few (25). These bioactive molecules are believed to influence DPSC migration, differentiation, proliferation and ultimately facilitate tertiary dentine deposition. However, MTA also is known to contain toxic elements, such as arsenic which raise concerns over its potential toxicity (79). Long-term success rates for MTA direct pulp capping are around 80% (57). With the current trends of regenerative medicine and dentistry, a failure rate of approximately 20% is unacceptable and a more reliable and predictable material is required.

1.2.2.2 BIODENTINE

Tricalcium silicate cements are the newest of the materials commonly used. Most studies suggest that these cements perform similarly to MTA (67). One of the more popular tricalcium silicate-based cements is Biodentine™. This material, is supplied as a powder and liquid. The powder is composed of tricalcium silicate (3CaO·SiO2), dicalcium silicate ($2CaO \cdot SiO_2$) and calcium carbonate ($CaCO_3$), with zirconium dioxide (ZrO_2) added to provide radiopacity (80). The liquid component is calcium chloride ($CaCl_2 \cdot 2H_2O$), which acts as an accelerator and water-reducing agent (80). The two phases are mixed in an amalgamator. Reported setting times vary between 12 minutes up to 85 minutes (80), making the setting time comparable to MTA. Biodentine™ also works in a similar way to MTA, with $Ca(OH)_2$ production imparting antimicrobial effects, and causing inflammation thought to upregulate the regenerative process of tertiary dentine deposition, and some cytotoxicity based upon $Ca(OH)_2$'s high alkalinity. Generally, Biodentine™ is considered to have better handling characteristics than MTA (81), higher compressive and flexural strength than MTA and a hardness similar to dentine (77).

1.2.3 HYDROGELS FOR PULP CAPPING

Tissue engineering, as a concept was first proposed in the USA in the 1980s as a potential answer to the scarcity of donors for organ transplantation (82). Classically, in a cell-based system, biodegradable scaffolds are seeded with cells and/or bioactive molecules (for example, growth factors) and implanted into the host, with the aim of inducing tissue growth. However, to obtain good results from this system, fine tuning of the three components is required (the cells, the scaffold or carrier and cell signalling) (82).

Regeneration of damaged and/or lost biological tissues is an on-going aim for researchers worldwide (15) and is an area of emerging research. However, many of the *in-vitro* systems poorly translate to *in-vivo* situations due to the differing processes of tissue maturation (82). With newer emerging technologies, such as gene editing, microfluidics, 3D printing, drug delivery and organoid systems, these technologies may be seen in clinics more and more frequently in the future as we overcome translational issues between the *in-vitro* and *in-vivo* differences (82).

As the coronal pulp is the area where tertiary dentinogenesis occurs, it stands to reason that the physiology of this area in carious teeth could be mimicked to facilitate reparative dentinogenesis.

The production of tertiary dentine is a delicate balance between regeneration and inflammation. It is widely believed that some degree of inflammation is required to initiate the reparative process, but that too much inflammation ultimately causes irreversible damage to the dental pulp, leading to pulp necrosis. Many of the PCAs available are highly alkaline, increasing pulpal inflammation in an already inflamed pulp. Current PCAs are not optimally designed to mimic the coronal pulp, as many are based upon a paste or powder, which is very different to the natural, highly hydrated environment in which tertiary dentinogenesis would normally occur. Therefore, if a PCA is designed to mimic the dental pulp, it may be able to produce a dentine bridge in a more controlled and reproducible manner, facilitating DPSC recruitment, colonisation and differentiation. Furthermore, a scaffold may have better handing properties than a paste, and potentially provide a good seal to the dental pulp due to swelling from absorption. Many scaffolds also have tuneable mechanical and physical properties that can be manipulated to create an optimally designed material.

To date, PCAs explored in the literature have generally failed to consider how their elastic moduli impact upon the biological performance of the material. This is likely due to a significant paucity of research exploring the elastic modulus of the dental pulp in disease and health. Without knowing the elastic modulus of the dental pulp in caries, where tertiary dentine is being produced, it is impossible to create a scaffold that mimics the physical environment of the dental pulp during tertiary dentinogenesis.

When considering tertiary dentinogenesis, we can use *ex-vivo* teeth as a biological model of DPSC migration and differentiation, which can be investigated to better understand some of the mechanical factors implicated in the migration and differentiation of DPSCs into odontoblasts. If we can understand the mechanical differences between dental pulps in carious and sound teeth, then we may be able to recreate the ideal environment for DPSC differentiation and migration. This information, in turn, can then be used to create an optimally designed dentinogenic scaffold for dental pulp capping, where DPSCs can differentiate into dentine-producing odontoblasts and seal the dental pulp without the need for exogenous bioactive molecules and cytotoxic dental materials based on alkaline preparations.

The elastic modulus of the dental pulp is important to elucidate because DPSCs are known to be mechanoreceptive cells, sensing changes in the elastic modulus of their surrounding tissue/scaffold, affecting their differentiation pathways; this is believed to be due (at least in part) to the action of Piezo1 channels (83). The role of Piezo 2 channels on DPSCs requires further elucidation to explore in more depth what role these channels have on DPSCs (83).

As no current commercially available PCA is perfect, with all having well documented flaws, considerable research has been undertaken exploring the use of other materials. Much of this has focused on naturally

derived materials, with a push towards regenerative dentistry using the DPC as a template. As such, most studies have focused on naturally derived scaffolds containing bioactive molecules known to be sequestered in dentine and released during bacterial ingress during caries and dentine destruction.

It seems that PCA design has historically focused on producing a material with similar characteristics to dentine – indeed Biodentine™ has similar hardness to dentine (77). This approach ignores the fact that the mineralisation in tertiary dentine occurs within the dental pulp; whether produced by DPSCs migrating and differentiating at the site of injury, or via dystrophic calcification by fibroblasts, the mineralisation occurs in the pulp and not within dentine. As such, if a dental material is to be designed to mimic the environment necessary for tertiary dentinogenesis, it should replicate the characteristics of the coronal dental pulp and not dentine. Making an environment more akin to the pulp could facilitate cellular infiltration into the PCA and diffusion of bioactive molecules through the scaffold, allowing tertiary dentinogenesis to occur in the dentine defect rather than beneath it; this in turn would save more coronal pulp and prevent obliteration (as can occur with MTA use (64,65)).

A hydrogel is a three-dimensional hydrophilic polymer, which is capable of absorbing a large quantity of water (84). In recent years, hydrogels have been explored for pulp capping. This has largely been achieved in the literature through adding bioactive molecules to the hydrogel scaffold and implanting the scaffold into a tooth (carious or sound). Bioactive molecules are naturally found in dentine, being intombed during dentinogenesis, and are released upon breakdown of the dentine due to caries. Bioactive molecules for pulp capping are covered in a comprehensive review by Whitehouse *et al.* (85), however, in brief, the main molecules explored for pulp capping in the literature are TGF-β1 (transforming growth factor β1), BMP2 (bone morphogenetic protein 2) and BMP7 (bone morphogenetic protein 7). The addition of bioactive molecules to a PCA scaffold has several impractical limitations, such as cost, the need for sustained release, short half-lives and the need to be provided at a suitable concentration to be effective while not damaging to the cells (85,86), limiting the practical application of these scaffolds.

Despite most scaffolds in the literature utilizing the addition of bioactive molecules to facilitate DPSC differentiation and dentine deposition, several studies have successfully demonstrated the deposition of mineral on unloaded scaffolds *in-vivo* (for example, Hu *et al*. (87) (using a collagen membrane), Koike *et al.* (88)(using a collagen sponge), Goldberg *et al.* (89)(using gelatin) and Matsunaga *et al*.(90) (using chitosan)). The ability of the pulp to produce reparative dentine without the need for exogenous bioactive molecules suggests that the bioactive molecules present in dentine (and the pulp) may be present in sufficient quantities for reparative dentine deposition, and as such the need for exogenous compounds may be unnecessary (85). These studies also demonstrate how a cell-free approach, without the need to harvest stem cells for insertion into a scaffold, may be a viable option for dental pulp capping.

One of the main drawbacks of the more popular scaffolds used in the literature for pulp capping (for example, collagen and gelatin, as mentioned above) is that they are frequently broken down by proteinases and reactive oxygen species (ROS) in the inflammation (91) – limiting their use in the inflammatory environment of the carious involved pulp. This can be advantageous if being utilized for the release of medicaments or bioactive molecules to enhance reparative dentinogenesis, however it can also be a negative property because breakdown prevents the scaffold remaining in situ during dentinogenesis, potentially exposing the pulp to toxic dental restorative materials or bacteria.

When designing a scaffold as a PCA, a suitable scaffold would need to have; biocompatibility, appropriate mechanical properties, biodegradability, capability to promote proliferation and differentiation of cells and interconnected porosity (14). There are a wide variety of scaffold options available, each with unique profiles of advantages and disadvantages for pulp capping.

Scaffolds are designed to provide a 3D template and microenvironment to facilitate cell adhesion, proliferation and differentiation aiding tissue repair. Tissue engineering systems often need to combine one or more of three integral components: biomaterial matrices, living cells, and bioactive molecules (86). However, as previously mentioned, the incorporation of bioactive molecules can be difficult to achieve and increases costs. In addition, the inclusion of cells extraneously (either from the donor in which they are to be reimplanted or from an exogenous source) adds complexity, cost and potential ethical contraindications. If a scaffold can be designed to utilise the existing endogenous stem cell population to facilitate the stem cell proliferation and differentiation, this would prevent the need for stem cells to be inserted into a scaffold before being used *in-vivo* (i.e. a ‘cell-free system’ can be designed).

Scaffolds for regeneration of the DPC can be broadly divided into natural and synthetic. Naturally derived scaffolds (for example; chitosan, alginate and collagen) are created from natural sources and form hydrogels capable of incorporating up to 99% water content. This is advantageous as it can mimic the hydrated state of natural tissues (14), however, broadly speaking they can have batch-to-batch variations and poor mechanical properties (92). Naturally derived scaffolds are generally biocompatible, inexpensive and easy to fabricate – making them an attractive option for DPC regeneration (14).

Synthetic scaffolds, like natural scaffolds, have mechanical, structural and biological properties unique to each material. These materials are designed to overcome some of the problems with natural scaffold materials such as low mechanical strength and variable degradation rates (86). Polylactic acid (PLA), polyglycolic acid (PGA), and polylactide-co-glycolide (PLGA) are some of the more commonly used synthetic polymers (14). These have good design flexibility having the advantages of tuneable

mechanical properties, viscosity, porosity and degradation (14). Typically, this is achieved by altering the copolymer ratio, molecular weight, and crystallinity of the synthetic scaffold materials.

Blended scaffolds are a mixture of one of more different materials. These can be synthetic or natural or a mixture of the two, aiming to modify the undesirable characteristics of one scaffold through the incorporation of another.

1.2.3.1 NATURAL HYROGEL SCAFFOLDS

Chitosan

Chitosan is a linear polysaccharide derived from chitin, which is found in the exoskeleton of marine crustaceans (for example shrimps and crabs), as well as some insects and the cell walls of fungi (14,93). Chitosan has numerous favourable properties such as being; biocompatible, biodegradable, antimicrobial, and osteo-inductive (14), but may not be suitable for people with certain allergies or religious or cultural practices (for example Judaism, vegetarians and vegans). Chitosan can be manufactured into numerous forms for delivery such as; membranes, gels, beads, scaffolds, and sponges (14) and has also been shown to promote DPSC proliferation (94). A significant advantage of chitosan is that it has antibacterial properties – which could be used to treat any residual caries (95).

When comparing collagen I, collagen III, gelatin and chitosan for the support and differentiation of DPSCs *in vitro*, collagen I and III outperformed chitosan which failed to support cell growth (96). However, chitosan has been used successfully for pulp capping drug and bioactive molecule delivery (for example, Li *et al.* (97) using TGF-β1 *in vivo* and Soares *et al.* (98) using Simvastatin) and has been used to support odontogenic differentiation (99).

Alginate

Alginate is a polysaccharide derived from brown seaweed, and is known to be biocompatible and have low immunogenicity (14,93). Alginate is generally considered to have low mechanical stiffness and uncontrolled degradation rates *in- vivo*, however this can be improved by increasing the calcium content (and therefore electrostatic cross-linkage) (14). Further modification with Arginine-glycine-aspartic acid promotes cell adhesion, proliferation and differentiation (100). Alginates have a good industrial track-record, being widely used in the pharmaceutical and biomedical industries (93).

Alginate has been successfully utilised to act as a carrier for TGF-β1 *in vitro* for pulp capping on human tooth slice culture (101). It has also been used to explore the controlled release of BMP-7 and TGF-β1 from alginate; in this study, 80% of each growth factor was released after 24 hours and 100% after 168 hours (102). In two other studies, rat and human DPSCs seeded onto unloaded alginate scaffolds were

implanted subcutaneously in mice with a culture medium containing β-glycerophosphate. In both cases, dentine was formed (103,104).

Collagen

Collagen is the most abundant protein in dentine (6) and the most commonly used natural scaffold material *in-vitro* for dental pulp capping. Collagen has been successfully used as a pulp capping agent and an *in-vivo* carrier for: TGF-β1 (87,105), BMP-2 (106,107), BMP-4 (106,107), BMP-7 (108–111) and GCSF (112).

In a study by Kim *et al.* comparing gelatin, collagen and chitosan, the authors found that collagen (types I and III) successfully supported the proliferation and differentiation of DPSCs – more so than the other materials (96). Collagen also supports DPSC adherence (11).

Collagen can be extracted from several allogenic sources (for example, bone, cartilage, tendon, muscle, skin) and is degraded by collagenase, which is present in even very mild inflammation (100), potentially limiting its use in the inflamed dental pulp. Although collagen has low immunogenicity in humans, its biological origin from animals could be a concern for certain patient groups (14)

Collagen fibrils have high tensile strength, and collagen's mechanical properties can be altered via cross-linking (for example with glutaraldehyde or diphenylphosphoryl azide) and the formation of hybrid scaffolds (for example with hydroxyapatite) (100). Interestingly, DPSCs are known to cause contraction of collagen lattices *in-vitro* which may prove a challenge for clinical application in dental pulp capping (113), as the contraction may affect the coverage of the exposed dental pulp.

Gelatin

Gelatin is derived from connective tissues, skin and bones of animals and produced by partial hydrolysis resulting in a mixture of peptides and proteins, with a chemical composition similar to collagen (14). Gelatin is inexpensive, biocompatible and biodegradable, it does not produce harmful by-products and exhibits low antigenicity (14). Gelatin can be modified to modulate cell adhesion and provide accessible functional groups (14). However, the disadvantages of gelatin include; mechanical properties very sensitive to temperature variation, low tensile strength, and because the material is derived from animals it is not suitable for all patients (14).

Gelatin, has been used successfully *in-vivo* as a carrier for; BMP-7 (89), BSP (89,114) and FGF-2 (115,116). Goldberg *et al.* also demonstrated that unloaded gelatin was capable of inducing tertiary dentinogenesis in rats in one of their control groups (89). Gelatin *in-vitro* has also demonstrated good properties of cell adhesion (with no statistical difference to collagen) (96), however in this study the

differentiation of DPSCs and mineralised tissue produced was less than that of collagen. Gelatin has also been used successful to produce an *in-vitro* DPC, using scaffolds of differing elastic moduli (12).

Fibrin

Fibrin is derived through polymerisation of fibrinogen (present in blood) and is an important component in wound healing and clotting (15). Fibrin has several attractive properties as a scaffold – it is inexpensive, biocompatible, has good cytological adhesion and can easily be obtained from autologous sources (eliminating immunogenicity issues) (15). However, fibrin has poor mechanical properties and suffers with shrinkage and although these can be improved upon through additives and modification of the polymerisation process, they cannot be overcome entirely (15). Fibrin does not have any antimicrobial properties, but again can be modified to incorporate these (for example with clindamycin) or through construction of a hybrid gel with chitosan (15).

Hyaluronic Acid

Hyaluronic acid is biodegradable, biocompatible, bioactive non-immunogenic and non-thrombogenic. It is a component of many extra-cellular matrix (ECM) environments (including the dental pulp), where it plays an integral role in in maintaining the structural organisation of the ECM and in activating various signalling pathways (15). Structurally, hyaluronic acid is a polysaccharide formed from alternating units of repeating disaccharide, D-glucuronic acid and N-acetyl-D-glucosamine, linked together via alternating β-1,4 and β-1,3 glycosidic bonds (15).

Hyaluronic acid has been extensively explored in the literature as a scaffold for regenerative endodontics, mainly for use as an injectable gel (15). However, hyaluronic acid is also readily degradable via hydrolysis and hyaluronidase action and often needs cross-linking or conjugation to stabilise it (15). Despite this, hyaluronic acid has demonstrated promise as a scaffold for dentine production *in-vivo* when inserted subcutaneously in mice (15).

Cellulose

Cellulose is a polysaccharide found largely in plant species (15). It is water insoluble and is stabilised via physical (ionic of hydrogen bonded) or chemical (using a cross linker between chains) methods (15). Physically stabilised cellulose gels are believed to behave in an unpredictable nature *in-vivo*, with issues of uncontrolled degradation and mechanical loading cited as potential issues (15). As such, chemically stabilised cellulose gels are more commonly used in the literature with siltation or the addition of hydroxyapatite showing some promise in *in-vtiro* models (15).

Agarose

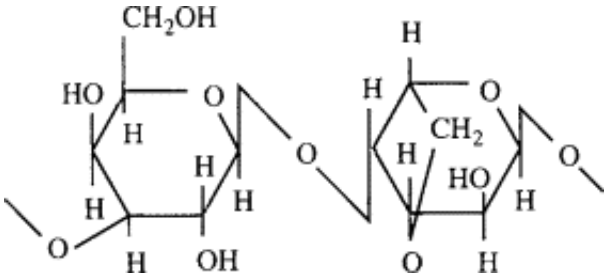

Figure 1.2.3.1 1: Chemical structure of agarose. Taken from Gustavsson *et al.* (117)

Agarose is a natural, biocompatible carbohydrate polymer with a strong background in being used in tissue regeneration (118). It is blendable, tunable (in terms of its mechanical characteristics and form), has a similar structure to extracellular matrix and is capable of allowing nutrient and oxygen filtration (118). Moreover, agarose has been shown to facilitate dentine remineralization *in-vitro* (119). See Table 1.2.3.1 1 for a full list of pros and cons for the biomaterial application of this material.

ADVANTAGES	DISADVANTAGES
Tunable forms – e.g. gels, fibers, injectable hydrogels	Poor cell adhesion due to inert nature
Similar structure to ECM (extra-cellular matrix); allows water, oxygen and nutrient transfer	Not degradable as humans do not synthesise agarase
Tunable porosity	
Because of the hydrogen bonding, relatively rigid structures can be made without toxic cross-linking agents (e.g. genipin).	
Good background in the literature with regards to tunable elastic modulus, necessary for assessing stem cell differentiation on gels of different moduli	
Blendable with other materials (e.g. silk)	
Biologically inert	
Can encapsulate medicaments	

Table 1.2.3.1 1: Pros and cons of agarose for biological scaffold creation (118)

Agarose is derived from red algae and is composed of repeated units of agarobiose (a disaccharide of D-galactose and 3,6-anhydro-L-galactopyranose)(118), see Figure 1.2.3.1 1. The oxygen and hydrogen in the side groups of the agarose chains supports agarose's self-gelling nature (118). The gelation and

melting points of agarose vary depending upon the molecular weight, w/v % concentration and the number of side groups present (118). Agarose permeability is also dependent upon this concentration (118). Within the gel, agarose chains are held together by hydrogen bonds. The gelation of agarose occurs in three steps: induction, gelation and pseudoequilibrium (118). The overall tetrahedral network produced by the agarose hydrogen bonding attracts not only further agarose chains, but also water (120), making agarose have a high swelling ratio, producing a highly aqueous environment, ideal for cell culture.

Despite agarose being an appealing biomaterial due to favourable characteristics (as per Table 1.2.3.1 1), it has not yet been explored as a scaffold for DPSC differentiation to induce dentinogenesis. As stated in Table 1.2.3.1 1, the lack of cellular adhesion makes it a difficult material to use in cell culture and this may be why it has not been previously explored as a dentinogenic scaffold.

The issue of cell attachment with agarose is due to a lack of any specific binding sites and the lack of any overall charge of the gel. Cell adhesion typically occurs due to one of several different methods and these can be broadly divided into 'non-receptor mediated' and 'receptor mediated', see Table 1.2.3.1 2 (121). Agarose needs to be modified to incorporate some of these binding formats to facilitate DPSC adhesion.

Non-receptor mediated binding	Receptor mediated
Hydrogen bonding Electrostatic interaction Polar interaction Ionic interaction	Minimum adhesion motif containing molecules (RGD (Arg-Gly-Asp)) found on collagen, vitronectin, fibronectin and many others Asp-Gly-Glu-Ala (DGEA) found on collagen Arg-Arg-Glu-Thr-Ala-Trp-Ala (RRETAWA) part of the α5β1 subunit for extracellular binding IKVAV (Ile-Lys-Val-Ala-Val) found on laminin YIGSR (Tyr-Iso-Gly-Ser-Arg) synthetic peptide based on laminin

Table 1.2.3.1 2: Summary of receptor and non-receptor mediated cellular binding to scaffolds (121–123)

The other key issue with using agarose as a biomaterial is its resistance to biological breakdown in the human body. Some authors have identified that exposure to agarase can facilitate sufficient scaffold degradation, whilst maintaining the produced tissue (124). However, for a PCA, the lack of degradability may not necessarily be a bad property; current PCAs do not degrade and for dentinogenesis to occur, the gel needs to be in place for a suitable period of time to facilitate this.

Agarose has been chosen for the scaffold material in this project due to its tuneable mechanical properties. This is integral to this work because exploration of the elastic modulus pertinent to DPSC differentiation into odontoblast-like cells requires a material that can be easily altered to adjust the elastic modulus. In addition, as this scaffold has not been previously explored with regards to facilitating DPSC differentiation and dentine deposition in the literature, it warrants exploration to determine whether this could be a viable alternative to more commonly used scaffold materials.

1.2.3.2 SYNTHETIC HYDROGEL SCAFFOLDS

PLGA

PLGA is a popular synthetic scaffold used in bioengineering and is a copolymer of lactic and glycolic acid (125). PLGA is synthesised by one of two methods; 1) direct polycondensation of lactic and glycolic acids, or 2) ring-opening polymerization or polyaddition of glycolides and lactides (125). The ratio of lactic acid to glycolic acid affects the properties of the material (for example, melting temperature and degradability) (125). PLGA is biocompatible, biodegradable, has mild inflammatory properties (100), and good mechanical characteristics (125). PLGA is porous, with pore size being controllable in manufacture (86,126). The size and inter-pore-connectivity affect the surface area, and therefore the release of bioactive molecules, making PLGA highly alterable for specific molecular release kinetics (86). The porosity also helps the penetration and proliferation of cells (86). A recent paper has proved that unloaded PLGA is capable of inducing reparative dentine formation in a rat model (127) and that the differentiation was influenced by surface porosity/topography, with the surface porosity of ~1-5µm/pore producing more dentine than a porosity of ~45µm. However, PLGA is most frequently used for pulp capping with other components added – for example with TGF-β1 and CaP (128) and with a beta-tricalcium phosphate-hydroxyapatite bioceramic (129).

PGA

PGA is similar to PLGA in its characteristics and is broken down in the body to glycolic acid, which is then excreted via metabolic pathways (14). PGA has been explored as a pulp capping agent with the addition of an enamel matrix derivative, but was not successful in producing a hard tissue barrier (130) and little further work has been done using this polymer for pulp capping.

PLA

PLA is broken down into lactic acid by the body and excreted via metabolic pathways and is similar to PLGA in characteristics (14), similar to PGA. However, PLA has not been used previously for pulp capping in the literature. PLA has been proven to be suitable for pulpal regeneration in a subcutaneously planted tooth slice within a murine model (131,132), but not for dental hard tissue formation.

2 RESEARCH AIMS AND OBJECTIVES

The aim of this project was to design, fabricate and characterise an *in-vitro* acellular scaffold, capable of being colonised by dental pulp stem cells (DPSCs) and sufficiently biomimetic to encourage their proliferation and differentiation into odontoblasts to facilitate dentine production. The design was based upon new mechanical findings gleaned from the pulp of *ex-vivo* teeth and linked to biological data.

Objective 1: To correlate and compare data on mechanical stiffness, RNA expression and histomorphology for the pulps of carious and sound teeth.

The stiffness of the pulp of carious and sound teeth was investigated using Atomic Force Microscopy (AFM) nanoindentation and correlated to RNA sequencing (RNAseq) data and confocal microscopy of pulpal histology. This provided data pertinent to nano and micro level changes in the pulp that link to biological activity. This was then used to inform objective two.

Objective 2: To create optimally designed dentinogenic hydrogel scaffolds.

Scaffolds based upon the ideal stiffness gleaned from Objective 1 were constructed from agarose and seeded with dental pulp stem cells (DPSCs). Confocal fluorescent microscopy was used to assess dentine production and differentiation of stem cells into odontoblasts. The scaffolds were characterised to provide vital information which may influence DPSC differentiation and dentine production.

Purpose of Research and Clinical Significance

The purpose of this research is to provide data demonstrating the elastic modulus of the dental pulp linked to histology and RNA sequencing data. This can ultimately be used in many aspects of dental research, such as pulpal replacements, furthering understanding of mechanisms of disease in dental caries, and facilitate a better understanding of mechanical factors impacting reparative dentinogenesis (including DPSC migration and differentiation), pulp capping scaffolds and materials..

3 ETHICS

For this work, ethical approval was first granted via Leeds Skeletal Tissue Bank to obtain teeth (Yorkshire and Humber, Leeds East Research Ethics Committee, 18/YH/0191), hereafter referred to as 'Tissue Bank Ethics'. However, after only low numbers of teeth were obtained with generally poor RNA yields, a separate full ethical application was submitted, with approval granted via North West Greater Manchester East Ethical Committee (REC reference: 21/NW/0106), hereafter referred to as 'Project Ethics'. The key differences, pertinent to this project, of these two collection methods, based on the ethical approvals, are outlined in Table 3 1.

Inclusion and exclusion criteria with regards to the teeth that were deemed suitable for this work are given in Table 3 2. Copies of the ethical approvals for this project are available in Appendix 1.

Leeds Skeletal Tissue Bank	**Project Ethics**
Includes patients under 18 years of age	Excludes patients under 18 years of age
Includes all teeth	Limited to teeth with intact pulps and secondary/permanent ('adult') teeth
Samples stored dry in a refrigerator	Samples stored in either RNALater, Phosphate Buffered Saline (PBS) or formalin, depending upon research application

Table 3 1: Differences between the two ethical approvals for this research

Criteria	Justification
Permanent 'adult' teeth only	Primary ('baby' or 'milk') teeth have different anatomy (e.g. larger pulp chambers comparative to size, and more bulbous crowns, and a different stem cell population), may have resorbed roots (possibly affecting the elastic modulus) and are overall smaller, potentially making AFM work and collecting sufficient tissue for a good RNA yield difficult.
Molar teeth only	These are the most common teeth extracted and have the largest pulps, facilitating easier RNA extraction and AFM force measurements. Selecting one type of tooth also increases reproducibility.
Intact pulp chamber	In some cases, the caries is so extensive that the pulp is destroyed, making measurement of the pulpal elastic modulus impossible. Similarly, with excessive secondary or tertiary dentine deposition, the pulp may become obliterated, leaving very little soft tissue for RNA extraction and AFM measurements. Also, teeth that have undergone endodontic 'root canal treatment' will not have pulpal tissue remaining.
Non-surgical extraction	If the tooth is fractured during extraction or surgically sectioned, this may change the elastic modulus of the sealed pulp.
Tooth must be unrestored if sound. May be unrestored or restored if carious.	As long as the pulp is intact, the presence of a restoration will not alter the ability for the tooth to be scanned if carious. For non-carious teeth, the tooth must be unrestored as previous disease activity may impact the soft tissue.
Must have extensive caries to be included in the 'carious' group	To ensure some degree of reproducibility with regards to the extent of caries acting on the pulp, only teeth with dentine caries will be used.

Table 3 2: Inclusion/exclusion criteria for teeth submitted for this research

4 CHARACTERISATION AND CORRELATION OF THE ELASTIC MODULUS OF THE DENTAL PULP, THE PULP TRANSCRIPTOME AND COLLAGEN BUNDLES IN SOUND AND CARIOUS TEETH

This section focuses on the research methods of Atomic Force Microscopy (AFM), RNA sequencing (RNAseq) and histomorphometric analysis using confocal microscopy within the pulps of carious and sound teeth. The information gleaned from the results of these methods informs scaffold production later in the thesis.

4.1 INTRODUCTION TO METHODS: ATOMIC FORCE MICROSCOPY, RNA SEQUENCING AND HISTOMORPHOMETRIC CONFOCAL FLUORESCENT MICROSCOPY

4.1.1 ATOMIC FORCE MICROSCOPY

AFM was invented in 1986 as a scanning probe microscope where image acquisition is based upon the deflection of a cantilever probe interacting with a sample's surface (133). Since its inception, AFM has been shown to be a useful tool in learning about the elastic modulus of samples and for nano-level interactions (for example folding and unfolding of proteins (133)). AFM assesses a sample's surface with a nano-scale probe, by either running the probe along the surface (to elucidate topography through moving the probe in the horizontal plane) or pressing/contacting the probe on the sample surface to determine the mechanical properties of the sample (by moving the probe in the vertical plane). The reverse surface of the cantilever force sensor has a gold coating which reflects a laser's beam onto a split photodetector. The deflection of the laser, caused by the probe's interaction with the surface, is identified by the photodetection system, producing topographic images or force profile data in the format of force curves (see Figure 4.1.1 1).

The elastic modulus, also known as 'Young's modulus', is a measure of a materials' elasticity, describing the linear relationship of uniaxial stress (force/area) to uniaxial strain (deformation as a fractional change compared to original size). It may sometimes be confused with 'stiffness', which is the resistance of an elastic material when a force is applied. The difference between elastic modulus and stiffness can be explained by the following example; a copper pipe and a copper wire will have the same elastic modulus but their stiffness will differ (134), in this way the elastic modulus is the intrinsic elastic material property of a sample.

When using the AFM for elastic modulus measurements, a force curve is produced demonstrating the force or cantilever deflection (y axis) against distance from sample surface (x axis) (see Appendix 2 for

an example force curve and Figure 4.1.1 1 for a schematic diagram of an AFM setup with a force curve), and from this the elastic modulus of the sample at the point of indentation can be calculated. This facilitates force measurements at the nano and micro-scale (which is currently the distance believed to be 'sensed' by cells (134,135)). With recent advances in AFM, it is now possible to study biological tissues in a non-destructive manner facilitating correlation between topographical and nanomechanical assessment using nanoindentation-based approaches. AFM has many advantages over other high resolution microscopy techniques for studying biological samples, such as the ability to measure samples in liquid environments, and the data can be analysed with well-accepted models, fit to the force curves produced (134).

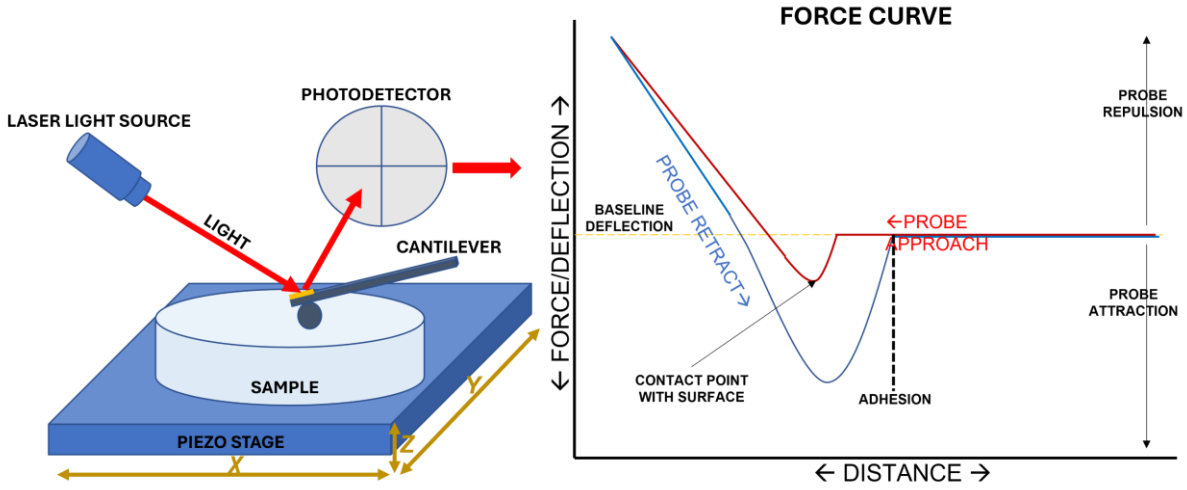

Figure 4.1.1 1: Schematic diagram of the basic setup of an AFM, with a laser reflecting off a cantilever, being detected by a photodetector. The photodetector detects the cantilever's movements, resulting in a force curve. The force curve records the cantilever/probe's approach to the surface and as the probe becomes attracted to the surface and the cantilever bends, the light deflection is detected by the photodetector. As the probe contacts with the sample's surface, the probe bends again as the atomic forces of the probe are repulsed by the sample's surface – again, this deflection to the cantilever is detected, before the probe is pulled away from the surface, the stage moved and the process repeated.

The basic setup for AFM traditionally includes: a cantilever, a detection system (typically a photodiode/laser system), a feedback loop to moderate the applied force and distance of the cantilever to the sample surface, a movement system (typically a piezo stage) to allow scanning (or indenting) of the sample in three dimensions and software to visualise and transform the data generated (133,136,137). See Figure 4.1.1 1 for a schematic diagram of an AFM.

When using AFM to measure the elastic modulus of a sample, the spring constant (stiffness) of the cantilever must first be known to allow calculation of the sample's elastic modulus with an accepted mechanics model (for example, Hertz). Although many cantilevers come with a pre-calibrated spring constant, it is necessary to confirm this with calibration in-house to ensure accurate force measurements. Most proprietary AFM software will accomplish this, and the basic process is given in the list below (136,137):

1) Align the laser to the reflective coating at the end of the cantilever (see Figure 4.1.1 1) – achieved by using an integrated camera to visualise the probe and the laser position.
2) Correct for virtual deflection (a mechanical correlation of the cantilever's deflection with movement in the Z-axis), off-setting the position of the photodetector so that the laser is aligned to a 'null' position before any measurements are taken.
3) Calculate Inverse Optical Lever Sensitivity (InvOLS) – achieved by measuring the slope on a force curve in the tip-sample contact region and is usually performed on a hard surface (such as a glass slide)
4) Determine the thermal resonance of the cantilever, from which the spring constant can be calculated using the equipartition of energy theorem, where 1/2kT of energy is ascribed to the cantilever vibration.

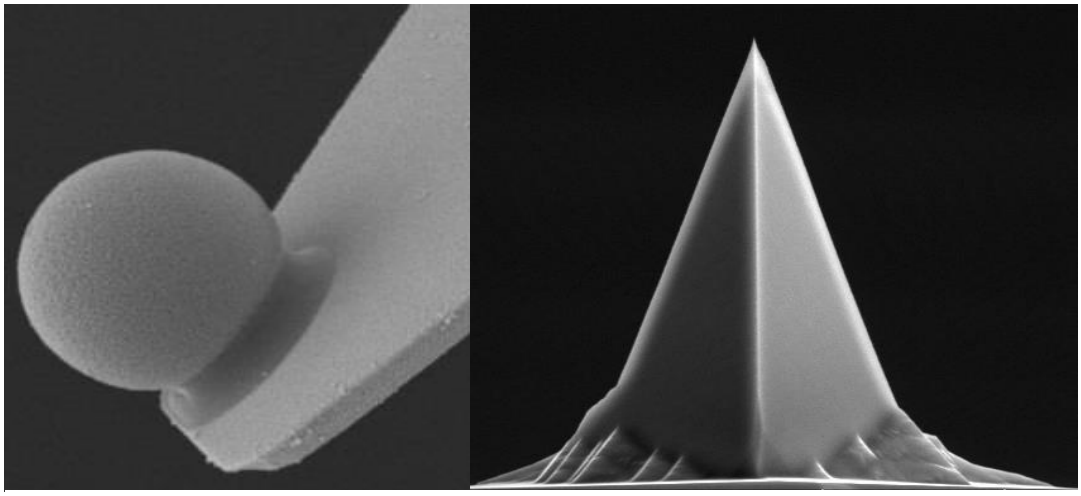

Figure 4.1.1 2: SEM images of a sphere-tipped AFM probe and a pyramidal AFM probe, taken from Apex Probes website, https://afm-probes.apexprobes.uk/. This is included to demonstrate some of the different tip dimensions available for AFM work. For the work in this thesis, a sphere-tipped probe/cantilever was used.

Cantilevers need to be carefully chosen for any AFM work as the size and shape of the tip is directly related to the resultant resolution of the surface topography and the area from which any elastic modulus

data is taken. The contact area of the probe tip is the ultimate determinant of resolution from within the image or measurement field, so smaller contact areas of pyramidal and cone-shaped tips result in higher resolution measurements than large sphere-shaped probes, as their contact area is typically smaller (see Figure 4.1.1 2 for example of some cantilever tips). For mechanical indentation measurements on soft samples (such as biological tissue), spherical bead-tipped probes are frequently used because sharp pyramidal or conical probes readily pierce the soft surface without the cantilever deflecting sufficiently. This means that the AFM cannot 'feel' the elasticity of the material because the nanoscale contact area between tip and sample does not give enough resistance for the cantilever to bend. Increasing the contact area, by using a micron-sized bead tip, means that the elastic modulus of very soft samples can be determined, but with lower maximum spatial resolution (134,138).

When examining *ex-vivo* tissue with AFM to determine its mechanical properties, the tissue needs to be fresh – cryosections and formalin fixed paraffin embedded sections have an altered elastic modulus, leading to non-representative measurements that poorly represent *in-vivo* mechanics (134,139). Biological samples need to be suitably hydrated too, as drying the tissue will lead to changes in the structure and elastic modulus. The sample also needs to be immobilised to prevent it floating or drifting during scanning - this is typically achieved with a biological adhesive such as poly-l-lysine or a glue, such as polyacrylate, attaching the sample to a glass slide. The tissue also needs to be thick enough to prevent the probe detecting the underlying glue or slide; indentations <10% of the sample's thickness are considered suitable for avoiding detection of the underlying hard surfaces (Bückle's rule) (134,140).

Very little work has been undertaken on mechanical testing of dental pulps in the literature. By contrast, much work has been achieved with regards to characterising the hard structures of the tooth, such as enamel and dentine in both health and disease (141–148). Without understanding the physio-mechanical properties of the living soft dental tissues, however, we cannot fully understand tooth physiology in health and pathological processes such as dental caries. As the pulp is encased by the dentine and enamel, it is difficult to explore in a non-destructive way, which may explain the paucity of research with regards to its mechanical properties. Assessing the dental pulp at the micro and nano-level facilitates a better understanding of the environment in which pulp cells reside, and how DPSCs migrate and differentiate within it, providing vital information that can be used to inform development of new dental materials and add to our expanding knowledge of the dental pulp in health and disease.

The only work to date looking at the elastic modulus of dental pulps was completed by Erisken *et al.*, who used dental pulps removed from porcine canines (149) and human third molars (150) to perform shear testing. This study, utilising bulk mechanical testing of dental pulps, is unique and welcome but has some significant disadvantages, limiting its clinical applications. Firstly, the group removed the dental pulp from the dentine encasing, disrupting the physiology of the pulp - as dental pulp is anchored to the dentine via the odontoblasts rimming the pulp, this method will negate any effect the odontoblasts

and the dentine will be having on the elastic modulus of the tissue. Secondly, the authors used bulk testing; this may be useful knowledge for large pulpal replacements (such as those used in root canal treatments/endodontics) to ensure the bulk mechanical function of the tooth during mastication. Current understanding, however, of the length-scale which is most pertinent for cellular interactions and their sensing of the environment suggests this is most likely at the μm and nm scale (134,135), though no definite consensus has been reached on this and the distance may well vary by cell type. If we wish to explore the biomechanics of the pulp at a level relevant to cellular function, we need to assess the elastic modulus of the pulp at a smaller scale. In summary, although Erisken *et al.*'s work is novel and the first completed on exploring the mechanical properties of the dental pulp, the issues with this work limit its use for biomimetic and regenerative dental biomaterials (149,150)

To overcome the issues above, a protocol has been designed for measuring the elastic modulus at the μm and nm scale, maintaining the dental pulp as much as possible within its hard tissue housing and using human *ex-vivo* tissue, to ensure the results are easily transferable for human biological application.

It is currently believed that, in addition to biochemical signalling, DPSCs interact with, and differentiate in response to, mechanical signals from the surrounding ECM or substrates. It is well established for many human tissues (including bone, cartilage and muscle) that scaffold and tissue stiffness affect the differentiation of mesenchymal stem cells, with documented reference values for the commitment of these cells to produce these tissue types (151). This approach of altering the scaffold or substrate modulus to affect the tissue type required for a particular role or function can be broadly applied to many biological tissues, to enable replacement and repair (152). Recent work demonstrated that scaffold stiffness affects dentinogenesis (12), but the optimum stiffness for dentinogenesis (*in-vitro* and *in-vivo*) is still not entirely known. Without this knowledge, we cannot understand the processes occurring in exogenous dentinogenesis within a scaffold, and as such, optimising this process becomes impossible. This information is pertinent for new PCA creation but can also be used to inform and improve current PCAs and pulpal replacements in endodontics.

Mechanotransduction via surface topography, substrate stiffness, Low Intensity Pulsed Ultrasound (LIPUS), dynamic hydrostatic pressure, mechanical stretching and pulsating fluid flow have all been shown to affect the differentiation and/or proliferation of DPSCs and are covered in a comprehensive review by Marrelli *et al.*(26). If a scaffold can be optimally designed to incorporate some of these mechanical features, it may be possible to create a dentinogenic scaffold capable of inducing odontogenic differentiation of DPSCs without the need for additional biological signals to be incorporated into the scaffold, making production cheaper, potentially easier, and more commercially viable. More importantly, it may produce more reliable and predictable outcomes for surgical procedures where tissue regeneration is the end goal (such as pulp capping in dentistry). When considering the practicalities of some of the

modalities discussed in Marrelli *et al.*'s review, some of the methods are difficult to employ at chairside in primary dental care (for example pulsating fluid flow). Therefore, this work focuses on substrate stiffness of the biomaterial to facilitate DPSC differentiation and hard tissue formation, with the aim of producing a hard tissue bridge capable of sealing a dental pulp.

4.1.2 HISTOMORPHOMETRIC CONFOCAL MICROSCOPY

Histomorphometric analysis is a method of quantitatively assessing the volume and organization of a tissue using microscopy. It can vary in complexity and application from simply measuring structures on a glass slide, to *in-vivo* assessment with fluorescent markers. This is a technique often employed in bone research (153), but has more recently been employed in analysis of soft tissues (154,155). It can involve rating by observers of specific histological structures (156) , which can be open to intra- and inter- rater variability, or by quantitatively measuring histological structures (157), which may be open to site-based selection bias.

As previously described, the dental pulp is predominantly formed of collagen type I, though other ECM proteins are also present, such as fibronectin, laminins, collagen type III and tenascin to name but a few. Changes in the expression of some of these ECM proteins between the healthy and carious state have been identified in previous RNAseq studies (158) and in other histological assessments of the dental pulp (159), and it is possible that changes to the ECM may account for any alterations in the elastic modulus using AFstudies. In addition to these changes, angiogenesis and neurogenesis occur in the carious pulp (160,161), which too may influence the outputs of RNAseq analysis and AFM data.

Confocal microscopy was created and patented in 1955 and facilitates the optical assessment of a slice within the tissue of interest, that may be many micrometers deep (162). It was not until the 1980s that confocal microscopes began to be used for biological applications and it became commercially available (163). Traditional light microscopy ("wide field microscopy") illuminates a tissue section by transmission of light through the tissue (which is traditionally prepared by fixing, paraffin embedding and sectioning). Therefore, this method illuminates the whole sample thickness, which can generate background 'noise', compromising the resolution of the image at the area of interest (162,163). Both traditional light microscopes and confocal microscopes can use fluorescence for imaging, whereby a fluorophore is used to stain an area, cell or structure of interest and a light beam is used to excite the fluorophore. The emitted light from the fluorophore is assessed by eye or computer. In traditional light microscopy used for fluorescence, background autofluorescence of structures, or fluorescence from stained structures deeper or superficial to the area of interest may lead to loss of contrast or resolution (163). The confocal microscope overcomes this issue by being able to focus the light beam on a small area inside the tissue (as small as 0.25µm, depending on the microscope and setup (163)), and creating

a ‘section’ through the tissue at the focal level required, thus eliminating fluorescence from unwanted sources. This section is usually 0.5-1.5µm thick (163), see Figure 4.1.2 1.

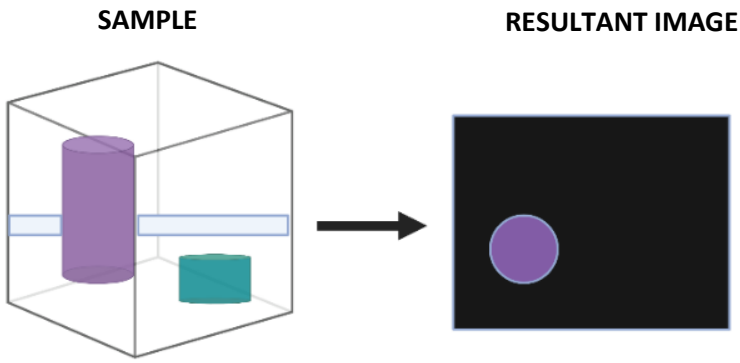

Figure 4.1.2 1: Schematic diagram demonstrating the ‘sectioning effect’ of confocal microscopy. The section in the focal plane is in pale blue, preventing fluorescence of deeper structures (in turquoise in the diagram) impacting on the image of the region of interest (region of interest being the purple structure).

Confocal microscopy exposes only a small area of the specimen to light, and only light from this small area is detected. This process of emitting light over a finely focused spot is repeated numerous times over the entire plane of focus, in a raster-scan pattern. As this is occurring, the illumination beam diverges above and below the focal plane, sending less light to areas out of focus and as such minimizing the amount of light passed to areas beyond the plane of interest, significantly reducing some of the ‘noise’ from out of focus features (163). A pinhole aperture removes out of focus light, as the illumination and detection systems are both focused on the same small area of the tissue, thus further reducing ‘noise’ from the specimen. These features impart the name ‘confocal’ to this microscopy system, as the specimen, illumination and detector all have the same focus, i.e. they are confocal (163) – see Figure 4.1.2 2.

The basic setup of a confocal microscope comprises of:

1. The microscope; upright or inverted. This will include a stage with x, y and z axis controls.
2. A light source. These are lasers, with varying emission wavelengths. Most confocal microscopes will have three to five lasers, emitting UV, blue, green, yellow or red light. These are often argon, krypton or helium ion lasers depending on the colour/wavelength of the light.
3. A scan head. This will contain the confocal aperture, shutter, filter wheels and scanning mirrors.
4. A detector. This is usually a photomultiplier tube.
5. A computer. This is necessary for image visualization, capture and processing.

Ultimately, these differences make confocal microscopy far superior to traditional light microscopy for highly detailed imaging necessary for accurate histomorphometric analysis. As with any technique, there are limitations to confocal microscopy – firstly, depth of imaging is limited by optical resolution and signal-to-noise ratio, secondly photobleaching of fluorophores limits the length and extent of imaging, thirdly phototoxicity can limit the use of confocal microscopy when imaging live samples (e.g. cells), and finally confocal microscopy is relatively expensive compared with other light microscopy techniques (162).

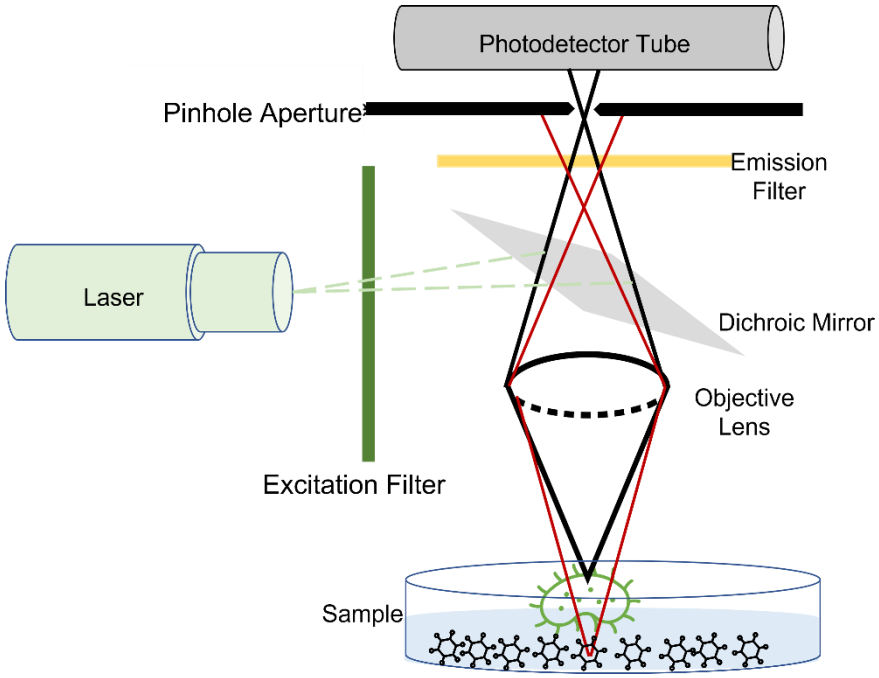

Figure 4.1.2 2: Schematic diagram of confocal microscopy and the effect of the pinhole aperture in removing light from out of focus areas. Black lines = area in focus, red lines = area out of focus

The purpose of this study was to analyse images acquired from dental pulps in a quantitative manner. This will allow assessment of the structures present and as such inferences can be made linking the histology of the dental pulp to AFM data and RNAseq data, allowing changes at the tissue-level to be linked to transcriptional and mechanical differences between carious and sound teeth. Confocal microscopy has been chosen for this due to its high resolution and optical accuracy.

When exploring the literature for histomorphometric analysis of the dental pulp, comparing carious and sound teeth, many of the studies are >40 years old, and these are more descriptive in nature than specifically 'histomorphometric' – for example, see (164–170) – these studies frequently utilise animal models and electron microscopy to image the dental pulp. These studies do not make use of modern advances in light microscopy, such as confocal microscopy. A recent paper has used lightsheet microscopy – a new and emerging technology that looks at structures within a tissue that has been

'cleared' to study tissue components in three-dimensions – to explore structures in the dental pulp, though their work mainly focused on nerves and vessels (171).

Of the few more recent histomorphometric analyses of highly collagenous tissues, studies have explored the arrangement of collagen fibres in skin and have utilized macros in ImageJ to automate measurements of fibre orientation (154,155,172). From the work Marcos-Garcés *et al*.(155), it seems that eosin staining for highly collagenous tissues is likely adequate for histomorphometric analysis as it shows comparable results in histomorphometric analysis to other differential stains (such as picrosirius red and Masson's trichrome). Using eosin has a key advantage over some other stains that may differentiate ECM components as it fluoresces, facilitating the image analysis via confocal microscopy, ensuring high resolution images for accurate measurements and this stain is relatively easy and inexpensive to do.

There are 28 different collagens, composed of >46 distinct polypeptide chains (173). Collagens I and III are found in the dental pulp (6) and these both have a fibrillar structure. Individual collagen fibrils are a triple helix of three polypeptide strands, these triple helices (known as 'tropocollagen'), assemble in a hierarchical manner to produce macroscopic tissues and tissue components (such as bone, tendons and in this instance, dental pulp) (173). Collagen I fibrils are formed of two α1 chains (coded for by *COL1A1* gene), and one α2 chain (coded for by *COL1A2* gene) whereas collagen III fibrils are formed of three α1 chains (173). Collagen I, as previously mentioned, is the main ECM component in dental pulp. Within the dental pulp, collagen I is produced by odontoblasts and fibroblasts, but fibroblasts also produce collagen III (170,174).

Several studies have highlighted a difference in the injured pulp compared to the sound pulp in relation to soft tissue changes. These have included assessment comparing carious and sound teeth and investigating the changes due to iatrogenic dentine damage (e.g. in cavity preparation). These changes include; increased vascularity (166), vasodilation (164), increased inflammatory cell infiltrate (164,166) and reduced collagen III, tenascin and fibronectin content (159). However, many of these studies are >30 years old, and qualitative in nature based upon generalized findings from light microscopy.

It is imperative to have a good understanding of any soft tissue changes in the dental pulp to better understand any micromechanical changes (detected by AFM), that may be impacting upon DPSC recruitment and differentiation as part of DPC healing and repair. By better understanding any soft tissue changes, and the impact that these may be having upon the micro-mechanical environment, we can learn about physical changes in the carious pulp that may be impacting tertiary dentine deposition. This information, in turn, may facilitate better strategies for tissue repair.

4.1.3 RNA SEQUENCING

Although all cells in a tissue have the same genome, the proteins they express can vary widely. This variability is influenced by many factors, including the individual's genome, the cells' function, health status and even time of day (175). Only a small fraction of the genome is expressed in mRNA form (which codes for the proteins expressed) at any given time. Thus, measuring mRNA provides a rich and detailed snapshot of cellular activity at a specific moment, in a specific environment.

Analysis of mRNA is a powerful tool for understanding biological processes in health and disease which begins with the isolation of mRNA from a tissue or cell sample. The mRNA is then reverse transcribed into cDNA, which is a double-stranded DNA molecule that is complementary to the mRNA. The cDNA is then sequenced, and the resulting sequence data is used to identify the genes that are being expressed.

By sequencing mRNA, researchers can identify which gene is being transcribed. This information can be used to track changes in gene expression over time, or to compare gene expression between different tissues or cell types (differential gene expression). Differential gene expression is achieved by assessing which genes are expressed and the abundance transcribed. It may be possible to link the changes in gene regulation to phenotypic, biological and mechanical changes to tissue by looking at differential gene expression, which can be useful in elucidating pathways of disease, repair, and health.

Transcriptomics of the dental pulp has historically focused on specific cell types isolated from the pulp (for example, DPSCs (176) and pericytes (177)) typically in an *in-vitro*/cell culture format, rather than focusing on the pulp as a whole tissue *ex-vivo*. In studies where the whole pulp has been examined, microarray analyses have generally been carried out, focusing on specific panels of genes (158,178–180).

To date, there is a paucity of literature on the use of next-generation sequencing (NGS) to compare differential gene expression between carious and sound teeth. NGS is a powerful tool for gene expression analysis that does not require the pre-selection of target genes, unlike microarrays, in this way NGS is more 'open-ended' asking 'what genes are expressed in this tissue?', rather than 'which genes from this list are expressed in this tissue?' and is therefore less susceptible to selection bias. Additionally, NGS can detect a wider range of gene expression levels than microarrays, as it outputs discrete read counts rather than signal intensity. This allows for more accurate quantification of gene expression, especially for genes with low expression levels (181). NGS is also able to detect novel transcripts, which would not be uncovered by a microarray (181), and the sensitivity and specificity of NGS is believed to be higher than that of a microarray (182). Microarray data normalization can be challenging. For example, a reference transcript (which is not expected to be up- or down-regulated) is needed, whereas in NGS, the number of reads across an entire genome can be used to normalize the results. This makes the interpretation of up- and down-regulation of genes in NGS potentially more reliable when comparing samples or groups of samples (differential expression). However, the advantages of

microarrays over NGS, are that microarrays are generally considered easier to perform, less expensive, less labour-intensive and microarray studies usually have more samples than NGS studies (due to the former reasons). As NGS RNA sequencing becomes more affordable, this powerful tool will be utilised more for dental research.

NGS is a type of DNA sequencing that has revolutionized the field of genomics. NGS is massively parallel, meaning that it can sequence millions of DNA fragments simultaneously. This is in contrast to Sanger sequencing, which can only sequence one DNA fragment at a time. In both Sanger sequencing and NGS, single strands of DNA are paired with bases that are colour-coded with a fluorescent dye. The different colours correspond to the four DNA bases: adenine (A), thymine (T), guanine (G), and cytosine (C). As the DNA polymerase adds nucleotides to the growing DNA strand, the fluorescent dyes are excited and emit light. The colour of the light emitted indicates which base was added. These fluorescent signals are arranged and then detected by a computer, and the sequence of the genome can be identified. NGS has several advantages over Sanger sequencing. It is faster, more efficient, and can sequence longer DNA fragments. The key differences between Sanger sequencing and NGS are that millions of strands of the template DNA are used in NGS, whereas in Sanger sequencing only one strand is used as the template, and in NGS the bases added to the template are all fluorescently tagged, whereas in Sanger sequencing non-tagged bases are also present that extend the replica strand until a fluorescent base is reached and the extension stops (183). As such, NGS is a vastly expanded version of Sanger sequencing (183). Putting this into perspective, 100 Sanger sequencers running 24/7, would require 3.5 years to sequence the entire human genome, whereas a single NGS machine could accomplish this feat in around one day (183).

NGS has been successfully used for single cell RNA Sequencing (scRNA-seq) of the whole dental pulp. A recent paper by Opasawatchai *et al*. (184), isolated dental pulp cells into 16 discrete cell populations and explored differential gene expression in these individual populations. Compared to whole-tissue RNA sequencing, scRNA-seq provides more insights into biological systems at a cellular level. This is because cells with greater abundance will contribute more reads and expression to the whole-tissue RNA sequencing output than cells with less abundance. For example, fibroblasts are the most abundant cell type in the dental pulp, whereas leukocytes and odontoblasts are relatively rare. scRNA-seq can account for this difference by sequencing individual cells, regardless of their abundance.

Although highly informative, the study by Opasawatchai *et al.* (184) does fall short on sample numbers as only four samples were included (though the authors do specify that it is a pilot study). In comparison, the microarray study by McLachan *et al.* included 23 samples (158) and the work by Pääkkönen *et al.*, included 104 samples (179). However, the microarray study by Pääkkönen *et al*.(179) did not include statistical analysis to verify the significance of the log2 fold changes identified in their results, nor did they account for false discovery, whereas the NGS work by Opasawatchai *et al*., (184) did as part of

their analysis pipeline (they used the R package DESeq2 (185)). In summary, the experimental work in the literature with regards to RNA sequencing analysis of the dental pulp comparing carious and sound teeth has limitations, whether that be in technique, sample number, or analysis, and as such this area warrants further exploration.

From the literature, examining sc-RNA-seq studies (184) and micro-array studies (158,178,179) of the dental pulp, several trends come to light when comparing carious and sound teeth. Firstly, carious teeth show upregulation of pro-inflammatory genes, such as genes from the CXC subfamily of chemokines, genes from the human leukocyte antigen complex (HLA), and immunoglobulins. These genes are involved in the recruitment and activation of immune cells, which contribute to the inflammatory response in carious teeth. Secondly, regenerative response demonstrated by the upregulation of anti-inflammatory genes (for example, *SERPINA3*) and genes associated with tissue formation (i.e. hard tissue formation, angiogenesis and neurogenesis) is found in carious teeth. Thirdly, general cell function upregulation is identified in carious teeth (for example, genes associated with cellular metabolism). Further trends demonstrate that generally more genes are upregulated in carious teeth, compared to sound, and the genes with the greatest fold changes are largely those associated with inflammation and immune response to pathogens (158,178) - this stands to reason considering the inflammatory response and leukocyte population that is only present in carious teeth (184). When looking specifically at sound teeth, compared to carious teeth, some DPSC genes are upregulated, such as those associated with hard tissue formation and cell cycling/growth/proliferation (158,184).

To summarise, AFM analysis can elucidate changes in the biomechanics of carious pulp. To better understand these changes, it is important to consider transcriptional changes in the host cells. Observing up- and down-regulation of genes can help us understand cellular functions and gene expression in carious pulp. Using NGS instead of microarrays can facilitate the exploration of genes not previously associated with healthy and carious pulps, furthering our understanding of the molecular landscape of tissue changes secondary to dental caries. The purpose of is the work presented here is to link the gene expression data of carious vs sound teeth to the mechanical and physical characteristics of the tissue, thereby inferring on the pulpal response to caries at a physical and cellular level. Also, NGS of the dental pulp will add to the literature of pulpal RNA data, facilitating comparisons and correlations to the findings of previous studies.

4.2 MATERIALS AND METHODS

4.2.1 AFM MATERIALS AND METHODS

Teeth were obtained from clinics at Leeds Dental Institute. Leeds Skeletal Tissue Bank provided carious teeth #1, #2, #3. #4 and sound teeth #1 and #2 for this work (through Tissue Bank Ethics). All other

teeth were obtained via Project Ethics. A total of 7 carious teeth and 7 sound teeth were used, submitted by three dental surgeons.

Teeth were stored in a refrigerator in phosphate buffered saline (PBS) for AFM. From experimental experience, it was not possible to use the same tooth for RNA sequencing and AFM as the whole pulp was needed to provide an adequate yield of RNA for RNA sequencing (see Section 4.2.3 for details in RNA extraction).

Once the teeth were obtained, they were sectioned into 4 pieces longitudinally in the mesio-distal plane; with two central slices (each 1.5mm thick) containing pulp – one section was used for AFM and one for histology, with the two end pieces discarded (the end pieces frequently contained little to no pulp). The teeth were sectioned using an Accutom 10 (Struers LLC, Cleveland, US). The section for histology was placed in formalin for 48 hours before processing (see Section 4.2.2).

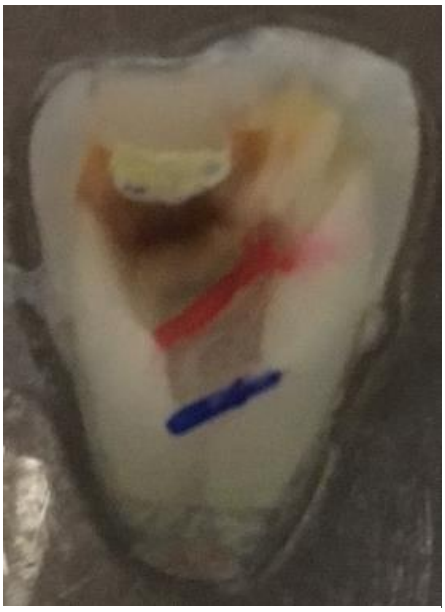

Figure 4.2.1 1: Image of a carious tooth prepared for AFM, with red ink marking the pulp roof and blue ink marking the pulp floor, making localisation using the AFM camera easier

The section for AFM was stuck to a clean glass slide using Vetbond tissue adhesive (3M, Bracknell, UK) (n-butyl cyanoacrylate), with a layer of dental silicone (Zhermack Elite Glass, Badia Polesine, Italy) introduced behind the soft pulp to support it. The silicone is an important step because the centre of the pulp sags without support, meaning the pulp becomes out of range for the AFM Z-piezo stage during the experiment. It is imperative that the samples for AFM are as flat as possible due to the limited range of the scanner (XY: 90µm, Z: 16µm) (134). Because the tissue slice is 1.5mm thick, the AFM elastic modulus measurements did not detect the underlying silicone with small indentations of the cantilever's tip (<10% of the sample's thickness, Bückle's rule (134,140,186)).

Once prepared, the tooth section on the slide is stored in PBS in a refrigerator until scanned (within 48 hours of sample preparation and the maximum time from extraction to scanning was 72 hours). The teeth are scanned under PBS to keep the tissue hydrated during nanoindentation measurements, to mimic the hydrated *in-vivo* state, and as PBS is isotonic, it will prevent excessive water movement into/out of the sample.

MFP 3D AFM (Oxford Instruments, Abingdon UK) was used for the AFM tooth experimental work. Before scanning each tooth, the cantilever was calibrated using Asylum Research (Oxford Instruments,

Abingdon, UK) proprietary software. The cantilevers used have a spherical tip, radius 1500nm (biosphere B1500-CONT). The cantilever tip is made from diamond-like carbon, with reflex gold coating, with a rectangular cantilever beam shape and a 0.2N/m spring constant and resonance frequency of 13kHz (Apex Probes, Bracknell, UK). Although the probes are pre-calibrated, there was still some variation in the true spring constant (0.19-0.42N/m) observed when calibrated in-house. The coronal aspect and floor of the pulp chamber were differentially marked with red and blue permanent ink markers to make orientation with the camera more straightforward (see Figure 4.2.1 1). The experimental setup for the AFM is shown in Figure 4.2.1 2.

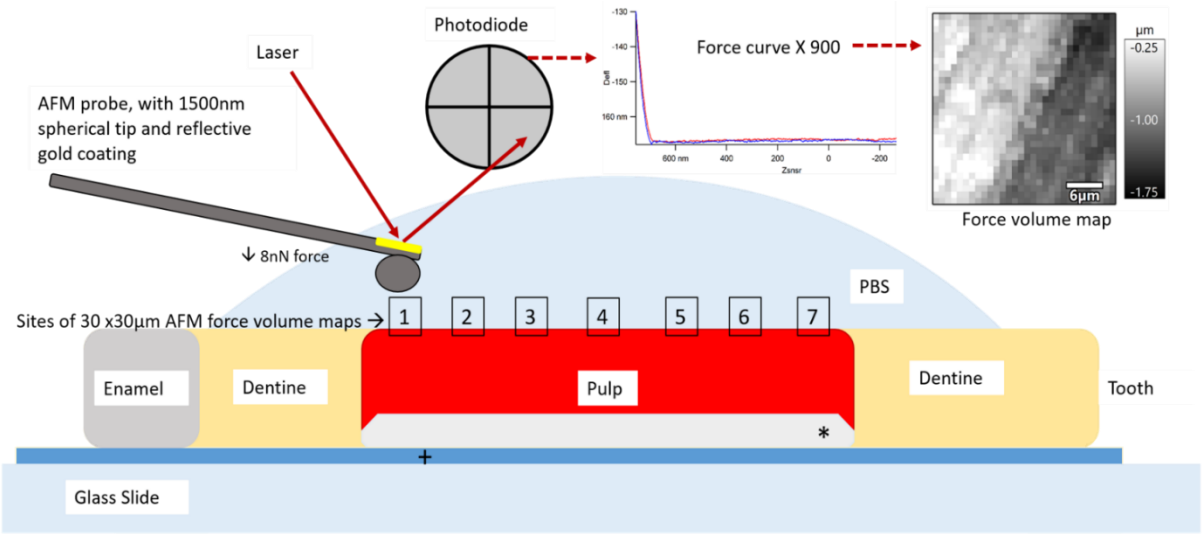

Figure 4.2.1 2: Schematic diagram showing the setup of a tooth slice for AFM of the dental pulp. * = dental silicone, + = glue. Seven force volume maps (FVMs)were produced from coronal (Site 1) to pulp floor (Site 7). Each FVM was composed of 900 individual force curves produced using a spherical-tipped cantilever. All measurements done under PBS to prevent the pulp drying out.

Once the cantilever was calibrated, the position on the pulp was identified using the microscope's camera and the probe lowered to the surface, with a few initial force curves created to ensure the working distance and maximum loading force (typically ~8 to 25nN) were appropriate and establish the location of the cantilever in relation to the pulpal anatomy. A force volume map (FVM) was then created consisting of 900 force curves over and array of 30µm x 30µm, such that each measurement is made within a 1x1um square area with a contact area of sub-micron squared. The microscope stage was then advanced using the mechanical XY stage so that the next force volume map can be created. This was repeated from the most coronal aspect of the dental pulp to the pulpal floor (at the cervical region of the tooth) in a straight line along the tooth long axis, until 7 FVMs are collected. A FVM is included in the AFM setup diagram in Figure 4.2.1 2. FVMs are a 3D array of the cantilever response at every position within the XYZ scan region. As the individual anatomy of each tooth varies and the total length of the pulps are different, there is no set specified distance between each force volume map but is typically in

the range 0.05mm-0.3mm. The start distance was 3µm (the point at which the cantilever starts the force curve) to prevent any dragging across the surface and avoid adhesion affecting the results, with a force distance of 1µm and a velocity of 2µm/s.

FVMs are used to provide information on surface topography, elastic modulus and surface adhesion across a specified area of the sample. FVMs are particularly useful for exploring elastic modulus, adhesion, indentation, and topography over a set area. A FVM is comprised of a set number of pixels, usually in a rectangle or square, with each pixel pertaining to an individual force curve and as such each pixel contains a wealth of information. FVM acquisition is usually automated, with size and velocity specified. Once one curve has been produced, the probe is lifted from the surface of the sample, the stage moved a set distance (as defined by the size of the FVM, the number of points per row and the number of rows), and another force curve produced. These are time-consuming to produce, as increasing velocity of the probe and stage often results in poor force curves.

Once created, the FVMs were analysed and the elastic modulus for each of the 900 force curves per map is calculated using proprietary software from Asylum Research (Oxford Instruments Company, Abingdon, UK). The elastic modulus was calculated by identifying the elastic portion of the curves and fitting the Hertz model to the curves; once one curve has been calculated the software will attempt to fit the model to all 900 curves. As it was not feasible to check the elastic modulus for each of the 900 curves individually, outliers are targeted and fitted to the curve manually as appropriate, or removed from analysis if the fit is too poor (the mean number of curves excluded from each FVM was 9.0 per 900, with a range of 0 to 51). An example of a 'good' curve (i.e. good fit to the Hertz model) and 'bad' curve (i.e. poorly fit)) are given in Appendix 2, and an example of a curve fit to the Hertz model is given in Appendix 3. Fit was determined qualitatively by eye and by using the ν-χ^2 value calculated by the software.

$$F = \frac{4E\sqrt{R}}{3(1-\nu^2)}(\delta)^{3/2}$$

Equation 4.2.1 1: Hertz model describing a sphere being compressed into a flat, elastic surface

For this research, the Hertz model was used to calculate the elastic modulus of each force curve. The Hertz model describes an incompressible sphere with radius (R), being pushed with a defined force (F), into a flat and elastic surface of a given elastic modulus (E). The relationship between F, applied by the sphere on the surface, and the indentation of the surface, δ, is then given by equation 4.2.1 1, where ν = Poisson's ratio (assumed to be 0.5, which is an appropriate value for materials assumed to remain unchanged under stress) (187).

A comparison of some of the most popular models for elastic modulus calculation from force curves are shown in Table 4.2.1 1.

Model	Advantages	Disadvantages
Hertz	Widely used Most simplistic Uses 'approach' curve	Assumes no adhesion Discounts viscoelasticity Only valid for small indentations (<10% sphere size)
Oliver-Pharr	Same as Hertz, but uses retraction curve Can be used for non-spherical tips Best choice for hard, non-biological samples where the elastic-plastic contact is assessed	As it is applied to the retraction curve, it is affected by adhesion and hysteresis Discounts viscoelasticity
JKR (Johnson-Kendall-Roberts)	Takes into account adhesion within the contact area	Applied to retraction curve, therefore not considering the traditional elastic portion of the curve As it is applied to the retraction curve, it is affected by adhesion and hysteresis Only suitable when the surface is much softer than the tip Assumes the soft surface will adhere to the tip Inappropriate at microscopic/nano levels for soft materials
DMT (Derjaguin, Muller and Toporov)	Considers attractive forces beyond the contact area	Only suitable for low-adhesion samples Requires a small tip radius
Sneddon	Used for conical/pyramidal indenters	Only valid for flat samples

Table 4.2.1 1: Comparison of different contact mechanics models to determine Young's modulus, (134,186,188–190)

The Hertz model was selected to calculate Young's modulus of the pulp tissue because a spherical indenter was used, the indentation depth was significantly smaller than the size of the cantilever, adhesion was generally low and it is the most commonly used model or analysis of biological samples

undergoing AFM (186). However, for the Hertz model to be correctly applied, the sample should ideally also be isotropic and homogenous, though for small indentations, and experiments where the sample size is considerably larger than the indenter, this has been demonstrated to be less crucial because at this level the load-indentation figures follow basic Hertzian mechanics and the sample can be considered an "elastic halfspace" (an isotropic and homogeneous material, expected to spread infinitely in all directions, with the superficial surface as a defined boundary) (186).

(134,186,188–190)For all of the sites, in all of the teeth, the data was non-parametric. Statistical analysis was carried out in R-studio to compare the sites within each tooth (Kruskal-Wallis tests completed using R studio package 'stats' (191), post-hoc analysis Dunn's test completed using R studio package 'dunn.test' (192)). To look for statistical differences between carious and sound teeth, both globally and at site-level, a linear mixed-effects statistical analysis model was needed to account for the multilevel grouping and nesting of the data. This is because each force curve cannot be considered a unique measurement when each curve belongs to a defined site, within a defined tooth; these are considered 'random effects' within this model. The multi-level nature of the data is further explained in Figure 4.2.1 3. The package lme4 was used in R studio to complete the linear mixed-effects model statistical analysis (193).

Data gathered from the patients included age and reason for extraction of the tooth. To assess for any correlation between age and elastic modulus of the pulp, Spearman's Rank correlation test was performed in R Studio.

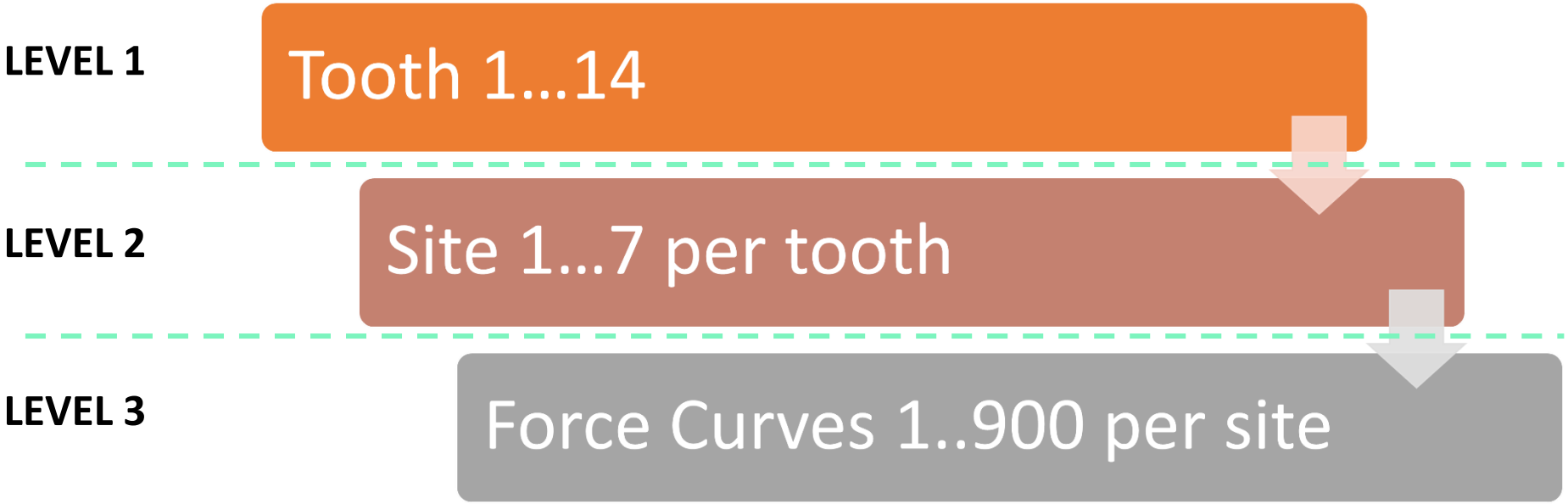

Figure 4.2.1 3: Multi-level nature of the AFM data, with random effects of the site and tooth displayed as a multi-level model

4.2.2 HISTOMORPHOMETRIC CONFOCAL MICROSCOPY MATERIALS AND METHODS

To investigate any changes in the elastic modulus of the teeth scanned in Section 4.2.1, histological assessment of these teeth was also performed. As collagen comprises the majority of the dental pulp, it is possible that changes in the collagen bundles are responsible for the changes in elastic modulus, though angiogenesis, neurogenesis and/or degradation of pulpal structures as part of necrotic changes could equally be causative.

One section of each tooth scanned on the AFM (sectioned on the Accutom 10 (Struers LLC, Cleveland, US), each section was 1.5mm)), was placed in neutral buffered formalin for 48 hours, and then decalcified using EDTA (20%, pH 7.8) for at least two months, until all calcium had been extracted from the specimens (this was assessed physically). The sections were dehydrated and embedded in paraffin wax, with sections sliced on a microtome into 7µm sections. Each section was dried overnight, dewaxed and rehydrated through graded alcohol, and stained with hematoxylin and eosin, then dehydrated again through graded alcohol and cleared with xylene. The sections were subsequently mounted with DPX and a coverslip. Two extra teeth to the 14 used for AFM were collected from clinics, one sound and one carious, and one section from each was taken and processed for histology as above (making the total number of teeth for histomorphometric analysis 16 (carious = 8, sound = 8)). The time from extraction to placing into formalin was a maximum of 24 hours. Table 4.2.2 1 summarises the staining process for each section.

PROCESS	ACTION	TIME
De-waxing	Submerge in xylene twice	10 minutes per submersion
Rehydrating	Submerge in 100% ethanol	3 minutes
	Submerge in 90% ethanol	3 minutes
	Submerge in 70% ethanol	3 minutes
	Submerge in running water	2 minutes
Stain with haematoxylin	Submerge in Harris's haematoxylin	3 minutes
'Blue' the haematoxylin	Submerge in running water	2 minutes
	Submerge in Scott's Tap Water	3 minutes
Stain with eosin	Submerge in eosin	3 minutes
Remove excess eosin	Submerge in running water	2 minutes
Dehydrate	Submerge in 70% ethanol	3 minutes
	Submerge in 90% ethanol	3 minutes
	Submerge in 100% ethanol	3 minutes
Clear the section	Submerge in xylene twice	3 minutes per submission

Table 4.2.2 1: Staining protocol used for Haematoxylin and Eosin staining

Sections were then scanned using the Leica SP8 confocal system with a Leica DM6-CS microscope (equipped with four lasers (405nm, 638nm, 488nm and 553nm)) (Leica Microsystems UK, Sheffield) using a x63 oil lens (and 1x optical zoom), using laser excitation to make the eosin fluoresce (excitation wavelength = 525nm and emission =546nm) (similar to the work by (154,155)).

Five images were captured from the top of the pulp, five from the middle and five near the bottom for each tooth (i.e. the pulpal floor, no root canal pulp was included). The odontoblast and cell-free zone were avoided for the coronal images – the cell-rich zone was imaged for this site. This was to avoid the dense neural plexus in the cell-free zone, where there are relatively few collagen bundles (194) and because of difficulty in imaging the odontoblast zone without including some dentine/predentine and the cell-free zone, which would affect later quantitative analysis.

The resultant images were loaded into ImageJ (version 1.54b, freely available from https://imagej.nih.gov/ij/index.html) for analysis, and Table 4.2.2 2 provides the parameters measured in each image.

PARAMETER MEASURED	MACRO/PROCESS
Number of fibres	Transects Macro
Width of fibres	Transects Macro
Area of fibres	Manual pixel counting
Orientation and alignment of fibres	Fourier Orientation Macro (Ratio) and OrientationJ (Coherence)

Table 4.2.2 2: Summary of parameters explored with histomorphometric analysis and the process used for each assessment

More teeth were submitted to the study than were scanned on the AFM; this is predominantly due to availability of the MFP3D AFM machine.

A total of 8 carious and 8 sound teeth were used for fibre analysis, culminating in 240 images (15 from each tooth).

Orientation Analysis

Marcos-Garcés *et al*. and Van Zuijlen *et al*. (154,155) found that the orientation of collagen bundles in soft tissue changed after a period of inflammation due to scarring. The protocol by Marco-Garcés *et al*. involved fluorescent imaging of eosin-stained sections of skin and measuring the collagen orientation/arrangement. They found that eosin performed as well as differential soft tissue stains (for

example Masson's Trichrome) for assessing collagen bundles and utilized this knowledge in their research (155) .

Broadly following their protocol, a macro was built ('Fourier Orientation Macro'). This essentially involved the following steps: 1) Applying an appropriate threshold (the same used for each image) 2) Making the image grayscale 3) Performing a Fourier Transform on the image and selecting only the pixels with a grayscale value >192.

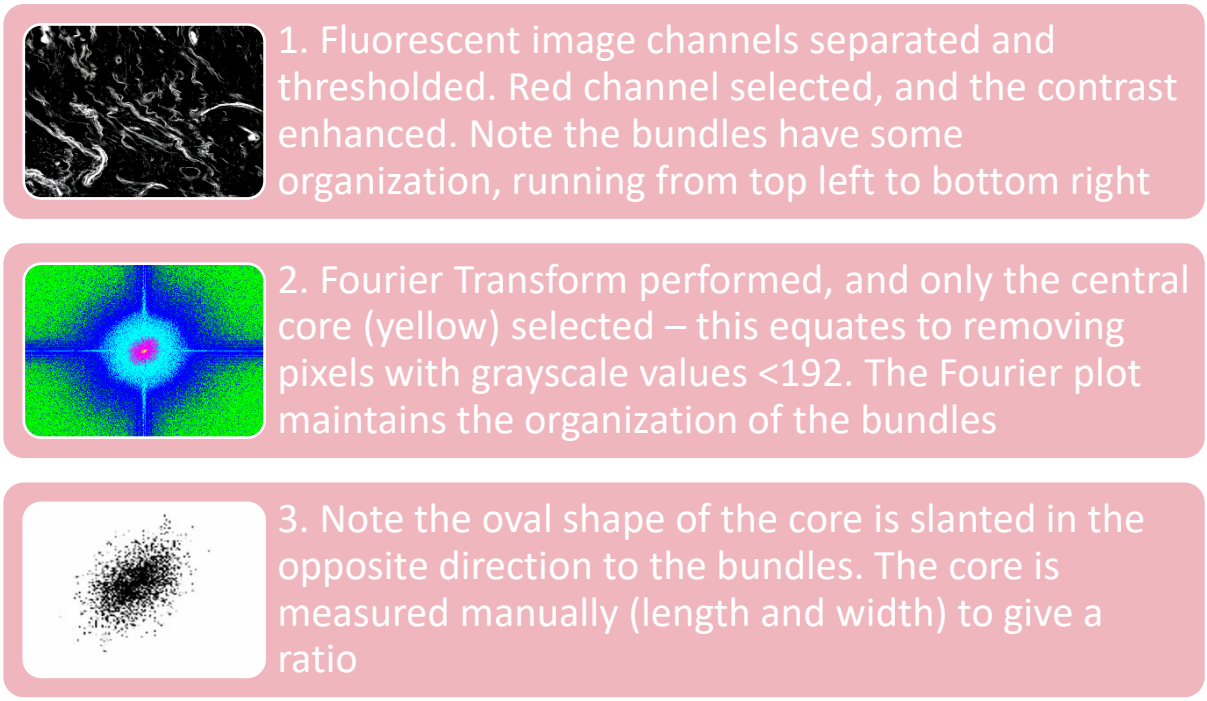

Figure 4.2.2 1: Overview of Fourier Orientation Macro Process

After steps 1-3 were completed (Figure 4.2.2 1), the image was measured manually. The previous steps have removed pixels with low grayscale values so that the downstream analysis focuses on the most prominent bundles only, and the Fourier Transform core orientation links to the orientation of the fibers (an elliptical core fits with organized fibers running in one direction, whereas a round core suggests the opposite). The selected 'central core' of the Fourier Transform is measured (width and length) manually in ImageJ. This results in a ratio value (width/length, 0.0-1.0), the closer to 1 the value is, the more randomly aligned the bundles are, the closer to 0, the more aligned/organized the bundles are (155).

In addition to the Fourier Orientation Macro, a widely available plugin was also used to assess the orientation of the fibers in the images, OrientationJ (195). For the OrientationJ analysis, the whole grayscale image (as per point 1 in Figure 4.2.2 1) was selected and the coherency value determined; this process was automated by the OrientationJ plugin. The programme measures the orientation of each pixel within the area selected, where each pixel is described by a value derived from the structure tensor produced for each image. The equations involved in the analysis for production of coherency values are

complex and discussed in more depth in (195). A coherency value closer to 0 means the fibres in the image are poorly aligned, a value closer to 1 means the fibres are well aligned.

A copy of the script for the Fourier Orientation macro (written in Java) created for this work, is provided in Appendix 4.

Pixel Counting Analysis

Within ImageJ, a pixel counting process is included as standard. To do this, a region of interest is selected (in this case, this was the whole image), and 'area fraction' measurement is taken – this is a % of the area that is not black i.e. a count of the pixels that are stained. This must be undertaken on a black and white image, which is produced by selecting the 'red' channel when splitting the image into red/blue/green channels. The resulting black and white image from the red channel is selected, the whole image is selected and the % area stained determined by measuring the area fraction.

Collagen Number Bundle and Width Analysis ('Transects Macro')

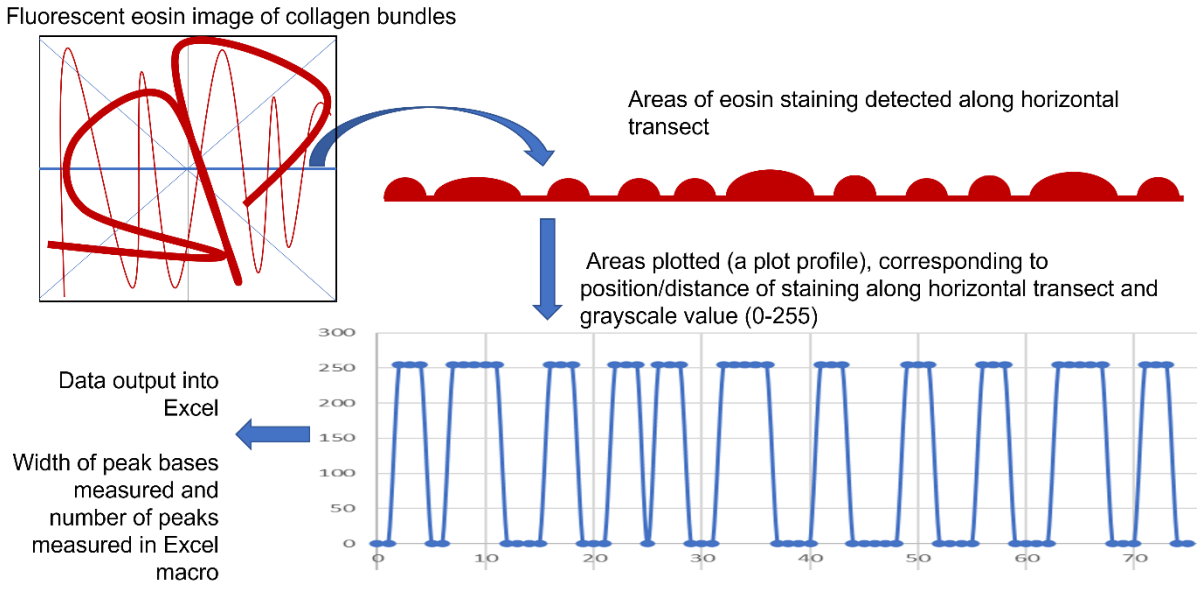

Figure 4.2.2 2: Summary of the Transects macro used in this study. The width of the peaks gives the width of the fibres and the number of peaks gives the number of fibres.

Analysing all of the fibres within each image would be difficult due to the number of images, the high level of detail within each image, the different orientations of the fibres and the different structures of the fibres, therefore transects through each image have been chosen as representative samples of the images. Two macros were developed to firstly collect the raw measurements and secondly to process the measurements. To make the images easier to analyse, the images were first made binary. For the

first macro, in ImageJ (written in Java), transects were selected (four in total – horizontal, vertical, and two diagonals) across each image, with measurements of the stained areas taken along each line, including the width of each area of staining and the number of areas stained. Quantifiable measurements were achieved by plotting the grayscale value against the distance along the transect ('plot profile'). The values from the plot were exported into Microsoft Excel. In Microsoft Excel, a macro was created (written in VBA) to measure the widths of the peaks of each stained area along the transect and to measure the number of these peaks. Copies of the scripts for both macros can be found in Appendix 4, and Figure 4.2.2 2 summarises the process.

Statistical Analysis

K-means clustering was completed to look identify clustering of the outputs. The ideal number of clusters was identified with a gap statistic plot.

For all of the parameters explored, linear mixed effect model was used to assess for statistical differences between carious and sound, with the site of the image (coronal/mid-pulp/pulp-floor) and individual teeth as random effects and carious/sound as a fixed effect.

It is a recognized limitation of this analysis that most structures of the pulp will be stained with eosin. However, as collagen is the main component of the pulp, the overall trends that will be identified are trusted to represent the collagen network of the pulp, even if additional pulpal components/structures such as capillaries are included in the analysis.

4.2.3 RNA SEQUENCING MATERIALS AND METHODS

4.2.3.1 PRE-SEQUENCING, SAMPLE PREPARATION

1. RNA extraction and quantification

A summary of the workflow for RNA extraction and preparation for sequencing is shown in Figure 4.2.3.1 1 and outlined in more depth below.

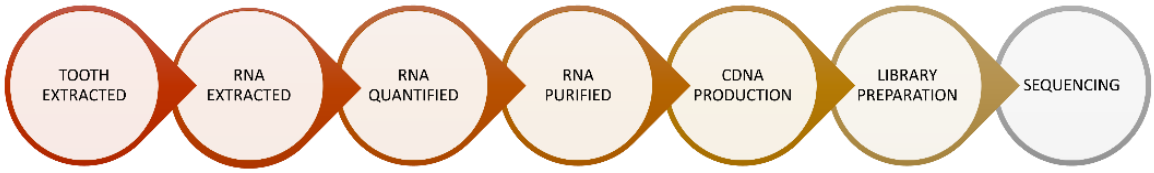

Figure 4.2.3.1 1: Workflow for preparing RNA for sequencing

Freshly extracted human teeth were collected from clinics based at the Leeds Dental Institute in accordance with the Project Ethics or Tissue Bank Ethics (as discussed earlier in Section 3).

Teeth #13, #25, #26, #27, #28, #29, and #30 were all obtained using Tissue Bank Ethics. Teeth #14, #15, #16, #17, #18, #19, #20, #21, #22, #23, #24 were all obtained using Project Ethics.

For the Project Ethics teeth, once extracted, the teeth were stored at room temperature in RNALater (Fisher Scientific UK, Loughborough, UK), before being transported to the laboratory, where they were then stored in a refrigerator at approx. 4°C. The time between tooth extraction and RNA isolation was a maximum of 72 hours; the manufacturers of RNALater specify that RNA stored in RNALater will be stable at room temperature for 1 week and at 4 °C for 1 month. For teeth obtained using Tissue Bank Ethics, the teeth were stored dry in a refrigerator (at 4°C), transported to the laboratory where they were again stored dry in a refrigerator before RNA extraction; maximum time between tooth extraction and RNA isolation was also 72 hours. It was not deemed feasible by clinical staff for teeth obtained using the Project Ethics to be stored in the refrigerator on clinic due to space limitations.

For RNA extraction, the teeth were fractured open using a benchtop woodwork vice that had been cleaned with 70% ethanol and RNAseZap (ThermoFisher Scientific, MA, USA). Once fractured open, the pulp was removed using a sterile dental excavator and barbed broaches and immediately placed into fresh DNA/RNAShield (part of the RNA extraction kit – see below), 700µL.

RNA was then extracted according to the manufacturer's instructions using the ZymoBIOMICS RNA Miniprep Kit (Zymo Research, CA, USA). The protocol is available from the Zymo Research website, https://zymoresearch.eu/collections/zymobiomics-rna-kits/products/zymobiomics-rna-miniprep-kit. Specific parameters that required modification and/or optimisation for pulp tissue included:

1) Agitating the sample in an Eppendorf on a vortex genie for 45 minutes (the manufacturer's protocol specifies "≥5minutes" on a bead beater) to suitably homogenise the tissue in the lysis tube.
2) A 10 minute lysozyme digestion step after the 'bead beating' step – this consisted of adding 50µL of freshly made lysozyme 10mg/mL to the sample and incubating at 37°C.
3) The supernatant regularly required more lysis buffer than the specified volume to ensure full cell lysis and prevent a cloudy supernatant. Increasing the lysis buffer volume made the whole sample volume too large for the spin columns, therefore the sample was split between three columns and as such, the RNA from each pulp was extracted in triplicate.

The extracted RNA was eluted in 50uL of RNase free water per column, and the RNA from each column pooled to return one sample per tooth (making 150uL per sample). DNase treatment was undertaken to remove any DNA from the sample according to the ZymoBIOMICS RNA Miniprep Kit. The RNA was stored at -80°C, including a small separate aliquot for quantification (2uL).

RNA quantification was completed using Quant-it RiboGreen RNA Assay Kit (ThermoFisher Scientific, MA, USA), plotting the fluorescence of the sample against a calibration curve as per the manufacturer's instructions.

2. cDNA synthesis, Library Preparation and sequencing

The total RNA extracted from the dental pulps includes RNA that is not relevant to the transcriptome and/or not amenable to sequencing (e.g. ribosomal RNA (rRNA), globin mRNA and transfer RNA) (196). Therefore, appropriate RNA depletion needs to be undertaken to remove unwanted RNA, leaving only mRNA. To achieve this, mRNA was purified from total RNA using poly-T oligo-attached magnetic beads.

The depleted RNA was fragmented. Hexamer primers are used for first strand and second strand cDNA synthesis, making a more stable cDNA product.

The cDNA was then randomly sheared into short fragments. The fragments were end-repaired, A-tailed and an Illumina adapter ligated. The library underwent size-selection, amplification and purification. The library preparation output was quantified with Qubit DNA assay (ThermoFisher Scientific, MA, USA) and real-time PCR. Agilent Bioanalyzer (Agilent, CA, USA) was used for size distribution detection. Once quantified, the libraries are pooled and sequenced on Illumina platforms. The library preparation kit used for this work was NEB Next® Ultra™ RNA Library Prep Kit and the platform used was Illumina Novaseq 6000.

For this work, cDNA synthesis, library preparation and sequencing was outsourced to Novogene (Novogene UK, Cambridge, UK). Appendix 5 contains a table showing the quality of the raw reads obtained from Novogene.

4.2.3.2 POST-SEQUENCING, DATA ANALYSIS

A total of 39 teeth underwent pulpal extirpation and RNA isolation, 18 teeth (all molars) yielded RNA amounts >50ng. Of these 18, only nine teeth were successfully sequenced and analysed, 6 carious and 3 sound. Most of the teeth that failed to be sequenced, failed at the library preparation stage, however one tooth (Tooth X30) was successfully sequenced but the reads failed to map to the indexed genome. As this process was outsourced, it is not possible to determine the exact reason behind these failures, but RNA quality could be a factor. The 18 teeth with RNA amounts >50ng are listed in Table 4.2.3.2 1, along with information on the tooth type, patient age, and whether the tooth was carious or sound.

A copy of all scripts run is available in Appendix 6. Full detail of the workflow is provided below, and Figure 4.2.3.2 1 also provides a pictorial overview of the workflow.

Tooth ID	Age	Tooth Type	Amount of RNA (ng)	Condition	Successfully Sequenced?	Ethics	RIN
#13	11	First Molar	493.32	SOUND	NO	Tissue Bank	-
#14	24	First Molar	1296.7	CARIOUS	YES	Project	3
#15	28	Third Molar	561.1	CARIOUS	YES	Project	2.5
#16	28	Third Molar	846	SOUND	YES	Project	2.3
#17	21	Third Molar	726.03	SOUND	YES	Project	2.1
#18	29	Second Molar	900.35	CARIOUS	YES	Project	2.4
#19	29	Third Molar	1036.78	CARIOUS	YES	Project	2.4
#20	24	Second Molar	113.88	CARIOUS	NO	Project	-
#21	37	Third Molar	1160.8	CARIOUS	YES	Project	2.3
#22	80	Second Molar	876.619	CARIOUS	NO	Project	3
#23	56	Second Molar	9019.805	CARIOUS	YES	Project	2.1
#24	45	Third Molar	2687.319	SOUND	YES	Project	2.8
#25	17	Third Molar	588.755	SOUND	NO	Tissue Bank	2.7
#26	7	First Molar	1732.164	CARIOUS	NO	Tissue Bank	2.6
#27	7	First Molar	1964.595	CARIOUS	NO	Tissue Bank	2.4
#28	11	First Molar	344.32	SOUND	NO	Tissue Bank	2.1
#29	24	Third Molar	56.579	SOUND	NO	Tissue Bank	2.5
#30	34	First Molar	238.06	CARIOUS	YES	Tissue Bank	2.8

Table 4.2.3.2 1: Summary of the patient demographics and samples that underwent RNA extraction. NB: Highlighted samples of the same colour belong to the same patient. RIN = RNA Integrity Number

Figure 4.2.3.2 1: Workflow of the post-sequencing analysis of the raw RNA reads

1. Read quality control and trimming

DNA sequence data were provided as Fastq files, which were uploaded to the Advanced Research Computer (ARC4) at the University of Leeds for processing. Unless otherwise specified, all analysis was undertaken using R version 3.6.2, "Dark and Stormy Night".

Adaptors were removed from the '3 end of the paired-end reads using the Cutadapt programme (197) in Linux, and reads were filtered using FastqCleaner (198), removing all reads below average quality score of 20. FastqCleaner is an online platform launched via R script. FastqCleaner confirmed the absence of adapters, and a summary of the quality of the reads after trimming and removal of poor quality reads is given in Table 4.2.3.2 2.

2. Read Mapping, Summarisation and Normalisation for Sample-level analysis and Principal Component Analysis

For reads to be mapped to a genome, an index must be created. An index was constructed using Rsubread (199) with Genome Reference Consortium Human Build 38 patch release 14 (GRCh38.p14) as its reference (200). The reads were aligned using the align() function in Rsubread(199). The resultant .bam files were summarised using the featurecounts() function in Rsubread (199) , with .txt and .csv files being produced.

For the reads of each sample to be comparable, allowing sample-level comparisons (for example in a principal component (PC) analysis), the reads need to be normalised. There are many different ways of normalising read data and the three main ways used in RNA sequencing analysis are; Trimmed Mean of M-values (TMM), Relative Log Expression (RLE) and Median Ratio Normalization (MRN) and a paper by Maza (201) discusses and compares these methods. For the data in this thesis (not including differential gene expression, which is discussed more below), TMM was selected because; i) it pre-normalises the counts by library sizes (for this data the library size has a range of 9,526,756 reads between the samples), ii) this method selects a reference sample from the samples input rather than relying on a mean of the samples, iii) TMM takes into account relative scaling factors and library size. For this data, R package EdgeR (202) has been used to make the reads comparable across all samples for PC analysis and Table 4.2.3.2 3 shows the library size and scale factors per sample as output by EdgeR and used in the calculations for normalisation.

PC analysis is a way of reducing the number of dimensions, or features, in a dataset. This is an important step because as the number of features (or in this case, genes) increases, the possible number of interactions between each of them increases exponentially, making assessment of any similarities between samples difficult (203). A way to assess for similarities between samples is by undertaking cluster analysis – more specifically K-means cluster analysis. Cluster analysis allows for division of datapoints (in the case of this work, it is the individual samples) into a set number of groups, so that the

datasets within these groups are comparable to each other and different to the datapoints in different clusters. In essence, it is summarising the outputs from numerous parameters for numerous datapoints (or samples) and comparing them to provide clustering of samples that show similar trends. K-means clustering is an unsupervised learning algorithm that places the samples into distinct groups that do not overlap on a plot (204). From this, trends and similarities in samples that share the same cluster can be explored and inferred.

3. Differential Gene Expression

Differential gene expression analysis allows for gene expression to be compared across two (or more groups).

DESeq2 package in R (185) was used to group the teeth into carious (n=6) and sound (n=3) and compare them. The comparison includes a statistical output (adjusted p-value (padj)) for each gene allowing comparisons between carious and sound pulps to be made at a gene level. For this research, a padj value of <0.05 was considered statistically significant. Genes that had no reads across all samples were removed from further analysis. Raw reads were input into DESeq2 as the package uses RLE normalisation by default.

To assess for correlations between total RNA amount and age, Pearson's Chi-squared test was also completed in R.

4. STRING analysis

STRING analysis is a way of exploring interactions between proteins and is facilitated by the STRING database (https://string-db.org/). This free to use database finds the proteins based upon the gene identifiers and looks for interactions between them to see if the proteins in a cohort form discrete networks. This is achieved by obtaining information from five key areas; genomic context predictions, high throughput lab experiments, (conserved) co-expression, automated textmining and previous knowledge from existing databases (205). The STRING networks produced assess for protein-protein links that result in a "functional association"(206).

Experimental and biochemical data in the STRING database comes from; the Database of Interacting Proteins (DIP) (https://dip.doe-mbi.ucla.edu/dip/Main.cgi), BioGRID (https://thebiogrid.org/), IntAct (https://www.ebi.ac.uk/intact/home), The Molecular INTeraction Database (MINT) (https://mint.bio.uniroma2.it/), RCSB Protein Data Bank (RCSB PDB) and Human Protein Reference Database (HPRD) (https://hprd.org/) (206). Curated data comes from five databases; Biocarta (https://mitelmandatabase.isb-cgc.org/) , BioCyc (https://biocyc.org/), Gene Ontology (https://geneontology.org/), Kyoto Encyclopaedia of Genes and Genomes (KEGG) (https://www.genome.jp/kegg/) and Reactome (https://reactome.org/) (206).

The output STRING analysis network demonstrates proteins as ‘nodes’ and the interactions as ‘edges’ in an interactive figure. The confidence of the interaction is denoted by the thickness of the line between the nodes and the evidence type is denoted by the colour (red = fusion evidence, green = neighbourhood evidence, blue = co-occurrence evidence, purple = experimental evidence, yellow = textmining evidence, lightblue = database evidence, black line = co-expression evidence).

For the work in this thesis, the STRING database will be used to explore protein networks from the differentially expressed genes and from the most abundantly expressed genes.

Sample and Read	Total sequences	Sequences Flagged as poor quality	Sequence Length	GC content
14, Read 1	45902808	0	2-150	50
14, Read 2	45902808	0	2-150	50
15, Read 1	43373194	0	2-150	51
15, Read 2	43577282	0	2-150	51
16, Read 1	46611746	0	2-150	51
16, Read 2	46611746	0	2-150	51
17, Read 1	39179061	0	2-150	51
17, Read 2	39179061	0	2-150	51
18, Read 1	34165529	0	2-150	49
18, Read 2	34165529	0	2-150	49
19, Read 1	36159599	0	2-150	49
19, Read 2	36159599	0	2-150	49
21, Read 1	37396014	0	2-150	49
21, Read 2	37396014	0	2-150	49
23, Read 1	41599222	0	2-150	48
23, Read 2	41599222	0	2-150	48
24, Read 1	40608463	0	2-150	47
24, Read 2	40608463	0	2-150	47

Table 4.2.3.2 2: Summary of the quality of the reads from the successfully sequenced dental pulps

Sample Name	Library Size	Scale Factor
X14	30579253	1.0563375
X15	28697321	1.0896296
X16	31745765	1.0537537
X17	25618276	1.1448218
X18	22215328	1.0728878
X19	23370697	1.1008817
X21	25680731	1.1149862
X23	27524698	0.9864969
X24	22739476	0.5543464

Table 4.2.3.2 3: Library Size and Scale Factor used for EdgeR

4.3 RESULTS

4.3.1 AFM RESULTS

KEY FINDINGS

1. There is a fall in the elastic modulus towards the centre of the pulp. This trend is more pronounced in sound teeth compared carious teeth.
2. At the most coronal aspect of the pulp, sound teeth have a statistically higher elastic modulus than carious teeth.
3. Carious teeth show fewer statistical differences in elastic modulus between the seven sites investigated compared sound teeth.

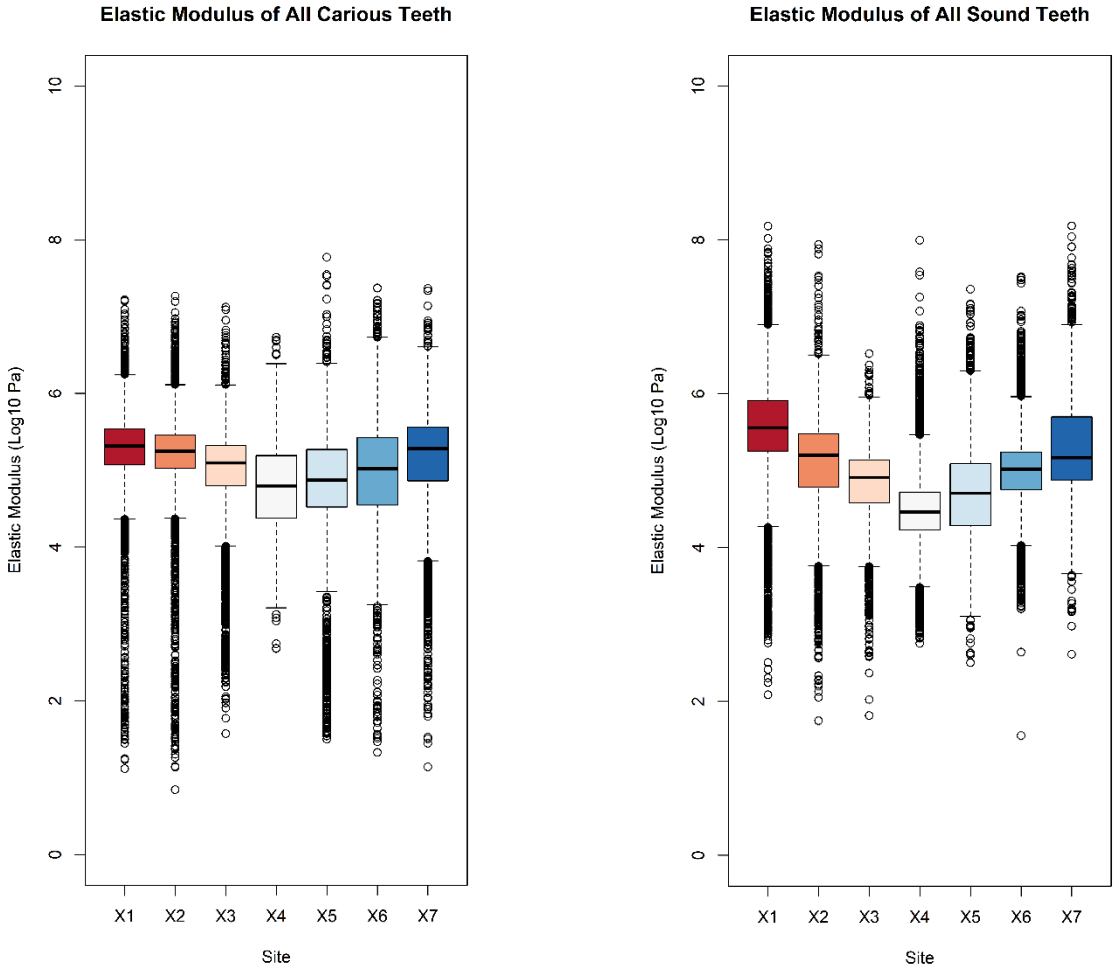

Figure 4.3.1 1: Box Plots of the Elastic Modulus Values for all Carious Teeth (n=7) and all Sound Teeth (n=7). Median values with interquartile ranges plotted. X1 = Site 1 (most coronal), X7 = Site 7, pulpal floor. Each site consists of 900 force curves per tooth (therefore 6300 measurements per site)

	Median (IQR) (kPa)		Range (kPa)		Carious vs sound comparison (p-value)
	Carious	Sound	Carious	Sound	
Site X1	**206** (118-348)	**362** (181-824)	0.01-16613	0.12-4399	0.023
Site X2	**178** (106-184)	**160** (62-303)	0.01-18524	0.11-87506	0.894
Site X3	**125** (63-212)	**82** (39-139)	0.04-13308	0.38-2040	0.057
Site X4	**63** (24-132)	**29** (17-53)	0.48-5383	0.57-99471	0.887
Site X5	**75** (33-187)	**51** (19-123)	0.03-59313	0.32-23026	0.813
Site X6	**106** (36-266)	**104** (57-175)	0.02-23628	0.44-33326	0.898
Site X7	**192** (73-364)	**148** (76-503)	0.01-23300	0.4-119	0.078

Table 4.3.1 1: Summary of elastic modulus values (kPa) for each site, including the results of multi-level mixed effects statistical test (p<0.05 = green, p>0.05 = pink). Site 1= Most coronal site of pulp, site 7 = pulpal floor.

The results of the AFM nanoindentation of the pulps reveal a consistent and strong trend in all cases – a fall in the elastic modulus from the most superior aspect of the pulp, to the centre, and then a rise in the elastic modulus towards the pulpal floor. This trend was present in all the teeth except Sound Tooth # 1, where the elastic modulus continues to decrease throughout the transition from superior to inferior – see Figures 4.3.1 1 and 4.3.1 2 and Table 4.3.1 1. There was a large range to the values obtained (Table 4.3.1 1), and these values could be down to experimental variance or heterogeneity of the dental pulp.

Comparing the elastic modulus values from all carious teeth grouped (n=7) against all sound teeth grouped (n=7), the median for each is 135kPa and 103kPa respectively – this difference is not statistically significant (б=-177, Standard Error (SE)= 132kPa, p-value = 0.18) when using a multilevel mixed effects model, with site and the individual tooth as predictors (193). The individual tooth accounted for 17.3% of variance in this model, and the site accounted for 0% of variance; in essence this means that the individual tooth has more effect on the spread of the data than the site.

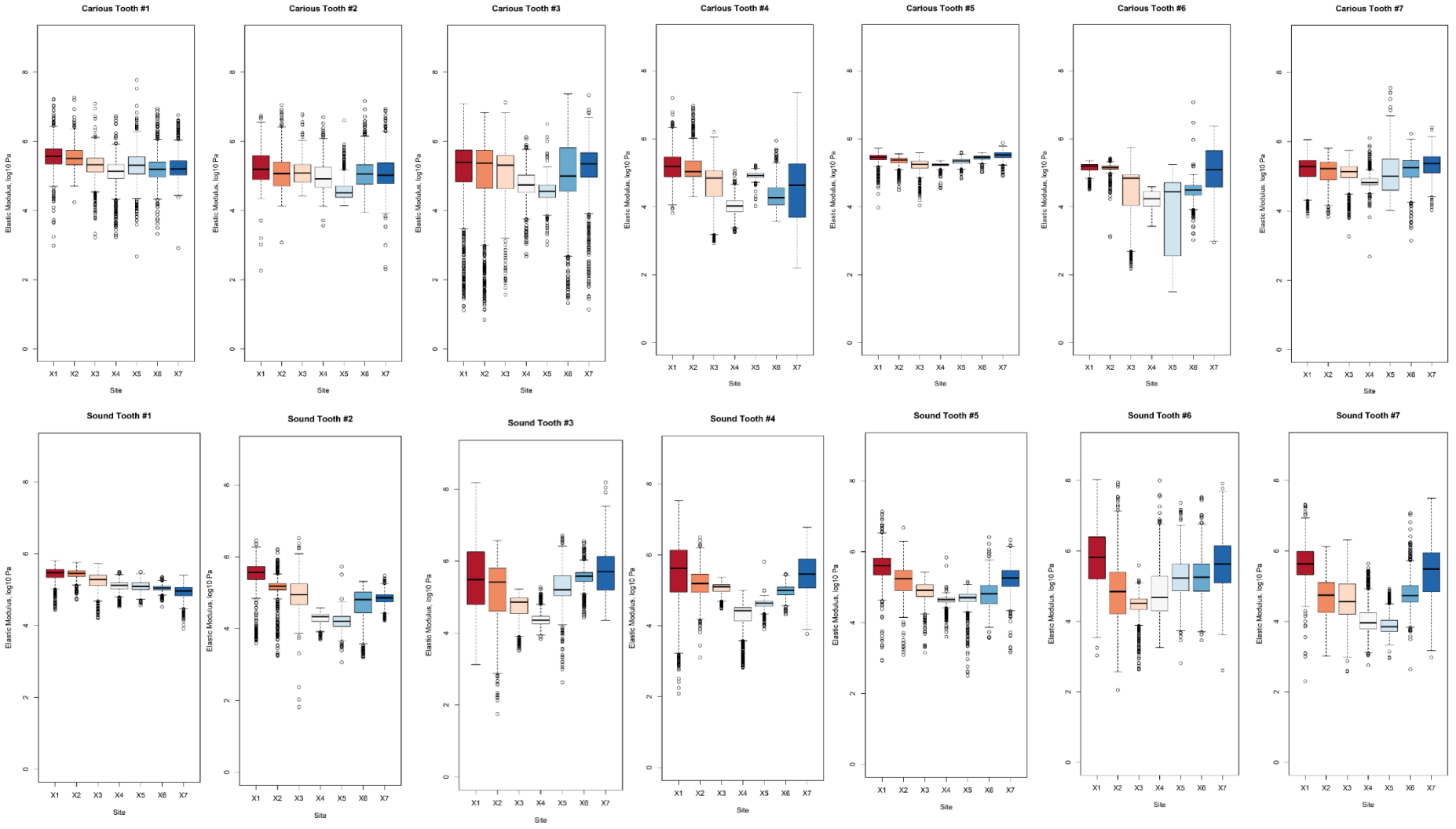

Figure 4.3.1 2: Boxplots of the Elastic Modulus Values for each Tooth. Carious = 7 teeth, sound = 7 teeth. X1 = Site 1 most coronal, X7 = Site 7, pulpal floor. Boxplots demonstrate medians and interquartile ranges. Figure demonstrates the common trend of a fall in the elastic modulus towards the centre of the tooth in carious and sound teeth.

When analysing in more detail at the elastic modulus values obtained for each site, carious pulps generally had a higher elastic modulus than sound pulps, and this was true across sites 3-7, but not sites 1 and 2 where the opposite was found (see Table 4.3.1 1 and Figure 4.3.1 1). This difference is statistically significant for site 1, but not other sites (Table 4.3.1 1). It can also be seen from the boxplots in Figures 4.3.1 1 and 4.3.1 2 and Table 4.3.1 1 that the interquartile range of the elastic modulus values towards the centre of the pulp (sites 3,4,5) were generally smaller than at other sites, suggesting that this area is more homogenous compared to other areas of the pulp; this trend was more pronounced in sound teeth compared with carious teeth.

All data for the AFM results section is skewed (non-parametric) hence why medians quoted in Table 4.3.1 1. Density plots are available in Appendix 7, displaying the skewness of the data.

	CARIOUS					
Pair-wise Site Comparison	1	2	3	4	5	6
1						
2	0.009					
3	<0.001	<0.001				
4	<0.001	<0.001	<0.001			
5	<0.001	<0.001	0.720	<0.001		
6	<0.001	<0.001	<0.001	<0.001	<0.001	
7	0.019	0.828	<0.001	<0.001	<0.001	<0.001
	SOUND					
Pair-wise Site Comparison	1	2	3	4	5	6
1						
2	0.009					
3	<0.001	<0.001				
4	<0.001	<0.001	0.744			
5	<0.001	<0.001	<0.001	0.011		
6	<0.001	0.0024	<0.001	<0.001	<0.001	
7	<0.001	<0.001	<0.001	<0.001	<0.001	<0.001
	ALL TEETH (CARIOUS AND SOUND TEETH GROUPED TOGETHER AS A WHOLE)					
Pair-wise Site Comparison	1	2	3	4	5	6
1						
2	0.016					
3	0.005	0.001				
4	0.001	<0.001	0.394			
5	0.003	<0.001	0.553	0.057		
6	0.006	0.038	0.074	0.001	0.176	
7	0.027	0.056	0.006	<0.001	0.003	0.009

Table 4.3.1 2: Results (p value) of Pairwise Multi-level Mixed Effects Tests. Non-significant results highlighted in pink(p>0.05) , significant results highlighted in green (p<0.05)

Site-level comparisons were undertaken, using a linear multi-level mixed effects model looking at sound teeth and carious teeth as subgroups and all teeth combined (i.e. comparing values from sound teeth at site 1 to values from sound teeth at site 2 etc, and then values from carious teeth at site 1 to values from carious teeth at site 2 etc.). The results of these are provided in Table 4.3.1 2. and show there are more areas of statistical difference in sound teeth than carious. Furthermore, when looking at all teeth (i.e. carious and sound combined), there are fewer areas of statistical significance towards the centre of the pulp. These tests were completed using the tooth and site as random effects in the multi-level mixed effects model (193).

The results of the Kruskal-Wallis test and post-hoc Dunn's test (192), performed on each individual tooth looking at pairwise comparisons of the seven sites, demonstrated fewer areas of statistical difference in carious teeth than in sound teeth at the individual tooth level. This also suggests more homogeneity in the elastic modulus across individual carious teeth than in individual sound teeth (see Appendix 8). It is important to note that this statistical test at an individual tooth level assumes all sites are independent from each other.

$$A=\pi(h^2 + a^2)$$

Equation 4.3.1 1: Archimedes' derivation of spherical cap, h = depth of indentation, a= radius of sphere at maximum indentation, π = Pi, A = Area of surface of sphere indented

Adhesion data between the AFM probe and pulp from the force curves was gathered and was found to be small, with a median of 271pN (for context, the indentation force was 8-25nN, see Section 4.1.1), justifying the use of the Hertz model for this research. Indentation data was also gathered, and was also found to also be small, with a median of 26nm. The spherical tip of the probe had a diameter of 3µm (3000nm), as such the indentation was ~0.9% of the sphere diameter. Therefore, the typical contact area of indentation would be ~0.247µm^2 (calculated using Archimedes' derivation of spherical cap formula (see Equation 4.3.1 1)).

Tooth Name	Tooth Type	Patient Age
Carious 1	UR7	24
Carious 2	LL6	10
Carious 3	LR6	11
Carious 4	LL6	17
Carious 5	LL7	28
Carious 6	UL7	28
Carious 7	LL7	53
Sound 1	LL8	24
Sound 2	UL6	9
Sound 3	LL8	36
Sound 4	LR8	25
Sound 5	LL8	26
Sound 6	LR7	53
Sound 7	UL7	20

Table 4.3.1 3: Ages of patients that submitted teeth used for AFM analysis

Age-related changes do occur in the pulp such as increased collagen fibre thickness, vascular changes, reduced odontoblast numbers and reduced pulp volume (207). On correlating age with the elastic modulus values, no correlation was found (Spearman's Rank correlation test in R returned a correlation coefficient (rho value) of 0.13, p-value=<0.05). The ages of the patients from whom the AFM teeth came are provided in Table 4.3.1 3, the mean age of all patients submitting teeth was 26. The mean age of patients submitting carious teeth was 24, and for sound teeth it was 28.

Interestingly, Carious Tooth #4 showed a slight increase in modulus at the centre of the pulp (Site X5) on assessing the histology of this tooth, this may have corresponded to a pulp stone – this is discussed further in Section 4.4.1.

From the FVMs, it is possible to reconstruct topography and indentation maps. As can be seen from Figure 4.3.1 3, which demonstrates the topography from the FVMs of Carious Tooth #7 and Sound Tooth #7, the surface of the samples in both carious and sound teeth was markedly heterogenous. Despite sites displaying differing topography, no consistent differences or patterns were identified between carious and sound teeth qualitatively and every tooth had very differing topographical features, with no specific features considered typical for carious or sound teeth, nor for any specific site.

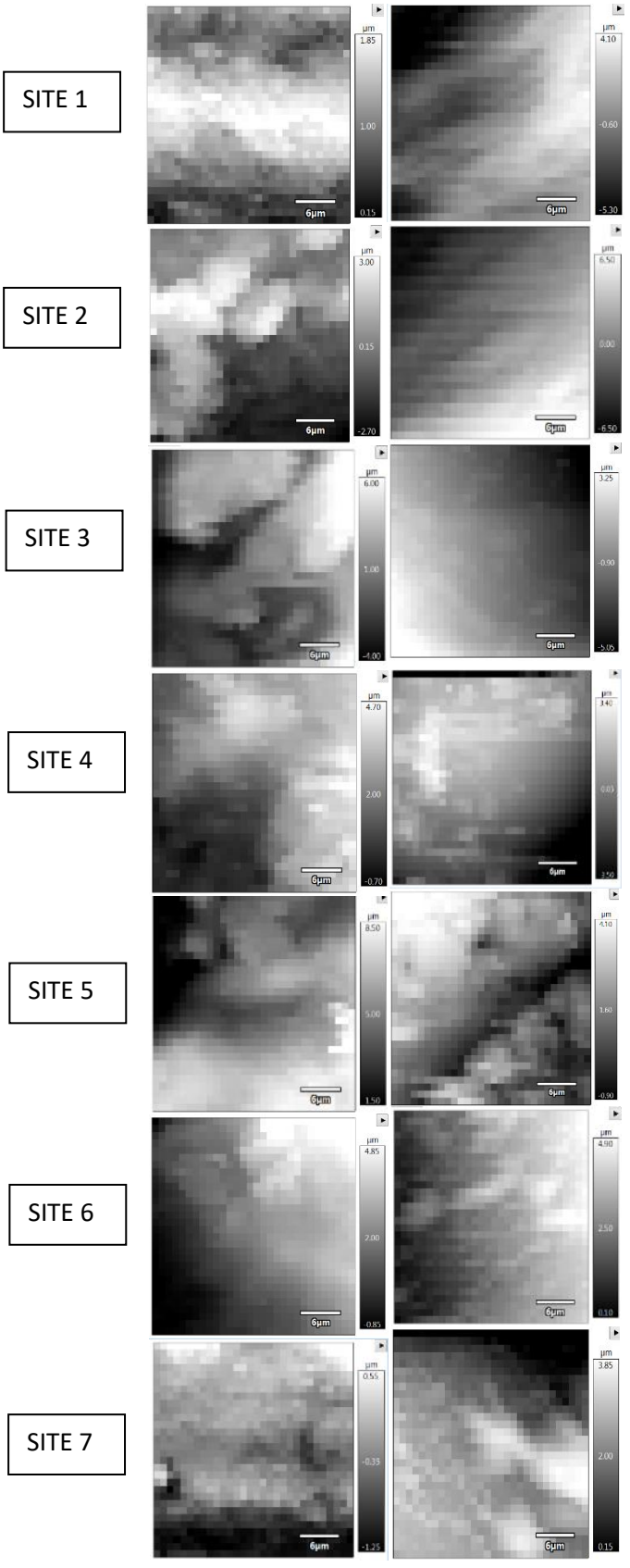

Figure 4.3.1 3: False Colour Map of the Topographical Data from the FVMs of two example Teeth

4.3.2 HISTOMORPHOMETRIC CONFOCAL MICROSCOPY RESULTS

KEY FINDINGS

1. Carious teeth showed more statistically significant differences between the sites of the pulp analysed compared with sound teeth – this is true for number of fibres, width of fibres, area of fibres and orientation of fibres.
2. Fibres were more aligned/organised in carious teeth than sound
3. There are more fibres in the pulps of sound teeth than carious .
4. There is a reduction in the width of fibres and the area of fibres (inferred from % area of pixels stained) towards the centre of the pulp in both carious and sound teeth.
5. The number of fibres in carious and sound teeth show opposing trends, with a fall in the number of fibres towards the centre of the pulp in carious teeth and a rise in the number of fibres towards the centre of the pulp in sound teeth.

A total of 240 images were analysed from 8 carious teeth and 8 sound teeth; 15 images per tooth from three zones of five images each. The three zones corresponded to the bottom, middle and top of the pulp, (i.e. the pulpal floor, the 'mid' point of the pulp and the pulpal roof (just apical to the cell free zone – hereafter termed 'coronal') respectively). The cell-free zone was avoided as it is believed to contain a dense vascular and neural network and little collagen (159). These teeth included all the 7 carious and 7 sound teeth from the AFM analysis plus one more from each group (as discussed early in methods – this was largely due to time constraints).

Qualitatively, there appeared to be some differences between the three pulpal sites investigated with confocal microscopy. Generally, the coronal pulp has more stained areas, more prominent collagen bundles and more aligned fibres than the other sites, and the mid-pulp seems to have the least aligned fibres and the least amount of staining. Figure 4.3.2 1 and Figure 4.3.2. 2 demonstrate examples of the original confocal images and the resultant Fourier Orientation Macro processes for sound teeth and carious teeth respectively.

The analyses in this section utilised the linear mixed effects statistical model, with the individual tooth and the site taken as random effects and (where applicable) carious (yes/no) as a predictor or 'fixed effect'. This was designed as a three-level model comprising of the observation(s)/measurement(s), then site, then individual tooth.

Five outcomes were investigated per image; number of fibres, width of fibres, area of pixels (% of image stained), coherence (from OrientationJ macro) and ratio (from Fourier Orientation macro).

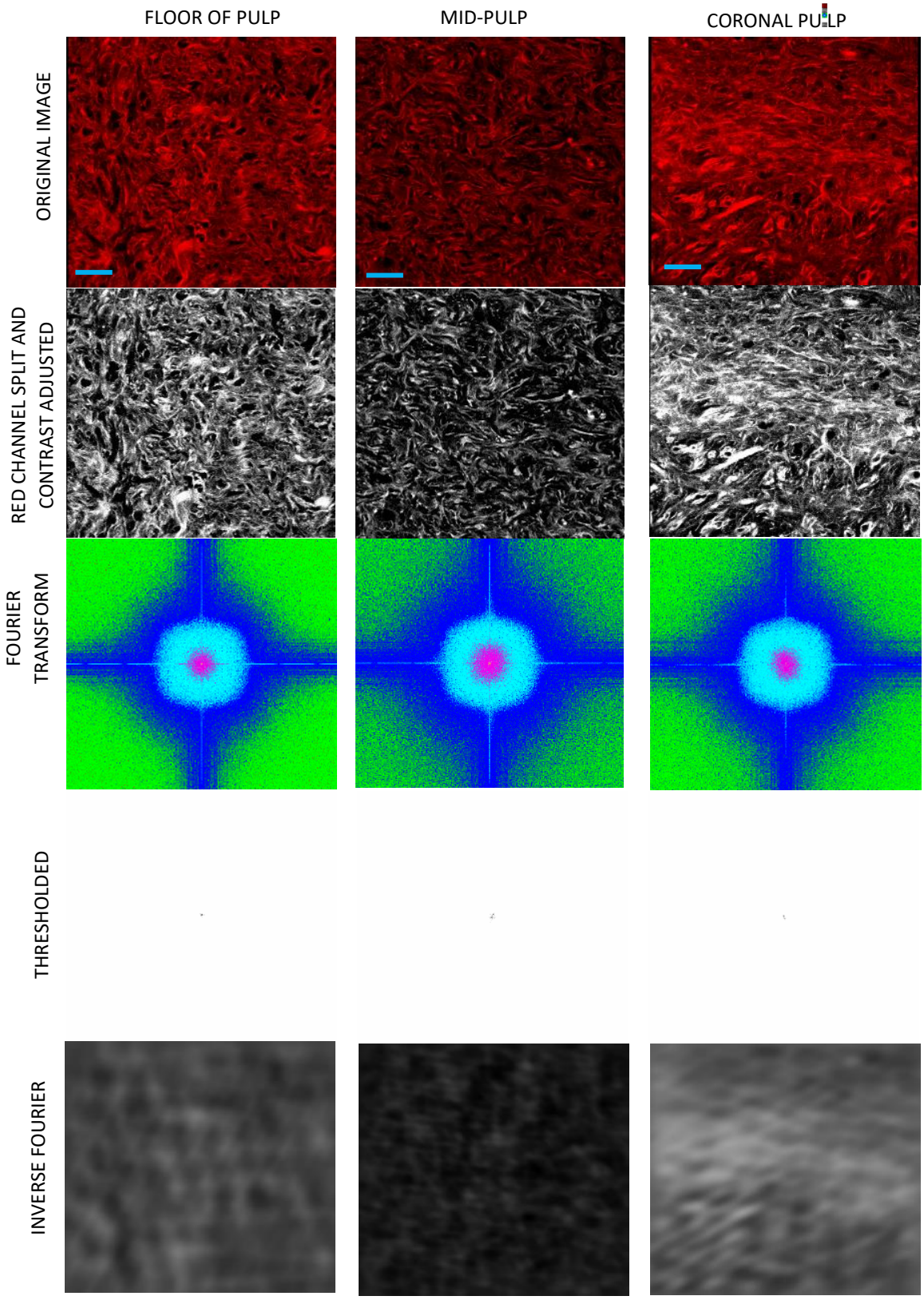

Figure 4.3.2 1: Fourier Orientation Macro for a sound tooth. 1) The image is split into channels, red channel selected with contrast enhanced 2) Fourier Transform is completed 3) Fourier plot is thresholded and the central core (black) measured to give a ratio. The inverse Fourier is the 'image' from the thresholded Fourier plot, demonstrating loss of detail but maintenance of directional trends. Scale bar = 50µm

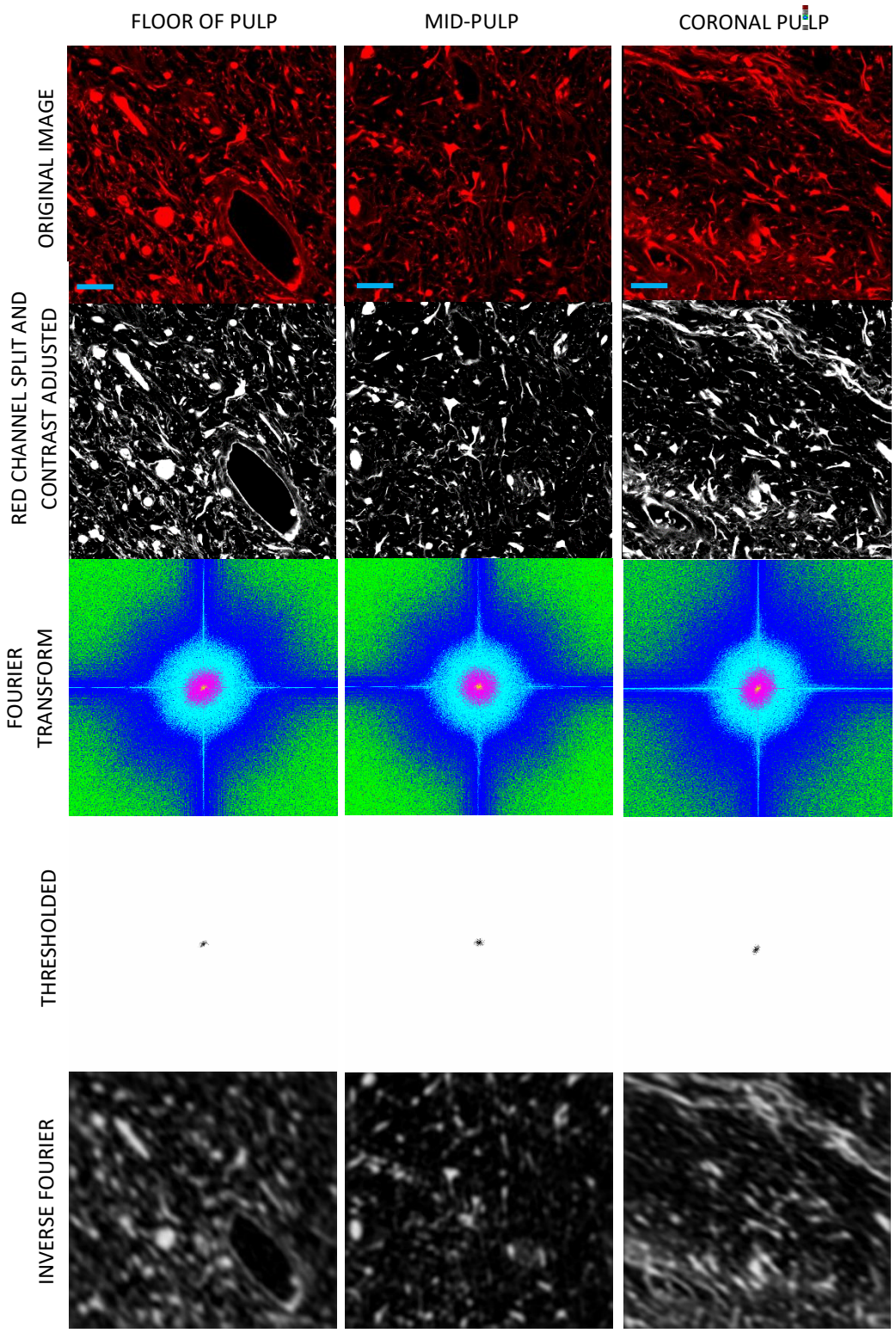

Figure 4.3.2 2: Fourier Orientation Macro for a carious tooth. 1) The image is split into channels, red channel selected with contrast enhanced 2) Fourier Transform is completed 3) Fourier plot is thresholded and the central core (black) measured to give a ratio. The inverse Fourier is the 'image' from the thresholded Fourier plot, demonstrating loss of detail but maintenance of directional trends. Scale bar = 50µm

No statistically significant correlations were observed between the five parameters investigated with confocal microscopy and patient age. Therefore, no correlation was identified between changes in the amount of collagen, collagen fibre number, collagen fibre width and collagen fibre orientation with age (Pearson's product-moment correlation and Spearman's Rank correlations in R both produced p-values >0.05 for each correlation).

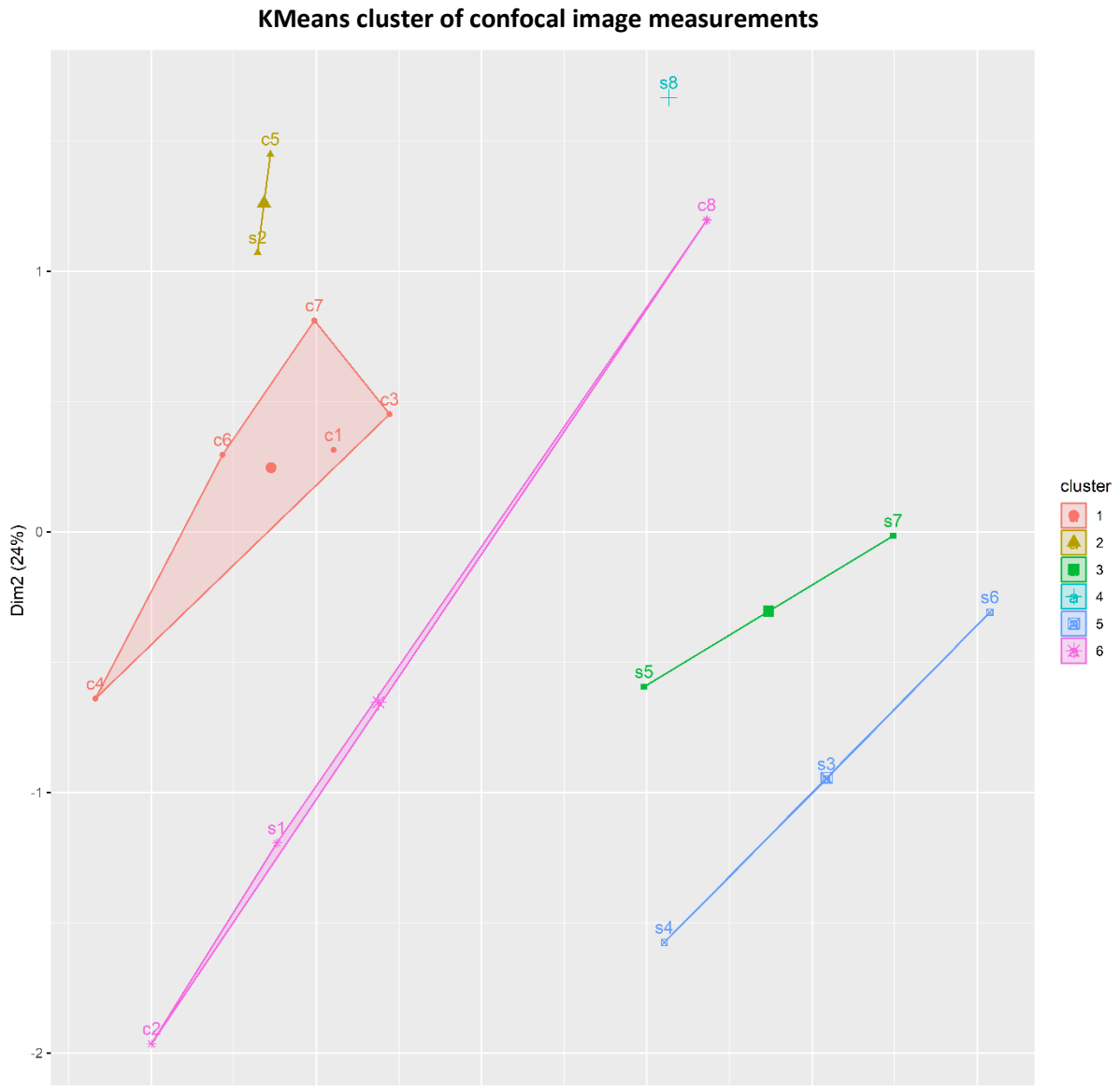

Figure 4.3.2 3: KMeans Cluster Plot for all parameters explored in the 240 confocal images of collagen bundles, S=Sound Tooth, C=Carious Tooth. Five clusters identified by gap statistic testing.

As can be seen in the k-means cluster plot in Figure 4.3.2 3, which demonstrates the clustering of individual teeth based upon the results of all five parameters measured, some of the clusters contain

only carious teeth (e.g. C1, C3, C4, C6 and C7 in cluster 1) and some contain only sound teeth (e.g. S3, S4 and S6 in cluster 5), demonstrating some similarities between carious and sound teeth in these groups. Five clusters were identified as optimal for this analysis using gap statistic testing (208) (using factoextra package in R). Clusters 2 and 6 contain a mix of carious and sound teeth and tooth S8 is in a cluster by itself.

Number of Collagen Fibres

The number of collagen fibres across the pulpal sites shows opposing trends in carious and sound teeth, with sound teeth displaying an increase in the number of collagen fibres towards the middle of the pulp, and carious teeth showing a fall in the number of collagen fibres towards the middle of the pulp (see Table 4.3.2 1 and Figure 4.3.2 4).

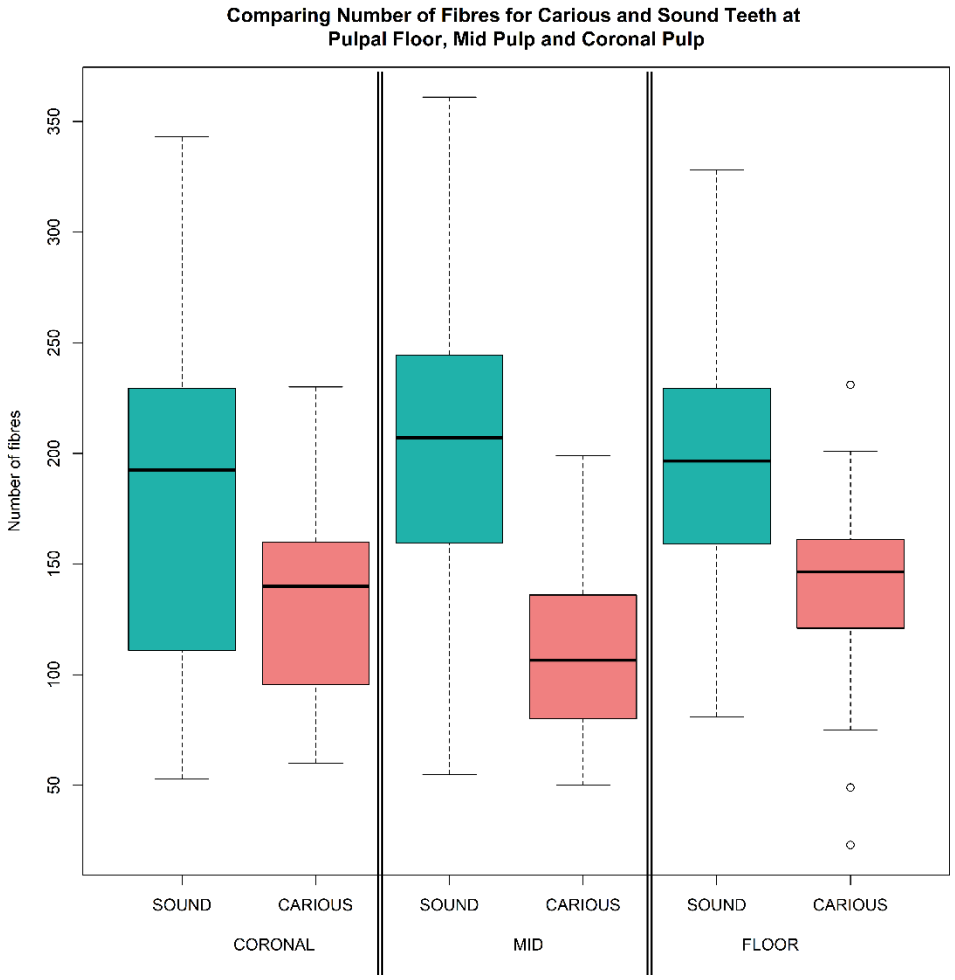

Figure 4.3.2 4: Number of collagen fibres, comparing sites and carious vs sound, results produced from the Transects macro. Comparing results from coronal pulp, mid pulp and floor of pulp f carious teeth (results in coral) and sound teeth (results in turquoise)

	MEAN (Standard Deviation (SD))		P-value
	SOUND	CARIOUS	
CORONAL	177.3 (76.1)	131.8 (39.2)	0.058
MID	198.8 (66.7)	110.8 (37.7)	<0.001
FLOOR	193.6 (50.0)	140.4 (40.5)	<0.001

Table 4.3.2 1: Statistics for the number of collagen fibres, comparing carious and sound for each site. Mean quoted as data is parametric. Statistical test = multilevel mixed effects model, p<0.05 = green, p>0.05 = pink

Comparing the number of collagen fibres of all sites combined, between carious and sound teeth resulted in a statistically significant difference (p value=<0.001), with sound teeth (mean =189.9, SD=65.3) having more fibers than carious (mean = 127.7, SD = 40.8), using multilevel linear mixed effects model. For this result and model, 55.69% of the variance was explained by the individual tooth and 0% explained by the site. This data was parametric (normally distributed), hence means as opposed to medians quoted above.

When assessing the coronal pulp, and comparing the outcomes for carious and sound teeth, no statistically significant difference is noted, despite sound teeth having a higher mean than carious. Analysis of MP and FP, revealed statistically significant differences between carious and sound teeth, with carious teeth having fewer fibres at these sites, see Table 4.3.2 1. This essentially indicates that sound teeth and carious teeth do not have statistically different numbers of fibres at the coronal aspect, whereas at the mid-pulp and pulp floor, carious teeth do have fewer fibres.

COMPARISSON	SOUND	CARIOUS	ALL TEETH
CP vs MP	0.069	0.010	0.970
CP vs FP	0.113	0.302	0.059
FP vs MP	0.536	<0.001	0.058

Table 4.3.2 2: Statistical comparisons the numbers of fibres counted from sites in carious teeth, sound teeth and all teeth, p<0.05 = green, p>0.05 = pink. P-value obtained from multi-level fixed effect model

When examining the outputs for carious teeth, the differences between the coronal pulp (CP) vs mid-pulp (MP), and floor of pulp (FP) vs MP, were both significant (see Table 4.3.2 2). No trend was identified when assessing all teeth together comparing CP, MP and FP sites; this is highlighted by the lack of statistical significance for these comparisons in Table 4.3.2 2. No statistically significant differences were noted when examining CP, MP and FP in sound teeth either (Table 4.3.2 2). These

statistical results were obtained using the linear mixed effects statistical model, with the site and tooth as random effects.

The lack of statistical difference seen when all teeth were compared is likely due to the opposing trends seen between carious and sound teeth, when these two cohorts were grouped together for the 'all teeth' comparison, the differences between the cohorts would become non-existent.

Width of Collagen Fibres

For both carious and sound teeth, the width of the fibres reduces towards the centre of the pulp (see Table 4.3.2 3 and Figure 4.3.2 5).

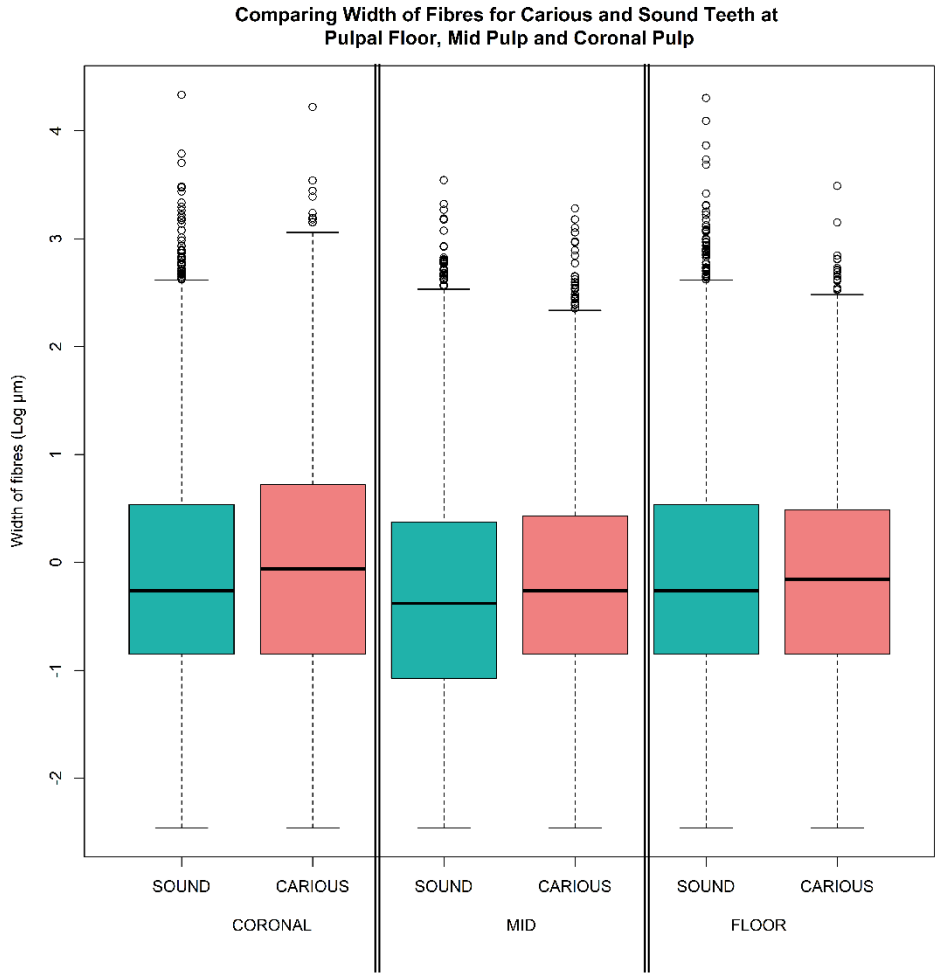

Figure 4.3.2 5: Width of collagen fibres, comparing sites and carious vs sound. Results from coronal pulp, mid pulp and floor of pulp from carious teeth (results in coral) and sound teeth (results in turquoise). Results produced from Transects macro.

Comparing the width of collagen bundles between carious and sound teeth (CP, MP and FP sites combined) resulted in a non-significant result (p value=0.893, carious median = 0.9µm (IQR: 0.4-1.6µm), sound median = 0.8µm (IQR: 0.4-1.7µm)). Median quoted as data is non-parametric. For this result and model, 0.04% of the variance was explained by the individual tooth and 0.06% explained by the site.

The results of comparing carious to sound, at each individual site (CP, FP and MP), resulted in no statistically significant differences, as per Table 4.3.2 3.

However, significant results were found for all comparisons of sites (CP, MP and FP) in carious teeth, and all teeth combined (i.e. carious and sound teeth groups) (see Table 4.3.2 4). A statistically significant difference for FP vs MP and CP vs MP in sound teeth was found, but not CP vs FP (see Table 4.3.2 4). This means that in sound teeth, the width of fibres is not statistically different between CP and FP.

	MEDIAN (IQR) (µm)		NUMBER OF FIBRES MEASURED		P-value
	SOUND	CARIOUS	SOUND	CARIOUS	
CORONAL	0.8 (0.4-1.7)	0.9 (0.4-2.1)	7093	5272	0.151
MID	0.7 (0.3-1.5)	0.8 (0.4-1.5)	7960	4432	0.975
FLOOR	0.8 (0.4-1.7)	0.9 (0.4-1.6)	7743	5707	0.202

Table 4.3.2 3: Comparison of statistics for carious vs sound at each site. P-value obtained from multilevel mixed-effect model, p<0.05 = pink. Number of fibres measured = total number of fibres across all sound/carious teeth (i.e. from 40 images)

COMPARISSON	SOUND	CARIOUS	ALL TEETH
CP vs MP	<0.001	<0.001	<0.001
CP vs FP	0.946	<0.001	<0.001
FP vs MP	<0.001	0.017	<0.001

Table 4.3.2 4: Statistical comparisons of the width of fibres from sites in carious teeth, sound teeth and all teeth, p<0.05 = green, p>0.05 = pink. P-value obtained from multi-level fixed effect model

Interestingly, even though the differences in medians and interquartile ranges (IQR) between each site were small (see Table 4.3.2 3 and boxplot in Figure 4.3.2 5), this still resulted in mostly statistically

significant results when comparing sites within carious and sound tooth subgroups, and all teeth (Table 4.3.2 4), this may be because the width of many fibres per image were included in the analysis, resulting in a large sample/observation size for each site (demonstrated by the 'number of fibres measured' column in Table 4.3.2 3).

These results essentially indicate that across the board there are statistically significant differences in the fibre widths between sites, but not in comparing the fibre width measurements between carious and sound teeth.

Area of Staining

The results of 'area of staining' are given as percentage (%) values. These values are the percentage of stained pixels per image analysed, equating to a percentage of the whole image. As such, if all the pixels in an image were stained, the value would be 100%, if none of the pixels were stained, the value would be 0%. This observation is used as a surrogate measure of the volume of collagen in each image.

Comparing the area (%) of pixels stained between all carious and sound teeth (all sites combined) resulted in a significant difference (p value = <0.001). For this result and model, 43.77% of the variance was explained by the individual tooth and 0% by the site. For this comparison, the data (all sites combined) for sound teeth is non-parametric and the data for carious teeth (all sites combined) is parametric. The median (and IQR) for the area of stained pixels in sound and carious teeth is 79.3% (62.6-74.7%) and 52.2% (40.5-52.4%), respectively. The mean (and SD) for the area of stained pixels in sound and carious teeth is 74.7% (17.7%) and 52.4% (16.6%), respectively. Both the median and mean confirm a higher % of area stained in sound teeth than carious, suggestive of more collagen present in sound teeth than carious, when looking at all sites (CP, MP and FP) combined.

Analysis at a site-level, demonstrated a decrease in the % of area covered by stained pixels in both carious and sound teeth (and all teeth, carious and sound combined) towards the centre of the pulp. This trend is most marked in carious teeth, as highlighted by statistically significant comparisons for CP vs MP, CP vs FP and MP vs FP, whereas the same comparisons resulted in no statistically significant differences in sound teeth (Table 4.3.2 5).

Table 4.3.2 6 summarises the statistics for the area of pixels stained in carious and sound teeth, broken down into the three sites analysed (CP, MP and FP); these data again highlight the trends of a decrease in the number of pixels stained towards the centre of the pulp, and that carious teeth generally had a lower % of pixels stained across the board. This table also demonstrates that the differences between the sites (FP, CP and MP) in carious teeth are more marked than the differences between the sites in sound teeth, mirroring the statistically significant differences identified. These trends are also presented in Figure 4.3.2 6.

COMPARISSON	SOUND	CARIOUS	ALL TEETH
CP vs MP	0.054	<0.001	<0.001
CP vs FP	0.978	0.019	0.076
FP vs MP	0.058	0.002	<0.001

Table 4.3.2 5: Statistical comparisons the area of fibres from sites in carious teeth, sound teeth and all teeth, p<0.05 = green, p>0.05 = pink. P-value obtained from multi-level fixed effect model

	MEDIAN (IQR) (%)		MEAN (SD) (%)		P-Value
	SOUND	CARIOUS	SOUND	CARIOUS	
CORONAL	83.8 (63.6-91.5)	57.9 (48.7-71.4)	76.5 (18.2)	59.7 (14.2)	0.011
MID	73.1 (59.3-87.2)	40.5 (31.6-55.4)	71.3 (19.6)	44.6 (17.0)	<0.001
FLOOR	79.5 (65.8-88.2)	51.8 (43.8-63.7)	76.4 (14.9)	63.7 (15.3)	<0.001

Table 4.3.2 6: Statistics for the Area of Pixels (%) per image stained. Coronal Carious and Floor Carious measurements = parametric distribution. All other distributions = non-parametric. Multi-level mixed effects statistical model used, p<0.05=green

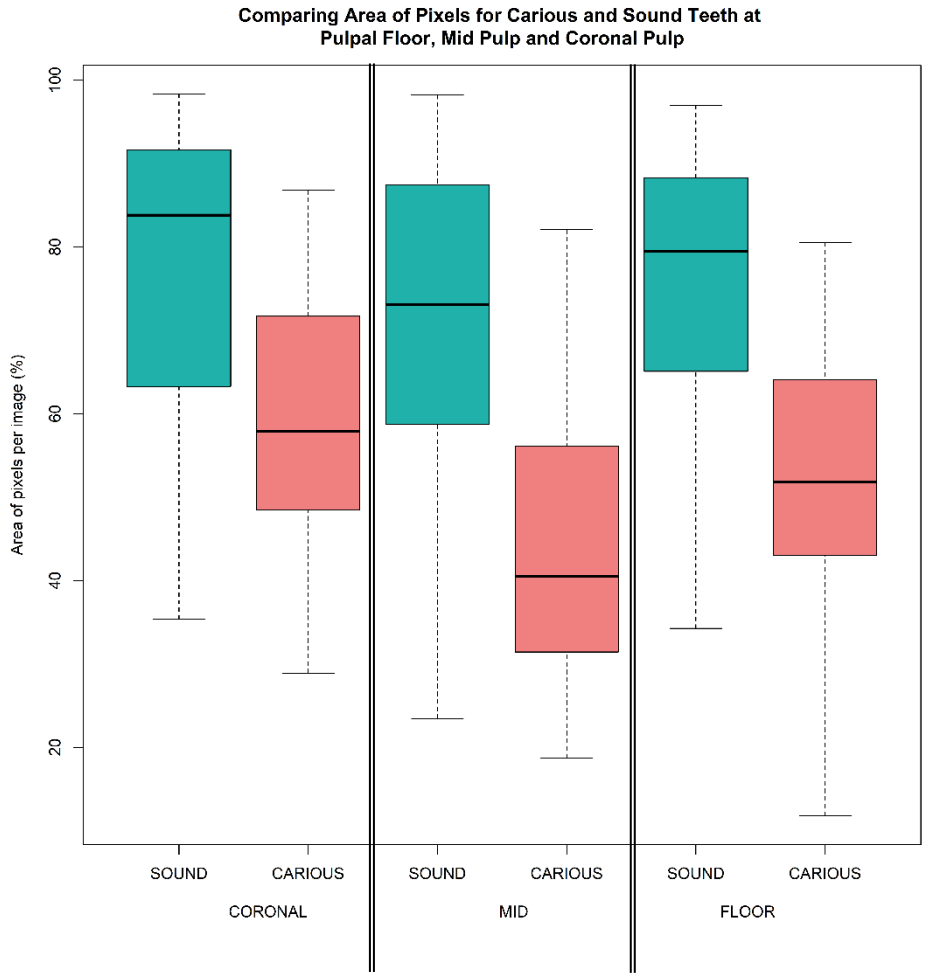

Figure 4.3.2 6: Area of collagen fibres, comparing sites and carious vs sound. Results obtained from pixel counter in ImageJ. Results from carious teeth in coral and sound teeth in turquoise.

Alignment of collagen bundles - Ratio (Fourier Orientation) and Coherence (OrientationJ)

The trends identified from the Fourier Orientation ratio reveal a higher ratio towards the middle of the pulp (suggesting the fibres here are less aligned/organized), and this is true for both carious and sound teeth (and all teeth combined), meaning the fibres in this area are less organized than the coronal aspect and floor – see Figure 4.3.2 7 and Table 4.3.2 7.

The trends elucidated from the OrientationJ coherence value reveal a lower value towards the middle of the pulp (suggesting the fibres here are less aligned/organized) in carious teeth, but a gradual increase in the orientation of the collagen fibres towards the floor of the pulp in sound teeth (Figure 4.3.2 8 and Table 4.3.2 8).

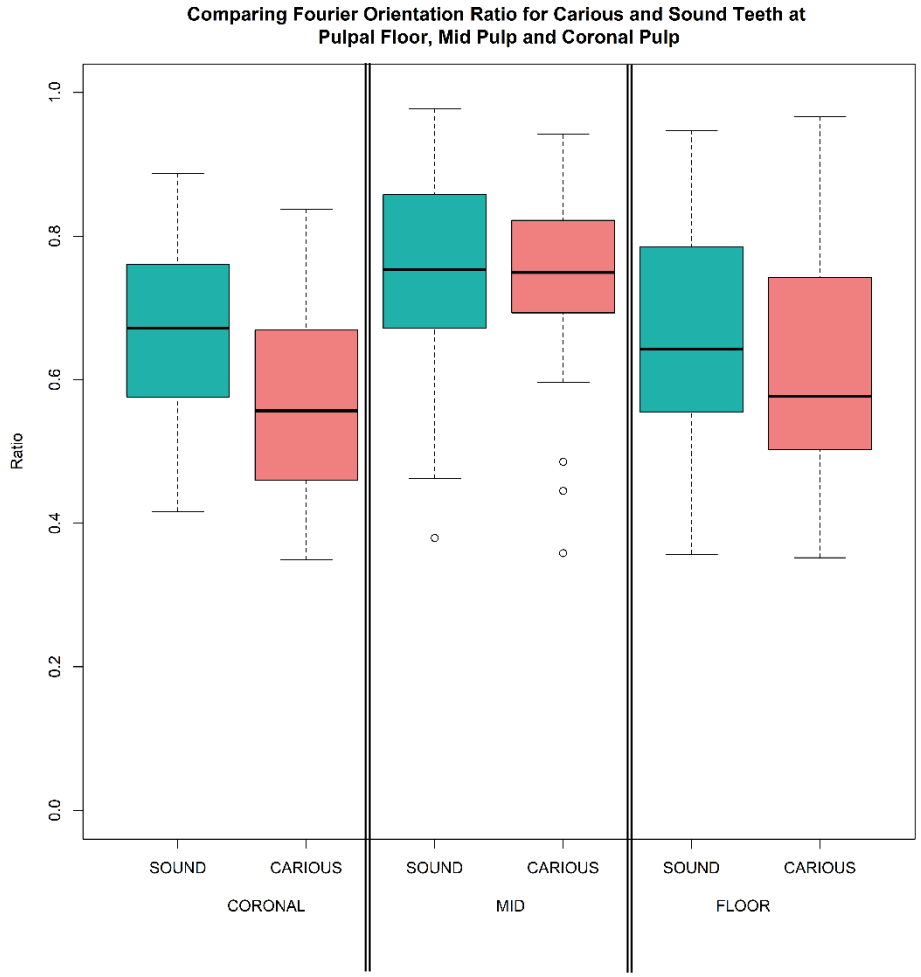

Figure 4.3.2 7: Organisation of collagen fibres, comparing sites and carious vs sound (results from Fourier Orientation Ratio), comparing carious teeth (coral) against sound teeth (turquoise). Figures closer to 1.0 = less aligned fibres, closer to 0 = more aligned.

	MEDIAN (IQR)		MEAN (SD)		P-Value
	SOUND	CARIOUS	SOUND	CARIOUS	
CORONAL	0.67 (0.58-0.78)	0.56 (0.46-0.67)	0.68 (0.12)	0.56 (0.12)	<0.001
MID	0.75 (0.69-0.85)	0.75 (0.70-0.82)	0.75 (0.14)	0.75 (0.13)	0.991
FLOOR	0.64 (0.56-0.78)	0.58 (0.51-0.74)	0.64 (0.14)	0.62 (0.17)	0.450

Table 4.3.2 7: Statistical analysis for Fourier Orientation ratio, comparing carious and sound for each site. Floor Carious and Mid Carious measurements = non-parametric distribution. All other distributions = parametric. Multi-level linear model results, p<0.05 = green, p>0.05 = pink

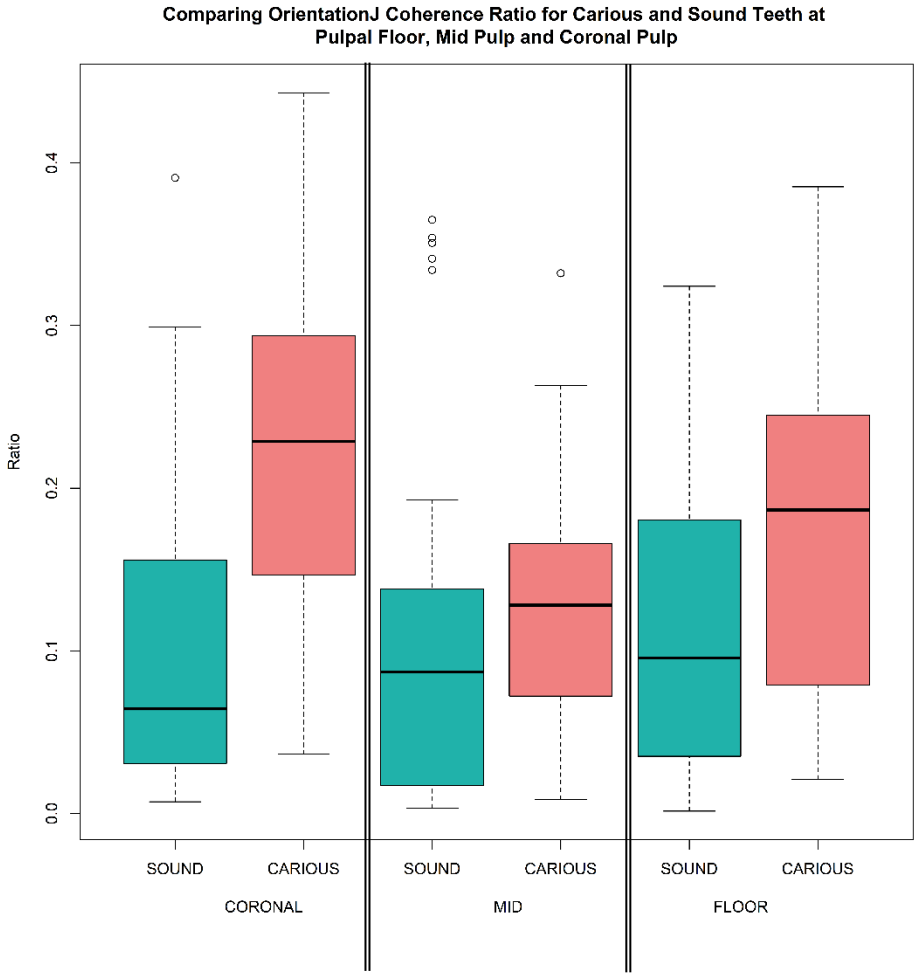

Figure 4.3.2 8: Organisation of collagen fibres, comparing sites and carious vs sound (results from OrientationJ Coherence value), comparing carious teeth (coral) against sound teeth (turquoise). Figures closer to 0 = less aligned, figures closer to 1 = more aligned.

	MEDIAN (IQR)		MEAN (SD)		P-Value
	SOUND	CARIOUS	SOUND	CARIOUS	
CORONAL	0.06 (0.03-0.16)	0.23 (0.15-0.29)	0 10 (0.10)	0.22 (0.10)	0.028
MID	0.09 (0.02-0.14))	0.13 (0.08-0.17))	0.10 (0.11)	0.12 (0.08)	0.648
FLOOR	0.10 (0.04-0.18)	0.19 (0.08-0.24)	0.11 (0.09)	0.18 (0.10)	0.075

Table 4.3.2 8: Statistics for OrientationJ coherence. All carious data = parametric distribution. All sound data = non-parametric distribution. Multi-level linear model results, p<0.05 = green, p>0.05 = pink

When examining the sites in carious and sound teeth, the data was mixed parametric and non-parametric, and a summary of the data is provided in Table 4.3.2 7 and Table 4.3.2 8. This shows that the difference between carious and sound teeth at CP is statistically different, whereas for sites MP and FP it was not. This trend is the same for both the OrientationJ output and the Fourier Orientation output.

The ratio derived from the Fourier Orientation macro and the coherence value from OrientationJ do share some similarities, as both programmes are created to measure the alignment of fibers. When studying the results of these measurements, the two outcomes correlate (proved by Spearman's correlation test completed in R, resulting in a rho value of -0.596 and a p value of <0.001), validating the design of the new macro and explaining the similarities in the statistical results for these two outcomes in Table 4.3.2 7 and Table 4.3.2 8. A graph showing the correlation between the two outcomes is provided in Appendix 9. The more randomly orientated the fibers in an image are, the closer to 0 the output of the coherence test in OrientationJ will be, whereas an output closer to 0 in the Fourier Orientation macro would mean the fibers are highly aligned, hence the negative correlation observed for these two variables.

Interestingly, a weak negative correlation was also found with the area of pixels stained and the coherence value from OrientationJ (Spearman's correlation test completed in R, resulted in a rho value of -0.328 and a p value of <0.001), but no correlation was detected with the area of pixels and the ratio from the Fourier Orientation macro (Spearman's correlation test completed in R, resulted in a rho value of -0.053 and a p value of 0.369). The negative correlation between pixel area and coherence essentially means that with more areas stained in the image, the more randomly orientated the fibers in the Image were (and vice-versa). This correlation was reflected by the statistical test results in Table 4.3.2 5 and Table 4.3.2 9.

Comparing the ratio from the Fourier Orientation macro between carious and sound teeth (all sites combined) resulted in a non-significant result (p value = 0.052). For this result and model, 11.22% of the variance was explained by the individual tooth and 0% explained by the site, using the linear mixed effect statistical model. This data was parametric (mean (and SD) for sound teeth = 0.70 (0.14), mean (and SD) for carious teeth = 0.64 (0.16)).

Comparing the coherence value from OrientationJ between carious and sound teeth (all sites combined) resulted in a statistically significant difference (p value = 0.005). For this result and model, 15.83% of the variance was explained by the individual tooth and 0% was explained by the site, using the linear mixed effects model. This data was non-parametric (median (and IQR) for sound teeth = 0.08 (0.03-0.15), median (and IQR) for carious teeth = 0.17 (0.09-0.24)).

For both the coherence (OrientationJ) and ratio (Fourier Orientation) outputs, when comparing the outputs at a site-level, no statistical difference was found for sound teeth CP vs FP, nor all teeth

combined CP vs FP whereas all site pair-wise comparisons in carious teeth were statistically significant (see Table 4.3.2 9 and Table 4.3.2 10).

COMPARISSON	SOUND	CARIOUS	ALL TEETH
CP vs MP	0.990	<0.001	<0.001
CP vs FP	0.777	0.006	0.081
FP vs MP	0.760	<0.001	0.004

Table 4.3.2 9: Statistical comparisons of the coherence value (from OrientationJ) from sites in carious teeth, sound teeth and all teeth, p<0.05 = green, p>0.05 = pink. P-value obtained from multi-level fixed effect model

COMPARISSON	SOUND	CARIOUS	ALL TEETH
CP vs MP	0.016	<0.001	<0.001
CP vs FP	0.549	0.040	0.270
FP vs MP	0.003	<0.001	<0.001

Table 4.3.2 10: Statistical comparisons of the ratio from the Fourier Orientation Macro from sites in carious teeth, sound teeth and all teeth, p<0.05 = green, p>0.05 = pink. P-value obtained from multi-level fixed effect model

4.3.3 RNA SEQUENCING RESULTS

KEY FINDINGS

1. More genes were upregulated in carious teeth compared with sound.
2. When looking at the differentially expressed genes, sound teeth and carious teeth form separate clusters.
3. The largest protein clusters formed from the differentially expressed genes have functions pertaining to neural function and immune response.
4. When determining protein clusters and functions from the 50 most expressed genes, functions related to iron/ferric ion binding, haemostatis, growth factor and signal receptor binding, extra-cellular matrix structure and intracellular cytoskeleton structure were identified.

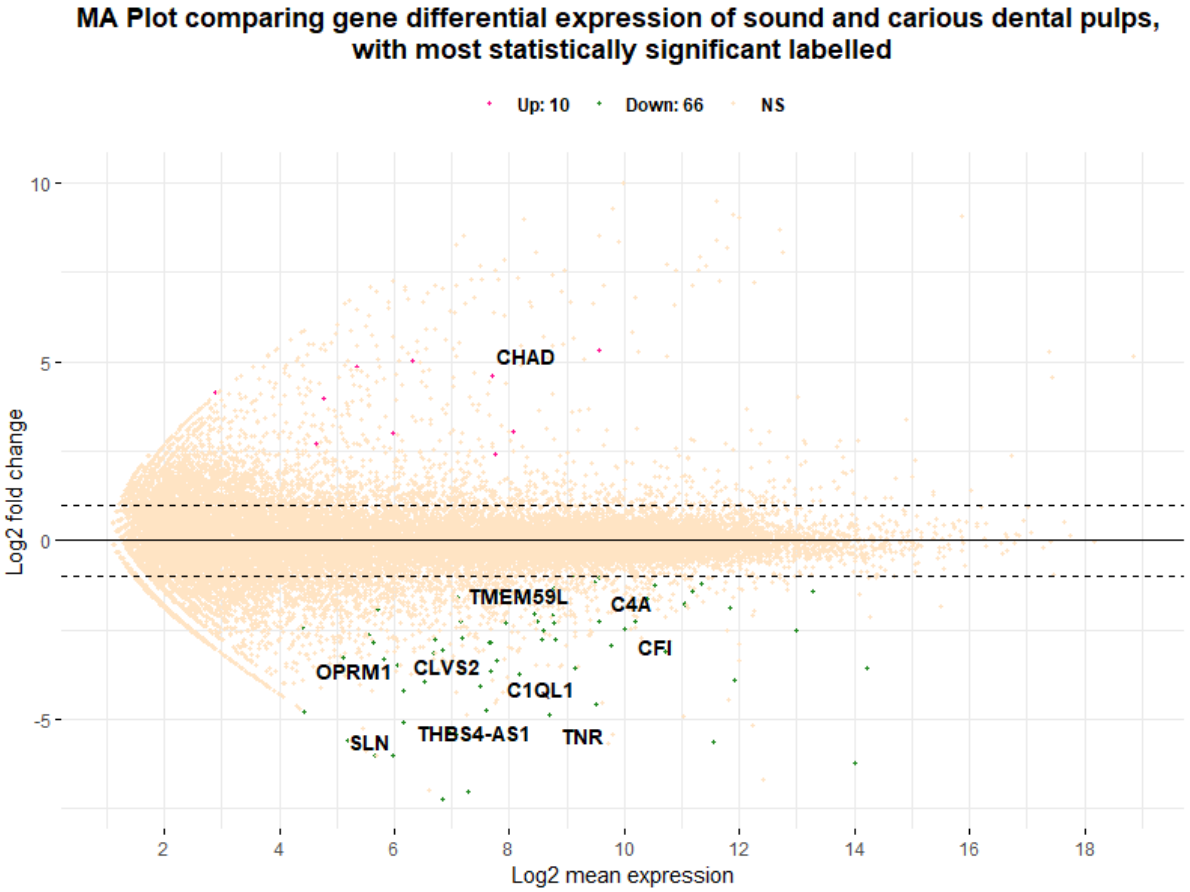

Figure 4.3.3 1: MA (Mean Average) plot demonstrating the differential expression of 76 genes (dots coloured red/green). Log2 fold changes <0 are carious-associated, >0 are sound-associated. Ten genes with the most marked statistical difference are labelled. Dotted lines are -2 and 2 Log2 fold change.

The results demonstrate there are 76 statistically significant differentially expressed genes (with a p value <0.05) when comparing sound to carious teeth. The results also demonstrated that the majority of these differentially expressed genes are upregulated in carious teeth, and this is the case for the top 10 genes that show the greatest difference between carious and sound teeth where only one gene (chondroadherin/*CHAD*) was upregulated in sound teeth. This is summarised in the MA plot in Figure 4.3.3 1. A list of these reads, including full gene name is available in Appendix 10. Normalised read counts for the top 10 genes with the most statistically significant difference are also displayed in Figure 4.3.3. 2.

A total of 2344 from 33279 mapped genes (i.e. excluding genes where no reads across all samples were detected) had a log2 fold change of >2 (1120 associated with sound teeth) or <-2 (1224 associated with carious teeth), and 60 of these had a p value <0.05 when comparing carious and sound teeth. This means that 16 of the 76 genes with a statistically significant (p value <0.05) differential expression have a log2 fold change of <2 and >-2 (LOC105379548, ALDH1A1, S100B, CPXM2, OSMR, ASB3, CPLX1, LOC105377896, CXCL12, MYH11, MC1R, CXXC5, TMEM176A, MATN2, GAR1, SMAD1 and TMEM176B).

The heatmap in Figure 4.3.3 3 shows the normalised reads for the 76 statistically significant differentially expressed genes, demonstrating some clustering for expression in the sound and carious teeth. It is clear from the heatmap that the differentially expressed genes all have relatively low read counts. Some of the differentially expressed reads include pseudogenes, genes with no known function (and as such are uncategorised), antisense RNA and splicesomal RNA. These have been included in the MA Plot (Figure 4.3.3 1) and heatmap (Figure 4.3.3 3) to demonstrate the abundance of these reads of unknown significance.

Figure 4.3.3 4 demonstrates the top 50 expressed genes overall (carious and sound teeth grouped together), with no clustering of carious and sound teeth evident. There was no statistically significant difference between carious and sound teeth for any of these top 50 reads (all had padj>0.05). These top 50 genes included one pseudogene and protein coding regions for immunoglobulins. Appendix 11 lists all of these reads, including full gene name in tabular form.

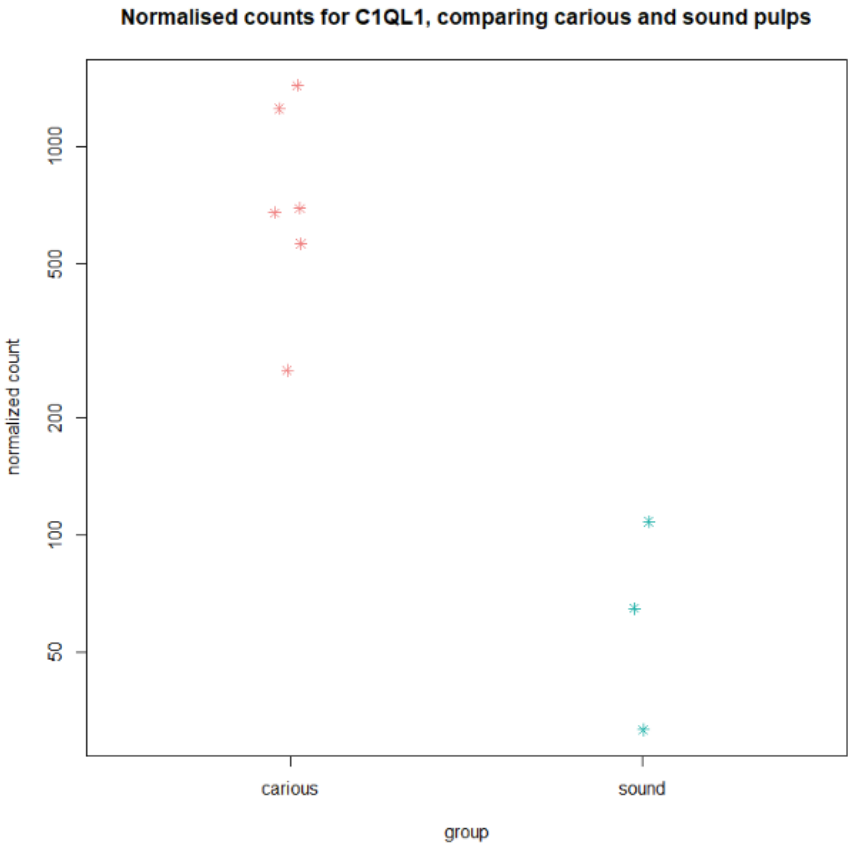

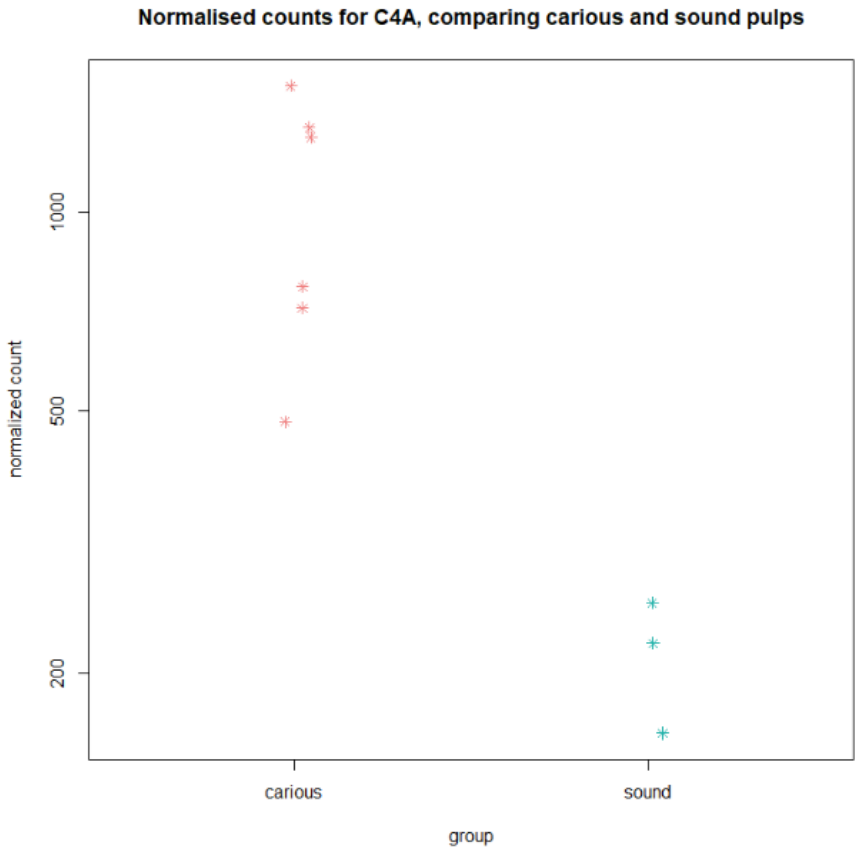

Figure 4.3.3 2: Plotted normalised counts for the 10 genes with the most statistically significant difference between the two groups – carious (in coral, one point per sample) and sound (in turquoise, one point per sample). These plots are included to demonstrate the variation in reads for the most statistically different genes.

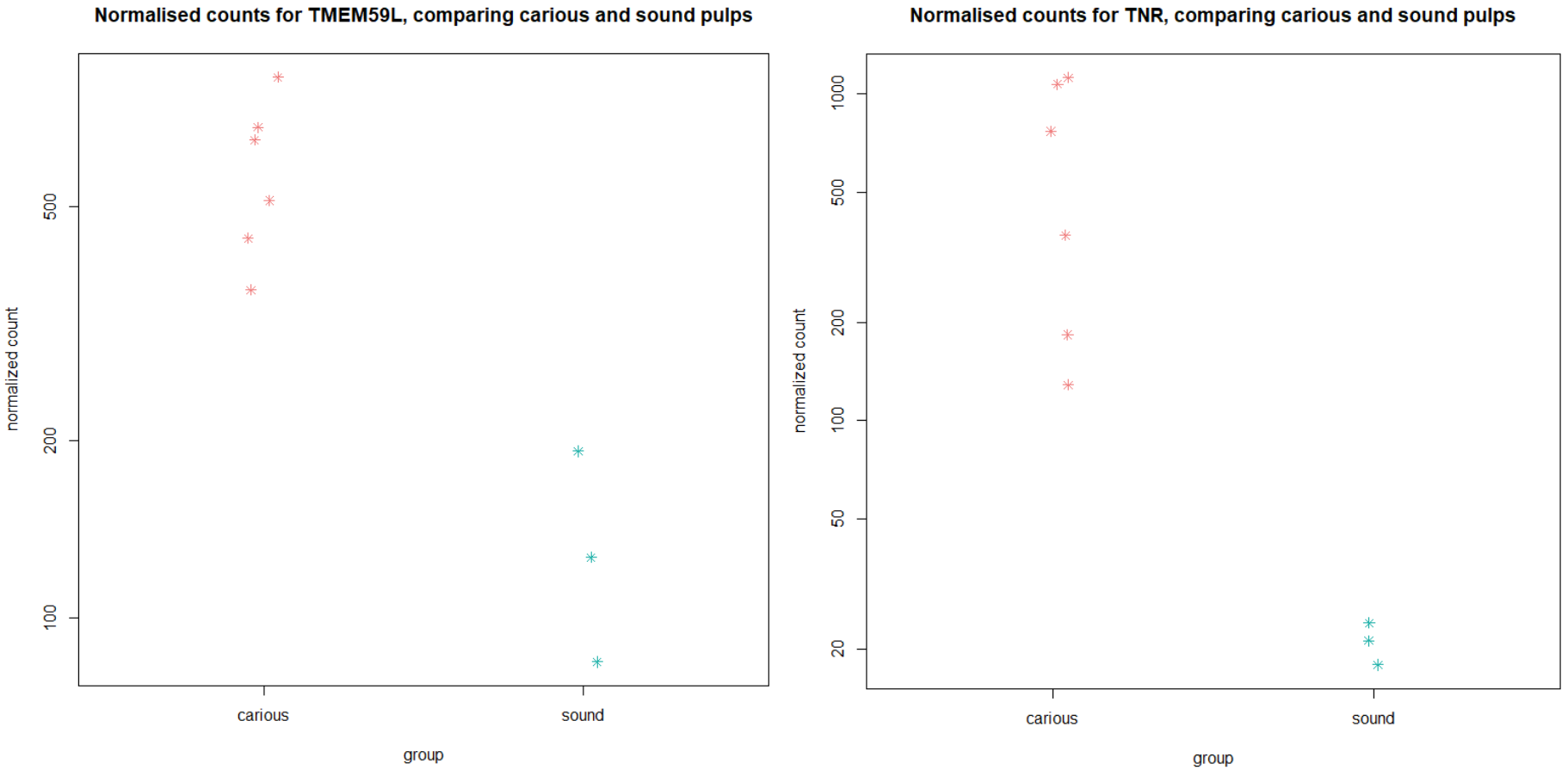

Figure 4.3.3 2: Plotted normalised counts for the 10 genes with the most statistically significant difference between the two groups – carious (in coral, one point per sample) and sound (in turquoise, one point per sample). These plots are included to demonstrate the variation in reads for the most statistically different genes(continued)

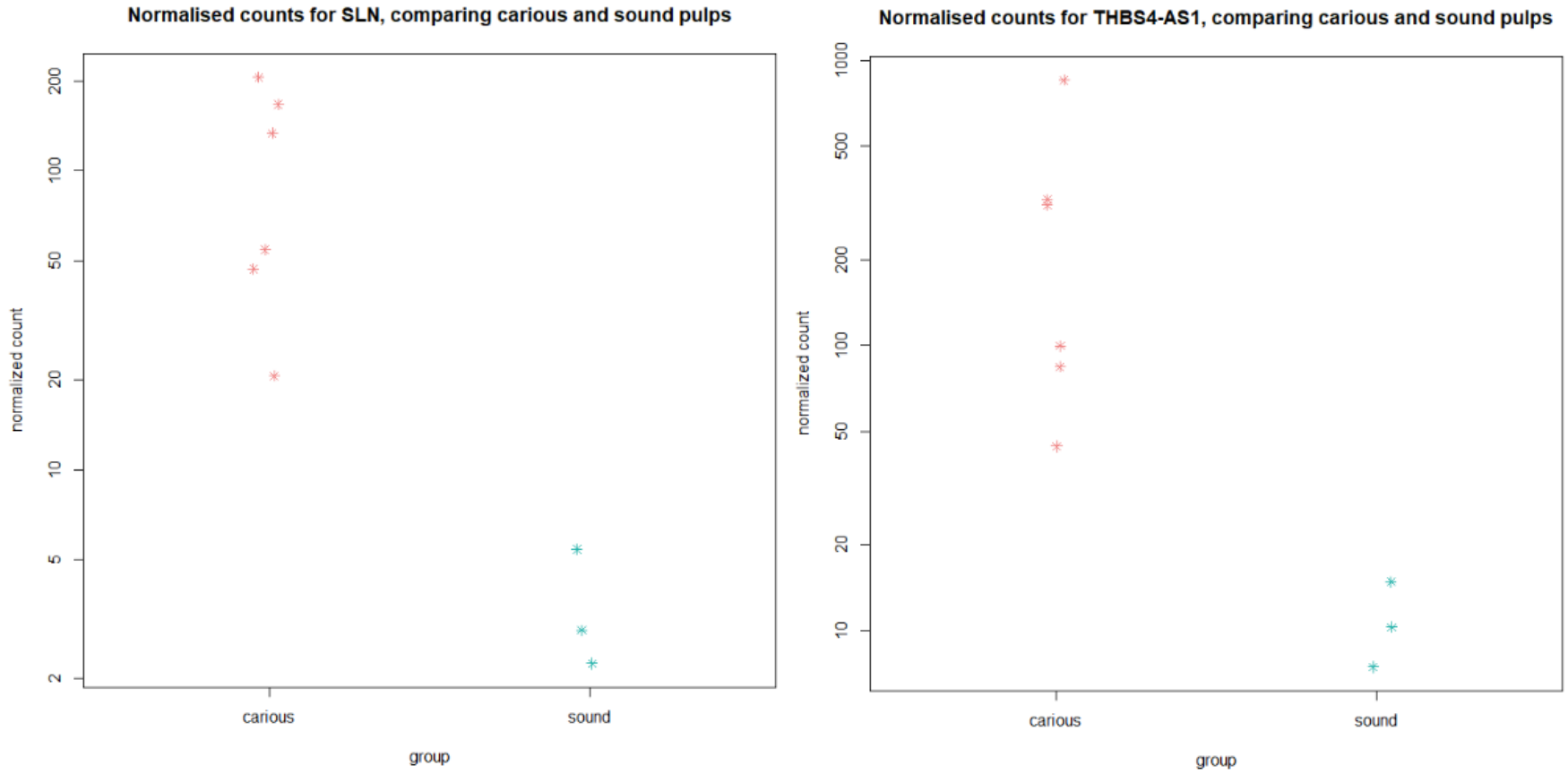

Figure 4.3.3 2: Plotted normalised counts for the 10 genes with the most statistically significant difference between the two groups – carious (in coral, one point per sample) and sound (in turquoise, one point per sample). These plots are included to demonstrate the variation in reads for the most statistically different genes(continued)

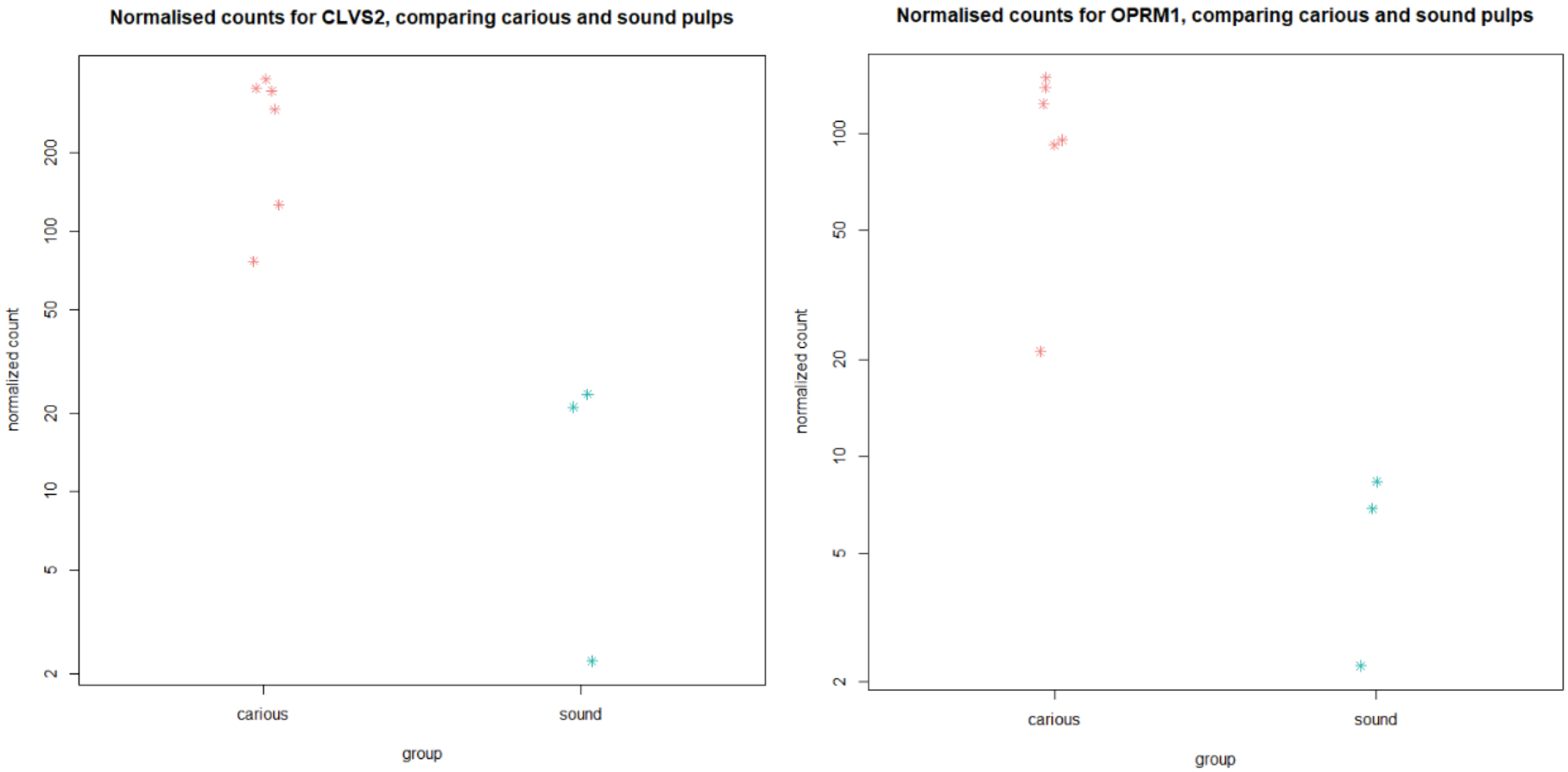

Figure 4.3.3 2: Plotted normalised counts for the 10 genes with the most statistically significant difference between the two groups – carious (in coral, one point per sample) and sound (in turquoise, one point per sample). These plots are included to demonstrate the variation in reads for the most statistically different genes(continued)

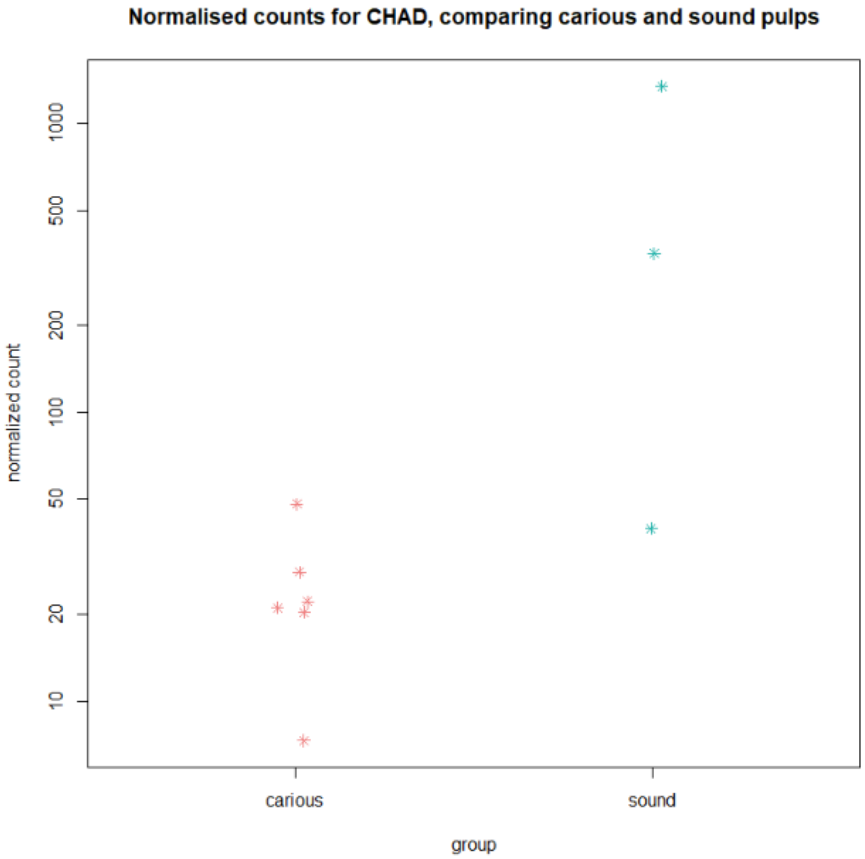

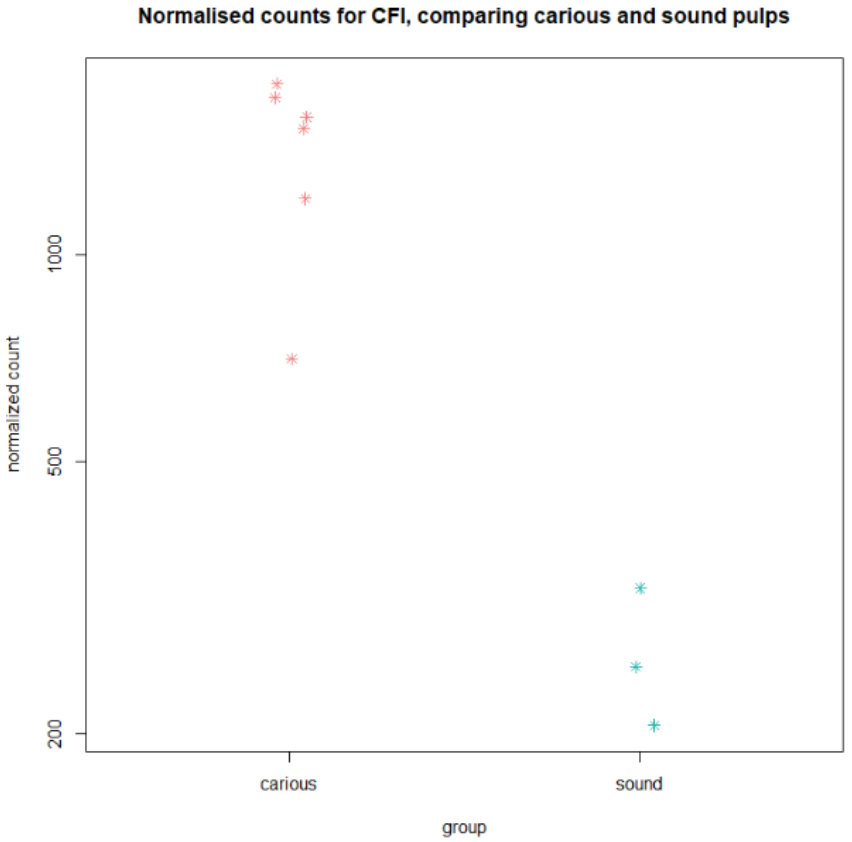

Figure 4.3.3 2: Plotted normalised counts for the 10 genes with the most statistically significant difference between the two groups – carious (in coral, one point per sample) and sound (in turquoise, one point per sample). These plots are included to demonstrate the variation in reads for the most statistically different genes(continued)

Figure 4.3.3 3: Heatmap of the 76 differentially expressed genes with padj value< 0.05, demonstrating clustering of carious (marked in coral) and sound teeth (marked in turquoise). Sample names across the bottom, gene symbols on the right.

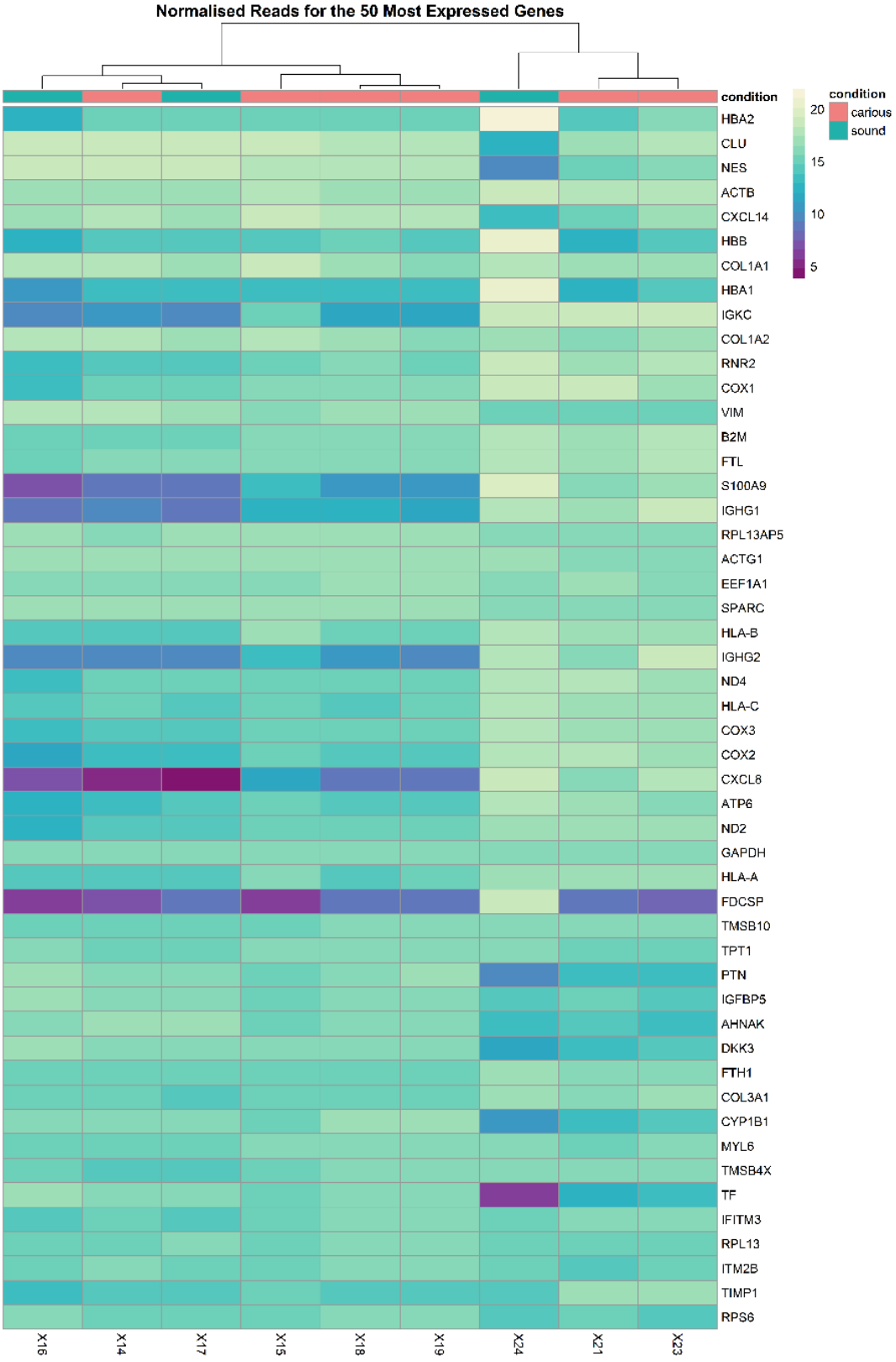

Figure 4.3.3 4: Heatmap of the top 50 most expressed genes (i.e. the genes with greatest abundance in carious and sound teeth). Note the lack of clustering between carious teeth (marked in coral) and sound teeth (marked in turquoise) and the abnormality of Sample X24. Sample names across the bottom, gene symbols on the right.

Principle Component (PC) analysis was also undertaken to determine clustering of genes from carious and sound pulps (Figure 4.3.3 5). There appears to be some pattern to the groups, with carious teeth being exclusively grouped below ~5 on the y axis, and carious teeth above ~5, but there is a spread across the plot. However, when k-means clustering was completed on the PC plot, X24 was one cluster and the remaining samples were another cluster, highlighting this sample as being different from the other teeth sequenced (see Appendix 12, produced with factoextra 1.0.6 in R).

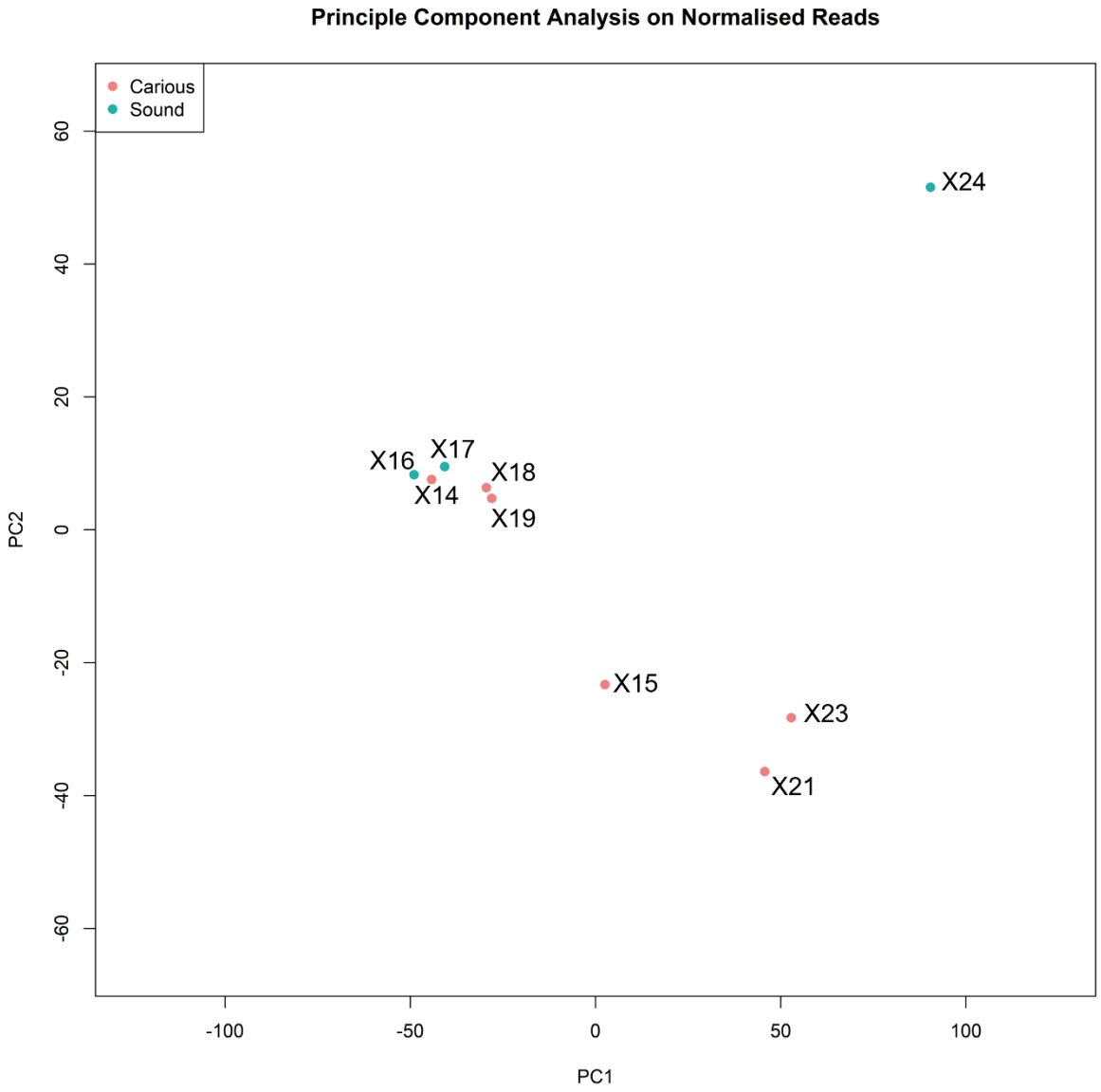

Figure 4.3.3 5: PC analysis plot, using normalised read counts (using TMM normalisation) demonstrating sound teeth (in turquoise) above ~5 on the y axis and carious teeth (in coral) below ~5 on the y axis.

Samples X15 and X16 were derived from one patient, and samples X18 and X19 also were derived from one patient. Samples X15 and X16 obtained from the same patient allows for an interesting comparison, as one of the samples (X15) is carious, and the other (X16) is sound. This allows for a direct assessment of the RNA changes due to caries excluding background genetic variability. As can be seen in the difference between these two samples on the PC plot (Figure 4.3.3 5), and the clustering of the heatmap in Figure 4.3.3 4, these samples do show some difference from each other in a small number of genes. As samples X18 and X19 come from the same patient, and are both carious, this explains their close proximity on the PC plot (Figure 4.3.3 5) and the heatmaps in Figures 4.3.3 4 and 4.3.3 3.

By using the STRING database (205) to analyse the 76 differentially expressed genes, 13 protein clusters were identified (input parameters included MCL clustering inflation parameter value of 2.5 and minimum confidence interaction value of 0.150) from 63/76 genes identified by the database. Six genes did not cluster; *SMAD1*, *NPIPA8*, *ASB3*, *PLEKHS1*, *CXXC5* and *WFDC2*. See Figure 4.3.3 6 for the network of these protein clusters, and Figures 4.3.3 7 and 4.4.4 8 for the individual 13 networks.

Cluster 1 is composed of genes largely associated with neural function and nervous system development. One pathway in this cluster is enriched – nuclear signalling by ERBB4 - with CXCL12, S100B and GFAP being actively involved in this pathway. Nuclear signalling by ERBB4 is believed to have neurogenerative functions (209). Eight proteins in this network are located in the synapse (TNR, LPAR3, SV2B, KCTD16, HTR1A, CPLX1, PTPRN, SLC1A1) and most of the proteins in this cluster have functions related to the nervous system and inflammation/immune response (209–211). As can be seen from Table 4.3.3 1, where genes upregulated in carious teeth are highlighted pink (log2 fold change <-2), and genes up regulated in sound teeth are highlighted green (log2 fold change >2), most of the genes in this network were upregulated in carious teeth. When looking at only those upregulated in carious teeth, two proteins are found in neural stem cells – GFAP and PROM1, further highlighting the neural component of this large cluster (210,211), but no further enrichment of Gene Ontology terms specific to the carious teeth in this network were found. No enrichment of Gene Ontology terms were found with the three proteins upregulated in sound teeth for this cluster.

Cluster 2 contains proteins associated with the immune response (209–211), and as can be seen in Table 4.3.3 1, there is upregulation of most of these in carious teeth (log2 fold change <-2) – GAR1 was also upregulated in carious teeth, was below the log2 fold change <-2 cut-off. The proteins in this cluster have strong associations, with shared biological processes (e.g. Gene Ontology terms such as “Defence Response”, and “Immune Response” are shared by six of the proteins (210,211)). In keeping with this, the same six proteins (C4A, C4B, COLEC11, CFI, GIG25, SAA1) are associated with the innate immune system Reactome pathway (212).

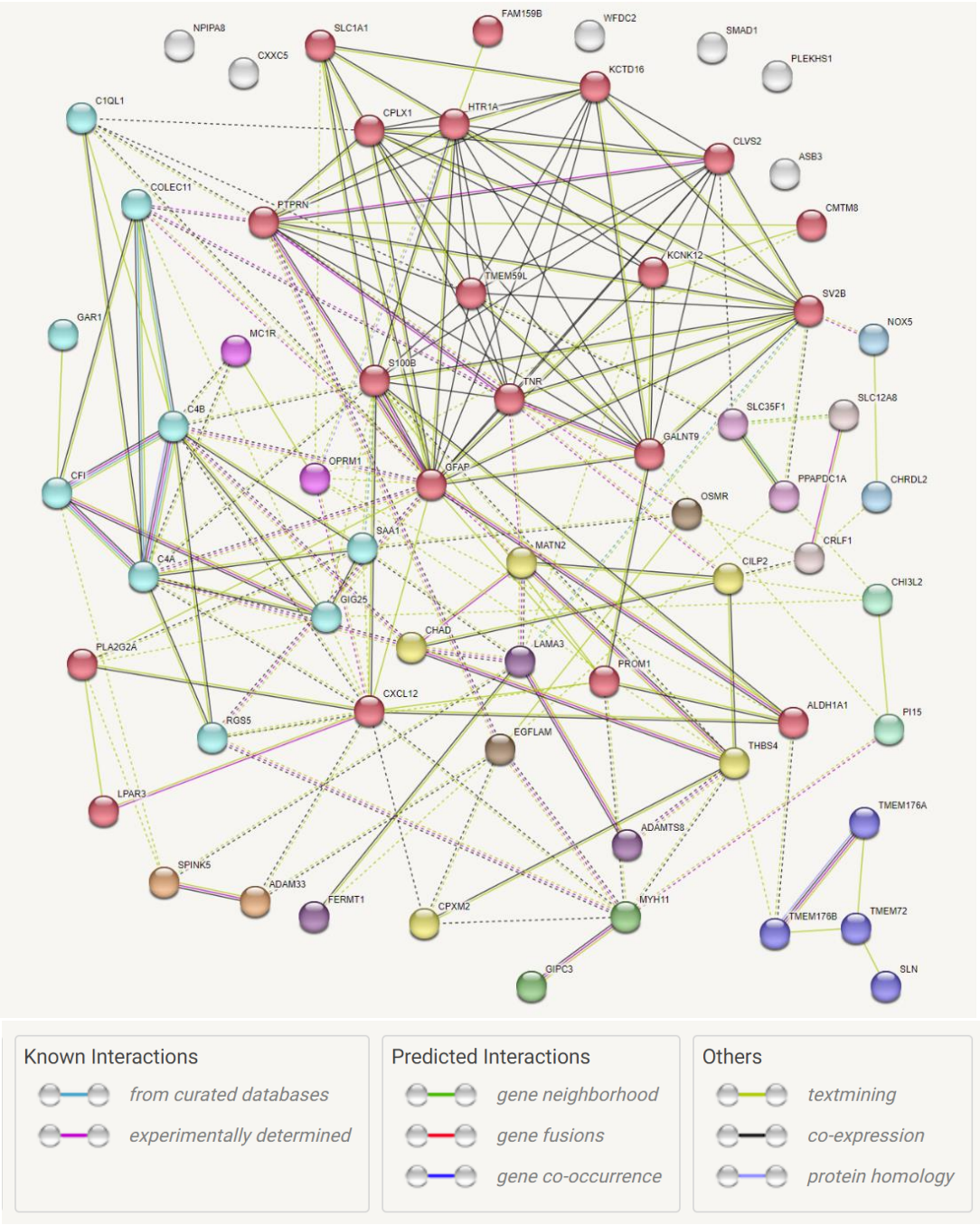

Figure 4.3.3 6: STRING Network analysis. Each cluster of proteins, derived from the differentially expressed genes, is differentially coloured, proteins not clustered = white. Thickness of the edges denotes the confidence of the interaction and the colour denotes the type of evidence (see legend above).

Cluster 3 contains proteins with functions associated with extracellular matrix maintenance (210,211). As can be seen in Table 4.3.3 1, more of these exhibit upregulation in sound teeth, compared to carious.

All of the proteins in cluster 4 are upregulated in carious teeth, however only 2 had log2 fold changes <-2. TMEM176A and TMEM176B are both associated with negative regulation of dendritic cell differentiation (210,211).

All of the proteins in cluster 5 are associated with integrin binding. LAMA3 and FERMT1 have shared functions related to cellular adhesion to the extracellular matrix (210,211)

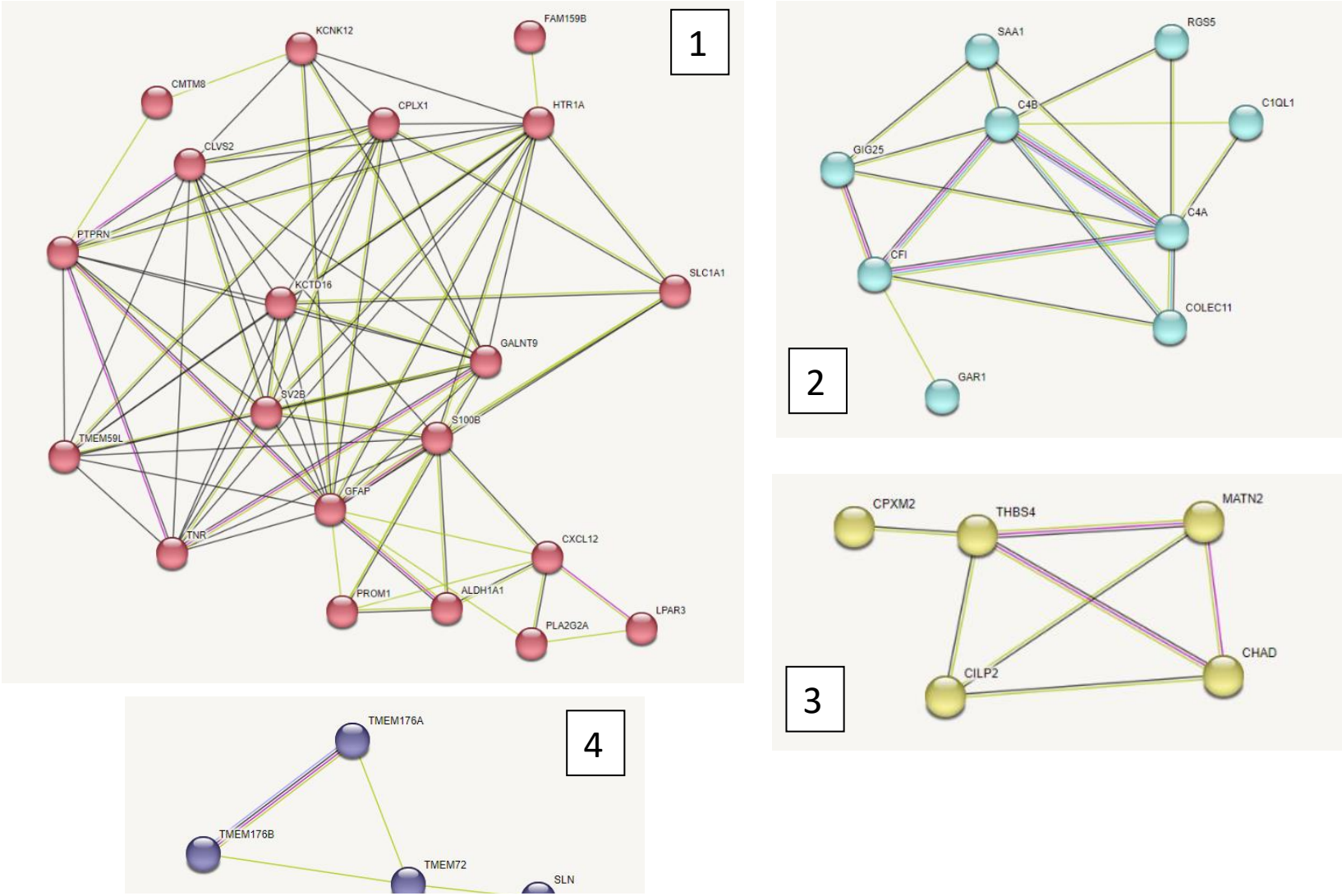

Figure 4.3.3 7: Clusters 1-4 from the STRING analysis – interaction legend as per Figure 4.3.3 6. These demonstrate the interactions between the proteins coded for by the differentially expressed genes identified in the STRING database.

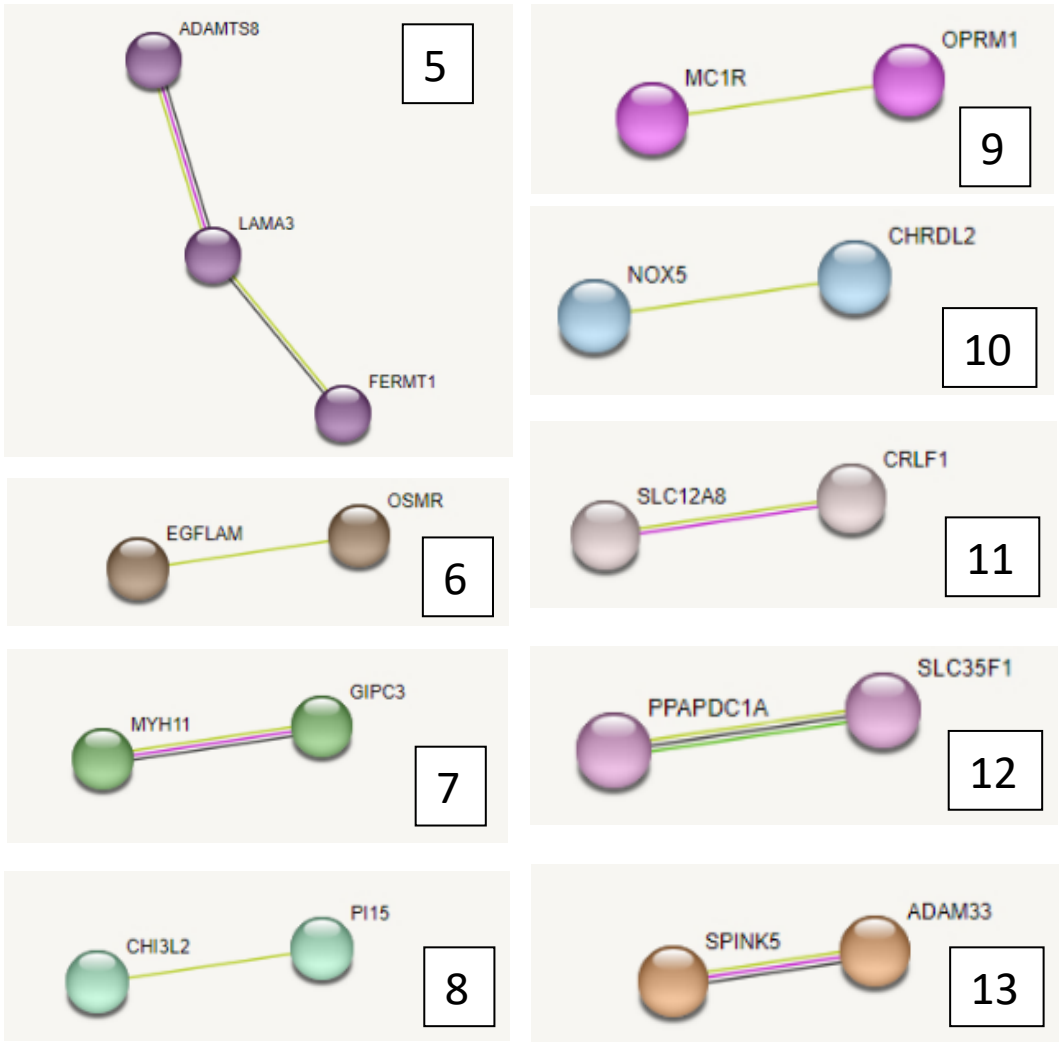

Figure 4.3.3 8: Clusters 5-13 from the STRING analysis - interaction legend as per Figure 4.3.3 6 These demonstrate the interactions between the proteins coded for by the differentially expressed genes identified in the STRING database.

.

Cluster	Number in cluster	Genes in Cluster
1	20	ALDH1A1, CLVS2, CMTM8, CPLX1, CXCL12, FAM159B, GALNT9, GFAP, HTR1A, KCNK12, KCTD16, LPAR3, PLA2G2A, PROM1, PTPRN, S100B, SLC1A1, SV2B, TMEM59L, TNR
2	9	C4A, C4B, C1QL1, CFI, COLEC11, GAR1, GIG25, RGS5, SAA1
3	5	CHAD, CILP2, CPXM2, MATN2, THBS4
4	4	TMEM72, TMEM176A, TMEM176B, SLN
5	3	LAMA3, FERMT1, ADAMST8
6	2	OSMR, EGFLAM
7	2	MYH11, GIPC3
8	2	PI15, CHI3L2
9	2	OPRM1, MC1R
10	2	NOX5, CHRDL2
11	2	SLC12A8, CRLF1
12	2	PPAPDC1A, SLC35F1
13	2	SPINK5, ADAM33

Table 4.3.3 1: Proteins in each cluster of the STRING Network. Pink proteins = log2 fold change <-2 associated with carious teeth. Green proteins = log2 fold change >2 associated with sound teeth

Figure 4.3.3 9 demonstrates the network formed by 46 of the most expressed genes across sound and carious teeth combined (input parameters included a MCL inflation parameter of 4.3 and a minimum confidence interaction level of 0.150). Four genes out of the top 50 that were input, were not identified on the STRING database, and as such were not included in the analysis. As can be seen, four clusters are identified in the network. One protein identified by the database, MTRNR2L8, did not cluster.

The proteins in Cluster 1 (see Table 4.3.3 2) encoded from the 50 most expressed genes have many functions. Broadly, they can be considered regulators of cellular processes. Molecularly, the proteins have functions pertaining to iron/ferric ion binding, haemostasis, growth factor and signal receptor binding, extra-cellular matrix structure and intracellular cytoskeleton structure (210,211). Significant Reactome pathways associated with these proteins include; Scavenging by Class A Receptors, Binding, Uptake of Ligands by Scavenger Receptors, Platelet activation, signalling and aggregation, ECM proteoglycans and Vesicle-mediated transport to name but a few (212).

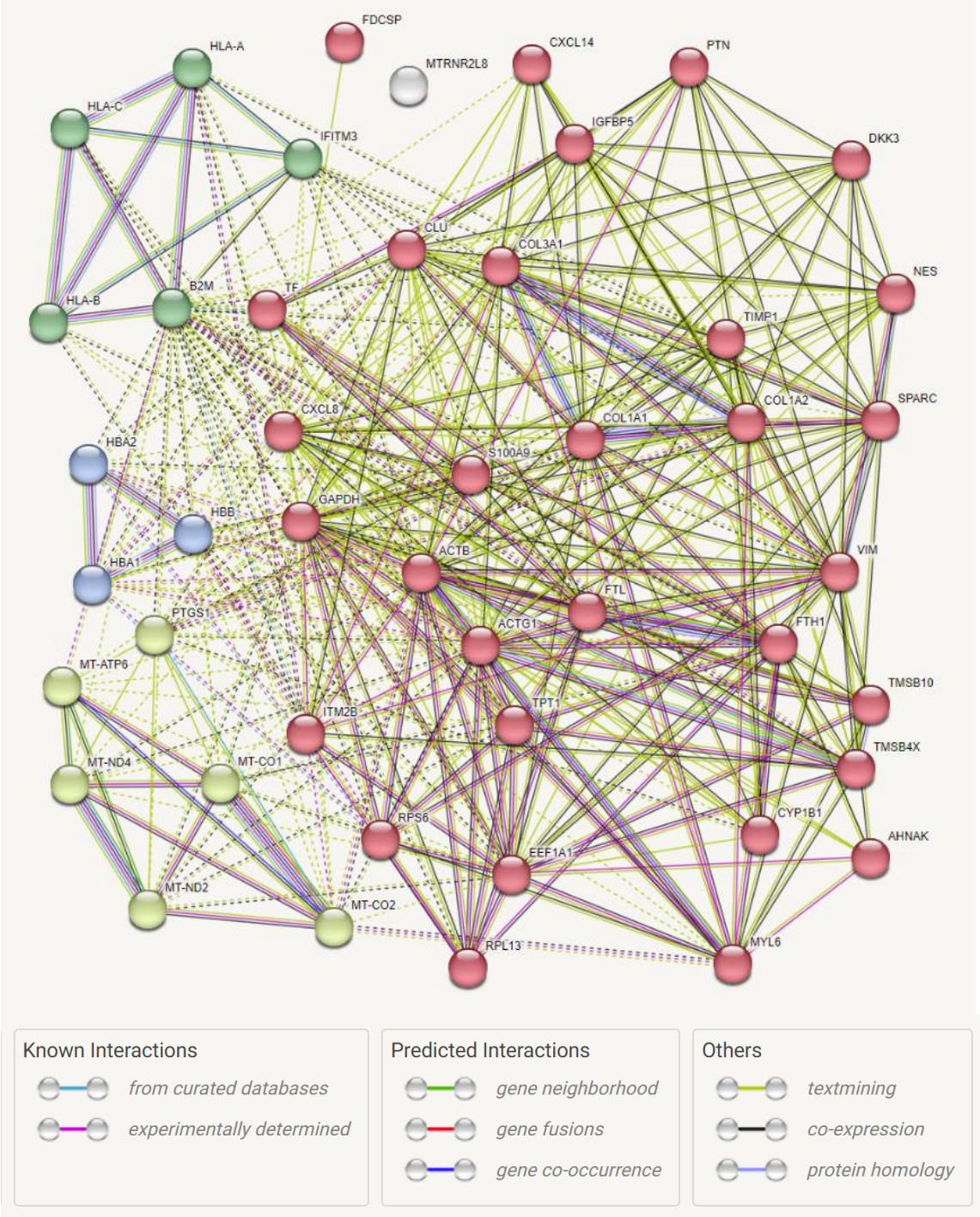

Figure 4.3.3 9: STRING Network analysis of the top 50 most expressed genes across both carious and sound teeth, differentially colour coded for each cluster. White = proteins that did not cluster. Each cluster of proteins, derived from the most abundantly expressed genes, is differentially coloured. Thickness of the edges denotes the confidence of the interaction and the colour denotes the type of evidence.

Cluster 2 is largely made up of mitochondrially encoded proteins. These are all involved in basic cytological functions pertaining to the respiratory chain and metabolism (210,211).

Cluster 3 includes proteins entirely involved in the immune response of the pulp, including the cytokine mediated response and antigen presentation (210,211).

Cluster 4 is made up of proteins only involved in haem binding and oxygen carrying (210,211). Interestingly, all three of the proteins in cluster 4 were upregulated in sound teeth, with a log2 fold change >2. Despite the large fold change, these three proteins did not have a statistically different expression between carious and sound teeth due to the Cook's cut-off employed by DESeq2 (which will not compute a p-value for outliers, and instead will provide an output of 'NA' in DESeq2). Cook's cut-off is discussed in more depth in the Discussion (Section 4.4.3).

Cluster	Number in cluster	Genes in Cluster
1	31	ACTB, ACTG1, AHNAK, CLU, COL1A1, COL1A2, COL3A1, CXCL14, CXCL8, CYP1B1, DKK3, EEF1A1, FDCSP, FTH1, FTL, GAPDH, IGFBP5, ITM2B, MYL6, NES, PTN, RPL13, RPS6, S100A9, SPARC, TF, TIMP1, TMSB10, TMSB4X, TPT1, VIM
2	6	MT-ATP6, MT-CO1, MT-CO2, MT-ND2, MT-ND4, PTGS1
3	5	BM2, HLA-A, HLA-B, HLA-C, IFITM3
4	3	HBB, HBA2, HBA1

Table 4.3.3 2: STRING Protein network analysis clusters of the 50 most expressed genes across carious and sound pulps. No gene had a log2 fold change <-2. Log2 fold change >2 = green text

It is important to note that although the numbers of genes involved in specific processes differ, this does not necessarily relate to differences in biological function; for example, although only a few genes were associated with extra-cellular matrix functions, *FERMT1* and *LAMA3* are some of the highest differentially expressed genes in sound teeth, with log2 fold changes of 4.85 and 5.33 respectively.

4.4 DISCUSSION

4.4.1 AFM DISCUSSION

All the pulps, whether of sound or carious teeth, showed a decrease of modulus towards the centre of the pulp. This trend of reduced modulus towards the centre of the pulp, could be due to the odontoblasts at the periphery of the pulp providing some mechanical stability to the soft tissues due to the odontoblasts being anchored into the dentine. This cannot be a consequence of the preparation of the

tooth slice for force mapping, as sufficient silicone was placed under the slice to adequately support the pulp. Odontoblasts are known to be mechanosensitive cells (213,214), reacting to thermal and osmotic changes, however this is the first time that the potential role of odontoblasts as mechanically stabilising cells within the dental pulp has been proposed. It has been hypothesised by Milos, Peters and Daly, that the tight odontoblastic rimming of the pulp and the continual deposition of dentine causes "increased mechanical compressive stress" and creates a "unique anatomical niche". This, they suggest, leads to a situation where the mechanical stresses at the odontoblast layer causes an inhibition in mitotic activity (215). Although at the time of force mapping the odontoblasts would likely be non-vital, their anchoring effect keeping the pulp attached to the dentine would still likely be a factor affecting the elastic modulus of the pulp as determined in this work. An alternative hypothesis relating to this is discussed by Kabartai *et al.*, who suggest that the pulp "suffers from a static compression because of the continuous formation of secondary dentin" (216), and argue that any increase in tissue pressure "can remain located within the part of the pulp where it was raised without spreading to involve the whole pulpal tissue", in essence the increased tissue pressure may be causing a localised increase in elastic modulus at the coronal aspect.

In-keeping with these hypotheses of increased mechanical stress due to the close proximity of the odontoblasts, the elastic modulus in sound teeth at Site 1 (which would be the area of the odontoblasts and/or just inferior to them) is higher than that of carious teeth at Site 1 (Table 4.3.1 1). If the odontoblast layer is disrupted due to odontoblast death from caries, it would stand to reason that the mechanical stress may reduce at Site 1, likely reducing the elastic modulus too. This reduction in mechanical stress could incite the proliferation of odontoblasts to seal the pulp if Milos, Peters and Daly's hypothesis on the tight proximity of odontoblasts in sound pulp preventing mitosis is correct (215).

The results of the AFM elastic modulus measurements of the dental pulp are generally significantly higher than those reported by other authors conducting bulk uniaxial compression on the pulp (149,150) (~5kPa compared to ~116kPa – the latter being the overall median of all AFM values from this work). This is likely due to the different modality of testing and maintaining a dentine encasing for testing by using tooth slices (as discussed in Section 4.1.1). From the literature, it is not uncommon for elastic modulus figures to vary with different modalities of testing (134,217,218). Heterogeneity at the micro- and nano- level will not be detected with bulk testing, whereas AFM will detect these differences and as such complex materials and biological tissues may have differing results depending upon the testing modality (134). Measurement at the microscale for biological samples does often produce larger elastic modulus values than at the macro scale (139,219). There is a general paucity in the literature of evaluating different mechanical testing methods on *ex-vivo* biological tissues, this area is however discussed in more depth in a paper by Akhtar *et al* (219), who demonstrate how the length-scale of

measurements of tissues (macro scale) over tissue components (micro scale) and individual proteins and molecules (nano scale) will result in increasing elastic modulus measurements, respectively.

The elastic modulus being much higher than expected (i.e. in comparison to the bulk modulus results from the literature) could draw into question whether dentine had been sampled at the coronal aspect and floor of the pulp, but the elastic modulus of dentine is typically in the region of 2.3 GPa (2300000 KPa) for peritubular dentine and 0.5 GPa (500000 KPa) for intertubular dentine (148), making this implausible. We do not know the elastic modulus of predentine, so it is difficult to determine whether some predentine was included in the measurements, but osteoid (which may be similar to predentine) has an elastic modulus around 200-300kPa, which could fit with some of the measurements at Site1 (220). The other sites have median elastic moduli figures matching that of kidney through to muscle (220).

As the AFM nanoindentation was conducted with only a slice of the tooth, the pulp was not fully encased as it would be *in-vivo*, therefore it is very likely that the elastic modulus is actually underestimated due to the disruption of the three-dimensional odontoblastic rim around the coronal pulp.

Contrary to what is sampled at Sites 1 and 2, all the other Sites (3, 4, 5, 6 and 7) (Table 4.3.1 1) have higher moduli in carious teeth and this difference is most notable towards the centre of the tooth (Site 4 has >2x difference between carious and sound medians). This suggests that the coronal aspect of the pulp, compared to all other areas is behaving differently. It is possible that inflammatory changes throughout the pulp are causing a general increase in the elastic modulus throughout carious teeth (explaining the difference found between the two states), but the disruption of the odontoblastic layer in carious teeth is leading to a reduction in modulus locally.

As previously mentioned, carious tooth 4 showed a higher elastic modulus at site 5 than at sites 4 and 6, which bucks the general trend of a lowering of the elastic modulus towards the centre of the pulp however this tooth had a large pulp stone present (see Figure 4.4.1 1). Pulp stones are theorised to have similar aetiology to tertiary dentine deposition and potentially the increase in modulus here and the subsequent calcification goes some way to supporting the idea that increased modulus of the pulp tissue is having some impact on dentine deposition (221) .

There is a rise in the elastic modulus around sites 6 and 7 found in most of the teeth. As odontoblasts are not found at the base of the dental pulp, they cannot be attributable to this finding. From assessing the collagen bundles in the pulp (Section 4.2.2), the bundles tend to run in parallel to the dentine at the edge of the pulp and are less organised towards the centre. It is possible that the elastic modulus trends seen at sites 6 and 7 (and indeed sites 1 and 2) are entirely caused by the organisation and orientation

of the collagen bundles of the pulp – both in carious and sound teeth. This is explored further in Sections 4.3.2 and 4.4.2.

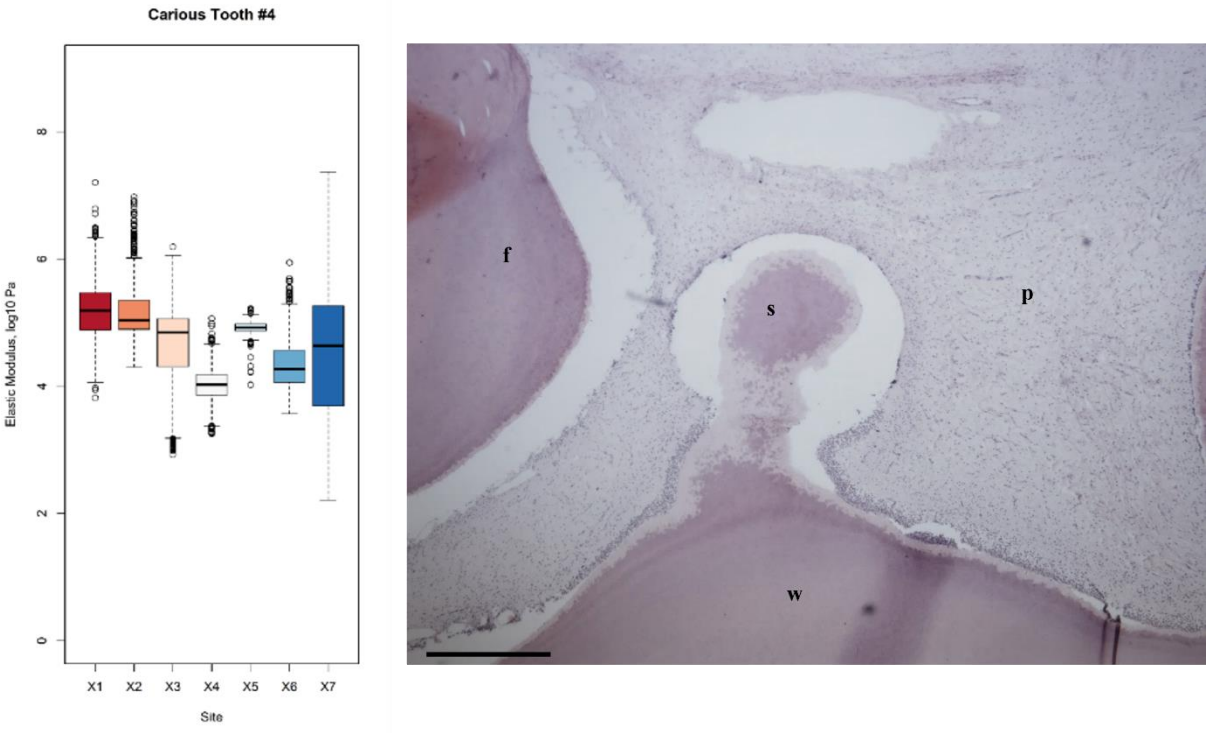

Figure 4.4.1 1: Histology of the pulp for Carious Tooth #4, s=Pulp Stone, p=Pulp, f=Floor of Pulp, w=wall of pulp, scale bar=250µm and the boxplot for Carious Tooth #4 AFM elastic modulus results (medians with interquartile ranges plotted), X1 = Site 1, most coronal, X7 = Site 7, pulpal floor

There has been much discussion in the literature about the location, number, biophysiology and biophysics of dental pulp stem cell niches. There is also no defined and agreed panel of DPSC markers to identify the niche(s) with immunohistochemistry, likely due to the presumed heterogeneity of DPSCs (222) . It is currently thought that there are numerous DPSC niches across the dental pulp and that these are associated with the capillary and neural network towards the centre of the pulp and in the cell rich zone (222,223), which would roughly correlate with sites 4-5 and sites 2-3 respectively in the data presented here. Sites 4-5 have the lowest elastic moduli for both carious and sound teeth; it could therefore be that these areas have some resistance to mechanical change caused by inflammation and tissue damage, possibly aiding in the maintenance of a pluripotent stem cell population. This theory has been discussed in a review by Al Madhoun *et al*., who state "DPSCs are mechanosensitive cells by default with the capacity to recognize mechanical signals and transform these stimuli into various cellular responses to sustain niche homeostasis" (222). It is possible the DPSCs in these areas are locally resisting the mechanical changes due to caries and as such are the cause behind the downward trend in elastic moduli maintained in carious teeth after they have been altered by caries. In further support of

this is the fact that DPSCs remain able to differentiate even in irreversible pulpitis, suggesting some resistance to surrounding inflammatory changes, including mechanical changes (224).

It is generally agreed that stem cell niches have certain characteristics, such as; tissue-specific and more generic cell populations, cell-cell interactions dependent on tight regulation and cell-cell contact, self-renewal and polarity determined by membrane-bound and secreted factors (e.g. Wnt and Notch), immune privilege, specific physical parameters influencing differentiation and maintenance and altered environmental factors (such as hypoxia) (222,225). Stem cells within and without their niches depend upon cues from their environment to proliferate, remain quiescent or differentiate, and these cues can be biochemical or physical. It is clear from the AFM data that there is a difference in the biomechanics at different sites of the pulp, with an increase in the elastic modulus in carious teeth towards the centre of the pulp when compared to sound teeth. This increase in elastic modulus at the centre of the tooth may affect the DPSC niches, leading to a localised increase in modulus around the DPSCs. Notably, it has been shown that an increased elastic modulus facilitates DPSC proliferation and differentiation down a hard tissue lineage (26,226), and this localised change may be having an effect *in-vivo*, playing a role in the proliferation of DPSCs and the cytological differentiation necessary for reparative dentine formation.

The increase in elastic modulus of pulp around the centre of carious teeth, as compared to sound teeth, may also be facilitating the migration of DPSCs out of their niche via durotaxis, as has been shown in fibroblasts (227) and other mesenchymal stem cells (228), where cells move from a soft substrate towards stiffer substrates. However, recent work has suggested that for DPSCs this may not be the case and the migration of DPSCs is not affected by different substrate elastic moduli (229). The work by Ehlinger *et al.* also found that DPSCs migrated with greater speed on softer substrates than harder substrates, linking this finding to focal adhesion size (229). It could be that the softer modulus of the most coronal pulp in carious teeth may be facilitating a quicker migration of DPSCs to the area of injury ready to differentiate into odontoblasts and begin reparative dentine deposition. These findings are also mirrored by the fact that there are fewer areas of statistical difference across the dental pulp in carious teeth, suggesting greater homogeneity across the pulp and a less marked drop in the modulus towards the centre of the pulp when compared to sound teeth (see Appendix 8). In essence, the homogeneity may be facilitating DPSC migration and differentiation in carious teeth by reducing gradients for the DPSCs to migrate through. Another explanation for there being more sites with a statistically significant difference in sound teeth would be that the healthy pulp contains numerous mechanically-defined ‘compartments’ (including compartments for DPSC niches), similar to the zones identified histologically, and when a pulp becomes inflamed the whole pulp is affected bringing in dysregulation of these discretely maintained environments, and as such loss of the compartmentalisation. Furthermore, it could be a combination of these two scenarios as they are not mutually exclusive.

Interestingly, the range in elastic modulus values is greater for carious teeth than sound teeth and this is true across most sites. With inflammation comes a mixed leukocyte population and inflammatory changes, such as angiogenesis, collagen breakdown, hard tissue formation and necrosis, which most likely reflects the greater range demonstrated for carious teeth compared to sound teeth.

A considerable confounding variable in these results is the age of the patient. With increasing age, the pulp size decreases due to the deposition of secondary dentine over time, which may affect the elastic modulus of the overall pulp and specifically the elastic modulus at the odontoblast layer (if the hypothesis by Milos, Peters and Daley (215) is correct). In addition to secondary dentine deposition, it is widely believed that pulpal collagen thickness increases with age (207), which again could lead to an increase in the elastic modulus of teeth from older patients. This work did not find any convincing correlation between age and the elastic modulus of the dental pulp, however the patients who submitted samples did not have a large age range (only one patient was over 50 years old), limiting this conclusion. With increased samples from patients of varying ages, any effects of age on the elastic modulus results could be better identified.

Another challenge with this work is the individual variability of teeth. The morphology of the tooth (and the pulp) is influenced by genetic, epigenetic and environmental factors which cannot be mitigated against in this study, without vastly increasing sample size (230). Specifically, the distance between each site on each tooth varied between 0.1 to 0.3mm to ensure that 7 FVMs could be produced per tooth. This may mean, for example, that Site 3 on one tooth will not be in the exact same relative location as Site 3 on another tooth. This variation was minimised as much as reasonably practicable by measuring the length of pulp and determining a reasonable interval for each FVM in each sample. FVMs are however a powerful tool in the armamentarium of scientists exploring mechanical properties over large areas (as is often the case when looking at *ex-vivo* tissue), each pixel/point contains information on the height of the sample surface, the adhesion at that point, the elastic modulus and indentation depth. This allows for images to be created to elucidate changes in mechanical and topographical parameters relative to other areas. The drawback of FVMs is that they are time-consuming to produce (each tooth in this study typically took between 10-16 hours to gain seven FVMs) and it can be difficult to create large FVMs over surfaces with a large z-range as the piezo stage can only compensate for a small degree of topographical height change before the AFM head height needs to be altered.

The disease status of the tooth is also an important consideration for this work. For all carious teeth used for AFM, extensive (i.e. dentine) caries was present, however no attempt was made to quantify this. This is a drawback to the study as it makes it impossible to link the changes in elastic modulus observed in carious teeth to the degree of caries present. For this work, the number of carious and sound teeth (n=7 for each group) was too small to conceivably produce a meaningful outcome for correlating

the degree of caries to the elastic modulus of the carious pulp. With greater numbers of teeth, this is something that could be explored in more depth.

The statistical individual variability of the teeth was accounted for in this work by use of a linear mixed-effects model approach. When comparing the overall elastic moduli of all carious vs all sound teeth, the variance of the individual tooth accounted for only 2% of the variance in the overall results, resulting in an insignificant difference. Similarly, when performing the analysis of site comparison between carious and sound teeth (i.e. comparing carious site 1 to sound site 1 etc.), the variance accounted for 2-6%. Although the variance is small, over such a large number of observations, this amounted to a large effect on the results, as simple statistical tests not accounting for the individual tooth variability resulted in statistically significant outcomes (for example, when a Wilcoxon rank-sum test is completed on comparing the same sites between carious and sound teeth, statistically significant outcomes are returned for all sites) whereas the multi level linear mixed effects model only returned one statistically significant comparison (comparing Site 1 in carious to Site 1 in sound teeth, Table 4.3.1 1). It is important to realise that the elastic modulus values for each site cannot be considered as isolated measurements because each site is within a single sample (i.e. one tooth), and as such simple statistical comparisons will not take into account the multi-level or nested effect of the data. The linear mixed effect model does have one key limitation; it is designed to work on parametric data, when the data for AFM analysis of the dental pulp is non-parametric. That being said, Schielzeth *et al*. explored the effects of different distributions of data on the model and found that the effects of distributions other than normal were small and that the model is very robust against violations of its assumptions (231).

Figure 4.3.1 4 demonstrates the variable topography of the dental pulp in two teeth. It would be tempting to assume the heterogeneity displayed in these FVMs correlates to specific pulpal structures (e.g. blood vessels, nerves, individual cells etc.) however, this cannot be confirmed without linking the tissue slice used for AFM with histology and knowing exactly where a FVM has been taken from. As previously discussed, the FVMs would be in different locations in each individual tooth, making linking to spatial histological features of the nm scale spurious. Compounding this further is the fact that the tissue slice was glued to a glass slide, making histological preparation and assessment after AFM measurements impossible. It is also important to consider that the sample preparation may be the cause of differences in topography (e.g. due to the blade used in the Accutom). Because it is impossible to link the topography to specific micro and nano-level structures, and the difficulty in excluding sample preparation as a potential cause for the surface level topography, these have not been assessed further and the images have been included only for interest and as a demonstration of some of the FVMs completed in this work.

As only molar teeth were used in this study for AFM, this work can only confidently be generalised to molar teeth. Molar teeth were selected due to the large pulp chamber size, and because they are the type of tooth most commonly extracted. No specific molar tooth type was selected (for example first molar, second molar or third molar) because this would have significantly limited the number of samples available for this project. It is likely that the trends demonstrated here (specifically; a reduction in the elastic modulus towards the centre of the tooth, a higher elastic modulus in sound teeth at the coronal aspect and a greater range in elastic moduli in carious teeth) would also be found in incisors, premolars and canines, but this cannot be proven without further work and the elastic modulus values could vary by tooth type. Pertinent to this is also the different morphologies of premolars, incisors and canines, compared to molars; if the odontoblast layer is having an effect on the elastic modulus, it stands to reason that the morphology of that layer may also affect the results. As has been shown by the results of the linear mixed methods model accounting for tooth individuality, even slight variance can have a large effect on the overall outcome.

None of the sound teeth used for this work had restorations present. This was deliberately chosen because the iatrogenic changes to the pulp secondary to cavity preparation and changes due to caries or trauma may have impacted on the pulpal mechanobiology (for example scarring from historical injuries).

In teeth where caries was present, the FVM measurements were made of the pulp inferior to this to provide elastic modulus measurements most pertinent to pulpal changes secondary to caries. It would be interesting to conduct a full study of the elastic modulus of the whole pulp in both carious and sound teeth because this may elucidate further information on the location and biophysical nature of the DPSC niche(s), and give more insight into the physical changes occurring in the pulp at a micro- and nano-level that may be influencing the behaviour of the cells. This may help with answering further questions that remain unanswered from this work – for example, with odontoblasts being at the lateral aspects of the pulp chamber, is the elastic modulus high here too? Does the elastic modulus vary over the root canals? Does the elastic modulus vary near blood vessels and nerves? Is the DPSC niche a unique area mechanically? Using AFM integrated with light, fluorescent or light sheet microscopy may be a way to facilitate this for future work. However, the optimisation of this technique on sufficiently thick, fresh, tissue slices would be difficult to accomplish, coupled with the time-scale involved in embarking upon such a feat; these challenges make the feasibility of this proposed work unlikely.

As the coronal pulp generally had the highest elastic modulus in each tooth, it is likely that the odontoblasts here are providing some mechanical stability. However, pulp stones and the floor of the pulp are not rimmed by odontoblasts. This means that the increase in modulus in these areas, as seen by the increase in modulus in Carious Tooth #4 adjacent to the pulp stone and the general finding of an

increase in elastic modulus at the floor of the pulp (site 7), must be due to something more than the odontoblasts providing mechanical stability to the pulp. As discussed later, the collagen bundles of the pulp may be the reason behind the increase in modulus at site 7.

4.4.2 HISTOMORPHOMETRIC CONFOCAL MICROSCOPY DISCUSSION

One key outcome of this work is the mapping of the collagen fibres in the dental pulp, and for the first time attempting to correlate these to mechanical changes seen in carious teeth. Although there are limitations to this work (explored in more depth below), several statistical differences have been identified in comparing carious and sound teeth and it is entirely possible that some of these may link to mechanical changes at the nano / micro level and with gene expression.

In exploring the differences between the sites (CP, MP and FP), it is clear that CP and FP are not very different from each other, and this can be seen qualitatively by examining the images in Appendix 13, and quantitatively in Tables 4.3.2 1 – 4.3.2 10 . Appendix 13 demonstrates all 240 images acquired in grayscale form. This trend is more marked in sound teeth than carious. For both the CP and FP, the fibres at these points run perpendicular to the dentine, and vessels in the pulp are known to follow this course (with collagen fibres running parallel (161,232)). The trend of CP and FP being similar is mirrored by the AFM elastic modulus data, as Site 1/Site 2 and Site 6/Site 7 had relatively high elastic moduli compared with other areas of the pulp.

MP appears to be the most different of the other sites, and again this correlates with the AFM data, with sites 3,4 and 5 having lower elastic moduli than the other sites. When inspecting the MP images (Appendix 13), the fibres in this area are more randomly orientated, generally sparser, and finer in appearance. This is more conspicuous in carious teeth and is validated by the quantitative findings of; statistically thinner fibres, statistically fewer fibres, statistically lower amount of fibres, and statistically less orientated/aligned fibres from the measurements taken, comparing MP to FP and MP to CP. Though less pronounced, this trend of MP being very different to FP and CP is still demonstrated in sound teeth, as the comparisons of MP vs FP, and MP vs CP, show more statistically significant differences than the comparison of CP vs FP in sound teeth. Again, this suggests that the pulpal core may be a distinct compartment of the pulp, as discussed in the AFM section (4.4.1), with specific mechanical characteristics, likely due to a distinct micro-environment. As the changes in the MP of carious teeth suggest less collagen is present, this raises the possibility that the proteinases in caries reach deep into the dental pulp, affecting more than just the coronal aspect and are causing soft tissue changes to the pulpal core. However, what bucks this trend is the fact that carious teeth had a higher elastic modulus than sound teeth for the core of the pulp (Sites 3/4/5 from the AFM data). The reduction of fibres, but increase in modulus makes it possible that the change in elastic modulus is more likely due to the structure and type of fibres present rather than the size and amount. For example, some of the fibres stained in the sound MP may be ones with a low elastic modulus, such as tenascin, laminins, collagen

III or fibronectins, and are more easily degraded by proteinases but as part of the pulpal response to healing, these are being replaced by fibres with higher elastic modulus, such as collagen I, so the fewer fibres present in the middle of carious pulps have a higher elastic modulus than the numerous fibres in sound dental pulps. Little work has been completed on the elastic modulus of individual extra-cellular matrix components, but it has been demonstrated that when assessing hybrid gels of collagen type I and collagen type III, the elastic modulus increases with collagen type III content up to 20%, but beyond this the elastic modulus drops (233), showing that the ratio between these fibres does have an impact on elastic modulus; further work on the elastic modulus of individual ECM fibres would be useful to better understand cellular environments and their mechanics. In-keeping with this theory of an altered ECM matrix component affecting the elastic modulus and fibre morphologies demonstrated, Martinez *et al.* found a significant reduction in tenascin, fibronectin and collagen III in the inflamed pulp compared to sound (159), and collagen III has a smaller width than collagen I (232), which fits with the width data trends (fibre width is greater in carious teeth). This is something that could be investigated further with differential staining of the different soft tissue components and structures of the pulp. An alternative hypothesis for this would be the alignment/organization of the fibres at this site being the factor behind a higher modulus in carious teeth than sound; although not statistically significant, a higher coherence value was identified for carious teeth. Either way, the fibrotic response to the inflammation may be creating an environment more conducive to DPSC migration and potentially differentiation, but this would require further investigation by exploring DPSC migration on scaffolds mimicking the ECM of the pulp from a carious tooth to better understand this process.

As mentioned in the AFM discussion, the disease status of the tooth is also an important consideration. No attempt was made to quantify the degree of carious ingress. This is a drawback to the study as it makes it impossible to link the changes to the fibres observed in carious teeth to the degree of caries in each teeth. With greater sample numbers, this could have been achieved.

There are some disadvantages to the methods employed in the collagen bundle analyses using confocal microscopy, and these are outlined below.

Firstly, eosin stains many structures within the pulp (red blood cells, cell cytoplasm, vessels and nerves to name but a few), therefore this analysis has likely overestimated the amount of collagen present; in essence the eosin stain lacks specificity. However, Marcos-Garcés *et al.* (155) found eosin to be as good as differential stains, such as Masson's trichrome, for distinguishing collagen banding for analysis in skin samples. The advantage of eosin over Masson's trichrome is that eosin fluoresces, making it suitable for fluorescent confocal microscopy. Immunohistochemistry (IHC) may have been another option for differentially staining collagen. The drawbacks of IHC are that it is costly, difficult to perform on decalcified dental tissue, and would only identify the antigens specific to the type of collagen the antibody is designed for (e.g. Type I, Type III, Type IV etc.). To differentially stain specific ECM

structures with IHC would mean multiple assessments on the same section ('multiplexing') to give a 'total view' of all of the fibres that may be contributing to a change in the elastic modulus – adding a further level of complexity. Skin, similar to pulp, is predominantly comprised of collagen (6), so it is reasonable to believe that similar methods can be employed in the collagen analyses for both. Furthermore, as collagen is the main component of the dental pulp, the eosin staining will mostly come from this protein. The work herein mirrored the work by Marcos-Garcés *et al*. (155), but it is a marked and recognized limitation of this research that vessels and nerves have not been differentially stained; an issue not raised in the discussion of Marcos-Garcés *et al*.'s work, despite vessels and nerves being present within the dermis. Other works have utilized eosin for confocal image analysis of soft tissue fibre arrangements (such as (154,172,234)), demonstrating that this is a well-utilised technique within the literature.

For this work, confocal microscopy was chosen to give the best resolution of the fluorescent fibres possible. As discussed in the materials and methods (4.2.2), this form of microscopy offers higher resolution than traditional fluorescent microscopy, ensuring the most accurate measurements possible.

Immunohistochemistry (IHC), with fluorescent dyes (immunofluorescence (IF)), or regular chromogens (such as DAB (3,3′-Diaminobenzidine)) would have been beneficial to differentiate between vessels, nerves and collagen bundles and this was attempted, but could not be accomplished on the tooth tissue – numerous parameters were explored to try to get this working, including; different antigen retrieval methods (protein (including different enzymes) and heat (including different buffers)), different incubation times, antibody concentrations, temperatures and differing blocking times and agents. IHC did work on tissue microarrays (positive controls) but would not work on the experimental tissue. After much consultation on the matter and exploration of experimental variables, it seems likely that the tissue was not perfused quickly enough with formalin to preserve the antigens for IHC. Based on the fact that it may have been up to 24 hours between extraction of the tooth and exposure to formalin (as most teeth were kept fresh for AFM prior to sectioning), it does seem plausible that this is the reason behind the IHC not working. Without differential staining of the structures in the pulp, it is very difficult to determine whether certain structures are vessels, nerves or collagen bundles. However, it is important to note that it is unlikely that the majority of fibres analysed were capillaries as the median widths of the bundles were 0.9 µm and 0.8µm (for carious and sound teeth respectively and the modal value for both was 0.3 µm), which are much smaller than the width of capillaries, which are typically ~ 9µm in width in the pulp (171). The thickness of a capillary walls is approximately 0.5µm (235), which could fit within the general ballpark of the measurements of the fibres assessed in this study; if the capillaries have been sectioned transversely, these could contribute to the overall fibre counts and measurements, and this possibility cannot definitively be excluded, though it seems unlikely that transversely cut capillaries could be making a marked contribution to the fibres analysed. Peripheral nerves vary in size from 7-12µm in the pulp, which also excludes the possibility that these fibres may be nerves (171).

Overall, eosin staining for this part of the project, despite its recognized limitation of poor specificity, has proved to be an acceptable, simple and time-efficient method for collating information regarding collagen distribution in key areas of the pulp that could then be correlated and compared with the AFM spatial information.

Secondly, as the whole pulp was not subjected to image analysis, the images may not be truly representative and are open to sampling bias. As fifteen individual images were taken of each tooth, the effects of this are likely to be small, but not inconsiderable. Whenever samples are taken, a balance needs to be reached between practicality (i.e. time in data preparation, acquisition and analysis) and gaining enough information from the experiment. As some statistically significant differences were identified in this work, it is likely that the number of images was indeed sufficient. However, more statistically significant outcomes may have been achieved with more images, more detailed exploration of parameters (for example, more transects when exploring the width and number of fibres) and more teeth to assess. As previously described, the collection of teeth was hampered by the global pandemic, and further teeth would have been beneficial to this project, though the time constraints of a PhD would have made analysis of significantly more teeth difficult.

Thirdly, for the Fourier Orientation macro, measurements of widths and measurements of the number of fibres performed, the image is simplified by removing the lesser-fluorescent areas (as part of the 'thresholding'). This would result in loss of fine detail, which may include small collagen fibres, and fibres not fully in the focal plane. It was necessary to threshold images to clearly delineate boundaries of fibres and sheets to glean understanding of the overall trend with regards to orientation of the fibres, but this will have resulted in some lost information with regards to smaller fibre orientation. When comparing some of the images between the original and the thresholded image, this is unlikely to have made a significant difference to the overall outcomes (see Figures 4.3.2 1 and 4.3.2 2). In addition to this, once the image has been Fourier transformed for the Fourier Orientation macro, only the central core is used to provide measurements for the orientation of the fibres – this excludes smaller, finer fibres from the analysis, focusing solely on the larger, more fluorescent fibres to give the orientation of the larger collagen structures. Again, this will result in some loss of information as background trends of smaller, less fluorescent fibres will not be included in the analysis - a copy of the inverse Fourier transform image is available in Figures 4.3.2 1 and 4.3.2 2 to demonstrate how the exclusion of smaller fibres outside of the central 'core' of the Fourier transform plot results in an image that displays the general orientation of the fibres. The advantages of this method are that the whole image is assessed, rather than relying on 'regions of interest' or transects, though the disadvantages are sufficient that it is prudent to consider using other methods with the Fourier Orientation macro (such as the OrientationJ plugin, which uses a completely different algorithm for orientation analysis) to provide more rigorous and reliable outcomes. It is important to realize that the two macros do measure different things, as the OrientationJ plugin assess the amount of fibres that follow the same direction i.e. that are 'coherent'

and expresses it as a ratio, whereas the Fourier Orientation macro provides a ratio for the orientation of the most prominent fibres in an image, so the two macros taken together probably provide a more detailed quantitative assessment of the alignment and orientation of the fibres in an image than either measurement taken alone. This being said, the methodology of utilizing Fourier transform to give a measurement of orientation has been used repeatedly in the literature, justifying its use herein (154,155,234).

For width measurements and measurements of the number of fibres, where collagen bundles overlap in the images, they would be wrongly counted as one fibre/bundle and possibly be considered wider than each separately, and some tortuous fibres would be counted more than once along one transect. However, as stated previously, the images are incredibly detailed, and there is no set methodology employed in the literature for this analysis. Ultimately, there needs to be a balance between loss of detail and ease of turning qualitative visual data into numeric data for quantitative analysis.

Looking at the images in a qualitative manner (Appendix 13), visually there appears to be some difference between the floor, middle and top of the pulp with regards to fibre orientation, and density, and this has resulted in some statistically significant differences numerically. The area of pixels and width of fibres both reduce towards the centre of the pulp and the fibres become less aligned; this is true for carious and sound teeth and mirrors the fall in elastic modulus towards the centre of the pulp identified in the AFM results. It is quite interesting that the trend of elastic modulus reducing towards the centre of the pulp links with the trend of a reduced width of fibres, area of fibres and reduced alignment of fibres from the histomorphometric analysis. It is entirely probable that the reduction in elastic modulus is at least associated with, but more likely caused by, this histological trend.

As the coronal aspect of the pulp is the area that is first (and as such most markedly) affected by caries, it stands to reason that this area is statistically different in carious teeth, with more aligned fibres present at this site in carious teeth than sound, and a smaller volume of fibres present (area stained %) than sound. This increase in alignment of fibres would fit with scarring mechanisms, as collagen fibres become more organized in scars (236).

An important confounding factor to add to this discussion is the fact that the cell-rich zone (where the coronal images were taken from) contains a capillary network that runs perpendicular to the dentinal tubules and it is entirely possible (and in some images very probable) that a reasonable proportion of the fibres identified in this analysis are in fact blood vessels. Studies have stated that collagen fibres (and nerves) in this area run parallel to these capillaries (232). Whether collagen fibres, nerve fibres or capillaries, it is likely that the increased volume of structures present in this site in sound teeth is the cause behind a higher elastic modulus value. Collagenases (such as the MMPs), oxidative damage and necrosis could all be plausible candidates behind the lower volume of fibres and lower number of fibres present in carious pulps. In linking the changes at the coronal aspect to the findings of the AFM data,

the histomorphometric CP area would likely fit with sites 2/3 in the AFM data – these areas have a slightly increased elastic modulus in carious teeth (not statistically significant), and it is possible that at this site, a mix of factors is impacting upon the mechanical properties; firstly, the loss of the odontoblastic rim is causing a reduction in the elastic modulus, simultaneously the increase in organization of the fibres at the CP is causing an increase in elastic modulus values, thus the overall change in elastic modulus becomes negligible – hence the lack of a statistically significant difference in elastic modulus at sites 2/3 despite differences at CP noticed between carious and sound on histomorphometric analysis.

Interestingly, the collagen fibre number analysis showed a statistically higher number of collagen fibres in sound teeth, and this is mirrored by the area of pixels. Again, the collagenases and proteinases present as part of the inflammatory process in carious teeth may be the cause behind this difference. The lower number of collagen fibres and overall collagen volume (area of pixels stained) could be beneficial in assisting with DPSC migration towards the coronal aspect of carious teeth, as the cells could move through less-dense networks to reach the area of injury, and in the migration of immune cells as part of the body's defense against caries (237). Partially degraded collagen has been shown to facilitate quicker migration and adhesion of pre-osteoblasts, and it is possible that the degradation may be helping the migration and adhesion of pre-odontoblast-like cells in reparative dentinogenesis (238). Denaturation of collagen exposes RGD binding sites which would facilitate cell adhesion and migration (239), so the breakdown of collagen may be integral to the healing and reparative mechanisms of the DPC.

With wound healing, collagen becomes organized into parallel, thick fibres (236). Although the results demonstrate some increase in fibre orientation and alignment in carious pulps, there is no statistically significant increase in fibre width when comparing carious and sound teeth. As healing occurs, the collagen fibres (generally) become organized prior to accumulating into thickened bundles as the tissue becomes scarred – it is highly plausible that the carious teeth in this study were extracted before thickening occurred, explaining the lack of any statistically significant difference between the two groups for fibre width (236). However, as part of this process, more collagen fibres are also deposited and there was no increase in collagen fibres found in carious teeth – to explain this, again, it is possible that the proteinases in the inflammation are the predominant driving force behind the changes, outweighing regenerative processes. Essentially, the carious teeth may be all at different points in the inflammatory/regenerative timeline and all experiencing different levels of inflammation, degeneration, regeneration and healing. However, the overall picture seems to be more one of degeneration than regeneration in the carious teeth in this study.

The histological assessment of the tissue in this research has focused upon the soft tissue changes, rather than linking to the type and degree of inflammation present in the pulp, or the level of carious ingress into the dentine. Future analyses could explore this further, however to do so rigorously would require

validation of a scoring system for inflammation assessment (including inter and intra-rater reliability testing) and more than one assessor (and likely numerous levels per tooth). It is possible now with deep learning for digital pathology to conduct histomorphometric analysis (240), however the costs associated with this emerging technology are currently prohibitive.

Accepting the fact that the staining of the images in this analysis will include vessels, nerves and ECM components other than collagen, it has still provided valuable insight into the organization of structures in the dental pulp and changes at a tissue-level from sound to carious. For example, whether the total area stained is due to an increase in collagen, nerves or vessels, there is still a marked difference between carious and sound teeth. Similarly, whether the organizational differences between the structures in carious and sound teeth are due to changes in the collagen, neurogenesis or angiogenesis, there is still a difference found, and this warrants further exploration to better understand the inflammatory process of the carious dental pulp. One way of exploring this further, is to analyse the transcriptomics to assess upregulation/downregulation of genes in carious and sound teeth – see Sections 4.3.3 and 4.4.3 for more information – to see if genes associated with angiogenesis/neurogenesis/collagen/ECM are upregulated or downregulated.

Assessment of the fluorescence of the images would have been a further parameter that could have been explored – this would have given an idea of the density of the fibres and would have been achievable by assessing the grayscale value of the images. However, for this work, the samples were not all stained and imaged in one batch. Therefore, slight variabilities will affect the intensity of the fluorescence (such as how recently the eosin had been refreshed, the gain set on the microscope, the thickness of the DPX (Dibutylphthalate Polystyrene Xylene) mountant and coverslip, and the laser intensity). Laser intensity and the gain were optimized for each image individually and this too may affect some of the other measurements as some smaller fibres may be less visible with less intense laser power or lower gain. This is an issue with fluorescent microscopy in general as it is more qualitative rather than a quantitative measure, and numerous repeats (as is the case in this study) can go someway to mitigate against this because slight variations in gain and laser intensity will have a smaller effect over a larger sample set.

Looking more qualitatively at the images, there do appear to be more ‘voids’ at FP than at MP or CP. This would fit with vessels, as it is known that larger vessels are present towards the bottom of the pulp, generally becoming smaller as they become more branched leading to the coronal pulp. Larger vessels typically have thicker walls. There was no statistically significant difference in width of fibres between CP and FP in sound teeth, but for carious teeth there was; looking at the median and IQR for these results, this is more likely due to changes at CP than at FP. Further supporting this is the case that the FP and CP in sound teeth are not statistically different to FP in carious teeth (p value = 0.098 for CP sound teeth to FP carious teeth). It is entirely possible that some of the differences seen between the sites are due to the thickness of vessel walls. However, if the thickness of the vessels was a significant

contributing factor to the width of fibre measurements, then a decrease in fibre thickness from the floor of the pulp up to the coronal aspect would be observed, when the trend shows a reduction towards the centre and rise again towards the CP. This finding suggests than even if the fibres do include vessels and nerves, they are not the bulk in terms of number of fibres measured in this analysis.

In addition to the larger vessels qualitatively visible in this histomorphometric analysis at FP, larger vessels have been demonstrated towards the floor of the pulp in other studies (171), and as previously stated vessels (particularly capillaries and small venules and arterioles) do have a lower elastic modulus than collagen type I. Site 7 in the AFM work showed a generally lower elastic modulus compared to site 1 (in both carious and sound teeth) and site 2 (sound teeth). Site 6 in the AFM work also showed a lower elastic modulus than sites 1 and 2 (carious and sound) and site 3 (carious). Linking this information with the lack of statistically different findings between CP and FP generally in this Histomorphometric analysis would suggest that the elastic modulus difference between these sites may again be due to the type of fibres making up FP having a lower elastic modulus than those at CP, rather than a difference in fibre number or arrangement. It is probable, based upon existing knowledge from the literature and qualitative assessment of the images presented in this work, that the difference in the elastic modulus between the coronal aspect of the pulp and the floor may be because of sampling of more vessels at a micro/nano level at the pulp floor, rather than a difference in the number/organization of collagen fibres.

A historic study into the collagen fibres of the dental pulp, digested and extracted different collagens and non-collagenous proteins from the coronal, mid and apical portions of the dental pulp in sound premolars and molars, to give a % dry weight for collagen and non-collagenous proteins for each of these pulpal areas (241). Although not completely comparable with the histomorphometric results produced in this work, because the study looked at the apical proportion of the pulp (i.e. in the root canals) rather than the pulpal floor, some interesting trends were found – firstly, the amount of collagen is highest at the centre of the pulp and the amount of non-collagenous proteins are lowest at the middle of the pulp. The number of collagen fibres in this histomorphometric analysis (for sound teeth) does fit with this trend, showing an increase in collagen fibre number towards the centre of the pulp. The fact that there is an opposing trend in carious teeth does suggest that the effects of caries on the dental pulp are having a profound influence on the central core of the pulp.

The issues with the specificity in this work means that the results should be viewed with caution. Although the histomorphometric image analysis does go someway to explain the mechanical changes of the dental pulp, this area could be explored further to draw more definitive conclusions. Recent work has utilized light sheet microscopy (171) to look at the neural and vascular networks within the dental pulp – using this technology to explore the differences in collagen bundles between carious and sound teeth could help to explain the differences in pulp mechanics identified from the AFM work.

4.4.3 RNA SEQUENCING DISCUSSION

Of the 76 differentially expressed reads, only 10 have higher expressions in sound teeth compared with carious; *CILP2, SLC12A8, FERMT1, HTR1A, LAMA3, NOX5, ADAM33, PLA2G2A, TRHDE-AS1* and *CHAD*, and this is further demonstrated by the MA plot in Figure 4.3.3 1. The large difference in genes associated with healthy and carious teeth (indicated by the log2 fold change on the MA Plot (Figure 4.3.3 1) has been demonstrated by previous RNAseq studies (such as (158,184)), and this work goes some way to further confirm the complex molecular changes present in carious teeth.

Collection of teeth for this aspect of the study was greatly hampered by the global pandemic, resulting in a low sample number. Greater numbers of teeth would have given more power to this study and would have likely elucidated more differences between carious and sound teeth, perhaps more closely correlated to the genes with a fold change >2/<-2. In addition, only permanent molar teeth were used for this work, limiting generalisability to all teeth; retrieval of RNA from incisors and premolars was attempted but the yields were too low to facilitate sequencing. This is most likely due to the volume of the pulp being small in incisors and premolars. As sound teeth are less frequently extracted compared with carious teeth, these were more difficult to obtain for this study, explaining the larger number of carious teeth compared to sound. It is not known whether there are differences between primary and secondary teeth at a transcriptional level (as primary teeth exfoliate, it is likely), so these data cannot be generalised to deciduous teeth. It could be argued that pooling the samples together would give greater biomass to the two groups of teeth (carious and sound), making comparisons between the two groups more valid and potentially easier. However, when these samples were prepared (prior to sending to Novogene for library preparation and sequencing), there were 18 samples (7 sound and 11 carious) so it was felt that pooling the samples was not necessary at this juncture; if it was apparent prior to sending the samples that only 9 would be suitable for sequencing and survive library preparation, pooling the samples may have given more power to the differences between carious and sound teeth. That being said, keeping the samples as individual specimens does have some advantages as it allows better understanding of individual variance and allows identification of outliers such as Sample 24 (discussed in more depth below).

Similar to the AFM work, all of the sound teeth used for RNA sequencing were unrestored, removing any possibility that prior restorative work will have impacted upon results.

Having some samples from the same patient (Samples X15 and X16, and Samples X18 and X19) does limit the power of this work as it ultimately reduces the generalisability to the population as a whole as fewer subjects have been included. However, it was difficult to get a large number of teeth for this project and recover a workable amount of RNA from each tooth. The inclusion of more than one sample from an individual may have skewed the results to some degree, as genetic similarity of the samples may lead to an overexpression of certain genes, yet as the marked difference between samples X15 and

X16 demonstrate on the PC plot, this genetic similarity does not appear to have such an impact as to counterbalance the differences in gene expression between carious and sound teeth (Figure 4.3.3 5). Furthermore, it is unlikely that the genetic similarity of two samples would affect the overall trends seen herein, but the statistical significance of some of the differences may have been different. For example, see Appendix 14 which shows the normalised reads for gene *CHRDL2* – Samples X18 and X19 on this plot both show lower reads for this gene compared to the rest of the carious teeth group - it could be that these lower reads skewed the data making the statistical significance of the sound/carious comparison less significant. Another example can be seen in Appendix 15, which shows the normalised reads for gene *S100B*, where samples X18 and X19 have higher reads than the rest of the carious cohort, perhaps making the statistical difference for this gene greater than would have been identified had these samples come from different patients.

To assess the effects of samples from the same patients further, the differential expression was rerun in DESeq2, omitting samples X18 (carious) and X15 (also carious), leaving three sound teeth and four carious. This resulted in 34 differentially expressed genes and within these 34, the 10 genes with the most marked difference between carious and sound as established in the initial DESeq2 output (*CFI, TNR, C1QL1, CLVS2, OPRM1, SLN, TMEM59L, THBS4-AS1, CHAD, C4A*) maintained their statistically significant difference ($p<0.05$). Of the 34 statistically differentially expressed genes in the rerun data, 31 are present in the original 76 differentially expressed genes (these 31 genes are listed in bold in the Table in Appendix 10). The three genes that were identified in the re-run differential gene expression analysis, that were not present in the original output are provided in Table 4.4.3 1.

Gene Name	Ensembl ID	Original p-value	Original log 2 fold change	Re-run p-value	Re-run log 2 fold change
RBP4	ENSG00000138207	0.09	3.4	<0.001	5.0
SHISA8	ENSG00000234965	0.07	-7.0	0.01	-7.2
LOC100131395	Uncharacterised	0.14	2.6	0.02	3.8

Table 4.4.3 1: Genes with statistically significant difference in expression between carious and sound teeth ($p<0.05$) present in the re-run differential expression analysis that were not present in the original data. Re-run data only includes one sample per patient. RBP4 = Retinol binding protein 4, SHISA8 = Shisa Family Member 8.

As the gene name 'Retinol binding protein 4'suggests, the protein encoded by this gene is largely involved in retinol transport, and this gene was upregulated in sound teeth. When exploring the literature around retinol and the dental pulp, retinoic acid was found to have a negative regulatory effect on MMP-2 in the dental pulp, and its upregulation in sound teeth may be inhibiting the effect of MMP-2, preventing inflammatory effects of this molecule on the healthy pulp (242) (please note, there was no log2 fold change >2/<-2 associated with *MMP-2* in either DESeq2 output). A recent paper also found

SHISA8 differentially expressed in their cohort of pulpitis vs normal teeth, and this gene is involved in the non-homologous end joining pathway, pertinent to the repair of double-strand breaks in DNA (243). The difference in the outputs of the two analyses demonstrates the effect of including more than one sample from the same patient on RNAseq NGS data, and how the statistical significance of the results herein should be viewed with some caution.

Overall, the amount of RNA retrieved from each tooth was low. Research has demonstrated that chilling teeth increases the volume of tooth tissue removed, as retrieval at room temperature results in the odontoblast layer remaining attached to the dentine (178) – for this experimental work, the teeth were all refrigerated upon arrival to the lab and prior to pulpal extirpation, and stored in RNALater (Fisher Scientific UK, Loughborough, UK), which has also demonstrated high RNA yields when extracting RNA from other tissues (244). There are two theories as to why RNA yields were poor: 1) The RNALater failed to infiltrate the pulp sufficiently, as discussed by Conde *et al*.(245), 2) The small, fibrous nature of the pulp and subsequent difficulties in fragmenting such tissue resulted in poor RNA yields. To ensure the best possible RNA retrieval in this work, two kits were trialled and the inclusion and exclusion of a lysozyme digestion step – the resultant combination of the ZymoKit (Zymo Research, CA, USA) and a lysozyme digestion used in this research is based upon the higher RNA yields found when using this combination. It is possible that another kit (such as RNeasy FibrousTissue Mini Kit (Qiagen, MD, USA)), or ensuring the sample was consistently stored in a refrigerator after extraction (on clinic prior to collection, the tooth was stored at room temperature) and transported chilled may have resulted in greater yields and thus permitted more samples to be suitable for sequencing. Any future work could include an assessment of different kits and techniques to maximise RNA yields for dental pulps.

The tooth tissue remaining after pulpal removal was not assessed histologically to check for soft tissue remnants attached to the dentine. This is a significant disadvantage as the extent of the pulpal odontoblast layer remaining attached to the dentine fragments cannot be assessed. Horst *et al*.,(246) have shown a difference in the genes expressed between the main pulp and the odontoblast layer using cDNA microarrays, and interestingly they found a marked increase in the number of genes expressed in the odontoblast layer of carious teeth compared to sound. In retrospect, assessment of the remaining hard tissue (as was done by McLachlan *et al*.,(178)) after pulpal extirpation would have been a useful step in protocol optimisation to ensure all of the pulp tissue was being removed – if not all of the pulp was removed, this may explain lower RNA yields for some of the teeth received. If the odontoblast layer was not retrieved, this too may go some way to explain the low reads of genes associated with odontoblasts – such as *DSPP* and *DMP1*, however it must be recognised that odontoblasts as a cell population are a relatively small percentage of the overall cellular component of the dental pulp.

When considering genes associated with tertiary dentinogenesis (for example, *DSPP*, *DMP1* and Nestin), no significant difference was found between the carious and sound cohorts. Similar results were reported by McLachlan *et al* (158). They postulated that this lack of difference was due to only a small reparative response in the teeth sampled and/or upregulation of these genes by odontoblasts is only occurring very locally within the pulp. Again, histological assessment may have helped with exploring this further. Another possibility is that the calcification seen in reparative dentinogenesis is actually dystrophic calcification by fibroblasts, and as such upregulation of genes specific to bone and dentine formation (such as *DSPP*(247)) would not be identified (as previously discussed in Chapter 1) – though this is an unpopular theorem behind tertiary dentinogenesis, some authors do believe this may be the case (16). The work by Galicia *et al*.(248), found that pulpitis with moderate-severe pain was associated with an upregulation in *DSPP*. However, when looking at the overall comparisons of pulpitis (regardless of pain intensity) vs sound teeth, no change in regulation of *DSPP* was found(248); although a direct comparison cannot be made with this work as pulpitis can be caused by many factors (though caries is the most common cause of pulpitis), pain is linked to the status of inflammation of the pulp (249) and more severe pain is related to partial pulpitis with necrosis. As such, it can be inferred by the work of Galicia *et al*.(248), that *DSPP* is upregulated in more severe cases of caries, and it could be that fewer cases of severe caries/pulpitis were included in the work by McLachlan *et al*.(158) and in this research, explaining the differences in *DSPP* expression found.

When examining the total amount of RNA obtained for all of the teeth collected in this study, a statistically significant association was found between patient age and amount of RNA collected (Person's Chi-squared test completed in R, $p=0.049$, with increasing RNA associated with increased age), however the amount of RNA retrieved was not related to whether the tooth was carious or not (Mann-Whitney-Wilcoxon Test, completed in R, $p=0.8219$). The increased RNA yield with age is unusual because the volume of the pulp decreases with age due to secondary dentine deposition. However, this could be explained due to differences in storage; teeth collected via the School of Dentistry's Skeletal Tissue Bank ('Tissue Bank Ethics') were stored in a refrigerator, dry (i.e. without any RNA preservative), and after poor RNA yields were obtained with this method, a separate full ethical application was submitted to obtain teeth directly from clinics ('Project Ethics'). The former method included patients under 18 years of age and the latter excluded patients under 18 years of age. Teeth collected according to the new protocol for RNA extraction and ethics were stored in RNALater as soon as they were extracted, preventing RNAse activity affecting resultant yields. In essence, the observed increase in RNA from more elderly individuals is likely due to differences in experimental procedures caused by a change in ethical approval, rather than a true difference in RNA amounts. Interestingly, age differences may account for some of the clustering of samples seen on the heatmap of most expressed genes though, as Samples X21, X23 and X24 (one group) were from the three eldest patients, Samples X18, X19 and X15 were from the next three eldest and X14, X16 and X17 were from

the youngest, though this is speculative and further work would be required to look at age-related gene expression of the dental pulp. Matching samples for gender and age across the two groups (carious and sound teeth) would have been the ideal scenario for this work, but sample collection was hindered by the global pandemic, limiting sample numbers and making this unfeasible. Larger studies could consider this option in future work. Due to the limited age range of the patients who submitted teeth to this aspect of the work, no firm conclusions can be drawn about the effects of aging on the transcriptional landscape of the pulp in this work.

Although information on patient age and reason for extraction was included in the data gathered at tooth collection as per the ethical approval (Project Ethics), without larger numbers of samples it is difficult to ascertain whether these factors have any bearing on the differential results obtained.

Early optimisation experiments attempted to use only part of the dental pulp for RNA extraction, leaving a slice for histological examination and slice for AFM, however it soon became apparent that the whole pulp was required to yield sufficient RNA for sequencing. Linking the findings directly to AFM data would have been advantageous, as outliers (such as X24) could be explored further, to see if any nano and micro-level differences in elastic modulus, away from the general trends, could be identified. Another parameter that would have been interesting to explore and correlate to the RNA findings would be microbiological assessment of biofilm of the tooth, and explore whether different gene expressions may be associated with different microbial interactions – particularly in carious teeth.

The quality of the RNA retrieved could have affected the results seen in this study. Although the RNA was stored at -80°C after isolation, RNAse-free plasticware and water used throughout RNA extraction and RNAse Zap (Fisher Scientific UK, Loughborough, UK), used to clean all surfaces and equipment during RNA extraction, the RNA Integrity Number (RIN) number (assessed by Novogene) was low for all samples (range: 2.1-3.0). RIN is an assessment of RNA quality and is affected by many factors such as tissue type, tissue environment *in-vivo* (for example, pyrexia prior to tissue removal), time between removing the tissue to RNA stabilisation/cryopreservation, and time from tissue isolation to RNA extraction to name but a few (250). To deal with low RIN samples, many studies use one of (or a mixture of) two methods; 1) Pick a cut-off RIN value, below which samples are not sequenced – this can lead to low quantities of samples in studies and there is no consensus on where this cut-off should be, 2) Employ the assumption that all transcripts will decay at a similar rate (therefore standard normalisation procedures will account for any variation identified in gene expression estimates)(250). For this work, the latter has been assumed. However, work by Romero *et al.*, has suggested that transcripts decay at different rates and that differential gene expression increases with RNA degradation due to different degradation times of different transcripts, and when RIN was included as a covariate in their analysis the differential gene expression dropped. They also found that RNA degradation (and therefore low RIN number) could be the cause of differential gene expression within the same individual (250).

Linking this to the work completed herein, Samples X15 and X16 (from the same patient) had RINs of 2.5 and 2.3 respectively, whereas Samples X18 and X19 (also from one patient) both had RINs of 2.4. It could be that the differences identified between X15 and X16 are due to differential RNA transcript degradation rather than due to the difference of carious vs sound, though this difference is really very small and it is difficult to infer any significant meaning from this difference. The work by Romero *et al*., does specify that transcripts are not entirely lost with RNA degradation and reducing RIN, just that their relative amounts vary with degradation and conclude that "as long as RIN scores are not associated with the effect of interest in the study…accounting for RIN scores explicitly can be an effective approach" for facilitating inclusion of poor quality samples in RNA sequencing studies (250). As the variation of RIN scores was relatively small in this study, their variation has not been accounted for in the analysis, as it is presumed the difference in outcomes will be small. However, more rigorous data analysis could account for the variation in RIN scores and provide more confidence to the results of the differentially expressed genes.

It is possible that time between tooth extraction and RNA extraction may have impacted on the RIN scores achieved. Although RNALater was used to stabilise the tissue retrieved via Project Ethics, it is plausible that the preservative did not penetrate the pulp due to the small apical opening of the root canal preventing adequate perfusion of the tissue (245). As RNA yields from tissue preserved in RNALater were fair (i.e. with teeth obtained via Project Ethics – see Table 4.2.3.2 1), no issues were detected with the RNA isolation technique until sequencing. Snap-freezing the tissue, as has been used previously in the literature (178), could be another option to preserve the pulpal tissues, however due to clinical restraints and the complexities of cross-site working, this was not feasible.

Further compounding the issue of RIN scores in this study is the method of library preparation used for this work. As RNA degradation occurs, less full-length poly-A RNA is retrieved with this method, leading to a library that is more 3' biased than other library preparation methods (such as rRNA removal methods) (251). Chen *et al.* trialled two other methods – Epicentre RiboZero rRNA Removal Kit (MRZH116, Epicentre Biotechnologies, Madison, WI, USA) (processed without the poly-A selection) and Ovation RNA-Seq FFPE System (7150, NuGEN Technologies Inc., San Carlos, CA, USA) to create cDNA, followed by TruSeq DNA Sample Preparation kit v2 (FC-121-2001, Illumina Inc., San Diego, CA,USA), both of which resulted in higher RINs (251).

RIN score seemed to have little effect on whether a sample was suitable for sequencing or not, as Sample X26 had a RIN of 2.6 yet did not survive library preparation, whereas samples with lower RIN scores did.

There is a general lack of consensus in the literature over RNA sequencing analysis tools, and different programmes may result in differing results (201). Although the analysis outputs in this manuscript are readily reproducible using the scripts in Appendix 6 and raw sequencing data, different choices in the

programmes run and different platforms may result in alternate outputs and this is a negative point pertinent to many RNA sequencing analyses, which will continue to be an issue for the foreseeable future.

From the heatmaps and the PC analysis, Sample X24 does appear to be an outlier. This tooth was unusual because it was extracted as part of a mandibular plating following bony fracture, as such the tooth was unerupted and completely embedded in the mandible. All other teeth in this study were (at least partially) erupted. This may go some way to explaining the reason behind the unusual results for this sample.

The DESeq2 package in R, used for the differential expression analysis, utilises by default a Cook's distance cut-off value of " .99 quantile of the F(p, m-p) distribution, where p is the number of coefficients being fitted and m is the number of samples." (252). Cook's distance is basically a way of detecting outliers in a dataset and excluding them if they are beyond a certain cut-off point, to prevent skewing of the data affecting resultant statistical differences. The Cook's distance cut off in DESeq2 resulted in 12316 genes being excluded from statistical analysis. Upon examining many of the plotted counts of these genes, Sample X24 does appear to be the outlier causing these genes to be excluded by the DESeq2 package.

Sample X24 has been retained in the results and analysis as it is a sound tooth and there are only three sound teeth included in this section of the project, and therefore removing it would greatly impact on the power of the data. However, the data was run again in DESeq2 to explore differential expression, with X24 removed. This resulted in 590 differentially expressed genes (padj<0.05) (roughly an eight fold increase in the number of differentially expressed genes) and of these, 28 had a log2 fold change <2 or>-2, with 546 of the differentially expressed genes showing a higher expression in carious teeth and 44 showing a higher expression in sound teeth. When comparing the two outputs (Figure 4.3.3 3 and Appendix 16), it can clearly be seen that the inclusion of X24 has a significant impact on the data, so much so that without the additional safety-net of Cook's cut off provided in DESeq2, it could erroneously be assumed that the results show a greater expression of genes with log2 fold change >2 (associated with sound teeth), rather than the higher number of genes associated with carious teeth. Interestingly, even with the exclusion of Sample X24, a small difference is still seen when Cook's cut off is applied, demonstrating that some outliers still exist even with the exclusion of Sample X24 (Figure 4.4.3 1).

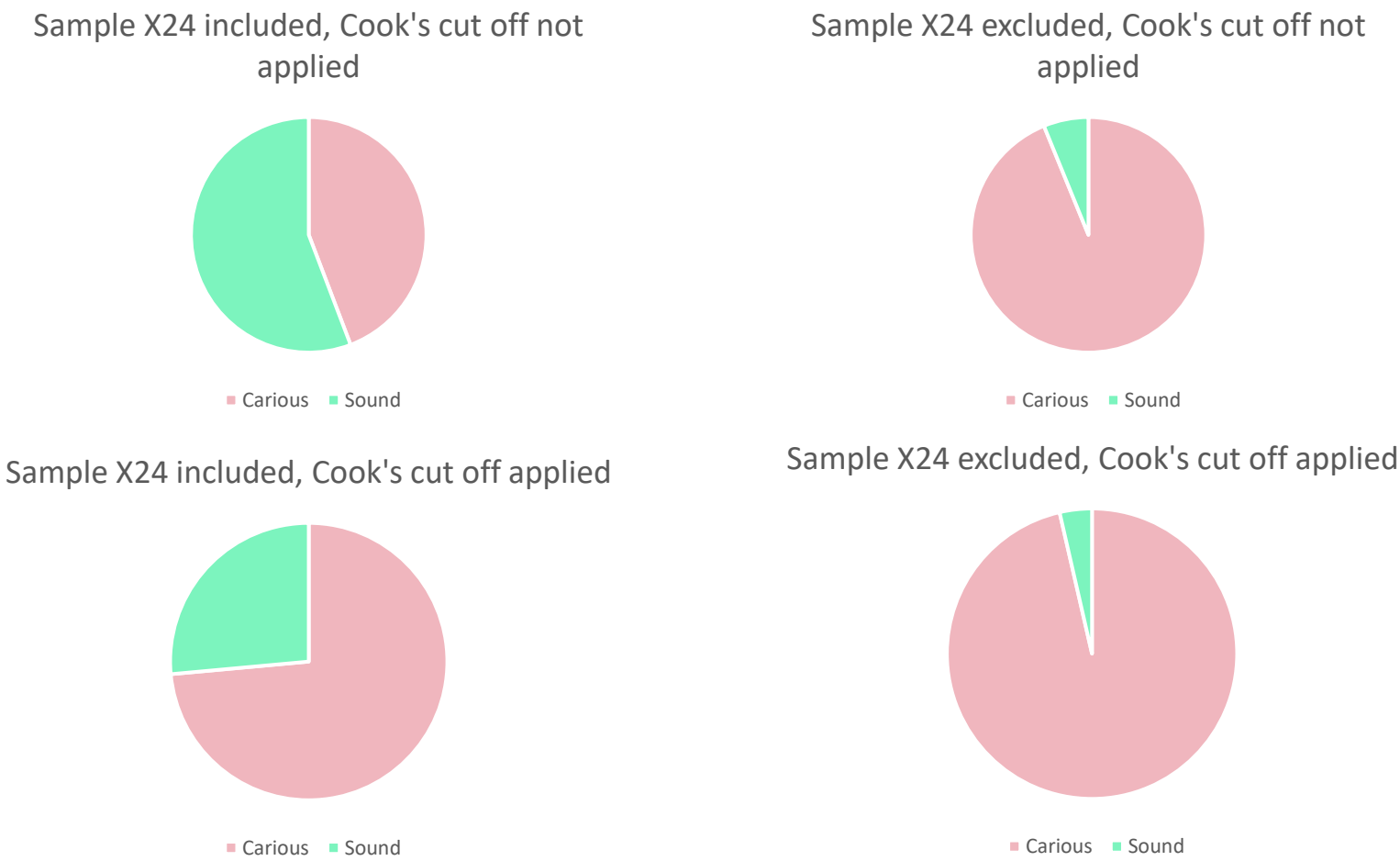

Figure 4.4.3 1 Genes with >log2 fold change, showing the differences in output when Sample X24 is, and is not, included in the data and when Cook's cut off is, and is not, applied. This demonstrates that without Cook's cut off, it could erroneously be concluded that there is a higher number of genes expressed in sound teeth than carious when Sample X24 is included, because of this tooth being an extreme outlier. It also demonstrates that some outliers still exist when Sample 24 is excluded form analysis

Appendix 16 includes a heatmap of the genes with the highest reads when X24 is excluded from analysis. Many genes associated with blood (e.g. *HBA2, HBA1*) are lost from the top 50 expressed genes when X24 is removed from analysis. As X24 appears to be such an outlier, the results with X24 included should be viewed with caution. However, the work by Opasawatchai *et al*., identified genes associated with haematopoietic stem cells in the dental pulp and other similarities with bone marrow, and as X24 was encased within bone, the results with X24 included may not be complete anomalies (184).

When looking in more depth at the genes with the highest expression overall (with X24 included, Figure 4.3.3 2), the most expressed genes within the pulp include many expected genes, such as genes encoding collagens and other ECM components, immune response, and oxygen binding.

The lack of any differential expression in the collagen I genes between carious and sound teeth verifies the paucity of statistical differences in the collagen bundling between carious and sound teeth identified in 4.3.3. Again, the evidence from the RNA sequencing data points to the possibility that the change in elastic modulus identified between carious and sound teeth is unlikely to be due to collagen I bundle restructuring as a result of scarring, inflammation and tissue damage. A lack of differential expression in collagen I genes was also identified in previous microarray studies (see supplementary data from (158), but this is inferred as no mention of collagen I genes is given in the supplementary tables of differentially expressed genes), though the work by Galicia *et al*.(248) and earlier work by McLachlan *et al*.(178), found differential expression of collagens in pulpitis and caries respectively, displaying the mixed outcomes for this in the literature.

As stated earlier, very few papers are available on next generation RNA sequencing comparing carious and sound teeth, with microarray analyses being far more common. A significant and novel feature of this research is the use of NGS for RNA sequencing of the whole pulp and this has resulted in the highlighting of several genes not previously associated with dental pulps in RNA studies (such as *NOX5*, *SPINK5* and *PROM1* to name but a few – see Appendix 10), and led to statistically significant differences in the genes expressed in carious teeth compared to sound.

Linking the findings of the differentially expressed genes herein to the genes identified in the literature of sc-RNA-seq and microarrays, Appendix 10 contains a table correlating the differentially expressed genes from this work with findings from the literature. In summary, most of the differentially expressed genes found in this work were not identified by other studies – this is likely because most of the comparable works utilised microarrays and the sc-RNA-seq work had relatively few differentially expressed genes.

Some of the reads that were determined to be statistically significant included (as previously mentioned) pseudogenes, uncategorised genes and splicesomal RNA reads. Pseudogenes are incredibly common and numerous in the human genome and it is not generally known what role these reads in our DNA

have, but it has been hypothesised that these genes may have a regulatory role in cellular functions by interacting with coding genes (253).

When analysing the literature surrounding the differentially expressed genes and focusing on the 10 with the greatest difference between carious and sound teeth, there is a general paucity of literature discussing the function of many of these genes in the pulp. When examining the literature surrounding these genes, *C4A* has the most research supporting its role in the pulp. Being a member of the complement family, it is actively involved in the pulpal immune response to caries (254). Horst *et al*., (246) explored gene expression using cDNA microarray of the dental pulp focusing on the cytokine network, but found only a marginal increase in expression of *C4A* in inflamed pulps and McLachlan *et al*. (158), found a 4.64 log2 fold increase in carious teeth. When looking further into the work by Horst *et al*., (246) other differences come to light in the genes associated with inflammation, for example their work found that *CXCL12* "was not significantly altered" when comparing carious and sound teeth, whereas this work has found the opposite, with *CXCL12* being significantly upregulated in carious teeth. Interestingly, the work by MacLachlan *et al* did also find a >3 log2 fold increase in *CXCL12* expression in carious teeth (158). The panel of genes studied in the microarray by Horst *et al*., (246) did not include a number of genes associated with inflammation that have shown a statistically significant difference in this research, for example; *CFI*, *C4B*, *COLEC11* and *C1QL1* – all of which are upregulated in carious teeth (this is true for both inclusion and exclusion of Sample X24)), demonstrating the power of NGS to elucidate more changes between conditions than microarrays. Should similar cDNA microarray work exploring inflammation-associated genes in the pulp be conducted in the future, it would be sensible to include the inflammation-associated differentially expressed genes demonstrated in this work. The number of teeth studied by Horst *et al*., (246) was significantly greater than the numbers studied in this piece of research, which may account for discrepancies between the results found by Horst *et al*. (115) and those herein but it is equally possible that the method of detection may be a key factor.

When examining the differentially expressed genes in STRING clusters with X24 removed, 466/590 genes were identified by the STRING database, and 14 clusters (with a MCL inflation parameter of 1.8 and minimum confidence interaction value of 0.150) (205). The largest of these clusters contained 395 proteins and these were largely involved in immune function.

Linking the RNA sequencing data to the AFM data, and considering potential tissue-level causes behind the lower elastic modulus at the coronal aspect of carious teeth, it is possible that the high immune response (as demonstrated by the RNA sequencing results) is the driver behind the changes. Collagenase activity associated with inflammation may have caused lower elastic modulus values at the coronal aspect of the pulp in carious teeth.

Neurogenesis is displayed in the healing pulp (255,256), and the resulting differential expression of genes associated with these activities (such as *GFAP*) further highlights the activity of this process in

the carious pulp. Neural genes were also part of the largest network identified in the STRING analysis of differentially expressed genes (205,210,211). Peripheral nerves have been demonstrated to have relatively high elastic modulus (~400-700 kPa (257)) and this coupled with the high expression of neural-related genes in carious teeth may go some way to explain the higher elastic modulus generally seen in carious teeth. As carious teeth generally had fewer fibres from the histomorphometric analysis and a lower % area stained when compared to sound teeth, it is unlikely that new nerve fibres are making a significant impact to the overall volume of the pulpal fibres and on balance, it is likely that the increased organisation of the fibres in carious teeth is behind the increase in elastic modulus.

When examining the 76 differentially expressed genes in more detail, and looking specifically at the largest log2 fold changes in carious teeth, many of the genes identified have no known function in the pulp, for example; *OR2I1P*, *TBC1D27P*, *CHI3L2*, *PLEKHS1* and *SHISAL2B*, making it difficult to infer what this differential expression may mean in terms of differences between carious and sound teeth at a tissue level, and further exploration of the roles of these genes in the pulp is warranted. When exploring the 9 differentially expressed genes with log2 fold changes >2 in sound teeth (excluding pseudogenes) (*CHAD*, *LAMA3*, *FERMT1*, *PLA2G2A*, *HTR1A*, *SLC12A8*, *CILP2*, *NOX5* and *ADAM33*), most have functions pertaining to extracellular matrix maintenance/production and immune function. Dysregulation of the extracellular matrix in carious teeth could be part of the cause behind the difference in elastic modulus seen in carious teeth compared to sound.

Confirmation of findings of specific genes of interest (for example *COL1A1* or *DSPP)* with RT-PCR or a microarray study of specific pathways of interest (e.g. Notch or wnt) would have been beneficial. This is particularly important for genes with shorter transcript lengths and lower abundance in the tissue being studied because RNAseq and PCR results may be discordant (258). This is believed to be largely due to normalisation strategies used in RNAseq analysis (258). In this work, because RNA yields were low, RT-PCR to confirm the RNAseq findings was not completed, however it would be prudent to consider this adjunct for future studies.

5. BIOMIMETIC HYDROGELS FOR DENTINOGENESIS

As previously discussed, DPSCs are believed to differentiate dependent upon various mechanical stimuli, as discussed in a review by Marrelli *et al*.(26). DPSCs are believed to be mechanosensitive cells and will differentiate along various lineages depending upon the stiffness of the substrate they are growing on, with hard tissue types generally being formed from DPSCs growing on substrates with higher elastic moduli (151). In making a biomimetic scaffold to encourage the differentiation of DPSCs in-vitro, the biomechanics of the substrate needs to be considered, as discussed earlier in Section 1.

From the work completed in Section 4.3.1, the elastic modulus at the nano/micro level of the pulp seems to be in the region of 29-362kPa in health and 63-206kPa in disease. This is a large range, and the material chosen to facilitate this large range needs to be easily tunable to ensure accurate, reproducible elastic modulus values so that the ideal elastic modulus for DPSC differentiation into odontoblasts can be discovered. Agarose has been chosen for this application and is discussed in more detail in 5.2.1. It is likely, though not proven, that in carious teeth where tertiary dentinogenesis is occurring, the DPSCs are differentiating towards the coronal aspect of the pulp, so the corresponding elastic modulus is likely to be closer to the region of 125-206kPa, fitting with the modulus found in sites 1 -3 in carious teeth.

The information gained from establishing the ideal elastic modulus for DPSC differentiation into odontoblasts will be useful for the dental scientific community and the field of bioengineering for multiple reasons. Firstly, in knowing there is gradient in the elastic modulus of the dental pulp, it may be possible to infer at what point in the pulp, during the migration of the DSPCs from their niche(s), differentiation into odontoblast-like cells occurs. Secondly, the information can be utilized to create biomimetic scaffolds that mimic the elastic modulus of the pulp at the point of DPSC differentiation, allowing dental pulp capping agents to be made that may be better than current applications. Thirdly, by determining the best elastic modulus for DPSC differentiation into odontoblasts based upon the figures from the dental pulp, it may be possible to demonstrate dentine formation on an agarose scaffold for the first time.

5.1 MATERIALS AND METHODS: AGAROSE GEL CONSTRUCTION

Throughout the work in this thesis, agarose gels were made using Lonza NuSieve 3:1 agarose (available from Lonza, Basel, Switzerland). This agarose was selected because it is advertised as a ‘strong gel’, suggesting the stiffness/elastic modulus of the gel may be tunable to match the relatively high elastic modulus of the pulp as determined by the previous AFM work.

Concentration of agarose was determined as w/v %. The liquid component of the gels was made up of HEPES (4-(2-hydroxyethyl)-1-piperazineethanesulfonic acid)) buffer (25mM, pH 7.4).

Early optimisation experiments resulted in marked batch-to-batch variation in mechanical properties and the results were poorly reproducible. As such, a protocol was designed and optimised to reduce variability as much as reasonably practicable.

The following reagents and equipment were used in this process:

1) Phosphate buffered saline (PBS)
2) Agarose – Lonza NuSieve 3:1, available from Lonza, Basel, Switzerland
3) HEPES buffer, 25mM, pH 7.4
4) Glass bijous, 30mL, available from International Scientific Supplies, Bradford, UK
5) Low adhesion 12-well plates, available from Sarstedt, Nümbrecht, Germany (suspension plates)
6) Bead bath
7) Water bath
8) Orbital shaker
9) 10mL syringe
10) Media; low glucose DMEM, 10% FBS, 2.5mM l-glutamine, 1% penicillin/streptomycin, all available from Sigma Aldrich, St Louis, USA – hereafter referred to as 'basal media'

Step	Stage	Process	Notes
1	Weighing agarose	Agarose was weighed out	Precise measurements were needed to ensure reproducibility (to 1mg)
2	Adding agarose to glass container and adding buffer	The weighed agarose was added in bulk to the glass container and the liquid component added. A small proportion of the liquid component (500uL) was used to rinse the weighing boat, this is then aspirated and returned to the whole sample.	Weighing boat rinsed to ensure all agarose is added
3	Orbital Shaker	Lids were added and the samples shaken by hand, before being placed on an orbital shaker for 15 minutes at 200 oscillations per minute.	Orbital shaken ensures the powder and liquid are well incorporated.
4	Bead Bath	The samples were then added to a bead bath set to 100°C for 25 minutes. Ensure the lids are tightly sealed.	Bead bath ensures even heat dispersion (c.f. a microwave which produces 'hot spots'). A bead bath avoids the issue of

			liquid evaporation that may occur in a water bath heated to 100℃.
5	Water bath	The samples were added to a water bath set to 50℃ for 20 minutes.	This ensures all samples are initially cooled at the same rate, but remain liquid.
6	Casting	The liquid gel was added to a 10mL syringe and syringed into 12-well plates, 1.5mL per well.	A syringe is needed because the agarose is too viscous to pass through a pipette tip. The gel should cover the whole base of the well plate to prevent cells preferentially adhering to the well plate.
7	Setting	The gels were left to solidify at room temperature for 45 minutes.	The lid must be kept off the well plates during this time – small beads of condensation can land on the gel surface affecting subsequent AFM nanoindentation work.
8	Sterilisation	PBS was added to the set gels to prevent dehydration (1mL per well), and the gels placed under UV light for 2 hours. The PBS was changed, and the gels placed in tissue culture incubator (37℃, 5% CO_2).	Sterilisation needed to prevent cell culture infection. As the gels and plates are clear, UV light will penetrate.
9	PBS changes and adding media	PBS is changed once more after 24 hours. PBS was then removed and replaced with basal media (low glucose DMEM, 10% FBS, 2.5mM l-glutamine, 1% penicillin/streptomycin, all available from Sigma Aldrich, St Louis, USA (1mL/well)) and left for three days before cells were seeded onto the gel.	Time is needed to ensure the media has infiltrated the gel sufficiently and replaced the PBS.

Table 5.1 1: Basic agarose gel construction protocol

The above method (Table 5.1 1) improved reproducibility of the elastic modulus values obtained in pilot work, however in early experiments it was evident that the cells were not adhering to the gels, as is well documented for agarose (118). To overcome this, the gels need to be modified.

Several methods of modification were explored, as per the table below (Table 5.1 2).

MODIFICATION	REFERENCES	OUTCOME	TECHNICAL ISSUES
Gelatin addition, making a hybrid gel of gelatin and agarose	(259–261)	Cell adhesion was still poor, and many cells were dead. See Appendix 21	None – the gels blended well and as they both need to be heated to form, the construction was relatively facile. Agarose/Gelatin composites ranged from 90%/10% to 60%/40% mixes
Collagen addition, making a hybrid gel of collagen and agarose	(262)	The collagen did not blend with the agarose at all, so these could not be reliably constructed	There is some evidence in the literature for collagen/agarose hybrid gels but the agarose needs to be low temperature setting to allow the gels to blend, which Nusieve 3:1 is not. Low temperature agarose would not achieve elastic moduli high enough to mimic pulp.
Fibronectin addition	(263)	This did produce good adhesion and reasonable viability on live/dead stains	The Fibronectin was also difficult to blend into the Nusieve agarose, resulting in 'clumpy' adhesion of cells. See Appendix 21.
Polydopamine addition	(264–266)	Polydopamine facilitated adhesion but turns the clear gels black	Live/dead staining demonstrated a high dead:live ratio and the black-coloured gels made assessing the cells with microscopy difficult. Issues have been raised with regards to polydopamine toxicity in the literature. See Appendix 21.
Laponite addition, making a hybrid gel of laponite and agarose	(267)	Cell adhesion was still poor – no significant improvement	Despite literature supporting the addition of laponite (267,268), to improve cellular adhesion of hydrogels, no improvement in cell adhesion was found, see Appendix 22. Laponite also exhibits autofluorescence, making cytological analysis by confocal microscopy difficult.

Table 5.1 2: Modifications trialled (and rejected) to improve cell adhesion to agarose

After the trials listed in Table 5.1 2, poly-l-lysine (PLL) was investigated. This produced good results in pilot experiments (see Appendix 23). The only issue that was found with poly-lysine coating is that when cells are cultured from day 1 in odontogenic media, adhesion was generally poor. However, if the cells are first cultured in basal media, this is not an issue. After many trials, it was felt that this may be due to the higher number of negatively charged amino acids in α-MEM compared to DMEM occupying the positively charged sites on the gels produced by the poly-lysine. This could not be proven unequivocally, but seemed to be the most plausible cause. As such, for all of the data presented in this chapter, the cells were routinely cultured in basal media first before the media was changed to α-MEM-based odontogenic media to facilitate initial attachment of the cells (see https://www.sigmaaldrich.com/deepweb/assets/sigmaaldrich/product/documents/223/143/d6046for.pdf and https://www.sigmaaldrich.com/deepweb/assets/sigmaaldrich/product/documents/176/585/m8042for.pdf for formulations of the two media).

From the literature, poly-lysine is used to coat surfaces for cellular attachment typically at concentrations of 0.1mg/mL and 0.01mg/mL. PLL and poly-d-lysine (PDL) have both been used successfully in the literature to facilitate cellular attachment to scaffolds(269–276) . However, to facilitate any migration of cells into the gels, it was decided to add the poly-lysine also to the agarose gel during construction, so that the poly-lysine was present throughout the gels rather than risk just coating the top surface. For PLL and PDL 0.01mg/mL, the poly-lysine samples used in this work were provided commercially at 0.1mg/mL concentration and diluted with PBS.

The protocol above (Table 5.1 1), was modified through several trials to incorporate the poly-lysine both as an additive throughout the gel and a coating, as follows:

1) At Step 2, half of the liquid component is added (i.e. if the total liquid volume required to give 8% w/v agarose is 5mL, 2.5mL HEPES is added)
2) Between Steps 4 and 5, the poly-lysine is warmed to 50°C in a water bath. This prevents the agarose gel setting on addition of the poly-lysine.
3) At Step 5, the remaining 50% liquid component is added to the molten agarose gel before the gel is placed into the water bath
4) After Step 8, PBS is removed and sterile poly-lysine is added as a coating to the agarose gel (500µL per well) and the gel placed in an incubator for 24 hours before being replaced with PBS again. After a further 24 hours, the PBS is replaced with media as per Step 9.

Further pilot work utilising AFM to assess the elastic modulus of the gels created using the protocol in Table 5.1 1 demonstrated that the elastic modulus in the range of 5 to 10% agarose would align best with the AFM data from the dental pulp.

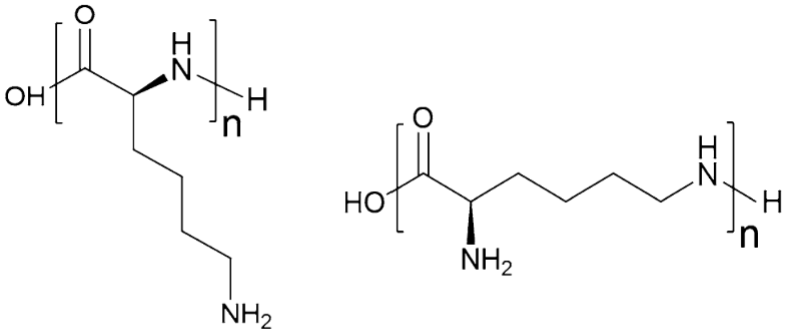

Figure 5.1 1: Chemical structures of α and ε poly-l-lysine. Modified from (277)

The poly-lysines trialled in the experimental works were:

1) Poly-l-lysine (150 000 – 300 000 Da, 0.1mg/mL, diluted in PBS, (Sigma Aldrich, St Louis, USA)
2) Poly-l-lysine (70 000-150 000 Da, 0.1mg/mL, diluted in PBS, (Culturex brand - from R&D Systems, Abingdon, UK)
3) Poly-d-lysine (70 000-150 000 Da, 0.1mg/mL, diluted in PBS, (Culturex brand - from R&D Systems, Abingdon, UK)

Poly-lysine comes in two distinct forms – α and ε (Figure 5.1 1). The main difference between the two is that α is synthetic (formed via a polycondensation reaction), whereas ε occurs naturally (produced from natural fermentation in some bacterial strains). Mixed molecules of the α and ε forms ('branched polylysine') also exist (278–280).

The α form is further divided into PLL and PDL, depending on the chirality of the central carbon in the lysine monomer. The precursor molecule for PLL occurs naturally (L-lysine), whereas the PDL precursor molecule is synthetic and both are used successfully for cell adhesion. In some instances, PDL is considered superior to PLL as the synthetic molecule has been shown to be more resistant to enzymatic degradation (278–280).

PLL and PDL have both been used in the literature for modifying scaffolds to facilitate cell adhesion. This is achieved due to the positive charge of the amino groups when at neutral pH (278–280) – see Figure 5.1 1.

PLL can polymerise further into alpha helices and beta sheets, being dependent upon temperature and pH; as both increase, the structure becomes more organised (279) (random coils>alpha helix>beta sheet). When at a neutral pH 7.4, the majority of the PLL present in solution will be in a random coil formation (281). As the pH increases and the PLL secondary structure becomes more organised, the

molecule becomes less positively charged (281). Based on the work by Stamou *et al*., it is unlikely that at pH 7.4 increasing the temperature of PLL will have any effect on the secondary structure of PLL (282).

5.2 MATERIALS AND METHODS: CELL CULTURE – LIVE/DEAD AND CYTOTOXICITY/VITALITY

Taking forwards the PDL and PLL modifications, gels were constructed over three percentages of agarose, 5%, 7% and 9% as the range for the dental pulp roughly correlated to 5-10% agarose gels. Three percentages were selected because doing 1% increments of gels between 5% and 10% would comprise of 6 different percentages of gels, coupled with the various poly-lysine coatings would produce too many variables to be assessed within the time constraints of this work. Beyond 9% the Nusieve agarose gel is also extremely viscous and difficult to handle and set without entrapping air bubbles within.

To optimise the viability of agarose as a hydrogel for DPSC differentiation, assessing the utility of the gels in terms of viability and cytotoxicity was paramount. This was achieved with three different methods,; i) a viability assay (Alamar Blue (AB)), ii) a cytotoxicity assay (Lactate Dehydrogenase (LDH)) iii) live/dead confocal microscopy.

For all cell culture work in this thesis, sterile media and sterile PBS were warmed prior to use in a water bath (35℃). All cells were used at passages 3-5 (as later passages have altered stem cell marker expression, reduced proliferation and altered differentiation capabilities and which fits with the passages used in the literature (283–285)). All DPSCs in this work were commercially purchased from Lonza (Basel, Switzerland). All cell work was completed in a sterile tissue culture hood. The tissue incubator was set at 37℃ with 5% CO_2. Cells were cultured initially in basal media in tissue culture flasks and split once the cells reached 80% confluence.

For passages and cell counting, media was removed from the flasks (T175 available from ThermoFisher, Waltham, MA, USA), the cells washed with PBS, and trypsin-EDTA added to the cell culture flasks. The flasks were then returned to the incubator for 15 minutes. The trypsin-EDTA/cell suspension was removed and centrifuged at 150g for 5 minutes, the supernatant was removed and basal media added to produce the desired concentration for cell counting. It is recommended that T175 flasks are seeded at 4.9 $x10^6$, and the working volume used for this work was 40mL per flask. Typically, it would take around four days for DPSCs to reach 80% confluency. Media was changed every two days.

Cell counting for seeding and passages was achieved by staining a sample of cell/media mix with Trypan blue (from ThermoFisher, Waltham, MA, USA), counting the cells using a haemocytometer and calculating the number of cells in the cell/media mix. The cell/media mix was then diluted

accordingly to give the desired concentration for seeding onto the gels and splitting into flasks for further culturing.

5.2.1 LIVE/DEAD CONFOCAL MICROSCOPY

Materials:

1. Ethidium homodimer I, 2mM in DMSO, (Generon, Slough, UK).
2. Hoechst 3342, 5mg/mL in water, (Generon, Slough, UK).
3. PBS (Phosphate buffered saline)
4. Basal media (low glucose DMEM, 10% FBS, 2.5mM l-glutamine, 1% penicillin/streptomycin, all available from Sigma Aldrich, St Louis, USA)
5. Odontogenic media, as per (286) (α-MEM, 20% FBS, 2.5mM l-glutamine, 100μM l-ascorbic acid 2-phosphate, 1% penicillin/streptomycin, 1.8mM monopotassium phosphate 10nM dexamethasone, all available from Sigma Aldrich, St Louis, USA)
6. Gels made as per Table 5.1 1, with poly-lysine additions.

It was clear from early pilot experiments that the cells had a somewhat distended cytoplasm, consistent with a secretory-stage phenotype when cultured on the agarose gels with poly-lysine coatings. This distended cytoplasm made quantification of live/dead with calcein AM/ethidium homodimer I (EH) staining difficult as EH is a nuclear stain, and calcein AM is a cytoplasm stain – see Appendix 23. Calcein AM/EH staining is commonly used in the literature (287), but frequently the issue with calcein AM being a cytoplasm stain and EH being a nuclear stain affecting quantification is not addressed. This difference in staining location makes cell counting difficult as it can be difficult to determine cell boundaries on the calcein AM stain and quantification of area stained (i.e. pixel counting) will always provide a higher result for live cells than dead due to the larger area covered by the cytoplasm. Cell counting programmes also struggle to find cell boundaries when the cells are clumped together in small groups or clusters, meaning this often needs to be marked by hand, making this process arduous for experiments with large numbers of images to analyse. As such, it was decided that a nuclear stain would be needed for both live and dead staining to make the results of live:dead easily comparable. These are not uncommonly used in the literature – for example, see (288,289).

For the live/dead staining, EH was used as a dead stain and Hoechst 3342 (H3342) was used as a counter nuclear stain. The rationale being the H3342 would stain all the nuclei, regardless of whether they are live or dead and the EH would only stain the dead cells. EH is a membrane-impermeable red stain, as such it can only enter cells that have a compromised membrane. H3342 is a nuclear blue stain, and binds to DNA and (to a lesser extent) RNA, and as such is a nuclear stain (290).

Confocal microscopy was used as outlined in Section 4.2.2. Emission and excitation wavelengths for EH are 528nm and 617nm respectively. Emission and excitation wavelengths for H3342 are 361nm and

497nm respectively. H3342 is similar to DAPI in its staining, but DAPI is usually used for fixed cells as it can be cytotoxic at the high concentrations needed for live staining; as such, H3342 provides an alternative to DAPI which is more suited to live cell staining.

Across each percentage of agarose (i.e. 5% 7% and 9%), three types of poly-lysine were trialled (PDL (Mw 70 -150 kDa) and PLL (Mws 70 – 150 kDa and 150 – 300 kDa)) at two different concentrations: 0.1mg/mL and 0.01mg/mL . The gels were made as per Table 5.1 1, with the modifications listed earlier. It would have been useful to trial PDL at molecular weight 150 – 300 kDa to make a further comparison against PLL, but this was not available as a ready-made solution commercially.

The combinations of the different agarose w/v concentrations and the different poly-lysine combinations resulted in 18 different gels. These are outlined in Table 5.2.1 1, and the abbreviations used throughout this thesis are given for each of the 18 gels.

	Poly-l-lysine (70 – 150 kDa) 0.1 mg/mL	Poly-l-lysine (70 – 150 kDa) 0.01mg/mL	Poly-l-lysine (150 – 300 kDa) 0.1mg/mL	Poly-l-lysine (150 – 300 kDa) 0.01mg/mL	Poly-d-lysine (70 – 150 kDa) 0.1mg/mL	Poly-d-lysine (70 – 150 kDa) 0.01mg/mL
5% Agarose	5LPLL0.1	5LPLL0.01	5HPLL0.1	5HPLL0.01	5LPDL0.1	5LPDL0.01
7% Agarose	7LPLL0.1	7LPLL0.01	7HPLL0.1	7HPLL0.01	7LPDL0.1	7LPDL0.01
9% Agarose	9LPLL0.1	9LPLL0.01	9HPLL0.1	9HPLL0.01	9LPDL0.1	9LPDL0.01

Table 5.2.1 1: The 18 combinations of poly-lysine and agarose percentages used in this thesis and the abbreviations used throughout

For this live/dead confocal experiment, three replicas of each of the 18 gel/poly-lysine combinations were made in 12 well plates, as per Table 5.2.1 1. The replicas were needed so that one gel per week could be imaged – the confocal microscope used in this work did not have an environment chamber and to facilitate clear imaging of the cells, the gels were imaged directly on the microscope stage meaning that they could not be returned to the incubator after imaging due to infection risk. This means that a different gel was used per timepoint, but each of these gels came from the same batch, and were made and seeded at the same time, in the same way.

This three-week experiment was repeated three times with separate batches of agarose gels made each time.

DPSCs (passage 3-6) were seeded onto the agarose scaffolds by removing the basal media that the gels had been left in, adding 1 x 10^5 cells in 300µL of basal media and statically seeding the cells onto the surface of the gel. This was achieved by carefully dropping the cell suspension onto the surface of the gel and ensuring the cell suspension was evenly coating the gel as much as possible. The seeded gels were then returned to the incubator for three hours. After this time, 600µL of media was then gently

added to each well and the gels returned again to the incubator, to give a final working volume of 900µL of media per well.

All gels were cultured in basal media for days 1-8 and then odontogenic media for days 8-21 (i.e. at day 8, the media was changed from basal media to odontogenic media). The gels were cultured in a cell culture incubator (set at 37℃ with 5% CO_2), with media changes every two days and 900µL of media per well.

The protocol for staining the gels is outlined below:

1. Dilute the EH in PBS to give a 4µM working solution.
2. Remove the media from the wells containing the seeded scaffolds.
3. Add 300µL of the EH working solution to each well
4. Return the well plate to the incubator for one hour
5. Dilute the H3342 to 1µg/mL in PBS.
6. Remove the plate from the incubator and remove the EH solution from the scaffold. Gently rinse with warm PBS.
7. Add 300µL of the H3342 solution and return the plate to the incubator for 30 minutes.
8. Remove the H3342 solution, rinse again with PBS.
9. Remove the gel from the plate and place on the confocal microscope stage.
10. Five images per gel were taken using x20 lens.

Three time points were used for measurements – 1 week, 2 weeks and 3 weeks. Five images were taken from each gel at each time point and the experiment was repeated three times. This resulted in 15 images per gel per timepoint. Three weeks was determined as the longest time point for cell culture, as this is often the shortest timepoint given for histological assessment of a calcified barrier for pulp capping to be successful, and as such any new material should be able to produce a mineralised barrier by this point to be comparable to current PCAs (291).

To calculate the live:dead ratio, a simple macro was implemented in ImageJ to split the channels into red, blue and green, and count the area stained in the red channel and the area stained in the blue channel. From this, a ratio was made of blue:red (e.g. 1.5:1), and from this ratio, the percentage more live than dead was calculated (e.g. 1.5:1 would be 50%). In addition to this, the total area stained was calculated by using the same macro on the ‘overlay’ image of red and blue (i.e. the image of EH and H3342 combined), this would provide an idea of the area of the gel covered by cells in total and as such give a measure of the adhesion between the cells and each gel/poly-lysine combination.

For the statistical analysis, repeated measures anova was used to look for statistical differences between the results at week 1, week 2 and week 3 for each gel, with a post-hoc Tukey’s test. To look for differences between the results for the gels at each timepoint, one-way anova was used to compare the

gels, with a post-hoc Tukey test. All statistics were undertaken using R-Studio (R 3.6.2, Dark and Stormy Night).

5.2.2 LDH ASSAY

Materials:

1. LDH assay kit (CyQUANT LDH cytotoxicity assay kit, Invitrogen, Waltham, MA, USA)
2. 96 well plates
3. Gels made as per Table 5.1 1 and Table 5.2.1 1, seeded with DPSC 1 x 10^5 per gel, passages 3-6
4. Basal media (as above)
5. Odontogenic media (as above)

The LDH assay has an advantage over the live/dead confocal because the same gel can be used for multiple time points. This is because the test is non-destructive as it utilises the media in which the gels are cultured in, leaving the scaffold untouched.

LDH assays are colorimetric and rely on quantifying the LDH, which is released from damaged cells. To detect the LDH present in the cell culture media, LDH catalyses the conversion of lactate to pyruvate, with NAD+ being reduced to NADH in the process. NADH is then oxidised back to NAD+ using diaphorase, which simultaneously converts a yellow tetrazolium salt into a red formazan product (292). LDH assays are frequently used in the literature, as are many other colorimetric assays (292). The disadvantage of the LDH assay compared to the confocal live:dead testing is that the cells are not visualised directly and the LDH is essentially used as a surrogate marker for cell death, though the LDH levels are deemed to be directionally proportional to cell death (292). However, as cells are not directly visualised, in a cell culture with very few cells, the LDH activity will be low, even if most of the cells are dead simply because of the low cell number, and when this is compared to a cell culture with a high number of cells, even if most of them are alive, the LDH activity may be higher simply because of the higher number of cells. As such, this assay should not be viewed as a measure of cell cytotoxicity alone (hence why in this work it has been coupled with an alamar blue assay and confocal live/dead experiment).

For the LDH assay, three scaffolds per gel/poly-lysine combination (as per Table 5.2.1 1) were made per experiment and the experiment was repeated three times (i.e. the initial setup is exactly the same as the setup for the live/dead confocal experiment). Media changes and cell seeding were also completed exactly the same as the confocal live/dead experiment (i.e. media changes every two days, initial culture in basal media for 8 days and odontogenic media thereafter).

Measurements were taken at Day 4, 8, 12, 16 and 20. One sample of media was taken for each of the gel triplicates at each time point and since the experiment was repeated three times, this culminated in

nine LDH readings per gel/poly-lysine combination, per timepoint. For each timepoint, a control was used (which comes as part of the LDH assay kit) to ensure the reagents were working effectively. Blank controls were also used of just media (as recommended in the LDH kit because of background LDH activity from the media).

As the measurements always occured on days when the media was to be changed (media was changed every two days, as standard), the samples were always taken before the media was changed, so the measurement of the LDH will be a representation of the previous two days' activity.

It was attempted in earlier experiments to quantify the readings against a 'standard curve' of cells by culturing a known number of cells overnight in a well plate and then adding DMSO to the plate to kill the cells, resulting in a LDH reading for a presumed number of dead cells. However, after trialling this over several timepoints in pilot work this did not prove feasible because i) a ready supply of cells was always needed every four days to create the curve with, ii) one could never be certain of the exact number of cells per well after culturing overnight (i.e. some may have proliferated, meaning the same number of cells added to the well was not the same number of cells killed in the well), iii) the number of dead cells may also be different to the cells seeded as not all of the cells may have been killed by the DMSO. As such, the LDH readings in the results sections are all of absorption and not calibrated to an exact cell number.

The LDH activity may be calculated by the following formula, where total cell death is calculated by adding DMSO to the total cell starting number:

(Absorbance of test samples-blank control (media))/(absorbance of positive control (total cell death)-blank control)

However, it was not feasible to have a ready supply of cells to use as a 'total cell death' reading for each timepoint, therefore the figures shown in the results are those of absorbance only.

The methodology for the LDH assay is listed below, however the protocol is also available in the kit.

1. Make up the LDH reaction mix (600µL of assay buffer added to 11.4mL of substrate stock solution)
2. 50µL of media is removed from each well and added to a 96 well plate
3. Include a 'blank' control of 50µL media in triplicate
4. Include a positive control of 50µL 1x LDH positive control into triplicate wells
5. 50µL of reaction mix is added to each well
6. Incubate, covered from light at room temperature for 30 minutes
7. Add 50µL stop solution to each well and cover from light
8. Read on plate reader; two readings at 490nm and 680nm. Subtract the 680

9. To calculate the absorbance, subtract the 680nm reading (the machine's background reading) from the 490nm reading

Statistical analyses of the results were undertaken using R-Studio. Similar to the confocal live/dead, this included repeated measures anova and post-hoc Tukey test to look for differences in the measurements at each time point for each gel. Differences between each of the 18 gel/poly-lysine combinations was assessed with a one-way anova and post-hoc Tukey's test.

5.2.3 AB ASSAY

Materials:

1. Alamar blue (AB) reagent (available from Invitrogen, Waltham, MA, USA)
2. Gels made as per Table 5.1 1 and Table 5.2.1 1, seeded with DPSC 1 x 10^5 per gel, passages 3-6
3. Basal media
4. Odontogenic media

The Alamar Blue (AB) Assay follows the same experimental design as the LDH assay; for each unique agarose%/poly-lysine combination, three gels were made and cultured over 20 days, with readings taken at day 4, 8, 12, 16 and 20, and the experiment was repeated three times.

Similar to LDH, AB works by sampling the media in which the gel is cultured, as such it is a non-destructive test and the same gel could be used over multiple time points.

AB assay is based upon the enzymatic reduction of AB (also known as resazurin) to resorufin. This results in a colour shift from blue/purple to pink as the resorufin is expelled from the viable cells (292). AB is regularly used as a measure of cell vitality (292). It is important to note that this is test of vitality – not viability. AB assesses the metabolic activity of cells and this is often used as a surrogate for viability as the two factors are linked, however because of this limitation it should not be viewed in isolation – hence the need for the confocal live/dead and the LDH assay.

The method for the AB assay is listed below.

1. 90µL of AB solution added to the media of each well.
2. Well plate returned to the incubator for 3 hours.
3. 50µL of media removed from each well and added to a 96 well plate
4. Read on plate reader (absorbance, 570-600nm)

Similar to the LDH assay, the AB was added to media before it was changed on each of the days, therefore the media was changed after the measurement. A well containing just media was also included with AB added as above, as a blank control – this was done 'fresh' for each measurement.

For some of the gels, AB would not be completely cleared from the media at the end of the incubation period (and was frequently taken up by the gel), as such it was not possible to use the same gel for the LDH assay as the AB assay, as the remaining AB may have affected the LDH reading due to both being colorimetric assays. Statistical tests were completed the same as the LDH assay.

5.2.4 BRIGHTFIELD MICROSCOPY

As part of regularly monitoring the scaffolds whilst being used for cell culture, the gels were frequently imaged using Brightfield microscopy to assess the status of the cells and assess for any infections in the culture.

Representative images of the gels were taken at various time points for completeness, interest and qualitative purposes. Some of the images taken are displayed in the results section, but these were not used for any quantitative analyses.

5.3 MATERIALS AND METHODS: MINERAL DEPOSITION AND CHARACTERISATION

5.3.1 CALCEIN STAINING

Calcein is a non-permanent cell dye that fluoresces green when bound to calcium. It is most commonly used as part of the live/dead, calcein AM/ethidium homodimer green/red stain frequently found in the literature. The ‘AM’ in calcein AM stands for acetoxymethyl and it is this compound which enables the calcein dye to cross the membrane of live cells, rendering them visible with confocal microscopy. However, calcein is also a calcium stain and without AM it cannot cross the phospholipid membrane and instead binds to extracellular calcium (293,294)

Alizarin red is more commonly used for cell culture work to demonstrate calcium deposition. However, as has been demonstrated in previous work (293), this stain tends to be less sensitive to mineral deposition and a certain ‘critical volume’ is often necessary to be picked up by the stain. As this work has not been attempted before, there was some doubt entering this experiment as to whether mineral deposition would occur, so calcein was chosen due to its higher sensitivity for extra-cellular calcium deposits than alizarin red. Von kossa is another option for looking at mineral deposition, but this was not chosen because it does not fluoresce and as such analysis would need to be completed using traditional light microscopy, which would be less accurate than fluorescent confocal microscopy (as is required for calcein staining). Table 5.3.1 1 lists the pros and cons for calcein, alizarin red and von kossa staining.

ALIZARIN RED		VON KOSSA		CALCEIN	
PROS	CONS	PROS	CONS	PROS	CONS
Most frequently used in the literature	Lengthy to prepare samples for staining (usually with fixing and histological processing)	As the stain precipitates an insoluble silver ion, further staining e.g. IHC can be done	Samples must be fixed – no live or real time staining	Simple and quick staining technique	Must be imaged with fluorescent microscopy which can be technique and operator sensitive
Can be used for light microscopy and fluorescent microscopy	Poor sensitivity	Commonly used in literature	Can be difficult to differentiate positive staining from the background haematoxylin	Fluorescent imaging – can be seen on confocal microscopy, therefore better resolution	Staining needs a long time to incubate
Well accepted technique	Samples must be fixed – no live or real time staining		Least sensitive	Better sensitivity than alizarin red	Less commonly used in literature
	pH affects staining		Needs light to develop – intensity affects speed of development	Will stain fixed and live cells	
	Can suffer diffusion artefact			Little to no background staining	
	Can show background staining				

Table 5.3.1 1: Comparison of different hard tissue staining methods used in the literature, with information adapted from (293–295)

As will be demonstrated in the results section for the cell culture work of the differing agarose gel/pol-lysine combinations (Section 5.6), gels incorporating PDL were the best performing. Taking this combination forwards, gels were constructed and cultured in odontogenic media or basal media, as per Table 5.3.1 2.

	BASAL MEDIA		ODONTOGENIC MEDIA	
	LPDL0.1	LPDL0.01	LPDL0.1	LPDL0.01
5% AGAROSE	5LPDL0.1_BM	5LPDL0.01_BM	5LPDL0.1_OM	5LPDL0.01_OM
7% AGAROSE	7PLDL0.1_BM	7LPDL0.01_BM	7PLDL0.1_OM	7LPDL0.01_OM
9% AGAROSE	9LPDL0.1_BM	9LPDL0.01_BM	9LPDL0.1_OM	9LPDL0.01_OM

Table 5.3.1 2: Abbreviations used in this thesis for the mineral deposition and cellular characterisation work, demonstrating the 12 media/poly-d-lysine/agarose concentration combinations

Materials:

4 Calcein solution: 1g/mL stock solution diluted in 0.1M NaOH, as per (293,294), sterile filtered
5 Gels constructed as per Table 5.3.1 2, seeded with DPSC 1 x 10^5 per gel, passage 5
6 Basal media
7 Odontogenic media
8 PBS

For this work, one gel per poly-lysine/agarose % combination was used for analysis, and these were made in duplicate so that one could be cultured in basal media, one in odontogenic media, resulting in 12 gels as per Table 5.3.1 2.

All gels were cultured for 8 days in basal media. At day 8, for half of the gels, the media was switched to odontogenic as per Table 5.3.1 2, the other half were continuously cultured in basal media.

Media changes took place every two days. At day 20, for all gels, the media was changed to basal media containing calcein at a concentration of 1µg/mL, with the calcein being diluted into the media.

After 24 hours culture in the calcein-containing media, the gels were removed from culture, rinsed with PBS and imaged using a confocal microscope (as per Section 4.2.2). Emission and excitation wavelengths for calcein are 488nm and 520nm respectively.

Five images per gel were taken with a x20 lens. In addition, Z-stack images were also produced for some of the gels to demonstrate the three-dimensional abundance of calcium deposition qualitatively.

This experiment was conducted twice, as such ten (two dimensional) images per gel were taken. A third experiment was begun but had to be aborted due to cell culture infection and was not repeated due to time constraints.

The images from the gels were analysed using ImageJ. For each image, the figure was split into three colour channels, the image made grayscale, and the pixels counted from the green channel to give a % of area covered. The results of culturing in basal media vs odontogenic media were compared with student's t-test. The results for all gels were compared using one-way anova with post-hoc Tukey's test. Statistical tests were completed using R in R-studio.

5.3.2 SCANNING ELECTRON MICROSCOPY (SEM)

Scanning electron microscopy (SEM) coupled with energy dispersive X-ray spectroscopy (EDS) were used to assess the structure of the mineral produced and the elements present in the mineral produced.

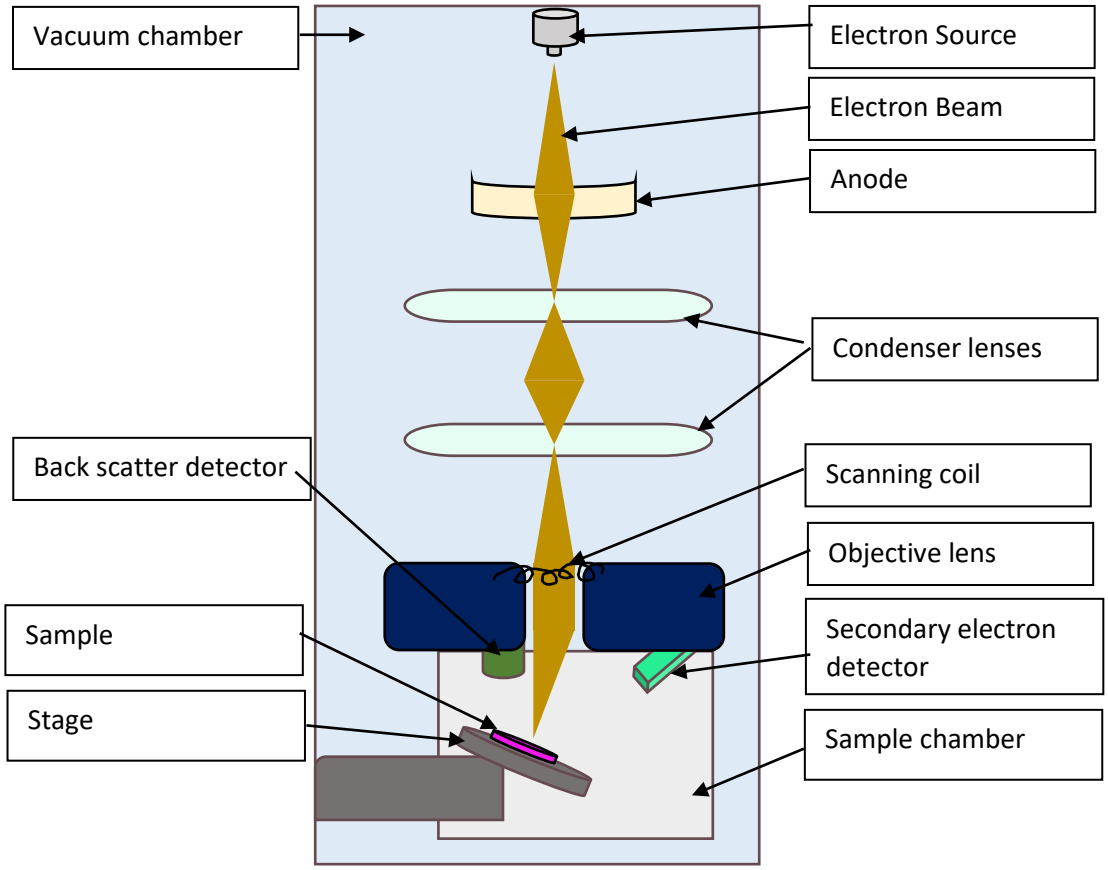

Figure 5.3.2 1: Schematic diagram of a SEM, demonstrating the standard setup required for scanning a sample.

SEM is a type of electron microscopy that has been used since the 1950s. Its basic setup is outlined in Figure 5.3.2 1. In essence, the SEM produces images based upon collecting electrons that have interacted with, and bounced back from, a sample. The collected electrons are converted to a signal which is then recapitulated into an image (296).

SEMs scan the surface of the sample in a raster fashion. As the electron beam moves over the surface, various emissions are created from the interaction between the sample surface and the electron beam; transmitted electrons, secondary electrons, backscattered electrons, characteristic X-rays to name but

a few (296). Identification of these emissions is achieved with various detectors, producing a 'secondary' electron signal (296).

For this work, the gels were imaged using a 'cold stage'. This is because in pilot work, dehydrating the sample prior to standard SEM resulted in the newly produced mineral becoming detached from the surface. With the SEM chamber held at a low pressure, and the sample kept cold, wet samples can remain fully hydrated and simultaneously ice crystal formation can be avoided (297).

As water sublimation is proportional atmospheric pressure, using the cold stage has numerous advantages over traditional 'ambient' SEM, listed below (297):

- Prevents water evaporation (particularly pertinent for hydrogel ultrastructure and composition and for cytological structures)
- Allows for non-invasive preparation of samples (e.g. fixing and/or dehydration)
- Prevent shrinkage artefacts

In tandem with the SEM of the gel surfaces to assess the mineral produced, EDS was undertaken. EDS is a process in which X-rays are fired at a sample and the emissions from the sample measured. The emissions are characteristic and relative to the elements present in a sample (298). An EDS spectra can be produced which has peaks present specific to the different elements in the sample (298). The advantage of using EDS in tandem with SEM is that the elements detected by the EDS can also be spatially mapped to the SEM images (298).

It has been assumed that the mineral on the gels cultured in odontogenic media is likely to be similar, regardless of the agarose %, and similarly the mineral produced on the gels cultured in basal media is likely to be similar regardless of the agarose %. Because of this, only two gels underwent SEM/EDS analysis; 7LPDL0.1 cultured in odontogenic media and 7LPDL0.1 cultured in basal media. These gels were chosen because they both had good amounts of mineral deposition and comparing two gels of the same percentage of agarose w/v allows for a more direct comparison of any differences caused by the media. It was not possible to assess all gels with SEM/EDS because of time constraints. Each gel took around one day (8 hours) to image and assess with EDS.

The two gels used were spare gels from the calcein experiment. As such, they were seeded with 1 $x10^5$ cells at passage 5 and cultured for 21 days. The basal media gels were cultured for the full 21 days in basal media. The odontogenic media gels were cultured in basal media for 8 days and odontogenic media for the remaining period.

To prepare the samples, the gels were removed from the well plates and small 4mm x 3mm x 2mm blocks were cut from the centre of the gels. The gels were placed on a sample holder and inserted into the cold stage.

Specific localisation of Ca, P, O was focused upon for the EDS analysis to establish whether or not the mineral produced is hydroxyapatite ($Ca_{10}(PO_4)_6(OH)_2$) (the inorganic, mineralised component of dentine).

5.4 MATERIALS AND METHODS: GEL CHARACTERISATION

The following parameters were determined for physical characterisation of the gels:

1. Elastic modulus, nano level (with AFM)
2. Elastic modulus, bulk level (with uniaxial compression)
3. Swelling ratio

5.4.1 AFM NANOINDENTATION OF GELS

For assessment of the elastic modulus of the gels, AFM force mapping was carried out, to compare directly with the pulp AFM work. It is also believed that the length scale at which cells 'sense' their environment is at the nano/micro level, making it most pertinent to cell work (134,135)

For this experiment, 21 gels were made; one of each of the poly-lysine/agarose combinations as per Table 5.2.1 1 and three plain agarose gels (5%, 7% and 9%). The gels were made as per Table 5.1 1 (with the poly-lysine modifications), however after setting, the gels were cut into 6mm x 4mm cylindrical samples (with a 6mm surgical punch and a depth-gauge) and stored in PBS buffer for 3 days in a refrigerator. Prior to scanning on the AFM, the gels were stuck to a glass slide using Vetbond adhesive (3M, Bracknell, UK). The AFM used was an MFP 3D (Asylum Research, Oxford Instruments, Abingdon UK) and the probe used was biosphere B1500-CONT (Apex Probes, Bracknell, UK); the same as for the pulpal AFM work.

For the scanning, 5 areas were chosen at random per gel, 20µm x 20µm, with 20 lines per image and 20 curves per line (1 um separation between force curves), resulting in 400 force curves per area (2000 curves per gel). The gels were scanned under PBS buffer, to keep them hydrated during the experiment.

The data and statistical analyses were carried out in the same way as the AFM pulp work – see Section 4.2.1. Each gel type was only measured once due to time constraints, however preliminary work demonstrated good reproducibility of AFM results with the modifications to Table 5.1 1 outlined on page 121.

5.4.2 UNIAXIAL COMPRESSION

Gels were made the same as for the AFM experiment above. Three cylinders per gel type were used and compressed to failure/fracture using BOSE Endura TEC ESG-3220.

Uniaxial compression applies a load on a sample in one direction until failure. In this case, the direction was in the long axis of the gel cylinder.

Elastic modulus at a bulk level is calculated by working out the equation for the slope on a stress-strain graph. The BOSE Endura calculates the stress and strain (based upon the dimensions of the gel and the force applied to it by the machine), allowing them to be plotted on a graph and the slope of the graph calculated. The graphs were plotted and the slope calculated in Microsoft Excel, an example of one of the graphs used for stress/strain analysis is in Appendix 24.

Statistical comparisons were completed in R and compared the different poly-lysine types and concentrations within subgroups of 5%, 7% and 9% agarose (Dunn's test), and the difference between 5%, 7% and 9% agarose gels in subgroups based upon poly-lysine type and concentration (t-test).

5.4.3 SWELLING RATIO

Swelling ratio is "the fractional increase in the weight of the hydrogel due to water absorption" (299). It can be calculated by:

$$\text{Swelling Ratio} = \frac{\text{Weight (swollen hydrogel)} - \text{Weight (dried hydrogel)}}{\text{Weight (dried hydrogel)}}$$

For this experiment, three cylinders were dissected out of each of the gels in Table 5.2.1 1. These cylinders were 6mm x 4mm in size, cut with a surgical punch (as per the AFM and uniaxial compression experiments). The gels were then stored in PBS for three days in a refrigerator. On the day of the experiment, the gels were returned to room temperature for 4 hours before starting the experiment.

The process of weighing the samples is as follows:

1. Add 20mL of PBS to a beaker and place on scales.
2. Record the weight of the beaker/PBS.
3. Add the gel cylinder to the beaker/PBS and record the weight.
4. Remove the gel from the beaker/PBS and place the gel in a dry well plate
5. Weigh the beaker/PBS again and record the weight.
6. Freeze-dry the cylinders of gel once all the gels have been weighed.
7. Weigh the dry gels directly on the scales and correlate to the respective hydrated weight of the gel to calculate the swelling ratio.

To calculate the weight of the hydrated hydrogel, calculate the average of the PBS/beaker weight from the measurements taken before and after the hydrogel was added to the PBS/beaker on the scales. Then, subtract this from the weight of the PBS/beaker with the gel added.

To account for any potential 'carry over' of PBS from the storage container to the PBS/beaker on the scales, the weight is taken before and after the gel is added to the PBS on the scales. This is important because 'carry over' of PBS into and out of the beaker on the scales could affect the overall weight of

the sample and thus the swelling ratio calculated. This cannot be avoided entirely, but this method may minimise the potential effects of this.

One way anova with post-hoc Tukey's test was run in R-Studio, with R 3.6.2 to compare the results of the swelling ratio.

5.5 MATERIALS AND METHODS: CELL DIFFERENTIATION

To assess whether the cells cultured on the gels have differentiated into odontoblasts, two methods were employed – immunofluorescence and reverse transcription PCR. It is difficult to determine irrefutably whether cells in culture are odontoblasts or osteoblasts and realistically the determination of this should be the result of a culmination of varying pieces of evidence taken together. Klein *et al.* (300), focus on this in a review and specify that discrimination of the supposed 'dentine' produced in cell culture from bone is integral to determine whether a cell/culture comprises of odontoblasts and/or dentine. It has been discussed by previous authors (301), that dentine and bone form a continuum and that ultimately the hard tissue expressed is a product of the environment. For these reasons, it is likely that hard tissue formed in culture is not likely to fit strictly into either a 'bone' or 'dentine' category. That being said, the work herein has attempted to determine whether the mineral produced on the gels is more likely a dentine phenotype or bone phenotype.

5.5.1 IMMUNOFLUORESCENCE

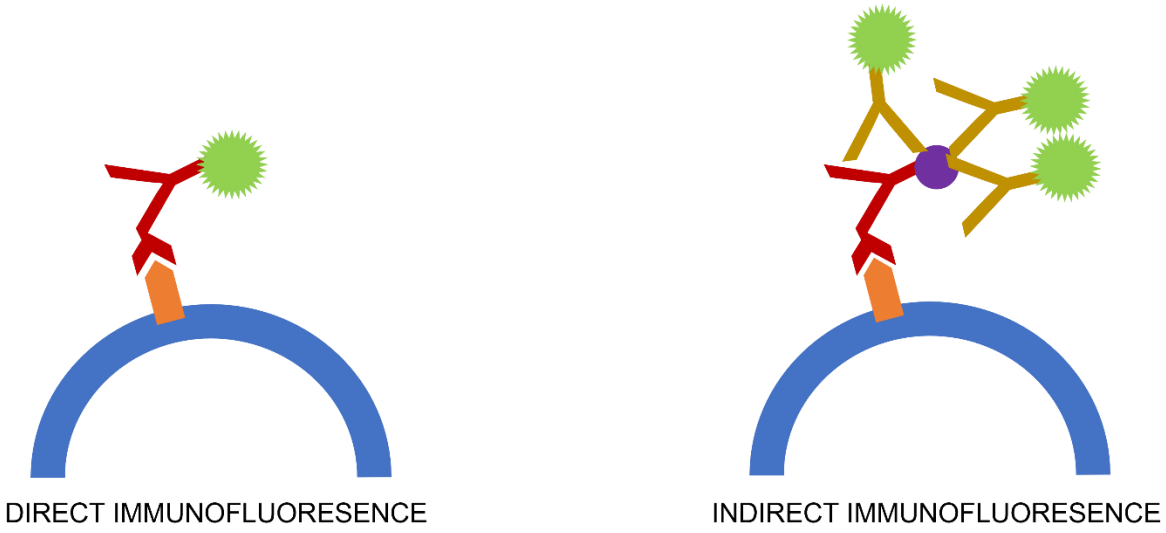

Figure 5.5.1 1: Schematic diagram comparing direct and indirect immunofluorescence. Direct immunofluorescence involves a single antibody binding to an antigen – in this scenario, the antibody is directly conjugated to a fluorophore (green). Indirect immunofluorescence involves numerous secondary antibodies (gold) binding to a primary antibody that targets the antigen of interest. The numerous secondary antibodies each contain a fluorophore (green), amplifying the signal.

Immunofluorescence is a method of using antibodies raised against antigens present on/in the cell of interest which are fluorescently tagged, so that they can be visualised on a microscope. There are two main methods of immunofluorescence – direct and indirect. In direct immunofluorescence, the fluorescent label is directly conjugated onto the antibody. In indirect immunofluorescence, a secondary antibody is used to attach to the primary antibody (which is attached to the cellular antigen) and the secondary antibody contains the fluorescent tag. Figure 5.5.1 1 provides a pictorial representation of the two methods. Table 5.5.1 1 gives a summary of the pros and cons of each method.

For this work, three antigens were chosen to target – dentine sialophosphoprotein (DSPP), dentine metalloprotein 1 (DMP1) and nestin. These are all found in odontoblasts and are considered markers of odontogenic differentiation and are used in the literature as markers of odontoblasts (49,300,302). DSPP and DMP1 are non-collagenous SIBLING (Small Integrin Binding Ligand N-linked Glycoprotein) family proteins (303). DSPP and DMP1 are both cleaved to become active in dentinogenesis (303). Until recently, DMP1 was considered specific to odontoblasts, but recent work found that it is also expressed in bone, brain and salivary glands and that the expression in bone is actually higher than that in dentine (304). DMP1 is expressed in odontoblasts and osteocytes (304). DSPP is also known to be expressed in bone, however DSPP in bone is believed to be at a level 1/400 of that in dentine (300,305).

DIRECT IMMUNOFLUORESENCE		INDIRECT IMMUNOFLUORESENCE	
PROS	CONS	PROS	CONS
Only one labelling step, so quicker	Conjugated antibodies are usually more expensive	Secondary antibodies are generally cheaper than conjugated antibodies	Additional steps, so more room for error and takes longer
Species cross reactivity is reduced because no secondary antibody is used	Fewer commercially available conjugated antibodies can make this option unfeasible	The same secondary can be used on numerous primary antibodies	Multiplexing to detect different antigens often needs numerous secondary antibodies.
As the fluorescent tag is conjugated to the antibody, background staining is reduced.	As the fluorescent signal is not amplified, the staining can be weaker than the staining seen in indirect immunofluorescence	Most target antigens have a commercially available primary antibody, giving greater flexibility	Species cross-reactivity can occur, where the secondary antibody binds non-specifically to targets.
		As numerous secondary antibodies can bind to the primary, the fluorescent signal is often stronger from indirect immunofluorescence	High immunoglobulin content in the background may result in non-specific background staining.
		Low abundance antigens or targets can be more readily detected due to signal amplification.	

Table 5.5.1 1: Comparison of direct and indirect immunofluorescence techniques (306)

Nestin is less specific as it is a general neural crest marker and some authors have found that it is not expressed in osteoblasts (302). Nestin is generally expressed during development, but can be re-expressed during pathological conditions and has been shown to be upregulated in odontoblasts during

caries as well as during primary dentinogenesis (307). Nestin has also been found to be upregulated in odontoblast-like cells derived from DPSCs cultured *in-vitro* (307).

To simplify the staining technique, direct immunofluorescence was selected. To prevent cross-talk between the different fluorophores, the fluorophores selected for conjugation had discrete excitation and emission profiles that could be modified with the band filters on the confocal to prevent cross-talk.

For this experimental work, only LPDL0.1 and LPDL0.01 were used as additives to the agarose. This is because, as discussed later in Sections 5.6.1 and 5.6.2, LPDL0.1 coated gels seemed to perform the best in terms of cell vitality, viability and adhesion at three weeks. LPDL0.01 was also used as a comparison to see if the LPDL concentration had any effect on cellular differentiation. Three agarose percentages were used; 5%, 7% and 9%.

Two gels of each LDPL/agarose combination (as per Table 5.5.1 2) were created; one of these gels was cultured for eight days in basal media and then 13 days in odontogenic media (21 days in total), the other was cultured for 21 days in basal media. Different media was used to assess to what extent the cell differentiation may be due to the elastic modulus of the gels and to what extent it may be due to the odontogenic media.

	5% Agarose	7% Agarose	9% Agarose
LPDL0.1	5LPDL0.1	7LPDL0.1	9LPDL0.1
LPDL0.01	5LPDL0.01	7LPDL0.01	9LPDL0.01

Table 5.5.1 2: LPDL and agarose combinations used for immunofluorescence

After 21 days, the gels were removed from the 12 well plate and the following method used to stain the cells for immunofluorescence:

Materials:

1. Conjugated antibodies – DSPP conjugated to AlexaFluor594, nestin conjugated to FITC, DMP1 conjugated to AlexaFluor680 - all available from Stratech, Ely, UK
2. DAPI counter stain, 1 µg/mL (Generon, Slough, UK)
3. 10% buffered formalin
4. PBS containing 0.1% Triton X-100
5. 2.5% Bovine Serum Albumin (BSA) in PBST (PBS with 0.1% Tween 20)
6. Basal media
7. Odontogenic media
8. PBS
9. Agarose gels made as per Table 5.5.1 2, seeded with DPSC 1 x 10^5 per gel, passage 4
10. DPSCs as control cells

11. Osteoblasts as control cells (from Lonza, Basel, Switzerland)

Method for immunofluorescence staining:

1. Fix gels for staining in formalin for 10 minutes at room temperature
2. Permeabilize cells with PBS/Triton X-100 – this step is necessary as all of the antigens are intracellular (i.e. not on the membrane), 4℃, 15 minutes
3. Block non-specific staining with 2.5% BSA in PBST for 30 minutes at room temperature
4. Dilute the antibodies to the following concentrations in 2.5% BSA in PBST: DSPP = 1:200, nestin = 1:200, DMP1 = 1:200
5. Add 300µL of each diluted antibody to the gel and incubate for 2 hours at 37℃, agitate occasionally. Protect from light.
6. Remove the antibody mixture, rinse with PBS twice.
7. Add the DAPI counterstain, 30 minutes, room temperature. Protect from light.
8. Image on confocal microscope, 5 images per gel at x20

Figure 5.5.1 2 shows the confocal microscopy setup for the fluorophores to prevent cross-talk. The same confocal microscope was used as per Section 4.2.2. A ‘frame-sequential’ scanning method was employed on the confocal; this means that for each frame, each fluorophore is excited and its emission recorded separately, thus preventing the emitted light from one fluorophore exciting another.

This experiment was only completed on one set of gels due to time constraints.

Osteoblasts were used as a control for the gels cultured with odontogenic media. DPSCs were used as a control for the gels cultured in basal media. Odontogenic differentiation was not expected in the cells cultured on the gels in basal media, as such the DPSCs are used as a control to see to what extent (if any) differentiation may occur solely due to the different gels the cells are grown on. As osteoblasts are known to express DMP1, DSPP and nestin, the osteoblasts are used as a control to see if the expression is higher or lower than the cells cultured on the gels. Proving a cell is an odontoblast rather than an osteoblast is difficult, but by using osteoblasts as a control to compare the expression of these odontoblast markers against, it may be possible to infer that it is more likely the cells are odontoblasts rather than osteoblasts.

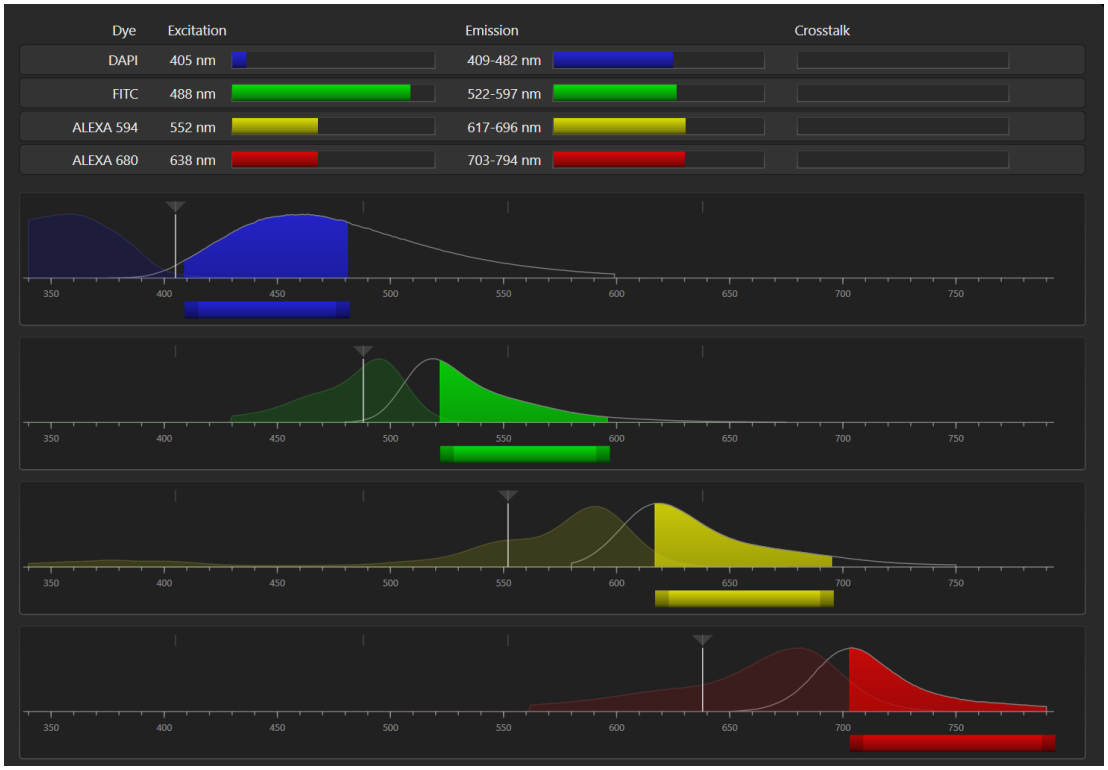

Figure 5.5.1 2: Confocal microscopy setup to prevent cross-talk of fluorophores, showing excitation and emission profiles as wavelengths in nm.

The DPSCs and osteoblasts used as controls were cultured on tissue culture polystyrene in 12 well plates (not low-adhesion). They were seeded at 1 x 10^5, passage three. The DSPCs were cultured in basal media for 21 days before undergoing immunofluorescent staining. The osteoblasts were cultured in odontogenic media for 21 days prior to staining with the odontoblast markers and imaging. In comparison to the gels, the cells cultured in the well plates on tissue culture polystyrene were stained and imaged in the well plates directly, whereas the gels were removed from the well plates to image on the confocal microscope.

To quantify the imaging results, each channel from the confocal image was selected individually and converted to grayscale. The pixels were then counted to give a quantifiable number per image. The grayscale pixel count for the DAPI channel was used to give a ratio against the immunofluorescent channels for DSPP, DMP1 and nestin (ratio = immunofluorescence pixels/DAPI pixels). This was done because the cell numbers on each gel will vary, so measuring the fluorescence in total for each gel would not give a suitable value to compare the antigen expression per cell (i.e. if a gel has lots of cells present, but little expression per cell, this may give a higher value overall than a gel with fewer cells but a lot of expression per cell). Statistical tests were carried out on the ratios produced as follows; i) two sample T-test and Welch's test (Welch's test performed when the standard deviation was >2x different between the two samples) comparing the results of the gels cultured in basal media vs those cultured in odontogenic media, ii) one-way anova with post-hoc Tukey's test to look for differences

between each of the gels. The statistical tests were completed in R-Studio, with R 3.6.2, Dark and Stormy Night.

5.5.2 REVERSE TRANSCRIPTION PCR AND COMPARATIVE PCR

Reverse transcription PCR (RT-PCR) is the synthesis of cDNA from RNA. RT-PCR can be used to convert a specific RNA transcript into cDNA and then amplify it – the amplification can then be quantified allowing comparison between samples (comparative PCR (cPCR)) (308,309). It can be used to provide information on the upregulation/downregulation of genes when compared to housekeeping genes. In this instance, RT-PCR is being used comparatively to see the difference in transcription of DSPP between different samples and compared against control cells (DPSCs and osteoblasts).

To quantify the amplified cDNA, quantitative PCR (qPCR) (also termed 'real-time PCR') needs to be undertaken. This is a method of measuring the amount of DNA present during PCR amplification (308,309).

For quantification of the DNA, SYBR green amplification/PCR was undertaken. This works by utilising a dye (SYBR green) which becomes fluorescent when bound to double stranded DNA. After the cDNA is denatured, the SYBR green binds to the double-stranded DNA as it is being produced and amplified. Once bound, SYBR green emits a fluorescence signal that can be detected and is directly proportional to the amount of double-stranded DNA present (310) .

For this work, six of each of the following gels were made; 5LPDL0.01, 5LPDL0.1, 7LPDL0.01, 7LPDL0.1, 9LPDL0.01, 9LPDL0.1. Six gels of each were necessary so that the experiment could be completed in triplicate for gels cultured in basal media and in odontogenic media (i.e. three of each gel type were cultured in basal media and three of each gel type were cultured in odontogenic media). The gels were made as per Table 5.1 1 with the modifications on page 121, seeded with DPSC 1 x 10^5 per gel, passage 5.

DSPP was chosen as this is the protein most used in the literature as a marker of odontoblastic differentiation (300).

DPSCs and osteoblasts were used as controls to compare the expression of DSPP from the gel-cultures against. The DPSCs and osteoblasts used as controls were cultured on tissue culture polystyrene in 12 well plates (not low-adhesion). They DPSCs were seeded at 1 x 10^5, passage five, the osteoblasts at the same concentration but passage 3. The DSPCs were cultured in basal media for 21 days before undergoing trypsin detachment. The osteoblasts were cultured in odontogenic media for 21 days prior to undergoing trypsin detachment.

In total, the gels were cultured for 21 days. For eight days, both sets of gels were cultured in basal media and at day eight, one of the sets was changed to odontogenic media.

Materials:

1) Trypsin-EDTA (from ThermoFisher, Waltham, MA, USA)
2) RNALater (FisherScientific UK, Loughborough UK)
3) PBS
4) ZymoBIOMICS RNA Miniprep Kit (Zymo Research, CA, USA)
5) High-Capacity cDNA Reverse Transcription Kit, by Applied Biosystems (available from ThermoFisher, Waltham, MA, USA)
6) Quant-it RiboGreen RNA Assay Kit (ThermoFisher Scientific, MA, USA)
7) RNAse Free water
8) Ultrapure water
9) DSPP primers (Forward = TCGCTGTTGTCCAAGAAG, Reverse = ATCCTCATCTGCTCCATTCC, from Eurogentec, Seraing, Belgium)
10) LightCycler 480 SYBR Green I Master Kit (Roche, Basel, Switzerland)
11) Roche LightCycler 480 Instrument II (Roche, Basel, Switzerland)

After three weeks, the cultured cells were trypsinized to remove them from the gels (or in the case of the control cells, from the polystyrene well plates) – the cells from the three same gels were pooled together to create a larger biomass. Cells from three wells of each type of control cell (DPSCs or osteoblasts) were also pooled. The cells were spun down to create a pellet using a centrifuge (150g for 5 minutes). RNALater was added to the cells to resuspend them and the cells were then spun down again. RNA was extracted from the cells using Zymokit and eluted into 50µL of RNAse free water. The primers were modified from (311).

Once the RNA was extracted, it was quantified using the Quant-it RiboGreen RNA assay kit and the RNA diluted to give 0.5µg/10uL per sample. The kit was used as per the protocol, available from https://www.thermofisher.com/document-connect/document-connect.html?url=https://assets.thermofisher.com/TFS-Assets%2FLSG%2Fmanuals%2FMAN0017977_highcap_cDNA_RT_UG.pdf .

The cDNA produced was diluted 5-fold. Three reactions were completed per gel type (i.e. the experiment was done in triplicate) following the protocol with the LightCycler kit. A control (also done in triplicate) using ultrapure water in place of cDNA was also used.

The LightCycler 480 Instrument measures the fluorescence emitted by the SYBR green. From this, a graph can be produced demonstrating number of cycles against the fluorescence. Once the fluorescence reaches a critical threshold, the number of cycles for that sample is recorded (CP value) (308) .

The lower the CP value, the fewer the cycles needed to reach the threshold for fluorescence and the greater the presence of the target DSPP, therefore CP is inversely proportional to the amount of DSPP

present (309,310). To better visualise this on a graph in the results section, the CP value has been subtracted from 100, so that the higher bars on the graph correlate to higher expression of DSPP.

No reference housekeeping genes were used in this experiment. Therefore the results are all comparative against each other, rather than against a background set value of expression.

T-test was completed to assess for statistically significant differences between the results from odontogenic media vs basal media for each gel type. One-way anova with post-hoc Tukey's test was completed to look for statistical differences between each gel in subgroups determined by the culture media. These tests were all completed in R-Studio, using R version 3.6.2.

5.6 RESULTS

5.6.1 ALAMAR BLUE ASSAY, LDH ASSAY AND CONFOCAL LIVE/DEAD

KEY FINDINGS

1. For most of the poly-lysine types used, the 0.1mg/mL poly-lysine additions performed better than the 0.01mg/mL additions – the exception to this was HPLL0.1 and HPLL0.01
2. The gels that performed the best overall (for viability and adhesion) had LPDL0.1 added
3. Generally, 5% gels performed better than 7% gels and 7% gels performed better than 9% gels
4. LPDL0.1 and HPLL0.1 incorporated gels had the best adhesion as shown by the largest values for area of fluorescence
5. Most of the results show an increase in cellular vitality/live cell number at 2 weeks culture

The results of the Alamar Blue assay (AB) and LDH assay (LDH) are best viewed together. This is because as viability goes up, the cytotoxicity usually would be expected to fall. In addition to this, if both the AB and LDH results are low, this may indicate few cells present, or similarly an abnormally high LDH and AB may be indicative of many cells being present and crowding causing cell death due to depletion of nutrients. The results of the AB and LDH assays are therefore shown on the same graphs (Figures 5.6.1 1-5.6.1 3).

Across most of the gels, a rise in the viability at day 12 is observed. In several cases, this is coupled with a fall in the cytotoxicity at day 12 too. As can be seen, 5% agarose with LPDL 0.1mg/mL, 9% agarose with LPDL 0.1 mg/mL and 7% agarose with LDPL 0.1mg/mL have the top 3 best viability

results respectively at day 12. Whereas 5% agarose with LPLL 0.1 mg/mL, 9% agarose with HPLL 0.01mg/mL and 7% agarose with HPLL 0.1mg/mL have the best cytotoxicity results at day 12 (better results = lower value for LDH). After a rise in viability towards the mid time point is seen, a fall towards the end time point is also identified. The cytotoxicity mirrors this trend to some extent, but largely appears flat across the range. The coatings that appear to have performed the worst are HPLL 0.1mg/mL and HPLL 0.01mg/mL in terms of viability (Figure 5.6.1 3), and this was true across all agarose percentages.

These assay results need to be viewed with caution because as previously mentioned, a very high number of cells or very low number of cells may give an inaccurate representation of the cytological environment (e.g. a low cytotoxicity may be recorded simply because there are very few cells present). Because of this, a live/dead stain was also completed using confocal imaging; this has the advantage of allowing the cells to be visualized and as such a sense of the number of cells present and their status can be better appreciated. The results of the live/dead confocal imaging and the area of cells stained can be seen in Figure 5.6.1 4 and Figure 5.6.1 5 respectively. These were also coupled with brightfield imaging to visualise the cell morphology.

The results of the live/dead confocal microscopy imaging reveal trends mirrored by the cytotoxicity and viability assays; a rise in live cells at the mid time point (in this case week 2) and a decrease again towards the final time point. Similar to the AB results, the gels that appear to have performed the best are the ones coated with LPDL0.1 (Figure 5.6.1 4).

The area occupied by the cells (as a surrogate measurement for the number of cells present) (Figure 5.6.1 5) shows two coatings as being the best; LPDL 0.1 and HPLL 0.1 and this is found across all agarose percentages. The trends in relation to area stained, also generally follow the same pattern of a rise towards the mid time point and a fall thereafter; this trend is weaker though for area stained than for the other parameters exploring cytotoxicity and viability.

Interestingly, across all agarose gels the coatings of a lower concentration of poly-lysine performed generally worse in terms of cytotoxicity and viability. The exception to this rule is the live/dead confocal results which show that for HPLL 0.1 and HPLL 0.01 coatings the opposite trend is seen; the lower concentration of the high molecular weight PLL outperformed the higher concentration of high molecular weight PLL.

Generally speaking, the higher the amount of the poly-lysine coating (i.e. 0.1mg/mL vs 0.01mg/mL), the higher the area of the gel covered by the cells (Figure 5.6.1 5). Again, this was generally found across all percentages of agarose.

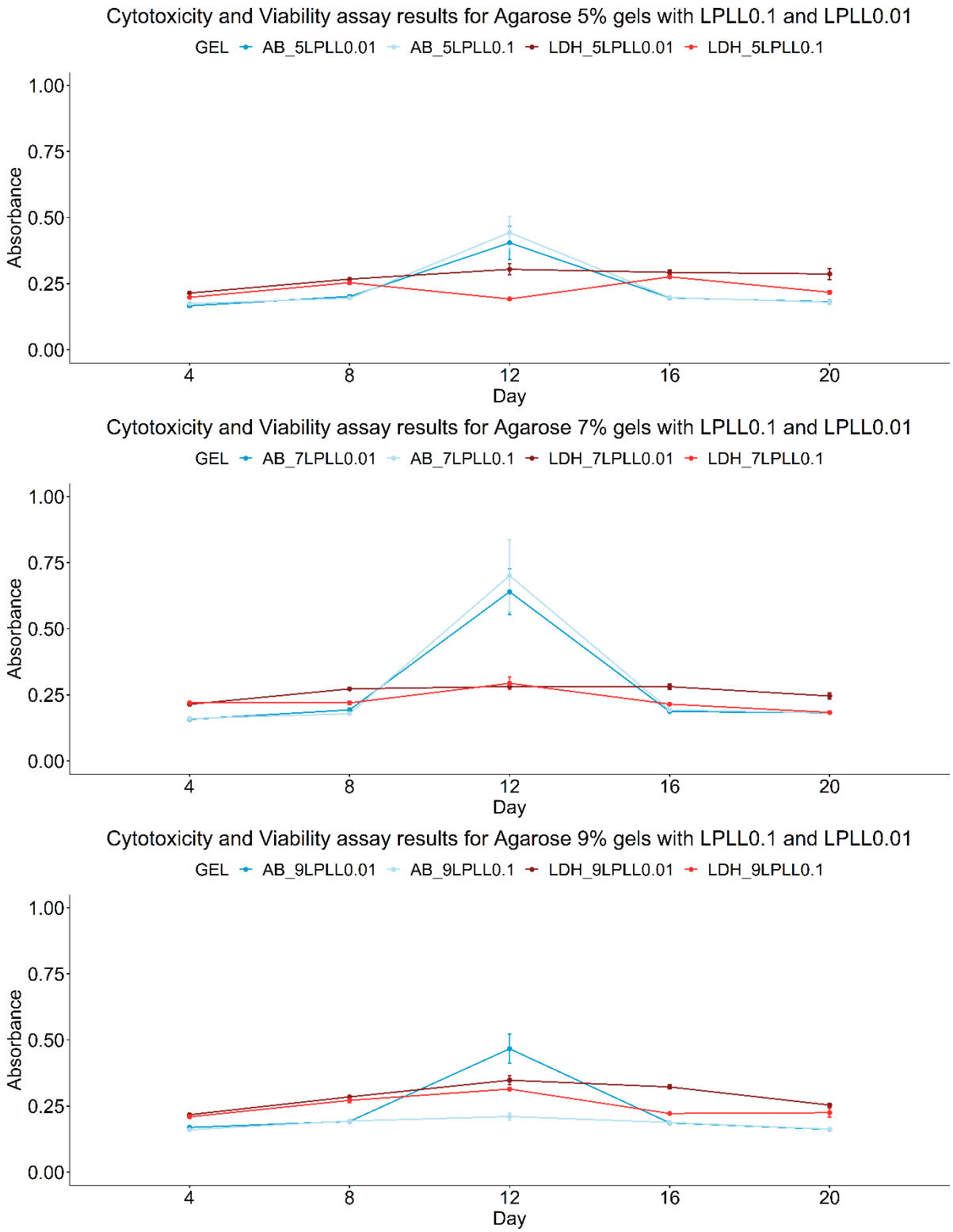

Figure 5.6.1 1: LDH and AB results for LPLL 0.1mg/mL (LPLL0.1) additive agarose gels and LPLL 0.01mg/mL (LPLL0.01) additive agarose gels across the five time points. AB results in blue, LDH results in red. Mean values plotted. Error bars = standard error.

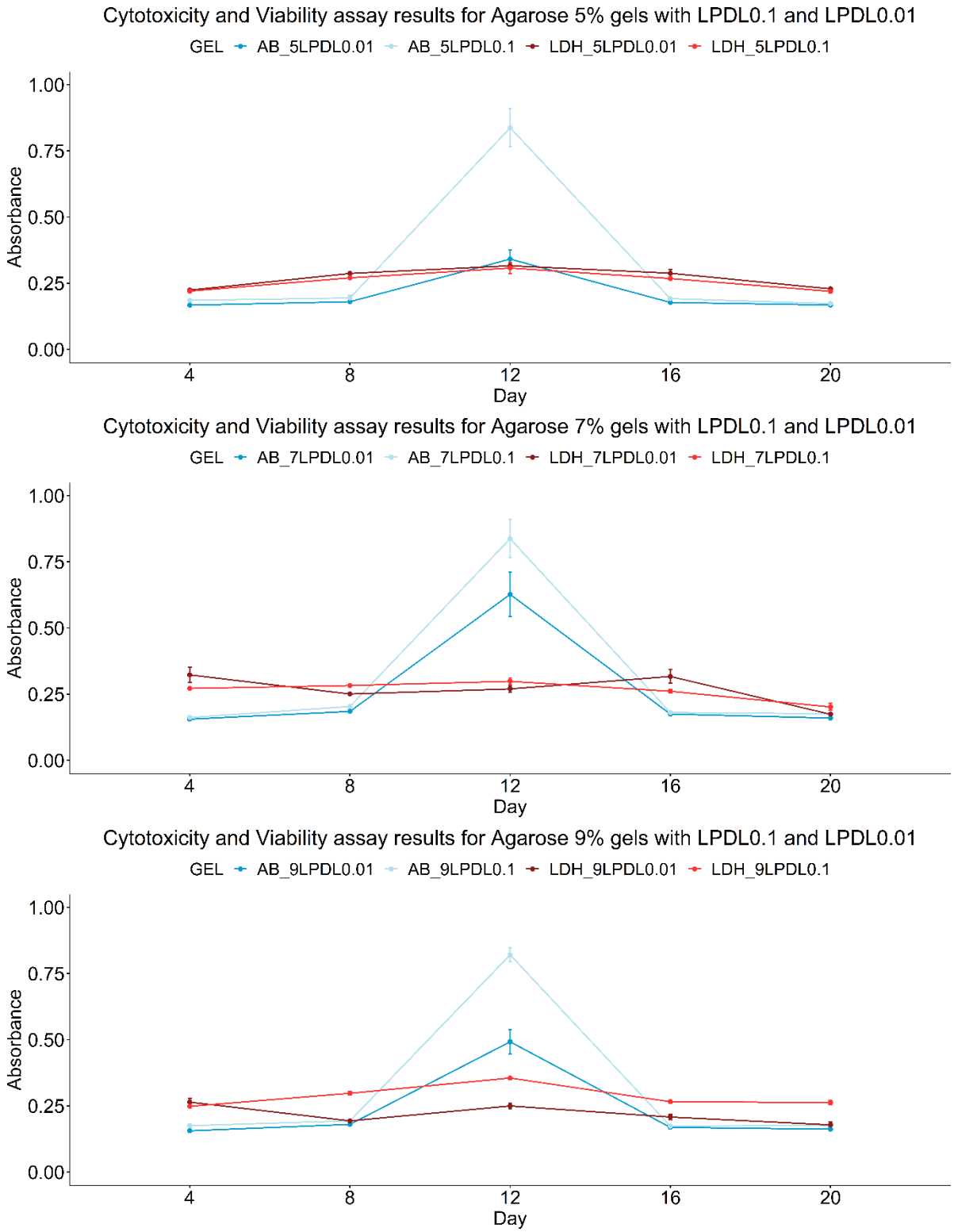

Figure 5.6.1 2: LDH and AB results for LPDL 0.1mg/mL (LPDL0.1) additive agarose gels and LPDL 0.01mg/mL (LPDL0.01) additive agarose gels across the five time points. AB results in blue, LDH results in red. Mean values plotted. Error bars = standard error.

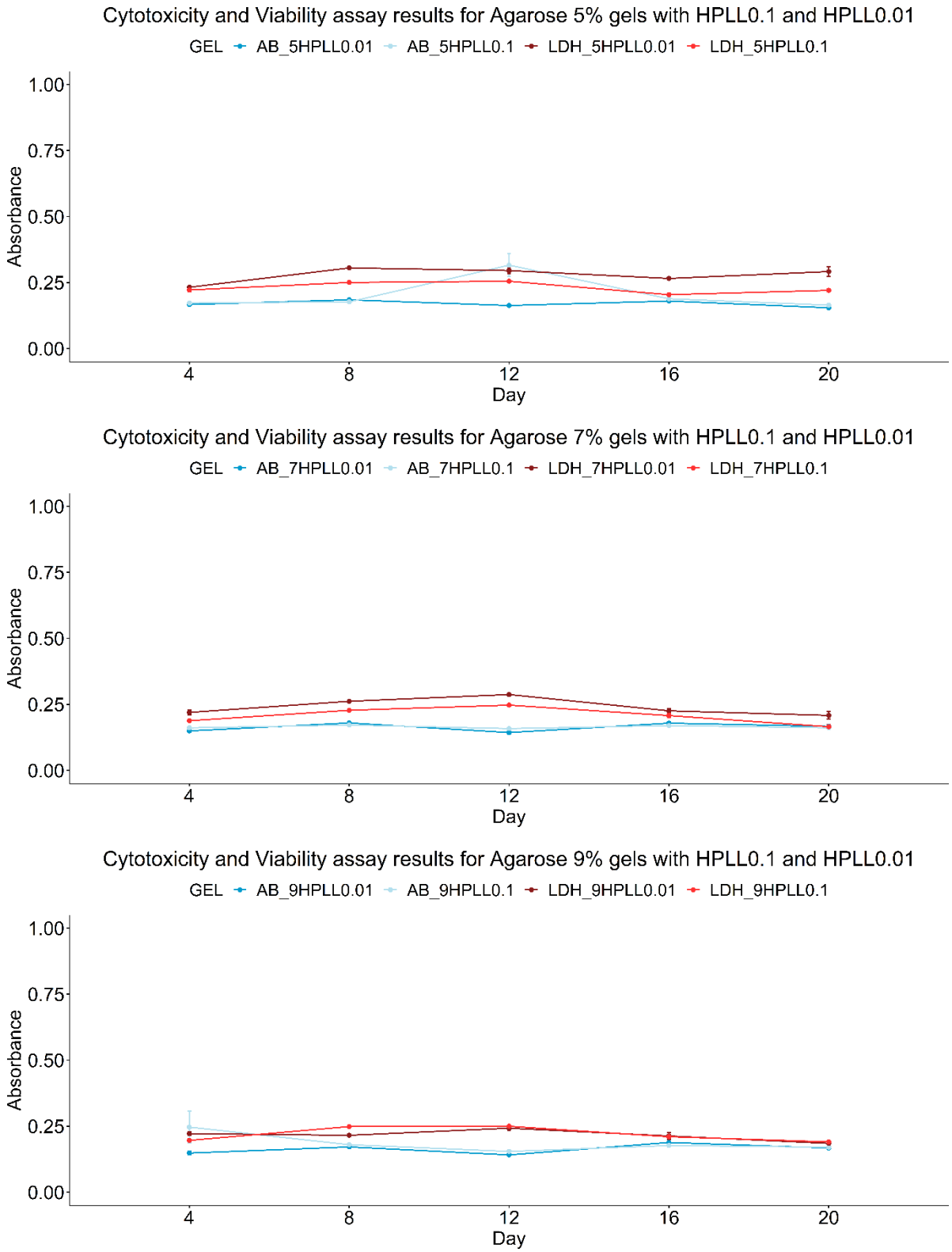

Figure 5.6.1 3: LDH and AB results for HPLL 0.1mg/mL (HPLL0.1) additive agarose gels and HPLL 0.01mg/mL (HPLL0.01) additive agarose gels across the five time points. AB results in blue, LDH results in red. Mean values plotted. Error bars = standard error.

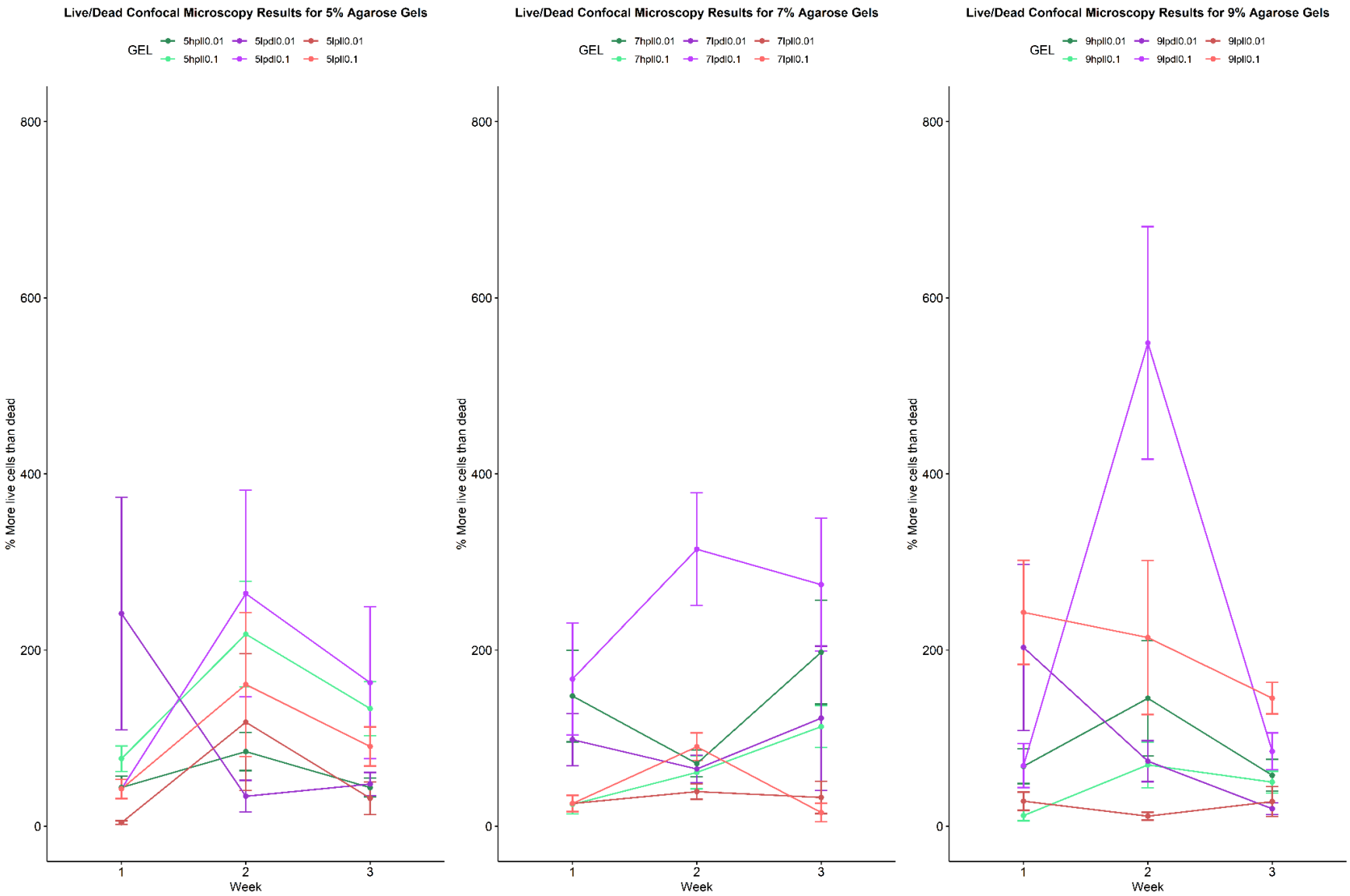

Figure 5.6.1 4: Live/dead confocal microscopy results, divided into percentages of agarose, means plotted with standard error

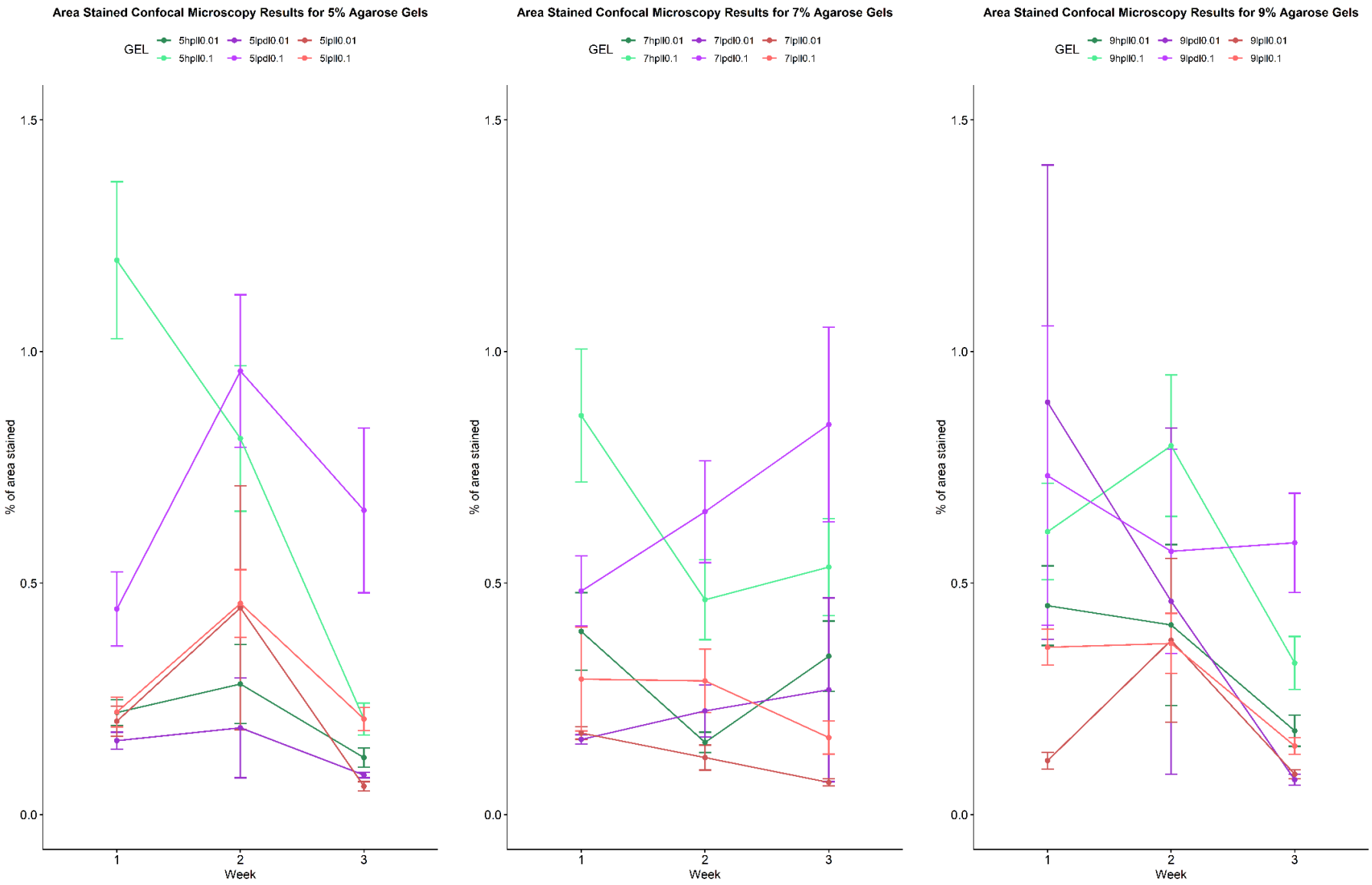

Figure 5.6.1 5: Area stained (%) confocal microscopy results, divided into percentages of agarose, means plotted with standard error

When statistically assessing the differences between the agarose gels and coating combinations with regards to the LDH and AB assays, some statistically significant outcomes were evident. The full results of the statistical tests for these assays can be found in Appendix 17. At day 4, the worst performing gel for cytotoxicity (LDH assay) (7% Agarose/LPDL 0.1) is statistically worse than most of the other 17 gels, and the best performing gel for vitality (AB assay) (9% agarose/HPLL0.1) is better than most of the 17 gels. Very few other statistically significant comparisons were found at Day 4.

At day 8 more statistically significant comparisons were identified, and more statistically significant differences were found for the 0.1mg/mL coatings than the 0.01mg/mL coatings of poly-lysine and increased statistical differences were found for the LDH assay than the AB assay.

At day 12, more statistical differences were found for the comparisons with the AB results than with the LDH results, and again the 0.1mg/mL coatings seemed to have resulted in more statistically significant comparisons than the 0.01mg/mL coatings. Of particular note, 5LPLL0.1 performed statistically well in terms of low cytotoxicity (LDH), 5LPDL0.1 and 9LPDL0.1 performed statistically well in terms of cellular vitality (AB).

At day 16, very few trends for the AB/LDH assays come to light. More statistically significant differences are seen in the LDH assay results than the AB results.

At day 20 the gels coated with the 0.01mg/mL poly-lysines have more statistically significant comparisons than the 0.1mg/mL poly-lysines. Of particular note, 5HPLL0.01 and 5LPLL0.01 performed particularly badly, and this was proved statistically.

A weak, but pertinent, finding also comes to light from looking at the statistical tables for the LDH and AB assays; for many of the comparisons of different agarose concentrations with the same coating, there is no statistically significant difference between the gels. For example, see Day 16 LDH cytotoxicity results for 5%, 7% and 9% agarose gels coated with LPDL 0.1 (these comparisons are all non-significant) and for the AB assay, the only comparison that is statistically significant for these gels is LPDL 0.1 with 5% agarose vs LPDL 0.1 with 9% agarose.

When assessing the statistical differences between time points for each individual gel for the AB and LDH assays (Appendix 18), very few trends are appreciable. That being said, LDH assays at day 8 seemed to produce more statistically significant comparisons for most gels. For the AB assay, the most statistically significant results were observed with comparisons including day 4. This does fit with the graphical data in Figures 5.6.1 1-5.6.1 3 to some degree as day 4 is the point where the AB assay is at its lowest value for most of the gels and day 8 is the point where the LDH assay is at its highest for most of the gels.

When assessing the statistical confocal live/dead results, very few statistically significant results were identified when comparing gels (Appendix 19). Example images of the live/dead stains are available in

Figures 5.6.1 6- 5.6.1 8. Indeed, for week 1, there were no statistically significant differences identified. At week 2, the best performing gel (9% agarose with LDPL 0.1) was statistically better than most other gels. At week 3, only two comparisons were statistically significant; i) 7% agarose with HPLL 0.01 and 7% agarose with LPLL 0.01, ii) 7% agarose with LPDL 0.1 and 7% agarose with LPLL 0.1. When assessing whether the changes for each gel over time are statistically significant (i.e. comparing the live/dead confocal results for an individual gel at time points week1, week 2 and week 3), again very few statistically significant results were evident (Appendix 20). Of these, 9LPDL0.1 had the most statistically significant differences between each of its time points – only week 1 vs week 3 resulted in a non-significant comparison. Where statistically significant differences were identified, these differences were found exclusively in gels coated with HPLL 0.1 and LPDL 0.1 and only for 7% gels and 9% gels.

When assessing the statistical test results for area stained (Appendix 19) comparing gel types, at week 1, only one statistically significant comparison comes to light; 5HPLL0.1 vs 9LPLL0.01; this stands to reason as these were the best and worst performing gels at this time point. At week 2, two comparisons resulted in a statistically significant difference; 5LPDL0.1 vs 7HPLL0.01 and 5LPDL0.1 vs 7LPLL0.01; again, this makes sense as 5LPDL0.1 was the best performing gel and 7HPLL0.01 and 7LPLL0.01 were the two worst performing gels. For week 3, most of the statistically significant comparisons involve gels coated with LDPL 0.1 (5%, 7% and 9% agarose), but interestingly no statistically significant differences were found between the three LPDL 0.1 coated gels (5%, 7% and 9% agarose) – see Appendix 19. This is important to note, because at week 3, the gels coated with LPDL 0.1 were the best performing in each of the agarose gel percentage cohorts (i.e. of the 5% agarose gels, the 7% agarose gels and the 9% agarose gels). When looking at an individual gel level, and comparing the outcomes for each week, 7% gels showed the least statistically significant differences when comparing different time points, and this can be appreciated by looking at Figure 5.6.1 5 which shows that the results for 7% gels had the least variability in their outputs for area stained compared to 9% and 5% gels. No other appreciable trends were found comparing the weekly outputs for the area stained at an individual gel level (Appendix 20).

When looking at all of the results combined for live and dead assessments (LDH assays, AB assays and confocal live/dead) and area, with outputs ranked from best to worst (ranking 1-18), and assessing these outputs on a heatmap (Figure 5.6.1 9), it is possible to identify some general trends. Firstly, the gels coated with 0.1mg/mL LPLL/LPDL/HPLL performed better than their counterparts with 0.01mg/mL coating. Secondly, coatings HPLL0.1 and LPDL0.1 appear to have performed best overall. Thirdly, when looking at HPLL0.1, LPDL0.1 and LPLL0.1 coatings, the 5% gels in these cohorts performed best. There is also an inverse relationship seen looking at LDH and AB outputs for HPLL 0.1 and LPDL0.1 coated gels; for HPLL0.1 gels, there was a poor AB output, but a good LDH output and for LPDL0.1 gels, there was a good AB output but a poor LDH output. The area for both of these cohorts

scored highly (Figure 5.6.1 9). The live/dead confocal output was slightly better for LPDL0.1 gels than HPLL0.1 gels.

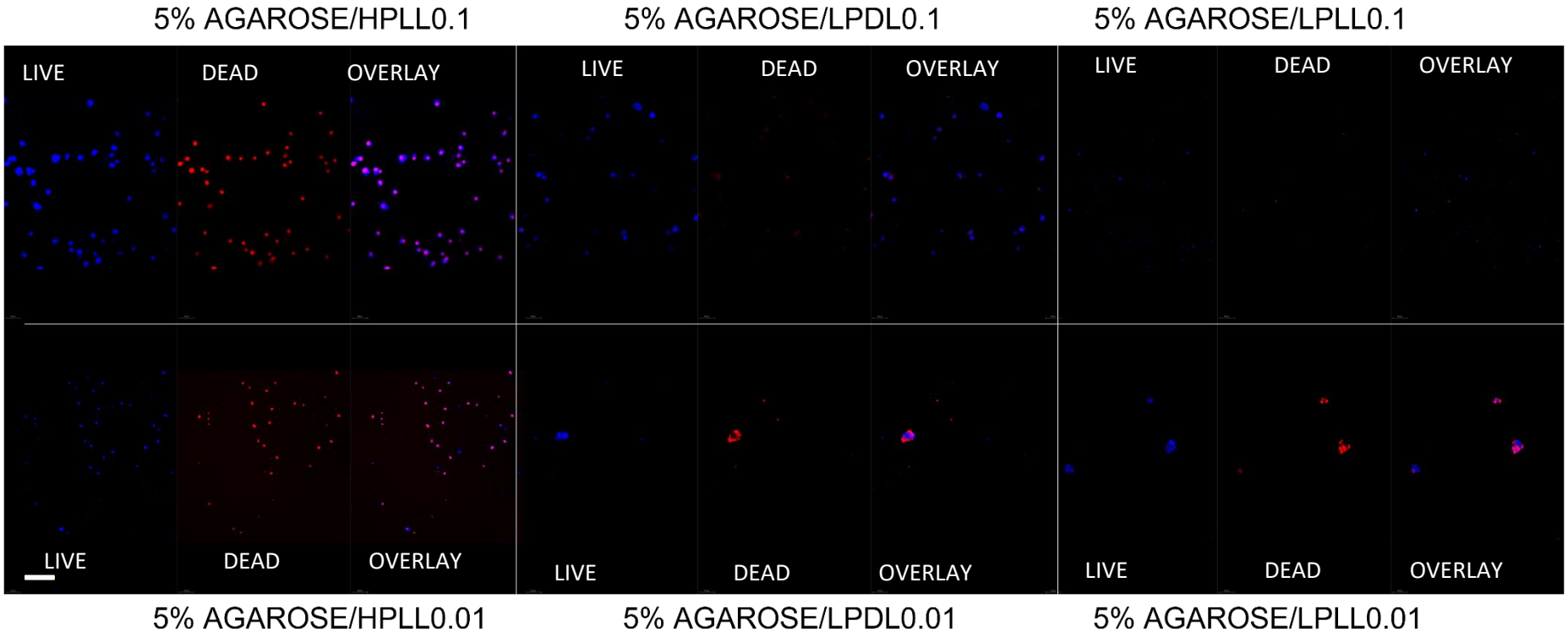

Figure 5.6.1 6: Example of images used for live/dead and area (%) analysis for 5% agarose gels. Scale bar = 100µm. Blue = H3342 stain, red = EH. Time point = week 3.

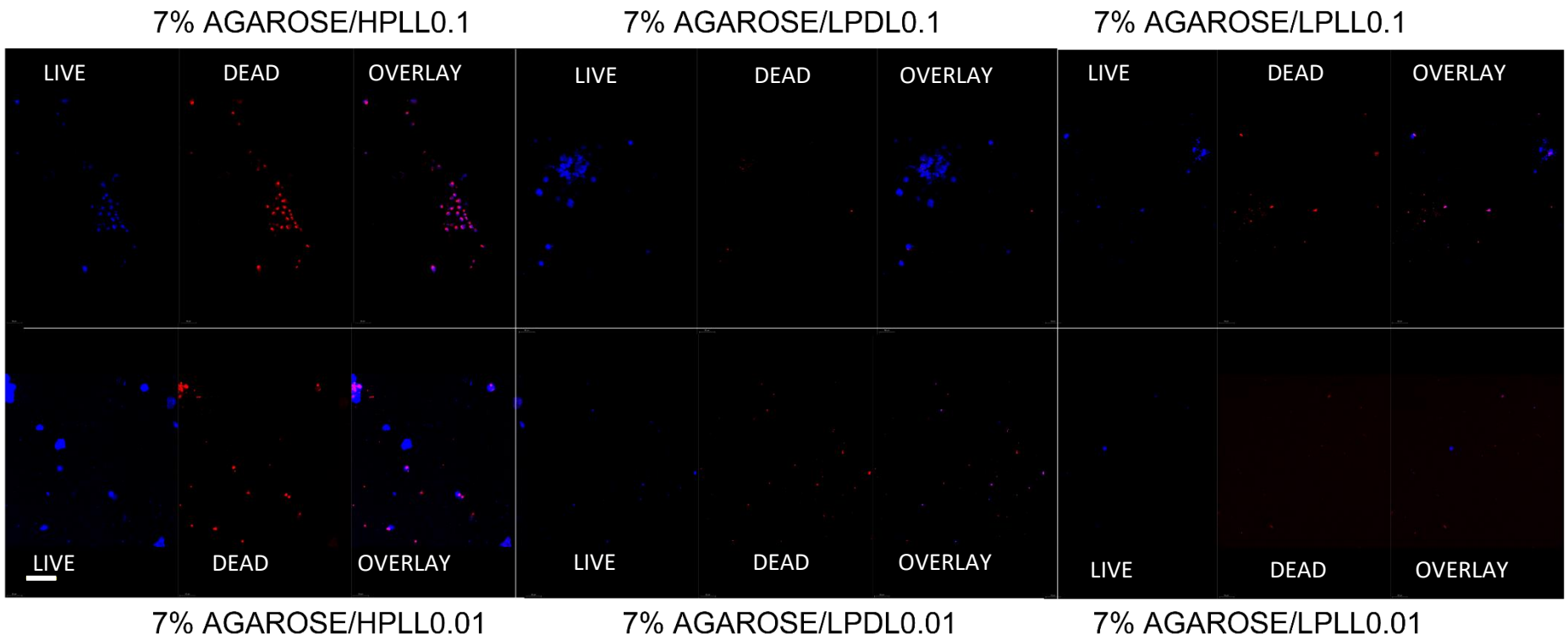

Figure 5.6.1 7: Example of images used for live/dead and area (%) analysis for 7% agarose gels. Scale bar = 100µm. Blue = H3342 stain, red = EH. Time point = week 3.

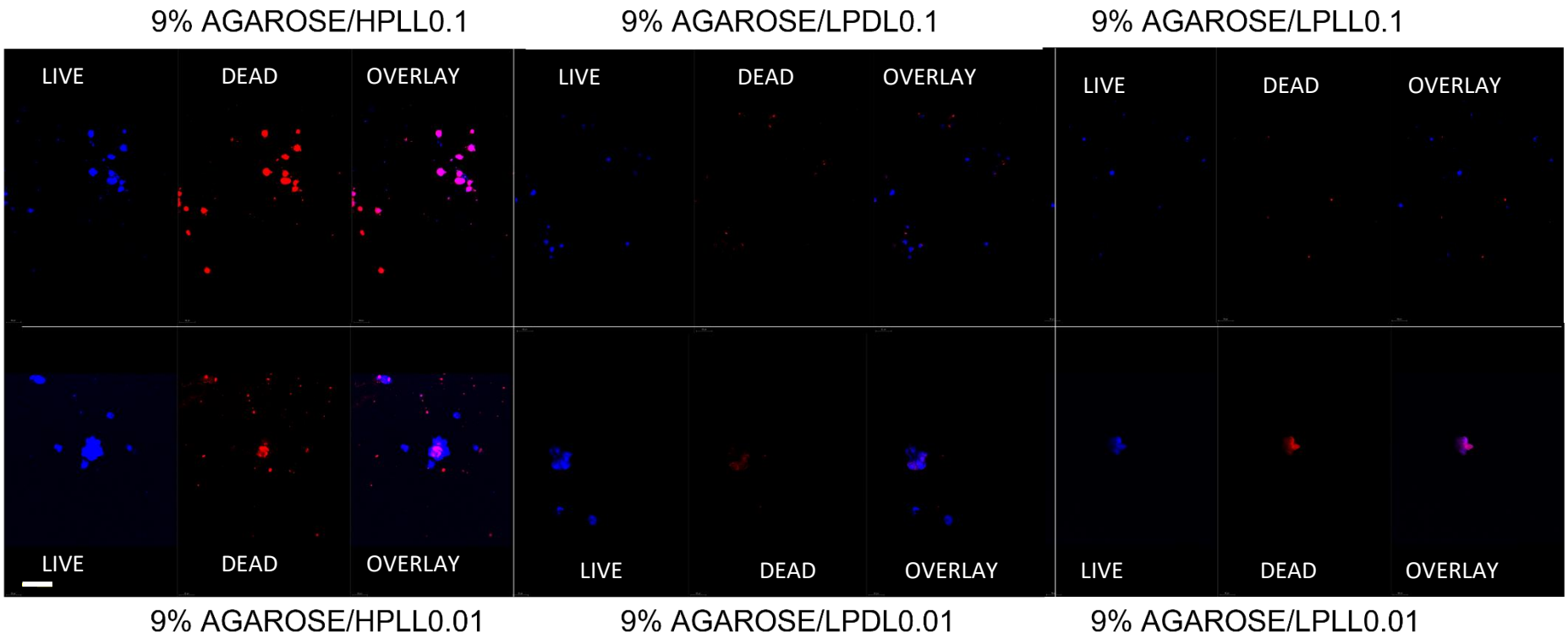

Figure 5.6.1 8: Example of images used for live/dead and area (%) analysis for 9% agarose gels. Scale bar = 100µm. Blue = H3342 stain, red = EH. Time point = week 3.

	HPLL0.1_5	HPLL0.1_7	HPLL0.1_9	HPLL0.01_5	HPLL0.01_7	HPLL0.01_9	LPLL0.1_5	LPLL0.1_7	LPLL0.1_9	LPLL0.01_5	LPLL0.01_7	LPLL0.01_9	LPDL0.1_5	LPDL0.1_7	LPDL0.1_9	LPDL0.01_5	LPDL0.01_7	LPDL0.01_9
LDH_1	12	1	2	14	8	11	3	9	4	6	5	7	10	17	15	13	18	16
LDH_2	6	4	5	10	9	2	8	3	13	11	14	15	12	16	18	17	7	1
LDH_3	6	3	5	10	9	2	1	11	15	13	8	17	14	12	18	16	7	4
LDH_4	1	2	4	10	8	5	13	6	7	16	14	18	12	9	11	15	17	3
LDH_5	11	1	6	18	8	5	9	4	12	17	14	15	10	7	16	13	2	3
AB_1	5	11	1	8	17	18	4	13	12	9	16	6	2	10	3	7	15	14
AB_2	16	17	13	1	14	18	4	15	6	3	8	7	5	2	9	11	10	12
AB_3	11	15	16	14	17	18	8	4	12	9	5	7	1	3	2	10	6	13
AB_4	5	17	14	11	12	6	1	3	7	2	8	9	4	10	16	13	15	18
AB_5	12	16	8	18	11	10	4	2	13	3	1	15	7	6	5	9	17	14
LD_1	7	15	18	12	5	8	10	13	3	17	14	16	11	4	9	1	6	2
LD_2	4	14	13	10	12	7	6	3	8	9	16	18	2	5	1	17	15	11
LD_3	4	6	10	13	1	9	7	18	12	14	15	17	3	2	8	11	5	16
AREA_1	1	3	5	13	9	7	12	11	10	14	15	18	8	6	4	17	16	2
AREA_2	2	6	3	13	17	12	9	14	11	8	18	10	1	4	5	16	15	7
AREA_3	7	4	6	12	5	9	8	10	11	18	17	13	2	1	3	14	16	15
TOTAL	110	135	129	187	162	147	107	139	156	169	188	208	104	114	143	200	187	151
RANKING	**3**	**6**	**5**	**14**	**12**	**9**	**2**	**7**	**11**	**13**	**16**	**18**	**1**	**4**	**8**	**17**	**14**	**10**

Figure 5.6.1 9: Heatmap demonstrating the performance of the 18 different gel concentration /poly-lysine combinations. Paler colour = worse performing. Darker colour = better performing. Gels ranked 1-18, with 1 being the best in each given output, 18 being the worst in each given output.

Key: LDH_1 = LDH outcome for reading 1 (4 days), LDH_2 = LDH outcome for reading 2 (8 days), LDH_3 = LDH outcome for reading 3 (12 days), LDH_4 = LDH outcome for reading 4 (16 days), LDH outcome for reading 5 (20 days). AB_1 = AB outcome for reading 1 (4 days), AB_2 = AB outcome for reading 2 (8 days), AB_3 = AB outcome for reading 3 (12 days), AB_4 = AB outcome for reading 4 (16 days), AB_5 = AB outcome for reading 5 (20 days). LD_1 = Live/dead confocal outcome for reading 1 (week 1), LD_2 = Live/dead confocal outcome for reading 2 (week 2), LD_3= Live/dead confocal outcome for reading 3 (week 3). AREA_1 = Area stained (confocal) for reading 1 (week 1), AREA_2 = Area stained (confocal) for reading 2 (week 2), AREA_3 = Area stained (confocal) for reading 3 (week 3).

5.6.2 BRIGHTFIELD CELL IMAGING

The morphology of the cells on the differently coated gels varied, with HPLL0.1 coated gels resulting in cells that remained tightly bound to the gel with a ball-like morphology. All other gels resulted in cells with a more spread out morphology. See Figure 5.6.2 1.

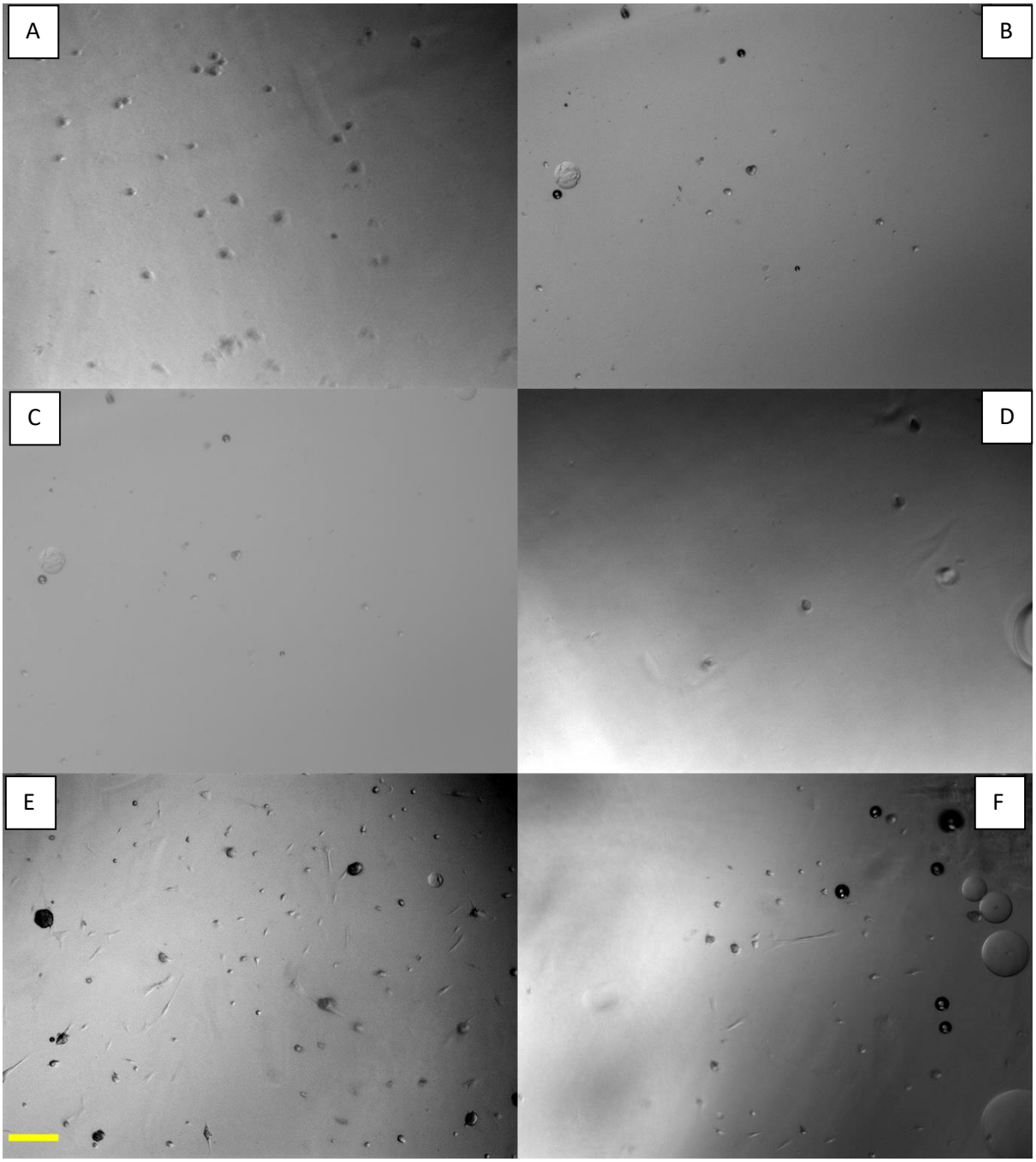

Figure 5.6.2 1: Representative brightfield images demonstrating the morphology of DPSCs growing on the agarose gels. A=7HPLL0.1, B= 7HPLL0.01, C=7LPLL0.1, D=7LPLL0.01, E=7LPDL0.1, F= 7LPDL0.01 Scale bar = 50µm. Timepoint = week 1

When assessing the morphology of the cells grown on different coatings, the LPDL 0.1mg/mL gels have a much more ‘spread-out’ morphology (Figure 5.6.2 1). From the brightfield images, it can also be appreciated how much more sparsely cellular coated the 0.01mg/mL gels were.

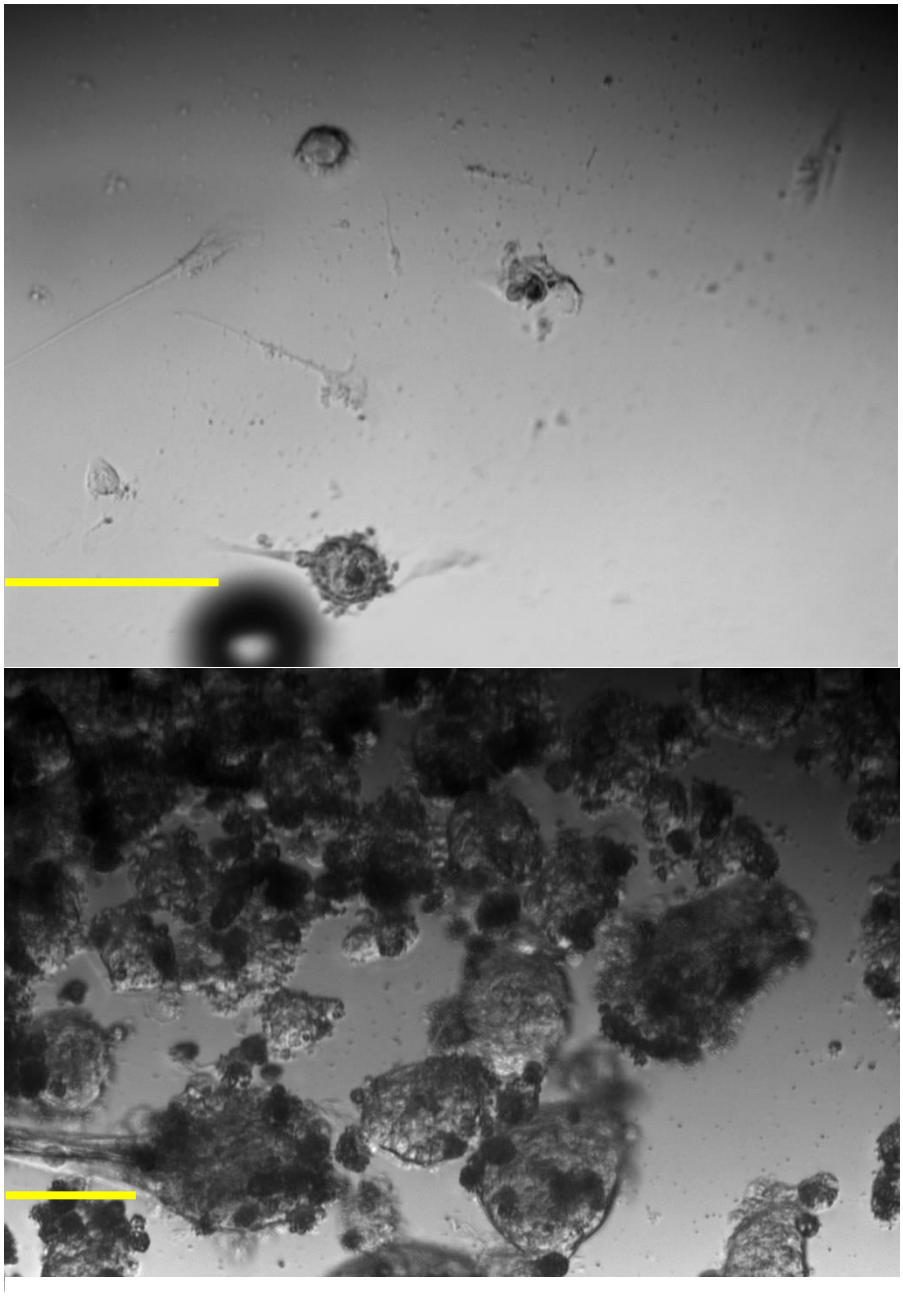

Figure 5.6.2 2:Brightfield images of DPSCs with a secretory phenotype, possibly laying down mineral, comparing odontogenic media and basal media. a) 9LPDL0.1 with basal media, B) 9LPDL0.1 with odontogenic media – scale bars both 50µm, week 2

After the odontogenic media was added, the cells displayed more of a secretory morphology and spicules of mineral began to be visible. With controls cultured in basal media, the cells did still appear to secrete a mineral substance but it was less prevalent in basal media, see Figure 5.6.2 2. In some areas, the mineral formed a thin coating/film across the gel surface, partially obscuring the cells (Figure 5.6.2 3). The mineral produced is explored later in the thesis. Occasional cells at this point also took on an odontoblast-like morphology (Figure 5.6.2 2).

Based upon the results of the LDH assay, AB assay, confocal live/dead, brightfield images and area stained assessments, it was decided that the LPDL 0.1 mg/mL and LPDL 0.01mg/mL gels would be taken forwards to use for dentinogenic scaffolds.

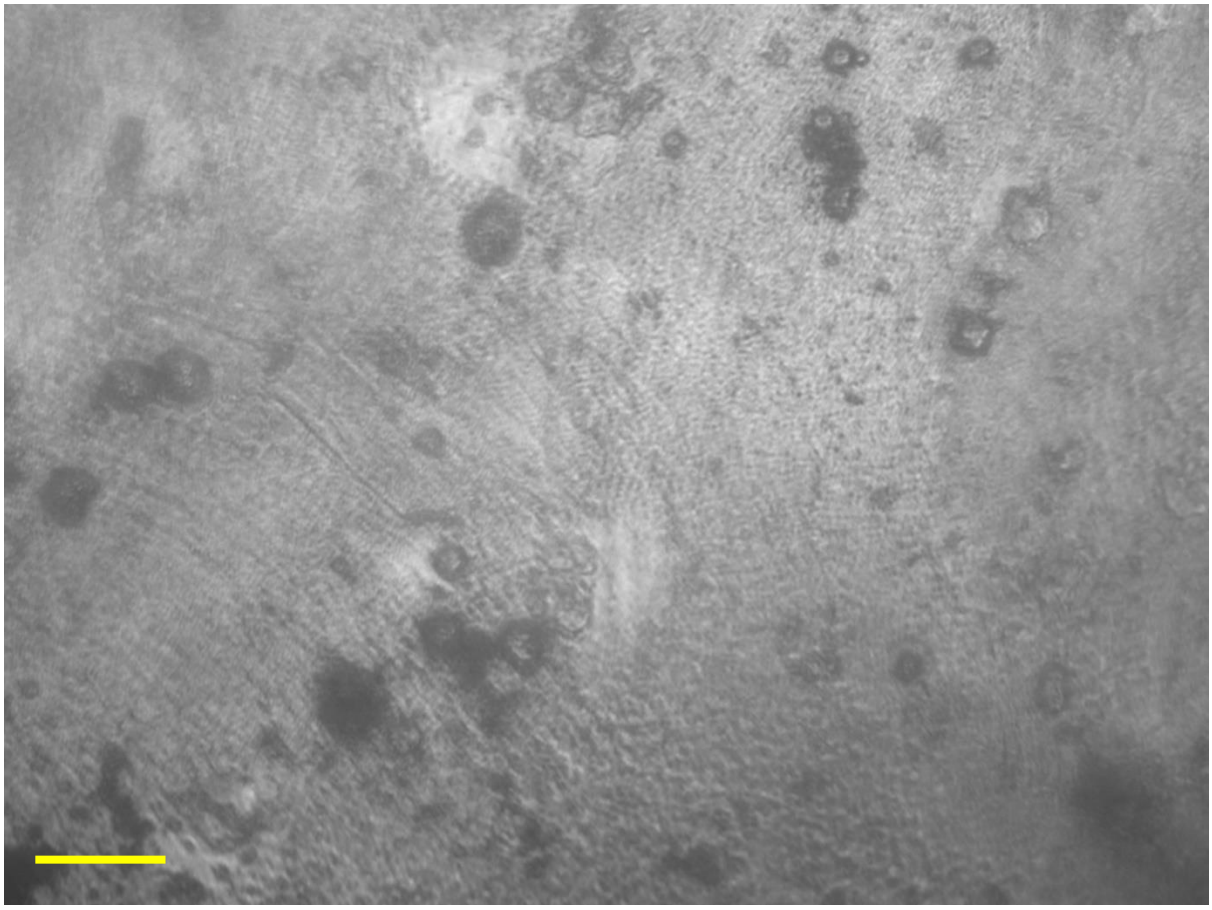

Figure 1.6.2 3: Brightfield image of 7LPDL0.1 (cultured in odontogenic media) gel with thin layer of mineral obscuring cells scale bar = 50µm

5.6.3 GEL CHARACTERISATION

KEY FINDINGS

1. There was an increase in elastic modulus with an increase in agarose % (for both AFM and uniaxial compression)
2. No trend was found between the type of poly-lysine added and the resulting elastic modulus for AFM results, but for uniaxial compression results a trend was seen HPLL>LPDL>LPLL.
3. Swelling ratio reduced with increasing agarose %, and therefore also reduced with increasing elastic modulus
4. For the majority of gels, the addition of any poly-lysine increased the swelling ratio

5.6.3.1 AFM

	HPLL0.01	HPLL0.1	LPDL0.01	LPDL0.1	LPLL0.01	LPLL0.1	PLAIN
5% M	47	94	77	41	63	76	126
IQR	80	21	29	16	43	27	23
7% M	50	113	79	96	69	170	178
IQR	15	24	29	21	38	50	53
9% M	65	194	87	122	79	170	200
IQR	16	145	50	45	36	132	89

Table 5.6.3.1 1: Median (M) and interquartile ranges (IQR) for the results of the elastic modulus AFM testing. All values in kPa

The results of the AFM from the gels were all non-parametric, hence medians and IQRs quoted.

The results show an increase in the elastic modulus with agarose %, as seen in Table 5.6.3.1 1 and Figure 5.6.3.1 1. The plain agarose gels all exhibited higher elastic moduli than the gels with poly-lysine added.

The 0.1mg/mL poly-lysine/agarose gels generally had a higher elastic modulus than the 0.01mg/mL poly-lysine gels – the exception to this was 5LPDL0.1 and 5LPDL0.01, where the results were the opposite.

The overall median (all poly-lysine gels and plain gels combined) of the 5%, 7% and 9% agarose gels is 75kPa, 99kPa, 108kPa respectively.

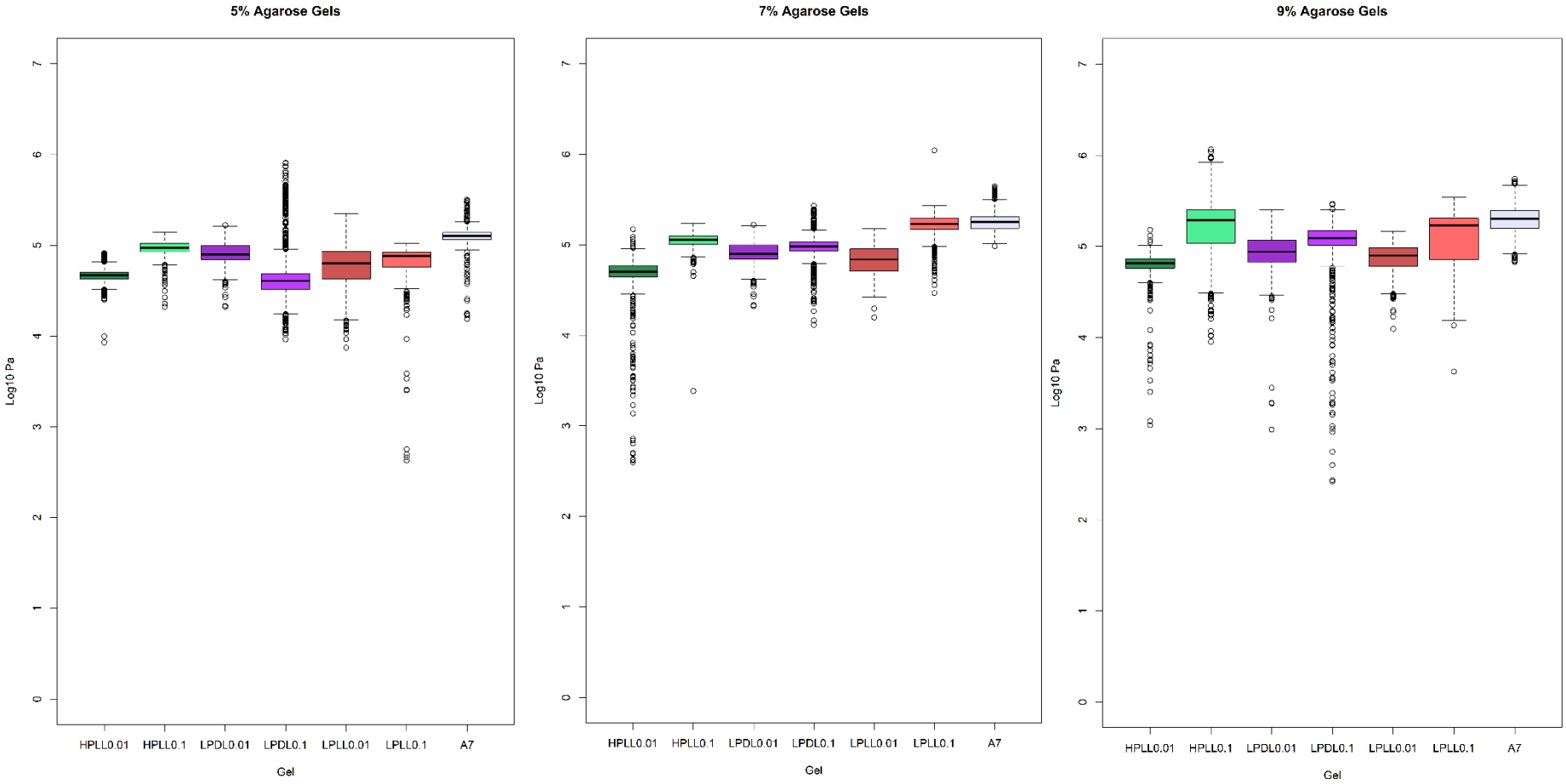

Figure 5.6.3.1 1: Box plots for the elastic modulus of different agarose %/poly-lysine combinations, separated into 5%, 7% and 9% agarose. Elastic modulus determined by AFM.

	HPLL0.01	HPLL0.1	LPDL0.01	LPDL0.1	LPLL0.01	LPLL0.1	PLAIN
5 vs 7	0.005	<0.001	0.100	<0.001	0.017	<0.001	<0.001
5 vs 9	<0.001	<0.001	0.001	<0.001	<0.001	<0.001	<0.001
7 vs 9	<0.001	<0.001	0.001	<0.001	<0.001	<0.001	<0.001

Table 5.6.3.1 2: Statistical test results (Dunn Test completed in R). Green =p<0.05, pink = p>0.05, p values quoted – comparing AFM elastic modulus results of different agarose concentrations within polylysine additive subgroups (i.e. comparing 5HPLL0.1 VS 7HPLL0.1 and 5LPLL0.1 vs 7LPLL0.1 etc.)

	HPLL0.01	HPLL0.1	LPDL0.01	LPDL0.1	LPLL0.01	LPLL0.1	PLAIN
HPLL0.01							
HPLL0.1	<0.001						
LPDL0.01	<0.001	<0.001					
LPDL0.1	0.0363	<0.001	<0.001				
LPLL0.01	<0.001	<0.001	<0.001	<0.001			
LPLL0.1	<0.001	<0.001	<0.001	<0.001	0.0161		
PLAIN	<0.001	<0.001	<0.001	<0.001	<0.001	<0.001	

Table 5.6.3.1 3: Statistical test results (Dunn Test, p value quoted) comparing AFM elastic modulus results of different poly-lysine additions for 5% agarose gels. Green =p value<0.05

	HPLL0.01	HPLL0.1	LPDL0.01	LPDL0.1	LPLL0.01	LPLL0.1	PLAIN
HPLL0.01							
HPLL0.1	<0.001						
LPDL0.01	<0.001	<0.001					
LPDL0.1	<0.001	<0.001	<0.001				
LPLL0.01	<0.001	<0.001	<0.001	<0.001			
LPLL0.1	<0.001	<0.001	<0.001	<0.001	<0.001		
PLAIN	<0.001	<0.001	<0.001	<0.001	<0.001	<0.001	

Table 5.6.3.1 4: Statistical test results (Dunn Test, p value quoted) comparing AFM elastic modulus results of different poly-lysine additions for 7% agarose gels. Green =p value<0.05

	HPLL0.01	HPLL0.1	LPDL0.01	LPDL0.1	LPLL0.01	LPLL0.1	PLAIN
HPLL0.01							
HPLL0.1	<0.001						
LPDL0.01	<0.001	<0.001					
LPDL0.1	<0.001	<0.001	<0.001				
LPLL0.01	<0.001	<0.001	<0.001	<0.001			
LPLL0.1	<0.001	<0.001	<0.001	1.000	<0.001		
PLAIN	<0.001	<0.001	<0.001	<0.001	<0.001	<0.001	

Table 5.6.3.1 5: Statistical test results (Dunn Test, p value quoted) comparing AFM elastic modulus results of different poly-lysine additions for 9% agarose gels. Green =p value<0.05, pink =p value>0.05

As can be seen in Table 5.6.3.1 2, the differences in the elastic modulus between each % of agarose when comparing the addition of the poly-lysines generally resulted in statistically significant differences in the elastic modulus of the gels. The only exception to this were 5LPDL0.01 vs 7LPDL0.01.

Statistically significant differences were identified across the board when assessing whether the poly-lysine additions could be affecting the elastic moduli for each agarose %. These can be seen in Tables 5.6.3.1 3-5.6.3.1 5. In all cases, the addition of poly-lysine resulted in a statistically significant difference between the plain gel and any of the gels with added poly-lysine (i.e. the addition of any poly-lysine resulted in a statistically significant difference when comparing the plain gel to the gel with the additive).

All comparisons were statistically significant for both 5% and 7% gels (Tables 5.6.3.1 3 and 5.6.3.1 4) and only for one comparison for the 9% gels (9LPDL0.1 vs 9LPLL0.1) was a non-statistically significant result found (Table 5.6.3.1 5). .

No trend was identified when exploring the type of poly-lysine added and the resulting elastic modulus.

5.6.3.2 UNIAXIAL COMPRESSION

The results of the uniaxial compression universally demonstrate a lower elastic modulus than the results obtained by AFM, see Figure 5.6.3.2 1 and Table 5.6.3.2 1.

For all poly-lysine additions, the agarose gel concentrations resulted in an expected, uniform trend of decreasing elastic modulus from 9% to 7% to 5% agarose. Interestingly, for all types of poly-lysine, the 0.1mg/mL additions resulted in a lower elastic modulus than the 0.01mg/mL additions.

Similar to the AFM results, any addition of poly-lysine resulted in a reduction in elastic modulus and this was true for all percentages of agarose gels. Therefore, the plain agarose gels had higher elastic modulus values than the ones where any poly-lysine was added – this mirrors the AFM results.

Interestingly, there is also a trend identifiable with regards to the type of poly-lysine added (which is different to the results generally found from the AFM work); the addition of HPLL0.01 resulted in the highest elastic modulus of all the gels across 5%,7% and 9% agarose gels where poly-lysine was added. Also, for 5% and 7% gels, HPLL0.1 addition resulted in the lowest elastic modulus values of all the gels. For 5% and 9% gels there is a slight trend also identifiable, with the poly-lysine type affecting the elastic modulus (HPLL>LPDL>LPLL) – this trend was not as strong for 7% gels.

Compared to the gels with poly-lysine additions, the pure agarose gels demonstrated a smaller standard deviation – see Table 5.6.3.2 1.

The overall mean values from the uniaxial compression test results for 5%, 7% and 9% gels were 165kPa, 247kPa and 378kPa respectively.

As can be seen in Table 5.6.3.2 2, for many of the agarose/poly-lysine gel combinations, the difference in w/v agarose concentration did not result in a statistically significant difference. However, the agarose gels with no poly-lysine added showed statistically significant differences between each percentage.

	HPLL0.01	HPLL0.1	LPDL0.01	LPDL0.1	LPLL0.01	LPLL0.1	PLAIN
5% M	255	11	175	161	149	140	261
SD	92	0.1	46	39	29	29	22
7% M	308	84	232	222	241	232	411
SD	29	64	49	16	45	56	13
9% M	496	480	406	280	234	229	518
SD	40	15	117	122	55	67	18

Table 5.6.3.2 1: Mean (M) values and standard deviation (SD) values for the results of the uniaxial compression tests

	HPLL0.01	HPLL0.1	LPDL0.01	LPDL0.1	LPLL0.01	LPLL0.1	PLAIN
5 vs 7	0.4272	0.187	0.216	0.098	0.049	0.086	0.001
5 vs 9	0.030	<0.001	0.061	0.222	0.098	0.134	<0.001
7 vs 9	0.004	0.006	0.108	0.491	0.873	0.956	0.002

Table 5.6.3.2 2: Statistical test results (Dunn Test completed in R). Green =p<0.05, pink = p>0.05, p values quoted – comparing uniaxial compression elastic modulus results of different agarose concentrations within polylysine additive subgroups (i.e. comparing 5HPLL0.1 VS 7HPLL0.1 and 5LPLL0.1 vs 7LPLL0.1 etc.)

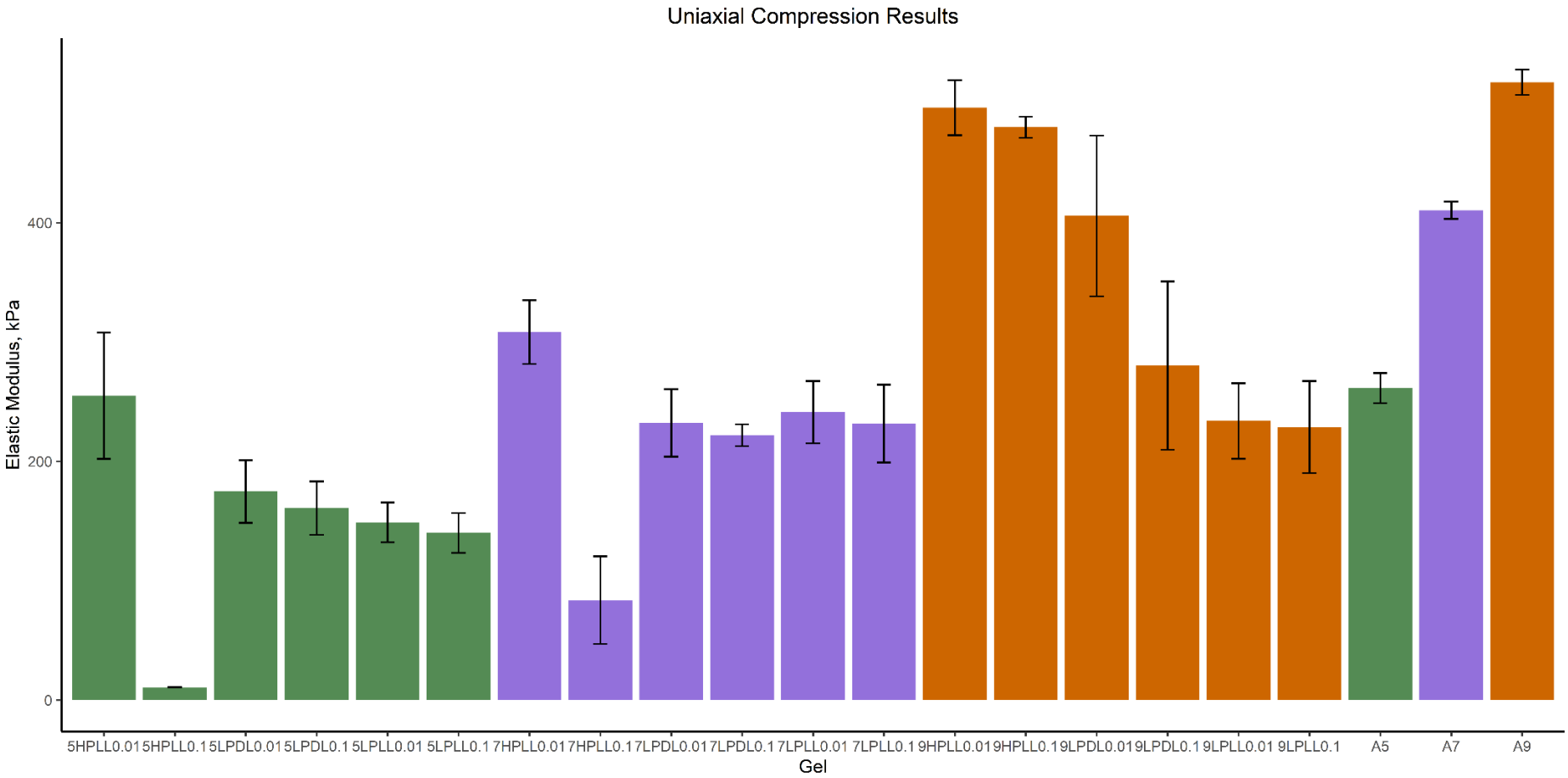

Figure 5.6.3.2 1: Elastic modulus determined by uniaxial compression results, mean results plotted with error bars showing standard deviation

When assessing for differences between the results from the gels at each percentage (i.e. looking solely at the 5% gels, 7% gels and 9% gels as subgroups), the only comparison that was statistically different was 7HPLL0.1 vs A7 (plain agarose) (padj 0.008), with Dunn's Test performed in R (data not shown).

5.6.3.3 SWELLING RATIO

As can be seen in Table 5.6.3.3 1, all of the gels had a water content above 99%, making them hydrogels as per the definition by Oyen (312). This was calculated by dividing the average dry weight per gel by the average hydrated weight per gel and multiplying it by 100.

GEL	% WATER BY WEIGHT
5HPLL0.01	99.963
5HPLL0.1	99.963
5LPDL0.01	99.966
5LPDL0.1	99.963
5LPLL0.01	99.967
5LPLL0.1	99.961
7HPLL0.01	99.952
7HPLL0.1	99.957
7LPDL0.01	99.957
7LPDL0.1	99.955
7LPLL0.01	99.954
7LPLL0.1	99.953
9HPLL0.01	99.954
9HPLL0.1	99.947
9LPDL0.01	99.948
9LPDL0.1	99.952
9LPLL0.01	99.957
9LPLL0.1	99.923
A5	99.953
A7	99.943
A9	99.933

Table 5.6.3.3 1: Swelling ratio results, water content of hydrated agarose gels by weight. A5 = plain 5% agarose, A7 = plain 7% agarose, A9 = plain 9% agarose

As can be seen in Figure 5.6.3.3 1, with increasing agarose concentration, there was a reduction in the swelling ratio. This indicates that gels of higher agarose concentration have less water content, as shown in Table 5.6.3.3 1.

Generally, the addition of any poly-lysine to the gels increased the swelling ratio, meaning more water was present in the poly-lysine/agarose gels than the pure agarose gels for each agarose % - the only exception to this was 9LPLL0.1, which had a lower swelling ratio than its pure agarose counterpart. This trend is generally not statistically significant, as can be seen in Table 5.6.3.3 2.

For the 5% agarose gels, there does seem to be a trend present, where the 0.01mg/mL poly-lysine gels (5HPLL0.01, 5LPLL0.01, 5LPDL0.01) all had higher swelling ratios than the 0.1mg/mL poly-lysine counterparts (5HPLL0.1, 5LPLL0.1, 5LPDL0.1). This trend was not mirrored in the 7% and 9% agarose gels.

There is no trend between the type of poly-lysine and the swelling ratio. This is corroborated by the statistical table (Table 5.6.3.3 2), comparing the results of all of the gels.

Most of the statistically significant results were found with comparisons involving 5LPDL0.01, 5LPLL0.01 and 9LPLL0.1. These gels have the highest and lowest swelling ratios.

As would be expected, the amount of water by weight has an inverse relationship with the percentage of agarose (i.e. with a higher agarose w/v %, the amount of water present reduces) – this is demonstrated in Table 5.6.3.3 1. As can also be seen in Table 5.6.3.3 1, the addition of any poly-lysine to the gel increases water content. The only exception to this is 9LPLL0.1, which has less water content than its pure agarose 9% counterpart.

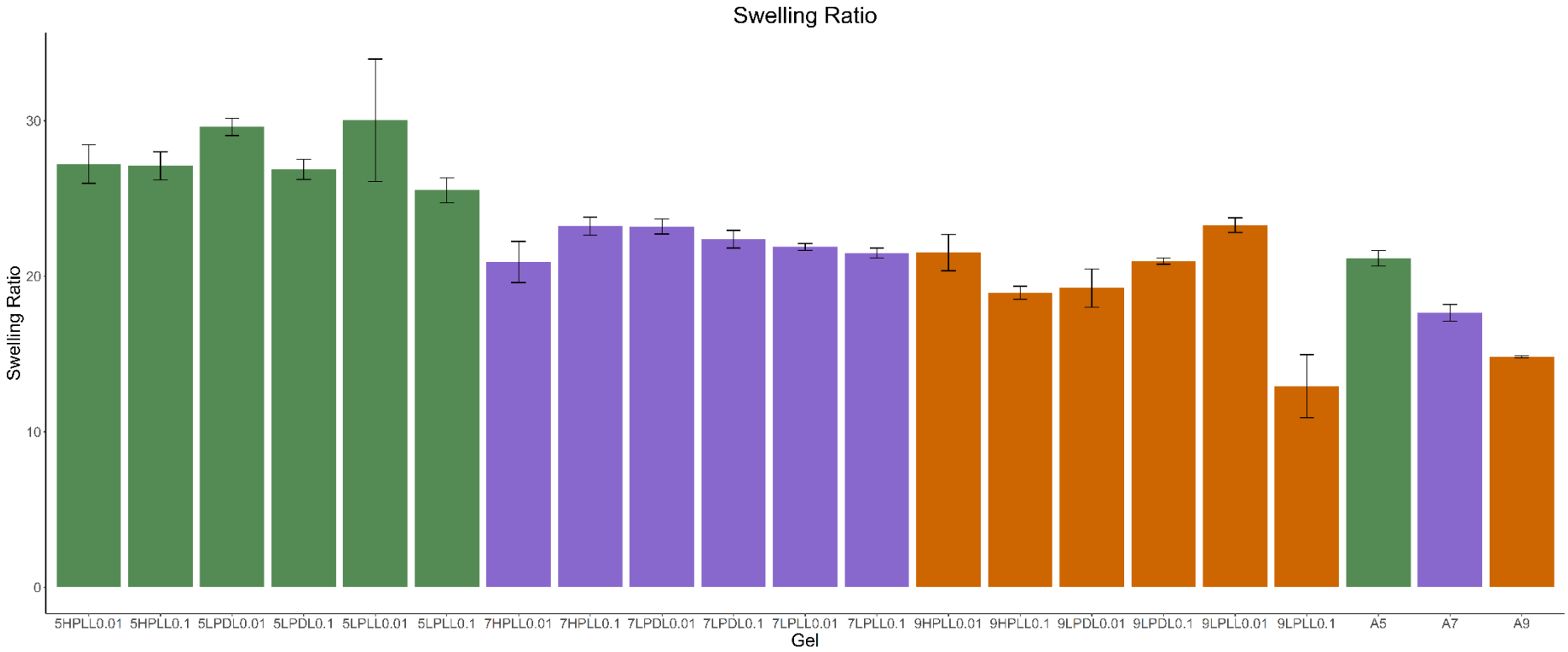

Figure 5.6.3.3 1: Mean swelling ratio with error bars showing standard deviation

SWELLING RATIO	5LPLL0.1	5LPLL0.01	5HPLL0.1	5HPLL0.01	5LPDL0.1	5LPDL0.01	7LPLL0.1	7LPLL0.01	7HPLL0.1	7HPLL0.01	7LPDL0.1	7LPDL0.01	9LPLL0.1	9LPLL0.01	9HPLL0.1	9HPLL0.01	9LPDL0.1	9LPDL0.01	A5	A7	A9
5LPLL0.1																					
5LPLL0.01	0.182																				
5HPLL0.1	1.000	0.603																			
5HPLL0.01	1.000	0.666	1.000																		
5LPDL0.1	1.000	0.515	1.000	1.000																	
5LPDL0.01	0.918	0.999	1.000	1.000	0.998																
7LPLL0.1	0.906	<0.001	0.468	0.409	0.556	0.037															
7LPLL0.01	0.958	0.001	0.590	0.527	0.678	0.059	1.000														
7HPLL0.1	1.000	0.011	0.941	0.912	0.969	0.253	1.000	1.000													
7HPLL0.01	0.746	<0.001	0.279	0.235	0.349	0.016	1.000	1.000	1.000												
7LPDL0.1	0.990	<0.001	0.754	0.696	0.827	0.106	1.000	1.000	1.000	1.000											
7LPDL0.01	1.000	0.010	0.937	0.907	0.966	0.247	1.000	1.000	1.000	1.000	1.000										
9LPLL0.1	<0.001	0.003	<0.001	<0.001	<0.001	<0.001	0.051	0.032	0.004	0.109	0.016	0.005									
9LPLL0.01	0.999	0.011	0.945	0.918	0.971	0.261	1.000	1.000	1.000	1.000	1.000	1.000	0.005								
9HPLL0.1	0.194	<0.001	0.0344	0.027	0.048	0.001	1.000	0.997	0.863	1.000	0.979	0.869	0.567	0.855							
9HPLL0.01	0.920	<0.001	0.495	0.434	0.583	0.041	1.000	1.000	1.000	1.000	1.000	1.000	0.046	1.000	0.999						
9LPDL0.1	0.785	<0.001	0.313	0.266	0.388	0.018	1.000	1.000	1.000	1.000	1.000	1.000	0.094	1.000	0.998	1.000					
9LPDL0.01	0.260	<0.001	0.051	0.040	0.0700	0.002	1.000	0.999	0.922	1.000	0.993	0.927	0.467	0.917	1.000	1.000	1.000				
A5	0.829	<0.001	0.358	0.307	0.438	0.023	1.000	1.000	1.000	1.000	1.000	1.000	0.078	1.000	1.000	1.000	1.000	1.000			
A7	0.046	<0.001	0.006	0.005	0.009	<0.001	0.942	0.882	0.473	0.991	0.752	0.483	0.919	0.463	1.000	0.932	0.986	1.000	0.977		
A9	<0.001	<0.001	<0.001	<0.001	<0.001	<0.001	0.190	0.130	0.025	0.344	0.073	0.026	1.000	0.024	1.000	0.175	0.308	0.836	0.266	0.998	

Table 5.6.3.3 2: Statistical results (p value from Dunn's test) comparing swelling ratios of each gel type. A5 = plain 5% agarose gel, A7 = plain 7% agarose gel, A9 = plain 9% agarose gel. Pink = p>0.05, green = p<0.05

5.6.3.4 CORRELATING UNIAXIAL COMPRESSION, AFM AND SWELLING RATIO RESULTS

Linking together the AFM and uniaxial compression results produces a significant trend – the addition of any poly-lysine results in a lower elastic modulus than is seen in pure agarose gels.

With increasing agarose concentration, the fold difference between the overall means of the gels for AFM and uniaxial compression increases (2.2x fold change for 5% gel, 2.5x fold change for 7% gel and 3.5x fold change for 9% gel). So, the difference between the two sets of elastic modulus results increases as the concentration of agarose increases (and as the overall elastic modulus values increase too).

As would be expected, the elastic moduli of the gels (with AFM and uniaxial compression) show a negative trend when correlated with swelling ratio – the greater the % of agarose (and so the greater the elastic modulus), the smaller the swelling ratio, and the less the water content of the gel.

5.6.4. CELL DIFFERENTIATION

5.6.4.1 IMMUNOFLUORESENCE

KEY FINDINGS

1. Expression of odontogenic markers DSPP, DMP1 and nestin was generally higher for gels cultured in odontogenic media than basal media on immunofluorescence
2. When comparing gels cultured in odontogenic media and basal media, more statistically significant differences were found for DMP1 and DSPP markers than nestin with immunofluorescence
3. Some cells showed an odontoblast-like morphology when cultured on 9% and 7% gels

To assess the differentiation of the cells, odontogenic markers NESTIN, DMP1 and DSPP were used for immunofluorescence on the agarose scaffolds at week 3, for the three chosen agarose percentages (5%, 7% and 9%). Scaffolds were seeded with cells as before, and cultured for 3 weeks. All gels were cultured in basal media for the first week, the gels were then split with one cultured in odontogenic media for the remaining two weeks and one in basal media for the remaining two weeks. Controls used were osteoblasts and DPSCs cultured on cell culture polystyrene. Osteoblasts were cultured in odontogenic media, DPSCs in basal media. Ratios for the fluorescence were calculated by using DAPI as a counter stain. As discussed in the methods, this was calculated as ratio = immunofluorescence pixels/DAPI pixels. The results of this can be seen in Figures 5.6.4.1 1-5.6.4.1 6. An example of one of the images captured provided in Figure 5.6.4.1 7, which demonstrates the IF staining.

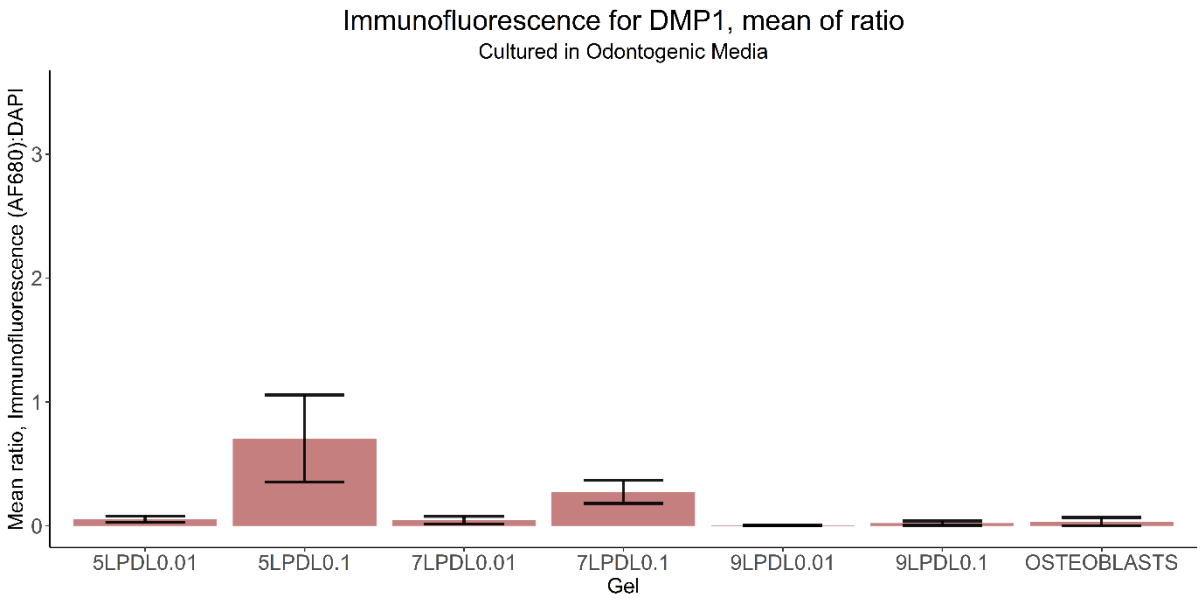

Figure 5.6.4.1 1: DMP1 immunofluorescence mean ratio (AF680:DAPI) with error bars showing standard deviation, all gels cultured in odontogenic media with osteoblasts as a control. Numerical figures in Table 5.6.4.1 1. Results from 5 images from 1 gel per bar.

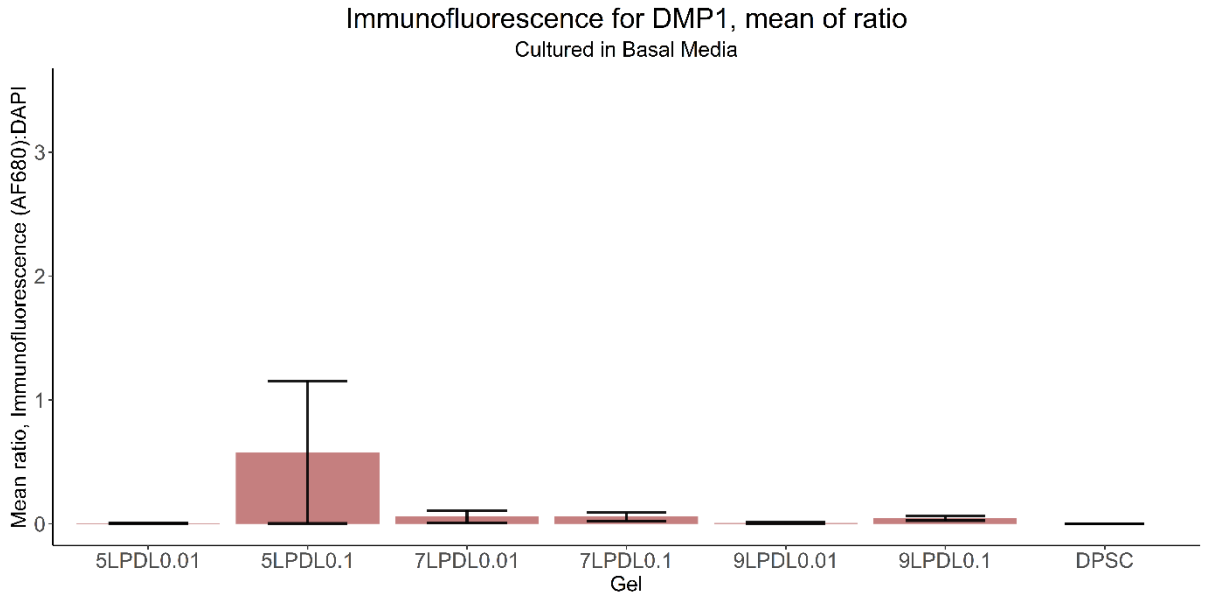

Figure 5.6.4.1 2: DMP1 immunofluorescence mean ratio (AF680:DAPI) with error bars showing standard deviation, all gels cultured in basal media with DPSCs as a control. Numerical figures in Table 5.6.4.1 1. Results from 5 images from 1 gel per bar.

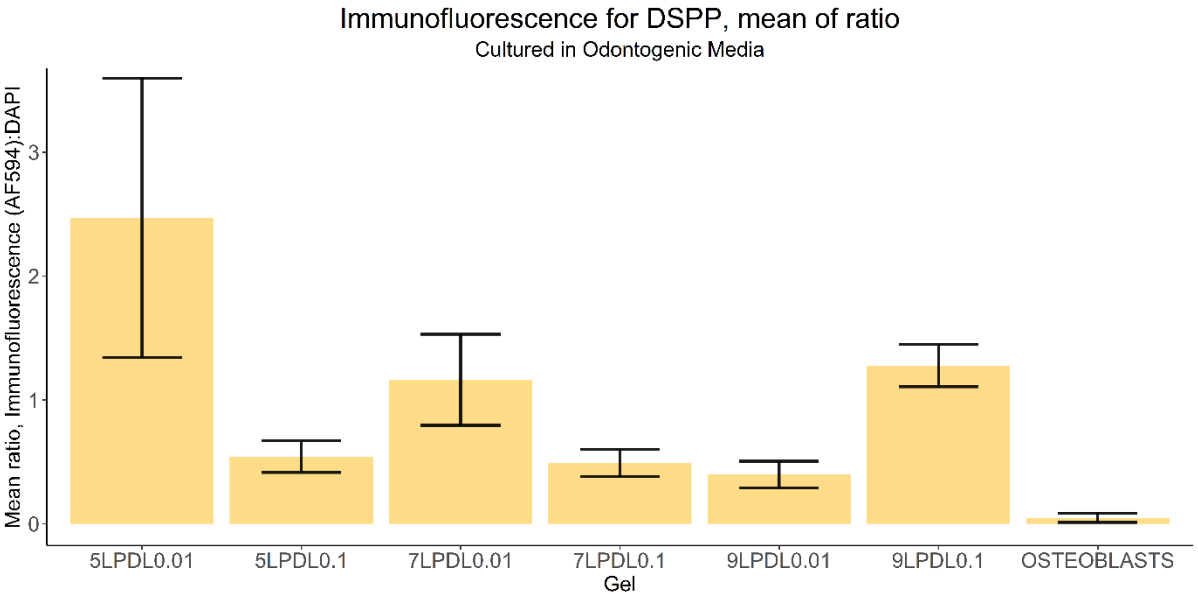

Figure 5.6.4.1 3: DSPP immunofluorescence mean ratio (AF594:DAPI) with error bars showing standard deviation, all gels cultured in odontogenic media with osteoblasts as a control. Numerical figures in Table 5.6.4.1 2. Results from 5 images from 1 gel per bar.

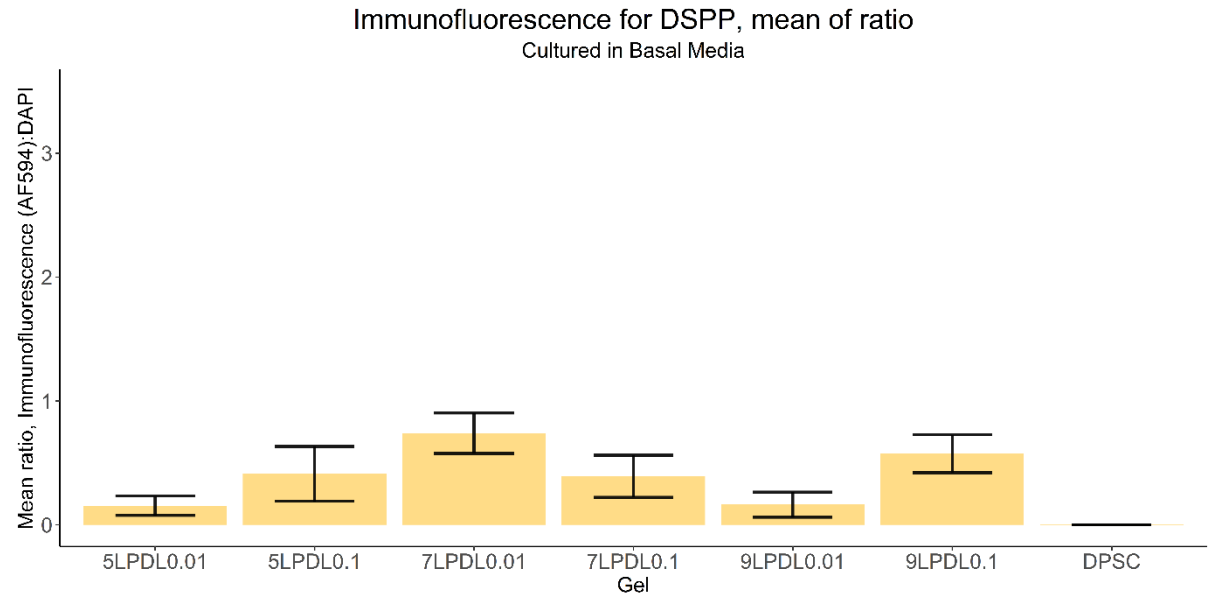

Figure 5.6.4.1 4: DSPP immunofluorescence mean ratio (AF594:DAPI) with error bars showing standard deviation, all gels cultured in basal media with DPSCs as a control. Numerical figures in Table 5.6.4.1 2. Results from 5 images from 1 gel per bar.

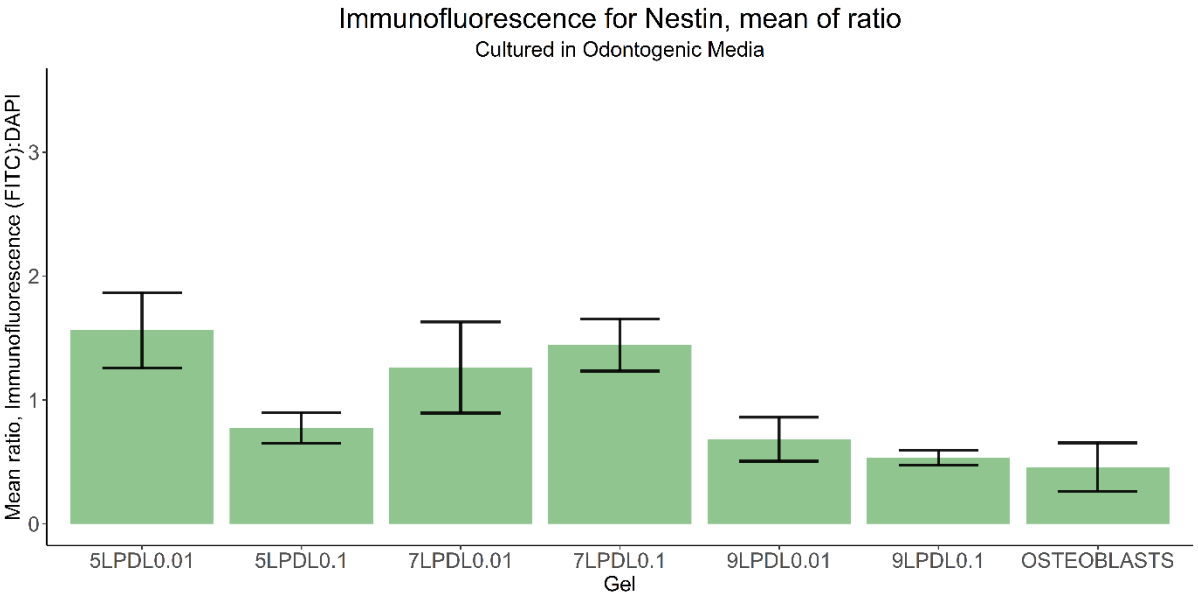

Figure 5.6.4.1 5: Nestin immunofluorescence mean ratio (FITC:DAPI) with error bars showing standard deviation, all gels cultured in odontogenic media with osteoblasts as a control. Numerical figures in Table 5.6.4.1 3. Results from 5 images from 1 gel per bar.

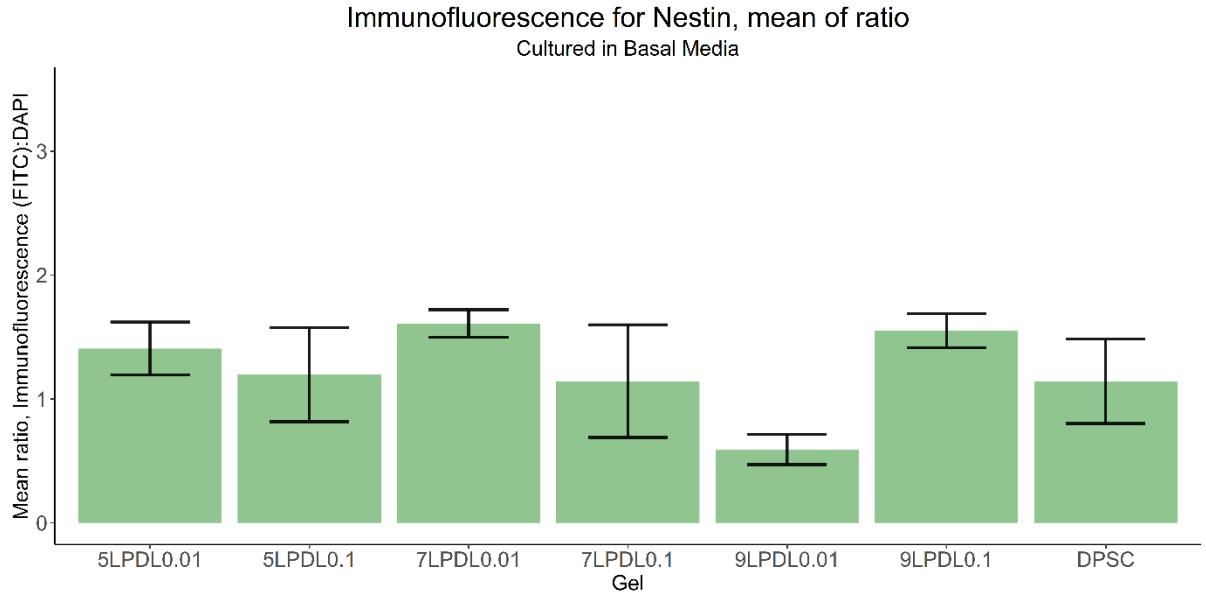

Figure 5.6.4.1 6: Nestin immunofluorescence mean ratio (FITC:DAPI) with error bars showing standard deviation, all gels cultured in basal media with DPSCs as a control. Numerical figures in Table 5.6.4.1 3. Results from 5 images from 1 gel per bar.

As can be seen in Figures 5.6.4.1 1-5.6.4.1 6 and Tables 5.6.4.1 1-5.6.4.1 3, odontogenic media produced a slightly higher expression for DMP1 and a markedly higher expression for DSPP when compared to basal media. For nestin, the opposite was found, whereby expression was higher for cells cultured in basal media, though the difference seems to be slight. As can be seen in Tables 5.6.4.1 1-5.6.4.1 3, the statistical differences between the gels cultured in odontogenic media vs basal media is most obvious for DMP1 expression. Nestin displayed the least number of differences between gels cultured in basal media vs odontogenic media, with only 9LPDL0.1 showing a statistically significant difference. Gel 7LPL0.01 had no statistical difference between odontogenic and basal media for the expression of any of the odontogenic markers investigated.

When comparing DPSCs cultured on gels vs DPSCs cultured on tissue culture polystyrene in basal media, only one gel showed any statistically significant difference; 7LPDL0.01 showed a statistically higher expression for DSPP (see Tables 5.6.4.1 4-5.6.4.1 6 for the statistical results and Figure 5.6.4.1 4 for the graph). This does suggest that the media is having an important impact on the differentiation of the DPSCs, potentially more so than the elastic modulus of the gel.

When comparing DPSCs cultured on gels vs osteoblasts cultured on tissue culture polystyrene in odontogenic media, statistical differences were seen for DMP1 (5LPDL0.1 vs osteoblasts), DSPP (5LPDL0.01 vs osteoblasts) and Nestin (5LPDL0.01 vs osteoblasts). Again, these are shown in Tables 5.6.4.1 4-5.6.4.1 6 and Figures 5.6.4.1 1, 5.6.4.1 3 and 5.6.4.1 5. In all of these instances of statistical difference, the gel is expressing more of the odontogenic marker than the cells cultured on tissue culture polystyrene. Also, in all of these instances, the statistical significance arises from the highest and lowest expressions for each odontogenic marker.

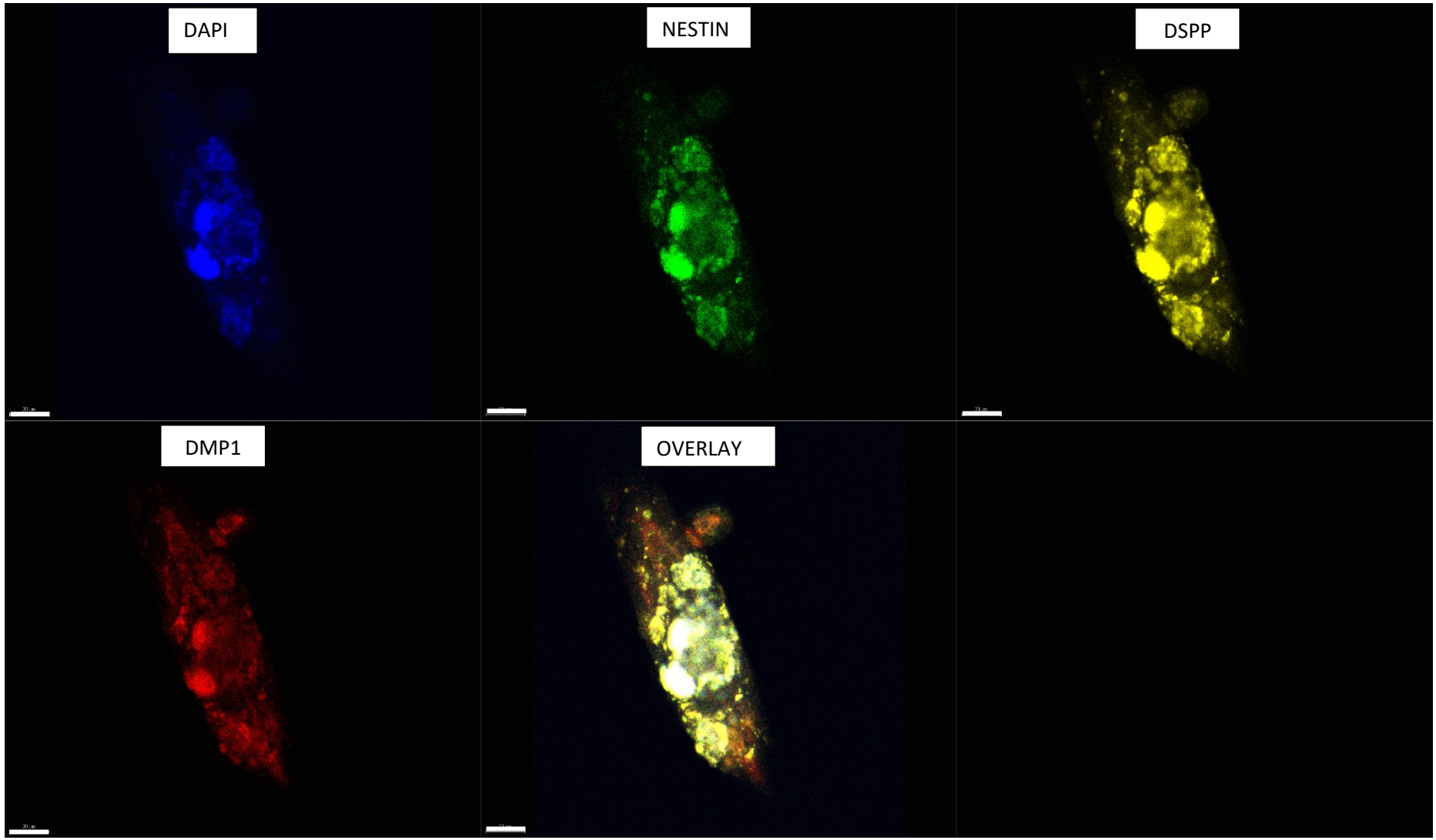

Figure 5.6.4.1 7: Example of confocal immunofluorescent imaging for 5LPDL0.1, cultured in odontogenic media at three weeks. Image represents a cluster of cells. Scale bar = 20µm.

	5LPDL0.01	5LPDL0.1	7LPDL0.01	7LPDL0.1	9LPDL0.01	9LPDL0.1
BASAL	0.004 (0.006)	0.577 (1.285)	0.057 (0.113)	0.057 (0.077)	0.007 (0.012)	0.044 (0.041)
ODONTO-GENIC	0.053 (0.057)	0.703 (0.788)	0.044 (0.069)	0.274 (0.207)	0.003 (0.003)	0.022 (0.039)
P-VALUE	0.019	0.036	0.522	0.042	0.014	0.055

Table 5.6.4.1 1: Statistical test results comparing the mean ratio of immunofluorescence for DMP1 on gels cultured in basal and odontogenic media. Independent samples t-test/Welch's test (Welch's test performed when standard deviation >2x difference between the two samples) completed in R. Pink =p>0.05, green =p<0.05. SD in brackets.

	5LPDL0.01	5LPDL0.1	7LPDL0.01	7LPDL0.1	9LPDL0.01	9LPDL0.1
BASAL	0.154 (0.177)	0.411 (0.494)	0.739 (0.365)	0.391 (0.380)	0.163 (0.227)	0.573 (0.341)
ODONTO-GENIC	2.469 (2.522)	0.542 (0.286)	1.163 (0.823)	0.491 (0.244)	0.397 (0.239)	1.277 (0.380)
P-VALUE	0.015	0.417	0.884	0.962	0.203	0.008

Table 5.6.4.1 2: Statistical test results comparing the mean ratio of immunofluorescence for DSPP on gels cultured in basal and odontogenic media. Independent samples t-test/Welch's test (Welch's test performed when standard deviation >2x difference between the two samples) completed in R. Pink =p>0.05, green =p<0.05. SD in brackets.

	5LPDL0.01	5LPDL0.1	7LPDL0.01	7LPDL0.1	9LPDL0.01	9LPDL0.1
BASAL	1.406 (0.478)	1.196 (0.849)	1.609 (0.248)	1.144 (1.017)	0.593 (0.273)	1.551 (0.303)
ODONTO-GENIC	1.561 (0.682)	0.775 (0.276)	1.262 (0.823)	1.444 (0.472)	0.683 (0.396)	0.532 (0.133)
P-VALUE	0.651	0.571	0.059	0.147	0.744	<0.001

Table 5.6.4.1 3: Statistical test results comparing the mean ratio of immunofluorescence for nestin on gels cultured in basal and odontogenic media. Independent samples t-test/Welch's test (Welch's test performed when standard deviation >2x difference between the two samples) completed in R. Pink =p>0.05, green =p<0.05. SD in brackets.

DMP1	5LPDL0.01	5LPDL0.1	7LPDL0.01	7LPDL0.1	9LPDL0.01	9LPDL0.1	DPSC	
5LPDL0.01		0.525	1.000	1.000	1.000	1.000	1.000	BASAL MEDIA
5LPDL0.1	0.042		0.633	0.633	0.532	0.606	0.517	
7LPDL0.01	1.000	0.034		1.000	1.000	1.000	1.000	
7LPDL0.1	0.931	0.337	0.901		1.000	1.000	1.000	
9LPDL0.01	1.000	0.020	1.000	0.810		1.000	1.000	
9LPDL0.1	1.000	0.026	1.000	0.855	1.000		1.000	
OSTEOBLASTS	1.000	0.030	1.000	0.882	1.000	1.000		
ODONTOGENIC MEDIA								

Table 5.6.4.1 4: Statistical results comparing DMP1 immunofluorescence expression results for each gel type when cultured in basal media or odontogenic media. P values quoted from Dunn's Test. Pink = p>0.05, green =p<0.05.

DSPP	5LPDL0.01	5LPDL0.1	7LPDL0.01	7LPDL0.1	9LPDL0.01	9LPDL0.1	DPSC	BASAL MEDIA
5LPDL0.01		0.861	0.094	0.900	1.000	0.397	0.988	
5LPDL0.1	0.018		0.674	1.000	0.878	0.983	0.424	
7LPDL0.01	0.141	0.964		0.613	0.102	0.981	0.017	
7LPDL0.1	0.015	1.000	0.948		0.914	0.970	0.483	
9LPDL0.01	0.011	1.000	0.907	1.000		0.421	0.983	
9LPDL0.1	0.195	0.922	1.000	0.896	0.837		0.106	
OSTEOBLASTS	0.003	0.989	0.640	0.994	0.998	0.533		
ODONTOGENIC MEDIA								

Table 5.6.4.1 5: Statistical results comparing DSPP immunofluorescence expression results for each gel type when cultured in basal media or odontogenic media. P values quoted from Dunn's Test. Pink = p>0.05, green =p<0.05.

NESTIN	5LPDL0.01	5LPDL0.1	7LPDL0.01	7LPDL0.1	9LPDL0.01	9LPDL0.1	DPSC	
5LPDL0.01		0.998	0.999	0.994	0.415	1.000	0.994	BASAL MEDIA
5LPDL0.1	0.240		0.941	1.000	0.736	0.971	1.000	
7LPDL0.01	0.966	0.761		0.901	0.182	1.000	0.900	
7LPDL0.1	1.000	0.427	0.998		0.807	0.944	1.000	
9LPDL0.01	0.144	1.000	0.592	0.281		0.236	0.810	
9LPDL0.1	0.056	0.989	0.327	0.122	0.999		0.944	
OSTEOBLASTS	0.034	0.960	0.227	0.077	0.993	1.000		
ODONTOGENIC MEDIA								

Table 5.6.4.1 6: Statistical results comparing <u>nestin</u> immunofluorescence expression results for each gel type when cultured in basal media or odontogenic media. P values quoted from Dunn's Test. Pink = p>0.05, green =p<0.05.

An interesting and incidental finding from the confocal microscopy was the presence of some cells exhibiting a polarized nucleus as is typical for an odontoblast, and not common for osteoblasts. These were mainly present on 7LPDL0.1 gels and 9LPDL0.1 gels cultured in odontogenic media. Examples of these can be found in Figure 5.6.4.1 8.

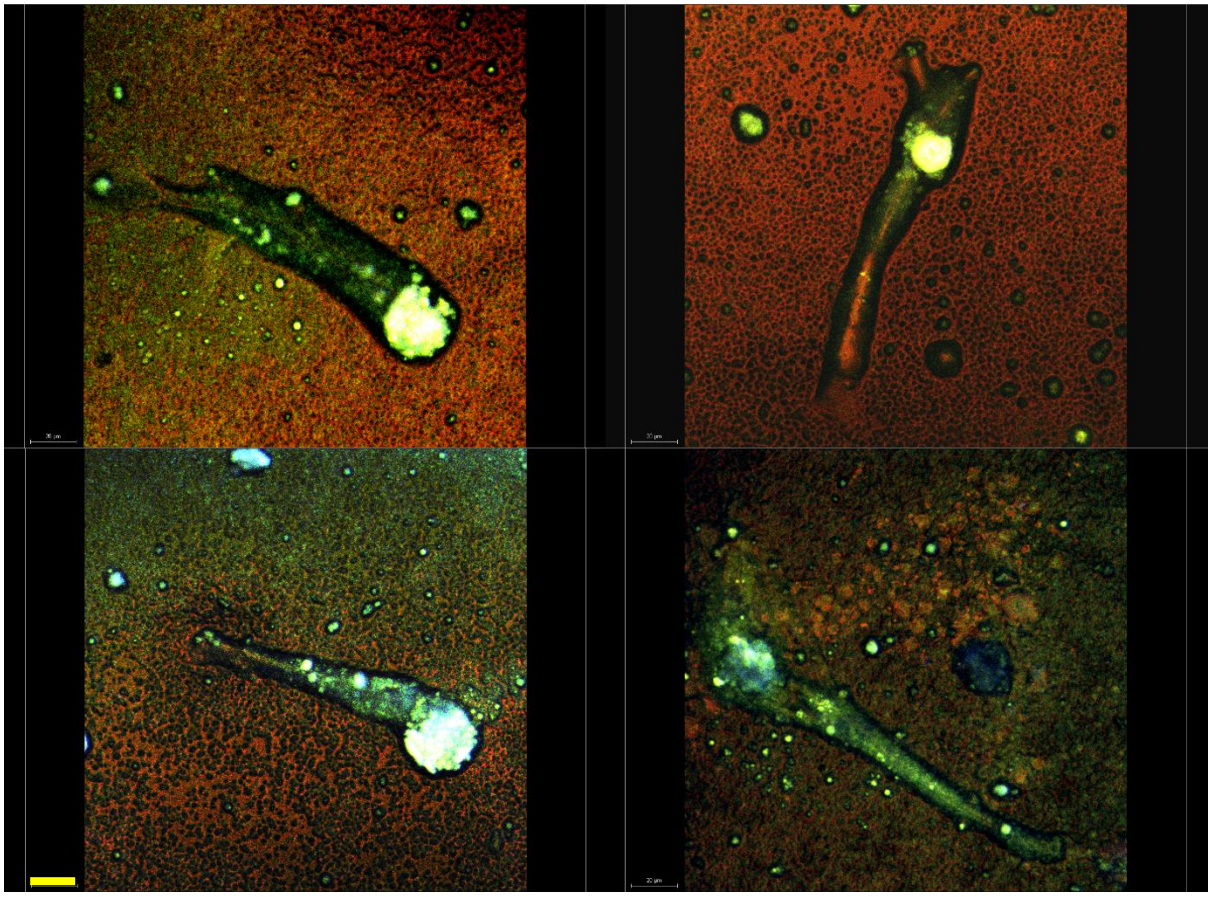

Figure 5.6.4.1 8: Cellular morphology images taken with confocal microscopy, following immunofluorescent staining. Scale bar = 20µm – please note that for these images the gain was deliberately raised relatively high to see the morphology of the cells, hence the strong background colouring.

5.6.4.2 REVERSE TRANSCRIPTION PCR

KEY FINDINGS

1. All of the gels cultured in odontogenic media had a higher expression of DSPP than the osteoblast controls – this was statistically significant for most gels
2. The gel with highest DSPP expression was 7LPDL0.1
3. When cultured in basal media, only 7LPDL0.1 had statistically higher expression of DSPP than the control DPSCs
4. When cultured in odontogenic media, only 7LPDL0.1 and 9LPDL0.1 had higher expression of DSPP than the control osteoblasts

As can be seen in the graph in Table 5.6.4.2 1 and Figure 5.6.4.2 1, the difference in DSPP expression between DPSCs and osteoblasts and the DPSCs cultured on gels is slight. However, 7LPDL0.1, cultured in odontogenic media has the highest expression and 5LPDL0.1, cultured in basal media has the lowest. For 7% agarose gels and 9% agarose gels, the expression of DSPP is higher with the 0.1mg/mL LPDL coating than the 0.01mg/mL LPDL coating – this is true for both basal media and odontogenic media. However, for 5% agarose gels, the converse is found with the 0.01mg/mL coatings producing a higher expression of DSPP in both basal media and odontogenic media.

For all of the gels cultured in odontogenic media, except 5LPDL0.1, expression of DSPP was higher than the osteoblast controls. For gels cultured in basal media, 5LPDL0.1 again had a lower expression than the control cells (DPSCs) as did 9LPDL0.01; this essentially means that the control of DSPCs in basal media falls within the range of values obtained for the experimental groups.

GEL	BASAL MEDIA	ODONTOGENIC MEDIA	PValue
5LPDL0.01	68.487 (0.512)	68.833 (0.311)	0.784
5LPDL0.1	62.160 (0.471)	67.190 (0.982)	0.010
7LPDL0.01	68.823 (0.266)	69.730 (0.454)	<0.001
7LPDL0.1	70.127 (0.447)	71.017 (0.454)	0.046
9LPDL0.01	65.133 (2.585)	68.207 (2.077)	0.020
9LPDL0.1	69.423 (0.723)	70.837 (0.422)	0.032
CONTROL	DPSCS 66.227 (0.979)	OSTEOBLASTS 66.505 (0.290)	0.350

Table 5.6.4.2 1: 100-CP RT-PCR results. Blue = higher expression than control, orange = lower expression than control. Statistical test = T-test comparing odontogenic media and basal media results, green =p value<0.05 and pink=p value>0.05

The control of water (i.e. blank control) for this experiment did not provide any reading, as would be expected.

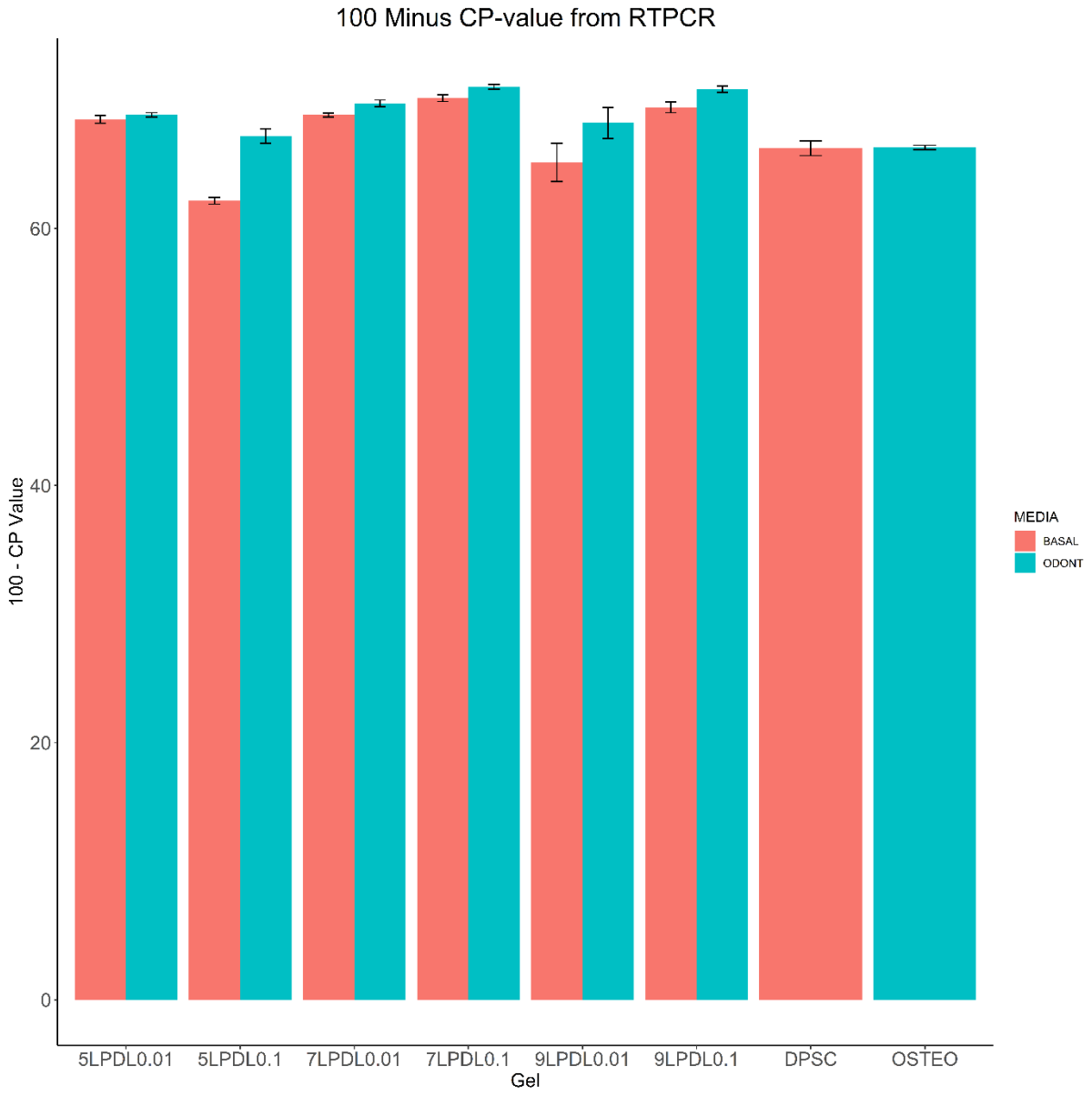

Figure 5.6.4.2 1: Bar plot of means from 100-CP values with error bars showing standard error. N.B. 100-CP chosen to deliberately demonstrate higher expression with lower CP value. Turquoise = results from gels cultured in odontogenic media (ODONT). Coral = results from gels cultured in basal media. OSTEO = Osteoblasts, DSPCS = Dental Pulp Stem Cells.

As can be seen in Table 5.6.4.2 1 and Figure 5.6.4.2 1, all of the gels cultured in odontogenic media produced higher expression of DSPP than osteoblasts. The greatest differences between the experimental gels and controls were seen in 7LPDL0.1 and 9LPDL0.1, and this was true for gels cultured in basal media and odontogenic media. For all of the gels, DSPP expression was highest when the gels were cultured in odontogenic media.

When looking for statistically significant differences, the controls (osteoblasts and DPSCs) did not have a statistically significant difference (Table 5.6.4.2 1). Statistically significant differences were found when comparing the results of the different culture media for each gel (Table 5.6.4.2 1) – the only exception to this was 5LPDL0.01.

As can be seen from Table 5.6.4.2 2, the only two gels cultured in odontogenic media with statistically higher DSPP expression than osteoblasts were 7LPDL0.1 and 9LPDL0.1. When looking at the gels cultured in basal media, only 7LPDL0.1 had higher DSPP expression than the DPSC controls.

As previously discussed in the methodology (Section 5.5.2), the CP value has an inverse relationship with expression, which is why the results are expressed as '100-CP value' so that the results with higher numerical figures are associated with higher expression for DSPP. A copy of the graph demonstrating the plot of cycles against fluorescence is available in Appendix 25.

DSPP RTPCR	5LPDL0.01	5LPDL0.1	7LPDL0.01	7LPDL0.1	9LPDL0.01	9LPDL0.1	DPSC	
5LPDL0.01		<0.001	1.000	0.934	0.120	1.000	0.637	BASAL MEDIA
5LPDL0.1	0.933		<0.001	<0.001	0.242	<0.001	0.026	
7LPDL0.01	1.000	0.464		0.989	0.182	1.000	0.431	
7LPDL0.1	0.684	0.045	0.999		0.807	1.000	0.038	
9LPDL0.01	1.000	0.999	0.961	0.316		0.015	0.998	
9LPDL0.1	0.787	0.066	0.997	1.000	0.412		0.163	
OSTEOBLASTS	0.486	1.000	0.103	0.005	0.835	0.008		
ODONTOGENIC MEDIA								

Table 5.6.4.2 2: Results of statistical tests, comparing each gel type in basal media and odontogenic media. Statistical test = Tukey's Test, pink = p value >0.05, green = p value <0.05

5.6.5 MINERAL DEPOSITION AND CHARACTERISATION

5.6.5.1 CALCEIN STAINING

KEY FINDINGS

1. Both gels cultured in basal media and gels cultured in odontogenic media produced mineral
2. For all gels, there was a statistically significant difference in the amount of mineral produced between gels cultured in basal media and those cultured in odontogenic media
3. The patterns of mineralisation show opposite trends for odontogenic media and basal media; with increasing agarose concentration, gels cultured in basal media showed more mineral, but with odontogenic media, the opposite was found
4. 5LPDL0.1 cultured in odontogenic media was statistically better than all other gels cultured in odontogenic media, with 7LPDL0.1 coming second in terms of mineral produced
5. Gels with 0.1mg/mL poly-lysine additions performed uniformly better then 0.01mg/mL poly-lysine additions – this trend was statistically significant for all gels cultured in basal media, but not all gels cultured in odontogenic media
6. For all of the gels except 9LPDL0.1, culturing in odontogenic media produced more mineral than basal media

As previously shown in the Brightfield images (Figure 5.6.2 2), deposition of mineral was evident even from early experiments. As previously discussed in the methodology, a calcein stain was used to assess the amount of mineral produced.

Figure 5.6.5.1 1 demonstrates representative images used in the analyses and quantification of these gels.

As discussed in the methodology (Section 5.3.1) for calcein staining, the calcein staining picking up on the outside of the mineral islands can be difficult to quantify because of imaging in one focal plane. To demonstrate this further, see Figure 5.6.5.1 2 which show examples of compiled Z-stacks for some of the gels and demonstrate the three-dimensional nature of the mineral produced.

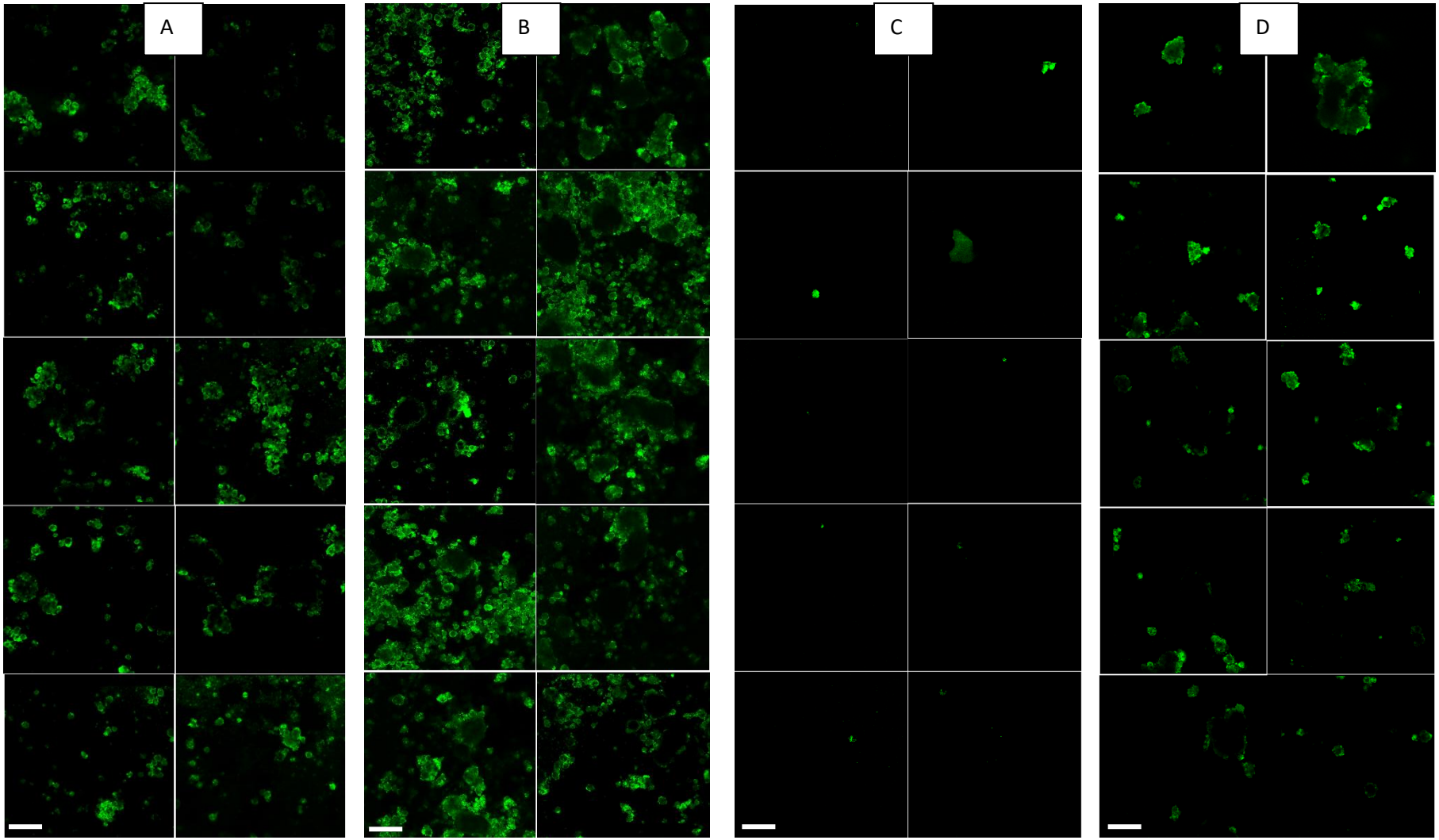

Figure 5.6.5.1 1: Examples of confocal 2D images of calcein staining. A= 5LPDL0.1 (basal media), B = 5LPDL0.1 (odontogenic media), C= 5LPDL0.01 (basal media), D= 5LPDL0.01 (odontogenic media) scale bar = 100µm. Experiment was conducted twice, with five images per gel produced (i.e. ten images per gel in total). Images taken at three weeks in culture.

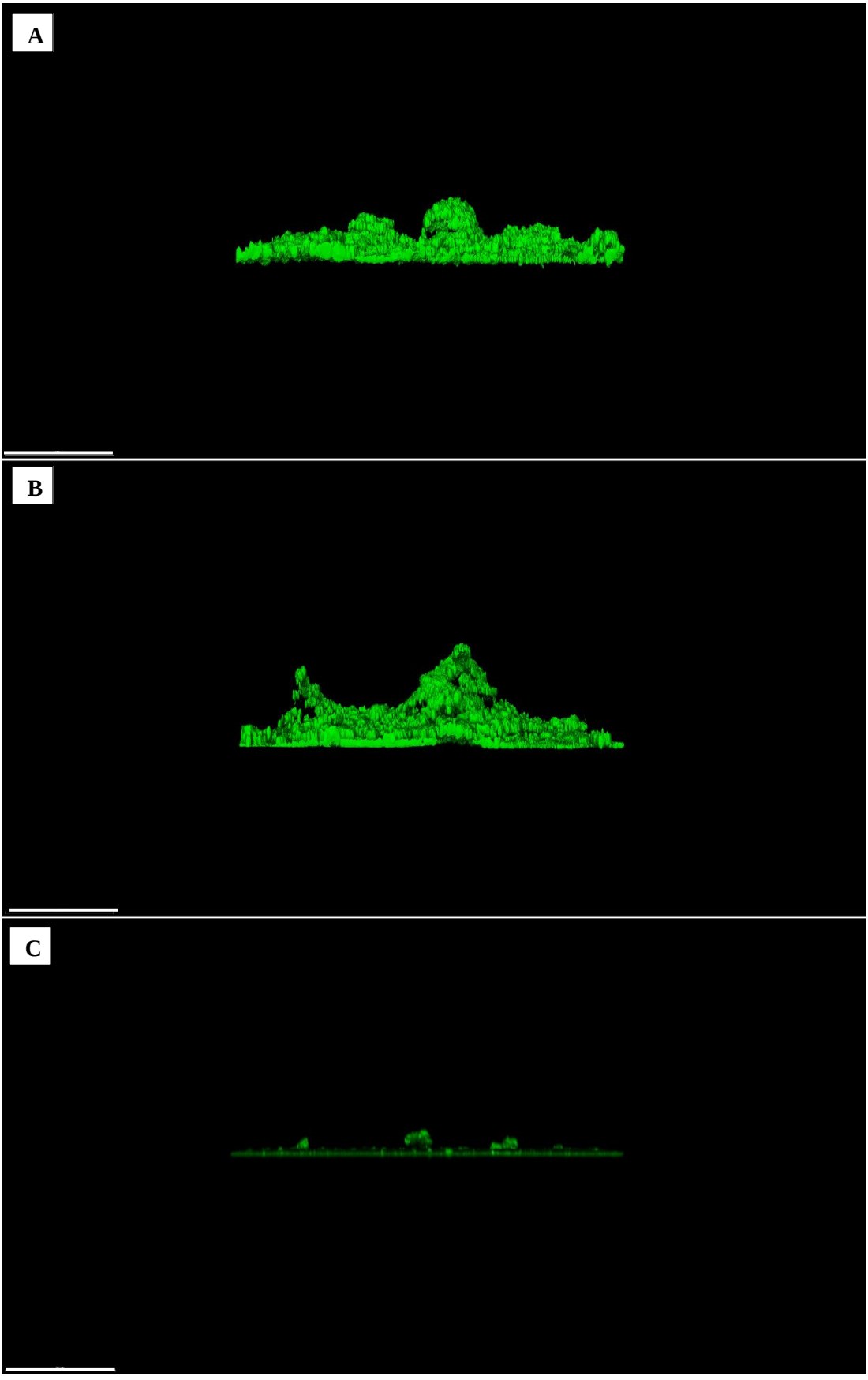

Figure 5.6.5.1 2: Z-Stacks of confocal images from calcein stained gels, cultured in odontogenic media. A=5LPDL0.1, B=7LPDL0.1, C=9LPDL0.1, scale bar = 200µm. Images taken at three weeks culture.

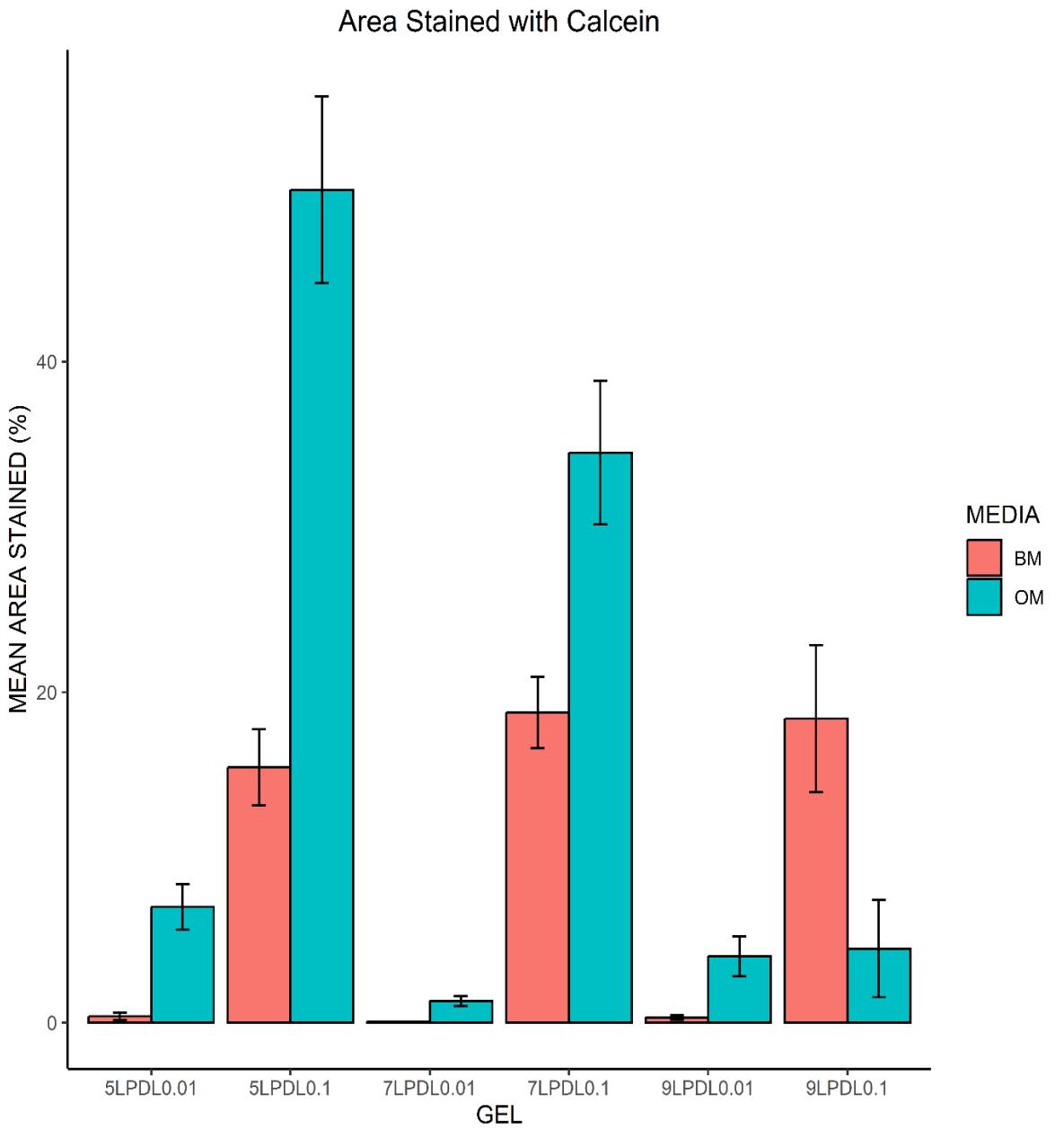

Figure 5.6.5.1 3:Bar chart showing mean area stained per gel in different culture mediums. Error bars= standard deviation. OM=Odontogenic media. BM = Basal media. Area stained is % of area stained with calcein across an image. Five images taken per gel, experiment completed twice, therefore ten images per gel in total.

Figure 5.6.5.1 3 shows the quantifiable results for the calcein staining. For the gels containing 0.01mg/mL LPDL, no discernable trend is identified linking the amount of mineral to the agarose concentration, but the gels cultured in odontogenic media produced more mineral than the ones cultured in basal media for all agarose concentrations.

For gels containing 0.1mg/mL LPDL, gels cultured in basal media generally showed an increase in mineral correlating with an increase in concentration of agarose. For the 0.1mg/mL LPDL gels cultured in odontogenic media, the opposite trend was seen (Figure 5.6.5.1 3).

Blank gels (i.e. agarose gels cultured without cells) produced no mineral in either basal or odontogenic media.

When comparing the gels cultured in basal media (Table 5.6.5.1 1), a very clear trend comes to light. Statistically significant differences are only seen when comparing gels coated with 0.01mg/mL LPDL against gels coated with 0.1mg/mL LPDL, regardless of the agarose concentration. No statistical differences were identified between agarose gel concentrations when looking at LPDL0.1mg/mL coated gels and 0.01mg/mL coated gels as subgroups. This suggests that for gels cultured in basal media, the coating density (or amount) of binding sites is more important than the gel elastic modulus because the differing agarose concentrations are not producing any statistically significant differences in the mineral produced, however the different LPDL coatings are.

When comparing the gels cultured in odontogenic media, (also in Table 5.6.5.1 1), two gels stand out as being statistically better than the others; 5LPDL0.1 and 7LPDL0.1. These gels produced statistically more mineral than all other gels. When comparing 5LPDL0.1 and 7LPDL0.1, 5LPDL0.1 produced statistically more mineral than 7LPDL0.1.

When looking at each agarose gel %, and comparing the gels coated with 0.1mg/mL LPDL vs 0.01mg/mL LPDL, 5% agarose and 7% agarose produce statistically significant differences, but 9% agarose shows no statistically significant difference.

The pattern is more complex for gels cultured in odontogenic media than in basal media; in some instances the difference in the coating is producing a statistically significant difference (e.g. comparing 5LPDL0.1 to 5LPDL0.01), but this is not universally observed (e.g. comparing 9LPDL0.1 to 9LPDL0.01). In some cases, the agarose percentage is resulting in statistically significant differences (e.g. 5LPDL0.1 vs 7LPDL0.1 vs 9LPDL0.1), but this trend is not mirrored for LPDL0.01 coated gels. These results suggest that the percentage of agarose is only a factor in the amount of mineral produced when the gels are coated with LPDL0.1 and not with LPDL0.01.

For all gels, there was a statistically significant difference between the amount of mineral produced in basal media vs odontogenic media (Table 5.6.5.1 2).

CALCEIN	5LPDL0.01	5LPDL0.1	7LPDL0.01	7LPDL0.1	9LPDL0.01	9LPDL0.1	
5LPDL0.01		<0.001	1.000	<0.001	1.000	<0.001	BASAL MEDIA
5LPDL0.1	<0.001		<0.001	0.917	<0.001	0.948	
7LPDL0.01	0.845	<0.001		<0.001	1.000	<0.001	
7LPDL0.1	<0.001	0.021	<0.001		<0.001	1.000	
9LPDL0.01	0.989	<0.001	0.993	<0.001		<0.001	
9LPDL0.1	0.995	<0.001	0.986	<0.001	1.000		
ODONTOGENIC MEDIA							

Table 5.6.5.1 1: Results of statistical tests for calcein staining, comparing each gel type in basal media and odontogenic media. Statistical test = Tukey's Test, pink = p value >0.05, green = p value <0.05

	5LPDL0.01	5LPDL0.1	7LPDL0.01	7LPDL0.1	9LPDL0.01	9LPDL0.1
BASAL	0.385 (0.722)	15.448 (7.275)	0.054 (0.045)	18.770 (6.801)	0.318 (0.457)	18.396 (14.112)
ODONTOGENIC	7.012 (4.336)	50.398 (17.872)	1.319 (0.954)	34.494 (13.746)	4.020 (3.861)	4.485 (9.324)
P-VALUE	<0.001	<0.001	0.002	0.006	0.014	0.020

Table 5.6.5.1 2: Results of statistical tests for calcein staining, comparing the results of each gel type in basal media vs odontogenic media. Means quoted with standard deviation in brackets. Statistical test = T-test (or Welch's test where standard deviation is >2x difference between the two samples), pink = p value >0.05, green = p value <0.05

For a summary of the comparative gel tests results, please see Table 5.6.5.1 3.

TEST	PARAMETER(S)	BEST PERFORMING GEL
AB ASSAY, LDH ASSAY AND LIVE/DEAD	VIABILITY, CYTOTOXICITY, ADHESION	5LPDL0.1
UNIAXIAL COMPRESSION	ELASTIC MODULUS, VALUES CLOSEST TO CORONAL PULP	5HPLL0.1, 7HPLL0.01
AFM	ELASTIC MODULUS, VALUES CLOSEST TO CORONL PULP	9HPLL0.1
SWELLING RATIO	MOST HYDRATED GEL	5LPLL0.01
IF DMP1 (ODONTOGNEIC MEDIA AND BASAL MEDIA)	HIGHEST RATIO OF STAINING TO DAPI	BASAL – 5LPDL0.1 OODNTOGENIC – 5LPDL0.1
IF DSPP (ODONTOGNEIC MEDIA AND BASAL MEDIA)	HIGHEST RATIO OF STAINING TO DAPI	BASAL – 7LPDL0.01 ODONTOGENIC – 5LPDL0.01
IF NESTIN (ODOTNOGENIC MEDIA AND BASAL MEDIA)	HIGHEST RATIO OF STAINING TO DAPI	BASAL – 7LPDL0.01 ODOTNOGENIC – 5LPDL0.01
REVERSE TRANSCRIPTION PCR (ODONTOGENIC AND BASAL MEDIA)	LOWEST CP VALUE	BASAL – 7LPDL0.1 ODONTOGENIC – 7LPDL0.1
MINERAL DEPOSTION (ODONTOGENIC AND BASAL MEDIA)	LARGEST AREA STAINED	BASAL – 7LPDL0.1 ODOTNOGENIC – 5LPDL0.1

Table 5.6.5.1 3: Summary Table of the comparative tests done to compare the agarose gels. Results demonstrate the best performing gel in each category explored.

5.6.5.2 SEM AND EDS

KEY FINDINGS

1. Gels cultured in both basal and odontogenic media produced mineral
2. The mineral from gels cultured in odontogenic media was in spherules, the mineral from gels cultured in basal media was in a more trabecular pattern
3. Mineral from gels cultured in odontogenic media had more calcium and phosphorus content than gels cultured in basal media, and the elements present were of a similar ratio to those seen in hydroxyapatite

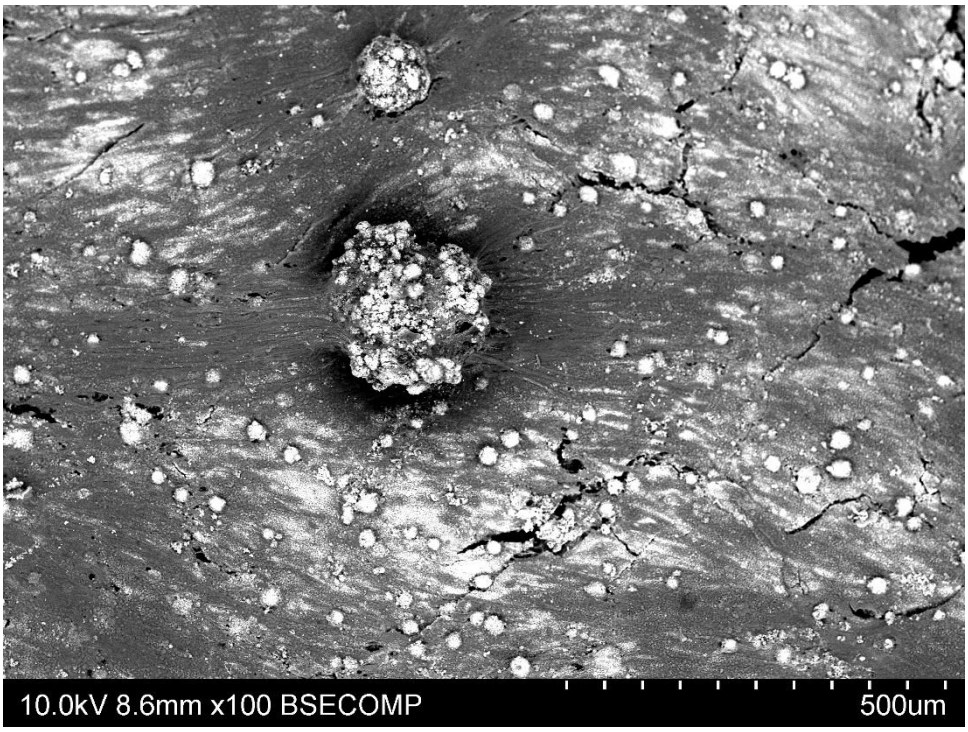

Figure 5.6.5.2 1: SEM back scatter (BSE) image of 7LPDL0.1 (cultured in odontogenic media). BSE used to show calcium ions, which are white in the image. Gel cultured for three weeks and imaged with a cold stage.

To assess the elemental contents of the mineral produced, EDS was completed on the best performing gel (7LPDL0.1), comparing basal media and odontogenic media. Hydroxyapatite ($Ca_{10}(PO_4)_6(OH)_2$) is the mineral component of both bone and dentine. As such, analysis of the mineral component of the gels will not determine whether the mineral produced is dentine or bone, but can determine that the elemental components are comparable with hydroxyapatite.

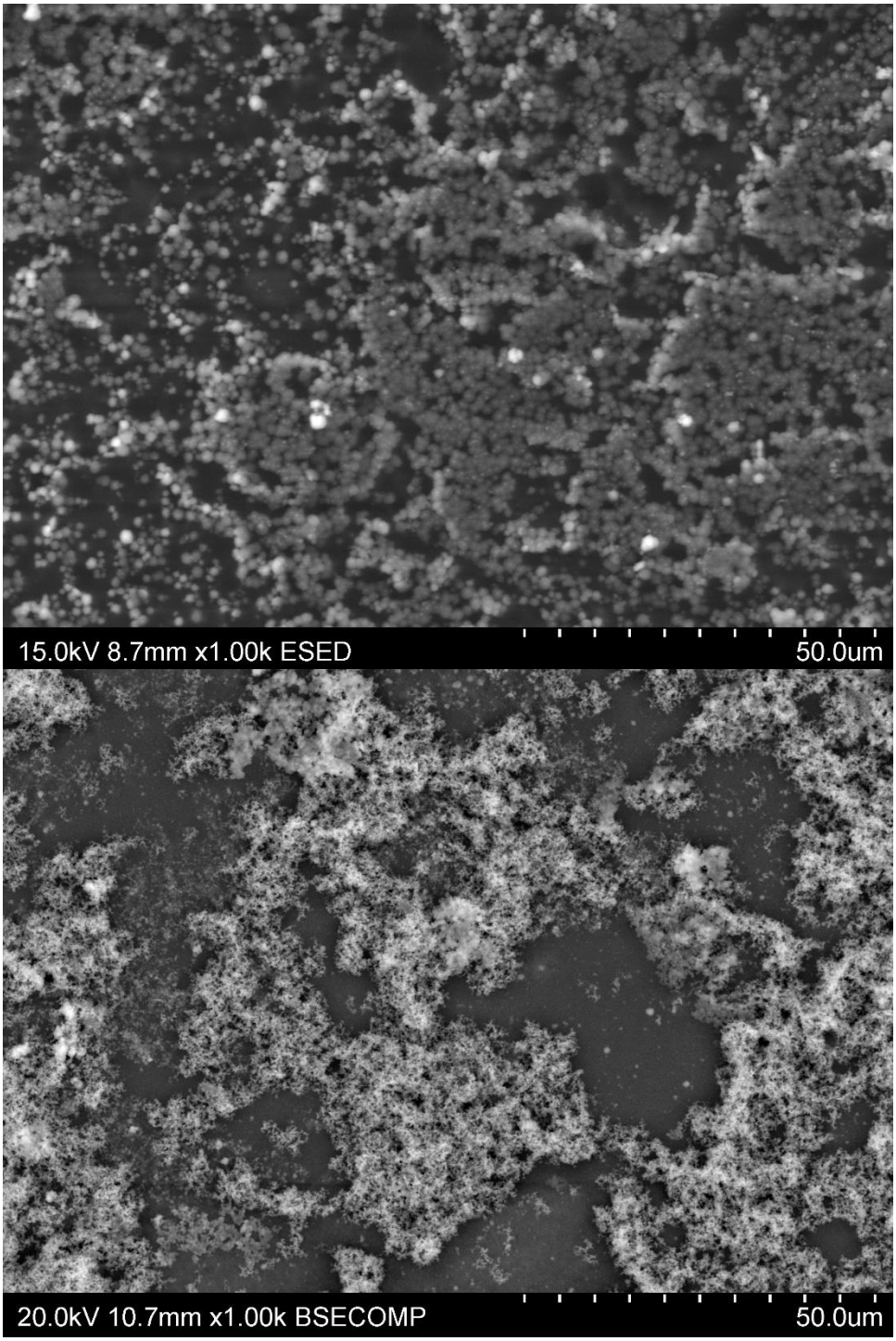

Figure 5.6.5.2 2: Two SEM images comparing the morphology of the mineral produced when the gel is cultured in basal media (bottom image) and odontogenic media (top image). Both gels were 7LPDL0.1, imaged after three weeks culture.

An SEM image of the mineral produced from 7LPDL0.1 (cultured in odontogenic media) is in Figure 5.6.5.2 1. As can be seen, the mineral was deposited in spherules, of varying size. Some of these

aggregated together to form large calcified masses. In these areas, the dense sheet-like organic component can also be appreciated.

When looking more closely at the mineral produced (Figure 5.6.5.2 2), there does seem to be a difference in the mineral produced on the gels cultured in basal media compared to the gels cultured in odontogenic media. The cells cultured on gels in odontogenic media produced more spherule-like deposits, whereas those in basal media produced more woven/trabecular deposits. To explore this further, EDS on the two gels was undertaken (Figures 5.6.5.2 3 and 5.6.5.2 4).

In Figure 5.6.5.2 4, showing the pictorial results of the EDS for the gel cultured in odontogenic media, it can clearly be seen that phosphorus and calcium locate to one of the mineralized spherules. Interestingly, carbon staining shows an inverse relationship with the spherule, demonstrating that the nodule is inorganic (i.e. mineral) in nature compared to the surrounding organic agarose gel. In-keeping with the mineral potentially being hydroxyapatite, oxygen is also present in the nodule.

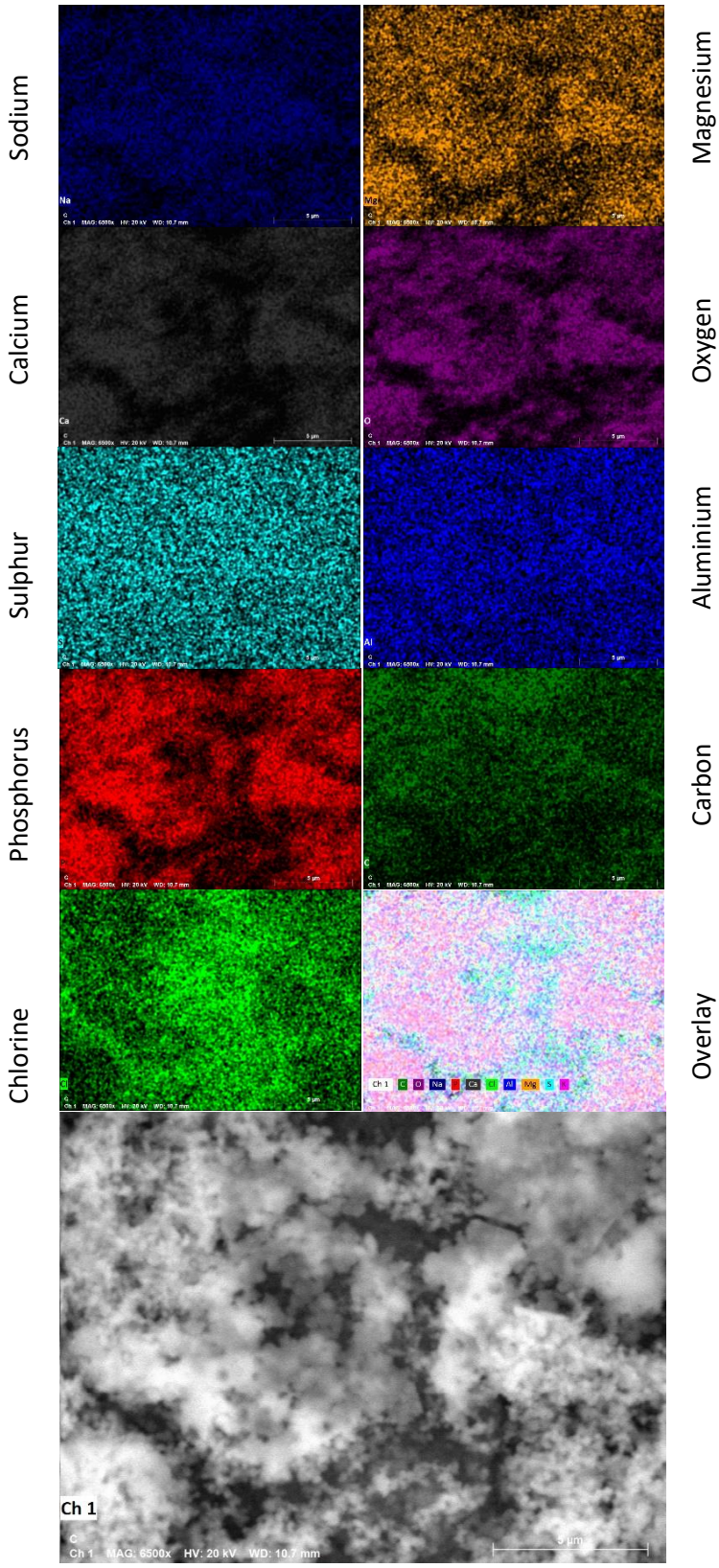

Figure 5.6.5.2 3: EDS elemental analysis of mineral produced on 7LPDL0.1 cultured in basal media for three weeks. Bottom image = SEM image of the area analysed. Elements detected by EDS labelled.

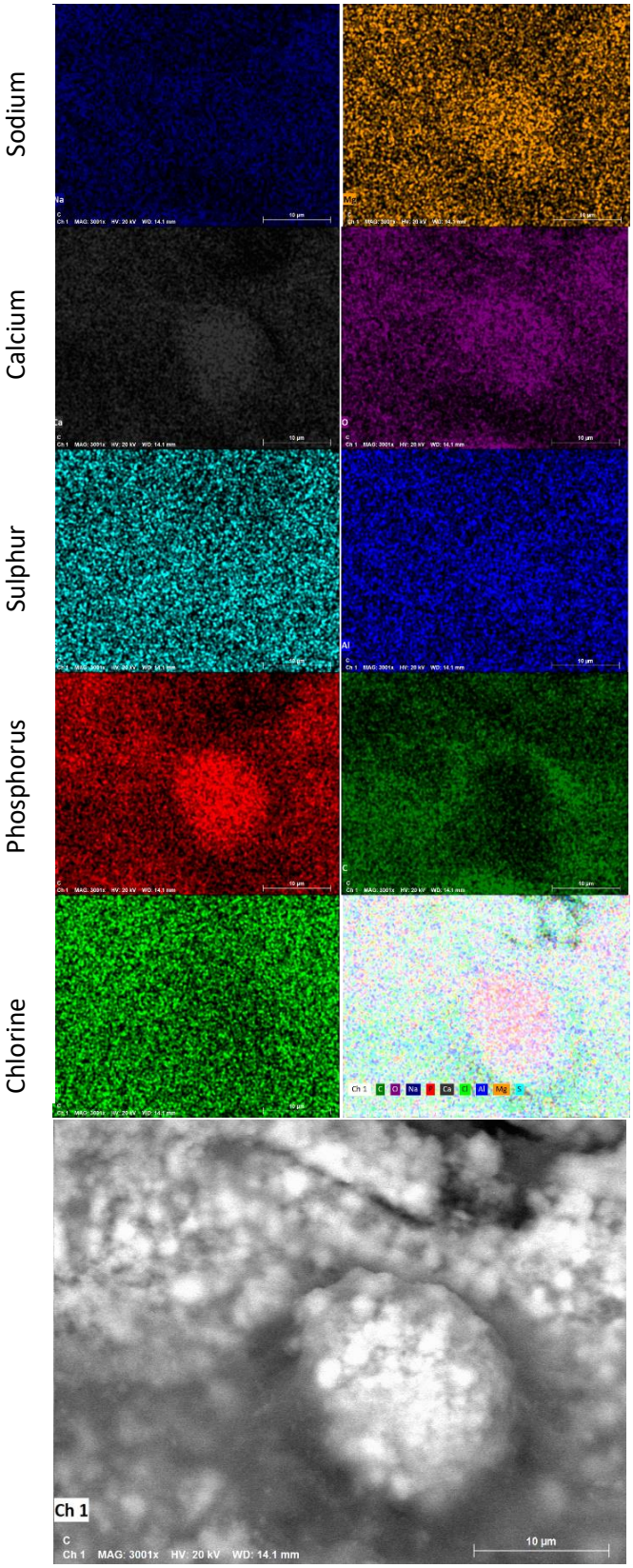

Figure 5.6.5.2 4: EDS elemental analysis of mineral produced on 7LPDL0.1 cultured in odontogenic media for three weeks. Bottom image = SEM image of the area analysed. Elements detected by EDS labelled.

	OM mass% norm, (relative error)	BM mass% norm, (relative error)
Carbon	28.09 (5.330	11.84 (5.58)
Oxygen	39.92 (5.24)	48.43 (5.08)
Sodium	3.1 (5.65)	12.45 (5.34)
Phosphorus	8.56 (2.66)	6.02 (2.47)
Calcium	17.49 (1.80)	9.72 (1.72)
Chlorine	1.8 (2.49)	7.86 (2.07)
Aluminium	0.28 (5.72)	0.96 (4.41)
Magnesium	0.44 (5.97)	1.61 (5.01)
Sulphur	0.31 (4.20)	0.37 (3.46)
Potassium	0 (0)	0.73 (2.41)

Table 5.6.5.2 1: EDS analysis results. Results quoted as % normalised mass. OM = odontogenic media, BM = basal media. Figures in brackets are relative error

As can be seen in Table 5.6.5.2 1, the mineral formed on the gel cultured in odontogenic media had much higher calcium and phosphorus content than the one cultured in basal media, as would be expected based on media composition.

Although the EDS analysis picked up on magnesium and aluminium being present in the mineral, this should be viewed with caution due to the error being greater than the normalized mass for both the basal media and odontogenic media gels. The 'uncontrolled' biological environment could also be the reason behind this, with trace elements being present in media, serum and other additives.

Although calcium, phosphorus and oxygen locate to mineralized areas of the gel in the basal-media cultured gel, chlorine, carbon, and sodium do too – a feature that is missing from the gels cultured in odontogenic media. This suggests the mineral from the gel cultured in basal media is different to the gel cultured in odontogenic media and unlikely to be hydroxyapatite. Also, as can be seen in Table 5.6.5.2 2, the elemental analysis of the Ca, P and O when seen as a ratio, supports the assumption that the mineral on the odontogenic media cultured gels is likely to be similar to hydroxyapatite ($Ca_{10}(PO_4)_6(OH)_2$), particularly taking into account the relative error.

	Ca	P	O
Hydroxyapatite	10	6	26
Mineral from odontogenic media cultured gels	11.39	5.78	26
Mineral from basal media cultured gels	5.22	3.23	26

Table 5.6.5.2 2: Comparing relative amounts of Ca, P and O from gels cultured in odontogenic media, gels cultured in basal media and hydroxyapatite

5.7 DISCUSSION

5.7.1 LIVE/DEAD STAINING AND ASSAYS

There is a well-written, concise review by Kamiloglu *et al*., that discusses the different methods of quantitative live/dead analysis, including the pros and cons of each method. No method is considered 'best practice'(292), and the ones chosen for this work have provided adequate results with their documented limitations. On balance, the triplicate method of assessing the cell status on the gels (i.e. the AB assay, the LDH assay and the live/dead confocal) provided a relatively robust analysis of the cell culture as only one or two of these methods are often used in the literature. The fact that the experiments were also done in triplicate allows for more confidence to be placed on the results. The use of the live/dead staining was possibly unnecessary as the AB and LDH assays provide a reasonable overview, however this analysis did give information on the adhesion of the cells and as such provide better context for the LDH and AB assays.

With many experiments, there are drawbacks to the methodology employed. One such issue with the AB assay is that the AB was taken up by the agarose gels, staining them blue/purple. This excess AB would then leach into the media the gels were cultured in after the media was changed. Because of this, the LDH assay could not be carried out on the same gels as the AB assay because both assays are colorimetric. However, the same batches were used for both assays.

The AB being uncontrollably leached from the gels into the media could also lead to inaccurate AB readings. This is because, if the AB from one reading is not completely removed from the gel/media, it could be leached into the media for the next reading. This would lead to differing amounts of AB being present in the media of each measurement as the amount of AB taken up and released by the gel is uncontrollable. This would lead to the results of the AB assay being inaccurately low after the first reading. As more variation was identified in the AB assay than the LDH assay (as seen by the larger standard error bars in Figures 5.6.1 1-5.6.1 3), it is possible that this may have been the causative factor behind the greater variation.

In pilot experiments, quantification of the vitality (AB) and cytotoxicity (LDH) assays was attempted by determining a calibration curve. This was carried out by adding a known quantity of cells to a well plate and leaving them to acclimatize overnight before killing the cells with DMSO (for the LDH assay) and harvesting the media, or adding AB to the cells and leaving them to incubate before harvesting the media. This proved to be poorly reproducible as the calibration curve regularly varied; this is likely because with this method the number of cells may vary due to proliferation overnight or the DMSO not killing all cells. Because there is no calibration curve, the measurements of fluorescence are all relative and not linked to a set, quantifiable cell number.

The live/dead staining for confocal posed some problems in the analysis. As can be seen Figures 5.6.1 6-5.6.1 8, the red and blue staining do not entirely overlap. It is difficult to pinpoint why this is. It could

be due to the different stains being used (e.g. one having a slightly higher affinity for nucleic acid than the other) or a technical limitation of the microscope. This lack of overlap sometimes led to a negative result (as the live to dead ratio was calculated by subtracting the red-stained area from the blue). Where this resulted in a negative value, it was assumed to be simply zero. Although authors have used similar methods in the literature (i.e. staining just nuclei with two different stains rather than the calcein AM/EH combination of a cytoplasmic and nuclear stain), none have cited this as a problem (313,314), as cell counting was used instead of pixel counting.

The live/dead confocal is open to selection bias as the operator could select areas that fit more with predetermined hypotheses and theories – blinding of the operator to the samples would have made this more robust but time limitations did not allow. Another option would have been to remove the cells from the cultured gels (with trypsin) and use flow cytometry to quantify the live and dead cell numbers; this would have been more accurate as an exact cell number could then be given overall per gel, rather than counting areas stained on representative images and remove selection bias.

The LDH assay, AB assay and live/dead confocal were employed in tandem in this research to provide the best possible assessment of the status of the cells on the gels. However, in retrospect, other methods may have been more appropriate, such as a picogreen assay to assess the amount of DNA as a marker for the number of cells on the gel; this would have had the advantage of assessing all of the cells on the gel rather than select areas as per the live/dead confocal measurements used. This would have involved making an additional gel that would be cultured for three weeks, the cells trypsinised, lysed and the DNA then quantified. In this scenario, DNA would be used as a surrogate marker for the number of cells present and the results would be quantifiable and comparable. However, plotting the DNA results against a calibration curve of a set number of cells, similar to as was attempted with the LDH/AB assays, would be problematic. Other types of viability assays could have been considered – for example, a Real-time viability assay (a luminometric assay based upon luciferase) – but all viability assays that are non-destructive work in a similar way (292).

The outcomes of the assays and live/dead confocal imaging resulted in two coatings performing best – HPLL0.1 and LPDL0.1. However, as was evident from Figure 5.6.1 9, HPLL0.1 performed poorly in the AB assay. As can be seen from the brightfield images in Figure 5.6.2 1, the cells cultured on the HPLL0.1 coated gels had a ball-like morphology and did not spread out on the gels. There is a link between the actin tension of the cytoskeleton to cellular metabolism (315,316) and it is probable that the higher molecular weight of the HPLL0.1 provided a lot of binding sites for the cells, meaning they adhered strongly to the gels and did not spread out – this in turn would mean the actin cytoskeleton was not under tension, which then likely affected the metabolism of the cells. In-keeping with this theory is the fact that (generally) more cells initially adhered to the HPLL0.1 coated gels, but over time, as the metabolism of the cell was affected, the cell may have died and detached, meaning the area covered by

cells decreased (see Figure 5.6.1 5). Interestingly, the growth and adhesion of primary cortical neurons has also been found to be affected by the concentration of PDL – the highest concentration of PDL resulted in small, rounded, singular cells that failed to mature (similar to the HPLL0.1 findings from this work) and the lower concentrations of PDL resulted in cells clustered together, which again failed to mature (280).

The AB figures for LPDL0.1 coated gels were generally quite high (particularly at approximately 2 weeks), and this trend was mirrored by the area stained by the cells – this likely means that the cells on the LPDL0.1 coated gels were proliferating. As this trend was generally seen after adding the odontogenic media, it is difficult to ascertain whether the increase in vitality around week 2 was due to an additive in the odontogenic media (adipose derived stem cells have been shown to proliferate faster in α-MEM than DMEM (317)) or would have occurred regardless, and this experiment would need to be repeated using basal media for three weeks to determine this. Interestingly, alkaline phosphatase (ALP) activity of mesenchymal stem cells undergoing osteogenic differentiation is generally thought to peak around 2 weeks, and it is possible that the increased metabolism found during odontogenic differentiation in culture at 14 days may link to this as osteogenic media is similar to odontogenic media (318).

A proliferation assay would have been a useful addition to the information gained for the LDH/AB assays (such as a BrdU proliferation assay), as this should then confirm the active proliferation of the DPSCs to giving a peak around week 2.

From early experimental work, the DPSCs easily adhered to the gels when seeded in basal media, but when they were seeded in odontogenic media, they would not attach. It is difficult to ascertain exactly why this happened but the higher amount of negatively charged amino acids in αMEM may be a contributing factor as they could be occupying the binding sites that would otherwise be taken by DPSCs. Due to this factor, all of the gels were seeded with DPSCs in basal media and cultured in basal media for one week before odontogenic media was added.

Overall, the LPDL0.1 coated gels performed best. LPLL0.1 gels would have had the same number of binding sites as LPDL0.1 gels due to the same molecular weight, so the difference between the LPLL0.1 and LPDL0.1 results really does seem to come down to the chirality of the carbon in the poly-lysine chains. Some works have suggested that PDL may be more resistant to enzymatic breakdown than PLL (319) and it may also have better resistance to breakdown from reactive oxygen species (ROS)(320) (useful in an inflamed environment, such as the carious-involved pulp). It is entirely possible that the results herein can be explained by the resistance of PDL to enzymatic breakdown by the DPSCs, resulting in better cellular adhesion and as such more successful cell culture.

5.7.2 CELL DIFFERENTIATION AND MINERAL DEPOSITION

It is difficult to determine irrefutably whether the cells cultured on the agarose gels have differentiated into odontoblasts. Determining cell differentiation is frequently achieved in the literature by using cell markers (either via immunohistochemistry or immunofluorescence) and/or reverse transcription PCR (300). For this work, it is particularly difficult as odontoblasts and osteoblasts share many cytological markers, so it can be hard to say whether the DSPCs have differentiated into an odontoblast or an osteoblast. It is good practice in pathology research to not rely on one marker to determine irrefutable differentiation of a cell into a particular lineage or cell-type (300) and this work has focused on using different markers and different methodologies to determine whether or not the cells cultured on the gels have differentiated into odontoblasts or not.

For this research, DSPP, DMP1 and nestin were chosen because they are often used in the literature for determining odontoblast-like cells in culture (300). DMP1, although first being identified in odontoblasts, is believed to have a higher expression in osteocytes than odontoblasts (304), while DSPP is expressed at a much higher level in odontoblasts than osteoblasts (300,305) . Nestin is a neural stem cell protein and intermediate filament (321), which is also expressed in odontoblasts (322). Nestin expression has been shown to be unaltered during osteogenic differentiation of bone-marrow derived mesenchymal stem cells, and it could be argued that the same is likely to happen during DPSC differentiation, making nestin unsuitable for determination of DPSC differentiation into odontoblasts during culture, however it is still not infrequently used (300). It is an interesting finding that the cells cultured in odontogenic media had lower expression of nestin with IF than the ones cultured in basal media. Nestin is known, however, to be expressed by odontoblast-like cells in reparative dentinogenesis (321), with expression levels gradually increasing following pulp capping (322). It is difficult to determine any definitive outcomes from the nestin IF as the results are so variable and with so few statistically significant differences between the gels and between culture in basal media and odontogenic media, therefore these results should be viewed with caution. It is entirely possible that the lack of any significant trends in nestin expression are mirroring the unaltered expression observed for nestin in osteogenic differentiation (300).

DMP1 has been shown to be a transcriptional promoter for DSPP during odontoblast differentiation and early dentine deposition (323). From the IF results, the gels with higher DMP1 expression had lower DSPP expression. To explain this, it is possible that there may be a ‘lag’ in the DSPP expression between DMP1 upregulation and subsequent DSPP upregulation, so the gels with higher DMP1 expression may later have higher DSPP expression. Furthermore, the gels with a higher DSPP expression and lower DMP1 expression may be demonstrating the evidence of a previously high DMP1 expression. To explore this further, expression of DMP1 and DSPP at different time points (and assessment of mineralization over different time points) and over a longer time period would be necessary.

Overall, due to the lack of statistically significant results from the IF experiments and some of the results bucking the trend of what would be expected (e.g. the nestin expression being higher in gels cultured in basal media than odontogenic media), it would be prudent for the experiment to be repeated (as it was only conducted once) to confirm the results and look for more statistically significant results. Time constraints meant this experiment was only conducted once. With repeats, other odontoblast markers and markers expressed during dentinogenesis could also be explored (for example, osteopontin, bone sialoprotein and matrix extracellular phosphoglycoprotein).

Using osteoblasts as a control allowed for the expression levels to be quantifiably compared in immunofluorescence and RT-PCR, so that it could be better determined whether the cells present on the gels had become osteoblasts or odontoblasts. However, these experiments were only conducted once (though the RT-PCR was done in triplicate for the one experiment), limiting the reliability of the results. Although DMP1 is believed to be more highly expressed in osteoblasts than odontoblasts, more DMP1 was expressed in several of the gel cultures than the osteoblasts cultured. It is possible that the secretory phases of the different cells may provide an explanation for this, with the gel culture cells being in a secretory phase and the osteoblasts not; as the DPSCs needed to differentiate first before beginning to lay down mineral, compared with the already differentiated osteoblasts, this is entirely possible. This work would need to be repeated to confirm this finding of differing DMP1 expression as it may be an anomaly. Furthermore, with repeats of this work, more statistical differences may have come to light and the results could be reviewed more confidently.

With the accepted limitation of the cell-differentiation experiments only being conducted once, the outcomes of this work have demonstrated that it is more likely that the cells had differentiated into odontoblasts than osteoblasts on some of the gels – namely 7LPDL0.1, 7LPDL0.01, 5LPDL0.01 and 9LPDL0.1. This is evidenced from the combined outcomes of the RT-PCR work, the morphology of the cells and the IF work. For 5LPDL0.1, the results are more mixed; the strong DMP1 expression found in the IF studies suggests the cells on this gel may be more osteoblast-like in nature. The AFM results for this gel placed the elastic modulus around 40kPa, which would fit with documented values for osteogenic differentiation of mesenchymal stem cells (324). It is entirely possible that a mixture of the low elastic modulus in 5LPDL0.1 and the higher concentration of LPDL (thus giving more binding sites for the cells) coupled together to create more osteoblast-like cells than odontoblasts. From the DMP1 expression, DSPP expression and AFM data, it is also possible that 5% agarose gels generally have an elastic modulus too low to facilitate odontoblast-like differentiation – the exception to this would be 5LPDL0.01, and for this gel it could be that the lower concentration of PDL is causing the DPSCs to be placed under more tension due to fewer electrostatic interactions with the gel surface and thus potentially affecting the cell metabolism and differentiation (315) This in turn could be the explanation behind the higher DSPP expression and lower DMP1 expression for this gel.

As much as is reasonably practicable, it has been shown that the cells cultured on the agarose gels are odontoblasts, and as such the mineral deposited may be more likely dentine than bone because of this. Dentine and bone are largely similar in their construction, with both being largely hydroxyapatite mineral, making differentiation between the two difficult. The main difference between the two is the gross morphological structure, with dentine having tubules and bone having lacunae. In tertiary dentine, the tubules are often absent and it can have a bone-like morphology (indeed, it is sometimes referred to as 'osteodentine'), so the absence of tubules would not necessitate the mineral formed on the gels to be bone. At a molecular level, the protein structure of bone and dentine do also differ, with different levels of certain proteins in each – and it is this difference that has been attempted to be demonstrated in the IF and RT-PCR accomplished in this work on gel-cultured DPSCs.

There are numerous different methods for assessing the amount of mineral produced on the gels. The more commonly used methods in the literature are von Kossa stains and alizarin red stains, and the pros and cons of each are discussed earlier in Table 5.3.1 1. ALP assays are also often conducted, though these are not a direct assessment of the mineral produced.

An ALP assay was considered for this work as it is frequently employed in the literature for determination of secretory odontoblast activity (300,325). However, ALP activity assessment would not be beneficial in differentiating between dentinogenesis and osteogenesis as ALP is active in both processes, and the presence of mineralized material has already been proven by the calcein staining, so the minimal additional information this assay may have given was not considered necessary. In addition, the assay involves the destruction of the cells – this means that for measurements to be taken over time numerous repeats of the gels would be necessary to give results at different time points, on top of the plethora of gels already created for the measurements of the live/dead confocal, LDH, AB, IF, RT-PCR and calcein staining. As such, this was not completed, but could be done in future work for comprehensiveness.

One key advantage to using calcein staining, that was not employed in this work, is its non-cell permanent nature and the way it does not interfere with cellular functions. As such, calcein staining can be used to show mineral deposition in real-time. Taking this work forwards, it would be interesting to see the mineral deposition over time for the gels to get a sense of the rate at different time points to help pin-point when cellular differentiation likely occurs and when mineral deposition is at its greatest and to see if this varies depending on the elastic modulus of the gel.

It is interesting that basal media produced mineral. In addition, the mineral produced by basal media, did contain calcium and phosphate as shown by EDS in the SEM – this can be explained by the presence of calcium ions and phosphate ions in the basal media (from $CaCl_2$ and sodium phosphate monobasic – see https://www.thermofisher.com/uk/en/home/technical-resources/media-formulation.48.html) and the presence of ALP in FBS (326). This suggests that even in the absence of the inductive odontogenic

media, the agarose gels with basal media are capable of being used for mineral production *in-vitro*. Mineral production in basal media increased with increasing elastic modulus, which does suggest that the elastic modulus of the gels is having an effect on mineral production. With odontogenic media, the opposite trend was found, which suggests that when calcium and phosphate ions are in abundance (as is the case in odontogenic media), increasing elastic modulus has a negative effect on mineral production, however when the mineral ions are more sparse (as in basal media), increasing elastic modulus has a positive effect on mineral production. Interestingly, the DSPP IF expression for basal media and odontogenic media also roughly follow this trend. DMP1 IF expression for odontogenic media only also follows the mineralization trend.

Although cells cultured on 7% and 9% gels in odontogenic media produced more of an odontoblast-like phenotype morphologically than 5% gels, they produced less mineral. It is possible that although the mineral produced is less in the 7% and 9% gels, the mineral in these gels may be more in-keeping with dentine than bone. This is supported by the RT-PCR odontogenic media results for 7LPDL0.1 and 9LPDL0.1 both being statistically higher than 5LPDL0.1.

It is difficult from the mixed *in-vitro* results to determine what would be the best gel for mineral formation in a pulp capping environment. Taking all the outcomes together, we might conclude that 5LPDL0.1 is the best gel scaffold; it had the highest mineral deposition (in odontogenic media) and performed well in the live/dead confocal, confocal cell adhesion (area measurement) and AB assay. However, it is important to consider that the cell culture environment and media are providing the optimum environment for DPSC differentiation and mineral deposition, so although 5LPDL0.1 appears to be the best performing it may be prudent to consider the results from the basal media as calcium and phosphate ions (although liberated from dentine during carious breakdown) may not be as abundant *in-vivo*. As such, 7LPDL0.1 may be a better choice – this gel performed the best for DSPP RT-PCR (both in odontogenic media and basal media, though not always statistically significant), displayed good mineral deposition for both basal and odontogenic media (suggesting the media may be less of a factor than the elastic modulus for this gel) and still had good outcomes in the confocal, AB and LDH outputs. The high DMP1 expression for 5LPDL0.1 also suggests that the mineral produced on this gel may be more like bone than dentine. In comparison, 7LPDL0.1 had lower DMP1 values, whilst still maintaining high DSPP values in RT-PCR, meaning this gel may possibly produce a more dentine-like mineral. In addition to this, 7LPDL0.1 and 9LPDL0.1 gels demonstrated an odontoblastic phenotype for some of the cells. Of course, with further work it is also possible that a '6LPDL0.1' gel may prove a happy medium between the two. The importance of a dentinogenic phenotype over a bone-producing phenotype to the cells and mineral produced is questionable considering that reparative dentine has an osteoid-like appearance, though it may still be informative, for dental material research and oral biology to know the ideal conditions for dentine deposition. Reparative dentine's osteoid-like appearance has the advantage of being more solid than dentine and lacking in tubules, meaning it is less likely to

facilitate bacterial ingress. The disadvantage to this morphology is that the compressive strength of reparative dentine is lower due to the lack of this regular, tubular structure. Although a tubular structure was not observed in the mineral produced in this study, it is considered by some authors to be preferable, as the dentinal tubular structure (when correctly orientated) will confer more strength to any dentine produced and should allow odontoblast-like cells to operate more like odontoblasts by providing some immunological and neurological functions (327). The AFM nanoindentation of pulp suggested that odontoblasts also may have a mechanically stabilizing function, and this is probably dependent upon being anchored into dentinal tubules, so this too may be a function that is realized if a tubular structure could be achieved.

The trends of the RT-PCR results do not match the IF results, but it is difficult to ascertain why this is the case. RT-PCR has generally been shown to have better sensitivity than IF in microbiological studies (328), though cross-over of this trend to the work herein may be limited, and there is a general paucity of literature comparing the outcomes and accuracies of the two methodologies. The RT-PCR used all of the cells from several gels, whereas the IF used only representative areas from the one gel type. These facts taken together mean that it is possible that the RT-PCR results are more reliable than the IF results. It may have been better, in retrospect, to also look at RT-PCR for DMP1 and nestin to give comparable results for all the markers explored with IF, to see if the lack of a correlation between the IF results was universal or just for DSPP. Furthermore, western blot (which is a semi-quantitative test to look for various proteins such as DSPP and DMP1), would have provided a further level of evidence to allow better determination and more confidence behind the RT-PCR and IF results (in essence a form of triangulation to culminate the results of several tests).

A good volume of mineral has been produced by the gels (as seen in Figures 5.6.5.1 1 and 5.6.5.1 2) over three weeks. Three weeks was determined as the ideal period of culture as Hargreaves and Cohen stated that a dentine bridge should be beginning to form within a maximum of thirty days following pulp cap (329), and as such for a new PCA to be viable, it should be able to produce mineral faster than the 30 days maximum period. As alluded to previously, more regular time intervals and potentially culturing the gels for longer would allow for greater and richer data capture so that mineralization and differentiation of the cells on the gels could be better studied.

Further analysis and quantification of the mineral produced on the gels would have been a good addition to this work. For example, the organic components of the gels could have been broken down and then weighing the mineral present to give more quantitative differences between the mineral production per gel.

5.7.3 GEL CHARACTERISATION

From the AFM results and the uniaxial compression results, the presence of any poly-lysine in the gels seems to cause a reduction in the elastic modulus, which is most likely due to disruption of the hydrogen

bonds holding the agarose together and the increased water content (as confirmed by the higher swelling ratio for gels containing poly-lysine). One study in the literature found that poly-lysine dots added to the surface of agarose gels resulted in an increased elastic modulus (330), compared to the adjacent uncoated agarose gels. This surface effect finding has not been identified in this work. It is probable that the addition of the poly-lysine to the bulk of the agarose gel, and the resulting lower modulus throughout the gel is overcoming any increase in elastic modulus at the surface of the gel.

Interestingly, the uniaxial compression elastic modulus results were higher than the AFM results. This is in contrast to the mechanical tests for pulpal tissue, where the AFM results identified in Section 4.3.1 resulted in a higher elastic modulus than the reported bulk values from the literature (149,150). No studies in the literature have compared elastic modulus values for high concentration agarose gels tested with bulk/macro uniaxial compression and nano/micro scale (via AFM), as such it is difficult to determine the reason behind this trend. The difference may be due to several factors. Firstly, the uniaxial compression test could not be undertaken in an aqueous environment, which is different to the AFM work; this could mean that the evaporation and water displacement during compression could lead to differing results. Secondly, as previously mentioned in the AFM pulpal discussion, the two testing modalities are fundamentally different in their approach and the models utilized in the elastic modulus calculations. As previously mentioned, the nano and micro scale is believed to be the level most pertinent to cellular function(134,135), and as such for this work, the AFM values are likely to be the most important when considering DPSC differentiation.

As previously highlighted, the swelling ratio roughly correlates with the AFM and uniaxial compression trends, with higher w/v agarose % associated with less water content and smaller swelling ratio and a higher elastic modulus. This trend seems logical because as the content of agarose increases, more agarose polymer chains would be present, with less space for water content, and previous studies have found a similar trend of increasing elastic modulus with increasing agarose concentration (331–333). Studies also show that pore size of agarose varies and correlates with agarose w/v % (amongst other factors) (334) - this again would fit with the swelling ratio because larger pore sizes would facilitate more water ingress and a potentially softer gel (i.e. a lower elastic modulus). Pore size was not explored in this work but could be accomplished with SEM for completeness. It would also be interesting to see how the addition of poly-lysine affects the pore size and structure of the agarose gels; if the theory of the poly-lysine disrupting the agarose tetrahedral structure is correct, then the pore size would likely be larger for gels with poly-lysine added than pure agarose gels.

The statistical results of the uniaxial compression tests and swelling ratio experiment should be viewed with caution as only three repeats were done. With more repeats, more certainty can be given to the trends identified.

It is widely accepted that cells may alter the scaffold that they are grown in or on (134); degradation of the gel or deposition of matrix may both affect the elastic modulus. Therefore, the ideal elastic modulus may be higher or lower than the values gained from the mechanical testing of the gels, as these tests were completed on unseeded gels. Testing the elastic modulus of gels cultured with live cells can be challenging due to maintenance of physiological conditions during testing. If physiological conditions are not maintained, apoptosis of cells may affect any ECM produced by the cells and as such the modulus produced by the experiment. This could be explored in future work.

5.7.4. LINKING THE AGAROSE CELL CULTURE RESULTS TO THE DENTAL PULP WORK

It is not currently known what the ideal modulus is for DPSCs to differentiate into odontoblasts. Some works have identified that the elastic modulus is important for odontogenic differentiation *in-vitro* (12), but full exploration of this process with DPSCs growing on a variety of substrate stiffnesses is lacking in the literature. From the literature, there are numerous figures quoted for the ideal elastic modulus for bone formation, but the ideal modulus is believed to be 20-60 kPa (covered in a concise review by Prouvé *et al.* (335). However it likely depends somewhat on what the cells are grown on and their attachment to the surface/substrate (134,336). As odontoblasts and osteoblasts share many similarities, as does the mineral produced by both, it is likely that the elastic modulus needed to differentiate odontoblasts is similar to that for osteoblasts. Based upon the works completed in this study, the best elastic modulus for odontoblastic differentiation links to an agarose concentration in the region of 5-7% (with a PDL 0.1mg/mL coating and addition), which corresponds to a range of 41-96kPa (based on the median elastic modulus values for 5LPDL0.1 and 7LPDL0.1 respectively). The reported values for osteoblastic differentiation would roughly fit within this range, however as noted in the review by Prouvé *et al.*, there is a general lack of studies exploring higher moduli for osteoblastic differentiation (335). Assuming an elastic modulus of 41-96 kPa to be the ideal for dentine-like mineral deposition and odontoblastic differentiation, this correlates with the sites 4 and 5 in carious teeth and site 3 and 5 in sound teeth (see Table 4.3.1 4). As below 5% agarose was not explored for cellular differentiation, it is difficult to determine whether gels below 5% w/v agarose would have facilitated better mineral deposition. However, based solely on the results herein, it would appear that DPSC differentiation may begin away from the central core of the tooth, at a midpoint between the core and coronal aspect. Towards the more coronal (and apical) areas, the elastic modulus of the pulpal tissue may be too high to facilitate good odontoblastic differentiation. It is also possible that the lower elastic modulus in the sound pulp at the core (site 4, 29kPa) may prevent odontoblastic differentiation, though exploration with lower modulus gels would be needed to prove this further. It would be interesting to explore in depth, and link the AFM results to, stem cell niches within the dental pulp to see if part of their ability to maintain a quiescent stem cell population may be based upon a reduced elastic modulus.

This work has not explored the infiltration of the cells into the gels. It would be ideal if the cells could infiltrate the gel, differentiate and begin dentinogenesis to replace the agarose pore spaces with dentine. In this way, the agarose scaffold will also act as a restoration and 'space filler' for the dental cavity. In its current state, the 5LPDL0.1 or 7LPDL0.1 gel would most likely be used as a thin, hydrogel membrane covering an exposed dental pulp. This membrane would facilitate DPSC colonization, differentiation and ultimate dentine deposition. Filling the cavity with dentine would result in potentially better aesthetics, better mechanical properties and improved pulpal vitality compared with some of the PCAs currently available. This is because the produced dentine would match the natural appearance of the tooth and impart similar mechanical and functional properties of the sound dentition. Improved pulpal vitality may also be possible due to the reduced cytotoxicity of agarose and reduced inflammation compared with many current PCA's highly alkaline formulations. As previously discussed in the introduction, some inflammation is necessary for regeneration in the pulp, but too much and the balance gets tipped into degradation and destruction (20). Another key advantage that has not been explored in this work for agarose as a PCA would be the addition of encapsulated medicaments and/or bioactive molecules into the scaffold; whether this be ions and growth factors to aid in mineralisation, DPSC chemotaxis and differentiation, or antimicrobials and anti-inflammatories to temper the inflammatory response to caries and treat any residual disease. The efficacy of these additions can only really be tested *in-vivo*, and animal studies would be warranted to explore this further.

As previously mentioned, agarose gels with a w/v% below 5% were not explored in this work because the initial AFM work found that gels with a 5-10% w/v agarose concentration fit with the coronal sites of the pulp, where DPSC differentiation to odontoblast-like cells is generally assumed to occur. However, from the findings herein, further exploration of lower percentage w/v agarose gels would be beneficial to determine if a lower % gel would be better than the 5-9% gels explored in this work.

One outcome of this work is the importance of cellular adhesion to the substrate in DPSC differentiation and metabolism; too little adhesion and the cells do not attach (as seen in LPLL0.01 and LPDL0.01 gels), too much adhesion and cellular metabolism is affected (as seen in HPLL0.1 gels). Linking this work to the RNAseq results, upregulation of some cellular adhesion proteins was identified in sound teeth. This may also suggest that the stronger integrin binding in sound teeth may prevent the differentiation and turnover of DPSCs, as seen in HPLL0.1 gels. Further work exploring specific integrins would be necessary both *ex-vivo* and *in-vitro* to explore the roles these play on the differentiation of DSPCs. Moreover, a recent study has also found that cell density is likely to be an important factor (potentially more so than substrate stiffness) in cell turnover and differentiation, highlighting the importance of considering the adhesion of cells to scaffolds and the resultant cellular density and intercellular interactions in stem cell fate in conjunction with substrate stiffness (337).

To link the DPSC/agarose gel culture to the RNA dental pulp work, it would have been interesting to sequence the DPSCs after the three week cell culture from the more successful gels. This would have given more insight into differential gene expression between the different gel types. However, to achieve enough biomass (and RNA) for this to be viable, the agarose gel culture would have needed to be completed on a large scale (at least 5 times). This would have provided a richer and more complex analysis than the IF and RT-PCR work completed in this work and potentially added to the evidence behind some of the gels successfully facilitating odontogenic differentiation.

A lot of statistical tests have been carried out in this work. With a p-value of 0.05, there is a 5% possibility each time a test is completed that the results are due to chance. Based upon this fact, and the extensive statistical tests completed herein, it is highly likely that some of the results are due to chance (either false-positive, “type I errors” or false-negative, “type 2 errors”). It is not possible to determine for certain which results may be subject to these errors, however they are more likely to be present in experiments with fewer technical and biological repeats. Decreasing the p-value to 0.01 can help with reducing the possibility of a type 1 error, however increasing it would reduce the possibility of a type 2 error. There is no ideal cutoff with regards to p-values and each experiment and field of scientific research uses different values. Overall, a p-value of 0.05 is considered acceptable in this field, but it is important to acknowledge the limitations of this in the statistical tests completed.

6. CONCLUSION AND FUTURE WORK

The work in this thesis has successfully met the objectives outlined in Section 2. In doing so, the microscale and nanoscale mechanics of the dental pulp have been explored and matched to structural changes and gene expression data. This has then been used to create a novel agarose scaffold capable of facilitating DPSC differentiation and hard tissue deposition.

This work has successfully demonstrated that an agarose gel scaffold can be effectively used to produce hydroxyapatite-like hard tissue and induce differentiation of DPSCs to odontoblast-like cells. The ideal elastic modulus for these DPSC scaffolds was in the range 41-96kPa, in line with the AFM work on the pulp in Chapter 4.3.1, however further exploration of lower elastic moduli would be prudent to confirm this as the most suitable modulus. The required elastic modulus correlated with 5% and 7% w/v agarose gels with poly-d-lysine addition and coating. Taking the agarose gel work forward, 3-D printing could be considered to help better pattern the gels to encourage a more dentine-like structure to the mineral produced.

When modifying the agarose gel to facilitate cell adhesion, poly-d-lysine (0.1mg/mL with a molecular weight of 70-150kDa) proved to be the most effective for DPSC differentiation and resultant mineral deposition. The poly-d-lysine addition to the gel reduced the effective elastic modulus, likely as a consequence of disruption of the hydrogen bonding in the agarose gel, leading to increased porosity and higher water content. SEM would be a good way to assess the gel structure further. Cellular adhesion has proved to be pertinent to DPSC metabolism and differentiation in this work, and the degree of cellular attachment has also proved a crucial factor in biomaterial design for DPSC differentiation. We are only just beginning to understand how cellular attachment may impact upon stem cell differentiation (for example see (315,316)) and exploration of this would be an interesting and worthwhile endeavor to better inform scaffold design.

When comparing mineral production in odontogenic and basal media, different trends were identified depending on the elastic modulus of the agarose gels. In odontogenic media, mineral production decreased with increasing elastic modulus, whereas in basal media, the opposite was found. Further work would be beneficial exploring mineralization in environments of differing ion concentration to see to what extent mineral ion abundance affects the volume of mineral produced when differing elastic modulus substrates are taken into account. Taking this project forwards, it would also be interesting and useful to assess mineralization in ‘real time’, to determine when peak mineralization occurs on the gels made in this thesis. This could be facilitated by ‘real time’ calcein staining.

The work in Chapter 4.3 has explored and determined the elastic modulus of the dental pulp at the micro and nano level and revealed this to be on a gradient, decreasing towards the pulp centre, as well as proved differences between the elastic modulus values of sound and carious teeth. Based upon confocal

histological images and RNAseq data, the changes in modulus between carious and sound teeth are likely due to differences in the volume and structure of collagen and other extracellular matrix fibres, potentially caused by differences in collagenase activities and/or dysregulation of the extracellular matrix in carious teeth. The elastic modulus range of the scaffolds, 41-96kPa, correlated with the values found closer to the centre of the pulp, which draws into question whether DPSCs differentiate before they migrate to the dentine-pulp interface or begin changing en-route.

Statistically significant differences in the elastic modulus between carious and sound teeth were found at the most coronal aspect of the pulp. This could be due to apoptosis of odontoblasts and inflammatory changes in carious teeth, such as ECM degradation. Odontoblasts may be providing some stability to the dental pulp due to their cytoplasmic projections anchoring them into the dentine, and when they undergo apoptosis, their loss may be reducing the elastic modulus locally.

Taking this work forwards, further exploration of the mechanics of the dental pulp is warranted to better understand the micromechanics of DPSC niches in health and disease so that we can better appreciate how mechanical changes are influencing DPSCs and build on existing knowledge for better pulpal replacements and therapeutics. Extensive literature exists on the mechanics of enamel and dentine, but very little work has been accomplished on the mechanics of the pulp and this work represents a significant step to address this void in the literature. Looking more closely at the micromechanics of stem cells niches in health and disease may allow us to better understand the process of DPSC migration and differentiation in reparative dentine. For example, we do not currently know if all stem cell niches share similar elastic properties or if they vary by tissue-type. Also, we do not know how the elastic modulus of stem cell niches change in disease and what influences this, nor do we know whether the elastic modulus of stem cell niches is playing a role in maintaining the pluripotency of the stem cells. The dental pulp offers a viable way of potentially exploring these avenues.

The RNAseq data provided herein adds to the growing literature on comparing the biological environment of carious and sound teeth, with genes associated with neurogenesis, inflammation and immune system response upregulated in carious teeth. Many genes not previously associated with pulpal biology were identified and further exploration of the roles of these genes in the pulp would lead to a better understanding of the mechanisms of pulpal disease. One tooth included in the cohort was unerupted, which has given a unique insight into the transcriptional landscape of an unerupted dental pulp and shown this to be very different to erupted teeth. Though not the focus of this project, it would be interesting to explore the transcriptional differences between unerupted and erupted teeth further to better understand the mechanisms of eruption. Some clustering was found linking age to RNAseq outputs in the top 50 most expressed genes, although sample numbers were quite limited. Again, though not the focus of this project, this finding has highlighted the impact ageing may play on the transcriptional environment of the dental pulp and a better understanding of the dental pulp in relation

to ageing would be of benefit to ensure that regenerative therapies will work in older patients, as research has shown that some commercial PCAs have age-dependent outcomes (80).

From the extensive data in this thesis, particularly with regards to the agarose gel work, future work could investigate predictive modelling using machine learning or mathematical modelling to forecast the possible characteristics of agarose gels and how well they may function as dentinogenic scaffolds. This would be beneficial in terms of reducing man power and laboratory-based time.

The aim of this project was to design, fabricate and characterise an *in-vitro* acellular biomimetic scaffold, capable of being colonised by DPSCs, and capable of facilitating dentine production. This work used new data from exploration of the dental pulp to inform scaffold design. This work has shown that agarose is a viable option for dentine production *in-vitro* when suitably modified with poly-d-lysine.

It is important to note that this is a basic science project. It provides only the initial scientific grounding behind a dentinogenic agarose scaffold. Should this scaffold be deemed a viable option for dental pulp capping, further work will be required to prove efficacy in animal models before human trials (including randomised control trials comparing existing PCAs to the agarose gel).

Current pulp therapies are largely based upon the production of a hard tissue barrier by using $Ca(OH)_2$ (either directly or indirectly via MTA leaching $Ca(OH)_2$). $Ca(OH)_2$ was first used as a PCA 100 years ago and the basic principles of placing an alkaline irritant directly onto a vital pulp to stimulate a hard tissue bridge have remained mostly similar in this time. Vital pulp therapies continue to evolve as our understanding of the dental pulp improves. With better understanding of the microscale (and even nanoscale) environment of the pulp, we can work towards producing therapies more geared towards regeneration rather than replacement or repair of dental tissues and design PCAs linked to an intimate understanding of the dental pulp in health and disease.

7. APPENDICES

APPENDIX 1

Ymchwil Iechyd a Gofal Cymru
Health and Care Research Wales

NHS
Health Research Authority

Dr Laura Whitehouse
Phd Student and StR in Oral and Maxillofacial Pathology
PhD Student - not employed
University of Leeds
Leeds
LS2 9JTN/A

Email: approvals@hra.nhs.uk
HCRW.approvals@wales.nhs.uk

01 April 2021

Dear Dr Whitehouse

HRA and Health and Care Research Wales (HCRW) Approval Letter

Study title:	**Linking Dental Pulp elastic moduli, RNA and histology**
IRAS project ID:	**294171**
Protocol number:	**N/A**
REC reference:	**21/NW/0106**
Sponsor	**University of Leeds**

I am pleased to confirm that **HRA and Health and Care Research Wales (HCRW) Approval** has been given for the above referenced study, on the basis described in the application form, protocol, supporting documentation and any clarifications received. You should not expect to receive anything further relating to this application.

Please now work with participating NHS organisations to confirm capacity and capability, in line with the instructions provided in the "Information to support study set up" section towards the end of this letter.

How should I work with participating NHS/HSC organisations in Northern Ireland and Scotland?
HRA and HCRW Approval does not apply to NHS/HSC organisations within Northern Ireland and Scotland.

If you indicated in your IRAS form that you do have participating organisations in either of these devolved administrations, the final document set and the study wide governance report (including this letter) have been sent to the coordinating centre of each participating nation. The relevant national coordinating function/s will contact you as appropriate.

Figure A1 1:Ethical approval for study ('Project Ethics')

Please see IRAS Help for information on working with NHS/HSC organisations in Northern Ireland and Scotland.

How should I work with participating non-NHS organisations?
HRA and HCRW Approval does not apply to non-NHS organisations. You should work with your non-NHS organisations to obtain local agreement in accordance with their procedures.

What are my notification responsibilities during the study?

The standard conditions document "*After Ethical Review – guidance for sponsors and investigators*", issued with your REC favourable opinion, gives detailed guidance on reporting expectations for studies, including:

- Registration of research
- Notifying amendments
- Notifying the end of the study

The HRA website also provides guidance on these topics, and is updated in the light of changes in reporting expectations or procedures.

Who should I contact for further information?
Please do not hesitate to contact me for assistance with this application. My contact details are below.

Your IRAS project ID is **294171**. Please quote this on all correspondence.

Yours sincerely,
Amber Ecclestone

Approvals Specialist

Email: approvals@hra.nhs.uk

Copy to: *Jean Uniacke*

Figure A1 1 (continued):Ethical approval for study ('Project Ethics') (continued)

UNIVERSITY OF LEEDS

School of Dentistry

Worsley Building

Clarendon Way

Leeds

LS2 9LU

+44 (0)113 3436210

Dear Laura

DREC ref: 140219/LW/269

Title: Creation and mechanical stimulation of dentinogenic scaffolds

I am pleased to inform you that the above Tissue Bank application has been accepted by the Dental Research Ethics Committee (DREC) for 16 teeth from the Tissue Bank.

Documents reviewed by the Committee

Document name	**Version number and date**
Tissue Bank application form	Signed 19.02.2019
Protocol	Version 1 14.02.2019

With best wishes for the success of your project.

For and on behalf of

Dr Jinous Tahmassebi

DREC Chair

Figure A1 2: Ethical approval from the local Leeds Skeletal Tissue Bank ('Tissue Bank Ethics')

APPENDIX 2

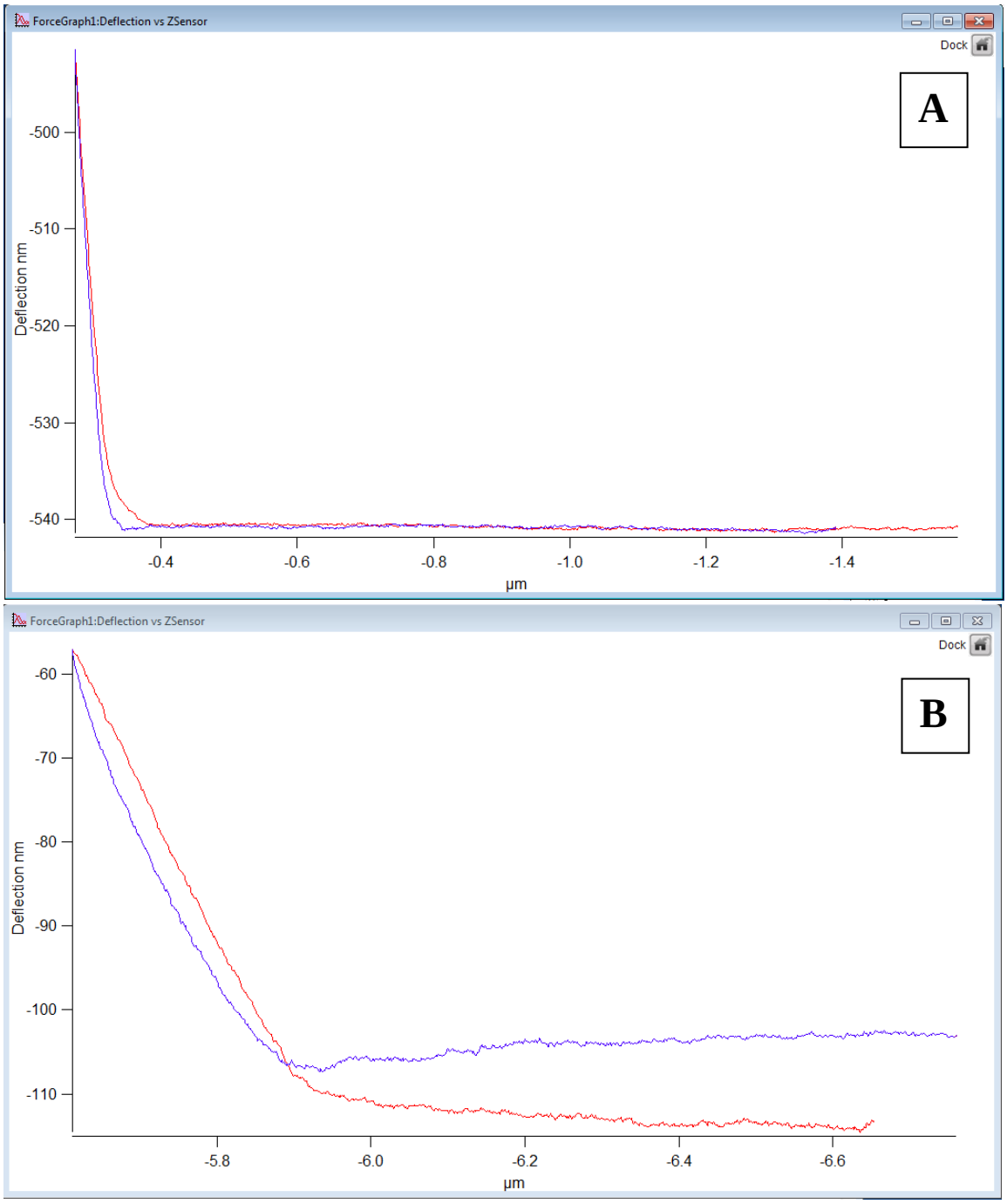

Figure A2 1: Comparing a 'good' curve (A), with a well-defined contact point, and clear approach and retraction lines, and a 'bad' curve (B), with a poorly defined contact point and irregular approach and retraction lines

APPENDIX 3

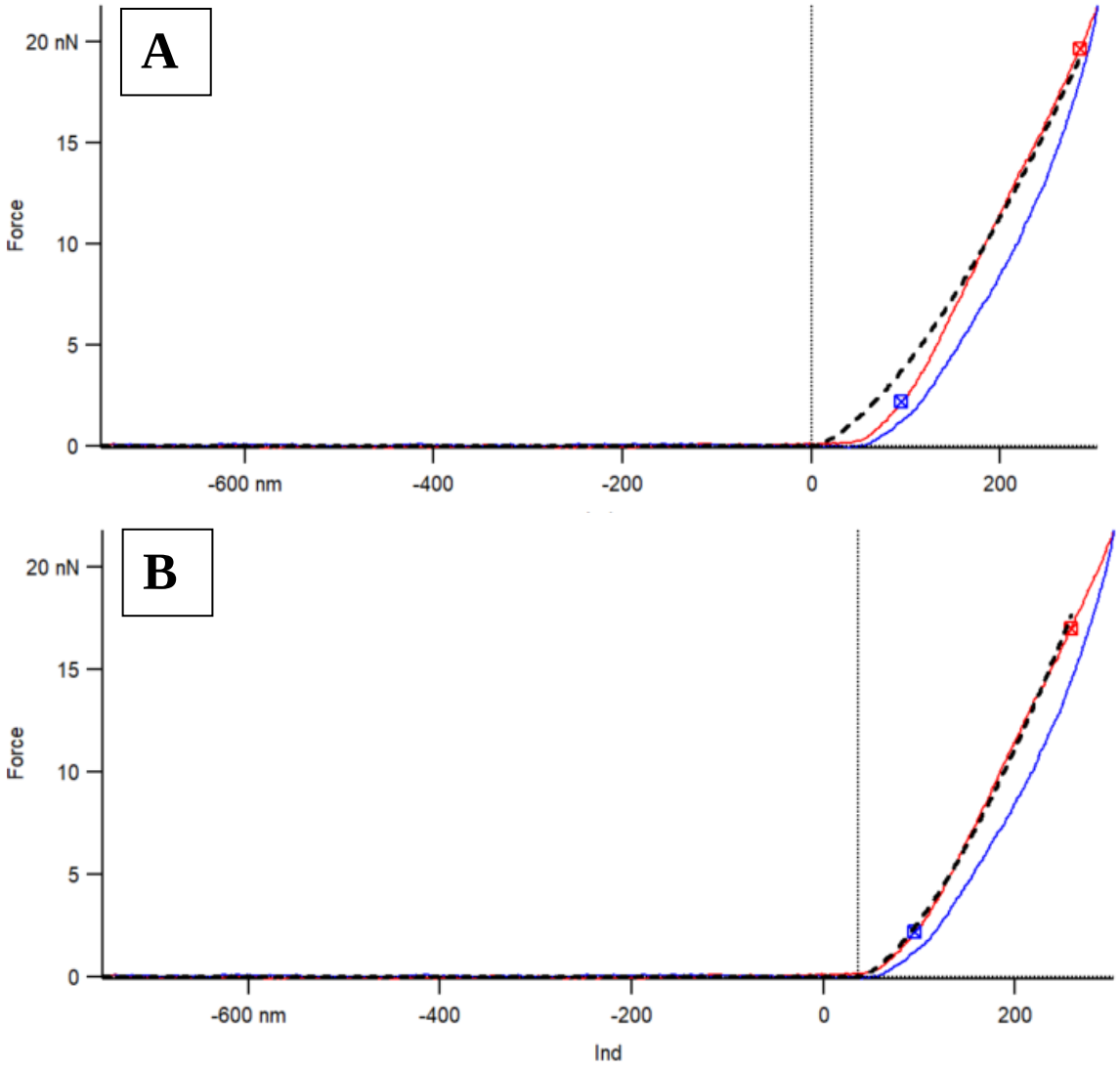

Figure A3 1: Fitting of a force curve with Hertz model. A= Before fit, B= After fit. Dotted line = Contact point

APPENDIX 4

FOURIER ORIENTATION MACRO:

```
open("FILEPATH.tif");
run("Set Scale...", "distance=585 known=50 unit=um global");
makeRectangle(963, 0, 2157, 2160);
run("Duplicate...", " ");
selectWindow("F_3.tif");
close();
selectWindow("F_3-1.tif");
run("Split Channels");
selectWindow("F_3-1.tif (red)");
selectWindow("F_3-1.tif (green)");
selectWindow("F_3-1.tif (blue)");
close();
close();
selectWindow("F_3-1.tif (red)");
//run("Brightness/Contrast...");
setMinAndMax(44, 210)
run("Apply LUT");
selectWindow("F_3-1.tif (red)")
run("FFT");
selectWindow("FFT of F_3-1.tif (red)")
run("BRGBCMYW");
//run("Threshold...");
setThreshold(192, 255);
run("Convert to Mask");
setOption("BlackBackground", false);
run("Convert to Mask");
run("Inverse FFT");
saveAs("Tiff", "FILENAME_AND_PATH.tif")
selectWindow("Inverse FFT of F_3-1.tif (red).tif")
//setTool("line");
```

```
makeLine(0, 3, 2157, 2160);
run("Plot Profile");
selectWindow("Plot of Inverse FFT of F_3-1.tif (red)");
Plot.showValues()
saveAs("Results", "FILENAME_AND_PATH.csv");
saveAs("Tiff", "FILENAME_AND_PATH.tif");
selectWindow("Plot of Inverse FFT of F_3-1.tif (red).tif")
close();
selectWindow("Inverse FFT of F_3-1.tif (red).tif")
//setTool("line");
makeLine(2154, 0, 6, 2149);
run("Plot Profile");
selectWindow("Plot of Inverse FFT of F_3-1.tif (red)");
Plot.showValues()
saveAs("Results", "FILENAME_AND_PATH.csv");
saveAs("Tiff", "FILENAME_AND_PATH.tif");
selectWindow("F_3-1.tif (red)");
saveAs("Tiff", "FILENAME_AND_PATH.tif");
selectWindow("F_3-1.tif (red).tif");
run("FFT");
selectWindow("FFT of F_3-1.tif (red).tif")
run("BRGBCMYW");
run("Duplicate...", " ");
selectWindow("FFT of F_3-1.tif (red)-1.tif")
saveAs("Tiff", "FILENAME_AND_PATH.tif");
//setTool("rectangle");
makeRectangle(846, 864, 2502, 2268);
run("Duplicate...", " ");
saveAs("Tiff", "FILENAME_AND_PATH.tif");
selectWindow("FFT of F_3-1.tif (red)");
run("Duplicate...", " ");
saveAs("Tiff", "FILENAME_AND_PATH.tif");
```

```
selectWindow("F_3-1.tif (red).tif")
makeLine(2154, 0, 0, 2154);
run("Plot Profile");
Plot.showValues()
saveAs("Results", "FILENAME_AND_PATH.csv");
selectWindow("F_3-1.tif (red).tif")
//setTool("line");
makeLine(0, 3, 2157, 2160);
run("Plot Profile");
saveAs("Results", "FILENAME_AND_PATH.csv");
```

TRANSECTS MACRO:

IMAGEJ:

```
open("FILENAME_AND_PATH_TO_PREVIOUS_GREYSCALE_FROM_FOURIER_ORIENTATION_MACRO.tif");
run("Options...", "iterations=1 count=1 black");
setOption("BlackBackground", true);
run("Convert to Mask");
//setTool("line");
makeLine(0, 2154, 2157, -3);
run("Plot Profile");
Plot.showValues()
saveAs("Results", "FILENAME_AND_PATH.csv");
close();
//setTool("line");
selectWindow("F_3-1.tif (red).tif");
makeLine(0, 6, 2157, 2163);
run("Plot Profile");
Plot.showValues()
saveAs("Results", "FILENAME_AND_PATH.csv");
close();
selectWindow("F_3-1.tif (red).tif");
makeLine(1050, 6, 1050, 2160);
```

```
run("Plot Profile");
Plot.showValues()
saveAs("Results", "FILENAME_AND_PATH.csv");
close();
selectWindow("F_3-1.tif (red).tif");
makeLine(2151, 1023, 0, 1023);
run("Plot Profile");
Plot.showValues()
saveAs("Results", "FILENAME_AND_PATH.csv");
close();
selectWindow("F_3-1.tif (red).tif");
close();
```

MICROSOFT EXCEL:

```
Sub gothroughall()
   Dim LR As Long, LC As Long, i As Long, j As Long
   Dim iRw As Integer
   Dim iCol As Integer
   Dim rng As Range
   Dim Count As Integer
   For i = 1 To 4000
   If ActiveCell.Value = "" Then
   Selection.End(xlDown).Select
   End If
   If ActiveCell.Value >= 0 Then
   Range("B" & i).Formula = ActiveCell.CurrentRegion.Rows.Count
   Selection.End(xlDown).Select
   End If
   ActiveCell.Offset(1, 0).Select
   Next i
End Sub
```

APPENDIX 5

Sample	Raw reads	Raw data	Effective(%)	Error(%)	Q20(%)	Q30(%)	GC(%)
TOOTH18	68671754	10.3	99.10	0.03	96.16	90.26	49.50
TOOTH16	93721478	14.1	98.85	0.03	96.39	90.69	51.50
TOOTH23	83584426	12.5	98.77	0.03	95.74	89.85	48.20
TOOTH17	78723880	11.8	99.07	0.03	96.44	90.80	51.30
TOOTH21	75104068	11.3	99.05	0.03	96.14	90.36	49.63
TOOTH14	92203662	13.8	99.02	0.03	96.41	90.77	50.92
TOOTH19	72620120	10.9	99.23	0.03	96.32	90.57	49.60
TOOTH24	81605834	12.2	98.89	0.03	95.36	89.12	46.80
TOOTH30	96931992	14.5	99.10	0.03	96.12	90.25	52.21
TOOTH15	87154564	13.1	99.12	0.03	96.25	90.49	51.49

Table A5 1: Quality of reads for teeth sequenced

APPENDIX 6

RNA-seq script:

Read Quality Control and Trimming:

```
cutadapt -a AGATCGGAAGAGCACACGTCTGAACTCCAGTCAC -o 14_1.fastq.gz
TOOTH14_1.fastq.gz
BiocManager::install("FastqCleaner")
library(FastqCleaner)
launch_fqc()
```

Build an Index and align reads:

```
BiocManager::install("Rsubread")

library(Rsubread)

buildindex(basename = "index3", reference
="/nobackup/denlwh/ref/GRCh38_latest_genomic.fa")

BiocManager::install("Rsubread")

library(Rsubread)

align(index="index3", readfile1="14_1.trimmed.fastq.gz",
readfile2="14_2.trimmed.fastq.gz", type="rna", input_format="gzFASTQ",
output_format = "BAM", PE_orientation="fr", nthreads = 6)
```

Read Summarisation:

```
Library(Rsubread)

fc<- featureCounts(files= "14_1.bam", annot.ext="index3",
isGTFAnnotationFile=TRUE, GTF.featureType= "exon", GTF.attrType=
"gene_id", useMetaFeatures=TRUE, allowMultiOverlap=FALSE,
strandSpecific=0, countMultiMappingReads=FALSE, isPairedEnd=TRUE,
requireBothEndsMapped=TRUE, checkFragLength=TRUE, minFragLength=50,
maxFragLength=600, countChimericFragments=FALSE)


write.csv(fc$counts, file= "14_1_counts.csv", quote=FALSE, row.names=TRUE)

write.table(fc$counts, file= "14_1_counts.txt", sep= "\t", quote=FALSE,
row.names=TRUE)
```

Normalisation:

```
BiocManager::install("edgeR")

library(edgeR)

count.data<-read.csv(file="all_counts.csv")
```

```
nrow(count.data)

keep<-rowSums(count.data)>=1

count.data.keep<-count.data[keep,]

count.data.keep<-count.data.keep+1

lib.size<-apply(count.data.keep, 2, sum)

scale.factors<-calcNormFactors(count.data.keep, method=”TMM”)

norm.data<-t(t(count.data.keep)/(scale.factors*lib.size))

norm.data<-log(norm.data)
```

Differential Gene Expression Analysis:

```
BiocManager::install(“DESeq2”)

Library(DESeq2)

count.data<-read.csv(file=”all_counts.csv”)

keep<-rowSums(count.data)>=1

count.data.keep<-count.data[keep,]

coldata<-data.frame(row.names=c(“X14”, “X15”, “X16”, “X17”, “X18”, “X19”, “X21”, “X23”, “X24”), condition=c(“Carious”, “Carious”, “Sound”, “Sound”, “Carious”, “Carious”, “Carious”, “Carious”, “Sound”))

dds<-DESeqDataSetFromMatrix(countData=count.data.keep, colData=coldata, design=~condition)

dds<-DESeq(dds, fitType=”local”)

res<-results(dds)
```

APPENDIX 7

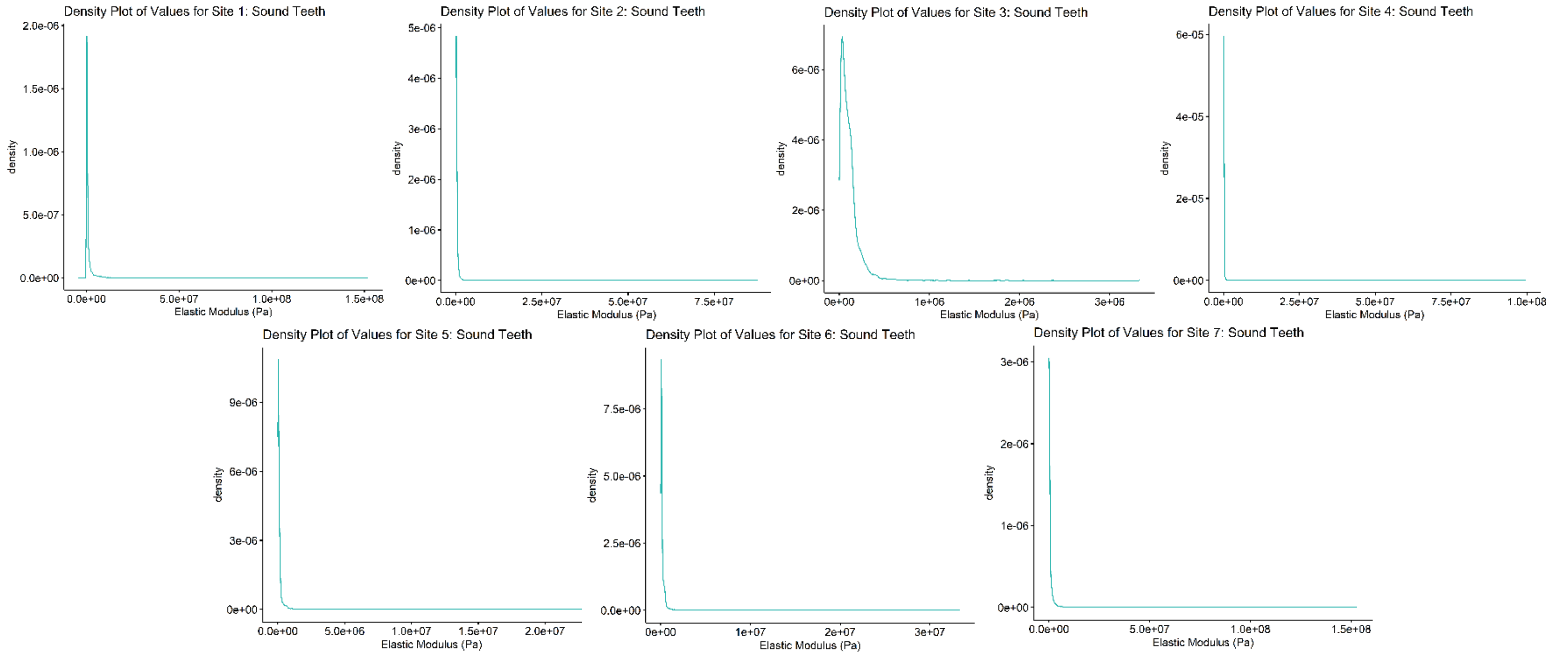

Figure A7 1: Density Plots for each site in Sound Teeth, AFM elastic modulus results

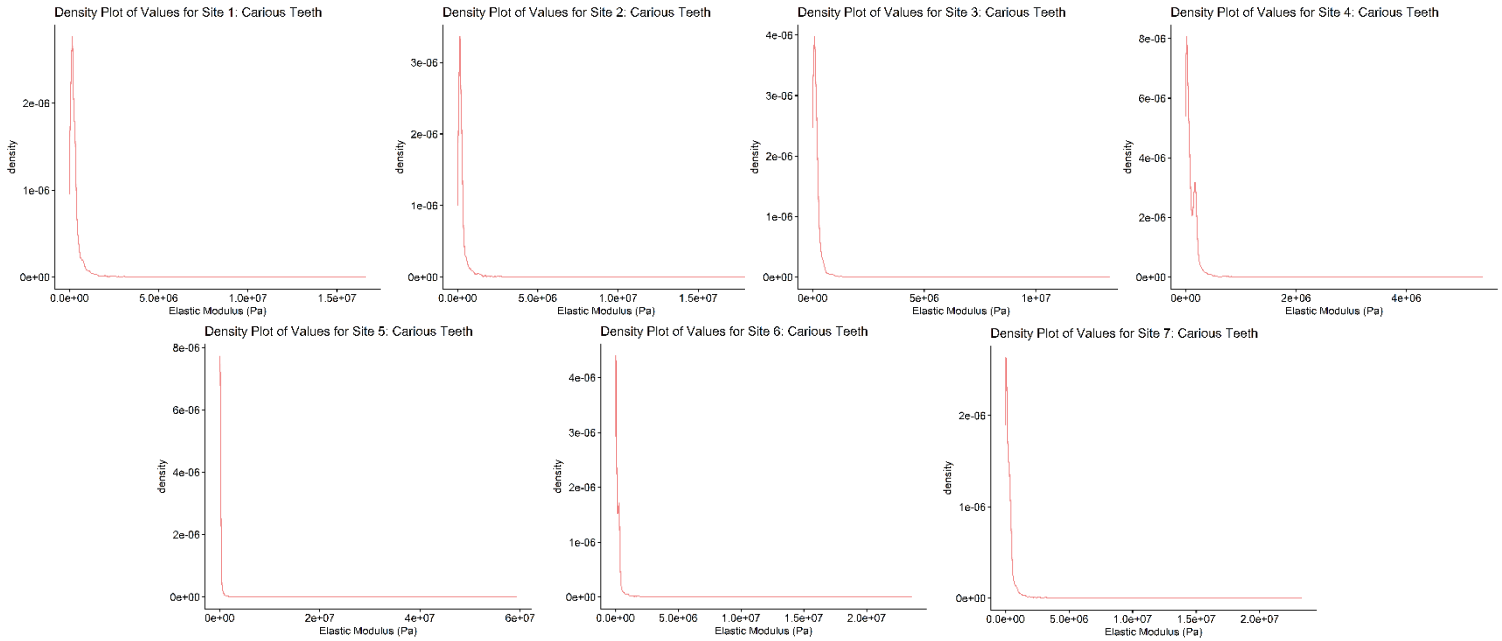

Figure A7 2: Density Plots for each site in Carious Teeth, AFM elastic modulus results

APPENDIX 8

CARIOUS TOOTH 1

	Comparison	Z	P.unadj	P.adj
1	1 - 2	1.30366064	1.923493e-01	3.846986e-01
2	1 - 3	14.34502090	1.144658e-46	1.602521e-45
3	2 - 3	13.04172385	7.083709e-39	8.500451e-38
4	1 - 4	25.50781046	1.614724e-143	3.390920e-142
5	2 - 4	24.20451341	1.994139e-129	3.988278e-128
6	3 - 4	11.15967798	6.422378e-29	7.064616e-28
7	1 - 5	14.41904145	3.927593e-47	5.891390e-46
8	2 - 5	13.11465514	2.714140e-39	3.528382e-38
9	3 - 5	0.06201406	9.505516e-01	9.505516e-01
10	4 - 5	-11.10698566	1.160097e-28	1.160097e-27
11	1 - 6	21.45346631	4.238598e-102	8.053336e-101
12	2 - 6	20.15016926	2.681955e-90	4.827518e-89
13	3 - 6	7.10646396	1.190537e-12	1.071484e-11
14	4 - 6	-4.05321402	5.051875e-05	2.020750e-04
15	5 - 6	7.05038597	1.784222e-12	1.427377e-11
16	1 - 7	18.49744120	2.165121e-76	3.680705e-75
17	2 - 7	17.19341747	2.974694e-66	4.759511e-65
18	3 - 7	4.14326543	3.423953e-05	2.054372e-04
19	4 - 7	-7.02263137	2.177281e-12	1.524097e-11
20	5 - 7	4.08468151	4.413731e-05	2.206866e-04
21	6 - 7	-2.96715867	3.005658e-03	9.016974e-03

Table A8 1: Post-hoc Dunn's Test results, with pairwise comparisons for all sites in Carious Tooth # 1, statistically significant results in green (p<0.05), non-statistically significant results in pink (p>0.05)

CARIOUS TOOTH 2

	Comparison	Z	P.unadj	P.adj
1	1 - 2	6.54554385	5.927926e-11	7.113511e-10
2	1 - 3	5.72495680	1.034601e-08	1.034601e-07
3	2 - 3	-0.82470107	4.095413e-01	1.000000e+00
4	1 - 4	11.95385661	6.198077e-33	9.297116e-32
5	2 - 4	5.40769320	6.384166e-08	5.745750e-07
6	3 - 4	6.23587897	4.492483e-10	4.941732e-09
7	1 - 5	31.96261114	3.609144e-224	7.579203e-223
8	2 - 5	25.42767278	1.246876e-142	2.369065e-141
9	3 - 5	26.26705228	4.564758e-152	9.129515e-151
10	4 - 5	20.03117331	2.946338e-89	4.714141e-88
11	1 - 6	6.91227650	4.769371e-12	6.200182e-11
12	2 - 6	0.35782367	7.204753e-01	1.000000e+00
13	3 - 6	1.18387552	2.364623e-01	1.000000e+00
14	4 - 6	-5.05721232	4.254295e-07	3.403436e-06
15	5 - 6	-25.10511779	4.372850e-139	7.871130e-138
16	1 - 7	6.97007023	3.167828e-12	4.434959e-11
17	2 - 7	0.41746767	6.763364e-01	1.000000e+00
18	3 - 7	1.24332336	2.137487e-01	1.000000e+00
19	4 - 7	-4.99603061	5.852238e-07	4.096566e-06
20	5 - 7	-25.03836646	2.337439e-138	3.973646e-137
21	6 - 7	0.05982673	9.522936e-01	9.522936e-01

Table A8 2: Post-hoc Dunn's Test results, with pairwise comparisons for all sites in Carious Tooth # 2, statistically significant results in green (p<0.05), non-statistically significant results in pink (p>0.05)

CARIOUS TOOTH 3

	Comparison	Z	P.unadj	P.adj
1	1 - 2	1.6272073	1.036931e-01	3.110792e-01
2	1 - 3	3.3186102	9.046662e-04	6.332663e-03
3	2 - 3	1.6988318	8.935088e-02	3.574035e-01
4	1 - 4	15.5227573	2.433648e-54	3.650472e-53
5	2 - 4	13.8742360	9.075488e-44	1.270568e-42
6	3 - 4	12.0901735	1.190351e-33	1.547456e-32
7	1 - 5	22.6552486	1.238435e-113	2.476870e-112
8	2 - 5	20.9981447	6.819721e-98	1.295747e-96
9	3 - 5	19.1729069	6.232675e-82	1.121882e-80
10	4 - 5	7.1435680	9.093892e-13	1.000328e-11
11	1 - 6	4.5311365	5.866722e-06	5.280050e-05
12	2 - 6	2.9111081	3.601494e-03	2.160896e-02
13	3 - 6	1.2065882	2.275908e-01	4.551815e-01
14	4 - 6	-10.8644481	1.702495e-27	2.042994e-26
15	5 - 6	-17.9419958	5.542816e-72	9.422787e-71
16	1 - 7	-0.8300769	4.064953e-01	4.064953e-01
17	2 - 7	-2.4445897	1.450170e-02	7.250851e-02
18	3 - 7	-4.1193575	3.799304e-05	3.039443e-04
19	4 - 7	-16.2422142	2.536030e-59	4.057648e-58
20	5 - 7	-23.3235617	2.557064e-120	5.369834e-119
21	6 - 7	-5.3227233	1.022252e-07	1.022252e-06

Table A8 3: Post-hoc Dunn's Test results, with pairwise comparisons for all sites in Carious Tooth # 3, statistically significant results in green (p<0.05), non-statistically significant results in pink (p>0.05)

CARIOUS TOOTH 4

	Comparison	Z	P.unadj	P.adj
1	1 - 2	1.177975	2.388064e-01	2.388064e-01
2	1 - 3	17.776380	1.077144e-70	1.184858e-69
3	2 - 3	16.601440	6.803893e-62	6.803893e-61
4	1 - 4	39.905584	0.000000e+00	0.000000e+00
5	2 - 4	38.735604	0.000000e+00	0.000000e+00
6	3 - 4	22.146841	1.118941e-108	1.790306e-107
7	1 - 5	9.658431	4.527464e-22	2.716478e-21
8	2 - 5	8.480219	2.247713e-17	8.990851e-17
9	3 - 5	-8.146530	3.745152e-16	1.123546e-15
10	4 - 5	-30.321056	6.051166e-202	1.089210e-200
11	1 - 6	30.544020	6.789273e-205	1.289962e-203
12	2 - 6	29.371391	1.274207e-189	2.166151e-188
13	3 - 6	12.769441	2.428912e-37	2.186020e-36
14	4 - 6	-9.387883	6.121807e-21	3.060903e-20
15	5 - 6	20.935788	2.528494e-97	3.792741e-96
16	1 - 7	20.247780	3.716152e-91	5.202612e-90
17	2 - 7	19.079144	3.763733e-81	4.516480e-80
18	3 - 7	2.560912	1.043978e-02	2.087956e-02
19	4 - 7	-19.476313	1.743950e-84	2.267135e-83
20	5 - 7	10.670306	1.401635e-26	1.121308e-25
21	6 - 7	-10.144129	3.519038e-24	2.463327e-23

Table A8 4: Post-hoc Dunn's Test results, with pairwise comparisons for all sites in Carious Tooth # 4, statistically significant results in green (p<0.05), non-statistically significant results in pink (p>0.05)

CARIOUS TOOTH 5

	Comparison	Z	P.unadj	P.adj
1	1 - 2	14.0366881	9.295628e-45	7.436502e-44
2	1 - 3	30.3628602	1.699709e-202	2.889505e-201
3	2 - 3	16.3197072	7.147766e-60	7.147766e-59
4	1 - 4	34.5163500	4.560534e-261	8.665015e-260
5	2 - 4	20.4911126	2.584199e-93	3.359459e-92
6	3 - 4	4.1942114	2.738226e-05	5.476452e-05
7	1 - 5	18.4585529	4.451082e-76	5.341299e-75
8	2 - 5	4.4243371	9.673885e-06	2.902166e-05
9	3 - 5	-11.8904459	1.326963e-32	7.961776e-32
10	4 - 5	-16.0667755	4.361939e-58	3.925745e-57
11	1 - 6	0.2890216	7.725648e-01	7.725648e-01
12	2 - 6	-13.7592691	4.480338e-43	3.136236e-42
13	3 - 6	-30.0988588	5.014847e-199	8.023755e-198
14	4 - 6	-34.2560950	3.538981e-257	6.370165e-256
15	5 - 6	-18.1848398	6.805402e-74	7.485942e-73
16	1 - 7	-8.8952979	5.826279e-19	2.330512e-18
17	2 - 7	-22.7917314	5.538209e-115	7.753493e-114
18	3 - 7	-38.9581158	0.000000e+00	0.000000e+00
19	4 - 7	-43.0596610	0.000000e+00	0.000000e+00
20	5 - 7	-27.1678800	1.556994e-162	2.335491e-161
21	6 - 7	-9.1886235	3.979004e-20	1.989502e-19

Table A8 5: Post-hoc Dunn's Test results, with pairwise comparisons for all sites in Carious Tooth # 5, statistically significant results in green (p<0.05), non-statistically significant results in pink (p>0.05)

CARIOUS TOOTH 6

	Comparison	Z	P.unadj	P.adj
1	1 - 2	1.428122	1.532567e-01	1.532567e-01
2	1 - 3	25.683961	1.766056e-145	2.295872e-144
3	2 - 3	24.233526	9.864508e-130	1.183741e-128
4	1 - 4	40.796554	0.000000e+00	0.000000e+00
5	2 - 4	39.333457	0.000000e+00	0.000000e+00
6	3 - 4	15.121005	1.177319e-51	1.059587e-50
7	1 - 5	36.564901	1.033777e-292	1.964176e-291
8	2 - 5	35.107837	5.118415e-270	9.213147e-269
9	3 - 5	10.929939	8.290433e-28	6.632346e-27
10	4 - 5	-4.165759	3.103182e-05	6.206364e-05
11	1 - 6	31.889926	3.682962e-223	5.892739e-222
12	2 - 6	30.437595	1.748281e-203	2.622422e-202
13	3 - 6	6.266767	3.686212e-10	1.474485e-09
14	4 - 6	-8.820448	1.140026e-18	7.980179e-18
15	5 - 6	-4.649270	3.331113e-06	9.993339e-06
16	1 - 7	8.212013	2.175112e-16	1.305067e-15
17	2 - 7	6.779432	1.206492e-11	6.032458e-11
18	3 - 7	-17.424268	5.399531e-68	5.399531e-67
19	4 - 7	-32.511483	7.338669e-232	1.247574e-230
20	5 - 7	-28.300831	3.375432e-176	4.725605e-175
21	6 - 7	-23.638329	1.556156e-123	1.711772e-122

Table A8 6: Post-hoc Dunn's Test results, with pairwise comparisons for all sites in Carious Tooth # 6, statistically significant results in green (p<0.05), non-statistically significant results in pink (p>0.05)

CARIOUS TOOTH 7

	Comparison	Z	P.unadj	P.adj
1	1 - 2	3.5049534	4.566872e-04	1.826749e-03
2	1 - 3	7.5562430	4.148785e-14	4.148785e-13
3	2 - 3	4.0404479	5.334922e-05	2.667461e-04
4	1 - 4	20.3726730	2.922806e-92	5.845612e-91
5	2 - 4	16.8358916	1.331674e-63	2.397013e-62
6	3 - 4	12.8106799	1.428772e-37	2.143158e-36
7	1 - 5	8.0685506	7.113761e-16	8.536513e-15
8	2 - 5	4.5696937	4.884376e-06	2.930625e-05
9	3 - 5	0.5502191	5.821691e-01	1.000000e+00
10	4 - 5	-12.1960572	3.262424e-34	4.567393e-33
11	1 - 6	0.1351622	8.924836e-01	8.924836e-01
12	2 - 6	-3.3671394	7.595228e-04	2.278569e-03
13	3 - 6	-7.4149351	1.216844e-13	1.095159e-12
14	4 - 6	-20.2208756	6.413477e-91	1.218561e-89
15	5 - 6	-7.9275712	2.234734e-15	2.458207e-14
16	1 - 7	-6.1517498	7.663271e-10	5.364290e-09
17	2 - 7	-9.6417876	5.325244e-22	6.922817e-21
18	3 - 7	-13.6948539	1.089794e-42	1.743670e-41
19	4 - 7	-26.4937619	1.143705e-154	2.401781e-153
20	5 - 7	-14.1755313	1.298567e-45	2.207563e-44
21	6 - 7	-6.2816707	3.349537e-10	2.679630e-09

Table A8 7: Post-hoc Dunn's Test results, with pairwise comparisons for all sites in Carious Tooth # 7, statistically significant results in green (p<0.05), non-statistically significant results in pink (p>0.05)

SOUND TOOTH 1

	Comparison	Z	P.unadj	P.adj
1	1 - 2	-1.398661	1.619146e-01	1.619146e-01
2	1 - 3	14.536049	7.160823e-48	7.160823e-47
3	2 - 3	15.943610	3.155862e-57	3.471448e-56
4	1 - 4	27.222326	3.534895e-163	4.948853e-162
5	2 - 4	28.637370	2.302771e-180	3.454157e-179
6	3 - 4	12.689320	6.777159e-37	4.066295e-36
7	1 - 5	28.694713	4.441073e-181	7.105717e-180
8	2 - 5	30.110581	3.522376e-199	5.988039e-198
9	3 - 5	14.162530	1.562643e-45	1.250115e-44
10	4 - 5	1.473621	1.405837e-01	2.811674e-01
11	1 - 6	34.959017	9.445913e-268	1.700264e-266
12	2 - 6	36.377583	9.630254e-290	1.829748e-288
13	3 - 6	20.438420	7.616522e-93	9.139826e-92
14	4 - 6	7.758330	8.605487e-15	4.302743e-14
15	5 - 6	6.285531	3.267352e-10	9.802055e-10
16	1 - 7	41.375272	0.000000e+00	0.000000e+00
17	2 - 7	42.797823	0.000000e+00	0.000000e+00
18	3 - 7	26.854213	7.531220e-159	9.790585e-158
19	4 - 7	14.172372	1.358334e-45	1.222501e-44
20	5 - 7	12.699162	5.976642e-37	4.183650e-36
21	6 - 7	6.408303	1.471480e-10	5.885919e-10

Table A8 8: Post-hoc Dunn's Test results, with pairwise comparisons for all sites in Sound Tooth # 1, statistically significant results in green (p<0.05), non-statistically significant results in pink (p>0.05)

SOUND TOOTH 2

	Comparison	Z	P.unadj	P.adj
1	1 - 2	9.489086	2.330691e-21	1.398415e-20
2	1 - 3	18.259292	1.745391e-74	1.745391e-73
3	2 - 3	8.767200	1.831649e-18	7.326595e-18
4	1 - 4	44.922439	0.000000e+00	0.000000e+00
5	2 - 4	35.447886	3.126630e-275	5.627934e-274
6	3 - 4	26.705407	4.073124e-157	6.109687e-156
7	1 - 5	49.411876	0.000000e+00	0.000000e+00
8	2 - 5	39.937211	0.000000e+00	0.000000e+00
9	3 - 5	31.196062	1.204858e-213	2.048258e-212
10	4 - 5	4.481983	7.395252e-06	1.479050e-05
11	1 - 6	27.509319	1.358238e-166	2.173180e-165
12	2 - 6	18.035580	1.024159e-72	9.217434e-72
13	3 - 6	9.288314	1.567522e-20	7.837611e-20
14	4 - 6	-17.382469	1.120245e-67	8.961964e-67
15	5 - 6	-21.864270	5.686769e-106	6.824123e-105
16	1 - 7	23.144421	1.654551e-118	2.150917e-117
17	2 - 7	13.662962	1.689696e-42	1.182787e-41
18	3 - 7	4.907162	9.240374e-07	2.772112e-06
19	4 - 7	-21.777319	3.807113e-105	4.187824e-104
20	5 - 7	-26.262849	5.098321e-152	7.137649e-151
21	6 - 7	-4.380245	1.185461e-05	1.185461e-05

Table A8 9: Post-hoc Dunn's Test results, with pairwise comparisons for all sites in Sound Tooth # 2, statistically significant results in green (p<0.05), non-statistically significant results in pink (p>0.05)

SOUND TOOTH 3

	Comparison	Z	P.unadj	P.adj
1	1 - 2	5.795653	6.805598e-09	3.402799e-08
2	1 - 3	22.758549	1.180889e-114	1.653245e-113
3	2 - 3	17.006488	7.351517e-65	8.821820e-64
4	1 - 4	32.567147	1.197419e-232	2.275095e-231
5	2 - 4	26.848673	8.740997e-159	1.311150e-157
6	3 - 4	9.867008	5.786493e-23	4.629195e-22
7	1 - 5	3.362400	7.726817e-04	2.318045e-03
8	2 - 5	-2.438288	1.475700e-02	2.951400e-02
9	3 - 5	-19.441283	3.454205e-84	4.490466e-83
10	4 - 5	-29.277909	1.982232e-188	3.568018e-187
11	1 - 6	-4.844710	1.267968e-06	5.071871e-06
12	2 - 6	-10.691292	1.118023e-26	1.118023e-25
13	3 - 6	-27.767636	1.067302e-169	1.707683e-168
14	4 - 6	-37.634643	0.000000e+00	0.000000e+00
15	5 - 6	-8.240854	1.709858e-16	1.196901e-15
16	1 - 7	-6.510163	7.506933e-11	4.504160e-10
17	2 - 7	-12.302496	8.781820e-35	9.660001e-34
18	3 - 7	-29.207400	1.561925e-187	2.655273e-186
19	4 - 7	-38.973205	0.000000e+00	0.000000e+00
20	5 - 7	-9.876208	5.279293e-23	4.751364e-22
21	6 - 7	-1.724568	8.460529e-02	8.460529e-02

Table A8 10: Post-hoc Dunn's Test results, with pairwise comparisons for all sites in Sound Tooth # 3, statistically significant results in green (p<0.05), non-statistically significant results in pink (p>0.05)

SOUND TOOTH 4

	Comparison	Z	P.unadj	P.adj
1	1 - 2	4.215211	2.495450e-05	7.486351e-05
2	1 - 3	8.431727	3.406002e-17	2.384202e-16
3	2 - 3	4.251881	2.119824e-05	8.479294e-05
4	1 - 4	41.148039	0.000000e+00	0.000000e+00
5	2 - 4	37.265597	5.923430e-304	1.125452e-302
6	3 - 4	33.038045	2.310001e-239	3.927002e-238
7	1 - 5	30.878359	2.332355e-209	3.731768e-208
8	2 - 5	26.901251	2.123459e-159	2.972843e-158
9	3 - 5	22.664377	1.006619e-113	1.308605e-112
10	4 - 5	-10.386937	2.843381e-25	2.274705e-24
11	1 - 6	12.262708	1.436192e-34	1.436192e-33
12	2 - 6	8.123882	4.515033e-16	2.709020e-15
13	3 - 6	3.881293	1.039028e-04	2.078055e-04
14	4 - 6	-29.106837	2.941418e-186	4.412127e-185
15	5 - 6	-18.747227	2.039530e-78	2.447436e-77
16	1 - 7	-2.688623	7.174729e-03	7.174729e-03
17	2 - 7	-6.939884	3.924233e-12	1.962116e-11
18	3 - 7	-11.170250	5.702036e-29	5.131832e-28
19	4 - 7	-43.978239	0.000000e+00	0.000000e+00
20	5 - 7	-33.680984	1.097651e-248	1.975771e-247
21	6 - 7	-15.007826	6.525159e-51	7.177675e-50

Table A8 11: Post-hoc Dunn's Test results, with pairwise comparisons for all sites in Sound Tooth # 4, statistically significant results in green (p<0.05), non-statistically significant results in pink (p>0.05)

SOUND TOOTH 5

	Comparison	Z	P.unadj	P.adj
1	1 - 2	14.268221	3.452740e-46	3.107466e-45
2	1 - 3	26.778742	5.715229e-158	8.572843e-157
3	2 - 3	12.510521	6.539371e-36	4.577560e-35
4	1 - 4	44.029039	0.000000e+00	0.000000e+00
5	2 - 4	29.760818	1.256413e-194	2.135902e-193
6	3 - 4	17.250297	1.113265e-66	1.224592e-65
7	1 - 5	39.292633	0.000000e+00	0.000000e+00
8	2 - 5	25.024412	3.316515e-138	4.643120e-137
9	3 - 5	12.513891	6.267743e-36	5.014195e-35
10	4 - 5	-4.736406	2.175417e-06	4.350833e-06
11	1 - 6	31.814792	4.041829e-222	7.275293e-221
12	2 - 6	17.546571	6.318174e-69	7.581808e-68
13	3 - 6	5.036049	4.752381e-07	1.425714e-06
14	4 - 6	-12.214247	2.609052e-34	1.565431e-33
15	5 - 6	-7.477841	7.555336e-14	3.022134e-13
16	1 - 7	11.105760	1.176130e-28	5.880649e-28
17	2 - 7	-3.162461	1.564414e-03	1.564414e-03
18	3 - 7	-15.672983	2.314575e-55	2.314575e-54
19	4 - 7	-32.923279	1.020830e-237	1.939578e-236
20	5 - 7	-28.186873	8.470368e-175	1.355259e-173
21	6 - 7	-20.709032	2.871688e-95	3.733194e-94

Table A8 12: Post-hoc Dunn's Test results, with pairwise comparisons for all sites in Sound Tooth # 5, statistically significant results in green (p<0.05), non-statistically significant results in pink (p>0.05)

SOUND TOOTH 6

	Comparison	Z	P.unadj	P.adj
1	1 - 2	22.0150381	2.066969e-107	3.307150e-106
2	1 - 3	34.7029657	7.107183e-264	1.492508e-262
3	2 - 3	12.8473543	8.900237e-38	1.157031e-36
4	1 - 4	23.2886858	5.772889e-120	9.813912e-119
5	2 - 4	1.4916034	1.358031e-01	2.716063e-01
6	3 - 4	-11.2369795	2.684094e-29	2.684094e-28
7	1 - 5	10.8912771	1.268489e-27	7.610932e-27
8	2 - 5	-10.9252732	8.727736e-28	6.109415e-27
9	3 - 5	-23.5761161	6.776939e-123	1.219849e-121
10	4 - 5	-12.2960611	9.509971e-35	1.046097e-33
11	1 - 6	11.0352241	2.584066e-28	2.325659e-27
12	2 - 6	-11.0166942	3.175064e-28	2.540051e-27
13	3 - 6	-23.8050847	2.958436e-125	5.621028e-124
14	4 - 6	-12.4002255	2.605893e-35	3.127072e-34
15	5 - 6	0.0274298	9.781169e-01	9.781169e-01
16	1 - 7	2.3956401	1.659137e-02	4.977412e-02
17	2 - 7	-19.5354434	5.486737e-85	7.681431e-84
18	3 - 7	-32.1921692	2.271544e-227	4.543088e-226
19	4 - 7	-20.8289604	2.365396e-96	3.548094e-95
20	5 - 7	-8.4763090	2.324509e-17	9.298037e-17
21	6 - 7	-8.5938909	8.407282e-18	4.203641e-17

Table A8 13: Post-hoc Dunn's Test results, with pairwise comparisons for all sites in Sound Tooth # 6, statistically significant results in green (p<0.05), non-statistically significant results in pink (p>0.05)

SOUND TOOTH 7

	Comparison	Z	P.unadj	P.adj
1	1 - 2	23.098519	4.791394e-118	6.707951e-117
2	1 - 3	25.010479	4.702248e-138	7.523596e-137
3	2 - 3	2.123699	3.369534e-02	3.369534e-02
4	1 - 4	42.238347	0.000000e+00	0.000000e+00
5	2 - 4	19.385488	1.023290e-83	1.023290e-82
6	3 - 4	17.102543	1.420675e-65	1.136540e-64
7	1 - 5	47.243210	0.000000e+00	0.000000e+00
8	2 - 5	24.428198	8.581540e-132	1.287231e-130
9	3 - 5	22.100908	3.097769e-108	3.717323e-107
10	4 - 5	5.019719	5.174710e-07	1.552413e-06
11	1 - 6	19.668271	4.033013e-86	4.436314e-85
12	2 - 6	-3.434706	5.931965e-04	1.186393e-03
13	3 - 6	-5.526657	3.263900e-08	1.305560e-07
14	4 - 6	-22.786705	6.211766e-115	8.075296e-114
15	5 - 6	-27.824670	2.182173e-170	3.709695e-169
16	1 - 7	7.257552	3.941588e-13	1.970794e-12
17	2 - 7	-16.013187	1.033764e-57	7.236351e-57
18	3 - 7	-18.002744	1.854014e-72	1.668612e-71
19	4 - 7	-35.372559	4.512328e-274	8.122190e-273
20	5 - 7	-40.427361	0.000000e+00	0.000000e+00
21	6 - 7	-12.555477	3.709382e-36	2.225629e-35

Table A8 14: Post-hoc Dunn's Test results, with pairwise comparisons for all sites in Sound Tooth # 7, statistically significant results in green (p<0.05), non-statistically significant results in pink (p>0.05)

APPENDIX 9

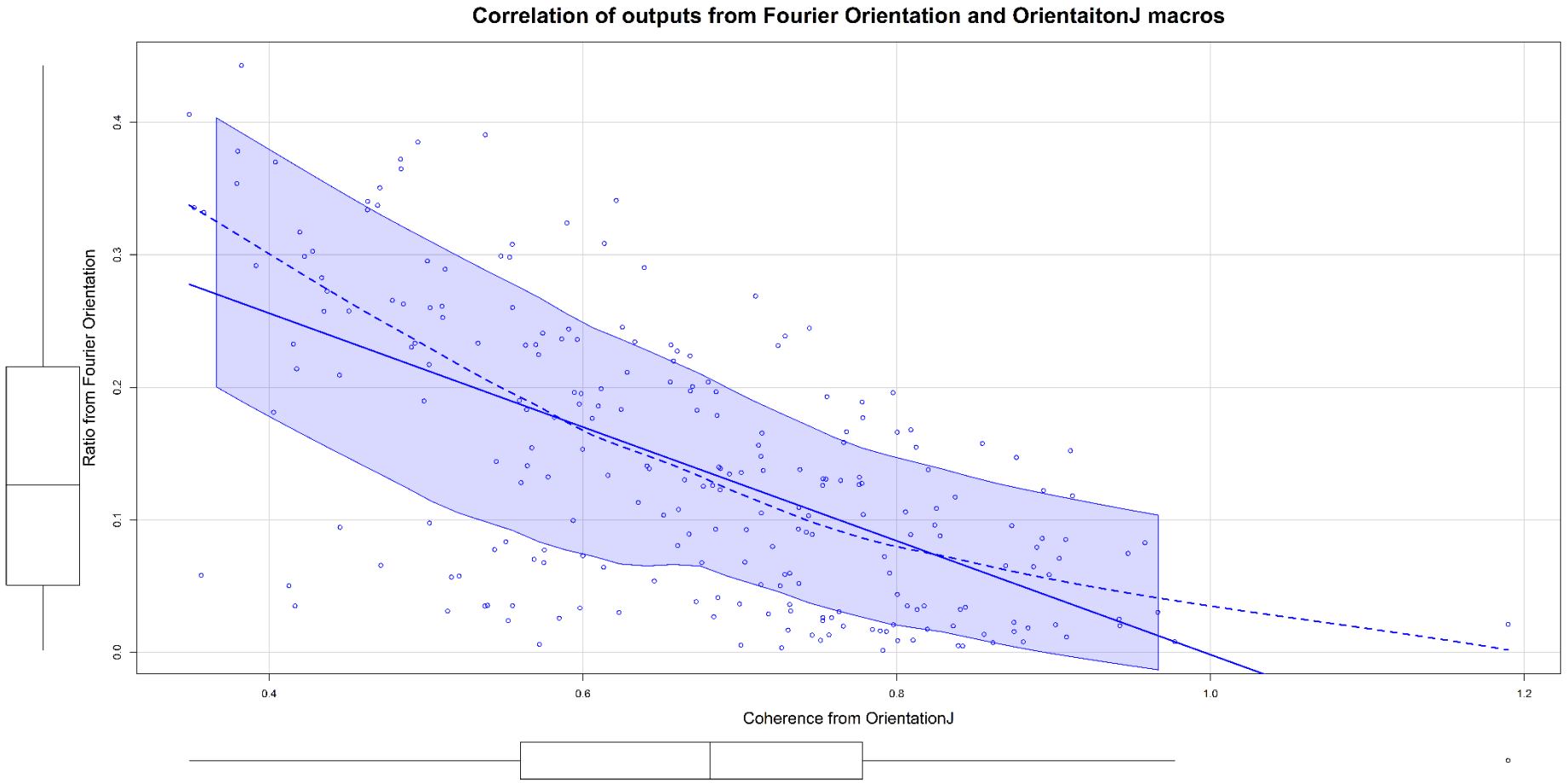

Figure A9 1: Correlation plot showing negative correlation between Coherence value and Ratio value for orientation of collagen fibres, including box plots to show data spread. Loess fit (shaded area and dotted line) and line of best fit (solid line) shown

APPENDIX 10

Gene Symbol	log2 Fold Change	padj	Ensembl ID	Gene Names	Found in Previous Studies?
CFI	-2.450037492	1.80E-09	ENSG00000205403	complement factor I	
TNR	-4.872211966	2.13E-09	ENSG00000116147	tenascin R	
C1QL1	-3.583572997	1.93E-07	ENSG00000131094	complement C1q like 1	
CLVS2	-4.058213145	5.05E-06	ENSG00000146352	clavesin 2	
OPRM1	-4.196044915	1.07E-05	ENSG00000112038	opioid receptor mu 1	
SLN	-5.070028951	1.99E-05	ENSG00000170290	sarcolipin	
TMEM59L	-2.105105894	2.32E-05	ENSG00000105696	transmembrane protein 59 like	
THBS4-AS1	-4.763692169	2.35E-05	ENSG00000249825	THBS4 antisense RNA 1	
CHAD	4.5939591	2.66E-05	ENSG00000136457	chondroadherin	
C4A	-2.264153308	2.69E-05	ENSG00000244731	complement C4A	Upregulated in carious teeth (158,246)
TMEM72	-4.59657122	5.07E-05	ENSG00000187783	transmembrane protein 72	
C4B	-2.255196596	0.000111	ENSG00000224389	complement C4B	
RGS5	-2.527735844	0.000247	ENSG00000143248	regulator of G protein signaling 5	
S100B	-1.78201907	0.000606	ENSG00000160307	S100 calcium binding protein B	
TRHDE-AS1	3.984901459	0.000736	ENSG00000236333	TRHDE antisense RNA 1	
PLA2G2A	5.050166911	0.001048	ENSG00000188257	phospholipase A2 group IIA	
ADAM33	2.44003219	0.00116	ENSG00000149451	ADAM metallopeptidase domain 33	
RNU1-2	-2.862398385	0.001379	ENSG00000207005	RNA, U1 small nuclear 2	
COLEC11	-2.275545447	0.002836	ENSG00000118004	collectin subfamily member 11	
NOX5	2.70160402	0.002836	ENSG00000290203	NADPH oxidase 5	
LAMA3	5.333560934	0.003716	ENSG00000053747	laminin subunit alpha 3	
GIPC3	-2.773504297	0.006261	ENSG00000179855	GIPC PDZ domain containing family member 3	
THBS4	-3.921479095	0.00667	ENSG00000113296	thrombospondin 4	Upregulated in carious teeth(158)
CRLF1	-3.103754871	0.006687	ENSG00000006016	cytokine receptor like factor 1	Upregulated in carious teeth(158)
PI15	-5.429187568	0.006765	ENSG00000137558	peptidase inhibitor 15	

PLPP4	-2.857632885	0.006765	ENSG00000203805	phospholipid phosphatase 4	
CMTM8	-2.773213916	0.007002	ENSG00000170293	CKLF like MARVEL transmembrane domain	
CXXC5	-1.231968361	0.007002	ENSG00000171604	CXXC finger protein 5	
GATA3-AS1	-6.011988181	0.007002	ENSG00000197308	GATA3 antisense RNA 1	
LOC105379548	-1.914952646	0.007002	ENSG00000288811	UNCATEGORISED	
MC1R	-1.342528541	0.007002	ENSG00000258839	melanocortin 1 receptor	
NPIPA8	-2.320561649	0.007235	ENSG00000214940	nuclear pore complex interacting protein family	
CHI3L2	-5.643372081	0.008191	ENSG00000064886	chitinase 3 like 2	Upregulated in carious teeth(158)
LOC124905321	-3.277714573	0.008191	ENSG00000275405	U1 Spliceosomal RNA	
HTR1A	4.127458255	0.009184	ENSG00000178394	5-hydroxytryptamine receptor 1A	
SLC35F1	-3.039733252	0.009471	ENSG00000196376	solute carrier family 35 member F1	
LOC110384692	-2.275225303	0.011754	ENSG00000244207	Complement C4A (Rodgers Blood Group)-Like	
PLEKHS1	-5.567803054	0.012027	ENSG00000148735	pleckstrin homology domain containing S1	
SHISAL2B	-4.807482697	0.012027	ENSG00000145642	shisa like 2B	
FERMT1	4.852572816	0.013539	ENSG00000101311	FERM domain containing kindlin 1	
KCNK12	-2.951057466	0.01356	ENSG00000184261	potassium two pore domain channel subfamily K	
PTPRN	-5.320199792	0.01356	ENSG00000054356	protein tyrosine phosphatase receptor type N	
RNU1-4	-2.636923257	0.01356	ENSG00000207389	RNA, U1 small nuclear 4	
OR2I1P	-7.035257982	0.013923	ENSG00000237988	olfactory receptor family 2 subfamily I member 1 pseudogene	
LPAR3	-3.350346305	0.016937	ENSG00000171517	lysophosphatidic acid receptor 3	
CHRDL2	-3.126449469	0.019123	ENSG00000054938	chordin like 2	
TMEM176B	-0.969344788	0.019696	ENSG00000106565	transmembrane protein 176B	
EGFLAM	-2.313436837	0.020295	ENSG00000164318	EGF like, fibronectin type III and laminin G	

WFDC2	-2.510161041	0.022025	ENSG00000101443	WAP four-disulfide core domain 2	
SPINK5	-2.768639356	0.022395	ENSG00000133710	serine peptidase inhibitor Kazal type 5	
SLC12A8	3.056542818	0.023022	ENSG00000221955	solute carrier family 12 member 8	
ADAMTS8	-3.963946621	0.024511	ENSG00000134917	ADAM metallopeptidase with thrombospondin	
SLC1A1	-2.066497127	0.024511	ENSG00000106688	solute carrier family 1 member 1	
OSMR	-1.605940213	0.028077	ENSG00000145623	oncostatin M receptor	
SAA1	-6.235967935	0.028624	ENSG00000173432	serum amyloid A1	
ALDH1A1	-1.860805276	0.028969	ENSG00000165092	aldehyde dehydrogenase 1 family member A1	
CILP2	3.028964816	0.028969	ENSG00000160161	cartilage intermediate layer protein 2	
KCTD16	-2.73059768	0.028969	ENSG00000183775	potassium channel tetramerization domain	
LINC01857	-6.027130523	0.028969	ENSG00000224137	long intergenic non-protein coding RNA 1857	
CPXM2	-1.751009089	0.029094	ENSG00000121898	carboxypeptidase X, M14 family member 2	
GFAP	-3.317259653	0.029094	ENSG00000131095	glial fibrillary acidic protein	
TMEM176A	-1.224026038	0.029094	ENSG00000002933	transmembrane protein 176A	
LOC105377896	-1.439270945	0.029214	UNCATEGORISED	UNCATEGORISED	
GALNT9	-3.641069347	0.029631	ENSG00000182870	polypeptide N-acetylgalactosaminyltransferase 9	
CXCL12	-1.433899538	0.029858	ENSG00000107562	C-X-C motif chemokine ligand 12	Upregulated in carious teeth(158), down regulated in odontoblast layer of carious teeth(246)
PROM1	-3.752096449	0.032026	ENSG00000007062	prominin 1	
SERPINA3	-3.543983711	0.033834	ENSG00000196136	serpin family A member 3	Upregulated in carious teeth(158,184)
SMAD1	-1.000386511	0.033834	ENSG00000170365	SMAD family member 1	
SV2B	-3.494288111	0.033834	ENSG00000185518	synaptic vesicle glycoprotein 2B	

2TBC1D27P	-7.232104558	0.033834	ENSG00000128438	TBC1 domain family member 27, pseudogene	
ASB3	-1.590336499	0.036021	ENSG00000115239	ankyrin repeat and SOCS box containing 3	
CPLX1	-1.56883595	0.037256	ENSG00000168993	complexin 1	
APOC1P1	-2.412448633	0.039047	ENSG00000291128	apolipoprotein C1 pseudogene 1	
GAR1	-1.025858333	0.039047	ENSG00000109534	GAR1 ribonucleoprotein	
MYH11	-1.396043827	0.039047	ENSG00000133392	myosin heavy chain 11	
MATN2	-1.162514612	0.043613	ENSG00000132561	matrilin 2	

Table A10 1: Differentially expressed genes. Shaded genes = 10 genes with greatest statistical difference between carious and sound teeth. Genes in bold = the 31 differentially expressed genes present in the re-run data when samples X18 and X15 are excluded.

APPENDIX 11

	baseMean	log2FoldChange	padj	Ensembl ID	Gene Name
HBA2	474234.6	5.170541	NA	ENSG00000188536	hemoglobin subunit alpha 2
CLU	293149	-0.04	0.999817	ENSG00000120885	Clusterin
NES	218676.4	0.132853	0.999817	ENSG00000132688	Nestin
ACTB	204104.6	0.507807	0.999817	ENSG00000075624	Actin Beta
CXCL14	181732.6	-0.95519	0.999817	ENSG00000145824	C-X-C motif chemokine ligand 14
HBB	177778	4.565491	NA	ENSG00000244734	hemoglobin subunit beta
COL1A1	172605.1	-0.03024	0.999817	ENSG00000108821	collagen type I alpha 1 chain
HBA1	172297.6	5.282846	NA	ENSG00000206172	hemoglobin subunit alpha 1
IGKC	158827	-0.18661	0.999817	ENSG00000211592	immunoglobulin kappa constant
COL1A2	137662	0.217236	0.999817	ENSG00000164692	collagen type I alpha 2 chain
RNR2	132334.7	0.963556	0.999817	UNCATEGORISED	RNA, Ribosomal 45S Cluster 2
COX1	126234.8	0.572191	0.999817	ENSG00000198804	Mitochondrially Encoded Cytochrome C Oxidase I
VIM	118235	0.147536	0.999817	ENSG00000026025	Vimentin
B2M	114206.9	0.200663	0.999817	ENSG00000166710	beta-2-microglobulin
FTL	113259.3	-0.06265	0.999817	ENSG00000087086	ferritin light chain
S100A9	108346.9	2.366164	0.999817	ENSG00000163220	S100 calcium binding protein A9
IGHG1	103274.6	0.100694	0.999817	ENSG00000211896	immunoglobulin heavy constant gamma 1
RPL13AP5	103051.2	-0.28671	0.999817	ENSG00000236552	ribosomal protein L13a pseudogene 5
ACTG1	100915.6	0.178383	0.999817	ENSG00000184009	actin gamma 1

EEF1A1	96676.4	-0.3757	0.999817	ENSG00000156508	eukaryotic translation elongation factor 1 alpha 1
SPARC	96138.23	-0.0587	0.999817	ENSG00000113140	secreted protein acidic and cysteine rich
HLA-B	80386.49	-0.16808	0.999817	ENSG00000234745	major histocompatibility complex, class I, B
IGHG2	79258.42	0.463851	0.999817	ENSG00000211893	immunoglobulin heavy constant gamma 2
ND4	77716.19	0.052654	0.999817	ENSG00000198886	Mitochondrially Encoded NADH:Ubiquinone Oxidoreductase Core Subunit 4
HLA-C	75927.82	0.929932	0.999817	ENSG00000204525	Major Histocompatibility Complex, Class I, C
COX3	71708.67	0.380734	0.999817	ENSG00000198938	Mitochondrially Encoded Cytochrome C Oxidase III
COX2	71612.78	0.477108	0.999817	ENSG00000198712	Mitochondrially Encoded Cytochrome C Oxidase II
CXCL8	66716.22	1.419352	0.999817	ENSG00000169429	C-X-C Motif Chemokine Ligand 8
ATP6	63502.74	0.508543	0.999817	ENSG00000198899	Mitochondrially Encoded ATP Synthase Membrane Subunit 6
ND2	62039.39	-0.70718	0.999817	ENSG00000198763	Mitochondrially Encoded NADH:Ubiquinone Oxidoreductase Core Subunit 2
GAPDH	61041.27	-0.07703	0.999817	ENSG00000111640	Glyceraldehyde-3-Phosphate Dehydrogenase
HLA-A	59733.2	0.028257	0.999817	ENSG00000206503	Major Histocompatibility Complex, Class I, A
FDCSP	59676	9.061527	NA	ENSG00000181617	Follicular Dendritic Cell Secreted Protein
TMSB10	59316.45	-0.2876	0.999817	ENSG00000034510	Thymosin Beta 10
TPT1	59285.66	0.111352	0.999817	ENSG00000133112	Tumor Protein, Translationally-Controlled 1
PTN	58219.49	0.269274	0.999817	ENSG00000105894	Pleiotrophin
IGFBP5	57472.14	0.554983	0.999817	ENSG00000115461	Insulin Like Growth Factor Binding Protein 5
AHNAK	54978.15	0.33749	0.999817	ENSG00000124942	AHNAK Nucleoprotein
DKK3	54649.93	0.406403	0.999817	ENSG00000050165	Dickkopf WNT Signaling Pathway Inhibitor 3
FTH1	53921.99	0.471558	0.999817	ENSG00000167996	Ferritin Heavy Chain 1

COL3A1	51662.94	0.143586	0.999817	ENSG00000168542	Collagen Type III Alpha 1 Chain
CYP1B1	51332.78	-0.21707	0.999817	ENSG00000138061	Cytochrome P450 Family 1 Subfamily B Member 1
MYL6	50977.83	-0.11382	0.999817	ENSG00000092841	Myosin Light Chain 6
TMSB4X	48370.34	-0.44015	0.999817	ENSG00000205542	Thymosin Beta 4 X-Linked
TF	48089.9	0.417972	0.999817	ENSG00000091513	Transferrin
IFITM3	47777.9	-0.79865	0.817226	ENSG00000142089	Interferon Induced Transmembrane Protein 3
RPL13	47593.3	-0.19502	0.999817	ENSG00000167526	Ribosomal Protein L13
ITM2B	46727.92	0.040229	0.999817	ENSG00000136156	Integral Membrane Protein 2B
TIMP1	46561.3	-1.82572	0.57421	ENSG00000102265	TIMP Metallopeptidase Inhibitor 1
RPS6	45715.34	-0.30782	0.999817	ENSG00000137154	Ribosomal Protein S6

Table A11 1: Top 50 genes with greatest abundance in sound and carious teeth combined. NB: where padj is 'NA', this has been highlighted as a potential outlier due to Cook's cut off in DESeq2.

APPENDIX 12

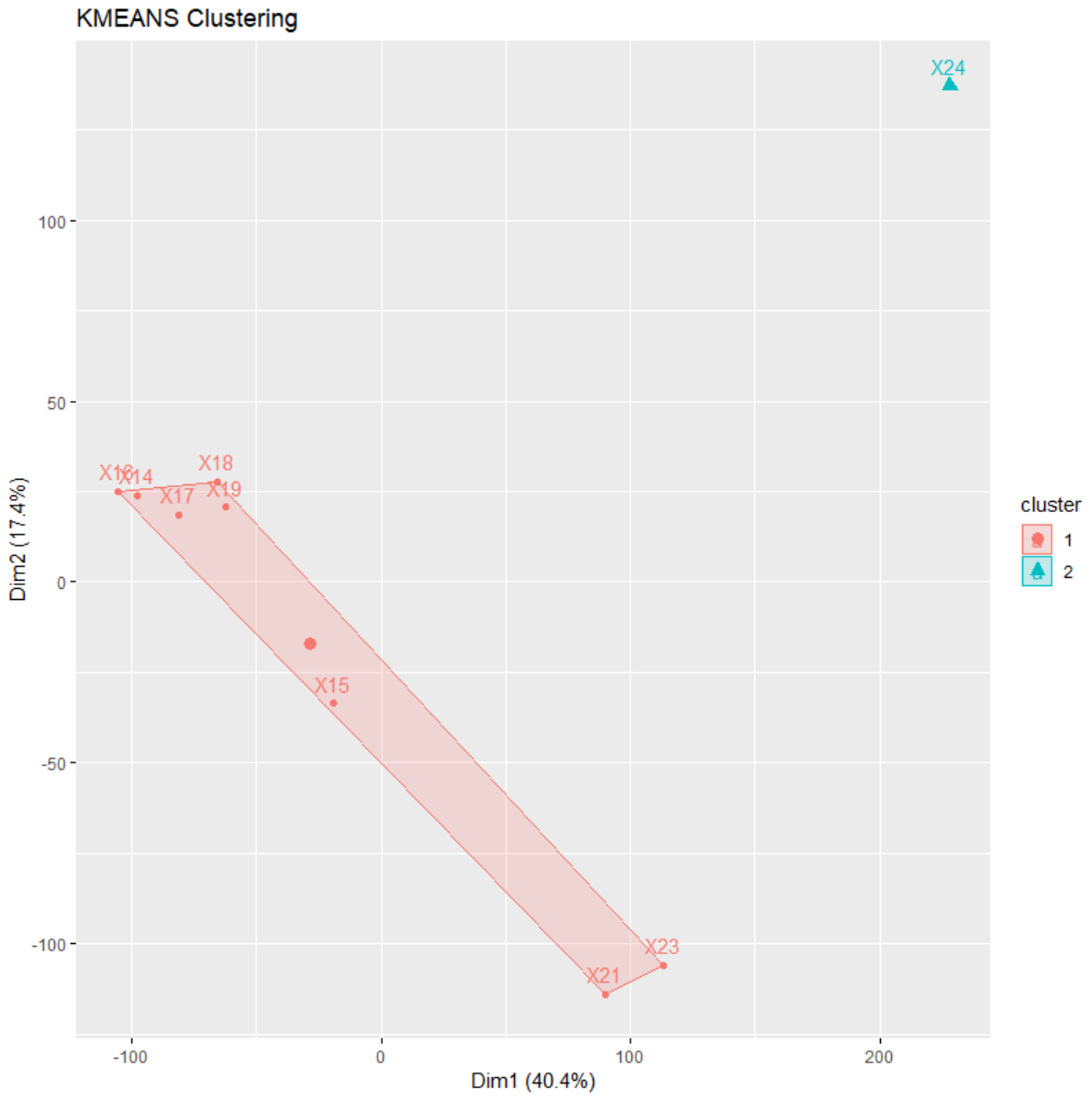

Figure A12 1: KMeans Cluster plot showing the two clusters identified and demonstrating X24 as a significant outlier.

APPENDIX 13

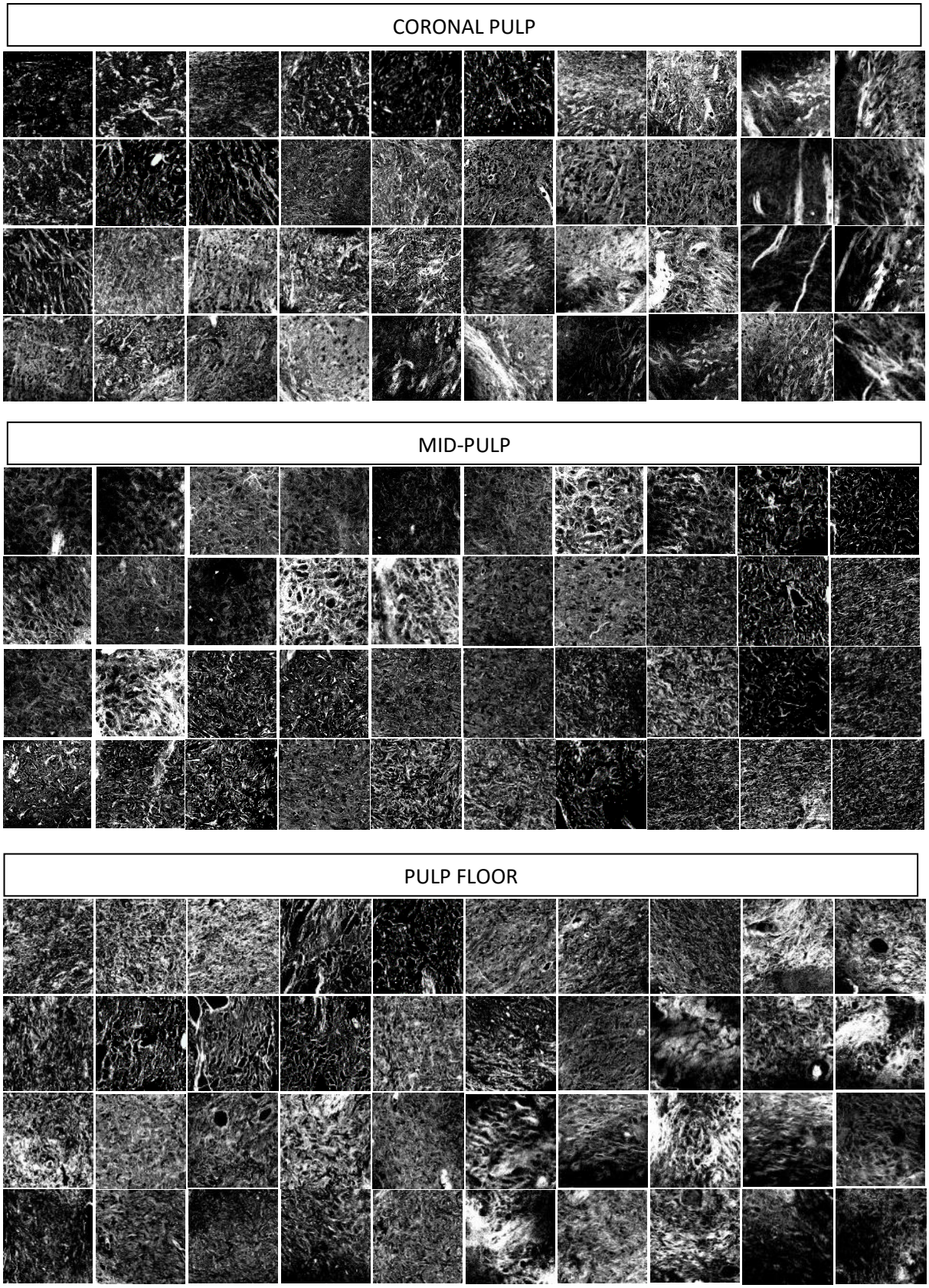

Figure A13 1: Comparison of grayscale images from the pulp floor, mid pulp and coronal pulp of sound teeth. Five images from each site across eight teeth.

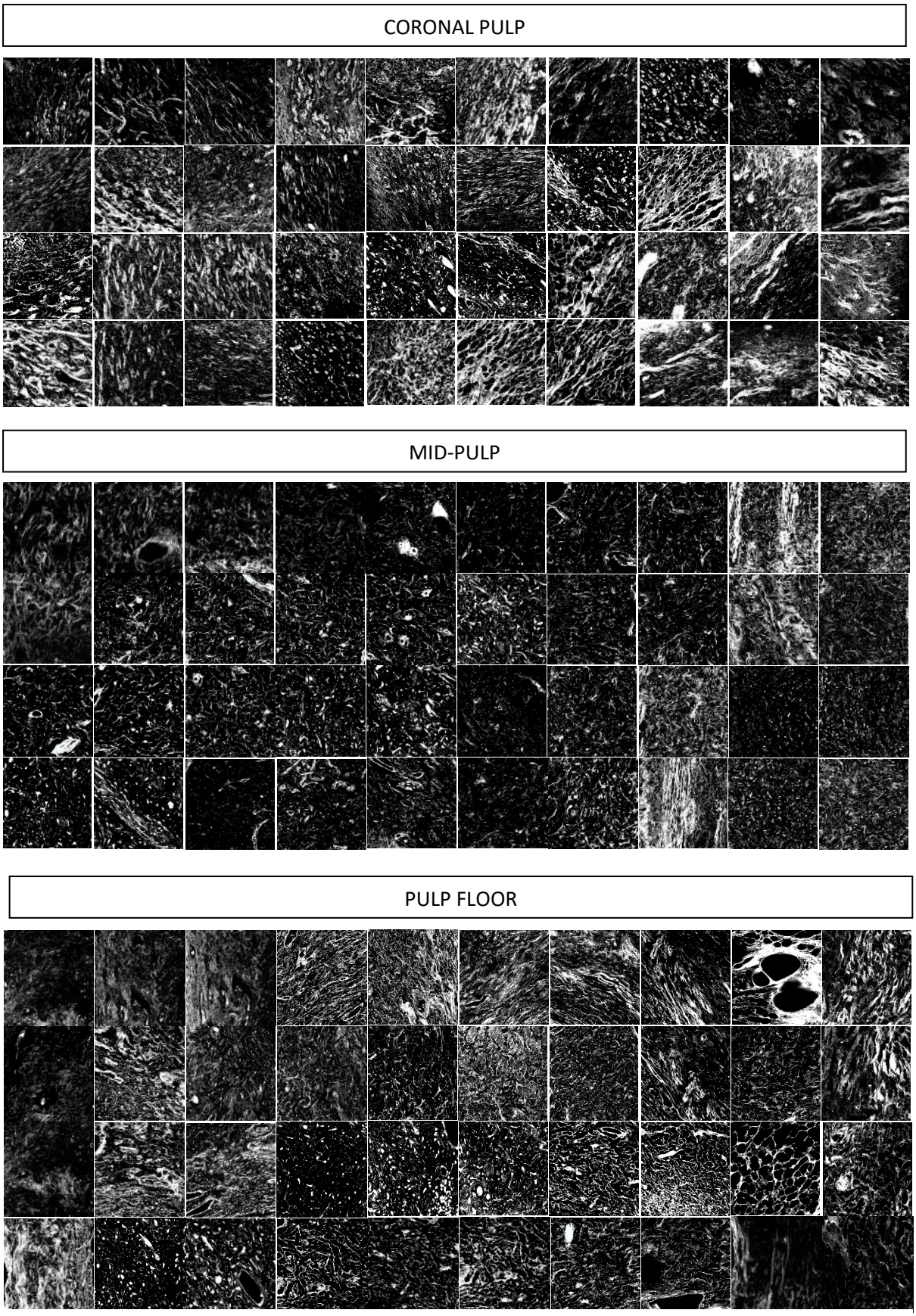

Figure A13 1: Comparison of grayscale images from the pulp floor, mid pulp and coronal pulp of carious teeth. Five images from each site across eight teeth.

APPENDIX 14

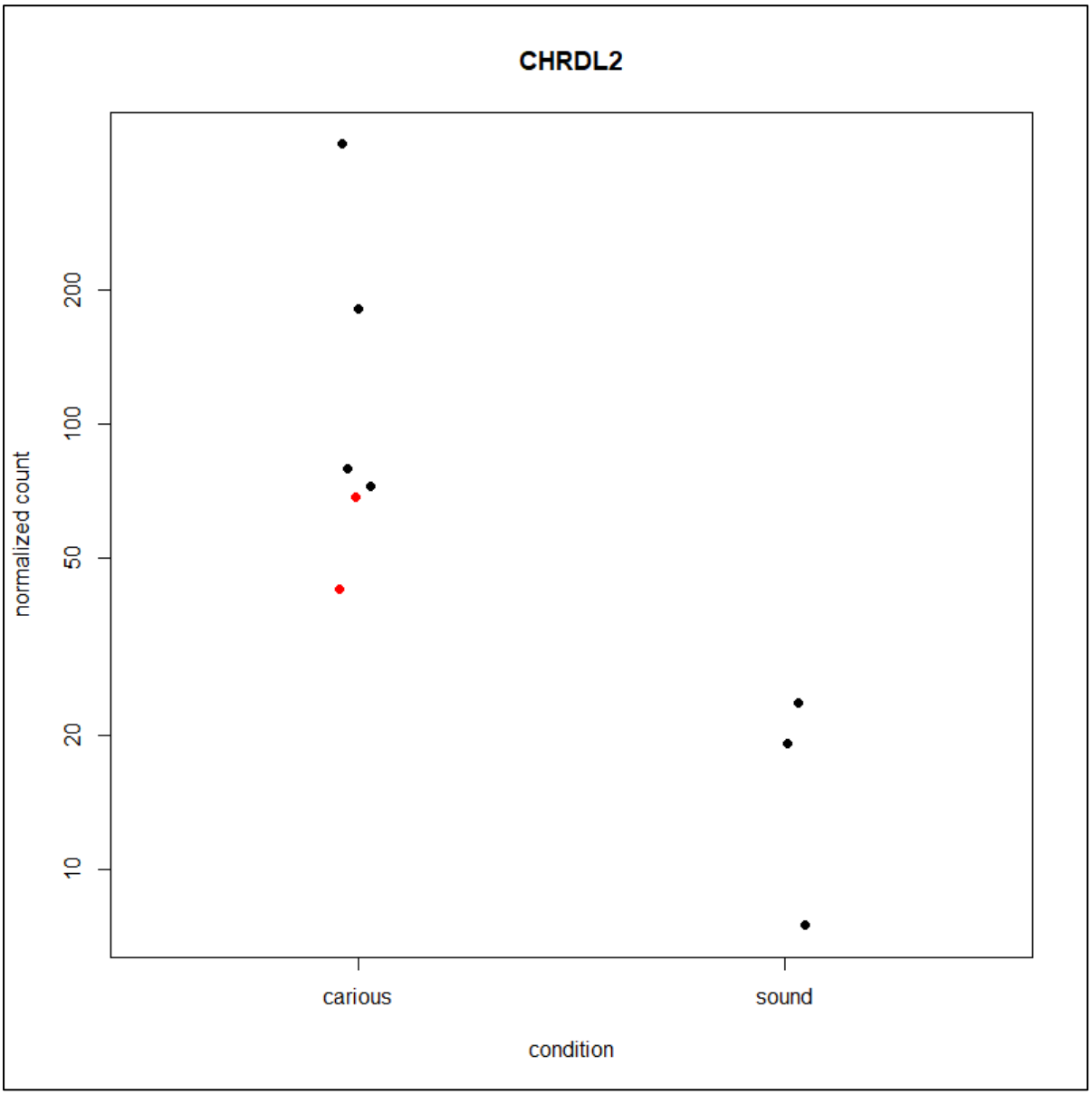

Figure A14 1 : Plot Counts plot CHRDL2, demonstrating X18 and X19 in red and showing how the inclusion of two samples from the same patient may skew the statistical outputs.

APPENDIX 15

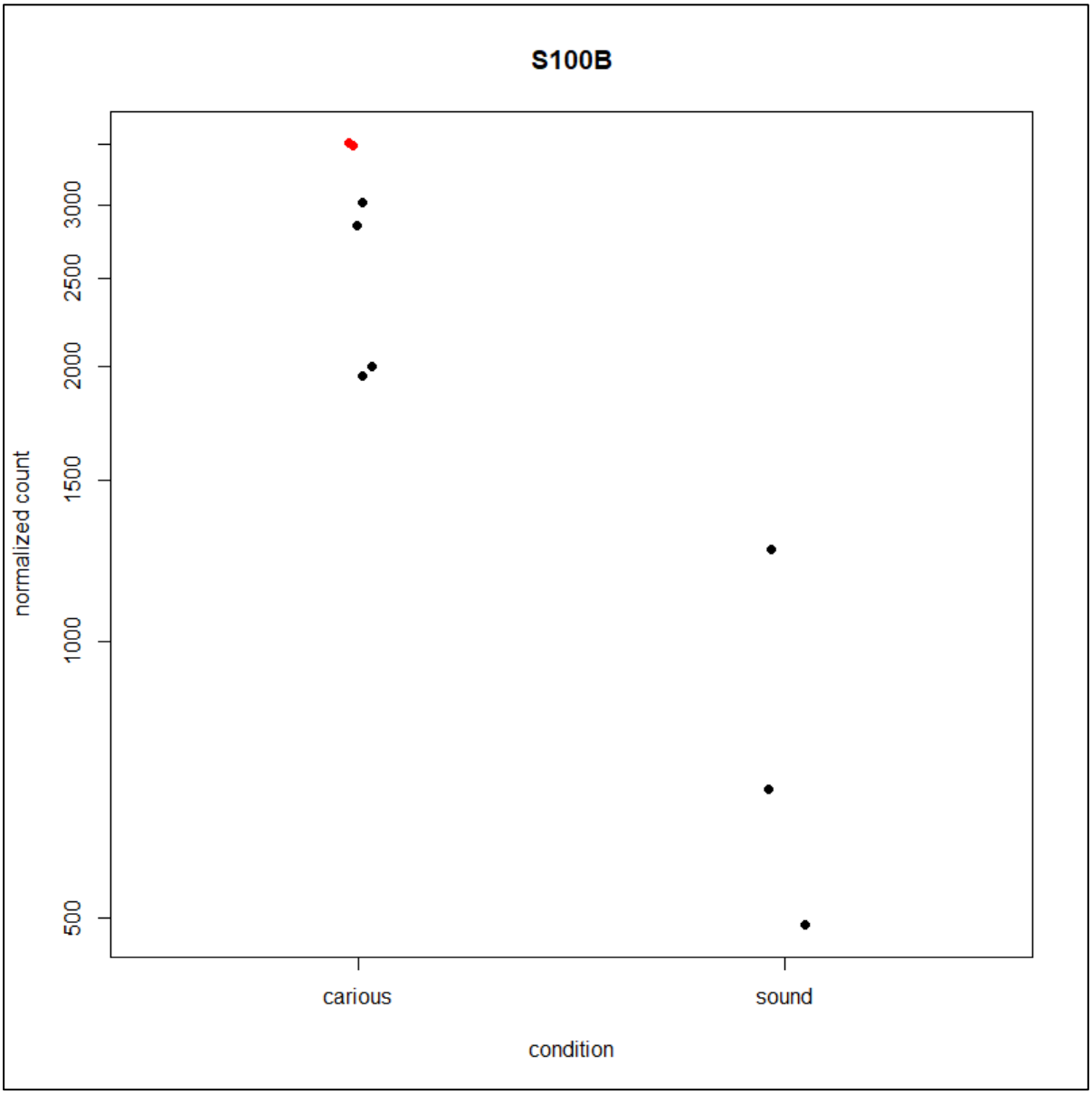

Figure A15 1 : Plot Counts plot S100B, demonstrating X18 and X19 in red and showing how the inclusion of two samples from the same patient may skew the statistical outputs.

APPENDIX 16

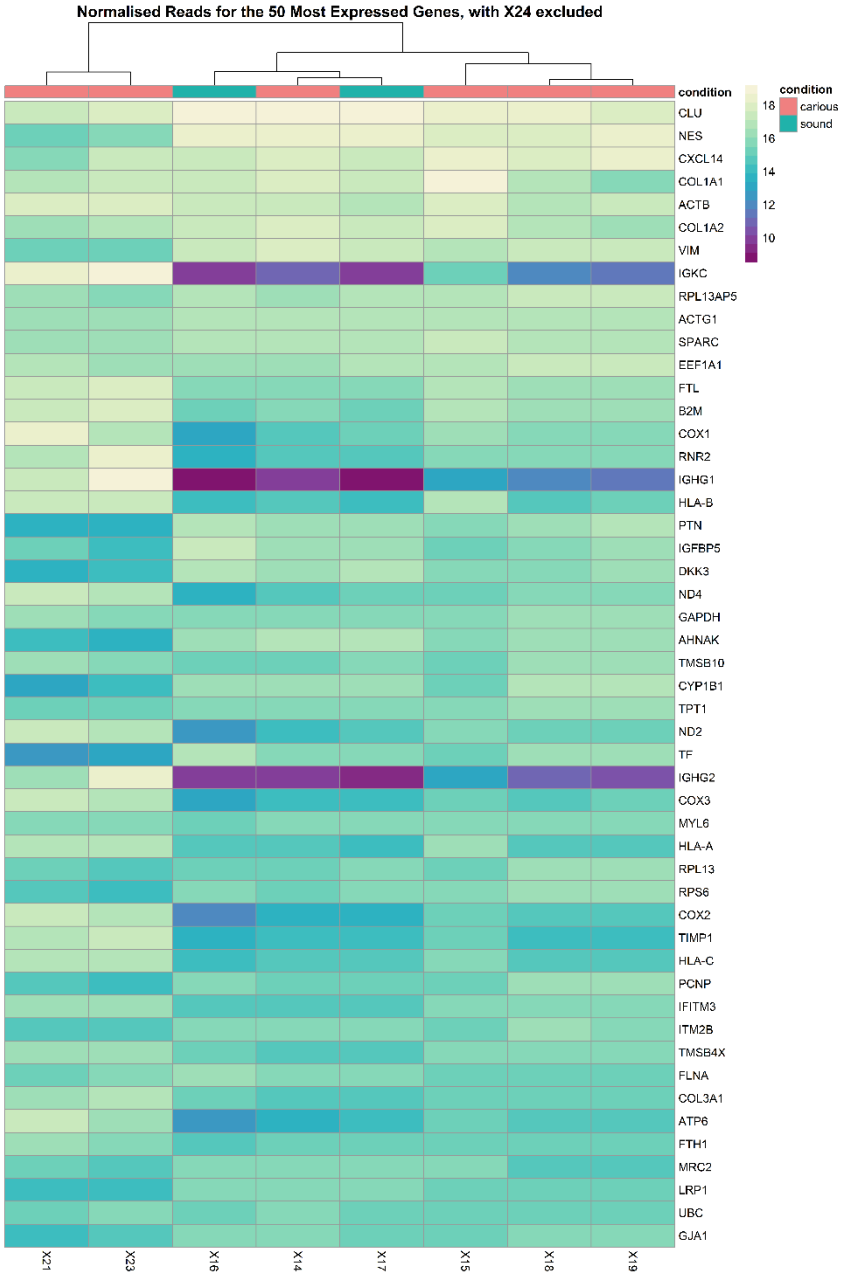

Figure A16 1: Heatmap of normalise reads for the 50 most abundant genes in carious and sound teeth, with X24 excluded from analysis

APPENDIX 17

DAY 4 LDH AND ALAMAR BLUE	5LPLL0.1	5LPLL0.01	5HPLL0.1	5HPLL0.01	5LPDL0.1	5LPDL0.01	7LPLL0.1	7LPLL0.01	7HPLL0.1	7HPLL0.01	7LPDL0.1	7LPDL0.01	9LPLL0.1	9LPLL0.01	9HPLL0.1	9HPLL0.01	9LPDL0.1	9LPDL0.01	
5LPLL0.1		1.000	1.000	1.000	1.000	1.000	1.000	1.000	1.000	0.100	1.000	1.000	1.000	1.000	1.000	1.000	1.000	0.574	ALAMAR BLUE
5LPLL0.01	0.441		1.000	1.000	1.000	1.000	1.000	1.000	1.000	1.000	1.000	1.000	1.000	1.000	0.022	1.000	1.000	1.000	
5HPLL0.1	1.000	1.000		1.000	1.000	1.000	1.000	1.000	0.415	1.000	1.000	1.000	1.000	1.000	1.000	1.000	1.000	1.000	
5HPLL0.01	0.222	0.320	1.000		1.000	1.000	1.000	1.000	0.841	1.000	1.000	1.000	1.000	1.000	0.024	1.000	1.000	1.000	
5LPDL0.1	1.000	1.000	1.000	1.000		1.000	0.610	0.105	0.056	1.000	0.106	0.100	0.134	1.000	1.000	1.000	1.000	0.123	
5LPDL0.01	1.000	1.000	1.000	1.000	1.000		1.000	1.000	1.000	1.000	1.000	1.000	1.000	1.000	0.025	1.000	1.000	1.000	
7LPLL0.1	0.102	1.000	1.000	1.000	1.000	1.000		1.000	1.000	1.000	1.000	1.000	1.000	1.000	0.008	1.000	1.000	1.000	
7LPLL0.01	0.281	1.000	1.000	1.000	1.000	0.233	1.000		1.000	1.000	1.000	1.000	1.000	1.000	0.005	1.000	1.000	1.000	
7HPLL0.1	1.000	0.292	1.000	0.035	0.19	0.120	0.350	0.266		1.000	1.000	1.000	1.000	1.000	0.010	1.000	1.000	1.000	
7HPLL0.01	1.000	1.000	1.000	1.000	1.000	1.000	1.000	1.000	1.000		1.000	1.000	1.000	0.926	0.001	1.000	1.000	1.000	
7LPDL0.1	<0.001	<0.001	0.007	0.056	0.005	0.012	0.004	<0.001	<0.001	0.003		1.000	1.000	1.000	0.011	1.000	1.000	1.000	
7LPDL0.01	<0.001	0.001	<0.001	<0.001	<0.001	<0.001	<0.001	<0.001	<0.001	<0.001	0.006		1.000	1.000	0.004	1.000	1.000	1.000	
9LPLL0.1	0.093	1.000	1.000	0.658	1.000	0.134	1.000	1.000	0.274	1.000	<0.001	<0.001		1.000	0.008	1.000	1.000	0.386	
9LPLL0.01	0.522	1.000	1.000	1.000	1.000	1.000	0.210	1.000	0.101	1.000	0.002	<0.001	1.000		0.033	1.000	1.000	1.000	
9HPLL0.1	1.000	1.000	1.000	0.171	1.000	0.059	0.510	0.592	1.000	1.000	<0.001	<0.001	0.473	0.265		0.001	1.000	0.004	
9HPLL0.01	1.000	1.000	1.000	1.000	1.000	1.000	1.000	1.000	0.242	1.000	0.006	<0.001	1.000	1.000	1.000		1.000	1.000	
9LPDL0.1	0.008	0.124	0.75	1.000	0.052	0.059	0.182	1.000	<0.001	0.823	1.000	<0.001	0.210	0.140	0.004	1.000		1.000	
9LPDL0.01	<0.001	0.007	1.000	1.000	0.039	1.000	0.032	0.006	<0.001	0.029	1.000	<0.001	0.001	0.015	<0.001	1.000	1.000		
	LDH																		

Table A17 1: Tukey's test comparing the results of each gel for LDH and AB assays at Day 4. Pink = p value >0.05, Green = p value <0.05

DAY 8 LDH AND ALAMAR BLUE	5LPLL0.1	5LPLL0.01	5HPLL0.1	5HPLL0.01	5LPDL0.1	5LPDL0.01	7LPLL0.1	7LPLL0.01	7HPLL0.1	7HPLL0.01	7LPDL0.1	7LPDL0.01	9PLL0.1	9LPLL0.01	9HPLL0.1	9HPLL0.01	9LPDL0.1	9LPDL0.01	
5LPLL0.1		1.000	0.174	1.000	1.000	0.829	0.061	1.000	0.009	0.067	0.004	0.62	1.000	1.000	0.142	0.008	1.000	0.392	ALAMAR BLUE
5LPLL0.01	<0.001		0.005	0.768	1.000	0.037	0.014	0.024	<0.001	1.000	1.000	1.000	1.000	1.000	0.032	<0.001	1.000	0.035	
5HPLL0.1	1.000	0.133		1.000	1.000	1.000	1.000	1.000	1.000	1.000	0.001	1.000	0.148	1.000	1.000	1.000	1.000	1.000	
5HPLL0.01	<0.001	<0.001	0.094		1.000	1.000	1.000	1.000	1.000	1.000	0.098	1.000	1.000	1.000	1.000	1.000	1.000	1.000	
5LPDL0.1	1.000	1.000	0.184	<0.001		1.000	1.000	1.000	0.012	1.000	0.011	1.000	1.000	1.000	1.000	0.011	1.000	1.000	
5LPDL0.01	<0.001	0.343	<0.001	0.981	1.000		1.000	1.000	1.000	1.000	0.155	1.000	0.737	1.000	1.000	1.000	1.000	1.000	
7LPLL0.1	<0.001	<0.001	<0.001	<0.001	<0.001	<0.001		1.000	1.000	1.000	0.510	1.000	0.618	1.000	1.000	1.000	1.000	1.000	
7LPLL0.01	1.000	1.000	0.049	<0.001	1.000	1.00	<0.001		0.027	1.000	1.000	1.000	1.000	1.000	1.000	0.024	1.000	1.000	
7HPLL0.1	0.072	<0.001	0.039	<0.001	<0.001	<0.001	1.000	<0.001		1.000	<0.001	0.447	0.022	0.044	1.000	1.000	0.020	1.000	
7HPLL0.01	1.000	1.000	0.058	<0.001	1.000	0.011	<0.001	1.000	<0.001		0.007	1.000	1.000	1.000	1.000	1.000	1.000	1.000	
7LPDL0.1	0.001	1.000	<0.001	0.039	1.000	0.128	<0.001	1.000	<0.001	0.120		0.155	1.000	0.156	0.010	<0.001	0.185	0.011	
7LPDL0.01	1.000	0.192	1.000	<0.001	0.679	<0.001	<0.001	1.000	0.033	1.000	<0.001		0.152	1.000	1.000	0.133	1.000	1.000	
9LPLL0.1	1.000	1.000	1.000	<0.001	1.000	1.000	<0.001	1.000	<0.001	1.000	1.000	1.000		1.000	0.132	0.020	1.000	1.000	
9LPLL0.01	<0.001	0.252	<0.001	1.000	0.246	1.000	<0.001	1.000	<0.001	0.036	1.000	<0.001	1.000		1.000	0.034	1.000	1.000	
9HPLL0.1	1.000	0.155	1.000	1.000	0.329	<0.001	0.001	0.017	0.111	0.286	<0.001	1.000	0.032	<0.001		0.884	1.000	1.000	
9HPLL0.01	<0.001	<0.001	<0.001	<0.001	<0.001	<0.001	1.000	<0.001	0.666	<0.001	<0.001	<0.001	<0.001	<0.001	<0.001		0.018	0.059	
9LPDL0.1	<0.001	<0.001	<0.001	1.000	0.003	1.000	<0.001	0.013	<0.001	<0.001	1.000	<0.001	0.007	1.000	<0.001	1.000		1.000	
9LPDL0.01	<0.001	<0.001	<0.001	<0.001	<0.001	<0.001	0.006	<0.001	<0.001	<0.001	<0.001	<0.001	<0.001	<0.001	<0.001	1.000	<0.001		
	LDH																		

Table A17 2: Tukey's test comparing the results of each gel for LDH and AB assays at Day 8. Pink = p value >0.05, Green = p value <0.05

DAY 12 LDH AND ALAMAR BLUE	5LPLL0.1	5LPLL0.01	5HPLL0.1	5HPLL0.01	5LPDL0.1	5LPDL0.01	7LPLL0.1	7LPLL0.01	7HPLL0.1	7HPLL0.01	7LPDL0.1	7LPDL0.01	9PLL0.1	9LPLL0.01	9HPLL0.1	9HPLL0.01	9LPDL0.1	9LPDL0.01	
5LPLL0.1		1.000	1.000	0.282	<0.001	1.000	1.000	1.000	0.236	0.038	1.000	1.000	0.526	1.000	0.237	0.035	0.001	1.000	ALAMAR BLUE
5LPLL0.01	1.000		1.000	0.811	<0.001	1.000	0.043	1.000	1.000	0.461	0.013	1.000	1.000	1.000	0.603	0.461	<0.001	1.000	
5HPLL0.1	0.038	1.000		1.000	<0.001	1.000	0.001	0.015	1.000	1.000	<0.001	0.025	1.000	1.000	1.000	0.580	<0.001	0.073	
5HPLL0.01	0.281	1.000	1.000		<0.001	0.135	<0.001	<0.001	1.000	0.815	<0.001	<0.001	0.433	0.033	1.000	0.145	<0.001	0.012	
5LPDL0.1	<0.001	1.000	1.000	1.000		<0.001	1.000	1.000	<0.001	<0.001	1.000	1.000	<0.001	0.002	<0.001	<0.001	0.006	<0.001	
5LPDL0.01	<0.001	1.000	0.049	1.000	1.000		0.003	0.040	0.102	0.074	<0.001	1.000	1.000	1.000	0.111	0.050	1.000	0.603	
7LPLL0.1	<0.001	1.000	1.000	1.000	1.000	1.000		1.000	<0.001	<0.001	1.000	1.000	<0.001	1.000	<0.001	<0.001	1.000	1.000	
7LPLL0.01	<0.001	1.000	1.000	1.000	1.000	1.000	1.000		<0.001	<0.001	1.000	1.000	<0.001	1.000	<0.001	<0.001	1.000	1.000	
7HPLL0.1	0.212	1.000	1.000	0.598	1.000	0.012	1.000	0.851		0.116	<0.001	<0.001	0.401	0.028	1.000	0.184	<0.001	0.005	
7HPLL0.01	<0.001	1.000	0.168	1.000	1.000	1.000	1.000	1.000	0.131		<0.001	<0.001	0.112	0.015	0.432	1.000	<0.001	0.009	
7LPDL0.1	<0.001	1.000	1.000	1.000	1.000	1.000	1.000	1.000	0.516	1.000		1.000	<0.001	0.322	<0.001	<0.001	1.000	1.000	
7LPDL0.01	0.002	1.000	1.000	1.000	1.000	1.000	1.000	1.000	1.000	1.000	1.000		<0.001	1.000	<0.001	<0.001	1.000	1.000	
9LPLL0.1	<0.001	1.000	0.300	1.000	1.000	1.000	1.000	1.000	0.017	1.000	1.000	1.000		0.294	0.432	0.135	<0.001	0.430	
9LPLL0.01	<0.001	1.000	<0.001	1.000	1.000	1.000	1.000	0.019	<0.001	1.000	1.000	0.002	0.093		0.024	0.014	0.004	1.000	
9HPLL0.1	0.498	1.000	1.000	1.000	1.000	0.019	1.000	1.000	1.000	0.120	0.531	1.000	0.027	<0.001		0.129	<0.001	0.005	
9HPLL0.01	0.063	0.046	0.113	0.282	0.026	0.004	1.000	1.000	1.000	0.907	0.202	1.000	0.007	<0.001	1.000		<0.001	0.061	
9LPDL0.1	<0.001	1.000	<0.001	0.369	1.000	0.143	0.047	0.004	<0.001	0.014	0.338	<0.001	0.131	0.210	<0.001	<0.001		0.012	
9LPDL0.01	0.114	1.000	1.000	1.000	0.655	0.019	1.000	1.000	1.000	1.000	1.000	1.000	0.026	<0.001	1.000	1.000	<0.001		
	LDH																		

Table A17 3: Tukey's test comparing the results of each gel for LDH and AB assays at Day 12. Pink = p value >0.05, Green = p value <0.05

DAY 16 LDH AND ALAMAR BLUE	5LPLL0.1	5LPLL0.01	5HPLL0.1	5HPLL0.01	5LPDL0.1	5LPDL0.01	7LPLL0.1	7LPLL0.01	7HPLL0.1	7HPLL0.01	7LPDL0.1	7LPDL0.01	9LPLL0.1	9LPLL0.01	9HPLL0.1	9HPLL0.01	9LPDL0.1	9LPDL0.01	
5LPLL0.1		1.000	1.000	0.002	1.000	<0.001	1.000	1.000	<0.001	0.001	0.005	<0.001	1.000	0.266	<0.001	1.000	<0.001	<0.001	ALAMAR BLUE
5LPLL0.01	1.000		1.000	0.006	1.000	0.001	1.000	1.000	<0.001	0.002	0.015	<0.001	1.000	1.000	<0.001	1.000	<0.001	<0.001	
5HPLL0.1	<0.001	<0.001		1.000	1.000	1.000	1.000	1.000	0.001	1.000	1.000	1.000	1.000	1.000	1.000	1.000	0.024	<0.001	
5HPLL0.01	1.000	0.121	0.002		1.000	1.000	0.176	1.000	1.000	1.000	1.000	1.000	1.000	1.000	1.000	1.000	1.000	1.000	
5LPDL0.1	1.000	1.000	0.001	1.000		0.038	1.000	1.000	<0.001	1.000	1.000	0.004	1.000	1.000	0.022	1.000	0.001	<0.001	
5LPDL0.01	1.000	1.000	<0.001	1.000	1.000		0.013	1.000	1.000	1.000	1.000	1.000	1.000	1.000	0.250	1.000	1.000	1.000	
7LPLL0.1	0.002	<0.001	1.000	0.031	0.018	<0.001		1.000	<0.001	0.045	1.000	0.001	1.000	1.000	0.007	0.999	<0.001	<0.001	
7LPLL0.01	1.000	1.000	<0.001	1.000	1.000	1.000	<0.001		0.003	0.401	1.000	1.000	1.000	1.000	1.000	1.000	0.062	0.002	
7HPLL0.1	<0.001	<0.001	1.000	0.005	0.003	<0.001	1.000	<0.001		0.673	1.000	1.000	0.001	0.004	1.000	0.001	1.000	0.138	
7HPLL0.01	0.035	<0.001	1.000	1.000	0.172	0.001	1.000	0.009	1.000		1.000	1.000	1.000	0.065	1.000	1.000	1.000	1.000	
7LPDL0.1	1.000	1.000	0.007	1.000	1.000	0.089	0.130	1.000	0.017	1.000		1.000	1.000	1.000	1.000	1.000	1.000	1.000	
7LPDL0.01	1.000	1.000	<0.001	0.026	0.044	1.000	<0.001	1.000	<0.001	<0.001	0.008		1.000	1.000	0.747	0.999	1.000	1.000	
9LPLL0.1	0.014	0.064	0.998	0.210	0.303	<0.001	1.000	0.003	0.436	1.000	0.171	<0.001		1.000	0.188	1.000	0.043	0.001	
9LPLL0.01	0.118	1.000	<0.001	0.007	0.012	1.000	<0.001	0.133	<0.001	<0.001	0.002	1.000	<0.001		0.705	1.000	0.205	0.002	
9HPLL0.1	0.001	<0.001	1.000	0.009	0.005	<0.001	1.000	<0.001	1.000	1.000	0.029	<0.001	1.000	<0.001		1.000	1.000	1.000	
9HPLL0.01	0.001	<0.001	1.000	0.019	0.011	<0.001	1.000	<0.001	1.000	1.000	0.056	<0.001	1.000	<0.001	1.000		0.029	<0.001	
9LPDL0.1	1.000	<0.001	0.002	1.000	1.000	1.000	0.030	1.000	0.005	1.000	1.000	0.027	0.190	0.007	0.009	0.018		1.000	
9LPDL0.01	<0.001	<0.001	1.000	0.005	0.003	<0.001	1.000	<0.001	1.000	1.000	0.018	<0.001	1.000	<0.001	1.000	1.000	0.005		
	LDH																		

Table A17 4: Tukey's test comparing the results of each gel for LDH and AB assays at Day 16. Pink = p value >0.05, Green = p value <0.05

DAY 20 LDH AND ALAMAR BLUE	5LPLL0.1	5LPLL0.01	5HPLL0.1	5HPLL0.01	5LPDL0.1	5LPDL0.01	7LPLL0.1	7LPLL0.01	7HPLL0.1	7HPLL0.01	7LPDL0.1	7LPDL0.01	9LPLL0.1	9LPLL0.01	9HPLL0.1	9HPLL0.01	9LPDL0.1	9LPDL0.01	
5LPLL0.1		1.000	1.000	0.787	1.000	1.000	1.000	1.000	0.018	1.000	1.000	0.005	1.000	0.022	1.000	1.000	1.000	0.026	ALAMAR BLUE
5LPLL0.01	0.002		1.000	0.329	1.000	1.000	1.000	1.000	0.005	0.103	1.000	0.001	0.047	0.007	0.015	0.684	1.000	0.008	
5HPLL0.1	1.000	0.001		1.000	1.000	1.000	0.025	0.025	1.000	1.000	0.155	1.000	1.000	1.000	1.000	1.000	0.600	1.000	
5HPLL0.01	<0.001	0.004	0.141		0.114	1.000	<0.001	<0.001	0.786	0.065	0.001	1.000	1.000	1.000	0.179	0.145	<0.001	1.000	
5LPDL0.1	1.000	0.003	1.000	0.001		1.000	1.000	1.000	0.193	1.000	1.000	0.070	1.000	0.554	1.000	0.684	1.000	1.000	
5LPDL0.01	1.000	0.027	1.000	0.009	1.000		1.000	0.321	0.777	1.000	1.000	1.000	1.000	1.000	1.000	1.000	1.000	1.000	
7LPLL0.1	1.000	<0.001	0.520	<0.001	0.439	0.051		1.000	0.002	0.310	1.000	<0.001	0.006	0.003	1.000	0.464	1.000	0.003	
7LPLL0.01	0.177	1.000	1.000	1.000	1.000	1.000	0.011		0.002	0.248	1.000	<0.001	0.006	0.002	1.000	0.171	1.000	0.003	
7HPLL0.1	0.174	<0.001	0.047	<0.001	0.102	0.008	1.000	<0.001		1.000	0.148	1.000	1.000	1.000	1.000	1.000	0.545	1.000	
7HPLL0.01	1.000	<0.001	1.000	<0.001	1.000	1.000	1.000	1.000	1.000		1.000	1.000	1.000	1.000	1.000	1.000	1.000	1.000	
7LPDL0.1	1.000	<0.001	1.000	<0.001	1.000	1.000	1.000	0.171	1.000	1.000		0.117	1.000	0.672	1.000	1.000	1.000	1.000	
7LPDL0.01	0.240	<0.001	0.461	<0.001	0.237	0.400	1.000	0.001	1.000	1.000	1.000		1.000	1.000	0.643	0.111	0.033	1.000	
9LPLL0.1	1.000	0.017	1.000	0.004	1.000	1.000	1.000	1.000	0.018	1.000	1.000	1.000		1.000	1.000	1.000	1.000	1.000	
9LPLL0.01	0.060	1.000	0.370	1.000	1.000	0.687	0.002	1.000	<0.001	1.000	0.177	<0.001	1.000		0.753	1.000	1.000	1.000	
9HPLL0.1	0.109	<0.001	0.760	<0.001	1.000	0.305	1.000	0.096	1.000	1.000	1.000	0.488	1.000	0.009		1.000	1.000	1.000	
9HPLL0.01	1.000	<0.001	0.470	<0.001	0.724	0.060	1.000	0.014	1.000	1.000	1.000	1.000	1.000	0.002	1.000		1.000	1.000	
9LPDL0.1	1.000	0.302	0.220	1.000	1.000	0.155	0.054	1.000	<0.001	1.000	0.015	<0.001	1.000	1.000	<0.001	<0.001		1.000	
9LPDL0.01	1.000	<0.001	1.000	<0.001	1.000	0.208	1.000	0.003	1.000	1.000	1.000	1.000	1.000	<0.001	1.000	1.000	<0.001		
	LDH																		

Table A17 5: Tukey's test comparing the results of each gel for LDH and AB assays at Day 20. Pink = p value >0.05, Green = p value <0.05

APPENDIX 18

5% AGAROSE/HPLL0.01						
DAY	4	8	12	16	20	ALAMAR BLUE
4		0.056	1.000	0.154	0.313	
8	<0.001		0.010	1.000	0.005	
12	1.000	0.001		0.019	0.284	
16	<0.001	<0.001	1.000		<0.001	
20	0.48	0.405	1.000	1.000		
LDH						

Table A18 1: Statistical test results (Post-hoc Tukey's test after repeated measures anova) assessing for statistical differences for 5HPLL0.01 gels, comparing different time points. LDH and AB assay results. Pink = p value>0.05, green = p value <0.05

5% AGAROSE/HPLL0.1						
DAY	4	8	12	16	20	ALAMAR BLUE
4		1.000	0.114	0.06	0.453	
8	0.002		0.137	0.138	0.01	
12	0.503	<0.001		0.249	0.091	
16	0.242	<0.001	0.361		<0.001	
20	0.095	<0.001	1.000	1.000		
LDH						

Table A18 2: Statistical test results (Post-hoc Tukey's test after repeated measures anova) assessing for statistical differences for 5HPLL0.1 gels, comparing different time points. LDH and AB assay results s. Pink = p value>0.05, green = p value <0.05

7% AGAROSE/HPLL0.1						
DAY	4	8	12	16	20	ALAMAR BLUE
4		0.305	1.000	0.022	1.000	
8	<0.001		0.046	1.000	0.060	
12	0.064	<0.001		0.004	1.000	
16	0.829	0.016	1.000		0.253	
20	0.0053	<0.001	<0.001	0.048		
LDH						

Table A18 3: Statistical test results (Post-hoc Tukey's test after repeated measures anova) assessing for statistical differences for 7HPLL0.1 gels, comparing different time points. LDH and AB assay results. Pink = p value>0.05, green = p value <0.05

7% AGAROSE/HPLL0.01						
DAY	4	8	12	16	20	ALAMAR BLUE
4		<0.001	0.124	<0.001	0.009	
8	0.009		<0.001	1.000	0.281	
12	1.000	0.002		<0.001	<0.001	
16	1.000	0.009	1.000		0.025	
20	1.000	0.002	0.219	1.000		
LDH						

Table A18 4: Statistical test results (Post-hoc Tukey's test after repeated measures anova) assessing for statistical differences for 7HPLL0.01 gels, comparing different time points. LDH and AB assay results. Pink = p value>0.05, green = p value <0.05

9% AGAROSE/HPLL0.01						
DAY	4	8	12	16	20	ALAMAR BLUE
4		0.173	1.000	0.007	0.287	
8	1.000		<0.001	0.060	0.837	
12	1.000	0.088		<0.001	<0.001	
16	1.000	1.000	1.000		0.003	
20	0.007	<0.001	0.047	0.213		
LDH						

Table A18 5: Statistical test results (Post-hoc Tukey's test after repeated measures anova) assessing for statistical differences for 9HPLL0.01 gels, comparing different time points LDH and AB assay results. Pink = p value>0.05, green = p value <0.05

9% AGAROSE/HPLL0.1						
DAY	4	8	12	16	20	ALAMAR BLUE
4		1.000	1.000	1.000	1.000	
8	<0.001		0.003	1.000	0.325	
12	0.107	<0.001		<0.001	0.024	
16	0.593	<0.001	1.000		0.455	
20	0.018	<0.001	<0.001	<0.001		
LDH						

Table A18 6: Statistical test results (Post-hoc Tukey's test after repeated measures anova) assessing for statistical differences for 9HPLL0.1 gels, comparing different time points. LDH and AB assay results. Pink = p value>0.05, green = p value <0.05

9% AGAROSE/LPLL0.1						
DAY	4	8	12	16	20	ALAMAR BLUE
4		<0.001	0.014	<0.001	1.000	
8	<0.001		1.000	1.000	<0.001	
12	<0.001	0.566		0.937	0.076	
16	1.000	<0.001	<0.001		0.003	
20	1.000	0.054	0.079	1.000		
LDH						

Table A18 7: Statistical test results (Post-hoc Tukey's test after repeated measures anova) assessing for statistical differences for 9LPLL0.1 gels, comparing different time points. LDH and AB assay results. Pink = p value>0.05, green = p value <0.05

9% AGAROSE/LPLL0.01						
DAY	4	8	12	16	20	ALAMAR BLUE
4		0.024	0.006	0.056	1.000	
8	<0.001		0.01	1.000	<0.001	
12	0.005	1.000		0.009	0.006	
16	<0.001	0.447	1.000		0.002	
20	0.234	0.001	0.019	0.001		
LDH						

Table A18 8: Statistical test results (Post-hoc Tukey's test after repeated measures anova) assessing for statistical differences for 9LPLL0.01 gels, comparing different time points. LDH and AB assay results. Pink = p value>0.05, green = p value <0.05

7% AGAROSE/LPLL0.01						
DAY	4	8	12	16	20	ALAMAR BLUE
4		0.035	0.005	0.001	0.017	
8	<0.001		0.010	1.000	1.000	
12	0.524	0.005		0.009	0.008	
16	0.002	1.000	0.003		0.244	
20	1.000	0.006	1.000	0.013		
LDH						

Table A18 9: Statistical test results (Post-hoc Tukey's test after repeated measures anova) assessing for statistical differences for 7LPLL0.01 gels, comparing different time points. LDH and AB assay results. Pink = p value>0.05, green = p value <0.05

7% AGAROSE/LPLL0.1						
DAY	4	8	12	16	20	ALAMAR BLUE
4		0.110	0.043	0.003	0.022	
8	1.000		0.050	0.054	1.000	
12	1.000	1.000		0.057	0.052	
16	0.425	0.109	1.000		0.043	
20	<0.001	0.002	0.024	<0.001		
LDH						

Table A18 10: Statistical test results (Post-hoc Tukey's test after repeated measures anova) assessing for statistical differences for 7LPLL0.1 gels, comparing different time points. LDH and AB assay results. Pink = p value>0.05, green = p value <0.05

5% AGAROSE/LPLL0.1						
DAY	4	8	12	16	20	ALAMAR BLUE
4		0.168	0.023	0.040	1.000	
8	<0.001		0.030	1.000	1.000	
12	<0.001	<0.001		0.038	0.027	
16	<0.001	1.000	<0.001		0.802	
20	1.000	0.004	0.018	<0.001		
LDH						

Table A18 11: Statistical test results (Post-hoc Tukey's test after repeated measures anova) assessing for statistical differences for 5LPLL0.1 gels, comparing different time points. LDH and AB assay results. Pink = p value>0.05, green = p value <0.05

5% AGAROSE/LPLL0.01						
DAY	4	8	12	16	20	ALAMAR BLUE
4		0.045	0.059	0.059	0.220	
8	<0.001		0.131	1.000	0.060	
12	0.888	1.000		0.116	0.082	
16	<0.001	1.000	1.000		0.248	
20	0.407	1.000	1.000	1.000		
LDH						

Table A18 12: Statistical test results (Post-hoc Tukey's test after repeated measures anova) assessing for statistical differences for 5LPLL0.01 gels, comparing different time points. LDH and AB assay results. Pink = p value>0.05, green = p value <0.05

5% AGAROSE/LPDL0.01						
DAY	4	8	12	16	20	ALAMAR BLUE
4		0.130	0.007	0.867	1.000	
8	<0.001		0.016	1.000	0.072	
12	0.018	0.009		0.011	0.009	
16	0.007	1.000	1.000		0.664	
20	0.262	<0.001	0.004	0.004		
LDH						

Table A18 13: Statistical test results (Post-hoc Tukey's test after repeated measures anova) assessing for statistical differences for 5LPDL0.01 gels, comparing different time points. LDH and AB assay results. Pink = p value>0.05, green = p value <0.05

5% AGAROSE/LPDL0.1						
DAY	4	8	12	16	20	ALAMAR BLUE
4		1.000	<0.001	0.504	0.072	
8	<0.001		<0.001	1.000	0.575	
12	0.725	1.000		<0.001	<0.001	
16	<0.001	0.570	1.000		0.002	
20	1.000	<0.001	0.454	1.000		
LDH						

Table A18 14: Statistical test results (Post-hoc Tukey's test after repeated measures anova) assessing for statistical differences for 5LPDL0.1 gels, comparing different time points. LDH and AB assay results. Pink = p value>0.05, green = p value <0.05

7% AGAROSE/LPDL0.1						
DAY	4	8	12	16	20	ALAMAR BLUE
4		<0.001	<0.001	0.054	0.156	
8	0.002		0.001	0.03	0.002	
12	0.398	0.01		<0.001	<0.001	
16	0.908	0.007	1.000		1.00	
20	<0.001	<0.001	0.009	0.015		
LDH						

Table A18 15: Statistical test results (Post-hoc Tukey's test after repeated measures anova) assessing for statistical differences for 7LPDL0.1 gels, comparing different time points. LDH and AB assay results. Pink = p value>0.05, green = p value <0.05

7% AGAROSE/LPDL0.01						
DAY	4	8	12	16	20	ALAMAR BLUE
4		<0.001	0.005	0.035	1.000	
8	0.721		0.008	0.07	<0.001	
12	0.027	0.066		0.006	0.006	
16	1.000	1.000	0.059		0.002	
20	0.007	<0.001	0.006	0.002		
LDH						

Table A18 16: Statistical test results (Post-hoc Tukey's test after repeated measures anova) assessing for statistical differences for 7LPDL0.01 gels, comparing different time points. LDH and AB assay results. Pink = p value>0.05, green = p value <0.05

9% AGAROSE/LPDL0.01						
DAY	4	8	12	16	20	ALAMAR BLUE
4		0.007	<0.001	0.041	1.000	
8	0.02		0.002	0.092	0.049	
12	0.05	1.000		0.001	<0.001	
16	0.004	1.000	1.000		1.000	
20	0.005	0.042	0.066	0.228		
LDH						

Table A18 17: Statistical test results (Post-hoc Tukey's test after repeated measures anova) assessing for statistical differences for 9LPDL0.01 gels, comparing different time points. LDH and AB assay results. Pink = p value>0.05, green = p value <0.05

9% AGAROSE/LPDL0.1						
DAY	4	8	12	16	20	ALAMAR BLUE
4		0.177	<0.001	1.000	1.000	
8	0.002		<0.001	0.007	0.05	
12	<0.001	0.112		<0.001	<0.001	
16	1.000	<0.001	0.001		1.000	
20	1.000	0.002	0.003	0.881		
LDH						

Table A18 18: Statistical test results (Post-hoc Tukey's test after repeated measures anova) assessing for statistical differences for 9LPDL0.1 gels, comparing different time LDH and AB assay results. Pink = p value>0.05, green = p value <0.05

APPENDIX 19

WEEK 1 AREA AND LIVE/DEAD	5LPLL0.1	5LPLL0.01	5HPLL0.1	5HPLL0.01	5LPDL0.1	5LPDL0.01	7LPLL0.1	7LPLL0.01	7HPLL0.1	7HPLL0.01	7LPDL0.1	7LPDL0.01	9PLL0.1	9LPLL0.01	9HPLL0.1	9HPLL0.01	9LPDL0.1	9LPDL0.01	
5LPLL0.1		1.000	1.000	1.000	1.000	1.000	1.000	1.000	1.000	1.000	1.000	1.000	1.000	1.000	1.000	1.000	1.000	1.000	
5LPLL0.01	1.000		0.132	1.000	0.719	1.000	1.000	1.000	1.000	1.000	1.000	1.000	1.000	1.000	1.000	1.000	1.000	1.000	
5HPLL0.1	0.220	0.176		1.000	1.000	1.000	1.000	1.000	1.000	1.000	1.000	1.000	1.000	1.000	0.719	1.000	1.000	1.000	
5HPLL0.01	1.000	1.000	0.217		1.000	1.000	1.000	1.000	1.000	1.000	1.000	1.000	1.000	1.000	1.000	1.000	1.000	1.000	
5LPDL0.1	1.000	1.000	0.936	1.000		1.000	1.000	1.000	1.000	1.000	1.000	1.000	1.000	1.000	1.000	1.000	1.000	1.000	
5LPDL0.01	1.000	1.000	0.109	1.000	1.000		1.000	1.000	1.000	1.000	1.000	1.000	1.000	1.000	1.000	1.000	1.000	1.000	
7LPLL0.1	0.506	1.000	1.000	0.500	1.000	1.000		1.000	1.000	1.000	1.000	1.000	1.000	1.000	1.000	1.000	1.000	1.000	
7LPLL0.01	1.000	1.000	0.132	1.000	1.000	1.000	1.000		1.000	1.000	1.000	1.000	1.000	1.000	1.000	1.000	1.000	1.000	
7HPLL0.1	1.000	1.000	1.000	1.000	1.000	1.000	1.000	1.000		1.000	1.000	1.000	1.000	1.000	1.000	1.000	1.000	1.000	
7HPLL0.01	1.000	1.000	1.000	1.000	1.000	1.000	1.000	1.000	0.379		1.000	1.000	1.000	1.000	1.000	1.000	1.000	1.000	
7LPDL0.1	1.000	0.164	1.000	0.574	1.000	0.104	1.000	0.139	1.000	1.000		1.000	1.000	1.000	1.000	1.000	1.000	1.000	
7LPDL0.01	1.000	1.000	0.112	1.000	0.571	1.000	1.000	1.000	1.000	1.000	0.167		1.000	1.000	1.000	1.000	1.000	1.000	
9LPLL0.1	1.000	0.702	0.947	0.777	1.000	0.095	1.000	0.052	0.526	1.000	1.000	0.061		1.000	1.000	1.000	1.000	1.000	
9LPLL0.01	1.000	1.000	0.044	0.756	0.174	1.000	1.000	1.000	1.000	1.000	0.116	0.496	1.000		1.000	1.000	1.000	1.000	
9HPLL0.1	0.133	1.000	0.001	0.052	1.000	0.052	1.000	0.063	1.000	1.000	1.000	0.119	1.000	0.072		1.000	1.000	1.000	
9HPLL0.01	0.629	0.191	0.006	1.000	1.000	0.513	1.000	0.711	0.972	1.000	1.000	0.696	1.000	0.401	1.000		1.000	1.000	
9LPDL0.1	1.000	1.000	1.000	1.000	1.000	1.000	1.000	1.000	1.000	1.000	1.000	1.000	1.000	1.000	1.000	1.000		1.000	
9LPDL0.01	1.000	1.000	1.000	1.000	1.000	1.000	1.000	1.000	1.000	1.000	1.000	1.000	1.000	1.000	1.000	1.000	1.000		
	AREA																		LIVE/DEAD

Table A19 1: Tukey's test comparing the results of each gel for live/dead confocal and confocal area stained at Week 1. Pink = p value >0.05, Green = p value <0.05

WEEK 2 AREA AND LIVE/DEAD	5LPLL0.1	5LPLL0.01	5HPLL0.1	5HPLL0.01	5LPDL0.1	5LPDL0.01	7LPLL0.1	7LPLL0.01	7HPLL0.1	7HPLL0.01	7LPDL0.1	7LPDL0.01	9PLL0.1	9LPLL0.01	9HPLL0.1	9HPLL0.01	9LPDL0.1	9LPDL0.01	
5LPLL0.1		1.000	1.000	1.000	1.000	1.000	1.000	1.000	1.000	1.000	1.000	1.000	1.000	1.000	1.000	1.000	0.006	1.000	LIVE/DEAD
5LPLL0.01	1.000		1.000	1.000	1.000	1.000	1.000	1.000	1.000	1.000	1.000	1.000	1.000	1.000	1.000	1.000	0.001	1.000	
5HPLL0.1	1.000	1.000		1.000	1.000	1.000	1.000	1.000	1.000	1.000	1.000	1.000	1.000	1.000	1.000	1.000	0.048	1.000	
5HPLL0.01	1.000	1.000	1.000		1.000	1.000	1.000	1.000	1.000	1.000	1.000	1.000	1.000	1.000	1.000	1.000	<0.001	1.000	
5LPDL0.1	1.000	1.000	1.000	0.422		1.000	1.000	1.000	1.000	1.000	1.000	1.000	1.000	1.000	1.000	1.000	0.274	1.000	
5LPDL0.01	1.000	1.000	0.915	1.000	0.104		1.000	1.000	1.000	1.000	1.000	1.000	1.000	1.000	1.000	1.000	<0.001	1.000	
7LPLL0.1	1.000	1.000	0.857	1.000	1.000	1.000		1.000	1.000	1.000	1.000	1.000	1.000	1.000	1.000	1.000	0.181	1.000	
7LPLL0.01	0.28	1.000	0.167	1.000	0.026	1.000	1.000		1.000	1.000	1.000	1.000	1.000	1.000	1.000	1.000	<0.001	1.000	
7HPLL0.1	1.000	1.000	1.000	1.000	1.000	1.000	1.000	0.838		1.000	1.000	1.000	1.000	1.000	1.000	1.000	<0.001	1.000	
7HPLL0.01	0.072	1.000	0.092	1.000	0.042	1.000	1.000	1.000	1.000		1.000	1.000	1.000	1.000	1.000	1.000	<0.001	1.000	
7LPDL0.1	1.000	1.000	1.000	1.000	1.000	1.000	1.000	0.355	0.214	0.152		1.000	1.000	1.000	1.000	1.000	0.033	1.000	
7LPDL0.01	1.000	1.000	0.171	1.000	0.179	1.000	1.000	1.000	1.000	1.000	0.219		1.000	1.000	1.000	1.000	<0.001	1.000	
9LPLL0.1	1.000	1.000	1.000	1.000	1.000	1.000	1.000	1.000	1.000	0.433	1.000	1.000		1.000	1.000	1.000	<0.001	1.000	
9LPLL0.01	1.000	1.000	1.000	1.000	1.000	1.000	1.000	1.000	1.000	1.000	1.000	1.000	1.000		1.000	1.000	<0.001	1.000	
9HPLL0.1	1.000	1.000	1.000	0.073	1.000	0.595	0.693	0.194	1.000	0.06	0.985	1.000	1.000	1.000		1.000	<0.001	1.000	
9HPLL0.01	1.000	1.000	1.000	1.000	1.000	1.000	1.000	1.000	1.000	1.000	1.000	1.000	1.000	1.000	1.000		0.003	1.000	
9LPDL0.1	1.000	1.000	1.000	1.000	1.000	1.000	1.000	1.000	1.000	1.000	1.000	1.000	1.000	1.000	1.000	1.000		<0.001	
9LPDL0.01	1.000	1.000	1.000	1.000	1.000	1.000	1.000	1.000	1.000	1.000	1.000	1.000	1.000	1.000	1.000	1.000	1.000		
	AREA																		

Table A19 2: Tukey's test comparing the results of each gel for live/dead confocal and confocal area stained at Week 2. Pink = p value >0.05, Green = p value <0.05

WEEK 3 AREA AND LIVE/DEAD	5LPLL0.1	5LPLL0.01	5HPLL0.1	5HPLL0.01	5LPDL0.1	5LPDL0.01	7LPLL0.1	7LPLL0.01	7HPLL0.1	7HPLL0.01	7LPDL0.1	7LPDL0.01	9PLL0.1	9LPLL0.01	9HPLL0.1	9HPLL0.01	9LPDL0.1	9LPDL0.01	
5LPLL0.1		1.000	1.000	1.000	1.000	1.000	0.569	1.000	1.000	1.000	1.000	1.000	1.000	1.000	1.000	1.000	1.000	1.000	
5LPLL0.01	0.022		0.143	1.000	1.000	1.000	1.000	1.000	1.000	1.000	1.000	1.000	1.000	1.000	1.000	1.000	1.000	1.000	
5HPLL0.1	1.000	0.349		0.808	1.000	1.000	0.623	1.000	1.000	1.000	1.000	1.000	1.000	0.099	1.000	1.000	1.000	0.404	
5HPLL0.01	1.000	1.000	1.000		1.000	1.000	1.000	1.000	1.000	1.000	1.000	1.000	1.000	1.000	1.000	1.000	1.000	1.000	
5LPDL0.1	1.000	<0.001	1.000	0.810		1.000	1.000	1.000	1.000	1.000	1.000	1.000	1.000	1.000	1.000	1.000	1.000	1.000	
5LPDL0.01	0.025	1.000	0.535	1.000	0.002		1.000	1.000	1.000	1.000	1.000	1.000	1.000	1.000	1.000	1.000	1.000	1.000	
7LPLL0.1	1.000	1.000	1.000	1.000	0.310	1.000		1.000	0.252	0.021	0.023	1.000	1.000	1.000	1.000	1.000	1.000	1.000	
7LPLL0.01	0.002	1.000	0.083	1.000	0.001	1.000	1.000		1.000	0.021	1.000	1.000	1.000	1.000	1.000	1.000	1.000	1.000	
7HPLL0.1	0.868	0.035	1.000	0.424	0.022	0.076	0.662	0.049		1.000	1.000	1.000	1.000	0.739	1.000	1.000	1.000	0.638	
7HPLL0.01	1.000	0.308	1.000	0.315	0.777	0.488	1.000	0.506	1.000		1.000	1.000	1.000	0.037	1.000	1.000	1.000	0.046	
7LPDL0.1	<0.001	1.000	<0.001	<0.001	1.000	<0.001	<0.001	<0.001	1.000	0.018		1.000	1.000	0.0400	1.000	1.000	1.000	0.049	
7LPDL0.01	1.000	1.000	1.000	1.000	0.237	1.000	1.000	1.000	1.000	1.000	0.002		1.000	1.000	1.000	1.000	1.000	1.000	
9LPLL0.1	1.000	1.000	1.000	1.000	0.014	0.41	0.629	0.128	0.356	1.000	<0.001	1.000		1.000	1.000	1.000	1.000	1.000	
9LPLL0.01	0.061	1.000	0.701	1.000	0.002	1.000	0.091	1.000	1.000	0.557	<0.001	1.000	0.641		1.000	1.000	1.000	1.000	
9HPLL0.1	1.000	0.041	1.000	0.234	1.000	1.000	0.093	0.079	1.000	1.000	0.012	1.000	0.421	0.112		1.000	1.000	1.000	
9HPLL0.01	1.000	0.881	1.000	0.242	0.033	0.907	1.000	1.000	0.054	1.000	<0.001	1.000	1.000	1.000	1.000		1.000	1.000	
9LPDL0.1	0.243	0.009	0.523	0.044	0.22	0.017	0.098	0.011	1.000	1.000	1.000	1.000	0.14	0.018	1.000	0.248		1.000	
9LPDL0.01	0.025	1.000	0.222	0.494	0.002	1.000	1.000	1.000	0.049	0.256	<0.001	1.000	0.035	1.000	0.021	1.000	0.013		
	AREA																		LIVE/DEAD

Table A19 3: Tukey's test comparing the results of each gel for live/dead confocal and confocal area stained at Week 3. Pink = p value >0.05, Green = p value <0.05

APPENDIX 20

	WEEK 1	WEEK 2
Agarose5%/LPLL0.1 LIVE/DEAD		
WEEK 2	0.561	
WEEK 3	0.345	1.000
Agarose 5%/LPLL0.01 LIVE/DEAD		
WEEK 2	0.609	
WEEK 3	0.429	1.000
Agarose 5%/HPLL0.1 LIVE/DEAD		
WEEK 2	0.100	
WEEK 3	0.309	0.228
Agarose 5%/HPLL 0.01 LIVE/DEAD		
WEEK 2	0.435	
WEEK 3	1.000	0.262
Agarose 5%/LPDL0.1 LIVE/DEAD		
WEEK 2	0.285	
WEEK 3	0.606	1.000
Agarose 5%/LPDL0.01 LIVE/DEAD		
WEEK 2	0.447	
WEEK 3	0.459	1.000
Agarose5%/LPLL0.1 AREA		
WEEK 2	0.052	
WEEK 3	1.000	0.004
Agarose 5%/LPLL0.01 AREA		
WEEK 2	1.000	
WEEK 3	0.002	0.486
Agarose 5%/HPLL0.1 AREA		
WEEK 2	0.06	
WEEK 3	<0.001	0.002
Agarose 5%/HPLL 0.01 AREA		
WEEK 2	1.000	
WEEK 3	0.038	0.327
Agarose 5%/LPDL0.1 AREA		
WEEK 2	0.043	
WEEK 3	1.000	1.000
Agarose 5%/LPDL0.01 AREA		
WEEK 2	1.000	
WEEK 3	0.004	1.000

Table A20 1: Statistical test results (Post-hoc Tukey's test after repeated measures anova) assessing for statistical differences for 5% gels, comparing different time points. Live/dead confocal results and area stained results. Pink = p value>0.05, green = p value <0.05

	WEEK 1	WEEK 2
Agarose7%/LPLL0.1 LIVE/DEAD		
WEEK 2	0.209	
WEEK 3	1.000	0.187
Agarose 7%/LPLL0.01 LIVE/DEAD		
WEEK 2	0.990	
WEEK 3	1.000	1.000
Agarose 7%/HPLL0.1 LIVE/DEAD		
WEEK 2	0.309	
WEEK 3	0.019	0.405
Agarose 7%/HPLL 0.01 LIVE/DEAD		
WEEK 2	0.813	
WEEK 3	1.000	0.092
Agarose 7%/LPDL0.1 LIVE/DEAD		
WEEK 2	1.000	
WEEK 3	1.000	1.000
Agarose 7%/LPDL0.01 LIVE/DEAD		
WEEK 2	1.000	
WEEK 3	1.000	1.000
Agarose7%/LPLL0.1 AREA		
WEEK 2	0.591	
WEEK 3	0.426	0.468
Agarose 7%/LPLL0.01 AREA		
WEEK 2	0.447	
WEEK 3	<0.001	0.242
Agarose 7%/HPLL0.1 AREA		
WEEK 2	0.009	
WEEK 3	0.072	1.000
Agarose 7%/HPLL 0.01 AREA		
WEEK 2	0.017	
WEEK 3	1.000	0.026
Agarose 7%/LPDL0.1 AREA		
WEEK 2	0.564	
WEEK 3	0.318	1.000
Agarose 7%/LPDL0.01 AREA		
WEEK 2	0.828	
WEEK 3	1.000	1.000

Table A20 2: Statistical test results (Post-hoc Tukey's test after repeated measures anova) assessing for statistical differences for 7% gels, comparing different time points. Live/dead confocal results and area stained results. Pink = p value>0.05, green = p value <0.05

	WEEK 1	WEEK 2
Agarose 9%/LPLL0.1 LIVE/DEAD		
WEEK 2	1.000	
WEEK 3	0.248	1.000
Agarose 9%/LPLL0.01 LIVE/DEAD		
WEEK 2	0.75	
WEEK 3	1.000	1.000
Agarose 9%/HPLL0.1 LIVE/DEAD		
WEEK 2	0.163	
WEEK 3	0.04	1.000
Agarose 9%/HPLL 0.01 LIVE/DEAD		
WEEK 2	0.843	
WEEK 3	1.000	0.666
Agarose 9%/LPDL0.1 LIVE/DEAD		
WEEK 2	0.012	
WEEK 3	1.000	0.003
Agarose 9%/LPDL0.01 LIVE/DEAD		
WEEK 2	0.738	
WEEK 3	0.274	0.085
Agarose 9%/LPLL0.1 AREA		
WEEK 2	1.000	
WEEK 3	<0.001	0.011
Agarose 9%/LPLL0.01 AREA		
WEEK 2	0.480	
WEEK 3	0.600	0.345
Agarose 9%/HPLL0.1 AREA		
WEEK 2	0.378	
WEEK 3	0.019	0.011
Agarose 9%/HPLL 0.01 AREA		
WEEK 2	1.000	
WEEK 3	0.041	0.666
Agarose 9%/LPDL0.1 AREA		
WEEK 2	0.663	
WEEK 3	0.679	0.939
Agarose 9%/LPDL0.01 AREA		
WEEK 2	0.825	
WEEK 3	0.405	0.966

Table A20 3: Statistical test results (Post-hoc Tukey's test after repeated measures anova) assessing for statistical differences for 9% gels, comparing different time points. Live/dead confocal results and area stained results. Pink = p value>0.05, green = p value <0.05

APPENDIX 21

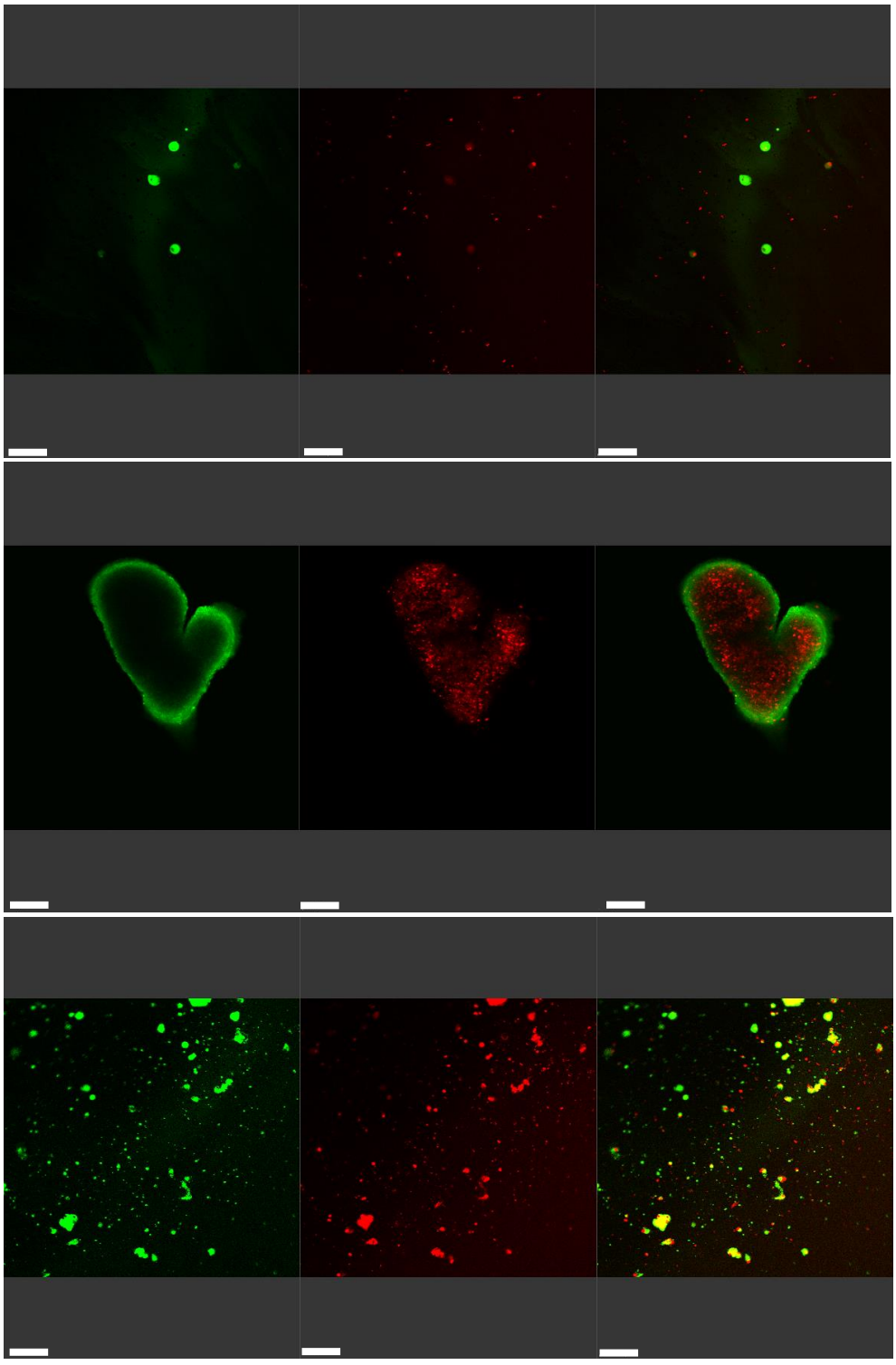

Figure A21 1: Demonstration of trials to improve cellular adhesion to agarose gels. A = Agarose/geltain hybrid (70% agarose, 30% gelatin), 5% gel. B = Fibronectin 0.01% addition with a 5% gel. C = Polydopamine coating 0.1mg, left to polymerise for 48 hours, 5% gel. All live/dead images taken at 1 week. Green = live (calcein AM stain). Red = dead (ethidium homodimer I). Scale bar = 100µm

APPENDIX 22

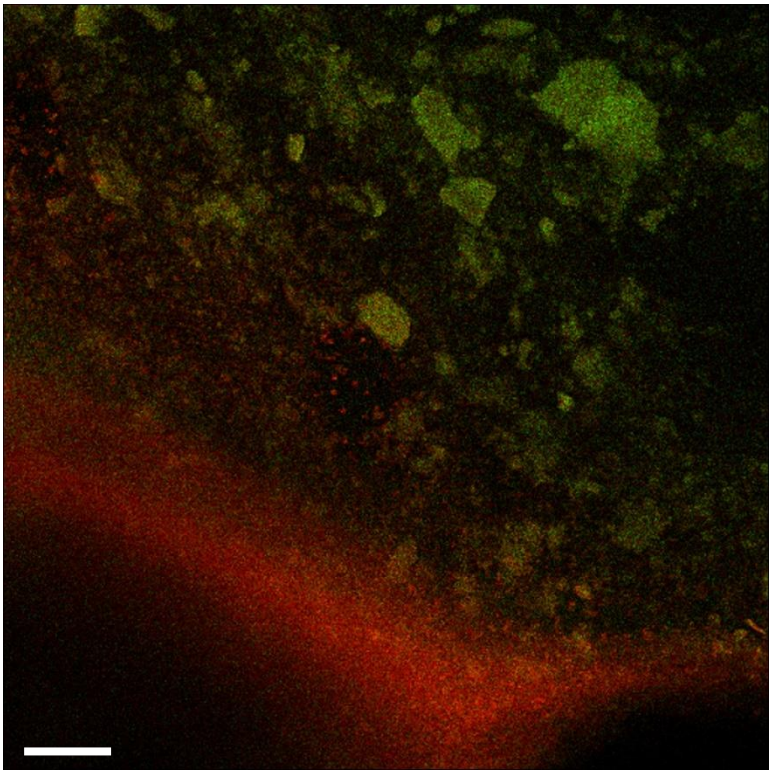

Figure A22 1: Laponite/agarose gel (50:50 mix, 7% gel). Note the autofluorescence of the laponite particles and the lack of cellular adhesion. Green stain = calcein AM, red stain = ethidium homodimer I. Scale bar = 100µm

APPENDIX 23

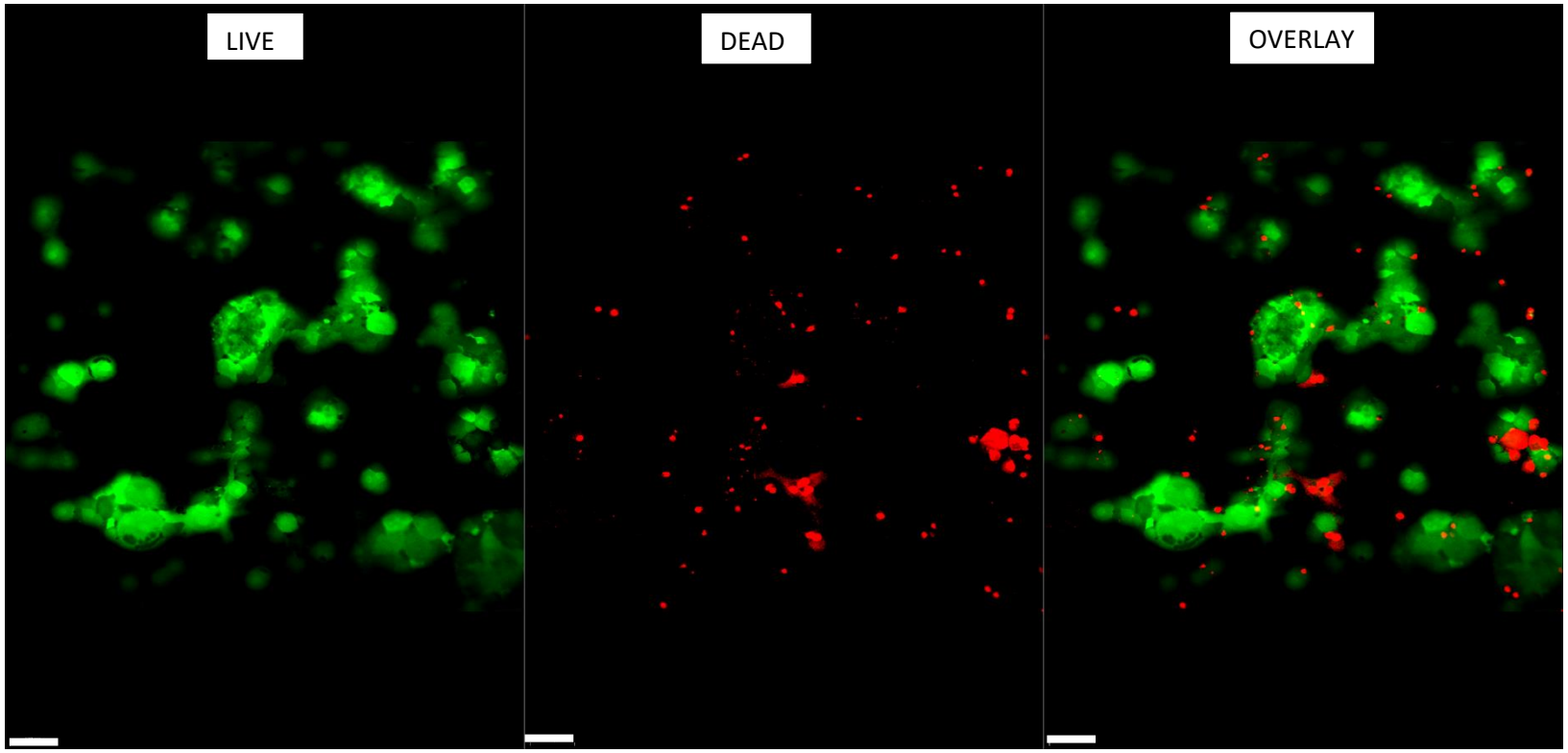

Figure A23 1: Pilot work on adding LPLL0.1 to agarose gels, demonstrating the large, distended cytoplasms of the DPSCs suggestive of secretory activity. Also note the large difference in area covered by the green cytoplasmic staining and the red nuclear staining making a live:dead ratio difficult. Staining with calcein AM (live cytoplasmic stain, green) and Ethidium Homodimer I (dead nuclear stain, red). Gel is 7LPLL0.1. Scale bar = 100µm

APPENDIX 24

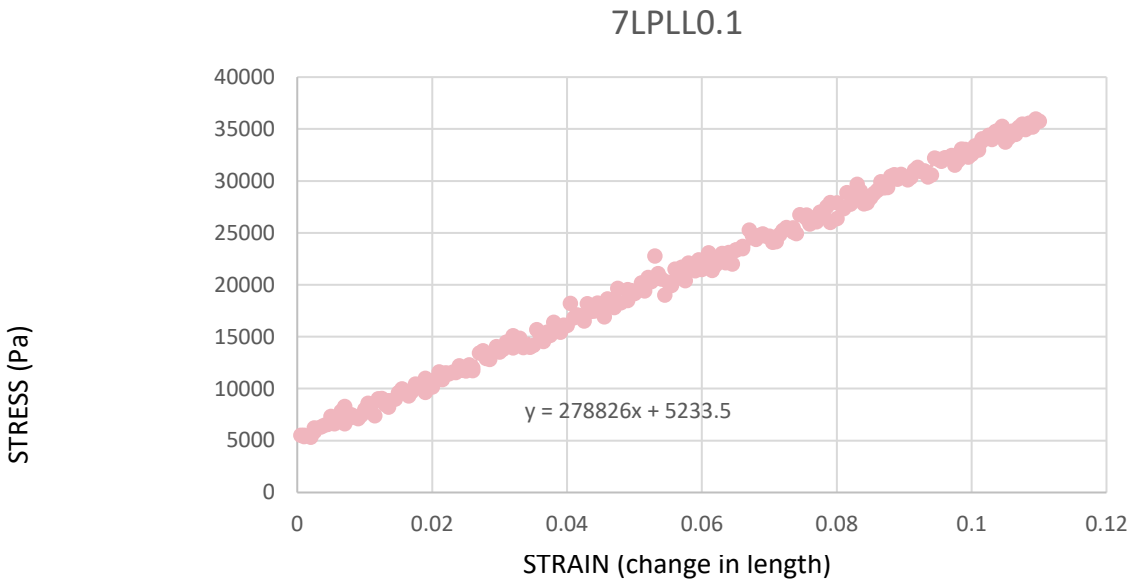

Figure A24 1: 7LPLL0.1 uniaxial compression stress/strain graph

APPENDIX 25

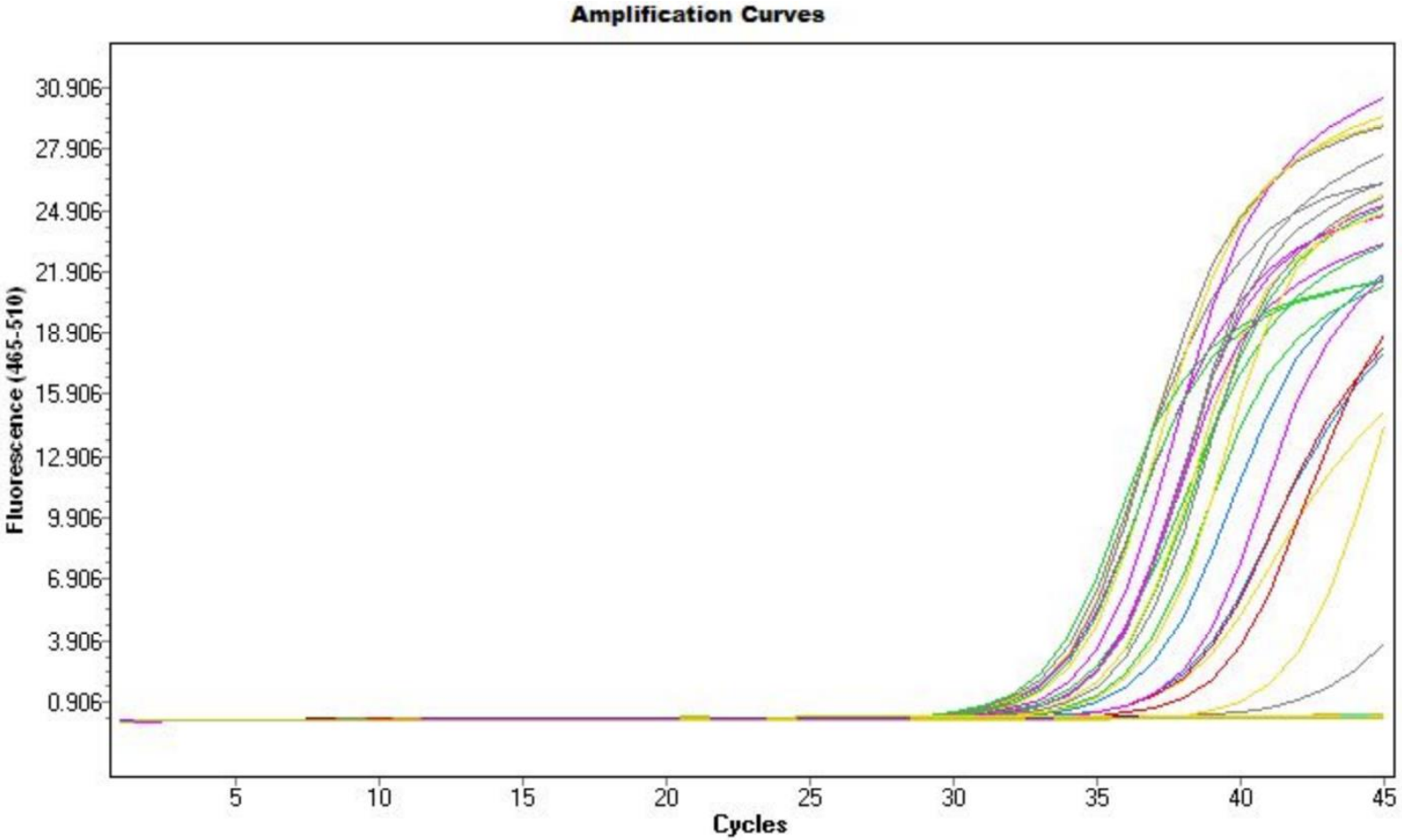

Figure A25 1: Roche Thermocycler output of amplification curves for DSPP RT-PCR

REFERENCES

1. World Health Organisation. Oral Health [Internet]. 2018 [cited 2019 Mar 1]. Available from: https://www.who.int/news-room/fact-sheets/detail/oral-health

2. Åkesson ML, Wärnberg Gerdin E, Söderström U, Lindahl B, Johansson I. Health-related quality of life and prospective caries development. BMC Oral Health [Internet]. 2016;16(1):15. Available from: https://doi.org/10.1186/s12903-016-0166-3

3. Cademartori MG, Gastal MT, Nascimento GG, Demarco FF, Corrêa MB. Is depression associated with oral health outcomes in adults and elders? A systematic review and meta-analysis. Clin Oral Investig. 2018;22(8):2685–702.

4. Peres MA, Macpherson LMD, Weyant RJ, Daly B, Venturelli R, Mathur MR, et al. Oral diseases: a global public health challenge. The Lancet. 2019 Jul;394(10194):249–60.

5. Tanaka R, Shibata Y, Manabe A, Miyazaki T. Mineralization potential of polarized dental enamel. PLoS One. 2009 Jun 19;4(6).

6. Sloan AJ. Biology of the Dentin-Pulp Complex. In: Stem Cell Biology and Tissue Engineering in Dental Sciences [Internet]. Elsevier; 2015. p. 371–8. Available from: http://dx.doi.org/10.1016/B978-0-12-397157-9.00033-3

7. Ahadian S, Akiyaman K, Alansari S, Alikhani M, Alikhani M, Arthur A, et al. Stem Cell Biology and Tissue Engineering in Dental Sciences [Internet]. Vishwakarma A, Sharpe P, Shi S, Ramalingam M, editors. Stem Cell Biology and Tissue Engineering in Dental Sciences. Boston: Elsevier; 2015. xxiii–xxx. Available from: https://linkinghub.elsevier.com/retrieve/pii/B9780123971579099963

8. Galler KM, Weber M, Korkmaz Y, Widbiller M, Feuerer M. Inflammatory response mechanisms of the dentine–pulp complex and the periapical tissues. Vol. 22, International Journal of Molecular Sciences. MDPI AG; 2021. p. 1–23.

9. Gronthos S, Mankani M, Brahim J, Robey PG, Shi S. Postnatal human dental pulp stem cells (DPSCs) *in vitro* and *in vivo*. Proceedings of the National Academy of Sciences [Internet]. 2000 Dec 5;97(25):13625–30. Available from: https://pnas.org/doi/full/10.1073/pnas.240309797

10. Smith AJ. Vitality of the dentin-pulp complex in health and disease: growth factors as key mediators. J Dent Educ [Internet]. 2003 Jun 1;67(6):678. Available from: http://www.jdentaled.org/content/67/6/678.abstract

11. Hashemi-Beni B, Khoroushi M, Foroughi MR, Karbasi S, Khademi AA. Tissue engineering: Dentin – pulp complex regeneration approaches (A review). Tissue Cell. 2017 Oct 1;49(5):552–64.

12. Qu T, Jing J, Ren Y, Ma C, Feng JQ, Yu Q, et al. Complete pulpodentin complex regeneration by modulating the stiffness of biomimetic matrix. Acta Biomater [Internet]. 2015 Apr 1 [cited 2019 Mar 7];16:60–70. Available from: https://www.sciencedirect.com/science/article/pii/S1742706115000392?via%3Dihub

13. Simon SR, Berdal A, Cooper PR, Lumley PJ, Tomson PL, Smith AJ. Dentin-pulp complex regeneration: from lab to clinic. Vol. 23, Advances in dental research. 2011. p. 340–5.

14. Moussa DG, Aparicio C. Present and future of tissue engineering scaffolds for dentin-pulp complex regeneration. Vol. 13, Journal of Tissue Engineering and Regenerative Medicine. John Wiley and Sons Ltd; 2019. p. 58–75.

15. Abbass MMS, El-Rashidy AA, Sadek KM, Moshy S El, Radwan IA, Rady D, et al. Hydrogels and dentin–pulp complex regeneration: From the benchtop to clinical translation. Vol. 12, Polymers. MDPI AG; 2020. p. 1–65.

16. Ricucci D, Loghin S, Lin LM, Spångberg LSW, Tay FR. Is hard tissue formation in the dental pulp after the death of the primary odontoblasts a regenerative or a reparative process? J Dent. 2014;42(9):1156–70.

17. Oh DH, Chen X, Daliri EBM, Kim N, Kim JR, Yoo D. Microbial etiology and prevention of dental caries: Exploiting natural products to inhibit cariogenic biofilms. Vol. 9, Pathogens. MDPI AG; 2020. p. 1–15.

18. Veiga N, Aires D, Douglas F, Pereira M, Vaz A, Rama L, et al. Scient Open Access Exploring the World of Science Dental Caries: A Review. J Dent Oral Health [Internet]. 2016;2. Available from: www.scientonline.org

19. Meyer F, Enax J, Epple M, Amaechi BT, Simader B. Cariogenic biofilms: Development, properties, and biomimetic preventive agents. Dent J (Basel). 2021 Aug 1;9(8).

20. Cooper PR, Holder MJ, Smith AJ. Inflammation and Regeneration in the Dentin-Pulp Complex: A Double-edged Sword. J Endod [Internet]. 2014 Apr;40(4):S46–51. Available from: https://linkinghub.elsevier.com/retrieve/pii/S009923991400082X

21. da Rosa WLO, Piva E, da Silva AF. Disclosing the physiology of pulp tissue for vital pulp therapy. Int Endod J. 2018;51(8):829–46.

22. Farooq I, Ali S, Khurram SA, Anderson P. Dentin. In: An Illustrated Guide to Oral Histology [Internet]. 2021. p. 35–53. Available from: https://doi.org/10.1002/9781119669616.ch3

23. Bleicher F, Richard B, Thivichon-Prince B, Farges JC, Carrouel F. Chapter 30 - Odontoblasts and Dentin Formation. In: Vishwakarma A, Sharpe P, Shi S, Ramalingam M, editors. Stem Cell Biology and Tissue Engineering in Dental Sciences [Internet]. Boston: Academic Press; 2015. p. 379–95. Available from: https://www.sciencedirect.com/science/article/pii/B9780123971579000345

24. Tomson PL. Dentine Extracellular Matrix Components Liberated by Calcium Silicate Cements and their effects on Dental Pulp Cells [Internet]. [Birmingham]: University of Birmingham; 2013 [cited 2023 Nov 21]. Available from: https://etheses.bham.ac.uk/id/eprint/4212/1/Tomson13PhD.pdf

25. Tomson PL, Lumley PJ, Smith AJ, Cooper PR. Growth factor release from dentine matrix by pulp-capping agents promotes pulp tissue repair-associated events. Int Endod J. 2017 Mar 1;50(3):281–92.

26. Marrelli M, Codispoti B, Shelton RM, Scheven BA, Cooper PR, Tatullo M, et al. Dental Pulp Stem Cell Mechanoresponsiveness: Effects of Mechanical Stimuli on Dental Pulp Stem Cell Behavior. Front Physiol [Internet]. 2018;9:1685. Available from: https://www.frontiersin.org/article/10.3389/fphys.2018.01685

27. Cai X, Gong P, Huang Y, Lin Y. Notch signalling pathway in tooth development and adult dental cells. Cell Prolif. 2011;44(6):495–507.

28. Simon S, Smith AJ, Lumley PJ, Cooper PR, Berdal A. The Pulp Healing Process: From Generation to Regeneration. Oral Wound Healing: Cell Biology and Clinical Management. 2013;313–32.

29. El karim IA, Cooper PR, About I, Tomson PL, Lundy FT, Duncan HF. Deciphering Reparative Processes in the Inflamed Dental Pulp. Vol. 2, Frontiers in Dental Medicine. Frontiers Media S.A.; 2021.

30. Howard C, Murray PE, Namerow KN. Dental pulp stem cell migration. J Endod. 2010 Dec;36(12):1963–6.

31. Sloan AJ, Waddington RJ. Dental pulp stem cells: What, where, how? Int J Paediatr Dent. 2009 Jan;19(1):61–70.

32. Dominici M, Le Blanc K, Mueller I, Slaper-Cortenbach I, Marini F, Krause D, et al. Minimal criteria for defining multipotent mesenchymal stromal cells. The International Society for Cellular Therapy position statement. Cytotherapy [Internet]. 2006 Jan 1;8(4):315–7. Available from: https://www.tandfonline.com/doi/abs/10.1080/14653240600855905

33. Bojic S, Volarevic V, Ljujic B, Stojkovic M. Dental stem cells--characteristics and potential. Histol Histopathol [Internet]. 2014 Jun;29(6):699–706. Available from: http://www.ncbi.nlm.nih.gov/pubmed/24446280

34. Lee SM, Zhang Q, Le AD. Dental Stem Cells: Sources and Potential Applications. Curr Oral Health Rep [Internet]. 2014 Mar 30;1(1):34–42. Available from: http://link.springer.com/10.1007/s40496-014-0012-0

35. Lymperi S, Ligoudistianou C, Taraslia V, Kontakiotis E, Anastasiadou E. Dental Stem Cells and their Applications in Dental Tissue Engineering. Open Dent J [Internet]. 2013;7:76–81. Available from: http://www.ncbi.nlm.nih.gov/pubmed/24009647

36. Alkharobi HE. Characterisation of Dental Pulp Cells Derived from Carious Teeth. [Leeds]: University of Leeds; 2016.

37. Alkharobi H, Beattie J, Meade J, Devine D, El-Gendy R. Dental pulp cells isolated from teeth with superficial caries retain an inflammatory phenotype and display an enhanced matrix mineralization potential. Front Physiol. 2017 Apr 28;8(Apr).

38. Alzer H, Kalbouneh H, Alsoleihat F, Abu Shahin N, Ryalat S, Alsalem M, et al. Age of the donor affects the nature of in vitro cultured human dental pulp stem cells. Saudi Dental Journal. 2021 Nov 1;33(7):524–32.

39. Hilkens P, Gervois P, Fanton Y, Vanormelingen J, Martens W, Struys T, et al. Effect of isolation methodology on stem cell properties and multilineage differentiation potential of human dental pulp stem cells. Cell Tissue Res. 2013 Jul;353(1):65–78.

40. Davies OG, Cooper PR, Shelton RM, Smith AJ, Scheven BA. A comparison of the in vitro mineralisation and dentinogenic potential of mesenchymal stem cells derived from adipose tissue, bone marrow and dental pulp. J Bone Miner Metab. 2015 Jul 23;33(4):371–82.

41. Alge DL, Zhou D, Adams LL, Wyss BK, Shadday MD, Woods EJ, et al. Donor-matched comparison of dental pulp stem cells and bone marrow-derived mesenchymal stem cells in a rat model. J Tissue Eng Regen Med. 2010;4(1):73–81.

42. Téclès O, Laurent P, Zygouritsas S, Burger AS, Camps J, Dejou J, et al. Activation of human dental pulp progenitor/stem cells in response to odontoblast injury. In: Archives of Oral Biology. Elsevier Ltd; 2005. p. 103–8.

43. Løvschall H, Tummers M, Thesleff I, E-m F, Activation PK. Activation of the Notch signaling pathway in response to pulp capping of rat molars. 2005;(9):312–7.

44. Nel S, Durandt C, Murdoch C, Pepper MS. Determinants of Dental Pulp Stem Cell Heterogeneity. Vol. 48, Journal of Endodontics. Elsevier Inc.; 2022. p. 1232–40.

45. Yamamura T. Differentiation of Pulpal Cells and Inductive Influences of Various Matrices with Reference to Pulpal Wound Healing. J Dent Res [Internet]. 1985 Apr 29;64(4):530–40. Available from: http://journals.sagepub.com/doi/10.1177/002203458506400406

46. Yu V, Damek-Poprawa M, Nicoll SB, Akintoye SO. Dynamic hydrostatic pressure promotes differentiation of human dental pulp stem cells. Biochem Biophys Res Commun. 2009 Sep 4;386(4):661–5.

47. Lee SK, Lee CY, Kook YA, Lee SK, Kim EC. Mechanical stress promotes odontoblastic differentiation via the heme oxygenase-1 pathway in human dental pulp cell line. Life Sci. 2010 Jan;86(3–4):107–14.

48. Yang H, Shu YX, Wang LY, Zou WL, Guo LY, Shao MY, et al. Effect of cyclic uniaxial compressive stress on human dental pulp cells in vitro. Connect Tissue Res. 2018 May 4;59(3):255–62.

49. Miyashita S, Ahmed NEMB, Murakami M, Iohara K, Yamamoto T, Horibe H, et al. Mechanical forces induce odontoblastic differentiation of mesenchymal stem cells on three-dimensional biomimetic scaffolds. J Tissue Eng Regen Med. 2017 Feb 1;11(2):434–46.

50. Rekow ED, Bayne SC, Carvalho RM, Steele JG. What Constitutes an Ideal Dental Restorative Material? Adv Dent Res. 2013 Oct 15;25(1):18–23.

51. Schwendicke F, Stolpe M. Direct pulp capping after a carious exposure versus root canal treatment: A cost-effectiveness analysis. J Endod. 2014;40(11):1764–70.

52. Edwards D, Stone S, Bailey O, Tomson P. Preserving pulp vitality: part two - vital pulp therapies. Br Dent J. 2021;230(3):148–55.

53. Miyashita H, Worthington H V., Qualtrough A, Plasschaert A. Pulp management for caries in adults: Maintaining pulp vitality. Cochrane Database of Systematic Reviews. 2016;2016(11).

54. Hilton TJ. Keys to Clinical Success with Pulp Capping: A Review of the Literature. Oper Dent. 2009;34(5):615–25.

55. Murray PE, Lumley PJ, Hafez AA, Cox CF, Smith AJ. Preserving the vital pulp in operative dentistry: 4. Factors influencing successful pulp capping. Dent Update. 2002;29(5):225–33.

56. Ritter A V. Direct Pulp-Capping Performed by Dental Students has a Success Rate Close to 60%. Direct Capping of Carious Pulp Exposures is Significantly Less Successful (33%) than

Direct Capping of Mechanical Pulp Exposures (92%). Journal of Evidence-Based Dental Practice. 2007;7(4):165–6.

57. Mente J, Hufnagel S, Leo M, Michel A, Gehrig H, Panagidis D, et al. Treatment outcome of mineral trioxide aggregate or calcium hydroxide direct pulp capping: Long-term results. J Endod [Internet]. 2014;40(11):1746–51. Available from: http://dx.doi.org/10.1016/j.joen.2014.07.019

58. Tüzüner T, Alacam A, Altunbas DA, Gokdogan FG, Gundogdu E. Clinical and radiographic outcomes of direct pulp capping therapy in primary molar teeth following haemostasis with various antiseptics: a randomised controlled trial. Eur J Paediatr Dent. 2012 Dec;13(4):289–92.

59. Stanley HR, Pameijer CH. Dentistry's friend: calcium hydroxide. Oper Dent. 1997;22(1):1—3.

60. Fitzgerald M. Cellular mechanics of dentinal bridge repair using 3H-thymidine. J Dent Res. 1979;58(SPEC.D):2198–206.

61. Schwendicke F, Brouwer F, Schwendicke A, Paris S. Different materials for direct pulp capping: systematic review and meta-analysis and trial sequential analysis. Clin Oral Investig. 2016;20(6):1121–32.

62. Farrugia C, Lung CYK, Schembri Wismayer P, Arias-Moliz MT, Camilleri J. The Relationship of Surface Characteristics and Antimicrobial Performance of Pulp Capping Materials. J Endod. 2018;44(7):1115–20.

63. Qureshi A, Soujanya E, Kumar N, Kumar P, Hivarao S. Recent advances in pulp capping materials: An overview. Journal of Clinical and Diagnostic Research. 2014;8(1):316–21.

64. Chisini LA, Conde MCM, Correa MB, Dantas RVF, Silva AF, Pappen FG, et al. Vital pulp therapies in clinical practice: Findings from a survey with dentist in southern Brazil. Braz Dent J. 2015;26(6):566–71.

65. da Rosa WLO, Cocco AR, Silva TM da, Mesquita LC, Galarça AD, Silva AF da, et al. Current trends and future perspectives of dental pulp capping materials: A systematic review. J Biomed Mater Res B Appl Biomater. 2018;106(3):1358–68.

66. Zhu C, Ju B, Ni R. Clinical outcome of direct pulp capping with MTA or calcium hydroxide: A systematic review and meta-analysis. Int J Clin Exp Med. 2015;8(10):17055–60.

67. Paula AB, Laranjo M, Marto CM, Paulo S, Abrantes AM, Casalta-Lopes J, et al. Direct Pulp Capping: What is the Most Effective Therapy?—Systematic Review and Meta-Analysis. Journal of Evidence-Based Dental Practice. 2018;18(4):298–314.

68. Fava LRG, Saunders WP. Calcium hydroxide pastes: Classification and clinical indications. Int Endod J. 1999;32(4):257–82.

69. Graham L, Cooper PR, Cassidy N, Nor JE, Sloan AJ, Smith AJ. The effect of calcium hydroxide on solubilisation of bio-active dentine matrix components. Biomaterials. 2006;27(14):2865–73.

70. Zafar K, Jamal S, Ghafoor R. Bio-active cements-mineral trioxide aggregate based calcium silicate materials: A narrative review. J Pak Med Assoc. 2020;70(3):497–504.

71. Youssef AR, Emara R, Taher MM, Al-Allaf FA, Almalki M, Almasri MA, et al. Effects of mineral trioxide aggregate, calcium hydroxide, biodentine and Emdogain on osteogenesis, Odontogenesis, angiogenesis and cell viability of dental pulp stem cells. BMC Oral Health. 2019 Jul 2;19(1).

72. Kim SY, Lee SM, Lee JH. Initial Cytotoxicity of Mineral Trioxide Aggregate (MTA) during Setting on Human Mesenchymal Stem Cells. Advances in Materials Science and Engineering [Internet]. 2019 Oct 16;2019:1–7. Available from: https://www.hindawi.com/journals/amse/2019/2365104/

73. Mestry SU, Kalmegh S, Mhaske ST. Mineral Trioxide Aggregates (MTA) in Dentistry: A Review on Chemistry, Synthesis Methods, and Critical Properties. Vol. 15, Silicon. Springer Science and Business Media B.V.; 2023. p. 2231–49.

74. Qudeimat MA, Alyahya A, Hasan AA, Barrieshi-Nusair KM. Mineral trioxide aggregate pulpotomy for permanent molars with clinical signs indicative of irreversible pulpitis: a preliminary study. Int Endod J. 2017 Feb 1;50(2):126–34.

75. Linsuwanont P, Wimonsutthikul K, Pothimoke U, Santiwong B. Treatment Outcomes of Mineral Trioxide Aggregate Pulpotomy in Vital Permanent Teeth with Carious Pulp Exposure: The Retrospective Study. J Endod. 2017 Feb 1;43(2):225–30.

76. Mestry SU, Kalmegh S, Mhaske ST. Mineral Trioxide Aggregates (MTA) in Dentistry: A Review on Chemistry, Synthesis Methods, and Critical Properties. Vol. 15, Silicon. Springer Science and Business Media B.V.; 2023. p. 2231–49.

77. Kaup M, Schäfer E, Dammaschke T. An in vitro study of different material properties of Biodentine compared to ProRoot MTA. Head Face Med. 2015 May 2;11(1).

78. Emara R, Krois J, Schwendicke F. Maintaining pulpal vitality: Cost-effectiveness analysis on carious tissue removal and direct pulp capping. J Dent. 2020;96(February):103330.

79. Kaur M, Singh H, Dhillon JS, Batra M, Saini M. MTA versus biodentine: Review of literature with a comparative analysis. Vol. 11, Journal of Clinical and Diagnostic Research. Journal of Clinical and Diagnostic Research; 2017. p. ZG01–5.

80. Lipski M, Nowicka A, Kot K, Postek-Stefańska L, Wysoczańska-Jankowicz I, Borkowski L, et al. Factors affecting the outcomes of direct pulp capping using Biodentine. Clin Oral Investig [Internet]. 2018 Jun 12;22(5):2021–9. Available from: http://link.springer.com/10.1007/s00784-017-2296-7

81. Zarrabi MH, Javidi M, Jafarian AH, Joushan B. Histologic assessment of human pulp response to capping with mineral trioxide aggregate and a novel endodontic cement. J Endod. 2010 Nov;36(11):1778–81.

82. Belleghem SM Van, Mahadik B, Snodderly KL, Fisher JP. 2.6.2 - Overview of Tissue Engineering Concepts and Applications. In: Wagner WR, Sakiyama-Elbert SE, Zhang G, Yaszemski MJ, editors. Biomaterials Science (Fourth Edition) [Internet]. Academic Press; 2020. p. 1289–316. Available from: https://www.sciencedirect.com/science/article/pii/B9780128161371000817

83. Lin Y, Ren J, McGrath C. Mechanosensitive Piezo1 and Piezo2 ion channels in craniofacial development and dentistry: Recent advances and prospects. Front Physiol [Internet]. 2022

Oct 21;13. Available from: https://www.frontiersin.org/articles/10.3389/fphys.2022.1039714/full

84. Ahmed EM. Hydrogel: Preparation, characterization, and applications: A review. Vol. 6, Journal of Advanced Research. Elsevier B.V.; 2015. p. 105–21.

85. Whitehouse L, Thomson N, Do T, Feichtinger G. Bioactive molecules for regenerative pulp capping. Eur Cell Mater. 2021 Nov 29;42:415–37.

86. Rambhia KJ, Ma PX. Controlled drug release for tissue engineering. J Control Release [Internet]. 2015/08/29. 2015 Dec 10;219:119–28. Available from: https://www.ncbi.nlm.nih.gov/pubmed/26325405

87. Hu CC, Zhang C, Qian Q, Tatum NB. Reparative dentin formation in rat molars after direct pulp capping with growth factors. J Endod. 1998;24(11):744–51.

88. Koike T, Polan MAA, Izumikawa M, Saito T. Induction of Reparative Dentin Formation on Exposed Dental Pulp by Dentin Phosphophoryn/Collagen Composite. Biomed Res Int [Internet]. 2014;2014:1–8. Available from: http://www.hindawi.com/journals/bmri/2014/745139/

89. Goldberg M, Six N, Decup F, Buch D, Soheili Majd E, Lasfargues JJ, et al. Application of bioactive molecules in pulp-capping situations. Adv Dent Res. 2001;15:91–5.

90. Matsunaga T, Yanagiguchi K, Yamada S, Ohara N, Ikeda T, Hayashi Y. Chitosan monomer promotes tissue regeneration on dental pulp wounds. J Biomed Mater Res A. 2006 Mar;76(4):711–20.

91. Kaczmarek-Szczepańska B, Polkowska I, Małek M, Kluczyński J, Paździor-Czapula K, Wekwejt M, et al. The characterization of collagen-based scaffolds modified with phenolic acids for tissue engineering application. Sci Rep. 2023 Dec 1;13(1).

92. Yang S, Leong KF, Du Z, Chua CK. The design of scaffolds for use in tissue engineering. Part I. Traditional factors. Tissue Eng. 2001;7(6):679–89.

93. Zhang L, Morsi Y, Wang Y, Li Y, Ramakrishna S. Review scaffold design and stem cells for tooth regeneration. Japanese Dental Science Review [Internet]. 2013 Feb;49(1):14–26. Available from: https://linkinghub.elsevier.com/retrieve/pii/S1882761612000610

94. Amir LR, Suniarti DF, Utami S, Abbas B. Chitosan as a potential osteogenic factor compared with dexamethasone in cultured macaque dental pulp stromal cells. Cell Tissue Res. 2014;358(2):407–15.

95. Osman ZF, Ahmad A, Noordin KBAA. Naturally derived scaffolds for dental pulp regeneration: a review. Gulhane Medical Journal. 2019;61(2):81.

96. Kim NR, Lee DH, Chung PH, Yang HC. Distinct differentiation properties of human dental pulp cells on collagen, gelatin, and chitosan scaffolds. Oral Surgery, Oral Medicine, Oral Pathology, Oral Radiology and Endodontology. 2009 Nov;108(5).

97. Li F, Liu X, Zhao S, Wu H, Xu HHK. Porous chitosan bilayer membrane containing TGF-β1 loaded microspheres for pulp capping and reparative dentin formation in a dog model. Dental Materials [Internet]. 2014;30(2):172–81. Available from: http://dx.doi.org/10.1016/j.dental.2013.11.005

98. Soares DG, Anovazzi G, Bordini EAF, Zuta UO, Silva Leite MLA, Basso FG, et al. Biological Analysis of Simvastatin-releasing Chitosan Scaffold as a Cell-free System for Pulp-dentin Regeneration. J Endod. 2018 Jun 1;44(6):971-976.e1.

99. Wu S, Zhou Y, Yu Y, Zhou X, Du W, Wan M, et al. Evaluation of Chitosan Hydrogel for Sustained Delivery of VEGF for Odontogenic Differentiation of Dental Pulp Stem Cells. Stem Cells Int [Internet]. 2019 Dec 19;2019:1–14. Available from: https://www.hindawi.com/journals/sci/2019/1515040/

100. Sharma S, Srivastava D, Grover S, Sharma V. Biomaterials in tooth tissue engineering: A review. Journal of Clinical and Diagnostic Research. 2014;8(1):309–15.

101. Dobie K, Smith G, Sloan AJ, Smith AJ. Effects of alginate hydrogels and TGF-β1 on human dental pulp repair in vitro. Connect Tissue Res. 2002;43(2–3):387–90.

102. Oliva-Rodríguez R, Pérez-Urizar J, Dibildox-Alvarado E, Martínez-Saldaña MC, Avelar-González FJ, Flores-Reyes H, et al. Design of a controlled release system of OP-1 and TGF-β1 based in microparticles of sodium alginate and release characterization by HPLC-UV. In Vitro Cell Dev Biol Anim. 2011;47(10):681–8.

103. Fujiwara S, Kumabe S, Iwai Y. Isolated rat dental pulp cell culture and transplantation with an alginate scaffold. Okajimas Folia Anat Jpn. 2006;83(1):15–24.

104. Kumabe S, Nakatsuka M, Kim GS, Jue SS, Aikawa F, Shin JW, et al. Human dental pulp cell culture and cell transplantation with an alginate scaffold. Okajimas Folia Anat Jpn. 2006;82(4):147–55.

105. Kunarti S. Pulp tissue inflammation and angiogenesis after pulp capping with transforming growth factor β1. Dental Journal (Majalah Kedokteran Gigi). 2008;41(2):88.

106. Nakashima M. Induction of Dentin Formation on Canine Amputated Pulp by Recombinant Human Bone Morphogenetic Proteins (BMP)-2 and -4. J Dent Res. 1994;73(9):1515–22.

107. Nakashima M. Induction of dentine in amputated pulp of dogs by recombinant human bone morphogenetic proteins-2 and -4 with collagen matrix. Arch Oral Biol. 1994;39(12):1085–9.

108. Rutherford RB, Spångberg L, Tucker M, Rueger D, Charette M. The time-course of the induction of reparative dentine formation in monkeys by recombinant human osteogenic protein-1. Arch Oral Biol. 1994;39(10):833–8.

109. Rutherford RB, Wahle J, Tucker M, Rueger D, Charette M. Induction of reparative dentine formation in monkeys by recombinant human osteogenic Protein-1. Arch Oral Biol. 1993;38(7):571–6.

110. Rutherford RB, Gu K. Treatment of inflamed ferret dental pulps with recombinant bone morphogenetic protein-7. Eur J Oral Sci. 2000;108(3):202–6.

111. Rutherford RB. Short communication BMP-7 gene transfer to in ¯ amed ferret dental pulps. 2001;7(26):422–4.

112. Iohara K, Murakami M, Takeuchi N, Osako Y, Ito M, Ishizaka R, et al. A Novel Combinatorial Therapy With Pulp Stem Cells and Granulocyte Colony-Stimulating Factor for Total Pulp Regeneration. Stem Cells Transl Med [Internet]. 2013 Jul 1;2(7):521–33. Available from: https://doi.org/10.5966/sctm.2012-0132

113. Chan CP, Lan WH, Chang MC, Chen YJ, Lan WC, Chang HH, et al. Effects of TGF-βs on the growth, collagen synthesis and collagen lattice contraction of human dental pulp fibroblasts in vitro. Arch Oral Biol. 2005;50(5):469–79.

114. Six N, Decup F, Lasfargues JJ, Salih E, Goldberg M. Osteogenic proteins (bone sialoprotein and bone morphogenetic protein-7) and dental pulp mineralization. J Mater Sci Mater Med. 2002;13(2):225–32.

115. Ishimatsu H, Kitamura C, Morotomi T, Tabata Y, Nishihara T, Chen KK, et al. Formation of Dentinal Bridge on Surface of Regenerated Dental Pulp in Dentin Defects by Controlled Release of Fibroblast Growth Factor-2 From Gelatin Hydrogels. J Endod [Internet]. 2009;35(6):858–65. Available from: http://dx.doi.org/10.1016/j.joen.2009.03.049

116. Kikuchi N, Kitamura C, Morotomi T, Inuyama Y, Ishimatsu H, Tabata Y, et al. Formation of Dentin-like Particles in Dentin Defects above Exposed Pulp by Controlled Release of Fibroblast Growth Factor 2 from Gelatin Hydrogels. J Endod. 2007;33(10):1198–202.

117. Gustavsson PE, Son PO. Chapter 6 - Monolithic Polysaccharide Materials. In: Švec F, Tennikova TB, Deyl Z, editors. Journal of Chromatography Library [Internet]. Elsevier; 2003. p. 121–41. Available from: https://www.sciencedirect.com/science/article/pii/S0301477003800222

118. Zarrintaj P, Manouchehri S, Ahmadi Z, Saeb MR, Urbanska AM, Kaplan DL, et al. Agarose-based biomaterials for tissue engineering. Carbohydr Polym [Internet]. 2018 May;187:66–84. Available from: https://linkinghub.elsevier.com/retrieve/pii/S014486171830078X

119. Cao CY, Li QL. Scanning electron microscopic analysis of using agarose hydrogel microenvironment to create enamel prism-like tissue on dentine surface. J Dent [Internet]. 2016 Dec;55:54–60. Available from: https://linkinghub.elsevier.com/retrieve/pii/S0300571216301919

120. Tako M, Tamaki Y, Teruya T, Takeda Y. The Principles of Starch Gelatinization and Retrogradation. Food Nutr Sci. 2014;05(03):280–91.

121. Bačáková L, Filová E, Rypáček F, Švorčík V, Starý V. Cell adhesion on artificial materials for tissue engineering. Physiol Res [Internet]. 2004;53(SUPPL. 1):S35–45. Available from: https://www.biomed.cas.cz/physiolres/pdf/53/53_S35.pdf

122. Mould AP, Burrows L, Humphries MJ. Identification of amino acid residues that form part of the ligand- binding pocket of integrin α5β1. Journal of Biological Chemistry. 1998 Oct 2;273(40):25664–72.

123. Morwood AJ, El-Karim IA, Clarke SA, Lundy FT. The Role of Extracellular Matrix (ECM) Adhesion Motifs in Functionalised Hydrogels. Molecules [Internet]. 2023 Jun 7;28(12):4616. Available from: https://www.mdpi.com/1420-3049/28/12/4616

124. Ng KW, Kugler LE, Doty SB, Ateshian GA, Hung CT. Scaffold degradation elevates the collagen content and dynamic compressive modulus in engineered articular cartilage. Osteoarthritis Cartilage [Internet]. 2009 Feb;17(2):220–7. Available from: https://linkinghub.elsevier.com/retrieve/pii/S1063458408002112

125. Martins C, Sousa F, Araújo F, Sarmento B. Functionalizing PLGA and PLGA Derivatives for Drug Delivery and Tissue Regeneration Applications. Adv Healthc Mater. 2018;7(1):1–24.

126. Rana D, Arulkumar S, Vishwakarma A, Ramalingam M. Considerations on Designing Scaffold for Tissue Engineering. In: Stem Cell Biology and Tissue Engineering in Dental Sciences [Internet]. Elsevier; 2015. p. 133–48. Available from: https://linkinghub.elsevier.com/retrieve/pii/B9780123971579000126

127. Li G, Xu Z, Yang M, Ning Y, Ye L, Jiang H, et al. Topographic Cues of a PLGA Scaffold Promote Odontogenic Differentiation of Dental Pulp Stem Cells through the YAP/β-Catenin Signaling Axis. ACS Biomater Sci Eng. 2023 Mar 13;9(3):1598–607.

128. Zhang W, Walboomers XF, Jansen JA. The formation of tertiary dentin after pulp capping with a calcium phosphate cement, loaded with PLGA microparticles containing TGF-β1. J Biomed Mater Res A. 2008;85(2):439–44.

129. Gala-Garcia A, Teixeira KIR, Wykrota FHL, Sinisterra RD, Cortés ME. Bioceramic/Poly (glycolic)-poly (lactic acid) composite induces mineralized barrier after direct capping of rat tooth pulp tissue. Braz Oral Res [Internet]. 2010 Mar;24(1):08–14. Available from: http://www.scielo.br/scielo.php?script=sci_arttext&pid=S1806-83242010000100002&lng=en&tlng=en

130. Olsson H, Davies JR, Holst KE, Schröder U, Petersson K. Dental pulp capping: Effect of Emdogain Gel on experimentally exposed human pulps. Int Endod J. 2005 Mar;38(3):186–94.

131. Cordeiro MM, Dong Z, Kaneko T, Zhang Z, Miyazawa M, Shi S, et al. Dental Pulp Tissue Engineering with Stem Cells from Exfoliated Deciduous Teeth. J Endod. 2008 Aug;34(8):962–9.

132. Sakai VT, Zhang Z, Dong Z, Neiva KG, MacHado MAAM, Shi S, et al. SHED differentiate into functional odontoblasts and endothelium. J Dent Res. 2010 Aug;89(8):791–6.

133. Peterman EJG. Single Molecule Analysis [Internet]. Second Edition. Peterman EJG, editor. New York, NY: Springer New York; 2018. (Methods in Molecular Biology; vol. 1665). Available from: http://link.springer.com/10.1007/978-1-4939-7271-5

134. Norman MDA, Ferreira SA, Jowett GM, Bozec L, Gentleman E. Measuring the elastic modulus of soft culture surfaces and three-dimensional hydrogels using atomic force microscopy. Nat Protoc [Internet]. 2021 May 14;16(5):2418–49. Available from: https://www.nature.com/articles/s41596-021-00495-4

135. Janmey PA, Fletcher DA, Reinhart-King CA. Stiffness sensing by cells. Physiol Rev. 2020;100(2):695–724.

136. AFMWorkshop. Measuring and Understanding Force Distance Curves [Internet]. [cited 2023 Mar 30]. Available from: https://www.afmworkshop.com/images/datasheets/Measuring-and-understanding-force-distance-curves-v2.pdf

137. Asylum Research An Oxford Instruments Company. SPM Applications Guide, User Guide 3, Version 16, Revision: A-2053 [Internet]. 2018 [cited 2023 Mar 30]. Available from: https://mmrc.caltech.edu/Asylum/Manuals/AR_ApplicationsGuide_16A.pdf

138. Akhtar R, Schwarzer N, Sherratt MJ, Watson REB, Graham HK, Trafford AW, et al. Nanoindentation of histological specimens: Mapping the elastic properties of soft tissues. J Mater Res. 2009 Mar;24(3):638–46.

139. McCarthy CM, Allardyce JM, Hickey SE, Walsh MT, McGourty KD, Mulvihill JJE. Comparison of macroscale and microscale mechanical properties of fresh and fixed-frozen porcine colonic tissue. J Mech Behav Biomed Mater. 2023 Feb 1;138.

140. Bückle H. The Science of Hardness Testing and its Research Applications. In: Westbrook JH, Conrad H, editors. Ohio: American Society of Metals; 1973. p. 472.

141. Kinney JH, Balooch M, Marshall GW, Marshall SJ. A micromechanics model of the elastic properties of human dentine. Arch Oral Biol [Internet]. 1999 Oct;44(10):813–22. Available from: https://linkinghub.elsevier.com/retrieve/pii/S0003996999000801

142. Marshall GW, Habelitz S, Gallagher R, Balooch M, Balooch G, Marshall SJ. Nanomechanical Properties of Hydrated Carious Human Dentin. J Dent Res [Internet]. 2001 Aug 8;80(8):1768–71. Available from: http://journals.sagepub.com/doi/10.1177/00220345010800081701

143. Habelitz S, Marshall SJ, Marshall GW, Balooch M. Mechanical properties of human dental enamel on the nanometre scale. Arch Oral Biol [Internet]. 2001 Feb;46(2):173–83. Available from: https://linkinghub.elsevier.com/retrieve/pii/S0003996900000893

144. Zheng L, Hilton JF, Habelitz S, Marshall SJ, Marshall GW. Dentin caries activity status related to hardness and elasticity. Eur J Oral Sci. 2003 Jun;111(3):243–52.

145. Barbour ME, Shellis RP. An investigation using atomic force microscopy nanoindentation of dental enamel demineralization as a function of undissociated acid concentration and differential buffer capacity. Phys Med Biol. 2007 Feb 21;52(4):899–910.

146. Pugach MK, Strother J, Darling CL, Fried D, Gansky SA, Marshall SJ, et al. Dentin caries zones: Mineral, structure, and properties. J Dent Res. 2009;88(1):71–6.

147. Lippert F, Parker DM, Jandt KD. In vitro demineralization/remineralization cycles at human tooth enamel surfaces investigated by AFM and nanoindentation. J Colloid Interface Sci. 2004 Dec 15;280(2):442–8.

148. Kinney JH, Balooch M, Marshall SJ, Marshall Jr. GW, Weihs TP. Atomic Force Microscope Measurements of the Hardness and Elasticity of Peritubular and Intertubular Human Dentin. J Biomech Eng [Internet]. 1996 Feb 1;118(1):133–5. Available from: https://doi.org/10.1115/1.2795939

149. Erisken C, Kalyon DM, Zhou J, Kim SG, Mao JJ. Viscoelastic properties of dental pulp tissue and ramifications on biomaterial development for pulp regeneration. J Endod. 2015 Oct 1;41(10):1711–7.

150. Ozcan B, Bayrak E, Erisken C. Characterization of Human Dental Pulp Tissue under Oscillatory Shear and Compression. J Biomech Eng. 2016;138(6):1–5.

151. Hiew VV, Simat SFB, Teoh PL. The Advancement of Biomaterials in Regulating Stem Cell Fate. Stem Cell Rev Rep [Internet]. 2018;14(1):43–57. Available from: https://doi.org/10.1007/s12015-017-9764-y

152. Breuls RGM, Jiya TU, Smit TH. Scaffold stiffness influences cell behavior: opportunities for skeletal tissue engineering. Open Orthop J. 2008 May 29;2:103–9.

153. Allen MR, Burr DB. Chapter 8 - Techniques in Histomorphometry. In: Burr DB, Allen MR, editors. Basic and Applied Bone Biology (Second Edition) [Internet]. Academic Press; 2019. p.

141–58. Available from: https://www.sciencedirect.com/science/article/pii/B9780128132593000087

154. Van Zuijlen PPM, De Vries HJC, Lamme EN, Coppens JE, Van Marle J, Kreis RW, et al. Morphometry of dermal collagen orientation by Fourier analysis is superior to multi-observer assessment. Journal of Pathology. 2002 Nov 1;198(3):284–91.

155. Marcos-Garcés V, Harvat M, Molina Aguilar P, Ferrandez Izquierdo A, Ruiz-Sauri A. Comparative measurement of collagen bundle orientation by Fourier analysis and semiquantitative evaluation: reliability and agreement in Masson's trichrome, Picrosirius red and confocal microscopy techniques. J Microsc [Internet]. 2017 Aug 20;267(2):130–42. Available from: https://onlinelibrary.wiley.com/doi/10.1111/jmi.12553

156. Heberer S, Al-Chawaf B, Hildebrand D, Nelson JJ, Nelson K. Histomorphometric analysis of extraction sockets augmented with Bio-Oss Collagen after a 6-week healing period: A prospective study. Clin Oral Implants Res. 2008 Dec;19(12):1219–25.

157. Caetano GF, Fronza M, Leite MN, Gomes A, Frade MAC. Comparison of collagen content in skin wounds evaluated by biochemical assay and by computer-aided histomorphometric analysis. Pharm Biol. 2016 Nov 1;54(11):2555–9.

158. McLachlan JL, Smith AJ, Bujalska IJ, Cooper PR. Gene expression profiling of pulpal tissue reveals the molecular complexity of dental caries. Biochim Biophys Acta Mol Basis Dis. 2005 Sep 25;1741(3):271–81.

159. Martinez EF, De Souza SOM, Correa L, de Araujo VC. Immunohistochemical Localization of Tenascin, Fibronectin, and Type III Collagen in Human Dental Pulp. J Endod [Internet]. 2000 Dec;26(12):708–11. Available from: http://linkinghub.elsevier.com/retrieve/pii/S0099239905608242

160. Conrads G, About I. Pathophysiology of Dental Caries. Caries Excavation: Evolution of Treating Cavitated Carious Lesions. Monogr Oral Sci [Internet]. 2018;1–10. Available from: https://www.karger.com/Article/FullText/487826

161. Wiśniewska K, Rybak Z, Szymonowicz M, Kuropka P, Kaleta-Kuratewicz K, Dobrzyński M. Detection of Lymphatic Vessels in Dental Pulp. Biology (Basel) [Internet]. 2022 Apr 21;11(5):635. Available from: https://www.mdpi.com/2079-7737/11/5/635

162. Nwaneshiudu A, Kuschal C, Sakamoto FH, Rox Anderson R, Schwarzenberger K, Young RC. Introduction to confocal microscopy. Journal of Investigative Dermatology. 2012;132(12):1–5.

163. Matsumoto B (Ed), Wright S J, Wright D J. Cell biological applications of confocal microscopy: Volume 70. 2nd ed. Matsumoto B, editor. Vol. 70, Methods in Cell Biology. San Diego, CA: Academic Press; 2002. 1–74 p.

164. Massler M, Pawlak J. The affected and infected pulp. Oral Surgery, Oral Medicine, Oral Pathology [Internet]. 1977 Jun;43(6):929–47. Available from: https://linkinghub.elsevier.com/retrieve/pii/003042207790086X

165. Breyan D, Schilder H. An electron microscopic study of collagen formation in the dental pulp of the human premolar and rat incisor. Oral Surgery, Oral Medicine, Oral Pathology [Internet]. 1977 Sep;44(3):437–55. Available from: https://linkinghub.elsevier.com/retrieve/pii/0030422077904157

166. Mjör IA, Tronstad L. Experimentally induced pulpitis. Oral Surgery, Oral Medicine, Oral Pathology [Internet]. 1972 Jul;34(1):102–8. Available from: https://linkinghub.elsevier.com/retrieve/pii/0030422072902782

167. Cutright DE, Bhaskar SN. Pulpal vasculature as demonstrated by a new method. Oral Surgery, Oral Medicine, Oral Pathology [Internet]. 1969 May;27(5):678–83. Available from: https://linkinghub.elsevier.com/retrieve/pii/0030422069901042

168. Rapp R, El-Labban NG, Kramer IRH, Wood D. Ultrastructure of fenestrated capillaries in human dental pulps. Arch Oral Biol [Internet]. 1977;22(5):317–9. Available from: https://linkinghub.elsevier.com/retrieve/pii/0003996977900292

169. Harrop TJ, Mackay B. Electron microscopic observations on healing in dental pulp in the rat. Arch Oral Biol [Internet]. 1968 Apr;13(4):365–85. Available from: https://linkinghub.elsevier.com/retrieve/pii/0003996968901659

170. Griffin CJ, Harris R. Ultrastructure of collagen fibrils and fibroblasts of the developing human dental pulp. Arch Oral Biol [Internet]. 1966 Jul;11(7):659–66. Available from: https://linkinghub.elsevier.com/retrieve/pii/0003996966900914

171. França CM, Riggers R, Muschler JL, Widbiller M, Lococo PM, Diogenes A, et al. 3D-Imaging of Whole Neuronal and Vascular Networks of the Human Dental Pulp via CLARITY and Light Sheet Microscopy. Sci Rep [Internet]. 2019 Jul 26;9(1):10860. Available from: https://www.nature.com/articles/s41598-019-47221-5

172. Verhaegen PDHM, van Marle J, Kuehne A, Schouten HJ, Gaffney EA, Maini PK, et al. Collagen bundle morphometry in skin and scar tissue: A novel distance mapping method provides superior measurements compared to Fourier analysis. J Microsc. 2012 Jan;245(1):82–9.

173. Shoulders MD, Raines RT. Collagen structure and stability. Vol. 78, Annual Review of Biochemistry. 2009. p. 929–58.

174. Bleicher F, Richard B, Thivichon-Prince B, Farges JC, Carrouel F. Odontoblasts and Dentin Formation. Stem Cell Biology and Tissue Engineering in Dental Sciences. 2015;379–95.

175. Couto Alves A, Glastonbury CA, El-Sayed Moustafa JS, Small KS. Fasting and time of day independently modulate circadian rhythm relevant gene expression in adipose and skin tissue. BMC Genomics. 2018 Sep 7;19(1).

176. Faruangsaeng T, Thaweesapphitak S, Khamwachirapitak C, Porntaveetus T, Shotelersuk V. Comparative transcriptome profiles of human dental pulp stem cells from maxillary and mandibular teeth. Sci Rep [Internet]. 2022 May 25;12(1):8860. Available from: https://www.nature.com/articles/s41598-022-12867-1

177. Yianni V, Sharpe PT. Transcriptomic Profiling of Dental Pulp Pericytes: An RNAseq Approach. Frontiers in Dental Medicine. 2020 Aug 25;1.

178. McLachlan JL, Smith AJ, Sloan AJ, Cooper PR. Gene expression analysis in cells of the dentine-pulp complex in healthy and carious teeth. Arch Oral Biol. 2003 Apr 1;48(4):273–83.

179. Pääkkönen V, Ohlmeier S, Bergmann U, Larmas M, Salo T, Tjäderhane L. Analysis of gene and protein expression in healthy and carious tooth pulp with cDNA microarray and two-dimensional gel electrophoresis. Eur J Oral Sci. 2005 Oct;113(5):369–79.

180. Liu L, Wang T, Huang D, Song D. Comprehensive Analysis of Differentially Expressed Genes in Clinically Diagnosed Irreversible Pulpitis by Multiplatform Data Integration Using a Robust Rank Aggregation Approach. J Endod. 2021 Sep 1;47(9):1365–75.

181. Wang Z, Gerstein M, Snyder M. RNA-Seq: A revolutionary tool for transcriptomics. Vol. 10, Nature Reviews Genetics. 2009. p. 57–63.

182. Wang C, Gong B, Bushel PR, Thierry-Mieg J, Thierry-Mieg D, Xu J, et al. The concordance between RNA-seq and microarray data depends on chemical treatment and transcript abundance. Nat Biotechnol. 2014 Sep 1;32(9):926–32.

183. Muzzey D, Evans EA, Lieber C. Understanding the Basics of NGS: From Mechanism to Variant Calling. Curr Genet Med Rep. 2015 Dec;3(4):158–65.

184. Opasawatchai A, Nguantad S, Sriwilai B, Matangkasombut P, Matangkasombut O, Srisatjaluk R, et al. Single-Cell Transcriptomic Profiling of Human Dental Pulp in Sound and Carious Teeth: A Pilot Study. Frontiers in Dental Medicine [Internet]. 2022 Jan 5;2. Available from: https://www.frontiersin.org/articles/10.3389/fdmed.2021.806294/full

185. Love MI, Huber W, Anders S. Moderated estimation of fold change and dispersion for RNA-seq data with DESeq2. Genome Biol. 2014 Dec 5;15(12).

186. Kontomaris S V., Malamou A. Hertz model or Oliver & Pharr analysis? Tutorial regarding AFM nanoindentation experiments on biological samples. Mater Res Express. 2020;7(3).

187. Costa KD. Single-cell elastography: Probing for disease with the atomic force microscope. Dis Markers. 2004;19(2–3):139–54.

188. Ren QM, Chen J, Li XN, Lv Y, Niu XL, Chen WY, et al. Effective elastic modulus of an intact cornea related to indentation behavior: A comparison between the Hertz model and Johnson-Kendall-Roberts model. Exp Eye Res [Internet]. 2021;209(June):108670. Available from: https://doi.org/10.1016/j.exer.2021.108670

189. Vlassov S, Oras S, Antsov M, Sosnin I, Polyakov B, Shutka A, et al. Adhesion and Mechanical Properties of PDMS-Based Materials Probed With AFM : A Review. Rev Adv Mater Sci. 2018;56:62–78.

190. Style RW, Hyland C, Boltyanskiy R, Wettlaufer JS, Dufresne ER. Surface tension and contact with soft elastic solids. Nat Commun. 2013;4:1–6.

191. R Core Team. R: A language and environment for statistical computing [Internet]. Vienna: R Foundation for Statistical Computing; 2019. Available from: https://www.r-project.org/

192. Dinno A. dunn.test: Dunn's Test of Multiple Comparisons Using Rank Sums [Internet]. 2017. Available from: https://cran.r-project.org/package=dunn.test

193. Bates D, Mächler M, Bolker B, Walker S. Fitting Linear Mixed-Effects Models Using **lme4**. J Stat Softw [Internet]. 2015;67(1). Available from: http://www.jstatsoft.org/v67/i01/

194. Bernick S, Nedelman C, Angeles L. Effect of aging on the human pulp. J Endod. 1975;1(3):88–94.

195. Rezakhaniha R, Agianniotis A, Schrauwen JTC, Griffa A, Sage D, Bouten CVC, et al. Experimental investigation of collagen waviness and orientation in the arterial adventitia

using confocal laser scanning microscopy. Biomech Model Mechanobiol. 2012 Mar;11(3–4):461–73.

196. ThermoFisher Scientific. Ribosomal RNA Depletion | rRNA Depletion [Internet]. [cited 2024 Mar 15]. Available from: https://www.thermofisher.com/uk/en/home/life-science/dna-rna-purification-analysis/rna-extraction/rna-applications/ribosomal-rna-depletion.html

197. Martin M. Cutadapt removes adapter sequences from high-throughput sequencing reads. EMBnet J [Internet]. 2011 May 2;17(1):10. Available from: http://journal.embnet.org/index.php/embnetjournal/article/view/200

198. Roser LG, Agüero F, Sánchez DO. FastqCleaner: an interactive Bioconductor application for quality-control, filtering and trimming of FASTQ files. BMC Bioinformatics [Internet]. 2019 Dec 28;20(1):361. Available from: https://bmcbioinformatics.biomedcentral.com/articles/10.1186/s12859-019-2961-8

199. Liao Y, Smyth GK, Shi W. The R package Rsubread is easier, faster, cheaper and better for alignment and quantification of RNA sequencing reads. Nucleic Acids Res [Internet]. 2019 May 7;47(8). Available from: https://academic.oup.com/nar/article/47/8/e47/5345150

200. National Library of Medicine NC for BI. GRCh38.p14. 2022 [cited 2023 Feb 5]. Genome assembly GRCh38.p14. Available from: https://www.ncbi.nlm.nih.gov/data-hub/genome/GCF_000001405.40/

201. Maza E. In papyro comparison of TMM (edgeR), RLE (DESeq2), and MRN normalization methods for a simple two-conditions-without-replicates RNA-seq experimental design. Front Genet. 2016 Sep 16;7(SEP).

202. Robinson MD, McCarthy DJ, Smyth GK. edgeR: A Bioconductor package for differential expression analysis of digital gene expression data. Bioinformatics. 2009 Nov 11;26(1):139–40.

203. GeeksforGeeks. Principal Component Analysis(PCA) [Internet]. 2023 [cited 2024 Mar 13]. Available from: https://www.geeksforgeeks.org/principal-component-analysis-pca/

204. GeeksforGeeks. K means Clustering – Introduction [Internet]. 2024 [cited 2024 Mar 13]. Available from: https://www.geeksforgeeks.org/k-means-clustering-introduction/?ref=lbp

205. Szklarczyk D, Gable AL, Lyon D, Junge A, Wyder S, Huerta-Cepas J, et al. STRING v11: Protein-protein association networks with increased coverage, supporting functional discovery in genome-wide experimental datasets. Nucleic Acids Res. 2019 Jan 8;47(D1):D607–13.

206. Szklarczyk D, Kirsch R, Koutrouli M, Nastou K, Mehryary F, Hachilif R, et al. The STRING database in 2023: protein-protein association networks and functional enrichment analyses for any sequenced genome of interest. Nucleic Acids Res. 2023 Jan 6;51(1 D):D638–46.

207. Baker A, Karpagaselvi K, Kumaraswamy J, Ranjini M, Gowher J. Role of dental pulp in age estimation:A quantitative and morphometric study. J Forensic Dent Sci. 2019;11(2):95.

208. Tibshirani R, Walther G, Hastie T. Estimating the Number of Clusters in a Data Set Via the Gap Statistic. J R Stat Soc Series B Stat Methodol [Internet]. 2001 Jul 1;63(2):411–23. Available from: https://academic.oup.com/jrsssb/article/63/2/411/7083348

209. Bateman A, Martin MJ, Orchard S, Magrane M, Ahmad S, Alpi E, et al. UniProt: the Universal Protein Knowledgebase in 2023. Nucleic Acids Res. 2023 Jan 6;51(D1):D523–31.

210. Carbon S, Douglass E, Good BM, Unni DR, Harris NL, Mungall CJ, et al. The Gene Ontology resource: Enriching a GOld mine. Nucleic Acids Res. 2021 Jan 8;49(D1):D325–34.

211. Ashburner M, Ball CA, Blake JA, Botstein D, Butler H, Cherry JM, et al. Gene ontology: Tool for the unification of biology. Vol. 25, Nature Genetics. 2000. p. 25–9.

212. Gillespie M, Jassal B, Stephan R, Milacic M, Rothfels K, Senff-Ribeiro A, et al. The reactome pathway knowledgebase 2022. Nucleic Acids Res. 2022 Jan 7;50(D1):D687–92.

213. Son AR, Yang YM, Hong JH, Lee SI, Shibukawa Y, Shin DM. Odontoblast TRP channels and thermo/mechanical transmission. J Dent Res. 2009;88(11):1014–9.

214. Magloire H, Couble ML, Thivichon-Prince B, Maurin JC, Bleicher F. Odontoblast: A mechano-sensory cell. J Exp Zool B Mol Dev Evol. 2009;312(5):416–24.

215. Milos NC, Peters E, Daley T. Odontoblasts in odontogenic tumors. Med Hypotheses. 2013 Sep;81(3):371–3.

216. Kabartai F, Hoffman T, Hannig C. Cellular reduction and pulp fibrosis can be related not only to aging process but also to a physiologic static compression. Dent Hypotheses. 2017 Apr 1;8(2):42–5.

217. Wu PH, Aroush DRB, Asnacios A, Chen WC, Dokukin ME, Doss BL, et al. A comparison of methods to assess cell mechanical properties. Nat Methods [Internet]. 2018 Jul 18;15(7):491–8. Available from: http://www.nature.com/articles/s41592-018-0015-1

218. Martinez-Vidal L, Murdica V, Venegoni C, Pederzoli F, Bandini M, Necchi A, et al. Causal contributors to tissue stiffness and clinical relevance in urology. Vol. 4, Communications Biology. Nature Research; 2021.

219. Akhtar R, Sherratt MJ, Cruickshank JK, Derby B. Characterizing the elastic properties of tissues. Materials Today [Internet]. 2011 Mar;14(3):96–105. Available from: https://linkinghub.elsevier.com/retrieve/pii/S1369702111700591

220. Sachot N, Engel E, Castano O. Hybrid Organic-Inorganic Scaffolding Biomaterials for Regenerative Therapies. Curr Org Chem. 2014 Nov 5;18(18):2299–314.

221. Ranjitkar S, Taylor JA, Townsend GC. A radiographic assessment of the prevalence of pulp stones in Australians. Aust Dent J. 2002;47(1):36–40.

222. Al Madhoun A, Sindhu S, Haddad D, Atari M, Ahmad R, Al-Mulla F. Dental Pulp Stem Cells Derived From Adult Human Third Molar Tooth: A Brief Review. Front Cell Dev Biol [Internet]. 2021 Oct 12;9. Available from: https://www.frontiersin.org/articles/10.3389/fcell.2021.717624/full

223. Shi S, Gronthos S. Perivascular niche of postnatal mesenchymal stem cells in human bone marrow and dental pulp. Journal of Bone and Mineral Research. 2003 Apr 1;18(4):696–704.

224. Wang Z, Pan J, Wright JT, Bencharit S, Zhang S, Everett ET, et al. Putative Stem Cells in Human Dental Pulp with Irreversible Pulpitis: An Exploratory Study. J Endod. 2010 May;36(5):820–5.

225. Lane SW, Williams DA, Watt FM. Modulating the stem cell niche for tissue regeneration. Nat Biotechnol. 2014;32(8):795–803.

226. Liu N, Zhou M, Zhang Q, Zhang T, Tian T, Ma Q, et al. Stiffness regulates the proliferation and osteogenic/odontogenic differentiation of human dental pulp stem cells via the WNT signalling pathway. Cell Prolif. 2018;51(2):1–10.

227. Lo CM, Wang HB, Dembo M, Wang YL. Cell movement is guided by the rigidity of the substrate. Biophys J. 2000;79(1):144–52.

228. Vincent LG, Choi YS, Alonso-Latorre B, del Álamo JC, Engler AJ. Mesenchymal stem cell durotaxis depends on substrate stiffness gradient strength. Biotechnol J. 2013 Apr;8(4):472–84.

229. Ehlinger C, Mathieu E, Rabineau M, Ball V, Lavalle P, Haikel Y, et al. Insensitivity of dental pulp stem cells migration to substrate stiffness. Biomaterials. 2021;275(June):120969.

230. Kondo S, Manabe Y. Analytical methods and interpretation of variation in tooth morphology. Vol. 58, Journal of Oral Biosciences. Japanese Association for Oral Biology; 2016. p. 85–94.

231. Schielzeth H, Dingemanse NJ, Nakagawa S, Westneat DF, Allegue H, Teplitsky C, et al. Robustness of linear mixed-effects models to violations of distributional assumptions. Methods Ecol Evol. 2020 Sep 1;11(9):1141–52.

232. Hillmann G, Geurtsen W. Light-microscopical investigation of the distribution of extracellular matrix molecules and calcifications in human dental pulps of various ages. Cell Tissue Res. 1997;289:145–54.

233. Ohto-Fujita E, Shimizu M, Sano S, Kurimoto M, Yamazawa K, Atomi T, et al. Solubilized eggshell membrane supplies a type III collagen-rich elastic dermal papilla. Cell Tissue Res. 2019 Apr 3;376(1):123–35.

234. Marcos-Garcés V, Rios-Navarro C, Gómez-Torres F, Gavara J, de Dios E, Diaz A, et al. Fourier analysis of collagen bundle orientation in myocardial infarction scars. Histochem Cell Biol. 2022 Nov 1;158(5):471–83.

235. Ashoor M, Khorshidi A, Sarkhosh L. Estimation of microvascular capillary physical parameters using MRI assuming a pseudo liquid drop as model of fluid exchange on the cellular level. Reports of Practical Oncology and Radiotherapy. 2019 Jan 1;24(1):3–11.

236. Mathew-Steiner SS, Roy S, Sen CK. Collagen in wound healing. Vol. 8, Bioengineering. MDPI AG; 2021.

237. Farges JC, Alliot-Licht B, Renard E, Ducret M, Gaudin A, Smith AJ, et al. Dental Pulp Defence and Repair Mechanisms in Dental Caries. Mediators Inflamm. 2015;2015.

238. Taubenberger A V., Woodruff MA, Bai H, Muller DJ, Hutmacher DW. The effect of unlocking RGD-motifs in collagen I on pre-osteoblast adhesion and differentiation. Biomaterials. 2010 Apr;31(10):2827–35.

239. Davis GE. Affinity of integrins for damaged extracellular matrix: αvβ3 binds to denatured collagen type I through RGD sites. Biochem Biophys Res Commun [Internet]. 1992 Feb;182(3):1025–31. Available from: https://linkinghub.elsevier.com/retrieve/pii/0006291X9291834D

240. Lucarelli N, Ginley B, Zee J, Mimar S, Paul AS, Jain S, et al. Correlating Deep Learning-Based Automated Reference Kidney Histomorphometry with Patient Demographics and Creatinine. Kidney360 [Internet]. 2023 Nov 14; Available from: https://journals.lww.com/10.34067/KID.0000000000000299

241. van Amerongen JP, Lemmens IG, Tonino GJM. The concentration, extractability and characterization of collagen in human dental pulp. Arch Oral Biol [Internet]. 1983;28(4):339–45. Available from: https://linkinghub.elsevier.com/retrieve/pii/0003996983900766

242. Kim JM, Kang SW, Shin SM, Kim DS, Choi KK, Kim EC, et al. Inhibition of matrix metalloproteinases expression in human dental pulp cells by all-trans retinoic acid. Int J Oral Sci. 2014 Aug 8;6(3):150–3.

243. Huang P, Wang F, Wang X, Meng X, Qiao W, Meng L. RNA-sequencing analysis reveals the potential molecular mechanism of RAD54B in the proliferation of inflamed human dental pulp cells. Int Endod J. 2023 Jan 1;56(1):39–52.

244. Mutter GL, Zahrieh D, Liu C, Neuberg D, Finkelstein D, Baker HE, et al. Comparison of frozen and RNALater solid tissue storage methods for use in RNA expression microarrays. BMC Genomics. 2004 Nov 10;5.

245. Conde MCM, Nedel F, Campos VF, Smith AJ, Nör JE, Demarco FF, et al. Odontoblast RNA stability in different temperature-based protocols for tooth storage. Int Endod J. 2012 Mar;45(3):266–72.

246. Horst O V, Horst JA, Samudrala R, Dale BA. Caries induced cytokine network in the odontoblast layer of human teeth. BMC Immunol [Internet]. 2011 Dec 24;12(1):9. Available from: https://bmcimmunol.biomedcentral.com/articles/10.1186/1471-2172-12-9

247. Monterubbianesi R, Bencun M, Pagella P, Woloszyk A, Orsini G, Mitsiadis TA. A comparative in vitro study of the osteogenic and adipogenic potential of human dental pulp stem cells, gingival fibroblasts and foreskin fibroblasts. Sci Rep. 2019 Dec 1;9(1).

248. Galicia JC, Henson BR, Parker JS, Khan AA. Gene expression profile of pulpitis. Genes Immun [Internet]. 2016 Jun 7;17(4):239–43. Available from: https://www.nature.com/articles/gene201614

249. Bender I. Pulpal Pain Diagnosis—A Review. J Endod [Internet]. 2000 Mar;26(3):175–9. Available from: http://linkinghub.elsevier.com/retrieve/pii/S009923990560951X

250. Gallego Romero I, Pai AA, Tung J, Gilad Y. RNA-seq: Impact of RNA degradation on transcript quantification. BMC Biol. 2014 May 30;12.

251. Chen EA, Souaiaia T, Herstein JS, Evgrafov O V, Spitsyna VN, Rebolini DF, et al. Effect of RNA integrity on uniquely mapped reads in RNA-Seq. BMC Res Notes [Internet]. 2014 Dec 23;7(1):753. Available from: https://bmcresnotes.biomedcentral.com/articles/10.1186/1756-0500-7-753

252. Love M, Anders S, Huber W. DESeq2: Differential gene expression analysis based on the negative binomial distribution [Internet]. DESeq2; 2023 [cited 2023 Nov 21]. p. 48–56. Available from: https://github.com/mikelove/DESeq2

253. Pink RC, Wicks K, Caley DP, Punch EK, Jacobs L, Francisco Carter DR. Pseudogenes: Pseudo-functional or key regulators in health and disease? RNA [Internet]. 2011 May;17(5):792–8. Available from: http://rnajournal.cshlp.org/lookup/doi/10.1261/rna.2658311

254. Giraud T, Rufas P, Chmilewsky F, Rombouts C, Dejou J, Jeanneau C, et al. Complement Activation by Pulp Capping Materials Plays a Significant Role in Both Inflammatory and Pulp Stem Cells' Recruitment. J Endod. 2017 Jul 1;43(7):1104–10.

255. Lundy FT, El karim I, Scheven BA. Current and Future Views on Pulpal Pain and Neurogenesis. In: Clinical Approaches in Endodontic Regeneration. Cham: Springer International Publishing; 2019. p. 19–36.

256. Goldberg M, Njeh A, Uzunoglu E. Is Pulp Inflammation a Prerequisite for Pulp Healing and Regeneration? Mediators Inflamm. 2015;2015.

257. Borschel GH, Kia KF, Kuzon WM, Dennis RG. Mechanical properties of acellular peripheral nerve. Journal of Surgical Research. 2003;114(2):133–9.

258. Sampathkumar NK, Sundaram VK, Danthi PS, Barakat R, Solomon S, Mondal M, et al. RNA-Seq is not required to determine stable reference genes for qPCR normalization. PLoS Comput Biol. 2022 Feb 1;18(2).

259. Ali AF, Ahmed MM, El-Kady AM, Abd El-Hady BM, Ibrahim AM. Synthesis of Gelatin-Agarose Scaffold for Controlled Antibiotic Delivery and its Modification by Glass Nanoparticles Addition as a Potential Osteomyelitis Treatment. Silicon [Internet]. 2021 Jun 15;13(6):2011–28. Available from: https://link.springer.com/10.1007/s12633-020-00576-1

260. Tripathi A, Kathuria N, Kumar A. Elastic and macroporous agarose-gelatin cryogels with isotropic and anisotropic porosity for tissue engineering. J Biomed Mater Res A. 2009;90(3):680–94.

261. Sakai S, Hashimoto I, Kawakami K. Synthesis of an agarose-gelatin conjugate for use as a tissue engineering scaffold. J Biosci Bioeng. 2007 Jan;103(1):22–6.

262. Cambria E, Brunner S, Heusser S, Fisch P, Hitzl W, Ferguson SJ, et al. Cell-Laden Agarose-Collagen Composite Hydrogels for Mechanotransduction Studies. Front Bioeng Biotechnol [Internet]. 2020 Apr 21;8. Available from: https://www.frontiersin.org/article/10.3389/fbioe.2020.00346/full

263. Chau DYS, Johnson C, MacNeil S, Haycock JW, Ghaemmaghami AM. The development of a 3D immunocompetent model of human skin. Biofabrication [Internet]. 2013 Jul 23;5(3):035011. Available from: https://iopscience.iop.org/article/10.1088/1758-5082/5/3/035011

264. Su T, Zhang M, Zeng Q, Pan W, Huang Y, Qian Y, et al. Mussel-inspired agarose hydrogel scaffolds for skin tissue engineering. Bioact Mater. 2021 Mar 1;6(3):579–88.

265. Chuah YJ, Koh YT, Lim K, Menon N V., Wu Y, Kang Y. Simple surface engineering of polydimethylsiloxane with polydopamine for stabilized mesenchymal stem cell adhesion and multipotency. Sci Rep [Internet]. 2015 Dec 9;5(1):18162. Available from: https://www.nature.com/articles/srep18162

266. Tsai WB, Chen WT, Chien HW, Kuo WH, Wang MJ. Poly(dopamine) coating of scaffolds for articular cartilage tissue engineering. Acta Biomater. 2011;7(12):4187–94.

267. Topuz F, Nadernezhad A, Caliskan OS, Menceloglu YZ, Koc B. Nanosilicate embedded agarose hydrogels with improved bioactivity. Carbohydr Polym. 2018 Dec 1;201:105–12.

268. Nair BP, Sindhu M, Nair PD. Polycaprolactone-laponite composite scaffold releasing strontium ranelate for bone tissue engineering applications. Colloids Surf B Biointerfaces. 2016 Jul 1;143:423–30.

269. Zheng S, Guan Y, Yu H, Huang G, Zheng C. Poly-l-lysine-coated PLGA/poly(amino acid)-modified hydroxyapatite porous scaffolds as efficient tissue engineering scaffolds for cell adhesion, proliferation, and differentiation. New Journal of Chemistry. 2019;43(25):9989–10002.

270. Yuan Y, Shi X, Gan Z, Wang F. Modification of porous PLGA microspheres by poly-L-lysine for use as tissue engineering scaffolds. Colloids Surf B Biointerfaces. 2018 Jan 1;161:162–8.

271. Kouhi M, Fathi M, Prabhakaran MP, Shamanian M, Ramakrishna S. Poly L lysine-modified PHBV based nanofibrous scaffolds for bone cell mineralization and osteogenic differentiation. Appl Surf Sci. 2018 Nov 1;457:616–25.

272. Kuo YC, Ku HF, Rajesh R. Chitosan/γ-poly(glutamic acid) scaffolds with surface-modified albumin, elastin and poly-L-lysine for cartilage tissue engineering. Materials Science and Engineering C. 2017 Sep 1;78:265–77.

273. Zhu J, Qi Z, Zheng C, Xue P, Fu C, Pan S, et al. Enhanced Cell Proliferation and Osteogenesis Differentiation through a Combined Treatment of Poly-L-Lysine-Coated PLGA/Graphene Oxide Hybrid Fiber Matrices and Electrical Stimulation. J Nanomater [Internet]. 2020 Feb 15;2020:1–15. Available from: https://www.hindawi.com/journals/jnm/2020/5892506/

274. Nisbet DR, Moses D, Gengenbach TR, Forsythe JS, Finkelstein DI, Horne MK. Enhancing neurite outgrowth from primary neurones and neural stem cells using thermoresponsive hydrogel scaffolds for the repair of spinal cord injury. J Biomed Mater Res A [Internet]. 2009 Apr 10;89A(1):24–35. Available from: https://onlinelibrary.wiley.com/doi/10.1002/jbm.a.31962

275. Crompton KE, Goud JD, Bellamkonda R V., Gengenbach TR, Finkelstein DI, Horne MK, et al. Polylysine-functionalised thermoresponsive chitosan hydrogel for neural tissue engineering. Biomaterials. 2007 Jan;28(3):441–9.

276. Hayman MW, Smith KH, Cameron NR, Przyborski SA. Growth of human stem cell-derived neurons on solid three-dimensional polymers. J Biochem Biophys Methods. 2005 Mar 31;62(3):231–40.

277. Hegde N, Velingkar V, Prabhakar B. An Update on Design and Pharmacology of Dendritic Poly(l-lysine). Vol. 25, International Journal of Peptide Research and Therapeutics. Springer Netherlands; 2019. p. 1539–62.

278. Shi C, He Y, Feng X, Fu D. ε-Polylysine and next-generation dendrigraft poly-L-lysine: Chemistry, activity, and applications in biopharmaceuticals. J Biomater Sci Polym Ed. 2015 Dec 12;26(18):1343–56.

279. Cieślik-Boczula K. Alpha-helix to beta-sheet transition in long-chain poly-L-lysine: Formation of alpha-helical fibrils by poly-L-lysine. Biochimie. 2017 Jun 1;137:106–14.

280. Stil A, Liberelle B, Guadarrama Bello D, Lacomme L, Arpin L, Parent P, et al. A simple method for poly-D-lysine coating to enhance adhesion and maturation of primary cortical neuron cultures in vitro. Front Cell Neurosci [Internet]. 2023 Jun 21;17. Available from: https://www.frontiersin.org/articles/10.3389/fncel.2023.1212097/full

281. Chittchang M, Alur HH, Mitra AK, Johnston TP. Poly(L-lysine) as a model drug macromolecule with which to investigate secondary structure and membrane transport, part I: physicochemical and stability studies. Journal of Pharmacy and Pharmacology. 2010 Feb 18;54(3):315–23.

282. Stamou A, Iatrou H, Tsitsilianis C. NIPAm-Based Modification of Poly(L-lysine): A pH-Dependent LCST-Type Thermo-Responsive Biodegradable Polymer. Polymers (Basel) [Internet]. 2022 Feb 18;14(4):802. Available from: https://www.mdpi.com/2073-4360/14/4/802

283. Yu J, He H, Tang C, Zhang G, Li Y, Wang R, et al. Differentiation potential of STRO-1+ dental pulp stem cells changes during cell passaging. BMC Cell Biol [Internet]. 2010 Dec 8;11(1):32. Available from: https://bmcmolcellbiol.biomedcentral.com/articles/10.1186/1471-2121-11-32

284. Chouaib B, Cuisinier F, Collart-Dutilleul PY. Dental stem cell-conditioned medium for tissue regeneration: Optimization of production and storage. World J Stem Cells. 2022;14(4):287–302.

285. Turrioni AP, Oliveira Neto NF de, Xu Y, Morse L, Costa CA de S, Battaglino R, et al. Proliferation rate and expression of stem cells markers during expansion in primary culture of pulp cells. Braz Oral Res [Internet]. 2021;35. Available from: http://www.scielo.br/scielo.php?script=sci_arttext&pid=S1806-83242021000100298&tlng=en

286. Jones TD, Naimipour H, Sun S, Cho M, Alapati SB. Mechanical Changes in Human Dental Pulp Stem Cells during Early Odontogenic Differentiation. J Endod [Internet]. 2015 Jan;41(1):50–5. Available from: https://linkinghub.elsevier.com/retrieve/pii/S0099239914007158

287. Gantenbein-Ritter B, Sprecher CM, Chan S, Illien-Junger S, Grad S. Mammalian Cell Viability [Internet]. Stoddart MJ, editor. Totowa, NJ: Humana Press; 2011. 127–217 p. (Methods in Molecular Biology; vol. 740). Available from: https://link.springer.com/10.1007/978-1-61779-108-6

288. Hu C, He S, Lee YJ, He Y, Kong EM, Li H, et al. Live-dead assay on unlabeled cells using phase imaging with computational specificity. Nat Commun [Internet]. 2022 Feb 7;13(1):713. Available from: https://www.nature.com/articles/s41467-022-28214-x

289. Xu R, Zhang Z, Toftdal MS, Møller AC, Dagnaes-Hansen F, Dong M, et al. Synchronous delivery of hydroxyapatite and connective tissue growth factor derived osteoinductive peptide enhanced osteogenesis. Journal of Controlled Release. 2019 May 10;301:129–39.

290. Ligasová A, Koberna K. Quantification of fixed adherent cells using a strong enhancer of the fluorescence of DNA dyes. Sci Rep [Internet]. 2019 Jun 18;9(1):8701. Available from: https://www.nature.com/articles/s41598-019-45217-9

291. Olsson H, Petersson K, Rohlin M. Formation of a hard tissue barrier after pulp cappings in humans. A systematic review. Vol. 39, International Endodontic Journal. 2006. p. 429–42.

292. Kamiloglu S, Sari G, Ozdal T, Capanoglu E. Guidelines for cell viability assays. Food Front. 2020 Sep 1;1(3):332–49.

293. White K, Chalaby R, Lowe G, Berlin J, Glackin C, Olabisi R. Calcein binding to assess mineralization in hydrogel microspheres. Polymers (Basel). 2021;13(14):1–8.

294. Serguienko A, Wang MY, Myklebost O. Real-Time Vital Mineralization Detection and Quantification during In Vitro Osteoblast Differentiation. Biol Proced Online [Internet]. 2018 Dec 1;20(1):14. Available from: https://biologicalproceduresonline.biomedcentral.com/articles/10.1186/s12575-018-0079-4

295. Puchtler H, Meloan SN, Terry MS. On The History and Mechanism of Alizarin and Alizarin Red S Stains for Caclium. The Journal of Histochemistry and Cytochemistry. 1969;17(2):110–24.

296. Postek MT, Vladár AE. Does your SEM Really tell the truth? - How would you know? Part 1. Scanning. 2013 Nov;35(6):355–61.

297. Sutton NA, Hughes N, Handley PS. A comparison of conventional SEM techniques, low temperature SEM and the electroscan wet scanning electron microscope to study the structure of a biofilm of Streptococcus crista CR3. Journal of Applied Bacteriology. 1994;76(5):448–54.

298. Miyoshi K. Surface Characterization Techniques: An Overview [Internet]. Cleveland, Ohio; 2002. Available from: www.sti.nasa.gov

299. Park H, Guo X, Temenoff JS, Tabata Y, Caplan AI, Kasper FK, et al. Effect of swelling ratio of injectable hydrogel composites on chondrogenic differentiation of encapsulated rabbit marrow mesenchymal stem cells in vitro. Biomacromolecules. 2009 Mar 9;10(3):541–6.

300. Klein C, Meller C, Schäfer E. Human Primary Odontoblast-like Cell Cultures—A Focused Review Regarding Cell Characterization. J Clin Med [Internet]. 2022 Sep 8;11(18):5296. Available from: https://www.mdpi.com/2077-0383/11/18/5296

301. Hall BK, Eckhard Witten P. Plasticity and Variation of Skeletal Cells and Tissues and the Evolutionary Development of Actinopterygian Fishes. In: Underwood C, Richter M, Johanson Z, editors. Evolution and Development of Fishes [Internet]. Cambridge: Cambridge University Press; 2019. p. 126–43. Available from: https://www.cambridge.org/core/books/evolution-and-development-of-fishes/plasticity-and-variation-of-skeletal-cells-and-tissues-and-the-evolutionary-development-of-actinopterygian-fishes/8D8B5AA655AA47E3E1AE1A5506107229

302. About I, Bottero MJ, De Denato P, Camps J, Franquin JC, Mitsiadis TA. Human dentin production in vitro. Exp Cell Res. 2000 Jul 10;258(1):33–41.

303. Martini D, Trirè A, Breschi L, Mazzoni A, Orsini G, Teti G, et al. Dentin matrix protein 1 and dentin sialophosphoprotein in human sound and carious teeth: An immunohistochemical and colorimetric assay. European Journal of Histochemistry. 2013 Oct 29;57(4):217–24.

304. Qin C, D'Souza R, Feng JQ. Dentin Matrix Protein 1 (DMP1): New and Important Roles for Biomineralization and Phosphate Homeostasis. J Dent Res [Internet]. 2007 Dec 8;86(12):1134–41. Available from: http://journals.sagepub.com/doi/10.1177/154405910708601202

305. Qin C, Brunn JC, Cadena E, Ridall A, Butler WT. Dentin sialoprotein in bone and dentin sialophosphoprotein gene expressed by osteoblasts. Connect Tissue Res. 2003;44(SUPPL. 1):179–83.

306. Abcam. Direct vs indirect immunofluorescence [Internet]. [cited 2023 Sep 12]. Available from: https://www.abcam.com/secondary-antibodies/direct-vs-indirect-immunofluorescence#:~:text=Direct%20IF%20uses%20a%20single,antibody%20is%20used%20for%20detection.

307. About I, Laurent-Maquin D, Lendahl U, Mitsiadis TA. Nestin expression in embryonic and adult human teeth under normal and pathological conditions. American Journal of Pathology [Internet]. 2000;157(1):287–95. Available from: http://dx.doi.org/10.1016/S0002-9440(10)64539-7

308. Schmittgen TD, Livak KJ. Analyzing real-time PCR data by the comparative CT method. Nat Protoc. 2008 May;3(6):1101–8.

309. Jalali M, Zaborowska J, Jalali M. Chapter 1 - The Polymerase Chain Reaction: PCR, qPCR, and RT-PCR. In: Jalali M, Saldanha FYL, Jalali M, editors. Basic Science Methods for Clinical Researchers [Internet]. Boston: Academic Press; 2017. p. 1–18. Available from: https://www.sciencedirect.com/science/article/pii/B9780128030776000011

310. Marmiroli N, Maestri E. Chapter 6 - Polymerase chain reaction (PCR). In: Picó Y, editor. Food Toxicants Analysis [Internet]. Amsterdam: Elsevier; 2007. p. 147–87. Available from: https://www.sciencedirect.com/science/article/pii/B9780444528438500079

311. Sabandal MMI, Schäfer E, Imper J, Jung S, Kleinheinz J, Sielker S. Simvastatin induces in vitro mineralization effects of primary human odontoblast-like cells. Materials. 2020 Oct 2;13(20):1–14.

312. Oyen ML. Mechanical characterisation of hydrogel materials. Vol. 59, International Materials Reviews. Maney Publishing; 2014. p. 44–59.

313. Yu AL, Birke K, Burger J, Welge-Lussen U. Biological Effects of Cigarette Smoke in Cultured Human Retinal Pigment Epithelial Cells. Boulton ME, editor. PLoS One [Internet]. 2012 Nov 14;7(11). Available from: https://dx.plos.org/10.1371/journal.pone.0048501

314. Omran MAA, Fabb SA, Dickson G. Biochemical and morphological analysis of cell death induced by Egyptian cobra (Naja haje) venom on cultured cells. Journal of Venomous Animals and Toxins including Tropical Diseases. 2004;10(3):219–41.

315. Fernie AR, Zhang Y, Sampathkumar A. Cytoskeleton Architecture Regulates Glycolysis Coupling Cellular Metabolism to Mechanical Cues. Vol. 45, Trends in Biochemical Sciences. Elsevier Ltd; 2020. p. 637–8.

316. Park JS, Burckhardt CJ, Lazcano R, Solis LM, Isogai T, Li L, et al. Mechanical regulation of glycolysis via cytoskeleton architecture. Nature. 2020 Feb 27;578(7796):621–6.

317. Riis S, Nielsen FM, Pennisi CP, Zachar V, Fink T. Comparative Analysis of Media and Supplements on Initiation and Expansion of Adipose-Derived Stem Cells. Stem Cells Transl Med. 2016 Mar 1;5(3):314–24.

318. Hanna H, Mir LM, Andre FM. In vitro osteoblastic differentiation of mesenchymal stem cells generates cell layers with distinct properties. Stem Cell Res Ther [Internet]. 2018 Dec

27;9(1):203. Available from: https://stemcellres.biomedcentral.com/articles/10.1186/s13287-018-0942-x

319. Jia F, Wang J, Peng J, Zhao P, Kong Z, Wang K, et al. D-amino acid substitution enhances the stability of antimicrobial peptide polybia-CP. Acta Biochim Biophys Sin (Shanghai). 2017 Oct 1;49(10):916–25.

320. Lee SK, Mortensen LJ, Lin CP, Tung CH. An authentic imaging probe to track cell fate from beginning to end. Nat Commun [Internet]. 2014 Oct 17;5(1):5216. Available from: https://www.nature.com/articles/ncomms6216

321. Okiji T, Yoshiba K. Reparative Dentinogenesis Induced by Mineral Trioxide Aggregate: A Review from the Biological and Physicochemical Points of View. Int J Dent [Internet]. 2009;2009:1–12. Available from: http://www.hindawi.com/journals/ijd/2009/464280/

322. Kuratate M, Yoshiba K, Shigetani Y, Yoshiba N, Ohshima H, Okiji T. Immunohistochemical Analysis of Nestin, Osteopontin, and Proliferating Cells in the Reparative Process of Exposed Dental Pulp Capped with Mineral Trioxide Aggregate. J Endod. 2008 Aug;34(8):970–4.

323. Narayanan K, Gajjeraman S, Ramachandran A, Hao J, George A. Dentin matrix protein 1 regulates dentin sialophosphoprotein gene transcription during early odontoblast differentiation. Journal of Biological Chemistry. 2006 Jul 14;281(28):19064–71.

324. Jhala D, Vasita R. A Review on Extracellular Matrix Mimicking Strategies for an Artificial Stem Cell Niche. Vol. 55, Polymer Reviews. Bellwether Publishing, Ltd.; 2015. p. 561–95.

325. Liu G, Xu G, Gao Z, Liu Z, Xu J, Wang J, et al. Demineralized Dentin Matrix Induces Odontoblastic Differentiation of Dental Pulp Stem Cells. Cells Tissues Organs [Internet]. 2015 Nov 17;201(1):65–76. Available from: https://doi.org/10.1159/000440952

326. Ansari S, Ito K, Hofmann S. Alkaline Phosphatase Activity of Serum Affects Osteogenic Differentiation Cultures. ACS Omega. 2022 Apr 19;7(15):12724–33.

327. Tjäderhane L, Carrilho MR, Breschi L, Tay FR, Pashley DH. Dentin basic structure and composition - an overview. Endod Topics. 2012;20:3–29.

328. Liolios L, Jenney A, Spelman D, Kotsimbos T, Catton M, Wesselingh S. Comparison of a multiplex reverse transcription-PCR-enzyme hybridization assay with conventional viral culture and immunofluorescence techniques for the detection of seven viral respiratory pathogens. J Clin Microbiol. 2001;39(8):2779–83.

329. Hargreaves KM, Cohen S. Cohen's Pathways of the Pulp. 10th ed. St Louis, Missouri: Mosby; 2010. 491–494 p.

330. Salerno M, Dante S, Patra N, Diaspro A. AFM measurement of the stiffness of layers of agarose gel patterned with polylysine. Microsc Res Tech. 2010 Oct;73(10):982–90.

331. Alam K, Umer J, Iqbal M, Hasan A. Measurements of Elastic Properties of Biological Hydrogels using Atomic Force Microscopy. J Phys Conf Ser [Internet]. 2020 Feb 1;1455(1):012012. Available from: https://iopscience.iop.org/article/10.1088/1742-6596/1455/1/012012

332. De Maria C, Rincon J, Duarte AA, Vozzi G, Boland T. A new approach to fabricate agarose microstructures. Polym Adv Technol. 2013 Oct;24(10):895–902.

333. Normand V, Lootens DL, Amici E, Plucknett KP, Aymard P. New insight into agarose gel mechanical properties. Biomacromolecules. 2000;1(4):730–8.

334. Pernodet N, Maaloum M, Tinland B. Pore size of agarose gels by atomic force microscopy. Electrophoresis. 1997;18(1):55–8.

335. Prouvé E, Rémy M, Feuillie C, Molinari M, Chevallier P, Drouin B, et al. Interplay of matrix stiffness and stress relaxation in directing osteogenic differentiation of mesenchymal stem cells. Biomater Sci. 2022 Jul 8;10(17):4978–96.

336. Wang YK, Chen CS. Cell adhesion and mechanical stimulation in the regulation of mesenchymal stem cell differentiation. Vol. 17, Journal of Cellular and Molecular Medicine. 2013. p. 823–32.

337. Venugopal B, Mogha P, Dhawan J, Majumder A. Cell density overrides the effect of substrate stiffness on human mesenchymal stem cells' morphology and proliferation. Biomater Sci. 2018 May 1;6(5):1109–19.